frontiers | Research Topics

Regulation of inflammation and metabolism in retinal neurodegenerative disorders

Edited by
Henri Leinonen, Ellen Tianwei Zhou, Zhongjie Fu, Anu Kauppinen and Brian G. Ballios

Published in
Frontiers in Neuroscience
Frontiers in Molecular Neuroscience

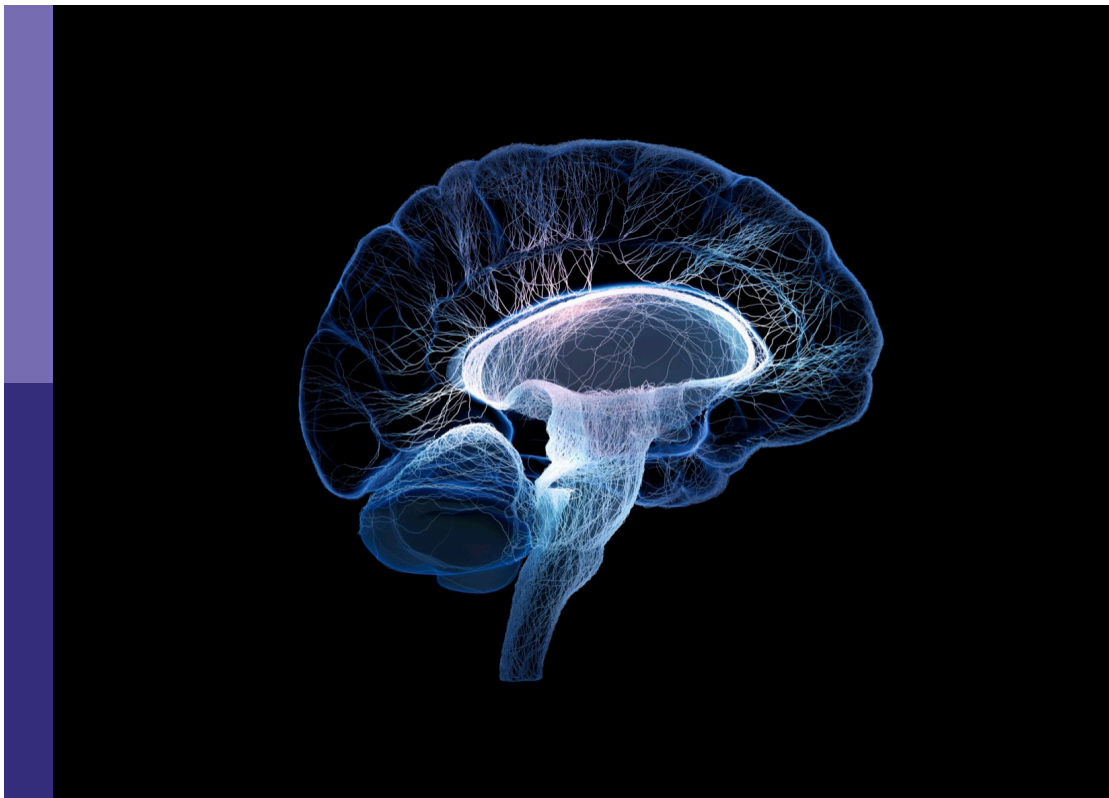

ISSN 1664-8714
ISBN 978-2-83251-083-4
DOI 10.3389/978-2-83251-083-4

About Frontiers

Frontiers is more than just an open access publisher of scholarly articles: it is a pioneering approach to the world of academia, radically improving the way scholarly research is managed. The grand vision of Frontiers is a world where all people have an equal opportunity to seek, share and generate knowledge. Frontiers provides immediate and permanent online open access to all its publications, but this alone is not enough to realize our grand goals.

Frontiers journal series

The Frontiers journal series is a multi-tier and interdisciplinary set of open-access, online journals, promising a paradigm shift from the current review, selection and dissemination processes in academic publishing. All Frontiers journals are driven by researchers for researchers; therefore, they constitute a service to the scholarly community. At the same time, the *Frontiers journal series* operates on a revolutionary invention, the tiered publishing system, initially addressing specific communities of scholars, and gradually climbing up to broader public understanding, thus serving the interests of the lay society, too.

Dedication to quality

Each Frontiers article is a landmark of the highest quality, thanks to genuinely collaborative interactions between authors and review editors, who include some of the world's best academicians. Research must be certified by peers before entering a stream of knowledge that may eventually reach the public - and shape society; therefore, Frontiers only applies the most rigorous and unbiased reviews. Frontiers revolutionizes research publishing by freely delivering the most outstanding research, evaluated with no bias from both the academic and social point of view. By applying the most advanced information technologies, Frontiers is catapulting scholarly publishing into a new generation.

What are Frontiers Research Topics?

Frontiers Research Topics are very popular trademarks of the *Frontiers journals series*: they are collections of at least ten articles, all centered on a particular subject. With their unique mix of varied contributions from Original Research to Review Articles, Frontiers Research Topics unify the most influential researchers, the latest key findings and historical advances in a hot research area.

Find out more on how to host your own Frontiers Research Topic or contribute to one as an author by contacting the Frontiers editorial office: frontiersin.org/about/contact

Regulation of inflammation and metabolism in retinal neurodegenerative disorders

Topic editors

Henri Leinonen — University of Eastern Finland, Finland
Ellen Tianwei Zhou — University of Toronto, Canada
Zhongjie Fu — Boston Children's Hospital, Harvard Medical School, United States
Anu Kauppinen — University of Eastern Finland, Finland
Brian G. Ballios — University of Toronto, Canada

Citation

Leinonen, H., Zhou, E. T., Fu, Z., Kauppinen, A., Ballios, B. G., eds. (2023). *Regulation of inflammation and metabolism in retinal neurodegenerative disorders*. Lausanne: Frontiers Media SA. doi: 10.3389/978-2-83251-083-4

Table of contents

frontiers | Frontiers in Neuroscience

TYPE Editorial
PUBLISHED 02 December 2022
DOI 10.3389/fnins.2022.1102385

OPEN ACCESS

EDITED AND REVIEWED BY
Jianhai Du,
West Virginia University, United States

*CORRESPONDENCE
Henri Leinonen
henri.leinonen@uef.fi
Zhongjie Fu
zhongjie.fu@childrens.harvard.edu

SPECIALTY SECTION
This article was submitted to Neurodegeneration, a section of the journal Frontiers in Neuroscience

RECEIVED 18 November 2022
ACCEPTED 22 November 2022
PUBLISHED 02 December 2022

CITATION
Leinonen H, Zhou TE, Ballios BG, Kauppinen A and Fu Z (2022) Editorial: Regulation of inflammation and metabolism in retinal neurodegenerative disorders. *Front. Neurosci.* 16:1102385. doi: 10.3389/fnins.2022.1102385

Editorial: Regulation of inflammation and metabolism in retinal neurodegenerative disorders

Henri Leinonen[1]*, Tianwei Ellen Zhou[2], Brian G. Ballios[2], Anu Kauppinen[1] and Zhongjie Fu[3]*

[1]Faculty of Health Sciences, School of Pharmacy, University of Eastern Finland, Kuopio, Finland, [2]Department of Ophthalmology and Vision Sciences, University of Toronto, Toronto, ON, Canada, [3]Department of Ophthalmology, Harvard Medical School, Boston Children's Hospital, Boston, MA, United States

KEYWORDS

neovascularization, retina, retinopathy, metabolism, inflammation

Editorial on the Research Topic
Regulation of inflammation and metabolism in retinal neurodegenerative disorders

Inflammation and metabolic alterations are two significant contributors to retinal degenerative disorders (RD) including diabetic retinopathy (DR), retinopathy of prematurity (ROP), glaucoma, and age-related macular degeneration (AMD). To facilitate research on new potential therapeutic targets, in this Research Topic we highlighted the role of inflammation and metabolism, as well as their interaction in disease progression.

Inflammation

DR and AMD are leading causes of vision loss in working-age adults and seniors, respectively (Bressler, 2004; Lee et al., 2015). DR initially manifests with cellular features of an inflammatory phenotype and reduced retinal blood flow due to arteriopathy, leading to hypoxia. Ischemia and reperfusion (I/R) injury can be used to model the hypoxic condition and screen therapeutic approaches to inhibit DR (Zheng et al., 2007). Goit et al. showed that anti-inflammatory α-melanocyte-stimulating hormone (α-MSH) alleviated I/R-induced retinal damage in diabetic mice under hyperglycemic condition. A follow-up study in non-diabetic conditions is warranted to better understand the mechanism, and local vs. systemic effects α-MSH should be clarified.

The degeneration of retinal pigment epithelium (RPE) cells results in the death of photoreceptors and to the loss of central vision in AMD (Kauppinen et al., 2016). Wong et al. provided an update about the interplay of RPE dysfunction and the innate immune system in AMD. It has long been held that the healthy eye is an immune-privileged environment and the subretinal space is devoid of microglia/macrophages. However, following the RPE damage, circulating mononuclear phagocytes (MP) can infiltrate into the subretinal space. The accumulation of MPs is likely meant to be a defense mechanism resulting in low-grade inflammation, called para-inflammation, maintaining tissue homeostasis. However, if the normal inflammation resolution mechanism fails, for instance, due to abnormal complement function, inflammation can shift from beneficial para- to detrimental pro-inflammatory state. Accordingly, MP factors that maintain the adaptive para-inflammation in aging RPE vs. those that trigger an overt pro-inflammatory response is a promising strategy for developing therapies to slow vision loss in AMD. Certain complement pathway inhibitors have slowed down dry AMD-associated geographic atrophy progression in Phase II trials. However, the clinical risk-to-benefit profile of these approaches requires close monitoring (Lin et al., 2021; Tolentino and Tolentino, 2022). Tao et al. reviewed the role of receptor-interacting protein kinase (RIPK)-dependent necroptosis in RD. Accumulating data from experimental models suggest that RIPK inhibition can reduce inflammation and necroptosis, phenomena that enhances each other, in various types of RD, including dry AMD. More research is needed to understand whether RIPK-dependent necroptosis could be a feasible drug target in AMD and/or other types of RD.

In retinal disorders, such as AMD, RPE cells suffer from the dysfunctionality of autophagy and mitochondria both of which contribute to the induction of inflammation and disturbed cellular metabolism (Kauppinen et al., 2016). Liu et al. suggested that suppressor of cytokine signaling 2 promotes autophagy activation by regulating glycogen synthase kinase 3β and mammalian target of rapamycin. Autophagy and inflammation are known to regulate each other in RPE cells and therefore autophagy activation could reduce inflammation (Kauppinen et al., 2016). Shu et al. demonstrated that the central pro-inflammatory cytokine tumor necrosis factor-alpha (TNF-α) enhanced inflammation and disturbed glycolysis and mitochondrial morphology in primary human RPE cells, suggesting an interaction between inflammation and metabolism. They also showed that the pre-treatment of RPE cells with dimethyl fumarate (DMF) prevented TNF-α-induced mitochondrial dysfunction and morphological abnormalities. In an animal model of Parkinson's disease, DMF protected the brain by activating autophagy and modulating neuroinflammation (Lastres-Becker et al., 2016). DMF has been associated with autophagy activation in human RPE cells (Catanzaro et al., 2020).

Metabolism

Metabolic alterations in the neural retina and the supporting cells (glia and RPE) contribute to retinal abnormalities including retinal vessel regression and proliferation (Joyal et al., 2018; Fu et al., 2019, 2021). Nilsson et al. provided an insight into the serum metabolome of extremely premature infants, which changed substantially in the neonatal period. No significant association between serum metabolome and retinopathy of prematurity and bronchopulmonary dysplasia was identified. Interestingly, circulating lipid and amino acid profile correlated with enteral energy intake. Further exploration of enteral vs. parenteral energy intake on premature complications is needed to personalize nutritional management in premature infants during the neonatal period. Shahandeh et al. summarized retinal iron metabolism and the clinical phenotypes of retinal changes including drusen-like deposits and progressive loss of visual function in iron disorders. Experimental studies also showed RPE damage and retinal dysfunction in mouse mutants with systemic iron loading and in mice with administration of exogenous iron. Further understanding of retinal pathology in systemic iron loading disorders is needed to develop therapies aimed at restoring retinal iron homeostasis. Pappenhagen et al. found that primary rat optic nerve head astrocytes had increased glycolysis under stretch stress, mimicking those findings that have been seen in glaucoma. Interestingly, the dependency of pyruvate and fatty acid as mitochondrial fuel increased in stretched optic nerve head astrocytes. Further validation in animal models *in vivo* would solidify the finding.

Clinical features and animal models of eye diseases

The increasing recognition that animals develop retinal diseases with similar traits to humans has provided a means for testing possible treatments and successful gene therapy trials. These animal models provided much insight into the underlying pathological mechanisms. Qiang et al. summarized the clinical, multimodal imaging, and pathological features of Type 3 macular neovascularization (MNV3), described the diversity of animal models, and compared their strengths and limitations. These models have revealed the roles of retinal hypoxia, inflammation, lipid metabolism, von Hippel–Lindau (VHL)–hypoxia-inducible factor (HIF) pathway, and retinoblastoma tumor suppressor (Rb)–E2F cell cycle pathway in the development of MNV3.

Collectively, this Research Topic includes original research and review articles regarding the contribution of inflammation and metabolic alterations to retinal disorders. Improved understanding of the disease mechanisms is

indispensable to the exploration of new potential therapeutic targets.

Author contributions

All authors listed have made a substantial, direct, and intellectual contribution to the work and approved it for publication.

Funding

This work was supported by NIH R01EY032492, NIH R01EY017017, Boston Children's Hospital (OFD/BTREC/CTREC Faculty Career Development Grant 97906, Pilot Grant 92214, and Ophthalmology Foundation 85010), Mass Lions Eye Foundation 77426 (ZF), Academy of Finland Grant 346295, Business Finland Grant 1689-31-2022, the Eye and Tissue Bank Foundation (Finland), Retina Registered Association (Finland), Sokeain Ystävät/De Blindas Vänner Registered Association (HL), and Foundation Fighting Blindness U.S. Career Development Award. CD-RM-0821-0806-UHN (BB).

Acknowledgments

As Topic Editors of this special issue, we sincerely thank all the authors and reviewers for their valuable contributions to this Research Topic.

Conflict of interest

The authors declare that the research was conducted in the absence of any commercial or financial relationships that could be construed as a potential conflict of interest.

Publisher's note

References

Bressler, N. M. (2004). Age-related macular degeneration is the leading cause of blindness. *JAMA* 291, 1900–1901. doi: 10.1001/jama.291.15.1900

Catanzaro, M., Lanni, C., Basagni, F., Rosini, M., Govoni, S., and Amadio, M. (2020). Eye-light on age-related macular degeneration: targeting nrf2-pathway as a novel therapeutic strategy for retinal pigment epithelium. *Front. Pharmacol.* 11, 844. doi: 10.3389/fphar.2020.00844

Fu, Z., Chen, C. T., Cagnone, G., Heckel, E., Sun, Y., Cakir, B. et al. (2019). Dyslipidemia in retinal metabolic disorders. *EMBO Mol. Med.* 11, e10473. doi: 10.15252/emmm.201910473

Fu, Z., Kern, T. S., Hellstrom, A., and Smith, L. E. H. (2021). Fatty acid oxidation and photoreceptor metabolic needs. *J. Lipid. Res.* 62, 100035. doi: 10.1194/jlr.TR120000618

Joyal, J. S., Gantner, M. L., and Smith, L. E. H. (2018). Retinal energy demands control vascular supply of the retina in development and disease: the role of neuronal lipid and glucose metabolism. *Prog. Retin. Eye Re.s* 64, 131–156. doi: 10.1016/j.preteyeres.2017.11.002

Kauppinen, A., Paterno, J. J., Blasiak, J., Salminen, A., and Kaarniranta, K. (2016). Inflammation and its role in age-related macular degeneration. *Cell Mol. Life Sci.* 73, 1765–1786. doi: 10.1007/s00018-016-2147-8

Lastres-Becker, I., Garcia-Yague, A. J., Scannevin, R. H., Casarejos, M. J., Kugler, S., Rabano, A., et al. (2016). Repurposing the NRF2 activator dimethyl fumarate as therapy against synucleinopathy in Parkinson's disease. *Antioxid. Redox Signal.* 25, 61–77. doi: 10.1089/ars.2015.6549

Lee, R., Wong, T. Y., and Sabanayagam, C. (2015). Epidemiology of diabetic retinopathy, diabetic macular edema and related vision loss. *Eye Vis. (Lond).* 2, 17. doi: 10.1186/s40662-015-0026-2

Lin, J. B., Halawa, O. A., Miller, J. W., and Vavvas, D. G. (2021). Complement inhibition for geographic atrophy: a tempting target with mixed results. *J. Clin. Med.* 10. doi: 10.3390/jcm10132890

Tolentino, M. J., and Tolentino, A. J. (2022). Investigational drugs in clinical trials for macular degeneration. *Expert. Opin. Investig. Drugs.* 31, 1067–1085. doi: 10.1080/13543784.2022.2113375

Zheng, L., Gong, B., Hatala, D. A., and Kern, T. S. (2007). Retinal ischemia and reperfusion causes capillary degeneration: similarities to diabetes. *Invest Ophthalmol. Vis. Sci.* 48, 361– doi: 10.1167/iovs.06-0510

frontiers in Neuroscience

REVIEW
published: 26 August 2021
doi: 10.3389/fnins.2021.734860

Clinical Pathological Features and Current Animal Models of Type 3 Macular Neovascularization

Wei Qiang[1,2†], *Ran Wei*[1,2†], *Yongjiang Chen*[3] *and Danian Chen*[1,2*]

[1] *Research Laboratory of Ophthalmology and Vision Sciences, State Key Laboratory of Biotherapy, West China Hospital, Sichuan University, Chengdu, China,* [2] *Department of Ophthalmology, West China Hospital, Sichuan University, Chengdu, China,* [3] *The School of Optometry and Vision Science, University of Waterloo, Waterloo, ON, Canada*

Type 3 macular neovascularization (MNV3), or retinal angiomatous proliferation (RAP), is a distinct type of neovascular age-related macular degeneration (AMD), which is a leading cause of vision loss in older persons. During the past decade, systematic investigation into the clinical, multimodal imaging, and histopathological features and therapeutic outcomes has provided important new insight into this disease. These studies favor the retinal origin of MNV3 and suggest the involvement of retinal hypoxia, inflammation, von Hippel–Lindau (VHL)–hypoxia-inducible factor (HIF)–vascular endothelial growth factor (VEGF) pathway, and multiple cell types in the development and progression of MNV3. Several mouse models, including the recently built *Rb/p107/Vhl* triple knockout mouse model by our group, have induced many of the histological features of MNV3 and provided much insight into the underlying pathological mechanisms. These models have revealed the roles of retinal hypoxia, inflammation, lipid metabolism, VHL/HIF pathway, and retinoblastoma tumor suppressor (Rb)–E2F cell cycle pathway in the development of MNV3. This article will summarize the clinical, multimodal imaging, and pathological features of MNV3 and the diversity of animal models that exist for MNV3, as well as their strengths and limitations.

Keywords: age-related macular degeneration (AMD), animal model, Type 3 macular neovascularization, retinal angiomatous proliferation (RAP), multimodal imaging, von Hippel – Lindau, hypoxia inducible factor (HIF), retinoblastoma gene (Rb1)

OPEN ACCESS

Edited by:
Zhongjie Fu,
Boston Children's Hospital, Harvard Medical School, United States

Reviewed by:
Leila El Matri,
Hedi Rays Institute of Ophthalmology of Tunis, Tunisia
José Carlos Rivera,
University of Montreal, Canada

****Correspondence:***
Danian Chen
danianchen2006@qq.com
orcid.org/0000-0002-6916-2978

† These authors have contributed equally to this work

Specialty section:
This article was submitted to Neurodegeneration, a section of the journal Frontiers in Neuroscience

Received: *01 July 2021*
Accepted: *29 July 2021*
Published: *26 August 2021*

Citation:
Qiang W, Wei R, Chen Y and Chen D (2021) Clinical Pathological Features and Current Animal Models of Type 3 Macular Neovascularization. Front. Neurosci. 15:734860. doi: 10.3389/fnins.2021.734860

INTRODUCTION

Type 3 macular neovascularization (MNV3) is a unique form of late-stage age-related macular degeneration (AMD), which has been discovered three decades ago, but its pathogenic mechanism is still elusive.

Age-Related Macular Degeneration

Age-related macular degeneration is the leading cause of legal blindness in aged individuals in developed countries (Klein et al., 2002; Mitchell et al., 2018; Fleckenstein et al., 2021). AMD is a multifactorial disease related to aging, genetic susceptibility, and environmental risk factors. AMD affects photoreceptors, retinal pigment epithelium (RPE), Bruch membrane, and the

choriocapillaris around the macular area (Fleckenstein et al., 2021). A systematic review showed that ∼8.7% of the worldwide population has AMD; there are nearly 196 million AMD patients all over the world in 2020, and this number will increase to ∼288 million in 2040 (Wong et al., 2014). According to the characteristics of the disease, AMD can be divided into two types: dry AMD and wet AMD (Ferris et al., 2013). Dry AMD accounts for about 85%, manifested as degeneration of RPE cells and photoreceptors; in severe cases, geographic atrophy (GA) forms. Wet AMD, also known as neovascular AMD (nAMD), accounts for about 15%, manifested as macular neovascularization (MNV). More than 80% of patients blinded by AMD are due to wet AMD (Miller, 2013). Clinically, AMD can be classified as early-stage (medium-sized and large drusen, pseudodrusen, and/or retinal pigment anomalies) and late-stage (nAMD and GA) (Klein et al., 2014; Mitchell et al., 2018).

Traditionally, nAMD is considered choroidal neovascularization (CNV) and is divided into occult (type 1) and classical (type 2) CNV (Macular-Group., 1991). Type 1 CNV refers to neovascular vessels confined to the sub-RPE space, and Type 2 refers to vessels proliferating above the RPE in the subretinal space (Gass, 1997). Recently, nAMD is renamed as MNV and classified into type 1 MNV, type 2 MNV, and type 3 MNV; polypoidal choroidal vasculopathy (PCV) is considered a subtype of type 1 MNV (also called aneurysmal type 1 neovascularization) (Spaide et al., 2020). Type 1 MNV is the occult (type 1) CNV, type 2 MNV is the classical (type 2) CNV, and type 3 MNV is retinal angiomatous proliferation (RAP) (Spaide et al., 2020).

Type 3 Macular Neovascularization

Type 3 macular neovascularization is an important subtype of nAMD (**Figure 1**), different from the type 1 or type 2 MNV as mentioned earlier (Yannuzzi et al., 2001; Freund et al., 2008). It was first reported in 1992, in which unusual RPE detachments were associated with retinal vessels that dove down into the deep retina and formed an angiomatous lesion (Hartnett et al., 1992). Kuhn et al. (1995) also described similar lesions by fluorescein and indocyanine green angiography and termed such lesions as chorioretinal anastomosis. Subsequently, it has also been referred to as deep retinal vascular anomalous complexes (RVACs) (Hartnett et al., 1996). Based on their clinical observation of 143 AMD eyes with intraretinal neovascularization (IRN), Yannuzzi et al. (2001) named this disease as RAP to suggest an intraretinal origin and proposed a three-stage model of progression including IRN (stage 1), subretinal neovascularization (SRN; stage 2), and CNV (stage 3). Gass et al. (2003) proposed a different explanation and suggested the term occult chorioretinal anastomosis (OCRA) to emphasize the choroidal origin of the intraretinal complex. Lacking a definitive sequential histopathologic evidence of its intraretinal vs. choroidal origin, in 2008, type 3 neovascularization was proposed for this entity (Freund et al., 2008) to emphasize the intraretinal location of the vascular complex and distinguish this type from type 1 and type 2 CNV previously described (Gass, 1997) rather than the clinically debated origins (Yannuzzi et al., 2008). MNV3 is the consensus term for this disease entity now (Spaide et al., 2020).

Epidemiology of Type 3 Macular Neovascularization

Type 3 macular neovascularization accounts for 15–20% of nAMD patients in white populations (Yannuzzi et al., 2008) and 4.5–11.1% among Asians (Song et al., 2009). When dye-based angiography and optical coherence tomography (OCT) were combined to identify lesion composition, MNV3 was found to be the presenting lesion type in 34.2% of eyes with newly diagnosed nAMD (Jung et al., 2014; Li et al., 2018). MNV3 usually occurs in individuals older than 75 years and is popular in women; the male-to-female ratio is about 1:2 (Marticorena et al., 2011; Tsai et al., 2017). There is a tendency toward bilateral involvement. It was found that 40% of the patients with unilateral MNV3 developed an MNV3 lesion in the fellow eye by 1 year, 56% by 2 years, and 100% by 3 years (Gross et al., 2005). The risk of fellow-eye involvement in MNV3 patients is significantly higher than that in typical nAMD patients (Yannuzzi et al., 2001).

Clinical Features of Type 3 Macular Neovascularization

The main clinical signs of MNV3 include superficial intraretinal hemorrhages and edema, hard exudates, pigment epithelial detachment (PED), and reticular pseudodrusen (RPD) (Maruko et al., 2007; Berenberg et al., 2012; Ueda-Arakawa et al., 2013; Kim et al., 2014, 2015; Ravera et al., 2016; Tsai et al., 2017). The combination of intraretinal hemorrhages, hard exudates, and PED is strongly associated with the presence of a connection between the retinal vasculature and the neovascular complex (Donati et al., 2006). The presence of small retinal hemorrhages, macular soft drusen, and RPD is highly predictive of MNV3, and especially intraretinal hemorrhages are a distinguishing feature from typical CNV (Yannuzzi et al., 2001; Kim et al., 2014; Tsai et al., 2017). RPE atrophy, GA, and focal hyperpigmentation are common features in the fellow eyes of MNV3 (Martins et al., 2018). RPD and a large area of soft drusen are risk factors for bilateral MNV3 (Miki Sawa et al., 2014; Marques et al., 2015; Chang et al., 2016).

Classification and Multimodal Imaging of Type 3 Macular Neovascularization

The three-stage classification proposed by Yannuzzi et al. (2001) is the most commonly used classification in clinical studies of MNV3, mainly based on clinical findings, fluorescein angiographic (FA), and indocyanine green angiographic (ICGA) findings (Yannuzzi et al., 2001; Tsai et al., 2017). FA revealed a feeding retinal arteriole dipping toward the RPE, forming "an angiomatous lesion" in the subretinal space. The FA features include intraretinal and subretinal leakage with indistinct margins or a vascularized PED, which simulates an occult (type 1) CNV pattern. With ICGA, the MNV3 is seen as a focal area of intense hyper-fluorescence corresponding to the neovascularization ("hot spot"). There is a late extension of the leakage within the retina from the IRN. Recently, multimodal imaging is also being widely applied in the diagnosis and classification of MNV3, including spectral domain optical

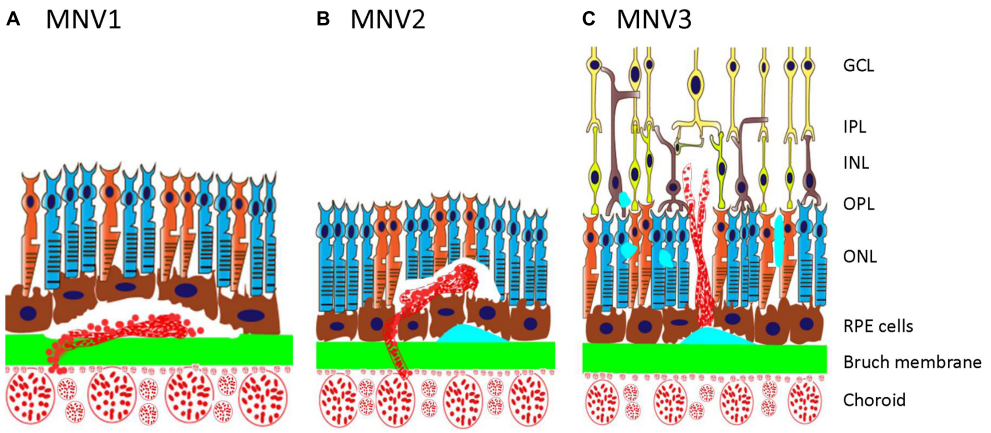

FIGURE 1 | Schematic showing type 1, type 2, and type 3 MNV. **(A)** Type 1 MNV is an ingrowth of vessels originating from the choriocapillaris into the sub-RPE space. **(B)** Type 2 MNV is the proliferation of new vessels arising from the choroid into the subretinal space. **(C)** Type 3 MNV is a downgrowth of vessels from the retinal vascular plexus toward the outer retina. GCL, ganglion cell layer; IPL, inner plexiform layer; INL, inner nuclear layer; OPL, outer plexiform layer; ONL, outer nuclear layer; RPE, retinal pigment epithelium; MNV, macular neovascularization.

coherence tomography (SD-OCT) and OCT angiography (OCT-A) (Ravera et al., 2016; Su et al., 2016).

Optical coherence tomography indicates that MNV3 is a focal hyperreflective lesion in the neurosensory retina with surrounding serous fluid (Brancato et al., 2002; Tsai et al., 2017). On high-resolution SD-OCT, the precursor lesion of MNV3 is punctate hyperreflective foci (HRF) in the outer retina (Nagiel et al., 2015). HRF represents two cell types, RPE cells that migrated into the outer retina and lipid-filled cells (Nagiel et al., 2015; Querques et al., 2015; Li et al., 2018). The IRN corresponded to a hyperreflective mass from the outer plexiform layer to the deeper layers and generally originated outside the fovea avascular zone (Matsumoto et al., 2010). The hyperreflective lesion often developed into sub-RPE within underlying drusen or drusenoid PED (Querques et al., 2013). These findings confirm the intraretinal localization of the MNV3, which is always associated with impressive exudative phenomena such as fluid, RPE elevation, and PED. Disruption of the external limiting membrane (ELM) and intraretinal edema internal to the PED are also common in MNV3 (Tsai et al., 2017). OCT-based classification suggested that the origin of MNV3 is from the deep retinal vascular plexus, followed by a disruption of outer retinal layers and penetration through the RPE (Su et al., 2016).

Spectral domain optical coherence tomography also revealed that the subfoveal choroid of MNV3 lesion is significantly thinner than that of age-matched control eyes (Yamazaki et al., 2014). Subfoveal choroidal thickness is considered a predictor of visual outcome and treatment response after anti-vascular endothelial growth factor (VEGF) treatment for typical exudative AMD. A thick choroid was correlated with a better treatment response (Kang et al., 2014). Anti-VEGF therapy on MNV3 can reduce the choroidal thickness significantly for a short time, and a thick choroid has been associated with a higher rate of recurrence of MNV3 (Kim et al., 2016). Thus, OCT is particularly suitable in planning the treatment of MNV3 and monitoring the disease, especially in the context of anti-VEGF therapy (Politoa et al., 2006; Fleckenstein et al., 2021).

Optical coherence tomography angiography is a non-invasive tool and provides independent analysis of blood flow based on motion contrast in the various retinal and choroidal layers (Fingler et al., 2008; Spaide et al., 2015). High-resolution volumetric blood flow information can be obtained to generate angiographic images in a matter of seconds, but no information on vascular wall integrity can be obtained; thus, OCT-A allows a detailed characterization and detection of MNV3, as the vessel structure is not obscured by dye leakage or dye staining of drusen (Perrott-Reynolds et al., 2019). OCT-A illustrates MNV3 lesions as distinct high-flow, tuft-like capillary networks (Borrelli et al., 2018). In the early stage of MNV3, there are frequently small claw-like lesions, which represent the sub-RPE neovascular tissues, connecting to high-flow, tuft-like lesions (Miere et al., 2015). In some cases, a "feeding" vessel can be observed in the neovascular complexes that communicated with inner retinal circulation (Kuehlewein et al., 2015).

Hyperreflective foci on structural SD-OCT represents a precursor lesion of MNV3 (Su et al., 2016). The relationship between HRF on SD-OCT and flow on OCT-A had also been studied. It was demonstrated that HRF on structural OCT corresponds to a small tuft of vessels on OCT-A but only after the development of intraretinal edema, a sign of active MNV3 (Kuehlewein et al., 2015; Tan et al., 2017). However, for nascent MNV3 lesions, detectable flow on OCT-A corresponded to intraretinal HRF on SD-OCT, although no signs of active MNV3 (i.e., intraretinal fluid or serous PED) were noted (Sacconi et al., 2018). Surprisingly, a recent observation suggested that intraretinal edema is not a sign of active MNV3. In that study, the fellow eyes of MNV3 patients had been monitored by structural SD-OCT and OCT-A. It was found that macular edema could occur before neovascularization, and in eyes with MNV3, there was widespread edema with a greater area than that of neovascularization. The intraretinal edema before the formation

of MNV3 lesion may be related to VEGF-mediated retinal vessel leakage (Spaide, 2019). Thus, the relationship between flow on OCT-A, HRF, and intraretinal fluid needs further investigation.

Histopathological Studies of Type 3 Macular Neovascularization

Surgically excised neovascular membranes from MNV3 eyes (a total of 15 specimens) were histopathologically analyzed in two reports (Lafaut et al., 2000; Shimada et al., 2006). It was found that neovascularization was growing out of the neuroretina into the subretinal space (Lafaut et al., 2000). The neovascular masses expressed VEGF and included macrophages and RPE cells. VEGF was also expressed in retinal vessels above the RPE and fibroblasts below the RPE. Hypoxia-inducible factors (HIF-1a and HIF-2a) were expressed in vascular endothelial cells and macrophages (Shimada et al., 2006). None of the cases of stage II lesions showed vascular connections to the choroid, which only was observed in stage III lesions (Shimada et al., 2006). These findings confirm that the initial lesion of MNV3 is IRN, which advances into the sub-RPE space and forms retinochoroidal anastomoses (RCAs).

Postmortem histopathological study of both eyeballs with MNV3 from an 87-year-old woman showed intraretinal vascular complexes in the outer retina and adjacent to the inner portion of the Bruch membrane. The complex had a circumscribed mass of endothelial cells and was surrounded by an eosinophilic matrix. The RPE cells enveloped the lesion. Cells of the angiomatous lesion expressed VEGF, although not as strong as the adjacent neurosensory retina. The RPE was also strongly positive for VEGF, but the choroid exhibited little VEGF expression (Monson et al., 2008; Klein and Wilson, 2011). Similar retinal glomerular angiomatous lesions with encapsulation are also reported in two MNV3 eyes with hematoxylin and eosin (H&E) staining (presented in **Figure 1**-supplement 4 of Luo et al., 2013). In one eye with MNV3, the glomerular IRN lesion had decreased expression of soluble vascular endothelial growth factor receptor 1 (sVEGFR1) (Luo et al., 2013). Interestingly, the above described retinal glomerular angiomatous lesion with encapsulation in four MNV3 eyes is similar to the concentric layers of proliferating endothelial cells induced by intravitreal injections of VEGF in the eyes of adult primates (Tolentino et al., 1996). It is also similar to the pathological structures of von Hippel–Lindau (VHL) gene mutation-related retinal capillary hemangioblastoma (RCH), which mainly have proliferating-endothelial cells and VHL-deficient foamy (lipid-filled) stromal cells (Park and Chan, 2012).

Postmortem histopathological features of an eye with MNV3 from a 93-year-old man treated with serial ranibizumab injections revealed a vascular complex located from the inner plexiform layer to the inner portion of the Bruch membrane. There were only sparse cells present within the structure of the complex. The RPE monolayer underlying the lesion was disrupted; however, the inner portion of the Bruch membrane was intact. The histopathologic findings corresponded to an area of hyperreflectivity on SD-OCT imaging, confirming the reported tomographic appearance of MNV3 lesions (Skalet et al., 2017).

Serial anti-VEGF treatment likely causes the decreased cellularity in the MNV3 lesion. Postmortem histopathological study of an eye with MNV3 from an 86-year-old woman treated with six intravitreal injections of bevacizumab revealed similar results (Li et al., 2018). High-resolution epoxy resin histologic results indicated that the retinal vascular complex was implanted into the sub-RPE basal laminar deposit. No connection between the choriocapillaris and the sub-RPE space was observed. Both RPE-derived and lipid-filled cells were correlated with clinical intraretinal hyperreflective foci. The sub-RPE space contained macrophages, lymphocytes, Müller cell processes, and subducted RPE cells (Li et al., 2018). The lipid-filled cells are similar to foamy cells found in RCH, which may indicate deregulated lipid metabolism and the VHL–HIF hypoxia pathway (Park and Chan, 2012; Wei et al., 2019).

These pathological studies are consistent with the multimodal imaging findings (Borrelli et al., 2018) and reinforce the proposed retinal (but not choroidal) origin of MNV3 and suggest the involvement of retinal hypoxia, inflammation, and multiple cell types (such as photoreceptors, Müller cells, RPE cells, macrophages, microglial cells, lipid-filled cells, and fibroblasts) in the development and progression of MNV3. The expression of VEGF/HIFs in the MNV3 lesion and/or surrounding cells (Shimada et al., 2006), decreased expression of sVEGFR1 in the MNV3 lesion (Luo et al., 2013), the structure of glomerular IRN (Monson et al., 2008; Klein and Wilson, 2011; Luo et al., 2013), and the existence of intraretinal lipid-filled cells beside IRN (Li et al., 2018) support the idea that the VHL–HIF–VEGF hypoxia pathway mediates the pathogenesis of MNV3.

Anti-vascular Endothelial Growth Factor and Anti-inflammation Therapy of Type 3 Macular Neovascularization

Before the advent of intravitreal anti-VEGF therapy, treatment outcomes were generally poor. Most MNV3 patients declined to 20/200 or worse visual acuity because of subretinal fibrosis or disciform scar formation (Bottoni et al., 2005). Thus, MNV3 was considered a particularly treatment-resistant form of AMD (Scott and Bressler, 2009), which may not be true now.

Intravitreal injection of triamcinolone acetonide (IVTA) in combination with photodynamic therapy (PDT) or focal laser photocoagulation is an option for treating retinal neovascularization before the advent of anti-VEGF therapy. Triamcinolone can suppress the inflammation cascade and reduce intraretinal vascular leakage. PDT/IVTA treatment had been used in many clinical studies treating MNV3, especially for stages II and III MNV3 (Gupta et al., 2010). The results were generally promising, as many eyes had stable or improved visual acuity or had complete resolution of vessel leakage (Freund et al., 2006; Montero et al., 2009). A study with a 3-year follow-up compared the therapeutic effects between anti-VEGF alone, PDT with anti-VEGF, and PDT with IVTA treatment of MNV3. Vision improved only in the group treated with PDT/IVTA, although the group treated with PDT/anti-VEGF had the best anatomical outcome. However, more patients who received IVTA developed GA and underwent cataract surgery (Rouvas et al., 2012).

Anti-VEGF therapy has achieved favorable outcomes in MNV3, especially if treatment was initiated during the

early stage of the disease (stages I and II). Early diagnosis of MNV3 is possible using multimodal imaging such as OCT/OCT-A now. For instance, 1 year after anti-VEGF treatment, the communication between deep retinal capillaries and the RPE/sub-RPE space on OCT-A disappeared, while the neovascular tuft persisted at the level of the deep retinal capillaries (Miere et al., 2017; Sacconi et al., 2021). Anti-VEGF treatment induced about 70% complete occlusion of the lesion at 2–3 years, and stable or improved visual acuity was obtained in 95% and 100% of eyes at 2 years and 3 years, respectively (Gharbiya et al., 2014).

However, anti-VEGF therapy can induce the development of GA and RPE rip. The long-term visual outcome of stage III lesions is still poor (Daniel et al., 2016), and recurrences are common after the cessation of treatment (Baek et al., 2016). In stage III, the lesion showed persistent leakage after treatment, and the rate of lesion occlusion is low (Malamos et al., 2018). Patients with MNV3 who had no lesion on an OCT-A scan after anti-VEGF treatment showed a lower recurrence rate and maintained visual acuity with fewer injections than those with persistent high-flow lesions on an OCT-A scan (Han et al., 2020). The incidence rate of massive subretinal hemorrhage increased steadily with time for stage III MNV3 (Lee et al., 2017; Han et al., 2020). The early sign of recurrence is detectable flow deepening from the deep retinal capillaries to the RPE/sub-RPE space using OCT-A (Sacconi et al., 2021).

ANIMAL MODELS OF TYPE 3 MACULAR NEOVASCULARIZATION

While epidemiological, pathological, multimodal imaging and therapeutic studies in humans have provided important clues toward the potential causes of MNV3, elucidation of its underlying mechanisms has only been possible using experimental animal models. Based on the pathological studies, retinal hypoxia and inflammation are obviously involved in the development of MNV3 through multiple cell types. Currently, there are seven major types of mouse model commonly used in the field, including three models directly related to the hypoxia pathway (retina-specific *VhlKO* mice, *Vegf* overexpression, and *sVEGFR1* knockout in mouse photoreceptors), two models related to abnormal lipid metabolism (*Vldlr*$^{-/-}$ mice and *Cyp27a1*$^{-/-}$ mice), one model related to cell migration pathway (endothelial cell-specific *Srf* knockout mice), and RNV3 (JR5558) mice that have mutations in genes regulating retinal polarity and inflammation (**Table 1**).

Retina-Specific *Vhl* Knockout Mice With or Without *Rb* Gene Knockout

As discussed above, the expression of VEGF/HIFs in MNV3 lesions and surrounding cells (Shimada et al., 2006) and the decreased expression of sVEGFR1 in MNV3 lesions (Luo et al., 2013) support the idea that the VHL–HIF–VEGF hypoxia pathway mediates the pathogenesis of MNV3. HIF is the master regulator of the response to hypoxia because HIF-α induces the transcription of genes involved in hypoxia adaptation, including erythropoietin (EPO) and VEGF (Schofield and Ratcliffe, 2004; Semenza, 2004). VHL tumor suppressor protein is a component of the E3 ubiquitin ligase complex that targets HIF-α for proteasomal degradation. Human VHL gene mutations cause VHL disease, a multisystem tumor syndrome associated with many tumors, such as brain hemangioblastoma and clear cell renal cell carcinomas (CCRCCs) (Lonser et al., 2003). RCH is the hallmark lesion of ocular VHL disease (Park and Chan, 2012). Histologically, RCH mainly consists of vascular endothelial cells and vacuolated "foamy" lipid-filled stromal cells likely due to VHL deficiency-induced abnormal lipid metabolism, also seen in the CCRCC and liver hemangioblastoma (Haase et al., 2001).

TABLE 1 | Animal models of MNV3.

	Mouse models	Genes	Target cells	Vascular origin	IRN	SRN	RCA	Photoreceptor degeneration	References
1	*alpha-Cre,VhlKO*	Vhl	Retinal progenitors	Retina	a few	NO	NO	Yes	Kurihara et al., 2010; Lange et al., 2011a
2	*Chx10-Cre,VhlKO*	Vhl	Retinal progenitors	Retina	a few	NO	NO	Yes	Wert et al., 2016
3	*alpha-Cre,Rb/p107/VhlTKO*	Rb/p107/Vhl	Retinal progenitors	Retina	Yes	Yes	Yes	Yes	Wei et al., 2019
4	*Opsin-Cre, VhlKO*	Vhl	Rods	Retina	NO	NO	NO	Yes	Lange et al., 2011b
5	*Pde6g-CreERT2, VhlKO*	Vhl	Rods	Retina	Yes	NO	NO	Yes	Zhang et al., 2019
6	*BP-Cre, VhlKO*	Vhl	Cones	Retina	Yes	NO	NO	Yes	Barben et al., 2018b
7	*Trp1-Cre, VhlKO*	Vhl	RPE cells	Retina	Yes	Yes	Yes	Yes	Lange et al., 2012
8	*rho/VEGF*	VEGF	Rods	Retina	Yes	Yes	NO	Yes	Tobe et al., 1998; Ohno-Matsui et al., 2002
9	*iCre-75, Vegfr1KO*	VEGFR1	Rods	Retina	Yes	Yes	NO	Yes	Luo et al., 2013
10	*Vldlr*$^{-/-}$	Vldlr	all Cells	Retina	Yes	Yes	Yes	Yes	Heckenlively et al., 2003
11	*Cyp27a1*$^{-/-}$	Cyp27a1	all Cells	Retina/Choroid	Yes	Yes	Yes	NO	Omarova et al., 2012
12	*Srf*$^{-/-}$	Srf	Adult endothelial cells	Retina	Yes	Yes	NO	Yes	Weinl et al., 2013
13	*RNV3 (JR5558)*	Crb1/Jak3	all Cells	Retina	Yes	Yes	NO	Yes	Hasegawa et al., 2014; Nagai et al., 2014; Chang et al., 2018

The foamy stromal cells are considered the actual tumor cells in the hemangioblastoma (Park and Chan, 2012). These histological features of RCH are similar to the pathological finding of retinal specimens from MNV3 patients, including glomerular IRN (Monson et al., 2008; Klein and Wilson, 2011; Luo et al., 2013) and intraretinal lipid-filled cells beside IRN (Li et al., 2018).

Several retina-specific *Vhl* knockout mice have been established using different Cre mouse lines and *Vhl* floxed mice. These studies shed great light on the action of the hypoxia pathway in the retina and elucidate many aspects of the pathogenesis of MNV3. Three studies using *Pax6* α-*Cre* or *Chx10-Cre* to knockout (KO) *Vhl* in retinal progenitors found that *VhlKO* delays the regression of hyaloid vessels and the development of retinal vessels (Kurihara et al., 2010; Lange et al., 2011a) or prompt retinal capillary dropout (Wert et al., 2016). Retinal vessel density was notably reduced in the Cre-expression area, while a few vessels were penetrating the outer nuclear layer (ONL) (Kurihara et al., 2010; Lange et al., 2011a). Both *Pax6* α-*Cre* and *Chx10-Cre*-mediated *VhlKO* retinas have upregulated Hif expression, severe retinal degeneration, and reduced electroretinogram (ERG) response. While these phenotypes resemble the early stage of human MNV3, paradoxically, high Hif does not induce extensive angiogenesis as expected but instead inhibits retinal angiogenesis in the murine *Vhl* null retina. Deleting *Vhl* in all retinal cells and vascular endothelial cells using *UBC-Cre*^{ER} also suppresses retinal angiogenesis (Arreola et al., 2018). The mechanism is unknown, but we figured this out (Wei et al., 2019).

We showed that retinoblastoma tumor suppressor (Rb) constrains the expression of some Hif target genes in the *Vhl*$^{-/-}$ retina. Deleting *Rb* induced extensive retinal neovascularization and autophagic ablation of photoreceptors in the *Vhl*$^{-/-}$ retina. Unexpectedly, triple knockout (*Rb/p107/Vhl*TKO) mice do not develop retinoblastoma as expected (Chen et al., 2004) but generate subretinal vascular growths resembling MNV3 and RCH (Wei et al., 2019). The subretinal MNV3/RCH-like lesions broke the RPE and Bruch membrane to form RCA. Most stromal cells in the MNV3/RCH-like lesions were Sox9^{+}, suggesting a Müller glia origin, and expressed Gal3, a marker of human brain hemangioblastoma (Al-Salam et al., 2013). RNA sequencing revealed that the complement pathway, extracellular matrix pathway, and phosphoinositide 3-kinase (PI3K) pathway are activated (Wei et al., 2019). This model has important implications in understanding the pathogenesis of MNV3, as this model mimics some important environmental risk factors such as smoking, which can inactivate the *Rb* gene (Dasgupta et al., 2006), and retinal hypoxia, which can inactivate the *Vhl* gene (Lonser et al., 2003).

Ptf1a-Cre-mediated *VhlKO* in amacrine and horizontal cells induced overdevelopment of deep and intermediate vascular plexuses without neovascularization (Usui et al., 2015). Two studies knocked out the *Vhl* gene in rod cells using *opsin-Cre* (Lange et al., 2011b) or *Pde6g-CreERT2* mice (Zhang et al., 2019). *Opsin-Cre*-induced photoreceptor hypoxia had no noticeable retinal vascular changes but had retinal degeneration at a late stage (Lange et al., 2011b; Barben et al., 2018a). Tamoxifen-induced *CreERT2*-mediated photoreceptor hypoxia can cause IRN/SRN, resembling the early stage of human MNV3 (Zhang et al., 2019). Knocking out *Vhl* in cone cells using *cone-opsin Cre (BP-Cre)* and *R91W;Nrl*$^{-/-}$ mice demonstrated that cone hypoxia could cause IRN, resembling early MNV3 (Barben et al., 2018b). All major phenotypes of *VhlKO* in retinal progenitors, amacrine and horizontal cells, rod, and cones can be rescued by *Hif1a* knockout, but not *Hif2a* knockout (Kurihara et al., 2010; Usui et al., 2015; Barben et al., 2018a; Barben et al., 2018b). Knocking out *Vhl* in RPE cells using *Trp1-Cre* induced IRN, SRN, and RCA, which cannot be rescued by *Hif1a* knockout, indicating these MNV3-like lesions are mediated by *Hif2a* (Lange et al., 2012).

These *VhlKO* models confirm the importance of retinal hypoxia, especially hypoxia of outer retinal cells, including photoreceptors and RPE cells, in the pathogenesis of MNV3. The Rb–E2F pathway can modulate the hypoxia response by regulating the expression of some Hif target genes. Only the *Rb/p107/Vhl TKO* model and RPE-specific *VhlKO* model can induce stage III MNV3.

Rho/VEGF and *IRBP/VEGF* Mice

Transgenic mice with bovine rhodopsin promoter-driven human VEGF165 expression in the photoreceptors (*rho/VEGF* mice) show focal areas of IRN and SRN originating from the deep capillary bed of the retina and vascular leakage (Okamoto et al., 1997). The *VEGF* transgene mRNA begins to express at postnatal day 6 (P6) and reaches a constant level between P14 and P21, but VEGF protein is only detected in some photoreceptors in focal areas. IRN lesions form at P14, and abnormal vessels reach the subretinal space by P18. In adult *rho/VEGF* retinas, blood vessels extend from the inner nuclear layer toward RPE to form an extensive plexus in the subretinal space. The SRN lesions are progressively engulfed by the RPE (Tobe et al., 1998).

Another doxycycline-inducible version of this transgenic mouse was also generated, including *rtTA-rho/TRE-VEGF* and *rtTA-IRBP/TRE-VEGF* mice (Ohno-Matsui et al., 2002). At 3 weeks–6 months of age, mice were treated with doxycycline in their drinking water or by daily subcutaneous injection. Doxycycline treatment induced IRN/SRN and tractional retinal detachment. The incidence of these phenotypes and their severity depended on doxycycline dosage (Ohno-Matsui et al., 2002).

These models, which present with features that mimic MNV3, demonstrate that overexpression of VEGF in photoreceptors is enough to induce IRN/SRN rather than CNV as RPE and Bruch membrane are intact. These models are similar to the rod/cone-specific *VhlKO* models (Barben et al., 2018b; Zhang et al., 2019). They are useful tools for investigating VEGF-induced early changes in the retina and are valuable models to test the effects of some angiogenesis inhibitors on retinal neovascularization (Liu et al., 2017).

Photoreceptor-Specific *VEGFR1* Knockout Mice

Retinal neurons can limit angiogenesis by titrating VEGF for vascular endothelial cells by expressing VEGFR1 and VEGFR2 (Luo et al., 2013; Okabe et al., 2014). Reducing the expression

of these receptors in retinal neurons may increase the available VEGF molecules for retinal vascular endothelial cells, thus inducing retinal neovascularization.

VEGFR1 (also called FLT-1) is widely expressed in many types of cells, including endothelial cells and neurons, and has diverse biological functions in different cell types. VEGFR1 is alternatively spliced to yield both soluble (sVEGFR1) and membrane-tethered (mVEGFR1) isoforms. Both isoforms bind VEGF-A with 10-fold higher affinity than VEGFR2, but mVEGFR1 has weak kinase activity in endothelial cells (Boucher et al., 2017). VEGFR1 acts as a decoy receptor by binding VEGFA and reducing VEGFR2 signaling (Gille et al., 2000); sVEGFR1 or sFLT-1 also saturates VEGFA and reduces VEGFA binding to VEGFR2 (Kendall and Thomas, 1993). VEGFR1 is therefore considered to be a negative regulator of angiogenesis due to its negative regulation of VEGFR2 signaling. *VEGFR1*$^{-/-}$ mice die at the embryonic stage, associated with aberrant endothelial cell proliferation and formation of disorganized vessels with partially obstructed lumens (Simons et al., 2016). Endogenous sVEGFR1 is both necessary and enough for corneal avascularity (Ambati et al., 2006). Retinal photoreceptors can express sVEGFR1 (Luo et al., 2013); thus, knocking out *sVEGFR1* in rods may free VEGF to promote angiogenesis. The *iCre-75* mouse is a rod-specific Cre transgenic mouse line, in which 4-kb mouse rhodopsin gene promoter drives the expression of Cre recombinase in rods (Li et al., 2005). Indeed, *Vegfr1 floxed/iCre-75* mice develop MNV3-like lesions at 1–3 months of age, with a penetrance of about 50–60% (Luo et al., 2013).

Vegfr2 is more abundantly expressed in retinal neurons than in retinal endothelial cells during the first week after birth but gradually decreases as development continues; at P13, only some Müller cells still express Vegfr2 (Okabe et al., 2014). Vegfr2 on retinal neurons can bind and engulf VEGF proteins around neurons. In neuron-specific deletions of *Vegfr2 (Pax6 α-Cre, Vegfr2 floxed)*, free VEGF proteins are markedly increased due to neurons insufficiently engulfing VEGF, which result in misdirected vertical angiogenic growth toward neurons and dense intraretinal vascular plexus. However, this mutant mouse has no MNV3 lesion (Domigan and Iruela-Arispe, 2014; Okabe et al., 2014). A major difference between the *sVEGFR1* deletion model (Luo et al., 2013) and the *Vegfr2* deletion model (Okabe et al., 2014) is the Cre mouse line, iCre-75 only expresses in rods, but Pax6 α-Cre can express in all retinal cells (Marquardt et al., 2001). These two *VEGFR* deletion models suggest free VEGF proteins around rods, but not all retinal neurons are critical for MNV3 lesion formation. It would be interesting to see if rod-specific deletion of *Vegfr2* can cause MNV3-like lesions.

Very Low-Density Lipoprotein Receptor Null (*Vldlr*$^{-/-}$) Mice

The very low-density lipoprotein receptor (*Vldlr*) gene is one of the functional candidate genes for a significant association with AMD in humans (Haines et al., 2006). Vldlr is an 86-kDa transmembrane protein that belongs to the low-density lipoprotein receptor (Ldlr) family. Vldlr is highly expressed in photoreceptors and can be detected in RPE cells and retinal vascular endothelial cells (Hu et al., 2008; Dorrell et al., 2009; Joyal et al., 2016).

Very low-density lipoprotein receptor null mice (B6;129S7-Vldlr^{tm1Her}/J, Jax Stock No.: 002529) have been shown to develop retinal neovascularization starting at ∼2 weeks of age with 100% penetrance but do not develop dyslipidemia. Normal and heterozygous mice do not have this phenotype (Frykman et al., 1995; Heckenlively et al., 2003; Hu et al., 2008). The progression of retinal lesions resembles human MNV3, including the three stages of IRN, SRN, and CNV or RCA. As early as P12, neovascular vessels from the outer plexiform layer grow into the avascular zone of the outer nuclear layer. From P15–P18, the new vessels gradually extend into the subretinal space. Focal RPE detachment was present in the early stage of SRN. RPE activation and subretinal fibrosis at lesion sites are in the late stage of SRN (Hu et al., 2008). Subretinal hemorrhages are evident by age ∼2 months. However, breaks in the Bruch membrane and RCA are not observed in mice less than 6 months of age, confirming the intraretinal origin of subretinal NV. RCA, secondary photoreceptor degeneration, and regression of the retinal neovascularization can be observed by age ∼8 months (Heckenlively et al., 2003; Li et al., 2007; Hu et al., 2008; Dorrell et al., 2009; Chen et al., 2020).

Fluorescein leakages are first noticeable at 3 weeks of age, and the number of leakage spots continues to increase with age and reaches a maximum level by 6 weeks. Leakage spots begin to reduce significantly after ∼8 months of age and are hardly noticeable at 12 months because of subretinal fibrosis or scarring (Heckenlively et al., 2003; Li et al., 2007; Hu et al., 2008). Although the numbers of subretinal sprouts are reduced in older mice, most intraretinal and subretinal vessels persist throughout the life of the *Vldlr*$^{-/-}$ mice (Dorrell et al., 2009). The morphology of the neovascular growths transits from initial vascular buds to balloon-shaped bulbs and then to mature angiomatous-like vascular tangles, reminiscent of the glomerular IRN found in postmortem human MNV3 lesions (Hu et al., 2008; Monson et al., 2008; Klein and Wilson, 2011; Luo et al., 2013).

Very low-density lipoprotein receptor null^{-} vascular lesions are associated with Müller glia activation at late stages, as demonstrated by glial fibrillary acidic protein (GFAP) expression, retinal rosette formation, and altered growth factor expression. VEGF and basic fibroblast growth factor (bFGF) expression increases in the photoreceptor layer around the IRN lesion from ∼4 weeks of age (Li et al., 2007). *Vldlr*$^{-/-}$ mice also develop chronic inflammation in the retina and RPE (Li et al., 2007; Chen et al., 2009; Dorrell et al., 2009). The increased VEGF levels observed in *Vldlr*$^{-/-}$ mice are initially suggested to be linked to the negative regulatory role of Vldlr on Wnt signaling, which targets VEGF (Chen et al., 2007). However, since Vldlr has important functions in cholesterol homeostasis, lipid metabolism, and transport (Tiebel et al., 1999), it is demonstrated that *AAV2-GRK1-shVldlr*-mediated *Vldlr* gene knockdown in photoreceptors alone can develop MNV3-like lesions, suggesting that photoreceptors can not only get energy from glucose but also use fatty acid (FA) β1 oxidation

(Joyal et al., 2016). It is demonstrated that impaired fatty acid uptake in *Vldlr*$^{-/-}$ mice results in a reduction of α-ketoglutarate, which decreases prolyl hydroxylase dehydrogenase activity and promotes the stabilization of Hif-1a. Subsequently, VEGF expressions increase in photoreceptors (Joyal et al., 2016). Thus, dysregulated energy metabolism might drive pathological neovascularization by stabilizing Hif1a and overexpression of VEGFA in *Vldlr*$^{-/-}$ photoreceptors.

Very low-density lipoprotein receptor is also the receptor of reelin and is essential for reelin signaling in neuronal migration and synaptic plasticity (Lane-Donovan and Herz, 2017). In *Vldlr*$^{-/-}$ mice, mistargeted neurites of horizontal cells act as a scaffold for growing neovascularization (Johnson et al., 2015). VEGFA produced by RPE cells in *Vldlr*$^{-/-}$ mice can induce subretinal infiltration of microglia/macrophages, which can migrate into the ONL and promote the formation of subretinal NV (Usui-Ouchi et al., 2020). Thus, overexpression of VEGFA in photoreceptors and RPE cells, mistargeted neurites of horizontal cells, and activated microglial cells are the three major mechanisms of retinal neovascularization in *Vldlr*$^{-/-}$ mice, which represent the function of Vldlr in lipid metabolism and reelin signaling, respectively.

The unique pathological features in the *Vldlr*$^{-/-}$ mouse model enable its wide use to investigate the potential mechanisms and treatments of retinal neovascularization, including antioxidants, neurotrophic factors, resveratrol, anti-inflammation, cellular bioenergetics, and transcriptional control (Dorrell et al., 2009; Joyal et al., 2016; Liu et al., 2017). For instance, the role of some pro-inflammatory factors involved in the development of MNV3 was investigated in the *Vldlr*$^{-/-}$ mouse. The expression of intercellular adhesion molecule (ICAM)-1, interleukin (IL)-18, tumor necrosis factor (TNF)-α, endothelial nitric oxide synthase (eNOS), and cyclooxygenase (COX)2 significantly increased in *Vldlr*$^{-/-}$ mouse retina and RPE (Li et al., 2007; Chen et al., 2009; Dorrell et al., 2009). Interestingly, the expression level of the suppressor of cytokine signaling 3 (SOCS3) decreased significantly in *Vldlr*$^{-/-}$ retinas, and daily SR1001 treatment increased the retinal Socs3 expression and significantly inhibited the MNV3 phenotypes (Sun et al., 2015). Furthermore, the expression of the master inflammatory regulator c-Fos increased in *Vldlr*$^{-/-}$ photoreceptors, which induced IL-6 and TNF expression, activated signal transducer and activator of transcription (STAT)3 and increased TNF-α-induced protein 3 (Tnfaip3) expression. Suppressing c-Fos reduced the pathological neovascularization and rescued visual function in *Vldlr*$^{-/-}$ mice (Sun et al., 2017; Wang et al., 2020).

Cyp27a1$^{-/-}$ Mice

Different cytochrome P450 (Cyp) enzymes play essential roles in maintaining cholesterol homeostasis, including cholesterol biosynthesis and elimination (Pikuleva, 2006). Cyp27a1 is a ubiquitously expressed mitochondrial sterol 27-hydroxylase that catalyzes the hydroxylation of cholesterol and other sterols at position C27 (Pikuleva, 2006). It is widely expressed in the retina and is the principal cholesterol hydroxylase in the retina where it accounts for the majority of enzymatic cholesterol elimination (Mast et al., 2011; Pikuleva and Curcio, 2014).

In humans, Cyp27a1 deficiency leads to cerebrotendinous xanthomatosis (CTX). CTX is a multi-symptom lipid storage disease whose typical clinical features include neurological dysfunction and tendon xanthomas (Björkhem and Hansson, 2010). CTX patients have some ocular abnormalities, such as juvenile bilateral cataracts, cholesterol-like crystals in the vitreous, premature retinal senescence with drusen and retinal vessel sclerosis, and cholesterol-like deposits along the vascular arcades (Cruysberg et al., 1995). Changes in *Cyp27a1*$^{-/-}$ mice, however, are less pronounced than those in humans. They lack classic symptoms of CTX, such as cataracts, brain and tendon xanthomas, and atherosclerosis. This may reflect distinct manifestations of sterol 27-hydroxylase deficiency in *Cyp27a1*$^{-/-}$ mice and CTX patients (Honda et al., 2001). Nevertheless, *Cyp27a1*$^{-/-}$ mice are associated with MNV3-like lesions, including RCA, and vascular leakage and focal depositions containing cholesterol along the Bruch membrane (Omarova et al., 2012).

Spectral domain optical coherence tomography examination reveals 3–10 small hyperreflective spots in the inferior retina of 6-week-old mutant mice. Most spots do not change with age, although some grow in diameters. Simultaneous disturbances in the outer plexiform layer (OPL) and RPE occur in all studied young *Cyp27a1*$^{-/-}$ mice. At 11 months old, large hyperreflective spots can be determined, and blends between the retinal and choroidal circulations can be found by the Doppler flow of SD-OCT. By 12 months, 63% of *Cyp27a1*$^{-/-}$ females and 84% of *Cyp27a1*$^{-/-}$ males have at least 1–2 large hyperreflective spots in both eyes. Histologically, small OPL hyperreflective spots are abnormally dilated blood vessels at 6 weeks old, and OPL disruption and torsion near the inner nuclear layer (INL)/OPL interface at 8 months old. Large lesions represent the formation of RCA involving blood vessels between the INL and choroid at 11 months old. Activated Müller cells can be observed along with the RCA also in the whole retina. Notably, focal lipid depositions along the Bruch membrane, similar to soft drusen and basal linear deposits in AMD, can be found. Pimonidazole labeling and Hif-1a staining suggest retinal and choroidal hypoxia in the *Cyp27a1*$^{-/-}$ mice, while the mechanism is still unknown (Omarova et al., 2012).

Unlike *Vldlr*$^{-/-}$ mice in which IRN comes from the retina, the neovascularization in *Cyp27a1*$^{-/-}$ mice seems to occur in both the retina and choroid. Unlike *Vldlr*$^{-/-}$ mice that have an abnormal ERG indicating secondary photoreceptor degeneration, *Cyp27a1*$^{-/-}$ mice have a normal ERG response measured at 2–12 months old as the retinal lesions occupy only a tiny retinal area (Chen et al., 2009; Dorrell et al., 2009; Omarova et al., 2012; Joyal et al., 2016). An important difference between human MNV3 and *Cyp27a1*$^{-/-}$ mice is that human MNV3 is more popular in women than men (Marticorena et al., 2011; Tsai et al., 2017), but *Cyp27a1*$^{-/-}$ males have a higher frequency of retinal/choroidal pathologies than females, as males had a greater elevation in the rate of cholesterol biosynthesis (2.6-fold in males vs. 1.7-fold in females) (Omarova et al., 2012). As

such, *Cyp27a1*$^{-/-}$ mice have not yet been widely used in the field of MNV3 study.

Srf$^{-/-}$ Mouse

Serum response factor (SRF) is a nuclear transcription factor modulating gene expression in concert with cytoskeletal assembly and disassembly, important for motile cell functions, such as cell migration, guided movement, engulfment, adhesion, and contraction (Olson and Nordheim, 2010). Myocardin-related transcription factors (MRTFs), including MRTF-A and MRTF-B, are key coactivators of SRF that link actin dynamics to SRF-mediated gene transcription (Gau and Roy, 2018). The activity of MTRFs is controlled by cytoskeletal actin dynamics, which is regulated by Rho-GTPase signaling (Posern and Treisman, 2006; Weinl et al., 2013). Numerous studies have demonstrated that loss of function of either MRTF or SRF causes defects in the actin cytoskeleton and migration of a diverse range of mammalian cells in certain physiological contexts, such as development, angiogenesis, hematopoiesis, and immune function (Gau and Roy, 2018).

Myocardin-related transcription factors-Serum response factor signaling is essential for angiogenesis and is regulated by VEGF. Endothelial cell (EC)-specific *SRF* deletion leads to aneurysms and hemorrhages from E11.5 and lethality at E14.5. Mutant embryos present a reduced capillary density and defects in EC migration, with fewer numbers of filopodia in tip cells and ECs showing defects in actin polymerization and intercellular junctions. Knockdown of *SRF* in ECs impaired VEGF-induced *in vitro* angiogenesis (Franco et al., 2008; Weinl et al., 2013). SRF is strongly expressed in a subset of ECs in active vascular sprouting regions, with the highest level observed in endothelial tip cells and stalk cells. SRF selectively controls tip cell invasion and filopodia formation but may not be related to vascular remodeling (Franco et al., 2013). SRF promotes the expression of VEGFR2, β-actin, and VE-cadherin, which is vital for the VEGF–VEGFR2 signaling (Franco et al., 2008). On the other hand, VEGF can promote MRTF nuclear accumulation (Weinl et al., 2013; Hinkel et al., 2014). VEGF also promotes SRF expression and increases SRF binding activity to DNA in ECs (Chai et al., 2004).

Pharmacological inhibition of MRTF–SRF signaling by CCG-1423 impedes endothelial cell migration and angiogenesis (Gau et al., 2017). Deletion of *SRF* in postnatal ECs at P1–P4 induces a significant delay in the development of the superficial vascular plexus and absence of deep vascular plexus, resembling major characteristics of inherited human retinal pathologies such as retinopathy of prematurity (ROP) and familial exudative vitreoretinopathy (FEVR), including Norrie's disease (Wang et al., 2012; Franco et al., 2013; Weinl et al., 2013).

However, *SRF* deletion in ECs induced in adult mice at 4–6 weeks of age triggers unwarranted IRN lesions, reminiscent of the human MNV3 (Weinl et al., 2013). These new vessels originate from retinal deep capillaries and develop non-uniformly distributed focal lesions. These lesions also have a thin ONL with secondary retinal degeneration, rupture of the RPE, lamination defects, and cell displacement within the INL and ONL. Interestingly, the mRNA level of VEGFA is unchanged in this model (Weinl et al., 2013). Chromatin immunoprecipitation (ChIP) experiments and *in vitro* siRNA knockdown prove that the Thbs1 gene, which encodes the Vldlr ligand thrombospondin 1, is a downstream target of SRF. This may partially explain the resemblance of intraretinal new vessels between adult EC-specific SRF deficiency mice and with the *Vldlr*$^{-/-}$ mice (Weinl et al., 2013; Joyal et al., 2016).

This adult mouse model with EC-specific SRF deficiency is unique, as there is no change of VEGF levels; it is also known that SRF promotes the expression of VEGFR2, which is vital for the VEGF–VEGFR2 signaling (Franco et al., 2008). Thus, this mouse model induces retinal neovascularization without upregulation of VEGF and VEGFR2. However, that *SRFKO* only induces IRN in adult but not young mouse matches the fact that AMD occurs in old persons. The molecular mechanism and the involvement of Vldlr ligand thrombospondin-1 in this model need to be further studied.

RNV3 (JR5558) Mice

RNV3 (B6.Cg-Crb1^{rd8} Jak3^{m1J}/Boc, Jax Stock No.: 005558) mice are also known as retinal vascularization 3 model, *NRV2* mice, and *JR5558* mice, which have mutations in the *Crb1* and *Jak3* genes (Chang et al., 2018). It was identified in a B6;129 mixed background strain with unique eye phenotypes through The Jackson Laboratory Eye Mutant Screening program (Won et al., 2011). This model was previously described by two groups (Hasegawa et al., 2014; Nagai et al., 2014). The first report indicated that the ectopic vascular vessels are choroidal in origin and infiltrated the RPE and intraretinal space (Nagai et al., 2014). The second group reported that the model captures the early stages of MNV3, with intraretinal vessels diving into the subretinal space but not breaching the Bruch membrane, and there was no RCA (Hasegawa et al., 2014). Now it is accepted that the lesions originate from the retina (Chang et al., 2018; Borrelli et al., 2020).

The major clinical manifestations are areas of retinal depigmentation. These depigmentation spots can be observed at P18 without fluorescein leakage. The lesions become well-demarcated and larger at P25, and some of the depigmented areas correspond to areas of fluorescein leakage. The retinal depigmented spots and areas of fluorescein leakage increase in number and size with age, with the maximal number of lesions reaching about 20 per eye at about 1 month. The areas of depigmentation correlate with the development of vascular leakage, indicating a vascular component to this disease phenotype. Around 2 months of age, some individual retinal depigmented spots appear to merge, generating larger areas of depigmentation. As with focal depigmentation, fluorescein leakages gradually decrease after P25 (Hasegawa et al., 2014; Nagai et al., 2014; Chang et al., 2018).

Histological studies indicate that new vessels begin to grow from INL at P15, extend into RPE, and form balloon-like vessel structures from P17 to P25. Photoreceptor cell degeneration can be observed where the ectopic vasculature disrupts the retinal structure. The neovascular lesions are enveloped by the RPE in the photoreceptor cell layer and subretinal space

by 3 months of age. By 8 months of age, mutants showed a much-reduced rod and cone ERG response compared to that of C57BL/6J wild-type controls. VEGF levels of the RNV3 retina are significantly higher than those of C57BL/6 control mice, and blockade of VEGF-A with a neutralizing monoclonal antibody can reduce the average number and size of neovascularization lesions (Hasegawa et al., 2014; Nagai et al., 2014; Chang et al., 2018). Thus, RNV3 neovascularization originates from the retinal vascular plexus and grows outward to the subretinal space, forming neovascularization structures at the RPE–Bruch membrane interface and mimicking the early clinical presentation of MNV3 in humans (Hasegawa et al., 2014; Chang et al., 2018). The balloon-like vessel structures of this model are similar to the retinal glomerular angiomatous lesions with encapsulation found in MNV3 patients (Monson et al., 2008; Klein and Wilson, 2011; Luo et al., 2013). Interestingly, the retinal new vessels show fenestrations along their contact with RPE, similar to the choriocapillaris (Hasegawa et al., 2014). RPE cells have the ability to induce fenestrations in endothelial cells of retinal vessels by encapsulating them (Burns and Hartz, 1992). Thus, RPE encapsulation is a possible mechanism, but further investigation is needed.

This mutant mouse model appears to have a recessive inheritance (Nagai et al., 2014; Borrelli et al., 2020). Genetic analysis localized *RNV3* to mouse chromosome 1 in a region containing the *Crb1* gene, *Cfh* (component factor h) gene, and Cfh-related genes 1 through 3 (*Cfhr1–Cfhr3*). High throughput whole-exome sequencing identified a single base deletion in the *Crb1* (crumbs family member 1) gene, which was previously reported to cause retinal degeneration 8 (*rd8*); no coding sequence variation was detected for *Cfh* and *cfhr1–cfhr3* genes (Mehalow et al., 2003; Nagai et al., 2014; Chang et al., 2018). The transcription activator-like effector nuclease (TALEN)-mediated oligonucleotide-directed repair (ODR) of this *Crb1* gene deletion rescued the posterior segment vascularization phenotype, indicating that *Crb1* mutation is necessary for the MNV3-like lesions in this mouse model (Low et al., 2014; Chang et al., 2018). Whole-exome sequencing also identified $Jak3^{m1J}$ gene mutation; however, this mutation alone cannot cause the MNV3-like lesions. When combined with the disruption in the *Crb1* gene, it can enhance the retinal vascular phenotype (Chang et al., 2018).

Crb1 is a membrane protein that establishes cell polarity and adhesion between cells. Crb1 is expressed in Müller glia cells and contributes to adherens junctions that constitute the external limiting membrane (ELM). The $Crb1^{rd8}$ mutant mice have retinal ELM fragmentation and outer retinal dysplasia but no new vascular lesions (Mehalow et al., 2003). The phenotypic difference between $Crb1^{rd8}$ and *RNV3* is most likely due to genetic background differences between the strains, for instance, the *Jak3* mutation in *RNV3* mice. Janus kinase 3 (Jak3) is critical for the normal development and function of the immune system, including B cells, T cells, and natural killer cells, thus affecting inflammation responses (Thomis et al., 1995). So, retinal polarity defects combined with abnormal inflammation response may drive the MNV3-like lesions in this model.

This model is a valuable platform to study the pathogenesis of MNV3, as well as for evaluating potential therapeutics, such as C-C chemokine receptor type 3 antagonists, simultaneous VEGF-A/ANG-2 neutralization, and DICER1 variant (OptiDicer) (Nagai et al., 2015; Foxton et al., 2019; Wright et al., 2020; Joussen et al., 2021). For instance, CCR3 is a receptor for multiple inflammatory CC chemokines. Immunostaining revealed that CCR3 expression was mainly localized to MNV3 lesions of *RNV3 (JR5558)* mice. $CCR3^{+}$ cells included IB4-stained blood endothelium cells, leukocytes, and macrophages but not RPE cells. The expression of CCR3 ligands (CCL11 and CCL24) increased in this mouse model, and they mainly were localized to the subretinal space and the RPE/choroid complex. Intravitreal injection of neutralizing antibodies against CCR3, CCL11, and CCL24 reduced MNV3 area and lesion number in these mice. Systemic administration of the CCR3 antagonists GW766994X and GW782415X had similar effects (Nagai et al., 2015).

CONCLUSION AND FUTURE DIRECTIONS

It is already three decades since the discovery of the clinical entity of MNV3 among AMD patients. MNV3 lesions originate from deep retinal vascular plexus, and clinically, it has three stages, including IRN, SRN, and RCA stages. MNV3 can be diagnosed and classified by clinical features, and multimodal imaging includes FA, ICGA, OCT, and OCT-A. Histopathological analysis reveals the expression of VEGF/HIFs, the structure of glomerular IRN, and the existence of intraretinal lipid-filled cells in MNV3 lesions and surrounding cells. These pathological studies suggest the involvement of retinal hypoxia, inflammation, and multiple cell types in the development and progression of MNV3. The structure of glomerular IRN and intraretinal lipid-filled cells are similar to histological features of human retinal hemangioblastoma (RCH), which also has foamy lipid-filled stromal cells.

The mouse models directly related to the hypoxia pathway (retina-specific *VhlKO* mice, *Vegf* overexpression, or *sVEGFR1* knockout in mouse photoreceptor) support the idea that outer retinal hypoxia is an initiation factor for MNV3. The RNV3 (JR5558) model indicates that the involvement of inflammation is necessary but not sufficient for MNV3 development. The $Vldlr^{-/-}$ mice, $Cyp27a1^{-/-}$ mice suggest lipid metabolism is vital for MNV3, while the adult EC-specific *SRF* deficiency mouse model supports that aging is a risk factor for MNV3. The finding that Rb can inhibit the Hif activity suggests that smoking or smoking-induced Rb inactivation may play a role in the pathogenesis of MNV3. These animal models also suggest the involvement of photoreceptors, RPE cells, Müller cells, and microglial cells.

Anti-inflammation strategies such as IVTA combined with PDT can improve the visual acuity of MNV3 patients but also induce GA, cataract, and other complications. Other strategies targeting inflammation factors, such as SOCS3, c-Fos, and CCR3/CCL11 or 24, had achieved encouraging results in MNV3 animal models but had not yet been tested in MNV3 patients.

Early-stage MNV3 can be treated by anti-VEGF therapy with favorable outcomes, while treatment of late-stage MNV3 is still a challenge. Thus, animal models that can develop retina-originated RCA are important for future studies, which include *Rb/p107/Vhl* TKO mice, RPE-specific *VhlKO* mice, and *Vldlr*$^{-/-}$ mice. How subretinal neovascularization broke the RPE and Bruch membrane is the key mechanism, and how to block this process will be the target of future therapy for late-stage MNV3.

A potential candidate target for the future treatment of late-stage MNV3 is the PI3K pathway, which is the downstream signaling pathway of most angiogenesis tyrosine kinase growth factor receptors such as EGFR, VEGFR, and platelet-derived growth factor receptor (PDGFR). PI3K pathway plays crucial roles in cell survival, migration, metabolism, and angiogenesis (Wert et al., 2016; Davies et al., 2019). Blockage of PI3K pathways inhibits retinal neovascularization and improves outcomes (Wert et al., 2016). PI3K pathway can also regulate autophagy to prevent oxidative injury (Zhang et al., 2020) or regulate the Sirtuin 1 (Sirt1)–E2F1 pathway to improve the antioxidative capability of RPE cells (Gong et al., 2020). Thus, it will be interesting to test if PI3K inhibitors can cure MNV3 on these late-stage MNV3 animal models.

AUTHOR CONTRIBUTIONS

WQ and DC conceived of and designed the manuscript, and all authors wrote, edited, and approved the manuscript.

FUNDING

This study was supported by a grant to DC from the National Natural Science Foundation of China (81870665).

REFERENCES

Al-Salam, S., Al-Salam, M., and Al Ashari, M. (2013). Galectin-3: a novel protein in cerebellar hemangioblastoma. *Int. J. Clin. Exp. Pathol.* 6, 853–861.

Ambati, B. K., Nozaki, M., Singh, N., Takeda, A., Jani, P. D., Suthar, T., et al. (2006). Corneal avascularity is due to soluble VEGF receptor-1. *Nature* 443, 993–997.

Arreola, A., Payne, L. B., Julian, M. H., De Cubas, A. A., Daniels, A. B., Taylor, S., et al. (2018). Von Hippel-Lindau mutations disrupt vascular patterning and maturation via Notch. *JCI Insight* 3:e92193.

Baek, J., Lee, J. H., Kim, J. Y., Kim, N. H., and Lee, W. K. (2016). Geographic atrophy and activity of neovascularization in retinal angiomatous proliferation. *Invest. Ophthalmol. Vis. Sci.* 57, 1500–1505. doi: 10.1167/iovs.15-18837

Barben, M., Ail, D., Storti, F., Klee, K., Schori, C., Samardzija, M., et al. (2018a). Hif1a inactivation rescues photoreceptor degeneration induced by a chronic hypoxia-like stress. *Cell Death Differ.* 25, 2071–2085. doi: 10.1038/s41418-018-0094-7

Barben, M., Schori, C., Samardzija, M., and Grimm, C. (2018b). Targeting Hif1a rescues cone degeneration and prevents subretinal neovascularization in a model of chronic hypoxia. *Mol. Neurodegener.* 13:12.

Berenberg, T. L., Metelitsina, T. I., Madow, B., Dai, Y., Ying, G.-S., Dupont, J. C., et al. (2012). The association between drusen extent and foveolar choroidal blood flow in age-related macular degeneration. *Retina* 32, 25–31. doi: 10.1097/iae.0b013e3182150483

Björkhem, I., and Hansson, M. (2010). Cerebrotendinous xanthomatosis: an inborn error in bile acid synthesis with defined mutations but still a challenge. *Biochem. Biophys. Res. Commun.* 396, 46–49. doi: 10.1016/j.bbrc.2010.02.140

Borrelli, E., Sarraf, D., Freund, K. B., and Sadda, S. R. (2018). OCT angiography and evaluation of the choroid and choroidal vascular disorders. *Prog. Retin. Eye Res.* 67, 30–55. doi: 10.1016/j.preteyeres.2018.07.002

Borrelli, E., Zerbini, G., Maestroni, S., Sacconi, R., Querques, L., Zucchiatti, I., et al. (2020). Multimodal imaging to detect in vivo responses to aflibercept therapy in a mouse model of type 3 neovascularization. *Ophthalmologica* 244, 193–199. doi: 10.1159/000513051

Bottoni, F., Massacesi, A., Cigada, M., Viola, F., Musicco, I., and Staurenghi, G. (2005). Treatment of retinal angiomatous proliferation in age-related macular degeneration: a series of 104 cases of retinal angiomatous proliferation. *Arch. Ophthalmol.* 123, 1644–1650. doi: 10.1001/archopht.123.12.1644

Boucher, J. M., Clark, R. P., Chong, D. C., Citrin, K. M., Wylie, L. A., and Bautch, V. L. (2017). Dynamic alterations in decoy VEGF receptor-1 stability regulate angiogenesis. *Nat. Commun.* 8:15699.

Brancato, R., Introini, U., Pierro, L., Setaccioli, M., Forti, M., Bolognesi, G., et al. (2002). Optical coherence tomography (OCT) angiomatous prolifieration (RAP) in retinal. *Eur. J. Ophthalmol.* 12, 467–472.

Burns, M. S., and Hartz, M. J. (1992). The retinal pigment epithelium induces fenestration of endothelial cells in vivo. *Curr. Eye Res.* 11, 863–873. doi: 10.3109/02713689209033484

Chai, J., Jones, M. K., and Tarnawski, A. S. (2004). Serum response factor is a critical requirement for VEGF signaling in endothelial cells and VEGF-induced angiogenesis. *FASEB J.* 18, 1264–1266. doi: 10.1096/fj.03-1232fje

Chang, B., Fitzmaurice, B., Wang, J., Low, B. E., Wiles, M. V., and Nishina, P. M. (2018). Spontaneous posterior segment vascular disease phenotype of a mouse model, rnv3, Is Dependent on the Crb1rd8 Allele. *Invest. Ophthalmol. Vis. Sci.* 59, 5127–5139. doi: 10.1167/iovs.18-25046

Chang, Y. S., Kim, J. H., Yoo, S. J., Lew, Y. J., and Kim, J. (2016). Fellow-eye neovascularization in unilateral retinal angiomatous proliferation in a Korean population. *Acta Ophthalmol.* 94, e49–e53.

Chen, D., Livne-Bar, I., Vanderluit, J. L., Slack, R. S., Agochiya, M., and Bremner, R. (2004). Cell-specific effects of RB or RB/p107 loss on retinal development implicate an intrinsically death-resistant cell-of-origin in retinoblastoma. *Cancer Cell* 5, 539–551. doi: 10.1016/j.ccr.2004.05.025

Chen, Q., Jiang, N., Zhang, Y., Ye, S., Liang, X., Wang, X., et al. (2020). Fenofibrate inhibits subretinal fibrosis through suppressing TGF-β-Smad2/3 signaling and Wnt signaling in neovascular age-related macular degeneration. *Front. Pharmacol.* 11:580884. doi: 10.3389/fphar.2020.580884

Chen, Y., Hu, Y., Lu, K., Flannery, J. G., and Ma, J. X. (2007). Very low density lipoprotein receptor, a negative regulator of the wnt signaling pathway and choroidal neovascularization. *J. Biol. Chem.* 282, 34420–34428. doi: 10.1074/jbc.m611289200

Chen, Y., Hu, Y., Moiseyev, G., Zhou, K. K., Chen, D., and Ma, J. X. (2009). Photoreceptor degeneration and retinal inflammation induced by very low-density lipoprotein receptor deficiency. *Microvasc. Res.* 78, 119–127. doi: 10.1016/j.mvr.2009.02.005

Cruysberg, J. R., Wevers, R. A., Van Engelen, B. G., Pinckers, A., Van Spreeken, A., and Tolboom, J. J. (1995). Ocular and systemic manifestations of *cerebrotendinous xanthomatosis*. *Am. J. Ophthalmol.* 120, 597–604. doi: 10.1016/s0002-9394(14)72206-8

Daniel, E., Shaffer, J., Ying, G. S., Grunwald, J. E., Martin, D. F., Jaffe, G. J., et al. (2016). Outcomes in eyes with retinal angiomatous proliferation in the comparison of age-related macular degeneration treatments trials (CATT). *Ophthalmology* 123, 609–616. doi: 10.1016/j.ophtha.2015.10.034

Dasgupta, P., Rastogi, S., Pillai, S., Ordonez-Ercan, D., Morris, M., Haura, E., et al. (2006). Nicotine induces cell proliferation by beta-arrestin-mediated activation of Src and Rb-Raf-1 pathways. *J. Clin. Invest.* 116, 2208–2217. doi: 10.1172/jci28164

Davies, E. M., Gurung, R., Le, K. Q., and Mitchell, C. A. (2019). Effective angiogenesis requires regulation of *phosphoinositide* signaling. *Adv. Biol. Regul.* 71, 69–78. doi: 10.1016/j.jbior.2018.11.008

Domigan, C. K., and Iruela-Arispe, M. L. (2014). Stealing VEGF from thy neighbor. *Cell* 159, 473–474. doi: 10.1016/j.cell.2014.10.008

Donati, M. C., Carifi, G., Virgili, G., and Menchini, U. (2006). Retinal angiomatous proliferation: association with clinical and angiographic features. *Ophthalmologica* 220, 31–36. doi: 10.1159/000089272

Dorrell, M. I., Aguilar, E., Jacobson, R., Yanes, O., Gariano, R., Heckenlively, J., et al. (2009). Antioxidant or neurotrophic factor treatment preserves function in a mouse model of neovascularization-associated oxidative stress. *J. Clin. Invest.* 119, 611–623. doi: 10.1172/jci35977

Ferris, F. L., Wilkinson, C. P., Bird, A., Chakravarthy, U., Chew, E., Csaky, K., et al. (2013). Clinical Classification of Age-related Macular Degeneration. *Ophthalmology* 120, 844–851.

Fingler, J., Readhead, C., Schwartz, D. M., and Fraser, S. E. (2008). Phase-contrast OCT imaging of transverse flows in the mouse retina and choroid. *Invest. Ophthalmol. Vis. Sci.* 49, 5055–5059. doi: 10.1167/iovs.07-1627

Fleckenstein, M., Keenan, T. D. L., Guymer, R. H., Chakravarthy, U., Schmitz-Valckenberg, S., Klaver, C. C., et al. (2021). Age-related macular degeneration. *Nat. Rev. Dis. Primers* 7:31.

Foxton, R. H., Uhles, S., Grüner, S., Revelant, F., and Ullmer, C. (2019). Efficacy of simultaneous VEGF-A/ANG-2 neutralization in suppressing spontaneous choroidal neovascularization. *EMBO Mol. Med.* 11:e10204.

Franco, C. A., Blanc, J., Parlakian, A., Blanco, R., Aspalter, I. M., Kazakova, N., et al. (2013). SRF selectively controls tip cell invasive behavior in angiogenesis. *Development* 140, 2321–2333. doi: 10.1242/dev.091074

Franco, C. A., Mericskay, M., Parlakian, A., Gary-Bobo, G., Gao-Li, J., Paulin, D., et al. (2008). Serum response factor is required for sprouting angiogenesis and vascular integrity. *Dev. Cell* 15, 448–461. doi: 10.1016/j.devcel.2008.07.019

Freund, K. B., Ho, I. V., Barbazetto, I. A., Koizumi, H., Laud, K., Ferrara, D., et al. (2008). Type 3 neovascularization: the expanded spectrum of retinal angiomatous proliferation. *Retina* 28, 201–211. doi: 10.1097/iae.0b013e3181669504

Freund, K. B., Klais, C. M., Eandi, C. M., Ober, M. D., Goldberg, D. E., Sorenson, J. A., et al. (2006). Sequenced combined intravitreal triamcinolone and indocyanine green angiography-guided photodynamic therapy for retinal angiomatous proliferation. *Arch. Ophthalmol.* 124, 487–492. doi: 10.1001/archopht.124.4.487

Frykman, P. K., Brown, M. S., Yamamoto, T., Goldstein, J. L., and Herz, J. (1995). Normal plasma lipoproteins and fertility in gene-targeted mice homozygous for a disruption in the gene encoding very low density lipoprotein receptor. *Proc. Natl. Acad. Sci. U.S.A.* 92, 8453–8457. doi: 10.1073/pnas.92.18.8453

Gass, J. D. (1997). *Stereoscopic Atlas of Macular Diseases*. St. Louis: C.V. Mosb.

Gass, J. D., Agarwal, A., Lavina, A. M., and Tawansy, K. A. (2003). Focal inner retinal hemorrhages in patients with drusen: an early sign of occult choroidal neovascularization and chorioretinal anastomosis. *Retina* 23, 741–751. doi: 10.1097/00006982-200312000-00001

Gau, D., and Roy, P. (2018). SRF'ing and SAP'ing - the role of MRTF proteins in cell migration. *J. Cell Sci.* 131:jcs218222.

Gau, D., Veon, W., Capasso, T. L., Bottcher, R., Shroff, S., Roman, B. L., et al. (2017). Pharmacological intervention of MKL SRF signaling by CCG-1423 impedes endothelial cell migration and angiogenesis. *Angiogenesis* 20, 663–672. doi: 10.1007/s10456-017-9560-y

Gharbiya, M., Parisi, F., Cruciani, F., Bozzoni-Pantaleoni, F., Pranno, F., and Abdolrahimzadeh, S. (2014). Intravitreal anti-vascular endothelial growth factor for retinal angiomatous proliferation in treatment-naive eyes: long-term functional and anatomical results using a modified PrONTO-style regimen. *Retina* 34, 298–305. doi: 10.1097/iae.0b013e3182979e62

Gille, H., Kowalski, J., Yu, L., Chen, H., Pisabarro, M. T., Davis-Smyth, T., et al. (2000). A repressor sequence in the *juxtamembrane* domain of Flt-1 (VEGFR-1) constitutively inhibits vascular endothelial growth factor-dependent phosphatidylinositol 3'-kinase activation and endothelial cell migration. *Embo. J.* 19, 4064–4073. doi: 10.1093/emboj/19.15.4064

Gong, C., Qiao, L., Feng, R., Xu, Q., Zhang, Y., Fang, Z., et al. (2020). IL-6-induced acetylation of E2F1 aggravates oxidative damage of retinal pigment epithelial cell line. *Exp. Eye Res.* 200:108219. doi: 10.1016/j.exer.2020.108219

Gross, N. E., Aizman, A., Brucker, A., Klancnik, J. M. Jr., and Yannuzzi, L. A. (2005). Nature and risk of neovascularization in the fellow eye of patients with unilateral retinal angiomatous proliferation. *Retina* 25, 713–718. doi: 10.1097/00006982-200509000-00005

Gupta, B., Jyothi, S., and Sivaprasad, S. (2010). Current treatment options for retinal *angiomatous* proliferans (RAP). *Br. J. Ophthalmol.* 94, 672–677. doi: 10.1136/bjo.2009.166975

Haase, V. H., Glickman, J. N., Socolovsky, M., and Jaenisch, R. (2001). Vascular tumors in livers with targeted inactivation of the von Hippel-Lindau tumor suppressor. *Proc. Natl. Acad. Sci. U.S.A.* 98, 1583–1588. doi: 10.1073/pnas.98.4.1583

Haines, J. L., Schnetz-Boutaud, N., Schmidt, S., Scott, W. K., Agarwal, A., Postel, E. A., et al. (2006). Functional candidate genes in age-related macular degeneration: significant association withVEGF,VLDLR, andLRP6. *Invest. Opthalmol. Vis. Sci.* 47, 329–335. doi: 10.1167/iovs.05-0116

Han, J. W., Cho, H. J., Kang, D. H., Jung, S. H., Park, S., and Kim, J. W. (2020). Changes in optical coherence tomography angiography and disease activity in type 3 neovascularization after anti-vascular endothelial growth factor treatment. *Retina* 40, 1245–1254. doi: 10.1097/iae.0000000000002562

Hartnett, M. E., Weiter, J. J., Garsd, A., and Jalkh, A. E. (1992). Classification of retinal pigment epithelial detachments associated with drusen. *Graefes Arch. Clin. Exp. Ophthalmol.* 230, 11–19. doi: 10.1007/bf00166756

Hartnett, M. E., Weiter, J. J., Staurenghi, G., and Elsner, A. E. (1996). Deep retinal vascular anomalous complexes in advanced age-related macular degeneration. *Ophthalmology* 103, 2042–2053. doi: 10.1016/s0161-6420(96)30389-8

Hasegawa, E., Sweigard, H., Husain, D., Olivares, A. M., Chang, B., Smith, K. E., et al. (2014). Characterization of a spontaneous retinal neovascular mouse model. *PLoS One* 9:e106507. doi: 10.1371/journal.pone.0106507

Heckenlively, J. R., Hawes, N. L., Friedlander, M., Nusinowitz, S., Hurd, R., Davisson, M., et al. (2003). Mouse model of subretinal neovascularization with choroidal anastomosis. *Retina* 23, 518–522. doi: 10.1097/00006982-200308000-00012

Hinkel, R., Trenkwalder, T., Petersen, B., Husada, W., Gesenhues, F., Lee, S., et al. (2014). MRTF-A controls vessel growth and maturation by increasing the expression of CCN1 and CCN2. *Nat. Commun.* 5:3970.

Honda, A., Salen, G., Matsuzaki, Y., Batta, A. K., Xu, G., Leitersdorf, E., et al. (2001). Differences in hepatic levels of intermediates in bile acid biosynthesis between Cyp27(-/-) mice and CTX. *J. Lipid Res.* 42, 291–300. doi: 10.1016/s0022-2275(20)31691-6

Hu, W., Jiang, A., Liang, J., Meng, H., Chang, B., Gao, H., et al. (2008). Expression of VLDLR in the retina and evolution of subretinal neovascularization in the knockout mouse model's retinal *angiomatous* proliferation. *Invest. Opthalmol. Vis. Sci.* 49, 407–415. doi: 10.1167/iovs.07-0870

Johnson, V., Xiang, M., Chen, Z., and Junge, H. J. (2015). Neurite Mistargeting and inverse order of intraretinal vascular plexus formation precede subretinal vascularization in *Vldlr* Mutant Mice. *PLoS One* 10:e0132013. doi: 10.1371/journal.pone.0132013

Joussen, A. M., Ricci, F., Paris, L. P., Korn, C., Quezada-Ruiz, C., and Zarbin, M. (2021). Angiopoietin/Tie2 signalling and its role in retinal and choroidal vascular diseases: a review of preclinical data. *Eye (Lond)* 35, 1305–1316. doi: 10.1038/s41433-020-01377-x

Joyal, J. S., Sun, Y., Gantner, M. L., Shao, Z., Evans, L. P., Saba, N., et al. (2016). Retinal lipid and glucose metabolism dictates angiogenesis through the lipid sensor Ffar1. *Nat. Med.* 22, 439–445. doi: 10.1038/nm.4059

Jung, J. J., Chen, C. Y., Mrejen, S., Gallego-Pinazo, R., Xu, L., Marsiglia, M., et al. (2014). The incidence of neovascular subtypes in newly diagnosed neovascular age-related macular degeneration. *Am. J. Ophthalmol.* 158, 769–779.e2.

Kang, H. M., Kwon, H. J., Yi, J. H., Lee, C. S., and Lee, S. C. (2014). Subfoveal choroidal thickness as a potential predictor of visual outcome and treatment response after intravitreal ranibizumab injections for typical exudative age-related macular degeneration. *Am. J. Ophthalmol.* 157, 1013–1021. doi: 10.1016/j.ajo.2014.01.019

Kendall, R., and Thomas, K. (1993). Inhibition of vascular endothelial cell growth factor activity by an endogenously encoded soluble receptor. *Proc. Natl. Acad. Sci. U.S.A.* 90, 10705–10709. doi: 10.1073/pnas.90.22.10705

Kim, J. H., Chang, Y. S., Kim, J. W., Lee, T. G., and Kim, C. G. (2015). Prevalence and genomic association of reticular pseudodrusen in age-related macular degeneration. *Retina* 35, 2604–2612.

Kim, J. H., Lee, T. G., Kim, J. W., Kim, C. G., Cho, S. W., and Han, J. I. (2014). Small retinal haemorrhages accompanied by macular soft drusen: prevalence, and funduscopic and angiographic characteristics. *Br. J. Ophthalmol.* 98, 1066–1072. doi: 10.1136/bjophthalmol-2013-304405

Kim, Y. K., Park, S. J., Woo, S. J., and Park, K. H. (2016). Choroidal thickness change after intravitreal anti-vascular endothelial growth factor treatment in retinal angiomatous proliferation and its recurrence. *Retina* 36, 1516–1526. doi: 10.1097/iae.0000000000000952

Klein, M. L., and Wilson, D. J. (2011). Clinicopathologic correlation of choroidal and retinal neovascular lesions in age-related macular degeneration. *Am. J. Ophthalmol.* 151, 161–169. doi: 10.1016/j.ajo.2010.07.020

Klein, R., Klein, B. E. K., Tomany, S. C., Meuer, S. M., and Huang, G.-H. (2002). Ten-year incidence and progression of age-related maculopathy: the beaver dam eye study. *Ophthalmology* 109, 1767–1779. doi: 10.1016/s0161-6420(02)01146-6

Klein, R., Meuer, S. M., Myers, C. E., Buitendijk, G. H., Rochtchina, E., Choudhury, F., et al. (2014). Harmonizing the classification of age-related macular degeneration in the three-continent AMD consortium. *Ophthalmic Epidemiol.* 21, 14–23. doi: 10.3109/09286586.2013.867512

Kuehlewein, L., Dansingani, K. K., Carlo, T. E. D., Filho, M.a.B, Iafe, N. A., Lenis, T. L., et al. (2015). Optical coherence tomography angiography of type 3 neovascularization secondary to age-related macular degeneration. *Retina* 35, 2229–2235.

Kuhn, D., Meunier, I., Soubrane, G., and Coscas, G. (1995). Imaging of chorioretinal anastomoses in vascularized retinal pigment epithelium detachments. *Arch. Ophthalmol.* 113, 1392–1398. doi: 10.1001/archopht.1995.01100110052025

Kurihara, T., Kubota, Y., Ozawa, Y., Takubo, K., Noda, K., Celeste Simon, M., et al. (2010). von Hippel-Lindau protein regulates transition from the fetal to the adult circulatory system in retina. *Development* 137, 1563–1571. doi: 10.1242/dev.049015

Lafaut, B. A., Aisenbrey, S., Vanden Broecke, C., and Bartz-Schmidt, K. U. (2000). Clinicopathological correlation of deep retinal vascular anomalous complex in age related macular degeneration. *Br. J. Ophthalmol.* 84, 1269–1274. doi: 10.1136/bjo.84.11.1269

Lane-Donovan, C., and Herz, J. (2017). The ApoE receptors Vldlr and Apoer2 in central nervous system function and disease. *J. Lipid Res.* 58, 1036–1043. doi: 10.1194/jlr.r075507

Lange, C., Caprara, C., Tanimoto, N., Beck, S., Huber, G., Samardzija, M., et al. (2011a). Retina-specific activation of a sustained hypoxia-like response leads to severe retinal degeneration and loss of vision. *Neurobiol. Dis.* 41, 119–130. doi: 10.1016/j.nbd.2010.08.028

Lange, C., Heynen, S. R., Tanimoto, N., Thiersch, M., Le, Y. Z., Meneau, I., et al. (2011b). Normoxic activation of hypoxia-inducible factors in photoreceptors provides transient protection against light-induced retinal degeneration. *Invest. Ophthalmol. Vis. Sci.* 52, 5872–5880. doi: 10.1167/iovs.11-7204

Lange, C. A., Luhmann, U. F., Mowat, F. M., Georgiadis, A., West, E. L., Abrahams, S., et al. (2012). Von Hippel-Lindau protein in the RPE is essential for normal ocular growth and vascular development. *Development* 139, 2340–2350. doi: 10.1242/dev.070813

Lee, J. H., Lee, M. Y., and Lee, W. K. (2017). Incidence and risk factors of massive subretinal hemorrhage in retinal angiomatous proliferation. *PLoS One* 12:e0186272. doi: 10.1371/journal.pone.0186272

Li, C., Huang, Z., Kingsley, R., Zhou, X., Li, F., Parke, D. W. II, et al. (2007). Biochemical alterations in the retinas of very low-density lipoprotein receptor knockout mice: an animal model of retinal angiomatous proliferation. *Arch. Ophthalmol.* 125, 795–803. doi: 10.1001/archopht.125.6.795

Li, M., Dolz-Marco, R., Messinger, J. D., Wang, L., Feist, R. M., Girkin, C. A., et al. (2018). Clinicopathologic correlation of anti-vascular endothelial growth factor-treated type 3 neovascularization in age-related macular degeneration. *Ophthalmology* 125, 276–287. doi: 10.1016/j.ophtha.2017.08.019

Li, S., Chen, D., Sauvé, Y., Mccandless, J., Chen, Y. J., and Chen, C. K. (2005). Rhodopsin-iCre transgenic mouse line for Cre-mediated rod-specific gene targeting. *Genesis* 41, 73–80. doi: 10.1002/gene.20097

Liu, C. H., Wang, Z., Sun, Y., and Chen, J. (2017). Animal models of ocular angiogenesis: from development to pathologies. *FASEB J.* 31, 4665–4681. doi: 10.1096/fj.201700336r

Lonser, R. R., Glenn, G. M., Walther, M., Chew, E. Y., Libutti, S. K., Linehan, W. M., et al. (2003). von Hippel-Lindau disease. *Lancet* 361, 2059–2067.

Low, B. E., Krebs, M. P., Joung, J. K., Tsai, S. Q., Nishina, P. M., and Wiles, M. V. (2014). Correction of the Crb1rd8 allele and retinal phenotype in C57BL/6N mice via TALEN-mediated homology-directed repair. *Invest. Ophthalmol. Vis. Sci.* 55, 387–395. doi: 10.1167/iovs.13-13278

Luo, L., Uehara, H., Zhang, X., Das, S. K., Olsen, T., Holt, D., et al. (2013). Photoreceptor avascular privilege is shielded by soluble VEGF receptor-1. *Elife* 2:e00324.

Macular-Group. (1991). Laser photocoagulation of subfoveal recurrent neovascular lesions in age-related macular degeneration. Results of a randomized clinical trial. Macular Photocoagulation Study Group. *Arch. Ophthalmol.* 109, 1232–1241. doi: 10.1001/archopht.1991.01080090056026

Malamos, P., Tservakis, I., Kanakis, M., Koutsiouki, C., Kiskira, E., Mylonas, G., et al. (2018). Long-Term results of combination treatment with single-dose ranibizumab plus photodynamic therapy for retinal angiomatous proliferation. *Ophthalmologica* 240, 213–221. doi: 10.1159/000487610

Marquardt, T., Ashery-Padan, R., Andrejewski, N., Scardigli, R., Guillemot, F., and Gruss, P. (2001). Pax6 is required for the multipotent state of retinal progenitor cells. *Cell* 105, 43–55. doi: 10.1016/s0092-8674(01)00295-1

Marques, J. P., Laíns, I., Costa, M., Pires, I., Cachulo, M. D. L., Figueira, J., et al. (2015). Retinal angiomatous proliferatio: a quantitative analysis of the fundoscopic features of the fellow eye. *Retina* 35, 1985–1991. doi: 10.1097/iae.0000000000000619

Marticorena, J., Leva, V. D., Cennamo, G. L., and Crecchio, G. D. (2011). Retinal angiomatous proliferation. *Curr. Drug Targets* 12, 199–205.

Martins, A., Farinha, C., Raimundo, M., Lopes, M., Santos, A. R., Melo, P., et al. (2018). Multimodal evaluation of the fellow eye of patients with retinal angiomatous proliferation. *Ophthalmic Res.* 59, 88–97. doi: 10.1159/000481262

Maruko, I., Iida, T., Saito, M., Nagayama, D., and Saito, K. (2007). Clinical characteristics of exudative age-related macular degeneration in Japanese patients. *Am. J. Ophthalmol.* 144, 15–22. doi: 10.1016/j.ajo.2007.03.047

Mast, N., Reem, R., Bederman, I., Huang, S., Dipatre, P. L., Bjorkhem, I., et al. (2011). Cholestenoic Acid is an important elimination product of cholesterol in the retina: comparison of retinal cholesterol metabolism with that in the brain. *Invest. Ophthalmol. Vis. Sci.* 52, 594–603. doi: 10.1167/iovs.10-6021

Matsumoto, H., Sato, T., and Kishi, S. (2010). Tomographic features of intraretinal neovascularization in retinal angiomatous proliferation. *Retina* 30, 425–430. doi: 10.1097/iae.0b013e3181bd2d95

Mehalow, A. K., Kameya, S., Smith, R. S., Hawes, N. L., Denegre, J. M., Young, J. A., et al. (2003). CRB1 is essential for external limiting membrane integrity and photoreceptor morphogenesis in the mammalian retina. *Hum. Mol. Genet.* 12, 2179–2189. doi: 10.1093/hmg/ddg232

Miere, A., Querques, G., Semoun, O., Ameen, A.a.E, Capuano, V., and Souied, E. H. (2015). Optical coherence tomography angiography in early type 3 neovascularization. *Retina* 35, 2236–2241. doi: 10.1097/iae.0000000000000834

Miere, A., Querques, G., Semoun, O., Amoroso, F., Zambrowski, O., Chapron, T., et al. (2017). Optical coherence tomography angiography changes in early type 3 neovascularization after anti-vascular endothelial growth factor treatment. *Retina* 37, 1873–1879. doi: 10.1097/iae.0000000000001447

Miller, J. W. (2013). Age-Related macular degeneration revisited – piecing the puzzle: the LXIX Edward Jackson Memorial Lecture. *Am. J. Ophthalmol.* 155, 1–35.e13.

Mitchell, P., Liew, G., Gopinath, B., and Wong, T. Y. (2018). Age-related macular degeneration. *Lancet* 392, 1147–1159.

Monson, D. M., Smith, J. R., Klein, M. L., and Wilson, D. J. (2008). Clinicopathologic correlation of retinal angiomatous proliferation. *Arch. Ophthalmol.* 126, 1664–1668. doi: 10.1001/archopht.126.12.1664

Montero, J. A., Ruiz-Moreno, J. M., Sanabria, M. R., and Fernandez-Munoz, M. (2009). Efficacy of intravitreal and periocular triamcinolone associated with photodynamic therapy for treatment of retinal angiomatous proliferation. *Br. J. Ophthalmol.* 93, 166–170. doi: 10.1136/bjo.2008.141903

Nagai, N., Ju, M., Izumi-Nagai, K., Robbie, S. J., Bainbridge, J. W., Gale, D. C., et al. (2015). Novel CCR3 antagonists are effective mono- and combination inhibitors of choroidal neovascular growth and vascular permeability. *Am. J. Pathol.* 185, 2534–2549. doi: 10.1016/j.ajpath.2015.04.029

Nagai, N., Lundh von Leithner, P., Izumi-Nagai, K., Hosking, B., Chang, B., Hurd, R., et al. (2014). Spontaneous CNV in a novel mutant mouse is associated with early VEGF-A-driven angiogenesis and late-stage focal edema, neural cell loss, and dysfunction. *Invest. Ophthalmol. Vis. Sci.* 55, 3709–3719. doi: 10.1167/iovs.14-13989

Nagiel, A., Sarraf, D., Sadda, S. R., Spaide, R. F., Jung, J. J., Bhavsar, K. V., et al. (2015). Type 3 neovascularization: evolution, association with pigment epithelial detachment, and treatment response as revealed by spectral domain optical coherence tomography. *Retina* 35, 638–647. doi: 10.1097/iae.0000000000000488

Ohno-Matsui, K., Hirose, A., Yamamoto, S., Saikia, J., Okamoto, N., Gehlbach, P., et al. (2002). Inducible expression of vascular endothelial growth factor in adult mice causes severe proliferative retinopathy and retinal detachment. *Am. J. Pathol.* 160, 711–719. doi: 10.1016/s0002-9440(10)64891-2

Okabe, K., Kobayashi, S., Yamada, T., Kurihara, T., Tai-Nagara, I., Miyamoto, T., et al. (2014). Neurons limit angiogenesis by titrating VEGF in retina. *Cell* 159, 584–596. doi: 10.1016/j.cell.2014.09.025

Okamoto, N., Tobe, T., Hackett, S. F., Ozaki, H., Vinores, M. A., Larochelle, W., et al. (1997). Transgenic mice with increased expression of vascular endothelial growth factor in the retina: a new model of intraretinal and subretinal neovascularization. *Am. J. Pathol.* 151, 281–291.

Olson, E. N., and Nordheim, A. (2010). Linking actin dynamics and gene transcription to drive cellular motile functions. *Nat. Rev. Mol. Cell. Biol.* 11, 353–365. doi: 10.1038/nrm2890

Omarova, S., Charvet, C. D., Reem, R. E., Mast, N., Zheng, W., Huang, S., et al. (2012). Abnormal vascularization in mouse retina with dysregulated retinal cholesterol homeostasis. *J. Clin. Invest.* 122, 3012–3023. doi: 10.1172/jci63816

Park, S., and Chan, C. C. (2012). Von Hippel-Lindau disease (VHL): a need for a murine model with retinal hemangioblastoma. *Histol. Histopathol.* 27, 975–984.

Perrott-Reynolds, R., Cann, R., Cronbach, N., Neo, Y. N., Ho, V., Mcnally, O., et al. (2019). The diagnostic accuracy of OCT angiography in naive and treated neovascular age-related macular degeneration: a review. *Eye (Lond)* 33, 274–282. doi: 10.1038/s41433-018-0229-6

Pikuleva, I. A. (2006). Cytochrome P450s and cholesterol homeostasis. *Pharmacol. Ther.* 112, 761–773. doi: 10.1016/j.pharmthera.2006.05.014

Pikuleva, I. A., and Curcio, C. A. (2014). Cholesterol in the retina: the best is yet to come. *Prog. Retin. Eye Res.* 41, 64–89. doi: 10.1016/j.preteyeres.2014.03.002

Politoa, A., Napolitano, M. C., Bandello, F., and Chiodini, R. G. (2006). The role of optical coherence tomography (OCT) in the diagnosis and management of retinal angiomatous proliferation (RAP) in patients with age-related macular degeneration. *Ann. Acad. Med. Singap.* 35, 420–424.

Posern, G., and Treisman, R. (2006). Actin' together: serum response factor, its cofactors and the link to signal transduction. *Trends Cell Biol.* 16, 588–596. doi: 10.1016/j.tcb.2006.09.008

Querques, G., Souied, E. H., and Freund, K. B. (2013). Multimodal imaging of early stage 1 type 3 neovascularization with simultaneous eye-tracked spectral-domain optical coherence tomography and high-speed real-time angiography. *Retina* 33, 1881–1887. doi: 10.1097/iae.0b013e3182923448

Querques, G., Souied, E. H., and Freund, K. B. (2015). How has high-resolution multimodal imaging refined our understanding of the vasogenic process in type 3 neovascularization? *Retina* 35, 603–613. doi: 10.1097/iae.0000000000000487

Ravera, V., Bottoni, F., Giani, A., Cigada, M., and Staurenghi, G. (2016). Retinal angiomatous proliferation diagnosis: a multiimaging approach. *Retina* 36, 2274–2281. doi: 10.1097/iae.0000000000001152

Rouvas, A. A., Chatziralli, I. P., Theodossiadis, P. G., Moschos, M. M., Kotsolis, A. I., and Ladas, I. D. (2012). Long-term results of intravitreal ranibizumab, intravitreal ranibizumab with photodynamic therapy, and intravitreal triamcinolone with photodynamic therapy for the treatment of retinal angiomatous proliferation. *Retina* 32, 1181–1189. doi: 10.1097/iae.0b013e318235d8ce

Sacconi, R., Battista, M., Borrelli, E., Miere, A., Corbelli, E., Capuano, V., et al. (2021). OCT-A characterisation of recurrent type 3 macular neovascularisation. *Br. J. Ophthalmol.* 105, 222–226. doi: 10.1136/bjophthalmol-2020-316054

Sacconi, R., Sarraf, D., Garrity, S., Freund, K. B., Yannuzzi, L. A., Gal-Or, O., et al. (2018). Nascent type 3 neovascularization in age-related macular degeneration. *Ophthalmol. Retina* 2, 1097–1106.

Sawa, M., Ueno, C., Gomi, F., and Nishida, K. (2014). Incidence and characteristics of neovascularization in fellow eyes of Japanese patients with unilateral retinal angiomatous proliferation. *Retina* 34, 761–767. doi: 10.1097/01.iae.0000434566.57189.37

Schofield, C. J., and Ratcliffe, P. J. (2004). Oxygen sensing by HIF hydroxylases. *Nat. Rev. Mol. Cell. Biol.* 5, 343–354. doi: 10.1038/nrm1366

Scott, A. W., and Bressler, S. B. (2009). Retinal angiomatous proliferation or retinal anastomosis to the lesion. *Eye* 24, 491–496. doi: 10.1038/eye.2009.311

Semenza, G. L. (2004). Hydroxylation of HIF-1: oxygen sensing at the molecular level. *Physiology (Bethesda)* 19, 176–182. doi: 10.1152/physiol.00001.2004

Shimada, H., Kawamura, A., Mori, R., and Yuzawa, M. (2006). Clinicopathological findings of retinal angiomatous proliferation. *Graefe's Arch. Clin. Exp. Ophthalmol.* 245, 295–300. doi: 10.1007/s00417-006-0367-6

Simons, M., Gordon, E., and Claesson-Welsh, L. (2016). Mechanisms and regulation of endothelial VEGF receptor signalling. *Nat. Rev. Mol. Cell. Biol.* 17, 611–625. doi: 10.1038/nrm.2016.87

Skalet, A. H., Miller, A. K., Klein, M. L., Lauer, A. K., and Wilson, D. J. (2017). Clinicopathologic correlation of retinal angiomatous proliferation treated with ranibizumab. *Retina* 37, 1620–1624. doi: 10.1097/iae.0000000000001672

Song, S. J., Youm, D. J., Chang, Y., and Yu, H. G. (2009). Age-related macular degeneration in a screened South Korean population: prevalence, risk factors, and subtypes. *Ophthalmic Epidemiol.* 16, 304–310. doi: 10.3109/09286580902999413

Spaide, R. F. (2019). New proposal for the pathophysiology of type 3 neovascularization as based on multimodal imaging findings. *Retina* 39, 1451–1464. doi: 10.1097/iae.0000000000002412

Spaide, R. F., Jaffe, G. J., Sarraf, D., Freund, K. B., Sadda, S. R., Staurenghi, G., et al. (2020). Consensus nomenclature for reporting neovascular age-related macular degeneration data: consensus on neovascular age-related macular degeneration nomenclature study group. *Ophthalmology* 127, 616–636.

Spaide, R. F., Klancnik, J. M. Jr., and Cooney, M. J. (2015). Retinal vascular layers imaged by fluorescein angiography and optical coherence tomography angiography. *JAMA Ophthalmol.* 133, 45–50. doi: 10.1001/jamaophthalmol.2014.3616

Su, D., Lin, S., Phasukkijwatana, N., Chen, X., Tan, A., Freund, K. B., et al. (2016). An updated staging system of type 3 neovascularization using spectral domain optical coherence tomography. *Retina* 36 Suppl 1, S40–S49.

Sun, Y., Lin, Z., Liu, C. H., Gong, Y., Liegl, R., Fredrick, T. W., et al. (2017). Inflammatory signals from photoreceptor modulate pathological retinal angiogenesis via c-Fos. *J. Exp. Med.* 214, 1753–1767. doi: 10.1084/jem.20161645

Sun, Y., Liu, C. H., Sangiovanni, J. P., Evans, L. P., Tian, K. T., Zhang, B., et al. (2015). Nuclear receptor RORα regulates pathologic retinal angiogenesis by modulating SOCS3-dependent inflammation. *Proc. Natl. Acad. Sci. U.S.A.* 112, 10401–10406. doi: 10.1073/pnas.1504387112

Tan, A. C. S., Dansingani, K. K., Yannuzzi, L. A., Sarraf, D., and Freund, K. B. (2017). Type 3 neovascularization imaged with cross-sectional and en face optical coherence tomography angiography. *Retina* 37, 234–246. doi: 10.1097/iae.0000000000001343

Thomis, D. C., Gurniak, C. B., Tivol, E., Sharpe, A. H., and Berg, L. J. (1995). Defects in B lymphocyte maturation and T lymphocyte activation in mice lacking Jak3. *Science* 270, 794–797. doi: 10.1126/science.270.5237.794

Tiebel, O., Oka, K., Robinson, K., Sullivan, M., Martinez, J., Nakamuta, M., et al. (1999). Mouse very low-density lipoprotein receptor (VLDLR): gene structure, tissue-specific expression and dietary and developmental regulation. *Atherosclerosis* 145, 239–251. doi: 10.1016/s0021-9150(99)00068-4

Tobe, T., Okamoto, N., Vinores, M. A., Derevjanik, N. L., Vinores, S. A., Zack, D. J., et al. (1998). Evolution of neovascularization in mice with overexpression of vascular endothelial growth factor in photoreceptors. *Invest. Ophthalmol. Vis. Sci.* 39, 180–188.

Tolentino, M. J., Miller, J. W., Gragoudas, E. S., Jakobiec, F. A., Flynn, E., Chatzistefanou, K., et al. (1996). Intravitreous injections of vascular endothelial growth factor produce retinal ischemia and microangiopathy in an adult primate. *Ophthalmology* 103, 1820–1828. doi: 10.1016/s0161-6420(96)30420-x

Tsai, A. S. H., Cheung, N., Gan, A. T. L., Jaffe, G. J., Sivaprasad, S., Wong, T. Y., et al. (2017). Retinal angiomatous proliferation. *Surv. Ophthalmol.* 62, 462–492.

Ueda-Arakawa, N., Ooto, S., Nakata, I., Yamashiro, K., Tsujikawa, A., Oishi, A., et al. (2013). Prevalence and genomic association of reticular pseudodrusen in age-related macular degeneration. *Am. J. Ophthalmol.* 155, 260–269.e2.

Usui, Y., Westenskow, P. D., Kurihara, T., Aguilar, E., Sakimoto, S., Paris, L. P., et al. (2015). Neurovascular crosstalk between interneurons and capillaries is required for vision. *J. Clin. Invest.* 125, 2335–2346. doi: 10.1172/jci80297

Usui-Ouchi, A., Usui, Y., Kurihara, T., Aguilar, E., Dorrell, M. I., Ideguchi, Y., et al. (2020). Retinal microglia are critical for subretinal neovascular formation. *JCI Insight* 5:e137317.

Wang, T., Tsirukis, D. I., and Sun, Y. (2020). Targeting neuroinflammation in neovascular retinal diseases. *Front. Pharmacol.* 11:234. doi: 10.3389/fphar.2020.00234

Wang, Y., Rattner, A., Zhou, Y., Williams, J., Smallwood, P. M., and Nathans, J. (2012). Norrin/Frizzled4 signaling in retinal vascular development and blood brain barrier plasticity. *Cell* 151, 1332–1344. doi: 10.1016/j.cell.2012.10.042

Wei, R., Ren, X., Kong, H., Lv, Z., Chen, Y., Tang, Y., et al. (2019). Rb1/Rbl1/Vhl loss induces mouse subretinal angiomatous proliferation and hemangioblastoma. *JCI Insight* 4, e127889.

Weinl, C., Riehle, H., Park, D., Stritt, C., Beck, S., Huber, G., et al. (2013). Endothelial SRF/MRTF ablation causes vascular disease phenotypes in murine retinae. *J. Clin. Invest.* 123, 2193–2206. doi: 10.1172/jci64201

Wert, K. J., Mahajan, V. B., Zhang, L., Yan, Y., Li, Y., Tosi, J., et al. (2016). Neuroretinal hypoxic signaling in a new preclinical murine model for proliferative diabetic retinopathy. *Signal Transduct. Target. Ther.* 1:16005.

Won, J., Shi, L. Y., Hicks, W., Wang, J., Hurd, R., Naggert, J. K., et al. (2011). Mouse model resources for vision research. *J. Ophthalmol.* 2011:391384.

Wong, W. L., Su, X., Li, X., Cheung, C. M. G., Klein, R., Cheng, C.-Y., et al. (2014). Global prevalence of age-related macular degeneration and disease burden projection for 2020 and 2040: a systematic review and meta-analysis. *Lancet Global Health* 2, e106–e116.

Wright, C. B., Uehara, H., Kim, Y., Yasuma, T., Yasuma, R., Hirahara, S., et al. (2020). Chronic Dicer1 deficiency promotes atrophic and neovascular outer retinal pathologies in mice. *Proc. Natl. Acad. Sci. U.S.A.* 117, 2579–2587. doi: 10.1073/pnas.1909761117

Yamazaki, T., Koizumi, H., Yamagishi, T., and Kinoshita, S. (2014). Subfoveal choroidal thickness in retinal angiomatous proliferation. *Retina* 34, 1316–1322. doi: 10.1097/iae.0000000000000086

Yannuzzi, L. A., Freund, K. B., and Takahashi, B. S. (2008). Review of retinal angiomatous proliferation or type 3 neovascularization. *Retina* 28, 375–384. doi: 10.1097/iae.0b013e3181619c55

Yannuzzi, L. A., Negrao, S., Iida, T., Carvalho, C., Rodriguez-Coleman, H., Slakter, J., et al. (2001). Retinal angiomatous proliferation in age-related macular degeneration. *Retina* 21, 416–434.

Zhang, L., Cui, X., Han, Y., Park, K. S., Gao, X., Zhang, X., et al. (2019). Hypoxic drive caused type 3 neovascularization in a preclinical model of exudative age-related macular degeneration. *Hum. Mol. Genet.* 28, 3475–3485. doi: 10.1093/hmg/ddz159

Zhang, Z. Y., Bao, X. L., Cong, Y. Y., Fan, B., and Li, G. Y. (2020). Autophagy in age-related macular degeneration: a regulatory mechanism of oxidative stress. *Oxid. Med. Cell. Longev.* 2020:2896036.

Conflict of Interest: The authors declare that the research was conducted in the absence of any commercial or financial relationships that could be construed as a potential conflict of interest.

Publisher's Note: All claims expressed in this article are solely those of the authors and do not necessarily represent those of their affiliated organizations, or those of the publisher, the editors and the reviewers. Any product that may be evaluated in this article, or claim that may be made by its manufacturer, is not guaranteed or endorsed by the publisher.

frontiers in Neuroscience

ORIGINAL RESEARCH
published: 08 November 2021
doi: 10.3389/fnins.2021.738022

Suppressor of Cytokine Signaling 2 Regulates Retinal Pigment Epithelium Metabolism by Enhancing Autophagy

*Xi-Yuan Liu, Rui Lu, Jing Chen, Jie Wang, Hong-Mei Qian, Gang Chen, Rong-Han Wu and Zai-Long Chi**

State Key Laboratory of Ophthalmology, Optometry and Visual Science, Eye Hospital and School of Ophthalmology and Optometry, Wenzhou Medical University, Wenzhou, China

Retinal pigment epithelium (RPE) serves critical functions in maintaining retinal homeostasis. An important function of RPE is to degrade the photoreceptor outer segment fragments daily to maintain photoreceptor function and longevity throughout life. An impairment of RPE functions such as metabolic regulation leads to the development of age-related macular degeneration (AMD) and inherited retinal degenerative diseases. As substrate recognition subunit of a ubiquitin ligase complex, suppressor of cytokine signaling 2 (SOCS2) specifically binds to the substrates for ubiquitination and negatively regulates growth hormone signaling. Herein, we explore the role of SOCS2 in the metabolic regulation of autophagy in the RPE cells. *SOCS2* knockout mice exhibited the irregular morphological deposits between the RPE and Bruch's membrane. Both *in vivo* and *in vitro* experiments showed that RPE cells lacking *SOCS2* displayed impaired autophagy, which could be recovered by re-expressing SOCS2. SOCS2 recognizes the ubiquitylated proteins and participates in the formation of autolysosome by binding with autophagy receptors and lysosome-associated membrane protein2 (LAMP-2), thereby regulating the phosphorylation of glycogen synthase kinase 3β (GSK3β) and mammalian target of rapamycin (mTOR) during the autophagy process. Our results imply that SOCS2 participates in ubiquitin-autophagy-lysosomal pathway and enhances autophagy by regulating GSK3β and mTOR. This study provides a potential therapeutic target for AMD.

Keywords: suppressor of cytokine signaling 2, retinal pigment epithelium, autophagy, ubiquitin, glycogen synthase kinase (GSK)-3β, mammalian target of rapamycin (mTOR)

OPEN ACCESS

Edited by:
Anu Kauppinen,
University of Eastern Finland, Finland

Reviewed by:
Kai Kaarniranta,
University of Eastern Finland, Finland
Yonju Ha,
University of Texas Medical Branch at Galveston, United States

***Correspondence:**
Zai-Long Chi
zailong.chi@eye.ac.cn

Specialty section:
This article was submitted to Neurodegeneration, a section of the journal Frontiers in Neuroscience

Received: *08 July 2021*
Accepted: *23 September 2021*
Published: *08 November 2021*

Citation:
Liu X-Y, Lu R, Chen J, Wang J, Qian H-M, Chen G, Wu R-H and Chi Z-L (2021) Suppressor of Cytokine Signaling 2 Regulates Retinal Pigment Epithelium Metabolism by Enhancing Autophagy. Front. Neurosci. 15:738022. doi: 10.3389/fnins.2021.738022

INTRODUCTION

Retinal pigment epithelium (RPE) serves critical functions in maintaining retinal homeostasis. Impairment of RPE functions such as metabolic regulation leads to the development of age-related macular degeneration (AMD). An important function of RPE is to digest the photoreceptor outer segment (POS) fragments daily to maintain photoreceptor function and longevity throughout

life. RPE undergoes various changes during aging, one of which is weakened autophagy (Giaime et al., 2017; Madeo et al., 2019). The disorder of RPE clearing POS fragments contributes to the accumulation of the intracellular residual bodies, eventually leading to the formation of drusen and development of AMD. AMD, a chronic disease of the macula, is the leading cause of irreversible blindness in the elderly individuals with a steep increase in the number of patients over age 65 years (Mitchell et al., 2018). Atrophic or dry AMD and neovascular or wet AMD are the two forms of AMD. To date, the treatments are limited to wet AMD and no effective treatment exists for dry AMD because the mechanism underlying AMD is still not fully understood. Thus, the discovery of a mechanism is critically needed to prevent or delay AMD progression. Reduced autophagy of RPE with age is one of the risk factors and accelerates the formation of drusen, which is composed of proteins, lipids, and minerals (Wang et al., 2010; Crabb, 2014). Proteomic analysis of drusen identified 129 proteins, most of which were insoluble and aggregate (Crabb et al., 2002; Hollyfield et al., 2003; Ohno-Matsui, 2011). Therefore, enhancing the degradation of metabolic proteins in RPE is one way to maintain retinal homeostasis.

Autophagy is essential for an organism as it improves protein and organellar quality control and helps to defer the age-related phenotypes (Hansen et al., 2018; Nakamura et al., 2019). Mammalian target of rapamycin (mTOR) is inactivated during autophagy initiation and plays a crucial role in regulating autophagy by directly interacting with or inhibiting autophagy-related genes (Kim and Guan, 2015; Saxton and Sabatini, 2017). Autophagy involves not only bulk autophagy but also selective autophagy. Ubiquitin acts as a specificity factor for selective autophagy and the ubiquitin-proteasome system (UPS). UPS is inclined to the rapid degradation of short-lived proteins in the young cells and autophagy selectively removes the long-lived protein aggregates and damaged or excess organelles during aging (Bence et al., 2001; Ravikumar et al., 2002; Gamerdinger et al., 2009). Various metabolic components ranging from protein aggregates, peroxisomes, ribosomes, and mitochondria can be specifically engulfed by autophagosomes through ubiquitination and ubiquitin-binding receptors such as sequestosome 1 (SQSTM1/p62, hereafter referred to as p62), neighbor of BRCA1 gene 1 (NBR1), nuclear dot protein 52 (NDP52), optineurin (OPTN), and toll-interaction protein (TOLLIP) (Kirkin et al., 2009; Thurston et al., 2009; Lu et al., 2014; Yamano and Youle, 2020). p62 serves as a scaffold for the formation of protein aggregates and acts as an autophagy receptor by linking the ubiquitin-tagged protein aggregates to autophagosomes (Dantuma and Bott, 2014; Parzych and Klionsky, 2014; Rogov et al., 2014; Zaffagnini et al., 2018). The ubiquitylated substrates are specifically degraded by a p62-dependent mechanism (Pankiv et al., 2007; Kim et al., 2008). Thus, it is likely that p62 acts as an adaptor between ubiquitylated proteins and autophagy.

Suppressor of cytokine signaling (SOCS) family proteins [SOCS 1–7 and cytokine inducible SH2-containing protein (CIS)] are essential regulators of cellular responses to cytokines *via* the regulation of Janus kinases/signal transducers and activator of transcription proteins signaling. SOCS2 expression is rapidly induced upon cytokine stimulation such as growth hormone (GH) and insulin-like growth factor (Turnley, 2005; Sarajlic et al., 2019). SOCS2 possesses an Src homology 2 (SH2) domain and a SOCS box, which is responsible for E3 ligase activity by assembly with the adaptors Elongin BC and Cullin 5 (Cul5) (Bulatov et al., 2015; Song et al., 2016; Chhabra et al., 2018). The Elongin BC-Cul5-SOCS box complex is stimulated by circulating GH and regulates GH receptors (GHR) through a negative feedback loop (Vesterlund et al., 2011). Glycogen synthase kinase 3β (GSK3β) is inhibited by serine phosphorylation in response to insulin or growth factors (Ge et al., 2013; Wei et al., 2021). GSK3β mediates the activation of mTOR by Wnt signaling and the inhibition of GSK3β increases the activation of mTOR (Inoki et al., 2006). GSK3β induces autophagy by phosphorylating unc-51 like autophagy activating kinase 1 (ULK1) in the adult hippocampal neural stem cells (Ryu et al., 2021). Inhibition of long non-coding RNA (lncRNA) X-inactive specific transcript (XIST) improves myocardial ischemia/reperfusion (I/R) injury by targeting miR-133a through inhibition of autophagy and regulation of SOCS2 (Li et al., 2019). SOCS2 is shown to be upregulated in Huntington's disease and involved in regulating autophagy by functioning as an E3 ligase (Cho et al., 2021). Another study indicates that the interaction between microtubule associated protein 1 light chain 3 (LC3) and SOCS2 was detected in astrocytes either in normal or in starvation conditions (Wang et al., 2014). The genome-wide association studies discover that SOCS2 is associated with visual loss belonging to vascular endothelial growth factor (VEGF)-related pathways in the patients with exudative AMD (Akiyama et al., 2018). Integrated bioinformatics analysis indicates that hypermethylated and low-expressed SOCS2 is related to AMD (Shen et al., 2020). In RPE, however, the role of SOCS2 in autophagy is largely unknown.

We report the function of SOCS2 on autophagy. During autophagy, SOCS2 colocalizes with ubiquitylated proteins, p62, lipidated LC3B, and lysosome-associated membrane protein2 (LAMP2) and regulates the phosphorylation of GSK3β and mTOR. Our results imply that SOCS2 may participate directly in the ubiquitin-autophagy-lysosomal pathway and enhance autophagy by regulating GSK3β and mTOR.

MATERIALS AND METHODS

Antibodies, Plasmids, and Chemicals

Anti-SOCS2 (#2779), β-actin (8H10D10) (#3700), phosphorylated mTOR (p-mTOR) (Ser2448) (#5536), mTOR (7C10), rabbit monoclonal antibody (mAb) (#2983), goat antirabbit immunoglobulin G (IgG) [horseradish peroxidase (HRP) linked] (#7074), and horse antimouse IgG (HRP linked) (#7076) were purchased from the Cell Signaling Technology (Danvers, Massachusetts, United States); anti-SQSTM1/p62 antibody (ab155686), anti-ubiquitin antibody (ab7254), anti-LAMP2 antibody-lysosome marker (ab25631), recombinant anti-GSK3β antibody (Y174) (ab32391), anti-GSK3β (phospho Y216 and Y279) (ab75745), and recombinant anti-LC3B antibody (ab192890) were purchased from the Abcam

(Discovery Drive Cambridge Biomedical Campus, Cambridge, United Kingdom). Antiadvanced glycation end product (AGE) carboxymethyl-lysine (CML) (MABN1837) was purchased from the Millipore (Billerica, MA, United States). Plasmid cytomegalovirus 3 (pCMV3)-Human-SOCS2-orange fluorescent protein (OFP) expression plasmid (HG11285-ACR), control vector OFP expression plasmids (CV025), pCMV3-Human-SOCS2-green fluorescent protein (GFP) (HG11285-ACG), and control vectors GFP expression plasmids (CV026) were purchased from the Sino Biological Incorporation (Wayne, PA, United States). The autophagy inhibitor chloroquine (CQ) diphosphate (c6628) was purchased from Sigma-Aldrich (St Louis, Mosby, United States).

Animals

All the animal studies were conducted according to the protocols approved by the Institutional Animal Care and Use Committee of Wenzhou Medical University and followed the Association for Research in Vision and Ophthalmology (ARVO) Statement for the Use of Animals in Vision Research and were in accordance with the approved institutional guidelines and regulations. C57BL/6 mice were purchased from the Vital River Laboratories (Beijing, China). SOCS2$^{-/-}$ mice were generated from C57BL/6 mice by using clustered regularly interspaced short palindromic repeats (CRISPR)/CRISPR-associated 9 (Cas9)-mediated genome engineering technology to delete the fragment of exon 3 by using gRNA1 (TTG GCA GTC GTT TTT CTA GT CGG) and gRNA2 (ATT CAG CTA AAA CTA CCT AA GGG) by the Cyagen Biosciences (Guangzhou, China). The mice were kept in the standard cages and fed *ad libitum*.

Cell Culture and Transfection

The adult retinal pigment epithelium-19 (ARPE-19) cells (CRL-2302) were purchased from the American Type Culture Collection (ATCC) (Manassas, VA, United States) and maintained in Dulbecco's Modified Essential Medium (DMEM)/F12 (011721ACS) (Boehringer Ingelheim, Shanghai, China) with 10% fetal bovine serum (FBS) (10099, Thermo Fisher Scientific, Wilmington, DE, United States), 100 units/ml penicillin and streptomycin (10378016, Thermo Fisher Scientific, Wilmington, DE, United States) at 37°C with 5% CO_2. For transfection, ARPE-19 cells reached 80% confluence. SOCS2 plasmids and control vectors were transfected with the Lipofectamine 3000 Transfection Kit (L3000015, Thermo Fisher Scientific, Wilmington, DE, United States) according to the instructions of the manufacturer.

Isolation and Primary Culture of Murine Retinal Pigment Epithelium

Primary RPE cells were isolated from wild-type (WT) C57BL/6 or SOCS2$^{-/-}$ mice at age of 6 weeks following the previously described method (Fernandez-Godino et al., 2016; Chinchilla et al., 2021). The single-layer RPE sheets were isolated and incubated in DMEM/F12 medium with 15% FBS at 37°C with 5% CO_2.

Real-Time Quantitative PCR

Total RNA was extracted by using TRIzol reagent (10296010, Invitrogen, Carlsbad, CA, United States) following the RNA preparation method and was quantified by using the Multiskan Go (Thermo Fisher Scientific, Wilmington, DE, United States) (Brown et al., 2018). Reverse transcription PCR was performed by using the GoScript Reverse Transcription System (A5001, Promega, Madison, WI, United States) following the instructions of the manufacturer. Quantitative real-time PCR was used to detect the messenger RNA (mRNA) expression of SOCS2 by using the iTaq^{TM} Universal SYBR® Green Supermix (172-5121, Bio-Rad, Philadelphia, PA, United States). The primers were listed as follows: mSOCS2-F (5′-3′ CTC AGT CAA ACA GGA TGG TAC T); mSOCS2-R (5′-3′ TAC TCA ATC CGC AGG TTA GTC); mGAPDH-F (5′-3′ GAG CCA AAA GGG TCA TCA TCT C); and mGAPDH-R (5′-3′ GTG AGC TTC CCG TTC AGC TCT); hSOCS2-F (5′-3′) GAGCTCGGTCAGACAGGATG; hSOCS2-R (5′-3′) AGTTGGTCCAGCTGATGTTTT; hGAPDH-F: ATC GTG GAA GGA CTC ATG ACC ACA; and hGAPDH-R: AGA GGC AGG GAT GAT GTT CTG GA. Real-time PCR was performed on a Q5 Real-Time PCR System (Applied Biosystems, Carlsbad, CA, United States). The expression of SOCS2 was calculated by comparing the threshold cycle numbers.

Duolink *in situ* Fluorescence

Cells on the glass slides were fixed with 4% paraformaldehyde (PFA) for 20 min and the experiment was performed by following the instructions of the manufacturer of Duolink *in situ* fluorescence (DUO92101-1KT, Sigma-Aldrich, St Louis, Mosby, United States). Cells of the experimental group were incubated with SOCS2 and ubiquitin or LAMP2 antibodies and cells of the negative group were incubated without antibodies. Mount slides with a minimal volume of Duolink *in situ* mounting medium with 4′,6-diamidino-2-phenylindole (DAPI) for 15 min before analyzing in the microscope.

Immunoblot

Retinal pigment epithelium cells were serum starved and treated with or without 30 μM CQ for 24 h. Immunoblots were performed as instructed in ECL immunoblot kits (1705061, Bio-Rad, Philadelphia, PA, United States). Protein bands were exposed and captured by using an imaging system (ChemiDoc XRS+, Bio-Rad, Philadelphia, PA, United States) and quantified by the ImageJ software (United States National Institutes of Health, Bethesda, MD, United States).

Immunofluorescent Staining

Retinal pigment epithelium cells were serum starved and treated with or without 30 μM CQ for 24 h. Immunofluorescence staining of LC3B, p62, ubiquitin, and LAMP2 was performed and images were captured under a confocal microscope (ZEISS, LSM710, Oberkochen, Germany) as described (Li et al., 2021).

Autophagic Flux of Retinal Pigment Epithelium *in vivo*

Adeno-associated virus (AAV) type 2 vectors with a tandem monomeric red fluorescent protein (mRFP)-GFP-LC3 construct (AAV2-mRFP-GFP-LC3, HB-AP2100001) were generated by the Hanbio Corporation Ltd. (Shanghai, China). AAV2-mRFP-GFP-LC3 was injected subretinally through the posterior part of the sclera as previously described (Ross et al., 2021). An eye of one adult mouse received 2 μl of the virus at a concentration of 1×10^{12} vg/ml. 2 weeks later, RPE/choroidal flat mounts were performed under a microscope. The fluorescence of the cells was visualized under a microscope (DMi8, LEICA, Wetzlar, Germany).

Histology

Eyes were enucleated from euthanized 1-year old mice, fixed in 4% paraformaldehyde solution, and embedded in paraffin. Tissue sections (5 μm thick) were stained with H&E before imaging. Images of the retina/RPE/choroid were collected.

Electron Microscopy

Eyes from 1-year old WT and SOCS2$^{-/-}$ mice were fixed in phosphate-buffered saline (PBS)-buffered glutaraldehyde (2.5%, pH 7.4). The cornea, iris, and lens were discarded. The retina/RPE/choroid was fixed one more time in PBS-buffered glutaraldehyde and PBS-buffered osmium tetroxide (0.5%). The retina/RPE/choroid was embedded in epoxy resin. Thin sections (90 nm) were collected on 200 μm mesh copper grids, dried for 24 h, and double-stained with uranyl acetate and lead citrate. Sections were viewed and imaged at 80 kV with a transmission electron microscope (Hitachi-7500, Hitachi Limited, Tokyo, Japan).

Statistical Analysis

The two-tailed unpaired *t*-test and the one-way ANOVA (GraphPad Prism, CA, United States) were used to calculate the *p*-value of the results. The data are expressed as the mean ± SEM. At least six mice including males and females were used in each group.

RESULTS

Suppressor of Cytokine Signaling 2$^{-/-}$ Mice Exhibit Abnormal Retinal Pigment Epithelium-Bruch's Membrane-Choriocapillaris Complex

Mice lacking SOCS2 exhibit gigantism, thickening dermis, and shortening lifespan (Casellas and Medrano, 2008; Gossing et al., 2021). To understand the biological function of SOCS2, SOCS2$^{-/-}$ mice were generated by deleting a 756-bp fragment in exon 3 through CRISPR/Cas9 technology (**Figure 1A**). The monolayer RPE sheets composed of pigmented and hexagonal RPE were isolated from mice as previously described (Fernandez-Godino et al., 2016) and RPE cells were cultured to obtain a large number of cells (**Figure 1B**). The expression of SOCS2 mRNA was confirmed in primary cultured RPE from WT, heterozygous, and homozygous mice (**Figure 1C**), while the protein expression of SOCS2 vanished in the RPE of SOCS2$^{-/-}$ mice (**Figure 1D**). Immunofluorescence of SOCS2 also confirmed that no SOCS2 expression takes place in the retina of SOCS2$^{-/-}$ mice (**Figure 1E**). SOCS2$^{-/-}$ mice weighted significantly (1.5-fold) more than their WT littermates at 10-week age (**Figure 1F**). For the study of fundus phenotypes accumulating with age, mice were selected from 1 year of age. More generally, the abnormal structures of retina were observed in SOCS2$^{-/-}$ mice such as the disorder of the nuclear arrangement of the outer nuclear layer (ONL), the unsmooth external limiting membrane, and the loose structure of the RPE (**Figure 1G**). The accumulation of CML adducts in Bruch's membrane was observed in SOCS2$^{-/-}$ mice (**Figure 1H**). CML is an AGE that results from oxidative stress and chemical glycation and accumulates with age in Bruch's membrane and drusen in AMD (Hariharan et al., 2011; Kim et al., 2013). SOCS2$^{-/-}$ mice showed thickened Bruch's membrane and irregular morphological deposits between the RPE and Bruch's membrane (**Figure 1I**).

Suppressor of Cytokine Signaling 2$^{-/-}$ Retinal Pigment Epithelium Exhibits Impaired Autophagy

Impaired autophagy leads to the progressive accumulations of proteins and other metabolites in the RPE, which, in turn, results in RPE toxicity and pathological conditions. To monitor the *in vivo* autophagic flux of RPE, AAV2-mRFP-GFP-LC3 was injected subretinally into adult WT and SOCS2$^{-/-}$ mice. The differentiation between autophagosomes and autolysosomes was captured by the tandem fluorescent mRFP-GFP-LC3 from RPE/choroid flat mounts (Ranieri et al., 2018). The number of autophagosomes could be evaluated by counting the yellow dots overlapped by GFP and mRFP. Green fluorescence is quenched in the acidic pH of the lysosome. The mRFP dots indicated autolysosome formation. More autophagosomes (yellow dots) and autolysosomes (RFP dots) were present in the RPE of WT mice compared to the RPE of SOCS2$^{-/-}$ mice (**Figures 2A,B**), suggesting that autophagy was impaired in the RPE of SOCS2$^{-/-}$ mice.

To further evaluate the autophagic activity of RPE from SOCS2$^{-/-}$ mice, *in vitro* cultured RPE cells were treated with or without autophagy inhibitor CQ, and a rescue experiment was performed by transfecting SOCS2-expressing plasmids. SOCS2$^{-/-}$ RPE had less LC3B puncta and the rescued group showed increased LC3B puncta than SOCS2$^{-/-}$ RPE (**Figures 2C,D**). The amount of p62 is negatively correlated with autophagic activity for its ultimate degradation by autophagy. The fluorescence intensity of p62 showed a slight difference (**Figures 2C,E**). The amount of LC3B and p62 was detected in cultured RPE cells by immunoblot (**Figure 2F**). Low LC3B-II/LC3B-I ratio was measured in SOCS2$^{-/-}$ RPE, whereas the heightened ratio was measured in rescued group and CQ enlarged this ratio by blocking the degradation of

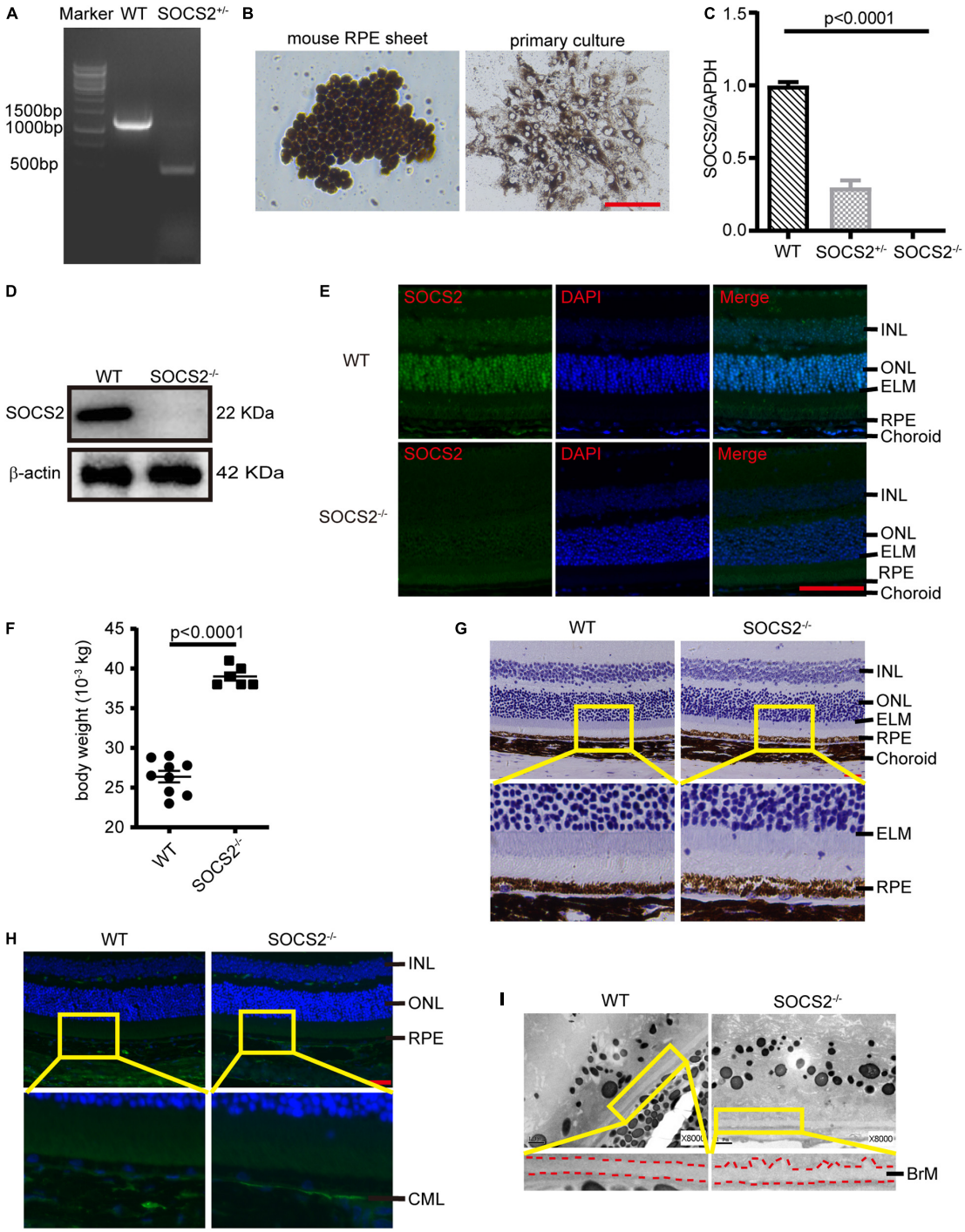

FIGURE 1 | Abnormal RPE-Bruch's membrane (BrM)-choriocapillaris complex of SOCS2$^{-/-}$ mice. **(A)** PCR screening of SOCS2$^{+/-}$ mice F1 founder to detect SOCS2 sequence from genomic DNA. **(B)** Primary culture of RPE cells isolated from WT mice. Scale bar, 200 μm. **(C)** Real-time quantitative PCR detected the mRNA expression of SOCS2 in the primary RPE of WT, heterozygote, and homozygote. Statistical significance was determined by using the one-way ANOVA. **(D)** Western blot detected the protein expression of SOCS2 in the RPE of WT and SOCS2$^{-/-}$ mice. **(E)** SOCS2 expression and location in the retina of WT and SOCS2$^{-/-}$ mice. Scale bar, 50 μm. **(F)** The body weights of the SOCS2$^{-/-}$ (n = 6, 8 weeks old, including males and females) and WT littermates (n = 9, 10 weeks old, including males and females). **(G)** The structures of the retinal-RPE-choroid were detected by histology in WT and SOCS2$^{-/-}$ mice (n = 6, 1-year old, including males and females). Scale bar, 50 μm. **(H)** CML was detected by immunofluorescence on the sections of retinal-RPE-choroid from WT and SOCS2$^{-/-}$ mice (n = 6, 1-year old, including males and females). Scale bar, 50 μm. **(I)** BrM and deposits were detected by transmission electron micrographs on the sections of retinal-RPE-choroid from WT and SOCS2$^{-/-}$ mice (n = 6, 1-year old, including males and females). Scale bar, 1 μm. Abbreviations: SOCS2, suppressor of cytokine signaling 2; mRNA, messenger RNA; INL, inner nuclear layer; ONL, outer nuclear layer; ELM, external limiting membrane; RPE, retinal pigment epithelium; WT, wild type.

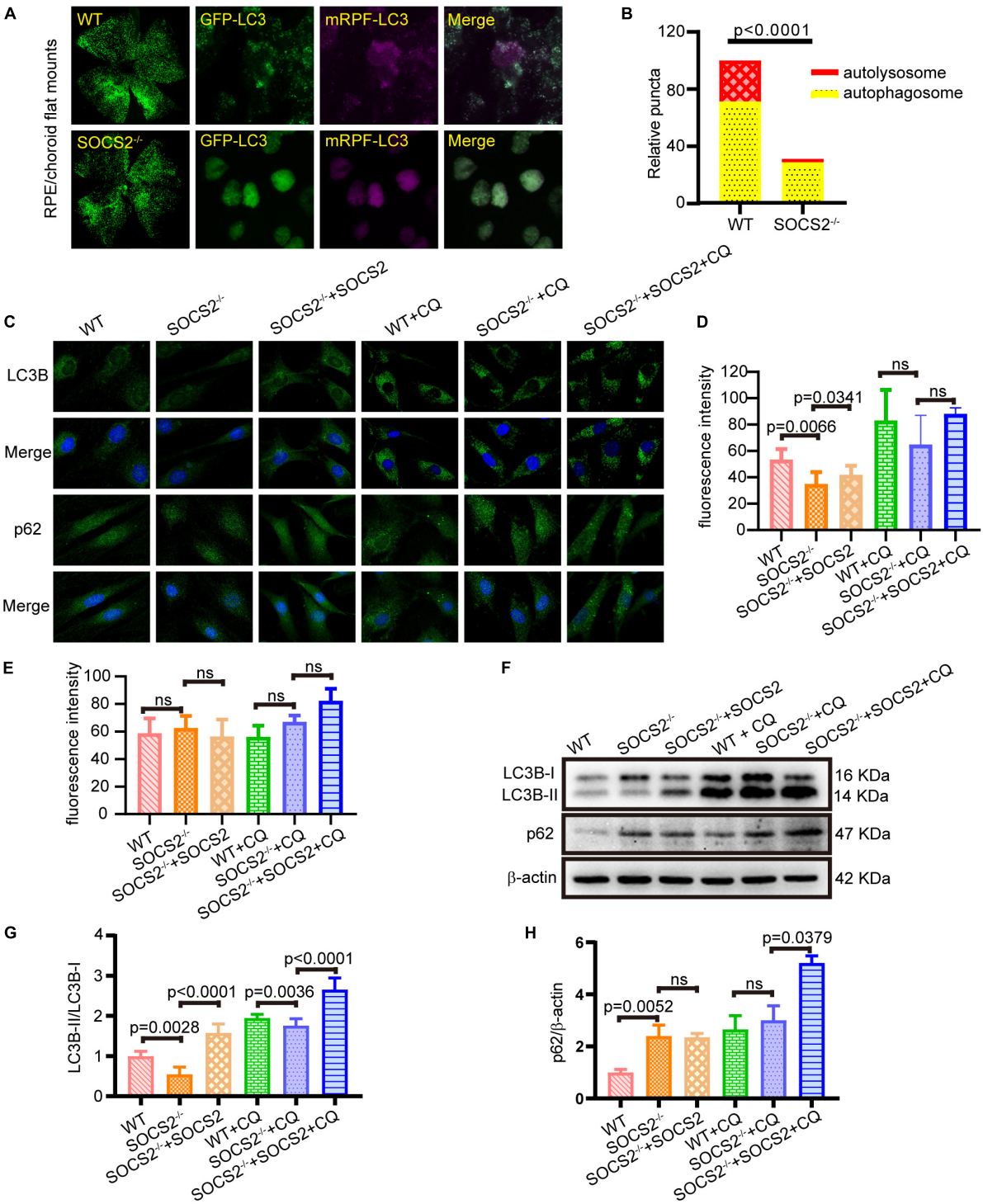

FIGURE 2 | RPE lacking the *SOCS2* gene exhibited impaired autophagy. **(A)** *In vivo*, autophagic flux was detected by injecting 2 μl of 1 × 10^{12} vg/ml adeno-associated virus 2 (AAV2)-mRFP-GFP-LC3 in the eyeball of adult WT and SOCS2$^{-/-}$ mice subretinally. About 2-weeks later, mice were starved for 24 h before euthanasia, and RPE/choroid flat mounts were isolated from mice (n = 8, 10-week old, including males and females). **(B)** The numbers of autophagosomes and autolysosomes were evaluated by counting yellow and RFP dots. Puncta dots per horizon are shown as the mean ± SEM. **(C)** LC3B puncta dots (green) and p62 puncta dots (green) were stained by immunofluorescence in mouse primary RPE cells that were starved and treated with or without 30 μM CQ for 24 h. One group of SOCS2$^{-/-}$ RPE re-expressed SOCS2 by transient transfection. **(D,E)** Fluorescence intensity of LC3B and p62 were quantified by the ImageJ software. **(F)** Immunoblotting for LC3B and p62 was performed in mouse primary RPE with different treatments. **(G)** The ratio of LC3B-II/LC3B-I was quantified by ImageJ software and normalized to β-actin. **(H)** p62 was quantified by ImageJ software and normalized to β-actin. Values for the control were set to 1. Statistical significance was determined by using the two-tailed unpaired *t*-test.

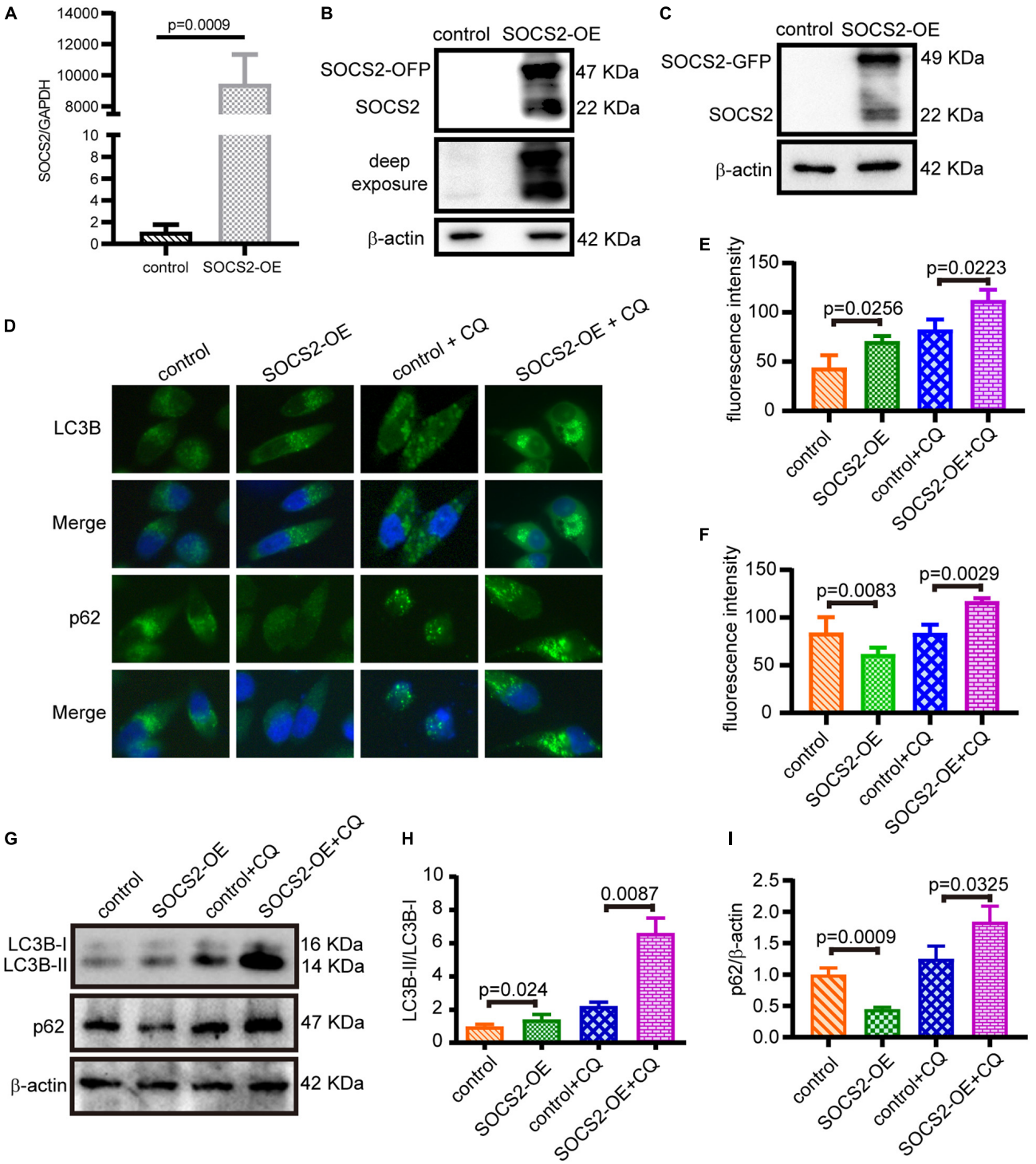

FIGURE 3 | SOCS2 promoted autophagy in ARPE-19 cells. **(A)** The mRNA expression of SOCS2 was detected by real-time quantitative PCR in ARPE-19 after transient transfection with pCMV3-Human-SOCS2-OFP expression plasmids or control vectors. The two-tailed unpaired *t*-test was used. **(B,C)** Western blot images of SOCS2-OFP and SOCS2-GFP were detected by the SOCS2 antibody to check the overexpression of SOCS2. **(D)** LC3B puncta dots (green) and p62 puncta dots (green) were stained by immunofluorescence in ARPE-19 cells transfected with pCMV3-Human-SOCS2-OFP expression plasmids or control vectors for 24 h, then cells were starved and treated with or without 30 μM CQ for 24 h. **(E,F)** Fluorescence intensity of LC3B and p62 was quantified by ImageJ software. **(G)** Western blot detected the expression of LC3B and p62 in SOCS2 overexpressing ARPE-19 cells that were treated with or without 30 μM CQ for 24 h. **(H)** The ratio of LC3B-II/LC3B-I was quantified by ImageJ software and normalized to β-actin. Values for the control were set to 1. **(I)** p62 was quantified by ImageJ software and normalized to β-actin. Values for the control were set to 1. Statistical significance was determined by using the two-tailed unpaired *t*-test.

LC3B-II (**Figure 2G**). More p62 was detected in SOCS2$^{-/-}$ RPE compared to WT RPE and more p62 stagnated in SOCS2 rescued RPE than SOCS2$^{-/-}$ RPE after CQ blocking autophagy (**Figure 2H**).

Overexpression of Suppressor of Cytokine Signaling 2 Promotes Autophagy in ARPE-19

To confirm the function of SOCS2 in RPE, SOCS2 overexpression (SOCS2-OE) models were established. Two sets of expression plasmids were employed in ARPE-19 by transient transfection, pCMV3-SOCS2-OFP plasmids or control vectors, and pCMV3-SOCS2-GFP plasmids or control vectors. The mRNA expression of SOCS2 increased around 9,000-fold in the SOCS2-OE group (**Figure 3A**) and the protein expression of SOCS2-GFP and SOCS2-OFP was detected (**Figures 3B,C**). To confirm the role of SOCS2 in autophagy, autophagic activity was evaluated in the SOCS2-OE model by detecting the immunofluorescence of LC3B and p62. Notably, the SOCS2-OE group had more LC3B puncta and less p62 puncta compared to the control. More LC3B and p62 stagnated in the SOCS2-OE model compared to control after CQ blocking autophagy (**Figures 3D–F**). The ratio of LC3B-II/LC3B-I consistently increased significantly in the SOCS2-OE model after CQ treatment, whereas p62 decreased in the SOCS2-OE group and more p62 was detected in the SOCS2-OE group after CQ treatment (**Figures 3G–I**).

Suppressor of Cytokine Signaling 2 Participates in a Ubiquitin-Autophagy-Lysosomal Pathway

As SOCS2 is a substrate recognition subunit of a ubiquitin ligase complex, to date, several proteins are identified as the substrates of SOCS2 such as GHR, erythropoietin receptor (EpoR), nuclear Dbf2-related kinase 1 (NDR1), and others (Vesterlund et al., 2011; Paul et al., 2017; Kung et al., 2019). Experiments of Duolink *in situ* fluorescence were performed in serum-starved ARPE-19 to detect the endogenous protein interaction of SOCS2 and ubiquitylated proteins. Red fluorescence indicated the colocalization of SOCS2 and ubiquitylated proteins (**Figure 4A**). To confirm the colocalization of SOCS2 and ubiquitylated proteins, either control-GFP or SOCS2-GFP was overexpressed in ARPE-19. The colocalization of SOCS2-GFP and ubiquitylated proteins were detected by the confocal microscopy with Z-stacked images (**Figure 4B**). The interaction of SOCS2-GFP and p62 was also detected by immunofluorescence and co-IP (**Figures 4C,D**). The p62 bodies were ubiquitin-containing protein aggregates (ubiquitin-positive inclusions) in the cytoplasm of ARPE-19 (**Figure 4E**). SOCS2 recognized the substrates for ubiquitination and p62 recruited ubiquitylated proteins for degradation. To check whether the ubiquitylated proteins recognized by SOCS2 were recruited to autophagosomes, the colocalization of SOCS2 and LC3B was detected by immunofluorescence and co-IP (**Figures 4F,G**).

After 24 h of CQ treatment, the colocalization of ubiquitin and a lysosome marker LAMP1 were reported (Zhan et al., 2016). To confirm the degradation of proteins identified by SOCS2 in the lysosome, experiments of Duolink *in situ* fluorescence were deployed to detect the endogenous protein interaction between SOCS2 and LAMP2 in ARPE-19. Red fluorescence indicated the colocalization of SOCS2 and LAMP2 (**Figure 4H**). To further identify the interaction of SOCS2 and LAMP2, SOCS2-OFP or control-OFP was expressed in ARPE-19 and the colocalization of SOCS2-OFP and LAMP2 was detected by confocal microscopy (**Figure 4I**). Earlier studies showed that the p62-mTOR complex translocated to the lysosome membrane in response to amino acid deprivation (Duran et al., 2011). In serum-starved ARPE-19, the interaction of p62 and p-mTOR was detected (**Figure 4J**). As additional evidence of SOCS2 locating in the lysosome, the interaction of SOCS2 and p-mTOR was also detected in starved ARPE-19 (**Figure 4K**). These findings imply that SOCS2 may directly participate in the ubiquitin-autophagy-lysosomal pathway.

Suppressor of Cytokine Signaling 2 Enhances Autophagy by Regulating the Phosphorylation of Glycogen Synthase Kinase 3β and Mammalian Target of Rapamycin in Retinal Pigment Epithelium

Suppressor of cytokine signaling 2 negatively regulates growth hormone signaling. GSK3β is inhibited in response to insulin or growth factors and negatively mediated activation of mTOR, but the relationship between SOCS2 and GSK3β has not been yet revealed. The expression of p-GSK3β (Tyr216) and GSK3β decreased (**Figures 5A–C**), whereas the phosphorylation of mTOR (Ser2448) significantly increased in SOCS2$^{-/-}$ RPE (**Figure 5D**). By contrast, SOCS2 overexpression increased the expression of GSK3β and p-GSK3β (**Figures 5E–G**), whereas the expression of p-mTOR decreased in the SOCS2-OE model (**Figure 5H**). These results imply that SOCS2 may enhance autophagy by regulating the phosphorylation of GSK3β and mTOR, both of which are involved in the regulation of autophagy.

DISCUSSION

The decreased autophagic ability of RPE with age is an important reason for drusen formation. Many studies reported that promoting autophagy protects RPE and contributes to maintaining retinal metabolism. The CD36 ligand-promoted autophagy protects RPE from oxidative stress (Dorion et al., 2021). The transcription factor EB (TFEB) inducer trehalose protects RPE against oxidative damage and cell death by upregulating autophagy (Abokyi et al., 2020). Metformin defenses hydrogen peroxide-induced oxidative damage in RPE by enhancing autophagy through activation of the AMP-activated protein kinase (AMPK) pathway (Zhao et al., 2020). Two recent studies described that SOCS2 is involved in autophagy in myocardial I/R and Huntington's disease (Li et al., 2019; Cho et al., 2021), but the underlying molecular mechanisms

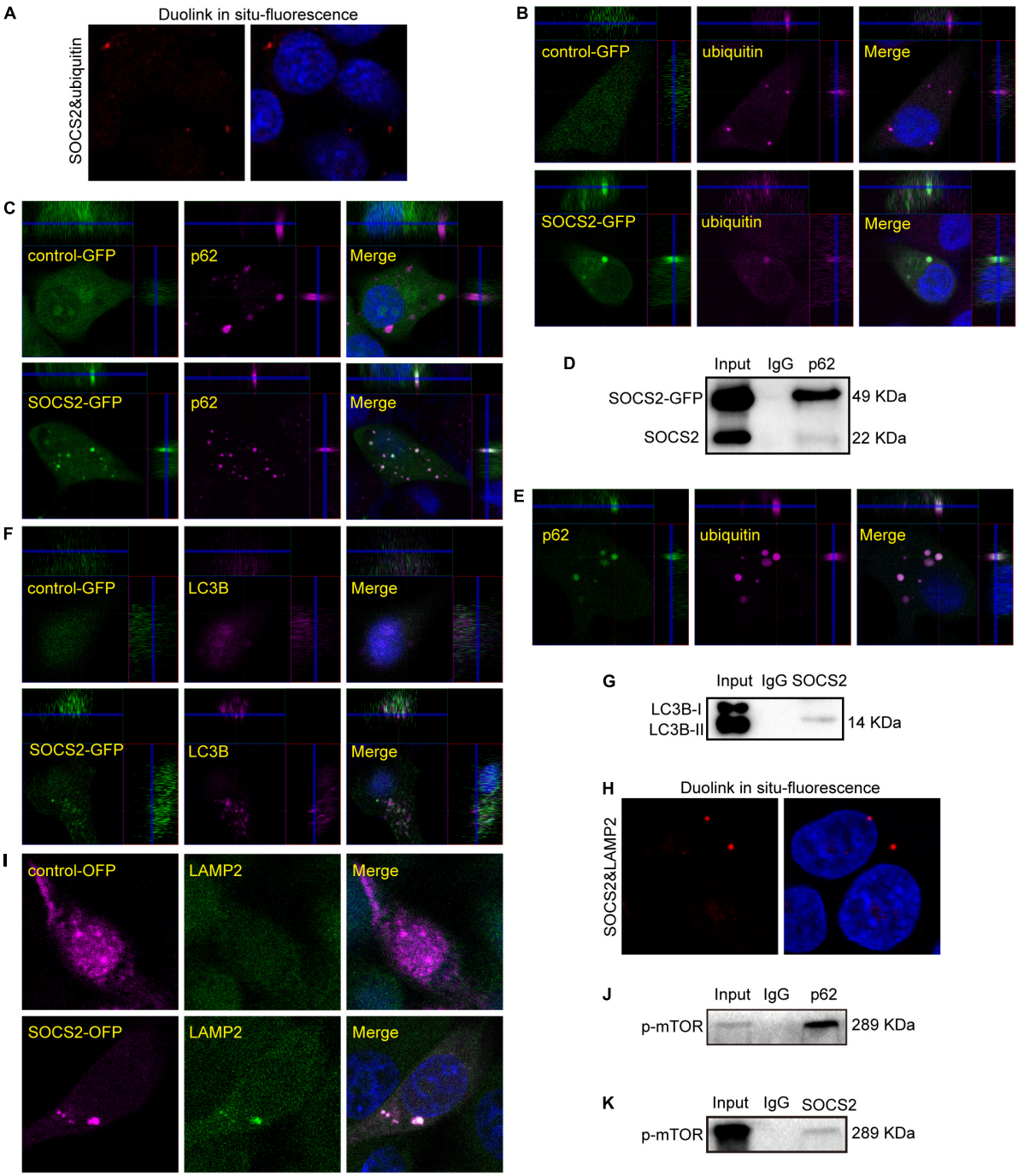

FIGURE 4 | Ubiquitylated proteins recognized by SOCS2 were transferred into autophagosomes and autolysosomes. **(A)** The endogenous detection of protein interaction between SOCS2 and ubiquitin was detected in starved ARPE-19 by Duolink *in situ* fluorescence. The red fluorescence indicated the interaction of SOCS2 and ubiquitin. **(B)** Immunofluorescence staining with ubiquitin (red) and DAPI (blue) was performed in starved ARPE-19 with transient transfection of GFP control vectors or SOCS2-GFP plasmids. The yellow dots indicated the colocalization of SOCS2 and ubiquitin in merged pictures. **(C)** Immunofluorescence staining with the antibody p62 (red) and DAPI (blue) in ARPE-19 with the same treatment of B. The yellow dots indicated the colocalization of SOCS2 and p62 in merged pictures. **(D)** The immunoprecipitation of p62 and SOCS2 was detected in ARPE-19 with the same treatment of B. **(E)** Immunofluorescence staining was performed with the antibodies against p62 (green) and ubiquitin (red) in starved ARPE-19. **(F)** Immunofluorescence staining with the antibody LC3B (red) in ARPE-19 with the same treatment of B. **(G)** The immunoprecipitation of LC3B and SOCS2 was detected in ARPE-19 with the same treatment of B. **(H)** The endogenous detection of protein interaction between SOCS2 and LAMP2 was detected in starved ARPE-19 by Duolink *in situ* fluorescence. The red fluorescence indicated the interaction of SOCS2 and LAMP2. **(I)** Immunofluorescence staining with the antibody LAMP2 in ARPE-19 after transient transfection of SOCS2-OFP plasmids or OFP control vectors. **(J,K)** The immunoprecipitation of p62 and phosphorylated mammalian target of rapamycin (p-mTOR), SOCS2, and p-mTOR were detected in ARPE-19 with the same treatment of B.

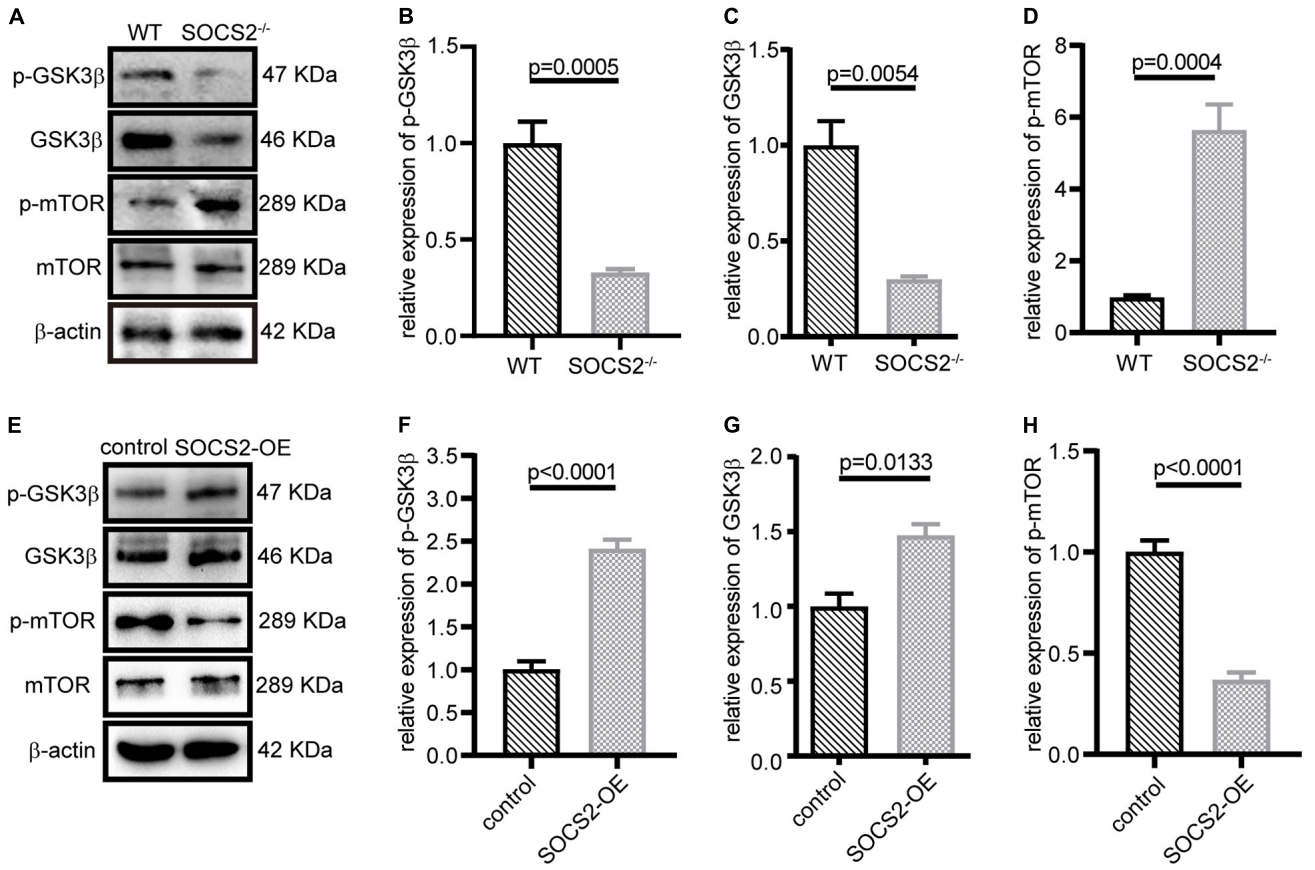

FIGURE 5 | SOCS2 regulated the phosphorylation of glycogen synthase kinase 3β (GSK3β) and mTOR. **(A)** Western blot images of p-GSK3β, GSK3β, and p-mTOR were detected in the primary RPE from WT and SOCS2$^{-/-}$. **(B,C,D)** Data shown are the mean of GSK3β, p-GSK3β, and p-mTOR bands quantified by ImageJ software and normalized to β-actin. Values for the control were set to 1. **(E)** Phosphorylation of GSK3β and mTOR was detected by immunoblot in ARPE-19 after transient transfection with SOCS2-OFP expression plasmids or OFP control vectors. **(F,G,H)** Data shown are the mean of p-GSK3β, GSK3β, and p-mTOR bands quantified by ImageJ software and normalized to β-actin. The two-tailed unpaired *t*-test was used.

for SOCS2 regulating autophagy are unclear. In this study, we explored that SOCS2 is the enhancement of autophagy in RPE by regulating mTOR and GSK3β.

Signal duration for the activated GHR is mainly controlled by SOCS2 (Sarajlic et al., 2019). The deletion of SOCS2 leads to overgrowth and abnormal metabolism, both of which may contribute to the accumulation of basal deposits between the RPE and Bruch's membrane. As SOCS2$^{-/-}$ mice are much heavier compared to the WT littermates, weight gain may be due not only to GH/insulin-like growth factor signaling but also to the accumulation of metabolic waste that cannot be removed properly by impaired autophagy. Basal deposits lead to structural and functional abnormity of RPE such as the blood-retinal barrier, phagocytosis, and light absorption, while RPE dysfunction accelerates the formation of basal deposits. This vicious cycle drives the damage to RPE.

The suppressor of cytokine signaling 2 is a substrate recognition subunit of a Cul5 E3 ubiquitin ligase complex. In this study, we found that SOCS2 colocalized not only with ubiquitylated proteins, but also with p62, LC3, and LAMP2 during autophagy. Ubiquitylated proteins were recruited by p62 to autophagosomes. LC3 is the most well-characterized autophagosome marker in mammalian cells. p62 binding directly to LC3 *via* a short LC3-interacting region (LIR) that serves as a mechanism to deliver autophagic cargo for degradation (Xu et al., 2014). LC3 binds to the crucial Trp/Phe/Tyr-X-X-Leu/Ile/Val (W/F/YXXL/I/V) motif in the LIR of proteins (Qiu et al., 2017; Sun et al., 2017). Four putative LIRs (W/F/YXXL/I/V) motifs were identified in the SOCS2 peptide sequence, implying that SOCS2 may directly bind with LC3 in the formation of autophagosomes.

Glycogen synthase kinase 3β is a serine/threonine kinase that mediates the inactivation of glycogen synthase and is inhibited by insulin signaling. Many studies reported that GSK3β is involved in autophagy. For example, GSK3β induces autophagy by phosphorylating ULK1 (Ryu et al., 2021) and C42 promotes autophagy by regulating the K-Ras/GSK3 signaling pathway in HCT116 cells (Niu et al., 2014). Inhibition of GSK3β stimulated mTOR signaling and inhibited autophagy through a rapamycin-sensitive mechanism during myocardial ischemia and IR (Zhai et al., 2011). Nimbolide negatively

regulates PI3K/Akt signaling with a consequent increase in p-GSK3β that inhibits autophagy (Sophia et al., 2018). GSK3β activation of mTOR inhibits autophagic and lysosomal activity in neurons (Rippin and Eldar-Finkelman, 2021). Ischemic post-conditioning ameliorates intestinal IR injury by evoking autophagy and inactivating GSK3β/nuclear factor erythroid 2-related factor 2 (Nrf2) pathway (Chen et al., 2020). However, none of the aforementioned studies identified the relationship between SOCS2 and GSK3β. We found that SOCS2 enhanced GSK3β activity in RPE. Low GSK3β expression was observed in SOCS2$^{-/-}$ RPE, which showed impaired autophagy. Conversely, overexpression of SOCS2 increased the activity of GSK3β and enhanced autophagy. A high positive correlation was observed between SOCS2 and GSK3β in RPE. We also found that SOCS2 negatively regulated mTOR, which is one of the pivotal factors for the regulation of autophagy. The overexpression of SOCS2 significantly inhibited the phosphorylation of mTOR. By contrast, RPE lacking the *SOCS2* gene showed much higher levels of phosphorylation of mTOR. Therefore, we concluded that SOCS2 is the enhancement of autophagy that may occur through the regulation of GSK3β and mTOR.

Loss of SOCS2 results in autophagic clearance defects due to inactive GSK3β and active mTOR signaling. Defective autophagy of RPE leads to detrimental aggregation, which is one of the clinical hallmarks of AMD. SOCS2$^{-/-}$ mice exhibit abnormal RPE-Bruch's membrane-choriocapillaris complex (**Figure 1**). It implies that defective autophagy is an important mechanism in the pathogenesis of AMD. Thus, identifying molecular targets that can regulate autophagy provides a new avenue for the treatment of AMD. Since the expression of SOCS2 were detected in the ONL of retina, and the SOCS2$^{-/-}$ mice show abnormal arrangement of the photoreceptor ONL, we speculate that SOCS2 is also involved in photoreceptor dysfunction and AMD pathology, but further experiments are needed in the future study. To date, AMD is an incurable disease, especially for dry AMD. Explored molecular mechanisms and possible therapeutic targets are a top priority. In this study, we performed both *in vitro* and *in vivo* experiments to investigate the role of SOCS2 in autophagy and found that SOCS2 participates directly in autophagy and enhances autophagy by regulating the phosphorylation of GSK3β and mTOR. This study outlined the process of SOCS2 involving autophagy and provided deeper insights into the molecular mechanisms, which may develop a potential therapeutic target for AMD.

DATA AVAILABILITY STATEMENT

The original contributions presented in the study are included in the article/supplementary material, further inquiries can be directed to the corresponding author.

ETHICS STATEMENT

The animal study was reviewed and approved by the Institutional Animal Care and Use Committee of Wenzhou Medical University.

AUTHOR CONTRIBUTIONS

Z-LC and X-YL investigated and designed the research and drafted the manuscript. Z-LC, X-YL, and GC analyzed the data. Z-LC, R-HW, and X-YL contributed to funding acquisition. X-YL, RL, JC, JW, R-HW, and H-MQ performed research. All authors contributed to the article and approved the submitted version.

FUNDING

This study was supported by the Natural Science Foundation of Zhejiang Province (LQ17H120006 and LY20H120004), the National Natural Science Foundation of China (81770918), and the initial Grant of Wenzhou Medical University Eye Hospital (KYQD150601).

ACKNOWLEDGMENTS

We thank all the past and current members of our laboratory for contributing to this project and their helpful comments on the manuscript.

REFERENCES

Abokyi, S., Shan, S. W., To, C. H., Chan, H. H., and Tse, D.Y. (2020). Autophagy upregulation by the TFEB inducer trehalose protects against oxidative damage and cell death associated with Nrf2 inhibition in human rpe cells. *Oxid. Med. Cell Longev.* 2020:5296341. doi: 10.1155/2020/5296341

Akiyama, M., Takahashi, A., Momozawa, Y., Arakawa, S., Miya, F., Tsunoda, T., et al. (2018). Genome-wide association study suggests four variants influencing outcomes with ranibizumab therapy in exudative age-related macular degeneration. *J. Hum. Genet.* 63, 1083–1091. doi: 10.1038/s10038-018-0493-0

Bence, N. F., Sampat, R. M., and Kopito, R. R. (2001). Impairment of the ubiquitin-proteasome system by protein aggregation. *Science* 292, 1552–1555.

Brown, R. A. M., Epis, M. R., Horsham, J. L., Kabir, T. D., Richardson, K. L., and Leedman, P. J. (2018). Total RNA extraction from tissues for microrna and target gene expression analysis: not all kits are created equal. *BMC Biotechnol.* 18:16. doi: 10.1186/s12896-018-0421-6

Bulatov, E., Martin, E. M., Chatterjee, S., Knebel, A., Shimamura, S., Konijnenberg, A., et al. (2015). Biophysical studies on interactions and assembly of full-size E3 ubiquitin ligase: suppressor of cytokine signaling 2 (SOCS2)-elongin BC-cullin 5-ring box protein 2 (RBX2). *J. Biol. Chem.* 290, 4178–4191. doi: 10.1074/jbc.M114.616664

Casellas, J., and Medrano, J. F. (2008). Lack of Socs2 expression reduces lifespan in high-growth mice. *Age* 30, 245–249. doi: 10.1007/s11357-008-9064-1

Chen, R., Zhang, Y. Y., Lan, J. N., Liu, H. M., Li, W., Wu, Y., et al. (2020). Ischemic Postconditioning Alleviates Intestinal Ischemia-Reperfusion Injury by Enhancing Autophagy and Suppressing Oxidative Stress through the Akt/GSK-3beta/Nrf2 Pathway in Mice. *Oxid. Med. Cel.l Longev.* 2020:6954764. doi: 10.1155/2020/6954764

Chhabra, Y., Wong, H. Y., Nikolajsen, L. F., Steinocher, H., Papadopulos, A., Tunny, K. A., et al. (2018). A growth hormone receptor SNP promotes lung cancer by impairment of SOCS2-mediated degradation. *Oncogene* 37, 489–501. doi: 10.1038/onc.2017.352

Chinchilla, B., Getachew, H., and Fernandez-Godino, R. (2021). Efficient Dissection and Culture of Primary Mouse Retinal Pigment Epithelial Cells. *J. Vis. Exp.* 168. doi: 10.3791/62228

Cho, K., Kim, S., and Choi, S. H. (2021). Suppressor of cytokine signaling 2 is induced in Huntington's disease and involved in autophagy. *Biochem. Biophys. Res. Commun.* 559, 21–27. doi: 10.1016/j.bbrc.2021.04.089

Crabb, J. W. (2014). The proteomics of drusen. *Cold Spring Harb. Perspect. Med.* 4:a017194.

Crabb, J. W., Miyagi, M., Gu, X., Shadrach, K., West, K. A., Sakaguchi, H., et al. (2002). Drusen proteome analysis: an approach to the etiology of age-related macular degeneration. *Proc. Natl. Acad. Sci. U. S. A.* 99, 14682–14687.

Dantuma, N. P., and Bott, L. C. (2014). The ubiquitin-proteasome system in neurodegenerative diseases: precipitating factor, yet part of the solution. *Front. Mol. Neurosci.* 7:70. doi: 10.3389/fnmol.2014.00070

Dorion, M. F., Mulumba, M., Kasai, S., Itoh, K., Lubell, W. D., and Ong, H. (2021). The CD36 Ligand-Promoted Autophagy Protects Retinal Pigment Epithelial Cells from Oxidative Stress. *Oxid. Med. Cell. Longev.* 2021:6691402. doi: 10.1155/2021/6691402

Duran, A., Amanchy, R., Linares, J. F., Joshi, J., Abu-Baker, S., Porollo, A., et al. (2011). p62 is a key regulator of nutrient sensing in the mTORC1 pathway. *Mol. Cell.* 44, 134–146. doi: 10.1016/j.molcel.2011.06.038

Fernandez-Godino, R., Garland, D. L., and Pierce, E. A. (2016). Isolation, culture and characterization of primary mouse RPE cells. *Nat. Protoc.* 11, 1206–1218. doi: 10.1038/nprot.2016.065

Gamerdinger, M., Hajieva, P., Kaya, A. M., Wolfrum, U., Hartl, F. U., and Behl, C. (2009). Protein quality control during aging involves recruitment of the macroautophagy pathway by BAG3. *EMBO J.* 28, 889–901. doi: 10.1038/emboj.2009.29

Ge, D., Dauchy, R. T., Liu, S., Zhang, Q., Mao, L., Dauchy, E. M., et al. (2013). Insulin and IGF1 enhance IL-17-induced chemokine expression through a GSK3B-dependent mechanism: a new target for melatonin's anti-inflammatory action. *J. Pineal. Res.* 55, 377–387. doi: 10.1111/jpi.12084

Giaime, E., Tong, Y., Wagner, L. K., Yuan, Y., Huang, G., and Shen, J. (2017). Age-Dependent Dopaminergic Neurodegeneration and Impairment of the Autophagy-Lysosomal Pathway in LRRK-Deficient Mice. *Neuron* 96:796–807.e6. doi: 10.1016/j.neuron.2017.09.036

Gossing, W., Radke, L., Biering, H., Diederich, S., Mai, K., and Frohme, M. (2021). The ElonginB/C-Cullin5-SOCS-Box-Complex Is a Potential Biomarker for Growth Hormone Disorders. *Biomedicines* 9:201. doi: 10.3390/biomedicines9020201

Hansen, M., Rubinsztein, D. C., and Walker, D. W. (2018). Publisher Correction: autophagy as a promoter of longevity: insights from model organisms. *Nat. Rev. Mol. Cell. Biol.* 19:611. doi: 10.1038/s41580-018-0048-4

Hariharan, N., Zhai, P., and Sadoshima, J. (2011). Oxidative stress stimulates autophagic flux during ischemia/reperfusion. *Antioxid. Redox. Signal.* 14, 2179–2190. doi: 10.1089/ars.2010.3488

Hollyfield, J. G., Salomon, R. G., and Crabb, J. W. (2003). Proteomic approaches to understanding age-related macular degeneration. *Adv. Exp. Med. Biol.* 533, 83–89. doi: 10.1007/978-1-4615-0067-4_11

Inoki, K., Ouyang, H., Zhu, T., Lindvall, C., Wang, Y., Zhang, X., et al. (2006). TSC2 integrates Wnt and energy signals *via* a coordinated phosphorylation by AMPK and GSK3 to regulate cell growth. *Cell* 126, 955–968. doi: 10.1016/j.cell.2006.06.055

Kim, J. Y., Zhao, H., Martinez, J., Doggett, T. A., Kolesnikov, A. V., Tang, P. H., et al. (2013). Noncanonical autophagy promotes the visual cycle. *Cell* 154, 365–376. doi: 10.1016/j.cell.2013.06.012

Kim, P. K., Hailey, D. W., Mullen, R. T., and Lippincott-Schwartz, J. (2008). Ubiquitin signals autophagic degradation of cytosolic proteins and peroxisomes. *Proc. Natl. Acad. Sci. U. S. A.* 105, 20567–20574. doi: 10.1073/pnas.0810611105

Kim, Y. C., and Guan, K. L. (2015). mTOR: a pharmacologic target for autophagy regulation. *J. Clin. Invest.* 125, 25–32.

Kirkin, V., Lamark, T., Sou, Y. S., Bjorkoy, G., Nunn, J. L., Bruun, J. A., et al. (2009). A role for NBR1 in autophagosomal degradation of ubiquitinated substrates. *Mol. Cell.* 33, 505–516.

Kung, W. W., Ramachandran, S., Makukhin, N., Bruno, E., and Ciulli, A. (2019). Structural insights into substrate recognition by the SOCS2 E3 ubiquitin ligase. *Nat. Commun.* 10:2534. doi: 10.1038/s41467-019-10190-4

Li, H., Chen, D., Sun, W., Chen, J., Luo, C., Xu, H., et al. (2021). KATP Opener Attenuates Diabetic-Induced Muller Gliosis and Inflammation by Modulating Kir6.1 in Microglia. *Invest. Ophthalmol. Vis. Sci.* 62:3. doi: 10.1167/iovs.62.2.3

Li, Z., Zhang, Y., Ding, N., Zhao, Y., Ye, Z., Shen, L., et al. (2019). Inhibition of lncRNA XIST Improves Myocardial I/R Injury by Targeting miR-133a through Inhibition of Autophagy and Regulation of SOCS2. *Mol. Ther. Nucleic Acids* 18, 764–773. doi: 10.1016/j.omtn.2019.10.004

Lu, K., Psakhye, I., and Jentsch, S. (2014). Autophagic clearance of polyQ proteins mediated by ubiquitin-Atg8 adaptors of the conserved CUET protein family. *Cell* 158, 549–563. doi: 10.1016/j.cell.2014.05.048

Madeo, F., Bauer, M. A., Carmona-Gutierrez, D., and Kroemer, G. (2019). Spermidine: a physiological autophagy inducer acting as an anti-aging vitamin in humans? *Autophagy* 15, 165–168. doi: 10.1080/15548627.2018.1530929

Mitchell, P., Liew, G., Gopinath, B., and Wong, T. Y. (2018). Age-related macular degeneration. *Lancet* 392, 1147–1159. doi: 10.1016/S0140-6736(18)31550-2

Nakamura, S., Oba, M., Suzuki, M., Takahashi, A., Yamamuro, T., Fujiwara, M., et al. (2019). Suppression of autophagic activity by Rubicon is a signature of aging. *Nat. Commun.* 10, 847. doi: 10.1038/s41467-019-08729-6

Niu, S., Yuan, D., Jiang, X., and Che, Y. (2014). 11'-Deoxyverticillin A (C42) promotes autophagy through K-Ras/GSK3 signaling pathway in HCT116 cells. *Protein Cell.* 5, 945–949. doi: 10.1007/s13238-014-0099-z

Ohno-Matsui, K. (2011). Parallel findings in age-related macular degeneration and Alzheimer's disease. *Prog. Retin. Eye Res.* 30, 217–238.

Pankiv, S., Clausen, T. H., Lamark, T., Brech, A., Bruun, J. A., Outzen, H., et al. (2007). p62/SQSTM1 binds directly to Atg8/LC3 to facilitate degradation of ubiquitinated protein aggregates by autophagy. *J. Biol. Chem.* 282, 24131–24145. doi: 10.1074/jbc.M702824200

Parzych, K. R., and Klionsky, D. J. (2014). An overview of autophagy: morphology, mechanism, and regulation. *Antioxid. Redox. Signal.* 20, 460–473. doi: 10.1089/ars.2013.5371

Paul, I., Batth, T. S., Iglesias-Gato, D., Al-Araimi, A., Al-Haddabi, I., Alkharusi, A., et al. (2017). The ubiquitin ligase Cullin5(SOCS2) regulates NDR1/STK38 stability and NF-kappaB transactivation. *Sci. Rep.* 7:42800. doi: 10.1038/srep42800

Qiu, Y., Zheng, Y., Wu, K. P., and Schulman, B. A. (2017). Insights into links between autophagy and the ubiquitin system from the structure of LC3B bound to the LIR motif from the E3 ligase NEDD4. *Protein Sci.* 26, 1674–1680. doi: 10.1002/pro.3186

Ranieri, R., Ciaglia, E., Amodio, G., Picardi, P., Proto, M. C., Gazzerro, P., et al. (2018). N6-isopentenyladenosine dual targeting of AMPK and Rab7 prenylation inhibits melanoma growth through the impairment of autophagic flux. *Cell Death Differ.* 25, 353–367. doi: 10.1038/cdd.2017.165

Ravikumar, B., Duden, R., and Rubinsztein, D. C. (2002). Aggregate-prone proteins with polyglutamine and polyalanine expansions are degraded by autophagy. *Hum. Mol. Genet.* 11, 1107–1117. doi: 10.1093/hmg/11.9.1107

Rippin, I., and Eldar-Finkelman, H. (2021). Mechanisms and Therapeutic Implications of GSK-3 in Treating Neurodegeneration. *Cells* 10:262. doi: 10.3390/cells10020262

Rogov, V., Dotsch, V., Johansen, T., and Kirkin, V. (2014). Interactions between autophagy receptors and ubiquitin-like proteins form the molecular basis for selective autophagy. *Mol. Cell.* 53, 167–178. doi: 10.1016/j.molcel.2013.12.014

Ross, B. X., Jia, L., Kong, D., Wang, T., Hager, H. M., Abcouwer, S. F., et al. (2021). Conditional Knock out of High-Mobility Group Box 1 (HMGB1) in Rods Reduces Autophagy Activation after Retinal Detachment. *Cells* 10:2010. doi: 10.3390/cells10082010

Ryu, H. Y., Kim, L. E., Jeong, H., Yeo, B. K., Lee, J. W., Nam, H., et al. (2021). GSK3B induces autophagy by phosphorylating ULK1. *Exp. Mol. Med.* 53, 369–383. doi: 10.1038/s12276-021-00570-6

Sarajlic, M., Neuper, T., Fohrenbach Quiroz, K. T., Michelini, S., Vetter, J., Schaller, S., et al. (2019). IL-1beta Induces SOCS2 Expression in Human Dendritic Cells. *Int. J. Mol. Sci.* 20:5931. doi: 10.3390/ijms20235931

Saxton, R. A., and Sabatini, D. M. (2017). mTOR Signaling in Growth, Metabolism, and Disease. *Cell* 169, 361–371. doi: 10.1016/j.cell.2017.03.035

Shen, Y., Li, M., Liu, K., Xu, X., Zhu, S., Wang, N., et al. (2020). Integrated bioinformatics analysis of aberrantly-methylated differentially-expressed genes and pathways in age-related macular degeneration. *BMC Ophthalmol.* 20:119. doi: 10.1186/s12886-020-01392-2

Song, H., Liu, B., Huai, W., Yu, Z., Wang, W., Zhao, J., et al. (2016). The E3 ubiquitin ligase TRIM31 attenuates NLRP3 inflammasome activation by promoting proteasomal degradation of NLRP3. *Nat. Commun.* 7:13727. doi: 10.1038/ncomms13727

Sophia, J., Kowshik, J., Dwivedi, A., Bhutia, S. K., Manavathi, B., Mishra, R., et al. (2018). Nimbolide, a neem limonoid inhibits cytoprotective autophagy to activate apoptosis *via* modulation of the PI3K/Akt/GSK-3beta signalling pathway in oral cancer. *Cell Death Dis.* 9:1087. doi: 10.1038/s41419-018-1126-4

Sun, A., Wei, J., Childress, C., Shaw, J. H. T., Peng, K., Shao, G., et al. (2017). The E3 ubiquitin ligase NEDD4 is an LC3-interactive protein and regulates autophagy. *Autophagy* 13, 522–537. doi: 10.1080/15548627.2016.1268301

Thurston, T. L., Ryzhakov, G., Bloor, S., Von Muhlinen, N., and Randow, F. (2009). The TBK1 adaptor and autophagy receptor NDP52 restricts the proliferation of ubiquitin-coated bacteria. *Nat. Immunol.* 10, 1215–1221. doi: 10.1038/ni.1800

Turnley, A. M. (2005). Role of SOCS2 in growth hormone actions. *Trends Endocrinol. Metab.* 16, 53–58. doi: 10.1016/j.tem.2005.01.006

Vesterlund, M., Zadjali, F., Persson, T., Nielsen, M. L., Kessler, B. M., Norstedt, G., et al. (2011). The SOCS2 ubiquitin ligase complex regulates growth hormone receptor levels. *PLoS One* 6:e25358. doi: 10.1371/journal.pone.0025358

Wang, L., Clark, M. E., Crossman, D. K., Kojima, K., Messinger, J. D., Mobley, J. A., et al. (2010). Abundant lipid and protein components of drusen. *PLoS One* 5:e10329. doi: 10.1371/journal.pone.0010329

Wang, S., Li, B., Qiao, H., Lv, X., Liang, Q., Shi, Z., et al. (2014). Autophagy-related gene Atg5 is essential for astrocyte differentiation in the developing mouse cortex. *EMBO Rep.* 15, 1053–1061. doi: 10.15252/embr.201338343

Wei, Z., Koya, J., and Reznik, S. E. (2021). Insulin Resistance Exacerbates Alzheimer Disease *via* Multiple Mechanisms. *Front. Neurosci.* 15:687157. doi: 10.3389/fnins.2021.687157

Xu, C., Feng, K., Zhao, X., Huang, S., Cheng, Y., Qian, L., et al. (2014). Regulation of autophagy by E3 ubiquitin ligase RNF216 through BECN1 ubiquitination. *Autophagy* 10, 2239–2250.

Yamano, K., and Youle, R. J. (2020). Two different axes CALCOCO2-RB1CC1 and OPTN-ATG9A initiate PRKN-mediated mitophagy. *Autophagy* 16, 2105–2107. doi: 10.1080/15548627.2020.1815457

Zaffagnini, G., Savova, A., Danieli, A., Romanov, J., Tremel, S., Ebner, M., et al. (2018). Phasing out the bad-How SQSTM1/p62 sequesters ubiquitinated proteins for degradation by autophagy. *Autophagy* 14, 1280–1282. doi: 10.1080/15548627.2018.1462079

Zhai, P., Sciarretta, S., Galeotti, J., Volpe, M., and Sadoshima, J. (2011). Differential roles of GSK-3beta during myocardial ischemia and ischemia/reperfusion. *Circ. Res.* 109, 502–511. doi: 10.1161/circresaha.111.249532

Zhan, J., He, J., Zhou, Y., Wu, M., Liu, Y., Shang, F., et al. (2016). Crosstalk Between the Autophagy-Lysosome Pathway and the Ubiquitin-Proteasome Pathway in Retinal Pigment Epithelial Cells. *Curr. Mol. Med.* 16, 487–495. doi: 10.2174/1566524016666160429121606

Zhao, X., Liu, L., Jiang, Y., Silva, M., Zhen, X., and Zheng, W. (2020). Protective Effect of Metformin against Hydrogen Peroxide-Induced Oxidative Damage in Human Retinal Pigment Epithelial (RPE) Cells by Enhancing Autophagy through Activation of AMPK Pathway. *Oxid. Med. Cell. Longev.* 2020:2524174. doi: 10.1155/2020/2524174

Conflict of Interest: The authors declare that the research was conducted in the absence of any commercial or financial relationships that could be construed as a potential conflict of interest.

Publisher's Note: All claims expressed in this article are solely those of the authors and do not necessarily represent those of their affiliated organizations, or those of the publisher, the editors and the reviewers. Any product that may be evaluated in this article, or claim that may be made by its manufacturer, is not guaranteed or endorsed by the publisher.

frontiers in Neuroscience

REVIEW
published: 03 February 2022
doi: 10.3389/fnins.2021.794809

Effects of Excess Iron on the Retina: Insights From Clinical Cases and Animal Models of Iron Disorders

*Ali Shahandeh[1], Bang V. Bui[1], David I. Finkelstein[2] and Christine T. O. Nguyen[1]**

[1] Department of Optometry and Vision Sciences, Faculty of Medicine, Dentistry and Health Sciences, University of Melbourne, Parkville, VIC, Australia, [2] Florey Department of Neuroscience and Mental Health, University of Melbourne, Parkville, VIC, Australia

Iron plays an important role in a wide range of metabolic pathways that are important for neuronal health. Excessive levels of iron, however, can promote toxicity and cell death. An example of an iron overload disorder is hemochromatosis (HH) which is a genetic disorder of iron metabolism in which the body's ability to regulate iron absorption is altered, resulting in iron build-up and injury in several organs. The retina was traditionally assumed to be protected from high levels of systemic iron overload by the blood-retina barrier. However, recent data shows that expression of genes that are associated with HH can disrupt retinal iron metabolism. Thus, the effects of iron overload on the retina have become an area of research interest, as excessively high levels of iron are implicated in several retinal disorders, most notably age–related macular degeneration. This review is an effort to highlight risk factors for excessive levels of systemic iron build-up in the retina and its potential impact on the eye health. Information is integrated across clinical and preclinical animal studies to provide insights into the effects of systemic iron loading on the retina.

Keywords: retina, iron, hemochromatosis, iron overload, retinal disorder

OPEN ACCESS

Edited by:
Ellen Tianwei Zhou,
University of Toronto, Canada

Reviewed by:
Joshua Dunaief,
University of Pennsylvania, United States
Michael L. H. Huang,
The University of Sydney, Australia

***Correspondence:**
Christine T. O. Nguyen
christine.nguyen@unimelb.edu.au

Specialty section:
This article was submitted to Neurodegeneration, a section of the journal Frontiers in Neuroscience

Received: *14 October 2021*
Accepted: *17 December 2021*
Published: *03 February 2022*

Citation:
Shahandeh A, Bui BV, Finkelstein DI and Nguyen CTO (2022) Effects of Excess Iron on the Retina: Insights From Clinical Cases and Animal Models of Iron Disorders. Front. Neurosci. 15:794809. doi: 10.3389/fnins.2021.794809

INTRODUCTION

Iron is essential for neuronal development and function (Lozoff et al., 2003). Iron plays key roles in neuronal metabolism, oxygen transport, oxidative phosphorylation, myelin production, and the synthesis of neurotransmitters, as reviewed in detail elsewhere (Crichton et al., 2011; Ward et al., 2014). However, abnormally high levels of intracellular iron, termed iron loading, can be neurotoxic and may lead to cellular injury. The exact mechanism of iron-induced neuronal degeneration is not yet fully understood; however, several mechanisms have been postulated. Perhaps, most well studied mechanism is the role of iron in mediating the formation of reactive oxygen species (ROS), a natural byproduct of Fenton reactions, which can contribute to tissue injury (Lloyd et al., 1997). In addition, high intracellular iron levels can affect the expression of several classes of genes including iron-dependent oxidative metabolism and the attendant oxidative stress genes (Casey et al., 1988; Ingrassia et al., 2019). Another suggested pathway through which errors in iron metabolism can be deleterious is ferroptosis, a recently identified form of cell death, which has been implicated in a number of central nervous system (CNS) diseases (Dixon et al., 2012; Guiney et al., 2017; Lane et al., 2018; Moreau et al., 2018; Masaldan et al., 2019).

To avoid the potential of iron toxicity, living organisms have developed homeostatic mechanisms, that regulate various proteins involved in iron import, storage, and export to maintain iron within a favorable physiological range. Most iron is tightly complexed with proteins or

other ligands, which restrict its redox potential. However, excess iron can build-up in the body in several ways including early life exposure to iron feeding (Hare et al., 2015); normal aging (Zecca et al., 2004), eating meat (heme-iron intake) (Haider et al., 2018), and acute toxicity from blood transfusions (Harmatz et al., 2000; Cunningham et al., 2004). In contrast low iron vegan and vegetarian diets have lower accumulation of iron and increased risk of iron deficiency with associated fatigue and impaired learning and concentration symptoms (Desmond et al., 2021). The retinal photoreceptors are the most highly energetically demanding tissue per weight in the whole body (Wong-Riley, 2010; Country, 2017), and photoreceptors are mitochondria-rich cells. The primary function of mitochondria is to generate energy in the form of adenosine triphosphate (ATP). Due to a lack of protective histones and proximity to the inner mitochondrial membrane, where oxidants are formed, mitochondrial DNA is vulnerable to oxidative damage (Gao et al., 2009; Lin et al., 2011). Iron-mediated damage to mitochondria is believed to be through various pathways including altered mitochondrial uptake of other metal ions (Jouihan et al., 2008), ferroptosis (Battaglia et al., 2020; Li et al., 2020) and oxidative damage leading to decreased synthesis of respiratory chain subunits encoded by the mitochondrial genome and further declines in cellular respiration. Mitochondrial iron homeostasis is crucial for normal physiology of the retina and any dysregulation in balance of the redox system in mitochondria has been associated with age-related retinal pathophysiology (Jarrett et al., 2008; Barot et al., 2011).

However, unlike the brain where iron-related pathology has received significant attention (Wessling-Resnick, 2017; Daglas and Adlard, 2018; D'Mello and Kindy, 2020), less is known about retinal susceptibility to iron loading. An improved understanding of iron's role in retinal health and disease conditions will guide the development of therapies for patients with hemochromatosis and possibly other iron overload conditions. We mainly focus on retinal structural and functional changes in clinical cases and preclinical models. This is particularly important because currently there is no routine clinical visual check–up for high-risk demographic such as patients with hemochromatosis or even people with high levels of dietary iron intake which may have been at risk of retinal iron accumulation and disease-related sequelae. Improving prognosis in people at risk, as some changes may be more easily attenuated or reversed than others are critical and subsequently treatments could be commenced before irreversible damage to the tissue occurs.

HEMOCHROMATOSIS

Iron build-up in the human body can arise as a result of genetic anomalies, one such example is hemochromatosis (HH) (Feder et al., 1996; Pietrangelo, 2003). HH is an autosomal recessive disorder characterized by increased iron absorption (Andrews, 1999), leading to excessive tissue iron deposition. A number of gene mutations have been found to underlie this phenotype as summarized in **Table 1**.

TABLE 1 | Summary of hemochromatosis phenotypes with their corresponding genes and clinical manifestations[a].

Types		Main clinical manifestations	Inheritance
Type 1	*HFE**	Late onset, >30 years old, mild to severe hepatomegaly, elevated aminotransferase levels, arthralgia, arthritis	Recessive
Type 2	Hemojuvelin *(HJV)*/ Hepcidin *(HAMP)*	Early onset, <30 years old, severe cardiomyopathy, arrhythmia, diabetes, hypogonadism	Recessive
Type 3	*TFR2*	Late onset, >30 years old, mild to severe hepatomegaly, elevated aminotransferase levels	Recessive
Type 4	Ferroportin (*SLC40A1*)	Late onset, >40 years old, mild hepatomegaly, elevated aminotransferase levels, arthralgia, arthritis	Dominant

[a]*Pietrangelo, 2004; Brissot and de Bels, 2006; Andrews, 2008; Fix and Kowdley, 2008; Powell et al., 2016.*

**Variation in this gene including C282Y, H63D, and S65C are associated with increasing risk of neurodegenerative disorders particularly Parkinson's disease.*

There are four main types of HH which have been identified based on their underlying genetic mutations. Type 1 forms the majority of HH cases and is attributed to homozygosity for a single nucleotide polymorphism (SNP) in the *HFE* gene located on chromosome 6p. This genetic variation causes the substitution of a cysteine with a tyrosine residue at amino acid 282 (C282Y) (Feder et al., 1996). The C282Y SNP has a carrier frequency of 10–20%, with 0.3–0.7% homozygosity in populations of northern European ancestry (Beutler et al., 2002; Allen, 2008). In non-Caucasian populations, however, this SNP is reported to have a low allele frequency (Merryweather-Clarke et al., 1997; Cullen et al., 1998).

Another allelic variant of the *HFE* gene involving the substitution of an aspartic acid with a histidine (H63D), has an even higher allele frequency that C282Y (Gochee et al., 2002; Adams, 2005). However, it generally does not appear to have considerable effects on iron status, even in the homozygous state. Inheritance of a dual polymorphism (H63D and C282Y) as a compound heterozygous genotype, however, can cause clinical hemochromatosis (Beutler et al., 1996; Jouanolle et al., 1997). *HFE* – associated hemochromatosis can also be due to a serine – to – cysteine substitution at amino acid position 65 (S65C) (Mura et al., 1999). This variation in the *HFE* gene is associated with the mild form of hemochromatosis and accounts for 7.8% of HH cases that were neither C282Y nor H63D substitutions (Mura et al., 1999).

Type 2 HH is due to mutations in the hemojuvelin gene (*HJV*) or the gene encoding hepcidin (*HAMP*); accounts for a very severe form of iron loading where iron accumulates rapidly in early postnatal life (Papanikolaou et al., 2004).

Mutations in the *TFR2* gene causes Type 3 HH in which homozygosity for the Y250X nonsense mutation in the *TFR2* gene is reported to be the most common cause (Camaschella et al., 2000). This mutation induces excessive iron loading with a similar phenotype to Type 1 HH, although patients exhibit greater variation in the severity of symptoms (Olynyk et al., 2008). Patients with mutations in both *TFR2* and *HFE* are

reported to have a severe iron loading phenotype (Pietrangelo et al., 2005; Rueda Adel et al., 2011; Del-Castillo-Rueda et al., 2012). The common feature of HH Types 1 to 3 is reduction of hepcidin expression which provides a possible mechanistic insight into build-up of iron in tissues (Brissot et al., 2019; Piperno et al., 2020).

Considering the importance of the hepcidin regulatory pathway in influencing body iron homeostasis, any mutation in the *SLC40A1* gene which encodes ferroportin; the molecular target for hepcidin results in Type 4 HH (Camaschella et al., 2000; Montosi et al., 2001; Callebaut et al., 2014). In this type of HH, mutation in *SLC40A1* gene either restricts the binding of hepcidin to ferroportin (Nemeth et al., 2004) or affects the ability of ferroportin to transport iron (Détivaud et al., 2013).

Most forms of hemochromatosis cause injury in peripheral tissues (heart and liver), however, it should be noted that the principal variants of the *HFE* gene can affect brain iron homeostasis and is considered as a risk factor for neurodegenerative disorders, particularly Parkinson's disease (Dekker et al., 2003; Guerreiro et al., 2006). In addition, hematochromatosis associated genes are expressed in the retina in a cell type specific manner (Gnana-Prakasam et al., 2008), which means retinal iron homeostasis may be disrupted in specific retinal cells by systemic iron loading conditions.

THE MAMMALIAN RETINA

The mammalian retina is an integral part of the CNS; capturing light energy (photons) and transforming it into a chemical signal to be passed onto the brain *via* electrical impulses. The retina has a multi–layered structure (see **Figures 1A,B**) composed of five main neuronal classes and supporting glia. Traditionally, it has been assumed that the retina is protected from systemic iron loading by the blood–retinal barrier, however, increasing evidence suggests that the blood–retinal barrier is unable to shield the retina against morbid levels of serum iron (Zhao et al., 2014). This is potentially problematic for the retina, given it is highly energetically demanding (Wong-Riley, 2010; Country, 2017), making it more likely vulnerable to metabolic and oxidative stress related to iron-loading. The potential for injury from excessive iron loading in the retina has become an area of research interest, particularly in conditions where the integrity of the blood–retina barrier is compromised. Indeed, studies have highlighted interactions between aging and iron homeostasis as potential pathological mediators for a number of retinal disorders including age-related macular degeneration (Dunaief, 2006; Biesemeier et al., 2015; Song et al., 2016; Čolak et al., 2018).

IRON METABOLISM AND RETINAL IRON HOMEOSTASIS

Dietary iron is the exclusive source of iron for mammals which consists of heme iron (e.g., meat or offal products) and non-heme iron (e.g., legumes, nuts, and seeds) sources (Bjorn-Rasmussen et al., 1974). Iron cannot be actively excreted through normal pathways such as the intestine or kidney and only small levels of iron can be discarded through sloughing of mucosal cells and desquamation, menstruation and other blood loss (Andrews, 1999; Miret et al., 2003; Kohgo et al., 2008). One of the earliest experiments to show a lack of execratory routs for iron was conducted by Widdowson and McCance (1937). The author orally administrated 1000 mg of ferric ammonium citrate per day to four volunteers over 36–46 days, and found that urinary and fecal output contained only trace amounts of unabsorbed iron (Widdowson and McCance, 1937). This work contributed to the current understanding that iron metabolism is a semi-closed system, with low levels of excretion (Kohgo et al., 2008). This closed system means that non-biodegradable iron can build-up in tissues over time, as reviewed elsewhere (Hahn et al., 2006, 2009; Hare et al., 2015, 2017; Shu and Dunaief, 2018). As iron is rare in our environment the body has adopted to store iron. In an iron replete modern diet, the abundance of iron is potentially contributing to health issues. Therefore, age-related accumulation of iron and its adverse effects may be a contributor to increased risk of neurodegeneration with age.

Dietary iron is chiefly absorbed in the upper part of the intestine through the apical side of the enterocyte brush border (Fuqua et al., 2012). After absorption across the gut, iron forms a complex, most notably with the iron carrier protein transferrin (TF), which chaperones iron in the circulation (Andrews, 1999; Meynard et al., 2014). A transferrin molecule can bind two molecules of ferric (Fe^{3+}) iron and is thought to be the main source of iron delivery to neurons in the CNS (Chua et al., 2007).

The specific locations of iron handling proteins in the retina as summarized in **Table 2** may provide clues as to functions that may be impacted by anomalies in iron metabolism and dysregulation. In the retina, transferrin is found in RPE cells, but it is also detectable in the neural retina including photoreceptor inner and outer segments, suggesting that iron is trafficked in the retina itself. Iron uptake from the choroidal circulation into the RPE cells is mediated by transferrin receptors 1 (TFR1), which has been found on basolateral and apical surfaces of RPE cells, suggesting that there is bi-directional iron movement across the RPE cells depending on the iron status of the retina (Yefimova et al., 2000; He et al., 2007). TFR1 has also been colocalized to the ganglion cell layer, inner nuclear layer, outer plexiform layer, and inner segment of photoreceptors (Yefimova et al., 2000; He et al., 2007).

Although TFR1 is the predominant protein responsible for cellular iron uptake, another homologous protein called transferrin receptors 2 (TFR2) also has a cooperative role in mediating retinal cellular iron uptake (Kawabata et al., 1999). The expression of TFR2 appears to be primarily in the RPE (Martin et al., 2006). TFR2 also serves as part of a feedback mechanism *via* its role as a membrane protein for serum iron levels. TFR2 is postulated to activate a downstream signaling pathway that leads to increase the iron-regulatory protein hepcidin. Increased levels of hepcidin, tightly influences intestinal iron absorption and macrophage iron recycling, helping to lower serum iron (Goswami and Andrews, 2006; Schmidt et al., 2008).

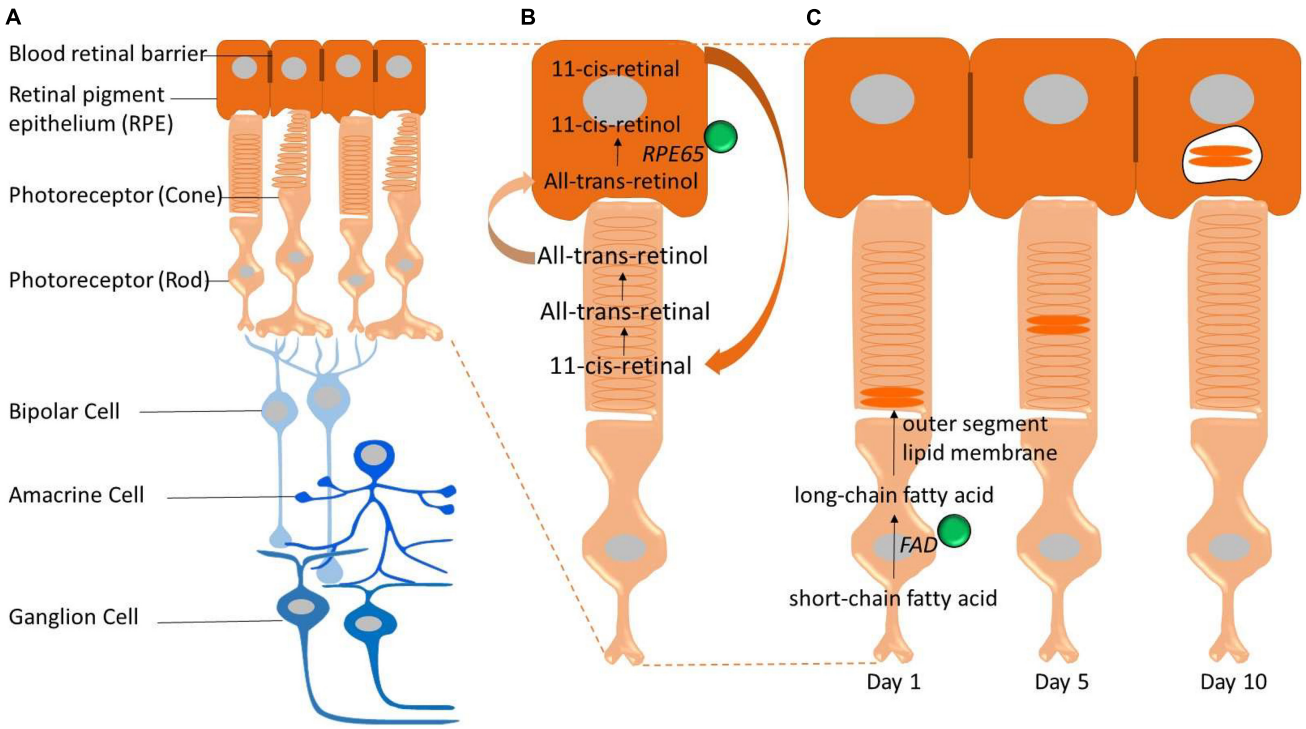

FIGURE 1 | Schematic representation of the retina and key pathways that involve iron (iron represented by green spheres). **(A)** The neural retina is isolated from the bloodstream (choroidal vessels) by the blood–retinal barrier. The outer blood–retinal–barrier is formed by tight junctions located between the retinal pigment epithelium (RPE). Photoreceptors convert light into electrical signals through the visual cycle and these electrical signals are communicated through the retina *via* the bipolar and ganglion cells. **(B)** Iron is required for the visual cycle. Regeneration of 11-cis-retinal, the chromophore of visual pigments in photoreceptor cells, is essential for vision and depends on an earlier reaction catalyzed by the iron-containing isomerase, retinal pigment epithelium-specific 65 kDa protein (RPE65). **(C)** Photoreceptor outer segments (rods and cones) are constantly synthesized and shed. This process is highly dependent on fatty acid desaturase (FAD) enzyme which is iron dependent to synthesize new membrane lipids.

TABLE 2 | Summary of the major iron-related proteins found in the retina.

	Protein	Function	Expression in retina
Iron import	Transferrin receptor 1 (TFR1)	Iron uptake	Ganglion cell layer, inner nuclear layer, outer plexiform layer, photoreceptor inner segment, RPE basolateral membrane, and choroid (Yefimova et al., 2000)
	Transferrin receptor 2 (TFR2)	Iron uptake	RPE (basolateral membrane) (Martin et al., 2006)
	Divalent metal transporter-1 (DMT-1)	Iron uptake	Rod bipolar cell bodies and axon termini, horizontal cell bodies, and photoreceptor inner segments (He et al., 2007)
Iron export	Ferroportin (SLC40A1)	Iron export	RPE, photoreceptor inner segments, inner and outer plexiform layers, and ganglion cell layer (Hahn et al., 2004a)
Iron storage	Ferritin (Ft)	Storage; anti-oxidant activity in association with p53 (Lee et al., 2009); regulator of angiogenesis (Coffman et al., 2009); receptor for hepcidin (Nemeth et al., 2004)	Photoreceptor inner segments, RPE, choroid, inner nuclear layer, and ganglion cell layer (He et al., 2007)
Iron regulatory	Hepcidin (HAMP)	Internalization of iron in association with ferroportin	Müller cells, photoreceptor cells, and RPE (Gnana-Prakasam et al., 2008; Hadziahmetovic et al., 2011a)
	Ceruloplasmin (CP)	Catalyzing the oxidization of Fe^{2+} to Fe^{3+} (ferroxidase)	Müller glia and RPE(Chen et al., 2003; Hahn et al., 2004b)
	Hephaestin (HEPH)	Catalyzing the oxidization of Fe^{2+} to Fe^{3+} (ferroxidase)	Müller glia and RPE (Hahn et al., 2004b)
	HFE	HFE in association with TFR2 regulates hepcidin (Wallace et al., 2009)	Restricted exclusively to basolateral membrane of RPE (Martin et al., 2006)
	Hemojuvelin (HJV)	Induces the expression of hepcidin (Babitt et al., 2006)	RPE (apical membrane facing neural retina), Müller glia, photoreceptors, and ganglion cells (Gnana-Prakasam et al., 2009b)

In addition, there is a non-transferrin-bound iron protein called divalent metal transporter-1 (DMT-1), which can contribute to transportation of ferrous iron across the plasma membrane or in some cases out of endosomal compartments (Gunshin et al., 1997). DMT-1 has been colocalized to rod bipolar cell bodies and axon termini, horizontal cell bodies and photoreceptor inner segments (He et al., 2007; Song and Dunaief, 2013).

Once iron is taken up into cells, it is primarily stored in ferritin, a large hollow symmetrical protein which is able to sequester around 4500 atoms of iron (Harrison and Arosio, 1996; Koorts and Viljoen, 2007; Arosio et al., 2009). In addition to the choroid and RPE, within the neural retina the regions with highest levels of iron and ferritin are found in the inner segment of photoreceptors, inner nuclear layer and the ganglion layer (Yefimova et al., 2000; He et al., 2007).

Iron efflux is regulated through a transmembrane protein called ferroportin. It is also known as an iron-regulated transporter 1 or solute carrier family 40 member 1 which exports iron from cells in the form of ferrous (Fe^{2+}) iron. Since ferrous iron must be oxidized to its ferric state to be regulated by systemic transferrin, ferroportin functions in conjunction with two extracellular multicopper ferroxidases, ceruloplasmin and hephaestin (Harris et al., 1999; Vulpe et al., 1999; Jeong and David, 2003; Ayton et al., 2013; McCarthy and Kosman, 2013). Ferroportin is found on most cells including retinal neurons and glia (Abboud and Haile, 2000; Donovan et al., 2000, 2005; Jeong and David, 2003; Hahn et al., 2004a). Ferroxidase enzymes including ceruloplasmin and hephaestin are also present in the retina, specifically in Müller glia and retinal pigment epithelial cells (Chen et al., 2003; Hahn et al., 2004b).

Another iron-regulatory protein which plays a crucial role in the maintenance of retinal iron homeostasis is hepcidin (Nicolas et al., 2001; Pigeon et al., 2001). Hepcidin is the main peptide hormone that regulates systemic iron. Hepcidin is primarily expressed by the liver and secreted into the bloodstream, and expression of hepcidin in retinal Müller cells, photoreceptor cells and RPE cells has been reported (Gnana-Prakasam et al., 2008; Hadziahmetovic et al., 2011a). Hepcidin regulates iron homeostasis by binding and antagonizing the only known mammalian iron exporter, ferroportin, leading to reduced cellular iron export thus limiting the amount of iron found in serum or extracellular fluid (Nemeth et al., 2004). Hepcidin also plays an important role in inhibiting the intestinal iron absorption (Ganz, 2005). Finally, hepcidin promotes sequestration of iron by macrophages which further reduce serum iron levels (Abreu et al., 2018).

ROLE OF IRON IN RETINAL PHYSIOLOGY

Iron is one of the most abundant metals in the retina (Ugarte et al., 2012), critical for retinal function *via* its role as an integral component of key retinal enzymes (Lohmann, 1964; Yau and Baylor, 1989; Yefimova et al., 2000; Moiseyev et al., 2006; Chen et al., 2009). The characterization of retinal iron content through histochemical approaches showed a heterogeneous distribution, with iron largely found at the choroid, RPE and the photoreceptors layer (Yefimova et al., 2000; Song and Dunaief, 2013). Similarly, iron colocalization at the RPE, choroid and to a lesser degree at the neural retain was confirmed using laser ablation-inductively coupled plasma-mass spectrometry (LA-ICP-MS) which is a sensitive technique that offers a fast and precise spatially resolved measurement of elements *in situ* at trace and ultra-trace levels (Pamphlett et al., 2020).

In the context of visual function, iron serves as a cofactor for the RPE-specific 65 kDa protein (RPE65), an enzyme required for the retinoid metabolic pathway, which is critical for the maintenance of light capturing chromophore levels in photoreceptors and thus phototransduction and visual adaption (Redmond et al., 2005; Moiseyev et al., 2006). The isomerohydrolase activity of RPE65 relies on the presence of metal ions (see **Figure 1B**). Iron is central to this process, as evidenced by findings that mutations in RPE65 iron coordinating result in a range of retinal dystrophies including Leber congenital amaurosis and some forms of retinitis pigmentosa (Thompson et al., 2000; Simovich et al., 2001; Redmond et al., 2005; Bereta et al., 2008).

In addition, iron is an essential cofactor of fatty acid desaturases enzymes which play an important role in photoreceptor outer segment disc biogenesis (**Figure 1C**; Shichi, 1969; Song and Dunaief, 2013); whereby old photoreceptor discs containing phototransduction proteins are completely replaced by new ones over the course of about 10 days (Young, 1967; Young and Bok, 1969; Chuang et al., 2007). In addition to the above retina specific role for iron, like the CNS, the retina expresses several iron-dependent enzymes including tyrosine hydroxylase (Ramsey et al., 1996), phenylalanine hydroxylase (Gottschall et al., 1982), and tryptophan hydroxylase (Kuhn et al., 1980) that are involved in the biosynthesis and regulation of neurotransmitters such as dopamine, serotonin, and melatonin (Kaushik et al., 2007). Therefore it is not surprising that the retina expresses a wide array of enzymes that utilize iron as a cofactor, including those involved in energy production; mitochondrial ferredoxins, Redfearn and King (1964) cytochromes (Slater, 1949), and aconitase (Dickman and Cloutier, 1950).

RETINAL CHANGES IN HEMOCHROMATOSIS

One way to consider the importance of iron to the retina and visual function is to examine what happens in those people who have an iron loading disorder. However, assessment of retinal changes in hemochromatosis patients remain limited. One of the earliest reports on the ocular manifestations of high levels of retinal iron loading in hemochromatosis patients was described by Maddox (1933). The author reported that there was normal visual acuity without overt retinal pathology in four cases (Maddox, 1933). Almost 40 years after Maddox,

further reports in those with hemochromatosis showed iron accumulation in the peripapillary (around the optic nerve) retinal pigment epithelium, ciliary epithelium (where aqueous humor is produced), corneal epithelium, and sclera (Davies et al., 1972; Roth and Foos, 1972). Drusen-like deposits, which are the prominent clinical feature of age-related macular degeneration, were also detected in these patients (Roth and Foos, 1972). In a more recent study, Menghini et al. (2018) examined 49 patients (∼15 years after diagnosis, average age at examination 60 years) with hemochromatosis and examined the retina *in vivo* using spectral domain optical coherence tomography, as well as short wavelength autofluorescence and color fundus images. Their results showed no retinal changes such as drusen, RPE alterations, or increased lipofuscin in any of the images.

In contrast, other case studies that examine histopathology and retinal function *via* electroretinography have indicated the possibility of retinal changes with hemochromatosis. Retinal abnormalities have been reported in a 49-year-old hemochromatosis patient with homozygosity for the C282Y polymorphism in the *HFE* gene. The patient was characterized by progressive loss of visual function assessed by full – field electroretinography (ERG) and abnormal RPE changes using retinal imaging (Zerbib et al., 2015). Electroretinographic examination at the initial visit revealed a 50% reduction in the rod response and no change in the cone response. Follow-up examinations 6-month later suggested that in addition to a diminished rod response there was a progression of cone dysfunction, with a 50% reduction in the cone response (Zerbib et al., 2015).

Recently, another case of ocular involvement in hereditary hemochromatosis was reported in a 39-year-old patient with a homozygous C282Y mutation in *HFE* gene, without any other mutations associated with inherited retinal dystrophies. The patient reported bilateral progressive blurry vision and recent onset photopsia and headaches. Electroretinograms demonstrated generalized rod and cone dysfunction with some central preservation of waveforms. There appeared to be no retinopathy progression at 6 month follow-up, after the patient had undergone treatment to normalize his iron levels (Bellsmith et al., 2020).

There remain limited studies exploring the relationship between the systemic iron loading disorders and retinal changes. The heterogeneity in findings between the few case reports and Menghini et al.'s (2018) study could derive from the methodologies employed, for example, electroretinography can be a more sensitive measure of temporary retinal dysfunction than optical coherence tomography, which may only detect more significant structural changes associated with longer term retina injury (Ledolter et al., 2015).

ANIMAL MODELS OF IRON DISORDERS OF THE RETINA

To gain further insight, preclinical studies have sought to examine in animal models the impact of systemic iron loading on retinal health. Broadly, three types of animal models have been developed including local administration of exogenous iron (e.g., intravitreal injection), oral delivery of iron (dietary iron supplementation), and genetically modified iron loading models.

It should be noted during the earliest stages of neonatal development when mammals nurse on their mother's milk, the blood–brain barrier is open to iron accumulation (Dwork, 1995; Kaur et al., 2007; Billings et al., 2016). Subsequently the blood–brain barrier becomes fully formed in early life and only then iron is acquired selectively through iron receptors proteins that mediate iron intake.

One of the earliest animal models of local administration of exogenous iron was conducted by Declercq et al. (1977). They examined the consequences of excess iron on retinal function and histopathology in an animal model of siderosis. Ten days after intravitreal injection of a solid iron foreign body into the rabbit eye, they reported reductions in both a- (photoreceptor) and b-wave (ON bipolar cells) amplitudes in conjunction with degeneration of the outer nuclear layer and RPE (Declercq et al., 1977). Subsequently, Doly et al. (1984) showed that intravitreal injection of a solution containing Fe^{2+} ascorbate into the rat's eyes selectively attenuated the b-wave in isolated retinal recordings (Doly et al., 1984). A similar study showed intravitreal injection of ferrous sulfate ($FeSO_4$) into mouse's eyes caused a reduction in the b-wave amplitude (Rogers et al., 2007). These data show that high levels of iron appear to reduce outer and middle retinal function.

The effects of high dietary iron were studied on 2-month-old mice by supplementing mice with 2% iron carbonyl for 3 or 10 months. Compared with a normal diet, dietary iron supplementation changed retinal mRNA levels of iron-responsive genes indicating a modest increase in iron in the RPE. However, even by 18 months of age there was little evidence of increased retinal iron and no retinal degeneration (Bhoiwala et al., 2015). The authors suggested that high levels of dietary iron can only modestly increase the level of iron deposition in the mouse RPE without causing RPE or retinal degeneration, which means the blood–retinal barrier is able to regulate iron levels (Bhoiwala et al., 2015).

The effects of acute systemic iron loading *via* intravenous injection were investigated by Song et al. (2016). Their study involved two cohorts of C57BL/6J male mice including a group of 2 months old mice administrated a weekly dose of 1.2 mg iron-sucrose for a total of 12 injections. These animals were examined at 12 months of age. The second cohort of mice at 10 weeks of age were subjected to two intravenous injections either with iron-sucrose or sucrose alone and euthanized 24 h after the last injection. Their results showed iron accumulated chiefly at the RPE and choroid in chronic exposure. Additionally, histological features similar to AMD such as Bruch's membrane thickening, RPE hypertrophy and vacuolization were noted in these mice. The second acute loading group displayed increased levels of ferritin mRNA and reduction of transferrin receptor mRNA within the RPE (Song et al., 2016).

Consistent with susceptibility of the choroid, RPE and outer retina, Song et al. (2016) reported a clinical case of a 43-year-old anemic patient who developed numerous retinal

drusen, the hallmark of AMD, within 11 months of intravenous iron therapy. The patient who had no prior ocular history had undergone infusion of 300 mg of iron-sucrose saline over 2 h three times a week. As the treatment progressed the patient noted delayed adaptation to low-light levels and difficulty reading at night. The patient's DNA was tested and revealed a high genetic risk for AMD. They concluded that iron therapy may have the potential to induce or exacerbate a form of retinal degeneration that shares features with AMD (Song et al., 2016).

It should be noted that the iron regulatory hormone, hepcidin is expressed in the neurosensory retina and may limit iron influx into the inner retina which would be another mechanism to protect the inner retina against high levels of iron (Baumann et al., 2019). Therefore, Shu et al. (2019) designed a study in which retina-specific hepcidin knockout mice were exposed to high systemic iron levels through daily intraperitoneal injection of 10 mg iron dextran for 5 days each week. Their results showed that while they could identify accumulation of high levels of iron in the RPE and retinal vascular endothelial cells of hepcidin knockout mice, there was no change in iron status of neurosensory retina. They reported no alterations in the retina–blood barrier and no signs of retinal degeneration. They concluded that the retinal–blood barrier can protect neurosensory retina from high doses of exogenously administered iron independent of retinal hepcidin production (Shu et al., 2019).

All of the studies analyzing the effects of acute exogenous iron-loading on retina showing similar patterns of iron distribution with RPE and choroid being the main sites of iron accumulation. However, the pathological effects of iron on retina seemed to be varied amongst these studies. Thus further studies of defective retinal iron homeostasis using both functional and histological outcome measures in genetically modified animal models of chronic iron loading could potentially provide a more comprehensive understanding of iron-induced retinal pathology.

Retinal Abnormalities in Genetically – Modified Animal Models of Systemic Iron Loading

Genetically modified animal models of chronic iron loading have been developed to recapitulate human iron loading diseases. One of the earliest mouse models of systemic iron loading was developed by disruption of a single ferroxidase, either *Cp* or *Heph*. A study has shown that the *Cp* knock-out mice at 18 months old showed increased retinal iron levels and degeneration of the retina (Patel et al., 2002) in alignment with aceruloplasminemia patients who have mutations in Cp (Wolkow et al., 2011). In contrast, other animal studies which selectively delete either *Cp* or *Heph* did not manifest any retinal iron loading or related pathology even at 2 years of age (Hahn et al., 2004b), suggesting that one ferroxidase can compensate for the functional loss of the other (Jiang et al., 2016). However, simultaneous disruption of *Cp* and *Heph* in double knockout mice led to substantial retinal iron build-up (more than 2.5-fold) at 6-month of age compared to wild-type mice (Hahn et al., 2004b; Hadziahmetovic et al., 2008). Double knockout mice showed photoreceptor degeneration, sub-retinal neovascularization and RPE hypertrophy, hyperplasia by 9 months of age (Hahn et al., 2004b). Retinal degeneration in these mice was progressive, becoming more severe by 12–13 months of age (Hadziahmetovic et al., 2008).

Another mouse model of systemic iron loading was developed by Wolkow et al. (2012). Their murine model combined systemic ceruloplasmin deletion with RPE-specific hephaestin knockout resulted in iron accumulation in the RPE by 3 months of age, which was accompanied with a range of pathological features. In contrast, photoreceptor-specific deletion of hephaestin had no substantial effect on iron levels in the neural retina, even with concomitant systemic deletion of ceruloplasmin (Wolkow et al., 2012). Together, these results indicate that hephaestin has a cell-autonomous role in the RPE.

A further mouse model was generated by a single nucleotide (G to A) switch of the transferrin gene to produce hypotransferrinemic $Hpx^{-/-}$ mice (Trenor et al., 2000). Homozygous $Hpx^{-/-}$ mice have no transferrin and injection of human transferrin is required for survival, but even then, only a minority of mice survive up to 2 months of age (Lederman et al., 2012). Despite administration of exogenous human transferrin, the amount of transferrin in the retina of $Hpx^{-/-}$ mouse decreased to 61% of wild-type levels (Dickinson and Connor, 1995). Interestingly, the total iron content in the retina was not different between $Hpx^{-/-}$ and wild-type mice. Although gross retinal structure appeared to be normal in $Hpx^{-/-}$ mouse, assessment of retinal function showed attenuation of scotopic and photopic electroretinogram amplitudes compared to wild-type mice at 1 and 2 months of age (Lederman et al., 2012).

Finally, abnormal systemic iron loading has also been modeled by disruption of the bone morphogenetic protein 6 (*Bmp6*) gene, a key iron regulator gene that acts through hepcidin. In *Bmp6* knockout mice ($Bmp6^{-/-}$) high levels of iron are found in the neural retina of male $Bmp6^{-/-}$ mice (fourfold compared to wild-type male mice) (Hadziahmetovic et al., 2011c). Male $Bmp6^{-/-}$ mice showed severe retinal pathology by ∼10 months of age, including RPE hypertrophy and hyperplasia, loss of overlying photoreceptors and outer nuclear layer thinning. It is of interest that male $Bmp6^{-/-}$ mice had almost 20-fold more iron in their RPE/choroid compared to female $Bmp6^{-/-}$ mice. Female $Bmp6^{-/-}$ mice showed no evidence of increased retinal iron loading and normal retinal morphology. The sexual dimorphism of iron effects in $Bmp6^{-/-}$ mice was studied by castration and ovariectomy. Higher levels of liver hepcidin was found in castrated $Bmp6^{-/-}$ males relative to non-castrated $Bmp6^{-/-}$ mice, while there was no evidence of abnormal hepcidin expression in ovariectomized females. The authors argued that higher iron accumulation in $Bmp6^{-/-}$ males may have arisen through additional suppressive effects of testosterone on hepcidin synthesis (Latour et al., 2014). These studies highlight that along with age, gender can affect levels of retinal iron loading in the retina (Hahn et al., 2006).

Whilst providing important insight, the genetic mouse models of iron dyshomeostasis introduced thus far are not genetically analogous to human hemochromatosis. Thus, further studies of mouse models with disruption of genes that predispose to heredity hemochromatosis could offer more clinical relevance.

Retinal Abnormalities in Genetically – Modified Animal Models of Hemochromatosis

In addition to the above models, preclinical studies have sought to disrupt genes that predispose to heredity hemochromatosis in humans. The expression of hemochromatosis-related genes in mouse retina (Martin et al., 2006) makes it a useful animal model to address the possibility of iron-induced retinal injury.

Iacovelli et al. (2009) hypothesized that the disruption of ferroportin (Type 4 hemochromatosis) within the retina could lead to aberrant iron accumulation during both development and adulthood in mammals. They generated a polycythemia (high concentration of red blood cells) mouse (Pcm) model, and the results showed that up to 7 weeks of age there was no difference between Pcm and wild-type mice. However, at 12 months of age there were signs of retinal degeneration and morphological changes in aging Pcm mice. Unfortunately, retinal iron levels were not reported for Pcm mice at 1 year of age (Iacovelli et al., 2009).

The hepcidin knockout mouse ($Hamp^{-/-}$) is another model of hemochromatosis (Type 2) that show age-dependent increases in retinal iron in the RPE/choroid and neural retina (Hadziahmetovic et al., 2011a). Retinal structure was normal at 3 months of age in $Hamp^{-/-}$ mice. Mild focal abnormalities became apparent by 9 months and by 18 months pathology was severe including RPE hyperplasia, accumulation of lipofuscin-like material in the RPE, loss of photoreceptor outer segments and subretinal neovascularization (Hadziahmetovic et al., 2011a). Histochemical analysis of retinal iron levels (Perls' staining) showed that the RPE and non-pigmented ciliary epithelium are the primary sites of retinal iron accumulation in $Hamp^{-/-}$ mice older than 9-month. $Hamp^{-/-}$ mice also showed changes in retinal iron-related genes and proteins, including reduced *Tfr1* mRNA levels, and increased retinal L-ferritin protein levels at 4 months of age (Hadziahmetovic et al., 2011a). It is noticeable that despite progressive retinal iron accumulation in $Hamp^{-/-}$ mice and previously described *Cp* and *Heph* double knockout mice, there is a down-regulation in transferrin-bound iron import proteins in the retina of these models. This contradiction was resolved by Sterling et al. (2017) showing upregulation of non-transferrin bound iron import proteins in these two mouse models of retinal iron accumulation.

Another mouse model of hemochromatosis (Type 2) is hemojuvelin knockout ($Hjv^{-/-}$) mice. This animal model showed early systemic iron loading in particular in the liver, pancreas and heart by two and a half months of age (Niederkofler et al., 2005), with little evidence of retina changes at this age. $Hjv^{-/-}$ mice showed retinal degeneration at 18 months of age as assessed by counting cell bodies in retinal cross sections (Gnana-Prakasam et al., 2012).

Finally, a mouse model of hemochromatosis Type 1, which is one of the most prevalent mutations seen in human is the *Hfe* knockout mouse ($Hfe^{-/-}$). This mouse model had normal retinas at 6 months of age. Assessment at 18 months of age revealed severe retinal abnormalities including loss of ganglion cells, uneven distribution of nuclei in the inner and outer nuclear layers, widespread hypertrophy of RPE cells and focal areas of RPE hyperplasia (Gnana-Prakasam et al., 2009a). In addition, $Hfe^{-/-}$ mice showed changes in iron – related proteins including increased levels of both H-ferritin and L-ferritin in photoreceptors, outer and inner plexiform layers and within the RPE, in addition to reduced *Tfr1* mRNA levels (Gnana-Prakasam et al., 2009b).

Summary of Animal Studies on Iron and Retina

The pathologic findings in animal models shows that too much iron in the eye leads to dysfunction of photoreceptors and downstream consequences on the inner retina. Under normal conditions it seems that the regulatory system including the blood–retinal barrier protects the retina from systemic dietary iron loading. However, high levels of serum iron can eventually damage the RPE, which then reduces support to photoreceptors. Additionally, disruption to genes associated with iron–regulation leads to iron build-up, particularly the RPE and photoreceptors, resulting in progressive photoreceptor and downstream inner retinal degeneration. There is some evidence that rod photoreceptor dysfunction precedes cone photoreceptor changes with iron accumulation in the RPE. The amount of retinal injury and rate of progression associated with systemic iron loading appears to be varied depending on the specific regulatory protein involved, in addition to the age and sex of the mice (Hahn et al., 2009). While there is an increasing interest in incorporating electroretinography and *in vivo* imaging, as well as gene expression changes in retinal studies in animal models of iron loading (Liu et al., 2021), the number of such studies are still limited. More comprehensive time course studies, particularly using complementary tools such as electroretinography and *in vivo* imaging to define the earliest retinal deficits would help to define the role of iron regulation on retinal degeneration. Current animal studies indicate that the major driving factor in retinal degeneration may be iron overload as opposed to the genetic mutation itself having a direct effect, even though many hemochromatosis molecules have been found in the retina (Gnana-Prakasam et al., 2009a). This is because in the genetic modification models retinal changes only manifest at older ages, a stage when iron has had a chance to over-accumulate. Furthermore, treating the *Cp-Heph* (Hadziahmetovic et al., 2011b) and *Hepc* (Song et al., 2014) knock out mouse with an iron-chelator decreased retinal iron levels, oxidative stress and ameliorated retinal degeneration. Given different sub-types of hemochromatosis are due to alterations in a variety of genes further interventional studies are still warranted in other animal models.

CONCLUSION

Iron is known to play a critical role in the metabolic activities of the retina particularly the RPE and photoreceptors, but also the inner retina. Studies of ocular manifestations of systemic iron loading remain confined to case reports (Hudson, 1953; Davies et al., 1972; Roth and Foos, 1972; Zerbib et al., 2015; Bellsmith et al., 2020), with only one study on cohort of hemochromatosis patients (Menghini et al., 2018). Few studies have systematically assessed retinal function aside from visual acuity. Cumulative evidence from animal studies, showed that polymorphisms and mutations in iron-modulating genes are associated with progressive retinal iron accumulation and retinal injury.

The exact pathophysiology of retinal abnormalities in systemic iron loading-disorders is still unclear. Improved understanding of the relationship between retinal iron imbalance and retinal pathology is likely to help in the development of therapeutic strategies that can restore retinal iron homeostasis and mitigate neurotoxicity.

AUTHOR CONTRIBUTIONS

AS wrote the first draft of the manuscript. CN, BB, and DF contributed to manuscript revision, read, and approved the submitted version. All authors contributed to the article and approved the submitted version.

FUNDING

This research was supported by the Australian Research Council Linkage grant LP160100126 (CN and BB).

REFERENCES

Abboud, S., and Haile, D. J. (2000). A novel mammalian iron-regulated protein involved in intracellular iron metabolism. *J. Biol. Chem.* 275, 19906–19912. doi: 10.1074/jbc.M000713200

Abreu, R., Quinn, F., and Giri, P. K. (2018). Role of the hepcidin-ferroportin axis in pathogen-mediated intracellular iron sequestration in human phagocytic cells. *Blood Adv.* 2, 1089–1100. doi: 10.1182/bloodadvances.2017015255

Adams, P. C. (2005). Screening for haemochromatosisproducing or preventing illness? *Lancet* 366, 269–271.

Allen, K. J. (2008). Population genetic screening for hereditary haemochromatosis: are we a step closer? *Med. J. Aust.* 189, 300–301. doi: 10.5694/j.1326-5377.2008.tb02043.x

Andrews, N. C. (1999). Disorders of iron metabolism. *N. Engl. J. Med.* 341, 1986–1995.

Andrews, N. C. (2008). Forging a field: the golden age of iron biology. *Blood* 112, 219–230. doi: 10.1182/blood-2007-12-077388

Arosio, P., Ingrassia, R., and Cavadini, P. (2009). Ferritins: a family of molecules for iron storage, antioxidation and more. *Biochim. Biophys. Acta* 1790, 589–599. doi: 10.1016/j.bbagen.2008.09.004

Ayton, S., Lei, P., Duce, J. A., Wong, B. X., Sedjahtera, A., Adlard, P. A., et al. (2013). Ceruloplasmin dysfunction and therapeutic potential for Parkinson disease. *Ann. Neurol.* 73, 554–559. doi: 10.1002/ana.23817

Babitt, J. L., Huang, F. W., Wrighting, D. M., Xia, Y., Sidis, Y., Samad, T. A., et al. (2006). Bone morphogenetic protein signaling by hemojuvelin regulates hepcidin expression. *Nat. Genet.* 38, 531–539. doi: 10.1038/ng1777

Barot, M., Gokulgandhi, M. R., and Mitra, A. K. (2011). Mitochondrial dysfunction in retinal diseases. *Curr. Eye. Res.* 36, 1069–1077.

Battaglia, A. M., Chirillo, R., Aversa, I., Sacco, A., Costanzo, F., and Biamonte, F. (2020). Ferroptosis and cancer: mitochondria meet the "iron maiden" cell death. *Cells* 9:1505. doi: 10.3390/cells9061505

Baumann, B. H., Shu, W., Song, Y., Sterling, J., Kozmik, Z., Lakhal-Littleton, S., et al. (2019). Liver-specific, but not retina-specific, hepcidin knockout causes retinal iron accumulation and degeneration. *Am. J. Pathol.* 189, 1814–1830. doi: 10.1016/j.ajpath.2019.05.022

Bellsmith, K. N., Dunaief, J. L., Yang, P., Pennesi, M. E., Davis, E., Hofkamp, H., et al. (2020). Bull's eye maculopathy associated with hereditary hemochromatosis. *Am. J. Ophthalmol. Case Rep.* 18:100674. doi: 10.1016/j.ajoc.2020.100674

Bereta, G., Kiser, P. D., Golczak, M., Sun, W., Heon, E., Saperstein, D. A., et al. (2008). Impact of retinal disease-associated RPE65 mutations on retinoid isomerization. *Biochemistry* 47, 9856–9865. doi: 10.1021/bi800905v

Beutler, E., Felitti, V. J., Koziol, J. A., Ho, N. J., and Gelbart, T. (2002). Penetrance of 845G–> A (C282Y) HFE hereditary haemochromatosis mutation in the USA. *Lancet* 359, 211–218. doi: 10.1016/S0140-6736(02)07447-0

Beutler, E., Gelbart, T., West, C., Lee, P., Adams, M., Blackstone, R., et al. (1996). Mutation analysis in hereditary hemochromatosis. *Blood Cells Mol. Dis.* 22, 187-194; discussion 194a-194b.

Bhoiwala, D. L., Song, Y., Cwanger, A., Clark, E., Zhao, L. L., Wang, C., et al. (2015). CD1 mouse retina is shielded from iron overload caused by a high iron diet. *Invest. Ophthalmol. Vis. Sci.* 56, 5344–5352. doi: 10.1167/iovs.15-17026

Biesemeier, A., Yoeruek, E., Eibl, O., and Schraermeyer, U. (2015). Iron accumulation in Bruch's membrane and melanosomes of donor eyes with age-related macular degeneration. *Exp. Eye Res.* 137, 39–49. doi: 10.1016/j.exer.2015.05.019

Billings, J. L., Hare, D. J., Nurjono, M., Volitakis, I., Cherny, R. A., Bush, A. I., et al. (2016). Effects of neonatal iron feeding and chronic clioquinol administration on the parkinsonian human A53T transgenic mouse. *ACS Chem. Neurosci.* 7, 360–366. doi: 10.1021/acschemneuro.5b00305

Bjorn-Rasmussen, E., Hallberg, L., Isaksson, B., and Arvidsson, B. (1974). Food iron absorption in man. applications of the two-pool extrinsic tag method to measure heme and nonheme iron absorption from the whole diet. *J. Clin. Invest.* 53, 247–255. doi: 10.1172/JCI107545

Brissot, P., and de Bels, F. (2006). Current approaches to the management of hemochromatosis. *Hematol. Am. Soc. Hematol. Educ. Prog.* 2006, 36–41. doi: 10.1182/asheducation-2006.1.36

Brissot, P., Troadec, M. B., Loréal, O., and Brissot, E. (2019). Pathophysiology and classification of iron overload diseases; update 2018. *Transfus Clin. Biol.* 26, 80–88. doi: 10.1016/j.tracli.2018.08.006

Callebaut, I., Joubrel, R., Pissard, S., Kannengiesser, C., Gerolami, V., Ged, C., et al. (2014). Comprehensive functional annotation of 18 missense mutations found in suspected hemochromatosis type 4 patients. *Hum. Mol. Genet.* 23, 4479–4490. doi: 10.1093/hmg/ddu160

Camaschella, C., Roetto, A., Cali, A., De Gobbi, M., Garozzo, G., Carella, M., et al. (2000). The gene TFR2 is mutated in a new type of haemochromatosis mapping to 7q22. *Nat. Genet.* 25, 14–15. doi: 10.1038/75534

Casey, J. L., Hentze, M. W., Koeller, D. M., Caughman, S. W., Rouault, T. A., Klausner, R. D., et al. (1988). Iron-responsive elements: regulatory RNA sequences that control mRNA levels and translation. *Science* 240, 924–928. doi: 10.1126/science.2452485

Chen, H., Lukas, T. J., Du, N., Suyeoka, G., and Neufeld, A. H. (2009). Dysfunction of the retinal pigment epithelium with age: increased iron decreases phagocytosis and lysosomal activity. *Invest Ophthalmol. Vis. Sci.* 50, 1895–1902. doi: 10.1167/iovs.08-2850

Chen, L., Dentchev, T., Wong, R., Hahn, P., Wen, R., Bennett, J., et al. (2003). Increased expression of ceruloplasmin in the retina following photic injury. *Mol. Vis.* 9, 151–158.

Chua, A. C., Graham, R. M., Trinder, D., and Olynyk, J. K. (2007). The regulation of cellular iron metabolism. *Crit. Rev. Clin. Lab Sci.* 44, 413–459.

Chuang, J. Z., Zhao, Y., and Sung, C. H. (2007). SARA-regulated vesicular targeting underlies formation of the light-sensing organelle in mammalian rods. *Cell* 130, 535–547. doi: 10.1016/j.cell.2007.06.030

Coffman, L. G., Parsonage, D., D'agostino, R. Jr., Torti, F. M., and Torti, S. V. (2009). Regulatory effects of ferritin on angiogenesis. *Proc. Natl. Acad. Sci. U.S.A.* 106, 570–575. doi: 10.1073/pnas.0812010106

Čolak, E., Žorić, L., Radosavljević, A., and Ignjatović, S. (2018). The association of serum iron-binding proteins and the antioxidant parameter levels in age-related macular degeneration. *Curr. Eye Res.* 43, 659–665. doi: 10.1080/02713683.2018.1437452

Country, M. W. (2017). Retinal metabolism: a comparative look at energetics in the retina. *Brain Res.* 1672, 50–57. doi: 10.1016/j.brainres.2017.07.025

Crichton, R. R., Dexter, D. T., and Ward, R. J. (2011). Brain iron metabolism and its perturbation in neurological diseases. *J. Neural. Transm (Vienna)* 118, 301–314. doi: 10.1007/s00702-010-0470-z

Cullen, L. M., Gao, X., Easteal, S., and Jazwinska, E. C. (1998). The hemochromatosis 845 G–>A and 187 C–>G mutations: prevalence in non-caucasian populations. *Am. J. Hum. Genet.* 62, 1403–1407. doi: 10.1086/301878

Cunningham, M. J., Macklin, E. A., Neufeld, E. J., and Cohen, A. R. (2004). Complications of β-thalassemia major in north America. *Blood* 104, 34–39. doi: 10.1182/blood-2003-09-3167

D'Mello, S. R., and Kindy, M. C. (2020). Overdosing on iron: elevated iron and degenerative brain disorders. *Exp. Biol. Med.* 245, 1444–1473. doi: 10.1177/1535370220953065

Daglas, M., and Adlard, P. A. (2018). The involvement of iron in traumatic brain injury and neurodegenerative disease. *Front. Neurosci.* 12:981. doi: 10.3389/fnins.2018.00981

Davies, G., Dymock, I., Harry, J., and Williams, R. (1972). Deposition of melanin and iron in ocular structures in haemochromatosis. *Br. J. Ophthalmol.* 56, 338–342. doi: 10.1136/bjo.56.4.338

Declercq, S. S., Meredith, P. C., and Rosenthal, A. R. (1977). Experimental siderosis in the rabbit: correlation between electroretinography and histopathology. *Arch. Ophthalmol.* 95, 1051–1058. doi: 10.1001/archopht.1977.04450060138014

Dekker, M. C., Giesbergen, P. C., Njajou, O. T., Van Swieten, J. C., Hofman, A., Breteler, M. M., et al. (2003). Mutations in the hemochromatosis gene (HFE). *Parkinson's Dis. Parkinsonism. Neurosci. Lett.* 348, 117–119. doi: 10.1016/s0304-3940(03)00713-4

Del-Castillo-Rueda, A., Moreno-Carralero, M. I., Cuadrado-Grande, N., Alvarez-Sala-Walther, L. A., Enriquez-De-Salamanca, R., Mendez, M., et al. (2012). Mutations in the HFE, TFR2, and SLC40A1 genes in patients with hemochromatosis. *Gene* 508, 15–20. doi: 10.1016/j.gene.2012.07.069

Desmond, M. A., Sobiecki, J. G., Jaworski, M., Płudowski, P., Antoniewicz, J., Shirley, M. K., et al. (2021). Growth, body composition, and cardiovascular and nutritional risk of 5- to 10-y-old children consuming vegetarian, vegan, or omnivore diets. *Am. J. Clin. Nutr.* 113, 1565–1577. doi: 10.1093/ajcn/nqaa445

Détivaud, L., Island, M. L., Jouanolle, A. M., Ropert, M., Bardou-Jacquet, E., Le Lan, C., et al. (2013). Ferroportin diseases: functional studies, a link between genetic and clinical phenotype. *Hum. Mutat.* 34, 1529–1536. doi: 10.1002/humu.22396

Dickinson, T. K., and Connor, J. R. (1995). Cellular distribution of iron, transferrin, and ferritin in the hypotransferrinemic (Hp) mouse brain. *J. Comput. Neurol.* 355, 67–80. doi: 10.1002/cne.903550109

Dickman, S. R., and Cloutier, A. A. (1950). Activation and stabilization of aconitase by ferrous ions. *Arch. Biochem.* 25, 229–231.

Dixon, S. J., Lemberg, K. M., Lamprecht, M. R., Skouta, R., Zaitsev, E. M., Gleason, C. E., et al. (2012). Ferroptosis: an iron-dependent form of nonapoptotic cell death. *Cell* 149, 1060–1072. doi: 10.1016/j.cell.2012.03.042

Doly, M., Braquet, P., Bonhomme, B., and Meyniel, G. (1984). Effects of lipid peroxidation on the isolated rat retina. *Ophthalmic. Res.* 16, 292–296. doi: 10.1159/000265332

Donovan, A., Brownlie, A., Zhou, Y., Shepard, J., Pratt, S. J., Moynihan, J., et al. (2000). Positional cloning of zebrafish ferroportin1 identifies a conserved vertebrate iron exporter. *Nature* 403, 776–781. doi: 10.1038/35001596

Donovan, A., Lima, C. A., Pinkus, J. L., Pinkus, G. S., Zon, L. I., Robine, S., et al. (2005). The iron exporter ferroportin/Slc40a1 is essential for iron homeostasis. *Cell Metab* 1, 191–200. doi: 10.1016/j.cmet.2005.01.003

Dunaief, J. L. (2006). Iron induced oxidative damage as a potential factor in age-related macular degeneration: the cogan lecture. *Invest. Ophthalmol. Vis. Sci.* 47, 4660–4664. doi: 10.1167/iovs.06-0568

Dwork, A. J. (1995). Effects of diet and development upon the uptake and distribution of cerebral iron. *J. Neurol. Sci.* 134, 45–51. doi: 10.1016/0022-510x(95)00207-i

Feder, J. N., Gnirke, A., Thomas, W., Tsuchihashi, Z., Ruddy, D. A., Basava, A., et al. (1996). A novel MHC class I-like gene is mutated in patients with hereditary haemochromatosis. *Nat. Genet.* 13, 399–408. doi: 10.1038/ng0896-399

Fix, O. K., and Kowdley, K. V. (2008). Hereditary hemochromatosis. *Minerva Med.* 99, 605–617.

Fuqua, B. K., Vulpe, C. D., and Anderson, G. J. (2012). Intestinal iron absorption. *J. Trace Elem Med. Biol.* 26, 115–119.

Ganz, T. (2005). Hepcidina regulator of intestinal iron absorption and iron recycling by macrophages. *Best Pract. Res. Clin. Haematol.* 18, 171–182. doi: 10.1016/j.beha.2004.08.020

Gao, X., Campian, J. L., Qian, M., Sun, X. F., and Eaton, J. W. (2009). Mitochondrial DNA damage in iron overload. *J. Biol. Chem.* 284, 4767–4775. doi: 10.1074/jbc.M806235200

Gnana-Prakasam, J. P., Martin, P. M., Mysona, B. A., Roon, P., Smith, S. B., and Ganapathy, V. (2008). Hepcidin expression in mouse retina and its regulation via lipopolysaccharide/toll-like receptor-4 pathway independent of Hfe. *Biochem. J.* 411, 79–88. doi: 10.1042/BJ20071377

Gnana-Prakasam, J. P., Tawfik, A., Romej, M., Ananth, S., Martin, P. M., Smith, S. B., et al. (2012). Iron-mediated retinal degeneration in haemojuvelin-knockout mice. *Biochem. J.* 441, 599–608. doi: 10.1042/BJ20111148

Gnana-Prakasam, J. P., Thangaraju, M., Liu, K., Ha, Y., Martin, P. M., Smith, S. B., et al. (2009a). Absence of iron-regulatory protein Hfe results in hyperproliferation of retinal pigment epithelium: role of cystine/glutamate exchanger. *Biochem. J.* 424, 243–252. doi: 10.1042/BJ20090424

Gnana-Prakasam, J. P., Zhang, M., Martin, P. M., Atherton, S. S., Smith, S. B., and Ganapathy, V. (2009b). Expression of the iron-regulatory protein haemojuvelin in retina and its regulation during cytomegalovirus infection. *Biochem. J.* 419, 533–543. doi: 10.1042/BJ20082240

Gochee, P. A., Powell, L. W., Cullen, D. J., Du Sart, D., Rossi, E., and Olynyk, J. K. (2002). A population-based study of the biochemical and clinical expression of the H63D hemochromatosis mutation. *Gastroenterology* 122, 646–651. doi: 10.1016/s0016-5085(02)80116-0

Goswami, T., and Andrews, N. C. (2006). Hereditary hemochromatosis protein, HFE, interaction with transferrin receptor 2 suggests a molecular mechanism for mammalian iron sensing. *J. Biol. Chem.* 281, 28494–28498. doi: 10.1074/jbc.C600197200

Gottschall, D. W., Dietrich, R. F., Benkovic, S. J., and Shiman, R. (1982). Phenylalanine hydroxylase. correlation of the iron content with activity and the preparation and reconstitution of the apoenzyme. *J. Biol. Chem.* 257, 845–849.

Guerreiro, R. J., Bras, J. M., Santana, I., Januario, C., Santiago, B., Morgadinho, A. S., et al. (2006). Association of HFE common mutations with Parkinson's disease, Alzheimer's disease and mild cognitive impairment in a portuguese cohort. *BMC Neurol.* 6:24. doi: 10.1186/1471-2377-6-24

Guiney, S. J., Adlard, P. A., Bush, A. I., Finkelstein, D. I., and Ayton, S. (2017). Ferroptosis and cell death mechanisms in Parkinson's disease. *Neurochem. Int.* 104, 34–48. doi: 10.1016/j.neuint.2017.01.004

Gunshin, H., Mackenzie, B., Berger, U. V., Gunshin, Y., Romero, M. F., Boron, W. F., et al. (1997). Cloning and characterization of a mammalian proton-coupled metal-ion transporter. *Nature* 388, 482–488. doi: 10.1038/41343

Hadziahmetovic, M., Dentchev, T., Song, Y., Haddad, N., He, X., Hahn, P., et al. (2008). Ceruloplasmin/hephaestin knockout mice model morphologic and molecular features of AMD. *Invest. Ophthalmol. Vis. Sci.* 49, 2728–2736. doi: 10.1167/iovs.07-1472

Hadziahmetovic, M., Song, Y., Ponnuru, P., Iacovelli, J., Hunter, A., Haddad, N., et al. (2011a). Age-dependent retinal iron accumulation and degeneration in hepcidin knockout mice. *Invest. Ophthalmol. Vis. Sci.* 52, 109–118. doi: 10.1167/iovs.10-6113

Hadziahmetovic, M., Song, Y., Wolkow, N., Iacovelli, J., Grieco, S., Lee, J., et al. (2011b). The oral iron chelator deferiprone protects against iron overload-induced retinal degeneration. *Invest. Ophthalmol. Vis. Sci.* 52, 959–968.

Hadziahmetovic, M., Song, Y., Wolkow, N., Iacovelli, J., Kautz, L., Roth, M. P., et al. (2011c). Bmp6 regulates retinal iron homeostasis and has altered expression in

age-related macular degeneration. *Am. J. Pathol.* 179, 335–348. doi: 10.1016/j.ajpath.2011.03.033

Hahn, P., Dentchev, T., Qian, Y., Rouault, T., Harris, Z. L., and Dunaief, J. L. (2004a). Immunolocalization and regulation of iron handling proteins ferritin and ferroportin in the retina. *Mol. Vis.* 10, 598–607.

Hahn, P., Qian, Y., Dentchev, T., Chen, L., Beard, J., Harris, Z. L., et al. (2004b). Disruption of ceruloplasmin and hephaestin in mice causes retinal iron overload and retinal degeneration with features of age-related macular degeneration. *Proc. Natl. Acad. Sci. U.S.A.* 101, 13850–13855. doi: 10.1073/pnas.0405146101

Hahn, P., Song, Y., Ying, G. S., He, X., Beard, J., and Dunaief, J. L. (2009). Age-dependent and gender-specific changes in mouse tissue iron by strain. *Experimental gerontology* 44, 594–600. doi: 10.1016/j.exger.2009.06.006

Hahn, P., Ying, G. S., Beard, J., and Dunaief, J. L. (2006). Iron levels in human retina: sex difference and increase with age. *Neuroreport* 17, 1803–1806.

Haider, L. M., Schwingshackl, L., Hoffmann, G., and Ekmekcioglu, C. (2018). The effect of vegetarian diets on iron status in adults: a systematic review and meta-analysis. *Crit. Rev. Food Sci. Nutr.* 58, 1359–1374. doi: 10.1080/10408398.2016.1259210

Hare, D. J., Arora, M., Jenkins, N. L., Finkelstein, D. I., Doble, P. A., and Bush, A. I. (2015). Is early-life iron exposure critical in neurodegeneration? *Nat. Rev. Neurol.* 11, 536–544. doi: 10.1038/nrneurol.2015.100

Hare, D. J., Cardoso, B. R., Raven, E. P., Double, K. L., Finkelstein, D. I., Szymlek-Gay, E. A., et al. (2017). Excessive early-life dietary exposure: a potential source of elevated brain iron and a risk factor for Parkinson's disease. *NPJ Parkinson's Dis.* 3:1. doi: 10.1038/s41531-016-0004-y

Harmatz, P., Butensky, E., Quirolo, K., Williams, R., Ferrell, L., Moyer, T., et al. (2000). Severity of iron overload in patients with sickle cell disease receiving chronic red blood cell transfusion therapy. *Blood* 96, 76–79.

Harris, Z. L., Durley, A. P., Man, T. K., and Gitlin, J. D. (1999). Targeted gene disruption reveals an essential role for ceruloplasmin in cellular iron efflux. *Proc. Natl. Acad. Sci. U.S.A.* 96, 10812–10817. doi: 10.1073/pnas.96.19.10812

Harrison, P. M., and Arosio, P. (1996). The ferritins: molecular properties, iron storage function and cellular regulation. *Biochim. Biophys. Acta* 1275, 161–203. doi: 10.1016/0005-2728(96)00022-9

He, X., Hahn, P., Iacovelli, J., Wong, R., King, C., Bhisitkul, R., et al. (2007). Iron homeostasis and toxicity in retinal degeneration. *Prog. Retin Eye Res.* 26, 649–673. doi: 10.1016/j.preteyeres.2007.07.004

Hudson, J. R. (1953). Ocular findings in haemochromatosis. *Br. J. Ophthalmol.* 37, 242–246. doi: 10.1136/bjo.37.4.242

Iacovelli, J., Mlodnicka, A. E., Veldman, P., Ying, G. S., Dunaief, J. L., and Schumacher, A. (2009). Brain and retinal ferroportin 1 dysregulation in polycythaemia mice. *Brain Res.* 1289, 85–95. doi: 10.1016/j.brainres.2009.06.098

Ingrassia, R., Garavaglia, B., and Memo, M. (2019). DMT1 expression and iron levels at the crossroads between aging and neurodegeneration. *Front. Neurosci.* 13:575. doi: 10.3389/fnins.2019.00575

Jarrett, S. G., Lin, H., Godley, B. F., and Boulton, M. E. (2008). Mitochondrial DNA damage and its potential role in retinal degeneration. *Prog. Retin Eye Res.* 27, 596–607. doi: 10.1016/j.preteyeres.2008.09.001

Jeong, S. Y., and David, S. (2003). Glycosylphosphatidylinositol-anchored ceruloplasmin is required for iron efflux from cells in the central nervous system. *J. Biol. Chem.* 278, 27144–27148. doi: 10.1074/jbc.M301988200

Jiang, B., Liu, G., Zheng, J., Chen, M., Maimaitiming, Z., Chen, M., et al. (2016). Hephaestin and ceruloplasmin facilitate iron metabolism in the mouse kidney. *Sci. Rep.* 6:39470. doi: 10.1038/srep39470

Jouanolle, A. M., Fergelot, P., Gandon, G., Yaouanq, J., Le Gall, J. Y., and David, V. (1997). A candidate gene for hemochromatosis: frequency of the C282Y and H63D mutations. *Hum. Genet.* 100, 544–547. doi: 10.1007/s004390050549

Jouihan, H. A., Cobine, P. A., Cooksey, R. C., Hoagland, E. A., Boudina, S., Abel, E. D., et al. (2008). Iron-mediated inhibition of mitochondrial manganese uptake mediates mitochondrial dysfunction in a mouse model of hemochromatosis. *Mol. Med.* 14, 98–108. doi: 10.2119/2007-00114.Jouihan

Kaur, D., Peng, J., Chinta, S. J., Rajagopalan, S., Di Monte, D. A., Cherny, R. A., et al. (2007). Increased murine neonatal iron intake results in Parkinson-like neurodegeneration with age. *Neurobiol. Aging* 28, 907–913. doi: 10.1016/j.neurobiolaging.2006.04.003

Kaushik, P., Gorin, F., and Vali, S. (2007). Dynamics of tyrosine hydroxylase mediated regulation of dopamine synthesis. *J. Comput. Neurosci.* 22, 147–160. doi: 10.1007/s10827-006-0004-8

Kawabata, H., Yang, R., Hirama, T., Vuong, P. T., Kawano, S., Gombart, A. F., et al. (1999). Molecular cloning of transferrin receptor 2. a new member of the transferrin receptor-like family. *J. Biol. Chem.* 274, 20826–20832. doi: 10.1074/jbc.274.30.20826

Kohgo, Y., Ikuta, K., Ohtake, T., Torimoto, Y., and Kato, J. (2008). Body iron metabolism and pathophysiology of iron overload. *Int. J. Hematol.* 88, 7–15. doi: 10.1007/s12185-008-0120-5

Koorts, A. M., and Viljoen, M. (2007). Ferritin and ferritin isoforms I: Structure-function relationships, synthesis, degradation and secretion. *Arch Physiol. Biochem.* 113, 30–54. doi: 10.1080/13813450701318583

Kuhn, D. M., Ruskin, B., and Lovenberg, W. (1980). Tryptophan hydroxylase. the role of oxygen, iron, and sulfhydryl groups as determinants of stability and catalytic activity. *J. Biol. Chem.* 255, 4137–4143.

Lane, D. J. R., Ayton, S., and Bush, A. I. (2018). Iron and Alzheimer's disease: an update on emerging mechanisms. *J. Alzheimer's Dis.* 64, S379–S395. doi: 10.3233/JAD-179944

Latour, C., Kautz, L., Besson-Fournier, C., Island, M. L., Canonne-Hergaux, F., Loreal, O., et al. (2014). Testosterone perturbs systemic iron balance through activation of epidermal growth factor receptor signaling in the liver and repression of hepcidin. *Hepatology* 59, 683–694. doi: 10.1002/hep.26648

Lederman, M., Obolensky, A., Grunin, M., Banin, E., and Chowers, I. (2012). Retinal function and structure in the hypotransferrinemic mouse. *Invest. Ophthalmol. Vis. Sci.* 53, 605–612. doi: 10.1167/iovs.11-7436

Ledolter, A. A., Monhart, M., Schoetzau, A., Todorova, M. G., and Palmowski-Wolfe, A. M. (2015). Structural and functional changes in glaucoma: comparing the two-flash multifocal electroretinogram to optical coherence tomography and visual fields. *Doc. Ophthalmol.* 130, 197–209. doi: 10.1007/s10633-015-9482-1

Lee, J. H., Jang, H., Cho, E. J., and Youn, H. D. (2009). Ferritin binds and activates p53 under oxidative stress. *Biochem. Biophys. Res. Commun.* 389, 399–404. doi: 10.1016/j.bbrc.2009.08.125

Li, N., Wang, W., Zhou, H., Wu, Q., Duan, M., Liu, C., et al. (2020). Ferritinophagy-mediated ferroptosis is involved in sepsis-induced cardiac injury. *Free Radic Biol. Med.* 160, 303–318. doi: 10.1016/j.freeradbiomed.2020.08.009

Lin, H., Xu, H., Liang, F. Q., Liang, H., Gupta, P., Havey, A. N., et al. (2011). Mitochondrial DNA damage and repair in RPE associated with aging and age-related macular degeneration. *Invest. Ophthalmol. Vis. Sci.* 52, 3521–3529. doi: 10.1167/iovs.10-6163

Liu, Y., Bell, B. A., Song, Y., Kim, H. J., Sterling, J. K., Kim, B. J., et al. (2021). Intraocular iron injection induces oxidative stress followed by elements of geographic atrophy and sympathetic ophthalmia. *Aging Cell* 20:e13490. doi: 10.1111/acel.13490

Lloyd, R. V., Hanna, P. M., and Mason, R. P. (1997). The origin of the hydroxyl radical oxygen in the fenton reaction. *Free Radic Biol. Med.* 22, 885–888. doi: 10.1016/s0891-5849(96)00432-7

Lohmann, W. (1964). The importance of sulfur and iron in the retina as determined by paramagnetic resonance studies. *Experientia* 20, 399–401. doi: 10.1007/BF02147991

Lozoff, B., De Andraca, I., Castillo, M., Smith, J. B., Walter, T., and Pino, P. (2003). Behavioral and developmental effects of preventing iron-deficiency anemia in healthy full-term infants. *Pediatrics* 112, 846–854. doi: 10.1542/peds.112.4.846

Maddox, K. (1933). The retina in haemochromatosis. *Br. J. Ophthalmol.* 17, 392–394. doi: 10.1136/bjo.17.7.392

Martin, P. M., Gnana-Prakasam, J. P., Roon, P., Smith, R. G., Smith, S. B., and Ganapathy, V. (2006). Expression and polarized localization of the hemochromatosis gene product HFE in retinal pigment epithelium. *Invest. Ophthalmol. Vis. Sci.* 47, 4238–4244. doi: 10.1167/iovs.06-0026

Masaldan, S., Bush, A. I., Devos, D., Rolland, A. S., and Moreau, C. (2019). Striking while the iron is hot: iron metabolism and ferroptosis in neurodegeneration. *Free Radic Biol. Med.* 133, 221–233. doi: 10.1016/j.freeradbiomed.2018.09.033

McCarthy, R. C., and Kosman, D. J. (2013). Ferroportin and exocytoplasmic ferroxidase activity are required for brain microvascular endothelial cell iron efflux. *J. Biol. Chem.* 288, 17932–17940. doi: 10.1074/jbc.M113.455428

Menghini, M., Prünte, C., Krayenbuehl, P. A., and Nowak, A. (2018). Assessment of drusen and other retinal degenerative changes in patients with hereditary hemochromatosis. *Retina* 38, 594–599. doi: 10.1097/IAE.0000000000001577

Merryweather-Clarke, A. T., Pointon, J. J., Shearman, J. D., and Robson, K. J. (1997). Global prevalence of putative haemochromatosis mutations. *J. Med. Genet.* 34, 275–278. doi: 10.1136/jmg.34.4.275

Meynard, D., Babitt, J. L., and Lin, H. Y. (2014). The liver: conductor of systemic iron balance. *Blood* 123, 168–176. doi: 10.1182/blood-2013-06-427757

Miret, S., Simpson, R. J., and Mckie, A. T. (2003). Physiology and molecular biology of dietary iron absorption. *Annu Rev. Nutr.* 23, 283–301. doi: 10.1146/annurev.nutr.23.011702.073139

Moiseyev, G., Takahashi, Y., Chen, Y., Gentleman, S., Redmond, T. M., Crouch, R. K., et al. (2006). RPE65 is an iron(II)-dependent isomerohydrolase in the retinoid visual cycle. *J. Biol. Chem.* 281, 2835–2840. doi: 10.1074/jbc.M508903200

Montosi, G., Donovan, A., Totaro, A., Garuti, C., Pignatti, E., Cassanelli, S., et al. (2001). Autosomal-dominant hemochromatosis is associated with a mutation in the ferroportin (SLC11A3) gene. *J. Clin. Invest.* 108, 619–623. doi: 10.1172/JCI13468

Moreau, C., Duce, J. A., Rascol, O., Devedjian, J. C., Berg, D., Dexter, D., et al. (2018). Iron as a therapeutic target for Parkinson's disease. *Mov. Disord* 33, 568–574. doi: 10.1002/mds.27275

Mura, C., Raguenes, O., and Férec, C. (1999). HFE mutations analysis in 711 hemochromatosis probands: evidence for S65C implication in mild form of hemochromatosis. *Blood* 93, 2502–2505.

Nemeth, E., Tuttle, M. S., Powelson, J., Vaughn, M. B., Donovan, A., Ward, D. M., et al. (2004). Hepcidin regulates cellular iron efflux by binding to ferroportin and inducing its internalization. *Science* 306, 2090–2093. doi: 10.1126/science.1104742

Nicolas, G., Bennoun, M., Devaux, I., Beaumont, C., Grandchamp, B., Kahn, A., et al. (2001). Lack of hepcidin gene expression and severe tissue iron overload in upstream stimulatory factor 2 (USF2) knockout mice. *Proc. Natl. Acad. Sci. U.S.A.* 98, 8780–8785.

Niederkofler, V., Salie, R., and Arber, S. (2005). Hemojuvelin is essential for dietary iron sensing, and its mutation leads to severe iron overload. *J. Clin. Invest.* 115, 2180–2186. doi: 10.1172/JCI25683

Olynyk, J. K., Trinder, D., Ramm, G. A., Britton, R. S., and Bacon, B. R. (2008). Hereditary hemochromatosis in the post-HFE era. *Hepatology* 48, 991–1001. doi: 10.1002/hep.22507

Pamphlett, R., Cherepanoff, S., Too, L. K., Kum Jew, S., Doble, P. A., and Bishop, D. P. (2020). The distribution of toxic metals in the human retina and optic nerve head: implications for age-related macular degeneration. *PLoS One* 15:e0241054. doi: 10.1371/journal.pone.0241054

Papanikolaou, G., Samuels, M. E., Ludwig, E. H., Macdonald, M. L., Franchini, P. L., Dube, M. P., et al. (2004). Mutations in HFE2 cause iron overload in chromosome 1q-linked juvenile hemochromatosis. *Nat. Genet.* 36, 77–82. doi: 10.1038/ng1274

Patel, B. N., Dunn, R. J., Jeong, S. Y., Zhu, Q., Julien, J. P., and David, S. (2002). Ceruloplasmin regulates iron levels in the CNS and prevents free radical injury. *J. Neurosci.* 22, 6578–6586.

Pietrangelo, A. (2003). Haemochromatosis. *Gut* 52(Suppl. 2), ii23–ii30.

Pietrangelo, A. (2004). Hereditary hemochromatosis—a new look at an old disease. *N. Engl. J. Med.* 350, 2383–2397. doi: 10.1056/NEJMra031573

Pietrangelo, A., Caleffi, A., Henrion, J., Ferrara, F., Corradini, E., Kulaksiz, H., et al. (2005). Juvenile hemochromatosis associated with pathogenic mutations of adult hemochromatosis genes. *Gastroenterology* 128, 470–479. doi: 10.1053/j.gastro.2004.11.057

Pigeon, C., Ilyin, G., Courselaud, B., Leroyer, P., Turlin, B., Brissot, P., et al. (2001). A new mouse liver-specific gene, encoding a protein homologous to human antimicrobial peptide hepcidin, is overexpressed during iron overload. *J. Biol. Chem.* 276, 7811–7819. doi: 10.1074/jbc.M008923200

Piperno, A., Pelucchi, S., and Mariani, R. (2020). Inherited iron overload disorders. *Trans. Gastroenterol. Hepatol.* 5:25. doi: 10.3324/haematol.2018.189845

Powell, L. W., Seckington, R. C., and Deugnier, Y. (2016). Haemochromatosis. *Lancet* 388, 706–716.

Ramsey, A. J., Hillas, P. J., and Fitzpatrick, P. F. (1996). Characterization of the active site iron in tyrosine hydroxylase. redox states of the iron. *J. Biol. Chem.* 271, 24395–24400. doi: 10.1074/jbc.271.40.24395

Redfearn, E. R., and King, T. E. (1964). Mitochondrial nadh2 dehydrogenase and nadh2 oxidase from heart muscle: possible existence of a ferredoxin-like component in the respiratory chain. *Nature* 202, 1313–1316. doi: 10.1038/2021313a0

Redmond, T. M., Poliakov, E., Yu, S., Tsai, J. Y., Lu, Z., and Gentleman, S. (2005). Mutation of key residues of RPE65 abolishes its enzymatic role as isomerohydrolase in the visual cycle. *Proc. Natl. Acad. Sci. U.S.A.* 102, 13658–13663. doi: 10.1073/pnas.0504167102

Rogers, B. S., Symons, R. C., Komeima, K., Shen, J., Xiao, W., Swaim, M. E., et al. (2007). Differential sensitivity of cones to iron-mediated oxidative damage. *Invest. Ophthalmol. Vis. Sci.* 48, 438–445. doi: 10.1167/iovs.06-0528

Roth, A. M., and Foos, R. Y. (1972). Ocular pathologic changes in primary hemochromatosis. *Arch. Ophthalmol.* 87, 507–514. doi: 10.1001/archopht.1972.01000020509003

Rueda Adel, C., Grande, N. C., Fernandez, E. A., Enriquez De Salamanca, R., Sala, L. A., and Jimenez, M. J. (2011). Mutations in HFE and TFR2 genes in a spanish patient with hemochromatosis. *Rev. Esp. Enferm Dig.* 103, 379–382. doi: 10.4321/s1130-01082011000700010

Schmidt, P. J., Toran, P. T., Giannetti, A. M., Bjorkman, P. J., and Andrews, N. C. (2008). The transferrin receptor modulates Hfe-dependent regulation of hepcidin expression. *Cell Metab* 7, 205–214. doi: 10.1016/j.cmet.2007.11.016

Shichi, H. (1969). Microsomal electron transfer system of bovine retinal pigment epithelium. *Exp. Eye Res.* 8, 60–68. doi: 10.1016/s0014-4835(69)80081-3

Shu, W., Baumann, B. H., Song, Y., Liu, Y., Wu, X., and Dunaief, J. L. (2019). Iron accumulates in retinal vascular endothelial cells but has minimal retinal penetration after IP Iron dextran injection in mice. *Invest. Ophthalmol. Vis. Sci.* 60, 4378–4387. doi: 10.1167/iovs.19-28250

Shu, W., and Dunaief, J. L. (2018). Potential treatment of retinal diseases with iron chelators. *Pharmaceuticals (Basel)* 11:112. doi: 10.3390/ph11040112

Simovich, M. J., Miller, B., Ezzeldin, H., Kirkland, B. T., Mcleod, G., Fulmer, C., et al. (2001). Four novel mutations in the RPE65 gene in patients with leber congenital amaurosis. *Hum. Mutat.* 18:164. doi: 10.1002/humu.1168

Slater, E. C. (1949). The measurement of the cytochrome oxidase activity of enzyme preparations. *Biochem. J.* 44, 305–318. doi: 10.1042/bj0440305

Song, D., and Dunaief, J. L. (2013). Retinal iron homeostasis in health and disease. *Front. Aging Neurosci.* 5:24. doi: 10.3389/fnagi.2013.00024

Song, D., Kanu, L. N., Li, Y., Kelly, K. L., Bhuyan, R. K., Aleman, T., et al. (2016). AMD-like retinopathy associated with intravenous iron. *Exp. Eye Res.* 151, 122–133. doi: 10.1016/j.exer.2016.08.008

Song, D., Zhao, L., Li, Y., Hadziahmetovic, M., Song, Y., Connelly, J., et al. (2014). The oral iron chelator deferiprone protects against systemic iron overload-induced retinal degeneration in hepcidin knockout mice. *Invest Ophthalmol Vis Sci* 55, 4525–4532. doi: 10.1167/iovs.14-14568

Sterling, J., Guttha, S., Song, Y., Song, D., Hadziahmetovic, M., and Dunaief, J. L. (2017). Iron importers Zip8 and Zip14 are expressed in retina and regulated by retinal iron levels. *Exp. Eye Res.* 155, 15–23. doi: 10.1016/j.exer.2016.12.008

Thompson, D. A., Gyurus, P., Fleischer, L. L., Bingham, E. L., Mchenry, C. L., Apfelstedt-Sylla, E., et al. (2000). Genetics and phenotypes of RPE65 mutations in inherited retinal degeneration. *Invest. Ophthalmol. Vis. Sci.* 41, 4293–4299.

Trenor, C. C., Campagna, D. R., Sellers, V. M., Andrews, N. C., and Fleming, M. D. (2000). The molecular defect in hypotransferrinemic mice. *Blood* 96, 1113–1118.

Ugarte, M., Grime, G. W., Lord, G., Geraki, K., Collingwood, J. F., Finnegan, M. E., et al. (2012). Concentration of various trace elements in the rat retina and their distribution in different structures. *Metallomics* 4, 1245–1254. doi: 10.1039/c2mt20157g

Vulpe, C. D., Kuo, Y. M., Murphy, T. L., Cowley, L., Askwith, C., Libina, N., et al. (1999). Hephaestin, a ceruloplasmin homologue implicated in intestinal iron transport, is defective in the sla mouse. *Nat. Genet.* 21, 195–199. doi: 10.1038/5979

Wallace, D. F., Summerville, L., Crampton, E. M., Frazer, D. M., Anderson, G. J., and Subramaniam, V. N. (2009). Combined deletion of Hfe and transferrin receptor 2 in mice leads to marked dysregulation of hepcidin and iron overload. *Hepatology* 50, 1992–2000. doi: 10.1002/hep.23198

Ward, R. J., Zucca, F. A., Duyn, J. H., Crichton, R. R., and Zecca, L. (2014). The role of iron in brain ageing and neurodegenerative disorders. *Lancet Neurol.* 13, 1045–1060. doi: 10.1016/S1474-4422(14)70117-6

Wessling-Resnick, M. (2017). Excess iron: considerations related to development and early growth. *Am. J. Clin. Nutr.* 106, 1600s–1605s. doi: 10.3945/ajcn.117.155879

Widdowson, E. M., and McCance, R. A. (1937). The absorption and excretion of iron before, during and after a period of very high intake. *Biochem. J.* 31:2029. doi: 10.1042/bj0312029

Wolkow, N., Song, D., Song, Y., Chu, S., Hadziahmetovic, M., Lee, J. C., et al. (2012). Ferroxidase hephaestin's cell-autonomous role in the retinal pigment epithelium. *Am. J. Pathol.* 180, 1614–1624. doi: 10.1016/j.ajpath.2011.12.041

Wolkow, N., Song, Y., Wu, T. D., Qian, J., Guerquin-Kern, J. L., and Dunaief, J. L. (2011). Aceruloplasminemia: retinal histopathologic manifestations and iron-mediated melanosome degradation. *Arch. Ophthalmol.* 129, 1466–1474. doi: 10.1001/archophthalmol.2011.309

Wong-Riley, M. T. (2010). Energy metabolism of the visual system. *Eye Brain* 2, 99–116.

Yau, K. W., and Baylor, D. A. (1989). Cyclic GMP-activated conductance of retinal photoreceptor cells. *Annu Rev. Neurosci.* 12, 289–327. doi: 10.1146/annurev.ne.12.030189.001445

Yefimova, M. G., Jeanny, J. C., Guillonneau, X., Keller, N., Nguyen-Legros, J., Sergeant, C., et al. (2000). Iron, ferritin, transferrin, and transferrin receptor in the adult rat retina. *Invest. Ophthalmol. Vis. Sci.* 41, 2343–2351.

Young, R. W. (1967). The renewal of photoreceptor cell outer segments. *J. Cell. Biol.* 33, 61–72. doi: 10.1083/jcb.33.1.61

Young, R. W., and Bok, D. (1969). Participation of the retinal pigment epithelium in the rod outer segment renewal process. *J. Cell. Biol.* 42, 392–403. doi: 10.1083/jcb.42.2.392

Zecca, L., Youdim, M. B., Riederer, P., Connor, J. R., and Crichton, R. R. (2004). Iron, brain ageing and neurodegenerative disorders. *Nat. Rev. Neurosci.* 5, 863–873. doi: 10.1038/nrn1537

Zerbib, J., Pierre-Kahn, V., Sikorav, A., Oubraham, H., Sayag, D., Lobstein, F., et al. (2015). Unusual retinopathy associated with hemochromatosis. *Retin. Cases Brief Rep.* 9, 190–194. doi: 10.1097/ICB.0000000000000135

Zhao, L., Li, Y., Song, D., Song, Y., Theurl, M., Wang, C., et al. (2014). A high serum iron level causes mouse retinal iron accumulation despite an intact blood-retinal barrier. *Am. J. Pathol.* 184, 2862–2867.

Conflict of Interest: The authors declare that this study received funding from an Australian Research Council Linkage grant LP160100126 with funding partners AstraZeneca and Biogen Inc. The funder was not involved in the study design, collection, analysis, interpretation of data, the writing of this article, or the decision to submit it for publication.

frontiers in Neuroscience

ORIGINAL RESEARCH
published: 17 February 2022
doi: 10.3389/fnins.2022.830884

Longitudinal Serum Metabolomics in Extremely Premature Infants: Relationships With Gestational Age, Nutrition, and Morbidities

Anders K. Nilsson[1], Abdellah Tebani[2,3], Daniel Malmodin[4], Anders Pedersen[4], Gunnel Hellgren[1,5], Chatarina Löfqvist[1,6], Ingrid Hansen-Pupp[7], Mathias Uhlén[3] and Ann Hellström[1]*

[1] Section for Ophthalmology, Department of Clinical Neuroscience, Institute of Neuroscience and Physiology, Sahlgrenska Academy, University of Gothenburg, Gothenburg, Sweden, [2] Department of Metabolic Biochemistry, UNIROUEN, INSERM U1245, CHU Rouen, Rouen University Hospital, Normandie University, Rouen, France, [3] Department of Protein Science, Science for Life Laboratory, KTH-Royal Institute of Technology, Stockholm, Sweden, [4] Swedish NMR Centre, University of Gothenburg, Gothenburg, Sweden, [5] Institute of Biomedicine, Sahlgrenska Academy, University of Gothenburg, Gothenburg, Sweden, [6] Institute of Health and Care Sciences, Sahlgrenska Academy, University of Gothenburg, Gothenburg, Sweden, [7] Department of Clinical Sciences, Pediatrics, Skåne University Hospital, Lund University, Lund, Sweden

OPEN ACCESS

Edited by:
Ellen Tianwei Zhou, University of Toronto, Canada

Reviewed by:
Shiro Tochitani, Suzuka University of Medical Science, Japan
Paul Allen Rosenberg, Boston Children's Hospital and Harvard Medical School, United States

***Correspondence:**
Anders K. Nilsson
anders.k.nilsson@gu.se

Specialty section:
This article was submitted to Neurodegeneration, a section of the journal Frontiers in Neuroscience

Received: *07 December 2021*
Accepted: *14 January 2022*
Published: *17 February 2022*

Citation:
Nilsson AK, Tebani A, Malmodin D, Pedersen A, Hellgren G, Löfqvist C, Hansen-Pupp I, Uhlén M and Hellström A (2022) Longitudinal Serum Metabolomics in Extremely Premature Infants: Relationships With Gestational Age, Nutrition, and Morbidities. Front. Neurosci. 16:830884. doi: 10.3389/fnins.2022.830884

An increasing number of extremely premature infants survive the neonatal period and beyond. Little is known about the maturation of the preterm infant's metabolome and its relation to the development of morbidities. Using 1H-NMR, we investigated the serum metabolic profile of 87 infants born at a gestational age (GA) <28 weeks [mean GA (SD) 25.4 (1.4) weeks] in samples longitudinally collected from birth to term equivalent age. The infant metabolome was analyzed in relation to GA, postnatal age, nutrition, and preterm morbidities. At postnatal day 1, low GA correlated with high levels of 3-hydroxyisobutyrate, acetate, acetoacetate, acetone, formate, glucose, and valine. Nearly all quantified metabolites displayed postnatal concentration changes. For example, the two phospholipid-related metabolites myo-inositol and ethanolamine displayed a similar decline from birth over the first weeks of life, irrespectively of GA. The proportion of enteral/parenteral energy intake in the first 28 days significantly correlated with mean levels of 52% of the analyzed metabolites. Low enteral energy intake was associated with high serum levels of 3-hydroxyisobutyrate, creatinine, glucose, glycerol, histidine, lactate, leucine, lysine, methionine, ornithine, phenylalanine, proline, threonine, and uridine. There were also significant correlations between high enteral intake and high serum levels of isoleucine and tyrosine. Retinopathy of prematurity (ROP) and bronchopulmonary dysplasia (BPD) outcomes were not significantly associated with metabolite levels in the neonatal period after correcting for multiple testing. In conclusion, the serum metabolome of extremely premature infants changes substantially in the neonatal period, largely driven by the gradual transfer from total parenteral nutrition to full enteral feeding. Further studies are needed to disentangle the intricate relationships between the metabolome, nutritional management, GA, and the development of preterm morbidities.

Keywords: bronchopulmonary dysplasia, enteral nutrition, parenteral nutrition, retinopathy of prematurity, ketone bodies, ethanolamine, one-carbon metabolism, human milk

INTRODUCTION

Advances in obstetrics and perinatal care over the last decades have dramatically improved the survival of infants born preterm. Despite improved survival, the prevalence of morbidities among extremely preterm infants (born <28 weeks of gestation) remains high, particularly among infants born at the lowest gestational ages (GAs) (Costeloe et al., 2012; Norman et al., 2019). Morbidities affecting preterm infants include intraventricular hemorrhage (IVH), necrotizing enterocolitis (NEC), sepsis, bronchopulmonary dysplasia (BPD), and retinopathy of prematurity (ROP). These morbidities pose immediate threats to infant health and may have long-term consequences for neurodevelopmental and behavioral outcomes (Mathewson et al., 2017; Pascal et al., 2018; Twilhaar et al., 2018). The neonatal period is an especially vulnerable time for extremely preterm infants with high risks for death and morbidities.

Metabolomics allows for the detection and quantification of an array of low molecular weight compounds derived from cellular metabolism or exogenous sources and has the potential to provide detailed insights into disease etiology and progression (La Frano et al., 2018; Ernst et al., 2020). Metabolomics is increasingly used in research settings and is a promising tool in precision medicine, especially in the context of clinical neonatology (Fanos et al., 2018). However, most metabolomics studies in preterm infant blood have focused on one or a few sampling occasions, while longitudinal studies during the neonatal period and beyond have been sparse and included few individuals.

The neonatal period of extremely preterm infants involves the gradual transfer from total or partial parenteral nutrition (PN) to full enteral nutrition (EN). Human milk is always the firsthand choice of enteral feed for preterm infants. In Sweden, all extremely preterm infants receive exclusively human milk, mother's own milk if available, otherwise, donor human milk, from the day of birth until usually 34 weeks postmenstrual age. Thereafter, a preterm formula may be introduced. Feeding tolerance is strongly linked to the GA at birth, and the most immature infants require the longest time to reach full enteral feeding. Therefore, an infant's metabolic profile depends on the GA and the postnatal age (Clark et al., 2014). Furthermore, the feeding regime influences the growth trajectory for the preterm infant (Power et al., 2019; Lund et al., 2020; Roggero et al., 2020), and poor growth gain during the 1st weeks of life is predictive for adverse morbidity outcomes, including severe ROP and BPD (Hellström et al., 2010; Chisholm et al., 2019).

Bronchopulmonary dysplasia and ROP are multifactorial diseases with certain common elements but also with distinct pathogenesis. ROP is a neurovascular disease characterized by dysregulated retinal vascularization that can lead to retinal detachment and permanent visual loss if not timely diagnosed and treated. The prevalence of ROP is higher in infants with low GA and low weight at birth (Hellström et al., 2013; Danielsson et al., 2021). BPD stems from pre and postnatal injury to the immature lung and affects almost 50% of extremely preterm infants born in high-income countries (Stoll et al., 2010; Hellström et al., 2021; Siffel et al., 2021). As for ROP, BPD involves disrupted vascular formation and is more common in infants with low GA and high supplemental oxygen.

Here, we assessed the serum metabolic profiles of extremely preterm infants from birth to term equivalent age and analyzed the metabolome in regards to GA, postnatal age, nutrition, and morbidities.

MATERIALS AND METHODS

Study Design

The current investigation was performed within the Donna Mega trial (ClinicalTrials.gov Identifier: NCT02760472). The Donna Mega trial is a single-center, randomized open-label trial designed to determine the effect of parenterally administered lipids with or without *n*–3 long-chain polyunsaturated fatty acids (LC-PUFAs) on growth and morbidity outcomes in infants born extremely preterm. Infants were randomly assigned an olive oil-based lipid parenteral emulsion (Clinoleic, Baxter Medical AB, Kista, Sweden) or a mixed-oil emulsion high in *n*–3 LC-PUFAs (Smoflipid, Fresenius Kabi, Uppsala, Sweden). The results of the primary outcomes of the trial have been previously published (Najm et al., 2017). Eligible for inclusion in the study were infants born at GA <28 weeks at the neonatal care unit at Sahlgrenska University Hospital in Gothenburg, Sweden, between April 2013 and September 2015. Infants born with major congenital malformations were excluded. Out of the 138 infants born at GA <28 weeks during the inclusion period, parents/legal guardians of 90 eligible infants agreed to participate after informed consent. Details of the nutritional strategy and nutritional data collection have been described in detail (Najm et al., 2017; Lund et al., 2020). Growth data (weight, length, and head circumference) were prospectively collected until term equivalent age and transformed into z-scores according to the growth reference by Niklasson and Albertsson-Wikland (2008).

Morbidities

Retinopathy of prematurity screening was performed as previously described (Löfqvist et al., 2018), and disease stages were classified using The International Classification of Retinopathy of Prematurity (2005). No/moderate ROP was defined as ROP stages 1–2, and Severe ROP as ROP stage 3 and/or Type 1 ROP. BPD was defined as the need for supplemental oxygen at 36 weeks postmenstrual age.

Blood Collection, Sample Preparation, and Metabolic Profiling

Infant blood samples were collected at postnatal days (PND) 1, 7, 14, and 28, and at postmenstrual age (PMA) 32, 36, and 40 weeks. The blood was allowed to clot at 4°C for a minimum of 45 min and a maximum of 2 h before centrifugation at room temperature at 1500 *g* for 10 min. The serum was then transferred into cryovials and stored at −20°C for up to 1 week before long-term storage at −80°C until analysis. All samples had been subjected to at least one, but less than five, freeze-thaw cycle before NMR analysis.

Serum samples (50 μl) were prepared and then analyzed on an Oxford 800 MHz magnet equipped with an Avance III HD console and 3 mm TCI cryoprobe (Bruker BioSpin). Details of sample processing and the ^{1}H NMR analysis have been published (Nilsson et al., 2020). Tentative annotations of peaks were made using ChenomX 8.3 (ChenomX Inc.) and the spectral data in the Human Metabolome Data Bank (Wishart et al., 2018). In total, 260 NMR features were detected in the serum samples. From these, 31 metabolites could be chemically and structurally annotated. In instances where multiple features represented a single metabolite, a strong well-separated peak was selected, or two or more peaks were summarized. All metabolite levels are reported as normalized NMR signals or as standardized values.

Ethics

The Donna Mega trial was approved by the Regional Ethical Review Board, Gothenburg (Dnr 303-11). Informed signed consent for all participants included in the study was obtained from their parents or legal guardians.

Statistical Analyses

Mann–Whitney *U*-test was used to compare continuous variables with non-normal distribution, and Spearman's rank test was applied to assess correlations between variables.

The area under the curve (AUC) for metabolites for PND 1–28 was calculated using the trapezoidal rule. The AUC was divided by the total number of days to yield a daily mean value. Only infants who had a complete sample series during their first 4 weeks of life (PNA 1, 7, 14, and 28) were included in this sub-analysis. In instances where no NMR signal could be detected and a peak intergraded, the minimum value/2 was imputed. Six out of 15593 (0.04%) values were imputed using this method.

For clustering, the NMR signal of each metabolite was first standardized with a standard deviation of 1 centered at 0. Then, the scaled values from all 503 samples were used to create the Euclidean distance matrix for dendrogram generation. Dendrograms showing metabolite levels in heatmaps have been clustered using the Ward2 algorithm, an implementation of Ward's minimum variance method implemented as "Ward.D2" in R package pheatmap (Kaufman and Rousseeuw, 2009; Murtagh and Legendre, 2014). Spearman correlation was used to compute the pairwise correlation. Multiple tests correction was performed with the Benjamini–Hochberg method.

Statistical analyses were performed using IBM SPSS Statistics version 27 (IBM Corp., Armonk, NY, United States) and R-Statistics Software (The R Foundation for Statistical Computing, Vienna, Austria).

RESULTS

Population Characteristics and Serum Sampling Scheme

Serum for ^{1}H NMR metabolomics was available from 87 out of 90 infants enrolled in the Donna Mega trial (Najm et al., 2017). The study infants' demographic and clinical data are presented in **Table 1** and the blood sampling scheme used is illustrated in **Figure 1**. In total, 503 serum samples collected at seven predetermined time points were analyzed (**Figure 1A**). Samples from the first four time points were collected based on chronological age [postnatal day (PND) 1, 7, 14, and 28], while the following samples were collected based on postmenstrual age [postmenstrual week (PMW) 32, 36, and 40) (**Figure 1B**).

Overview of the Infant Metabolome

Thirty-one serum metabolites could be unambiguously annotated and quantified in all samples (**Supplementary Table 1**). To overview the data, mean metabolite levels across the sample time points were subjected to hierarchical clustering and visualized in a heatmap (**Figure 2**). For assessing the impact of GA on the metabolome, infants were subdivided into three groups based on GA at birth: below 25 weeks GA (n = 33), 25–26 weeks GA (n = 36), and 27 weeks GA (n = 18). There was apparent clustering both according to sampling time and GA at birth. Overall, samples from the two lower GA groups (<25 and 25–26 weeks) clustered together and showed larger variability in metabolite levels between time points than samples from the group of infants with the highest GA (27 weeks). Samples collected at PND 1 and PND7 in the two lower GA groups formed a cluster defined by high levels of acetone, creatinine, and phenylalanine. Furthermore, PND 1 samples from GA <27 weeks infants displayed high 3-hydroxyisobutyrate, ethanolamine, and myoinositol levels, among other metabolites. At PMW 40, samples from all three GA groups clustered together, indicating a transient change in the metabolome in infants born at the lowest GAs occurring in the neonatal period.

Influence of Gestational Age at Birth on Metabolites the First Day of Life

At PND 1, levels of 7 (23%) of the analyzed metabolites were significantly correlated with GA at birth (**Figure 3** and **Supplementary Table 2**). Notably, all metabolites associated with GA at birth displayed negative correlations.

TABLE 1 | Demographic data of the study population (n = 87).

Variable	Value
Gestational age at birth, mean (SD), wks	25.4 (1.4)
Birth weight, mean (SD), g	780 (224)
Birth zWeight, mean (SD)[a]	−0.86 (1.36)
Birth weight small for gestational age[b], *n* (%)	12 (14)
Male, *n* (%)	50 (57)
Retinopathy of prematurity (ROP), stages 0–2	47/78
Retinopathy of prematurity (ROP), stages 3 or Type I	31/78
Bronchopulmonary dysplasia (BPD)[c], *n* (%)	39/78 (50)
Death before 40 weeks PMA, n (%)	9 (10)

[a] *Calculated according to Niklasson and Albertsson-Wikland (2008).*
[b] *BW <−2 SD.*
[c] *Supplemental O_2 at 36 weeks PMA.*

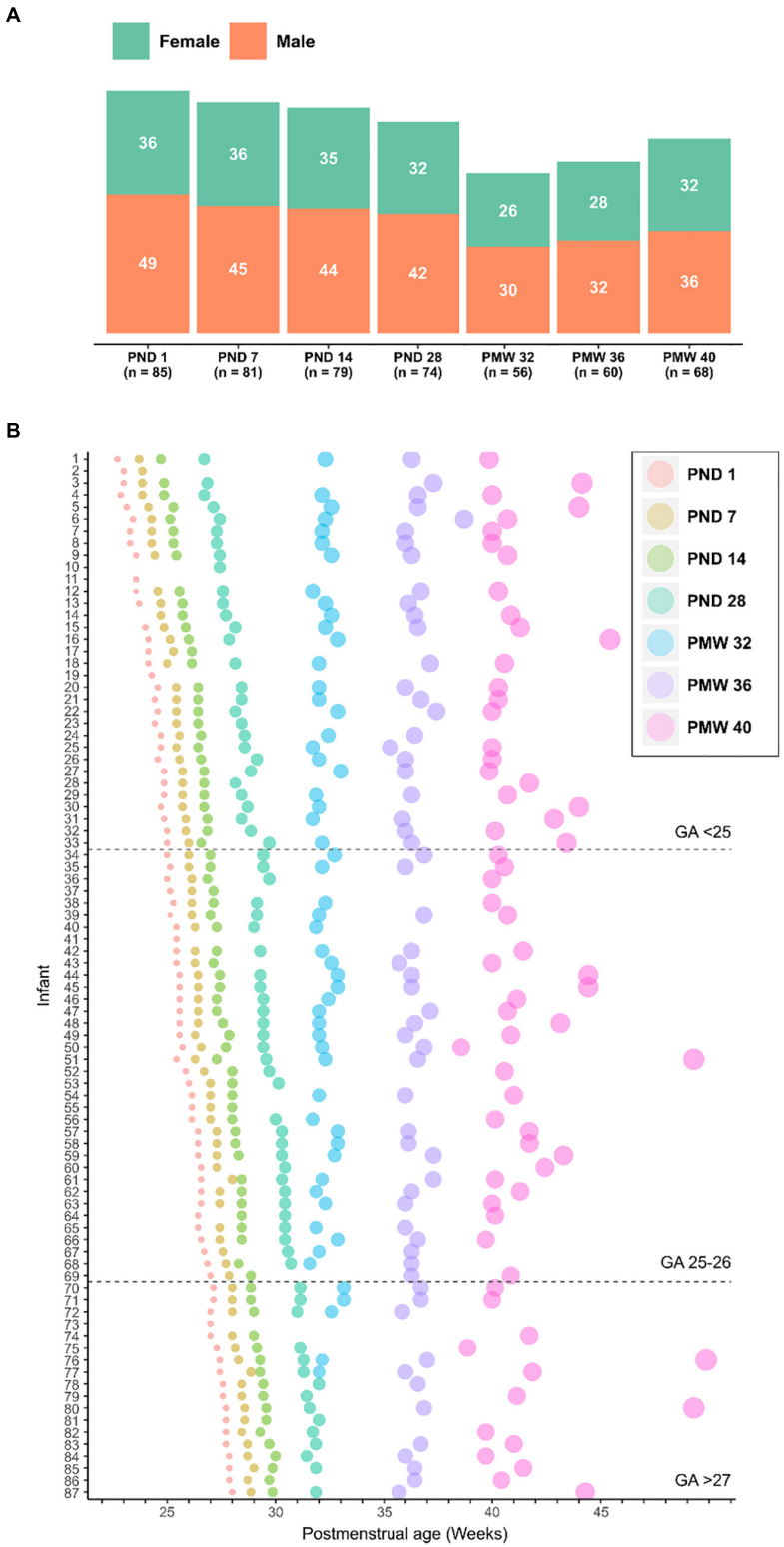

FIGURE 1 | Overview of analyzed samples. **(A)** Number of samples collected at seven time points used for serum metabolomics presented by gender. **(B)** Longitudinal serum sampling scheme for all infants included in the study. Infants are sorted by gestational age at birth. The size of the dot at sampling is proportional to the postnatal age of the infant and the color indicates the sampling time point accordingly to legend. GA, gestational age; PND, postnatal day; PMW, postmenstrual week.

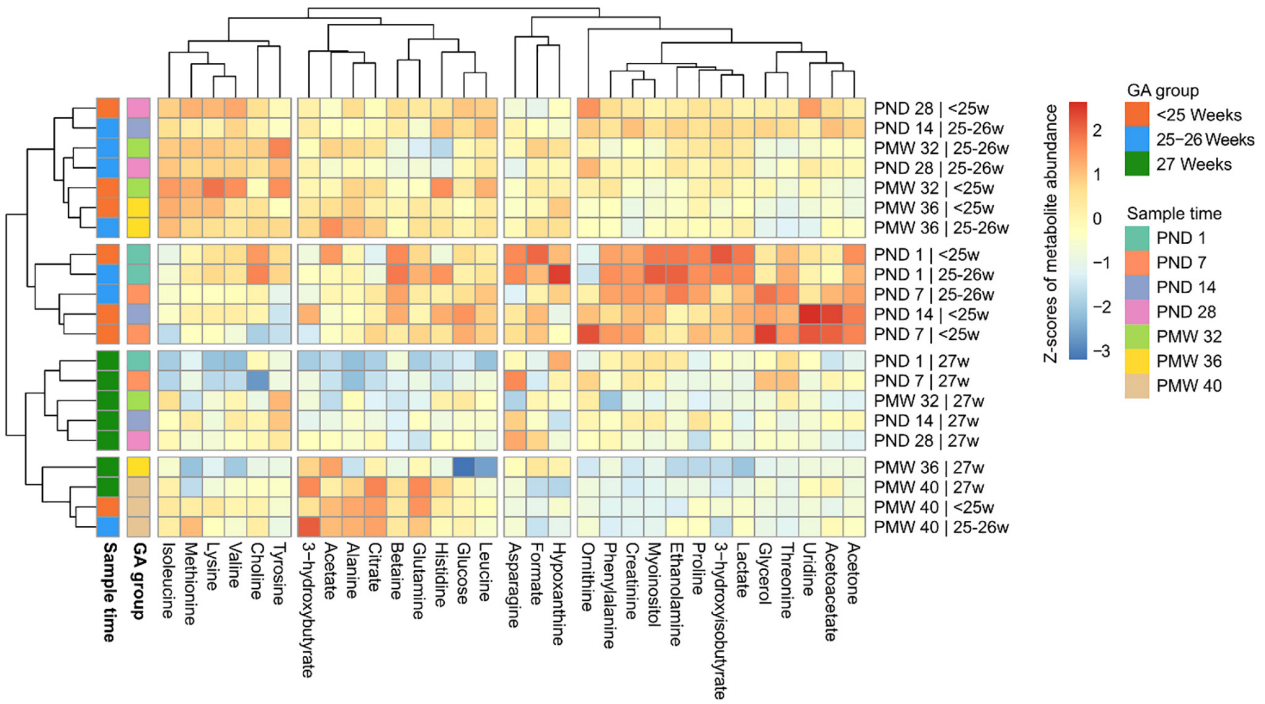

FIGURE 2 | Heatmap of metabolite levels over the study period stratified by gestational age (GA) at birth: <25 weeks, 25–26 weeks, or 27 weeks. Each metabolite was scaled using the mean value and standard deviation and centered at 0. Intensities from blue to red display relative metabolite levels in standard deviations. Both rows and columns have been hierarchically clustered based on metabolite abundances at specified time points for each GA group. Thus, metabolites that show similar abundance patterns across the study period group together vertically, and time points for each GA group that show similar metabolite abundance patterns group horizontally. Breaks in the heatmap indicate clusters from the dendrograms; the number of clusters was manually specified. PND, postnatal day; PMW, postmenstrual week.

Longitudinal Changes in the Infant Metabolome

Figure 4 shows all analyzed metabolites longitudinally plotted with individual samples colored according to time point. The same metabolites presented by the three GA groups are shown in **Figure 5**. As seen in both the heatmap (**Figure 2**) and longitudinal plotting of the data (**Figures 4**, **5**), the most pronounced metabolome changes occurred during the neonatal period, i.e., between birth and postnatal day 28. Specifically, this period was also defined by differences in metabolite levels between the three GA groups. Some metabolites, however, also displayed abundance changes in the later part of the study period (e.g., citrate, glutamine, and lysine).

Relationships Between Nutritional Management, Growth, and the Infant Metabolome

Next, we explored relationships between the infant metabolome, growth, and nutritional parameters by correlating data collected the first 28 postnatal days (**Figure 6**). About half of the nutritional variables were significantly associated with metabolite levels (**Figure 6A**). Variables related to parenteral nutrition formed a cluster and were positively correlated with serum levels of glycerol, threonine, and ornithine (**Figure 6B**). Contrary, nutritional variables related to enteral nutrition formed a cluster together with choline and tyrosine. Surprisingly, donor milk and mother's own milk were found in two separate clusters. Standardize weight (zWeight) and head circumference (zHC) formed a small cluster together with asparagine.

Enteral Nutritional Intake and the Serum Metabolome

To further understand how nutritional management influences the metabolome, we compared the % enteral of total energy intake (kcal/kg/d) PND 1–28 with mean metabolite levels. Only infants with complete metabolic profiles from PND 1 to PND 28 were included (n = 69). Isoleucine and tyrosine displayed positive correlations with % enteral energy intake, whereas many other (14/31) metabolites were negatively associated, including glycerol, threonine, and creatinine (**Figure 7A**). Next, infants were dichotomously grouped based on if they had high (>median) or low (<median) enteral energy intake PND 1–28 (**Supplementary Table 3**). **Figures 7B–E** show examples of metabolites that significantly differed between infants with high and low enteral energy intake. Among these examples, the daily mean glycerol and threonine levels were two-fold higher in infants who received little enteral intake compared to infants with high enteral intake.

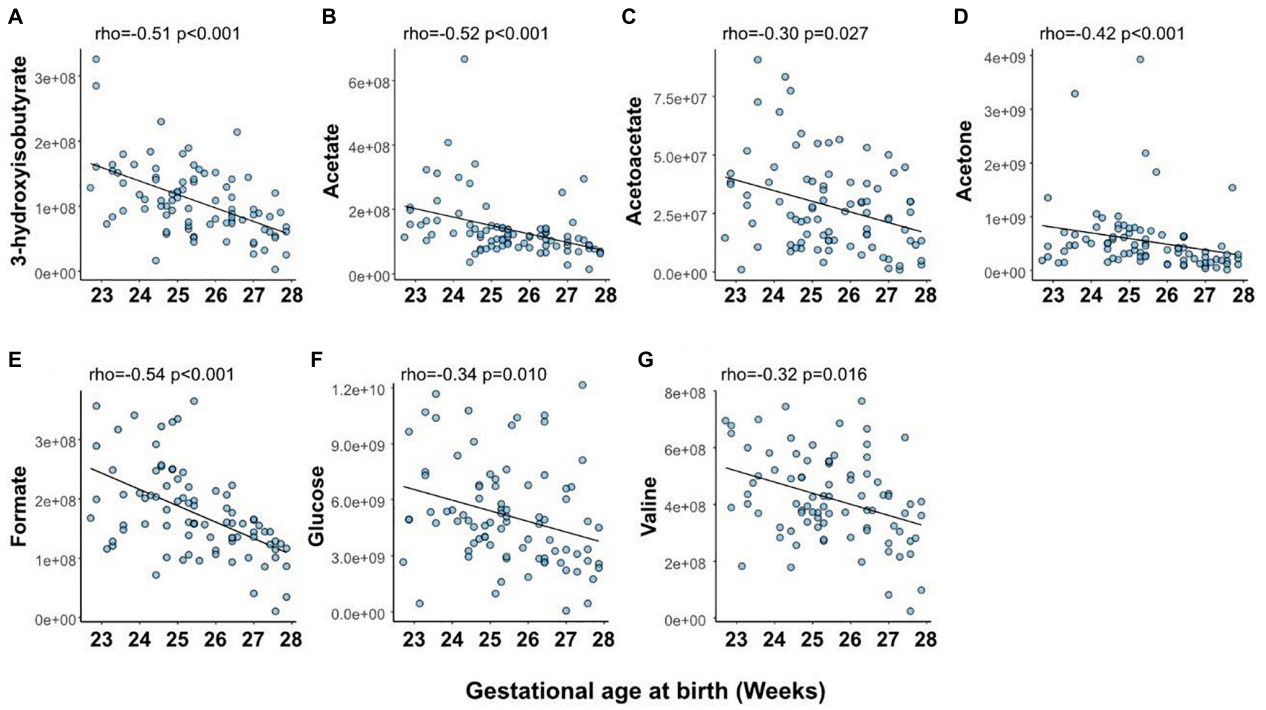

FIGURE 3 | Relationship between gestational age at birth and serum levels of metabolites at postnatal day (PND) 1: 3-hydroxyisobutyrate **(A)**, acetate **(B)**, acetoacetate **(C)**, acetone **(D)**, formate **(E)**, glucose **(F)**, and valine **(G)**. Shown are Spearman's correlation coefficient (rho) and *p*-value for the association between metabolite levels and gestational age. *p*-values have been false discovery rate adjusted using the Benjamini-Hochberg method. *Y*-axis shows normalized NMR signal.

Associations Between the Serum Metabolome and Morbidities

To identify metabolites associated with the development of preterm morbidities, we compared mean daily metabolite levels PND 1–28 with ROP and BPD outcomes. Before correction for multiple testing, 10 metabolites differed significantly between infants who developed no/mild ROP (stages 0–2, n = 39) and infants who developed severe ROP (stage 3 and/or Type 1 ROP, n = 29) (**Supplementary Table 4**). However, after false discovery rate correction, no metabolite remained statistically significant. Similarly, three metabolites differed significantly between infants who did not (n = 36) or did develop BPD (n = 32), but none remained significant after false discovery rate correction (**Supplementary Table 4**).

DISCUSSION

We longitudinally followed the serum metabolome of extremely preterm infants from birth to term equivalent age. Our results show that the metabolome of the infants undergoes substantial composition changes during the early perinatal period, strongly influenced by the feeding regime, and moreover, relates to GA at birth.

The levels of seven serum metabolites on PND 1 significantly correlated with GA at birth (3-hydroxyisobutyrate, acetate, acetoacetate, acetone, formate, glucose, and valine). Valine has previously been shown to be the amino acid with the most considerable concentration difference between extremely preterm and full-term infants, demonstrating a GA dependence (Wilson et al., 2014). Apart from valine, the identified metabolites constituted non-amino acid compounds and showed limited overlap with metabolites related to GA in very- and moderately preterm infants (Ernst et al., 2020). Formate can be produced from various sources and is a critical component in one-carbon metabolism, including the metabolic pathways of folate, choline, and methionine. The concentration of formate is higher in fetal plasma than in maternal plasma (Washburn et al., 2015; Brosnan et al., 2019). It has been suggested that high fetal formate supports increased one-carbon metabolism during late gestation when extensive growth occurs (Brosnan et al., 2019). We found that low GA at birth was associated with higher serum formate at PND 1. The implications of this finding need further studies. Acetoacetate, acetone, and 3-hydroxybutyrate are ketone bodies that generally increase in the blood under fasting conditions, a high-fat diet, suckling, and during the second half of the pregnancy. Ketone bodies are formed from the breakdown of fatty acids and are used as fuel when glucose is unavailable or needed for anabolism. Further metabolism of acetone yields lactate and acetate, among other compounds. Ketone bodies can freely cross the placenta, and maternal-fetal concentrations are closely related at delivery (Paterson et al., 1967). We found infant ketone levels at PND 1 to be lower in infants born at higher GAs. The increase in acetoacetate observed at PND 7 and 14, especially

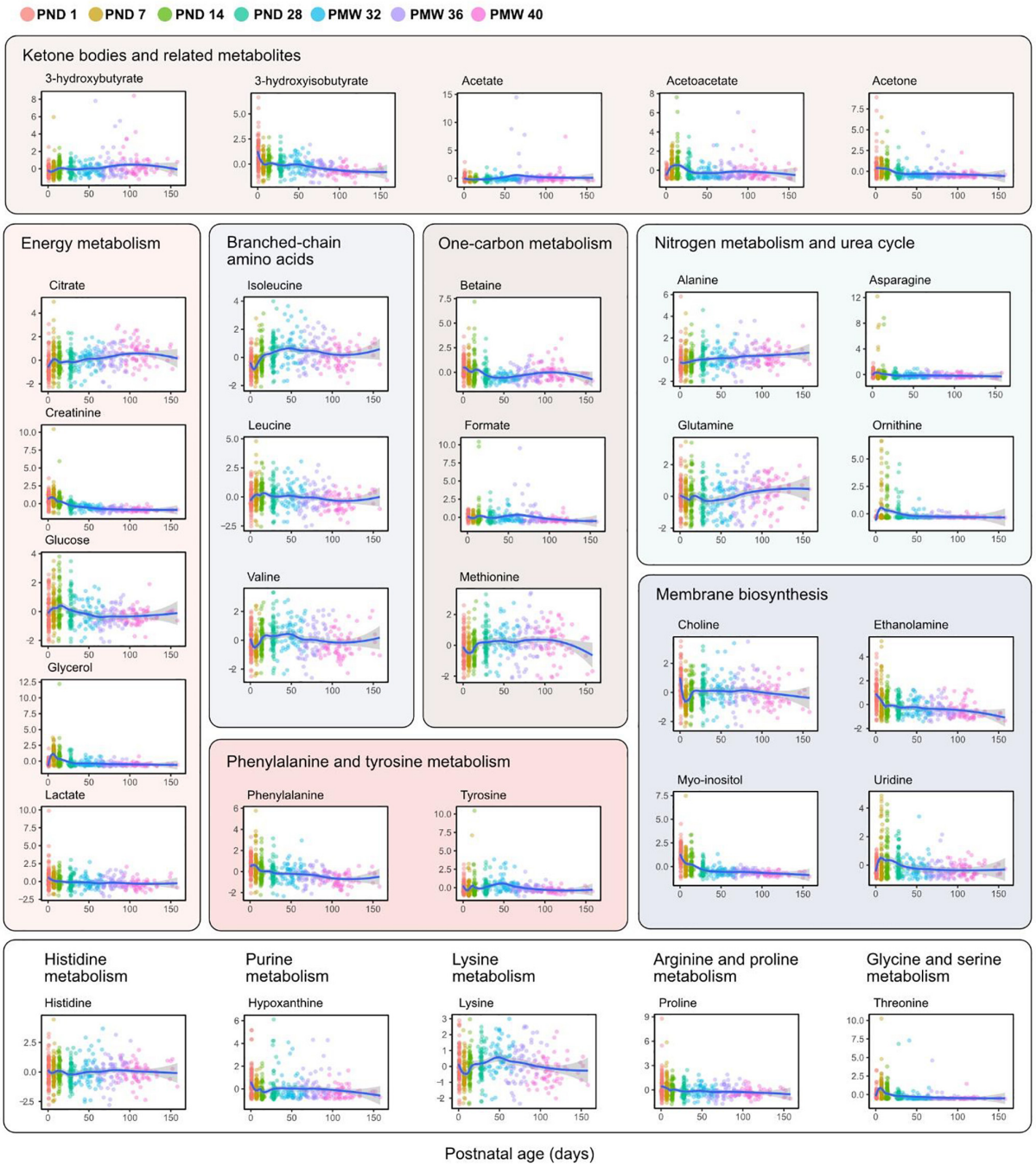

FIGURE 4 | Metabolite levels over postnatal age (days). Individual sample values are plotted and colored according to time point as indicated in the legend. Lines represent smoothed conditional means with 95% confidence intervals (shaded areas). *Y*-axis shows z-score normalized metabolite abundances.

in lower GAs, likely reflects a high intake of parenteral lipids and increased plasma lipid levels.

Serum myo-inositol and ethanolamine followed a similar decline after birth to reach plateau levels around PND 28. Both of these metabolites are essential components of membrane phospholipids. A postnatal decrease in myo-inositol is known to occur in preterm infants (Brion et al., 2021), and attempts have been made to restore myo-inositol levels to reduce morbidity, particularly respiratory distress syndrome and ROP (Hallman et al., 1992; Phelps et al., 2018). However, a recent systematic review concluded that myo-inositol supplementation to preterm infants did not reduce adverse outcomes (Howlett et al., 2019). To the best of our knowledge, decreasing serum levels of ethanolamine following extremely preterm birth has

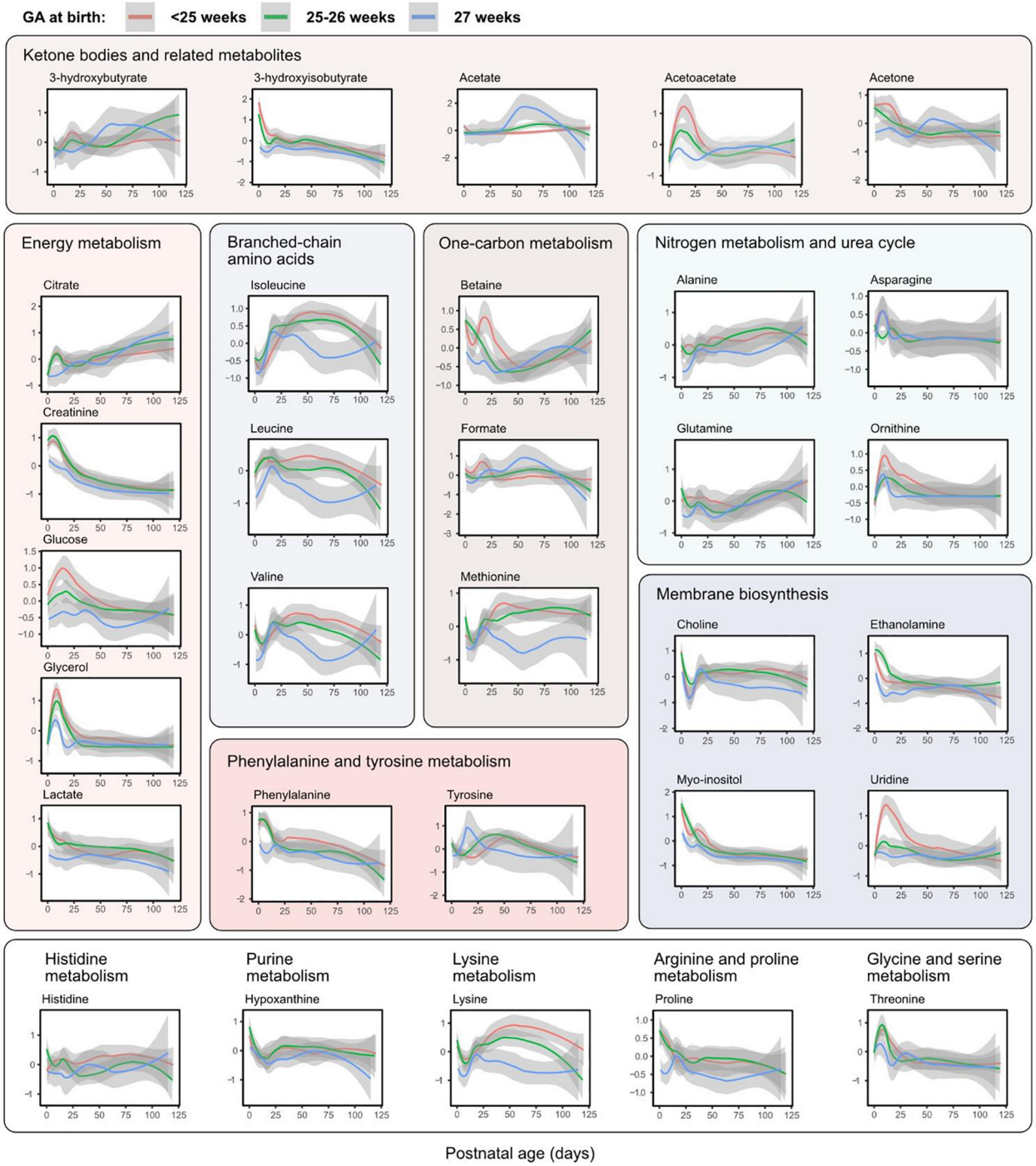

FIGURE 5 | Metabolite levels over postnatal age (days) by gestational age (GA) group. Accordingly to the legend, metabolite levels were stratified by GA at birth. Lines represent smoothed conditional means with 95% confidence intervals (shaded areas). Means are only shown up to day 120 due to few samples in each group at later time points. Y-axis shows z-score normalized metabolite abundances.

not previously been reported, although urine metabolomics has identified ethanolamine to decline with postnatal age in full-term infants (Scalabre et al., 2017). Ethanolamine is a precursor for the synthesis of phosphatidylethanolamine and phosphatidylcholine, the two most abundant phospholipids in humans, and circulating ethanolamine can act as a growth factor to stimulate hepatocyte proliferation (Sasaki et al., 1997; Kume et al., 2006). The consequences of a postnatal

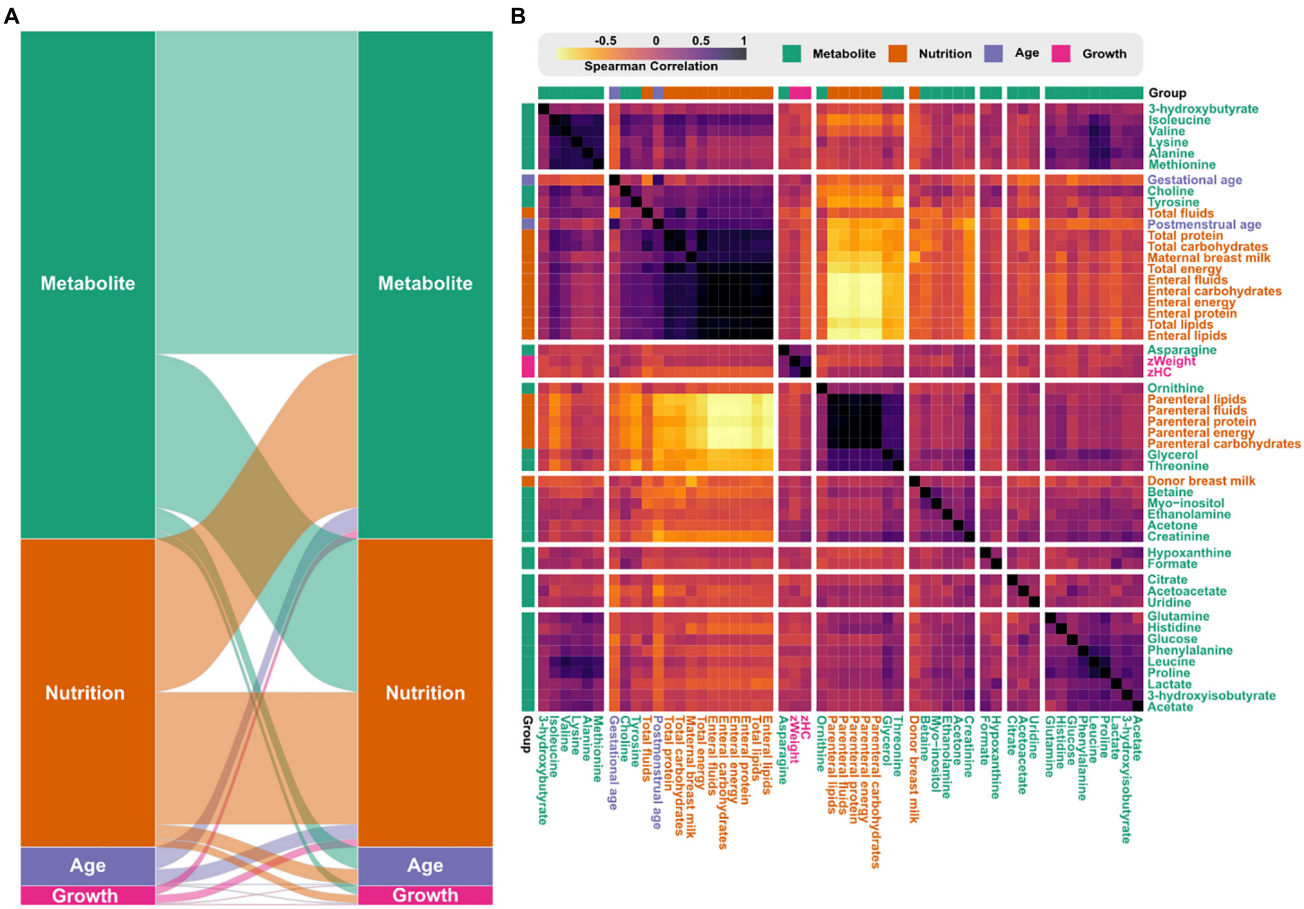

FIGURE 6 | Correlations between nutritional intake, growth, and the infant serum metabolome. **(A)** Flow diagram showing the correlations within and between variables groups based on Spearman correlations above 0.5. Link-width is proportional to the number of features correlating between the variable groups. **(B)** Heatmap with hierarchical clustering based on the pairwise Spearman correlations between variables. Color reflects the Spearman's rank correlation coefficient accordingly to the legend.

loss of serum ethanolamine in preterm infants warrant further research.

We correlated infant serum metabolites with growth parameters and nutritional data collected over the first 4 weeks of infant life. Choline, a compound involved in one-carbon metabolism and phospholipid synthesis, correlated positively with enteral nutrition. Choline is not present in PN solutions, and we previously reported that high parenteral intake is associated with lower infant serum choline (Nilsson et al., 2020). Somewhat surprisingly, the mean intake (ml/kg) of human donor and mother's own milk, respectively, were grouped into two separate clusters. This might reflect differences in the nutritional composition between mother's own milk and donor milk [reviewed in Hård et al. (2019)], or reflect that the two types of milk are used to different extents during the neonatal period. The strongest (positive) association for z-score weight and head circumference was with asparagine. Other studies have identified metabolites, included asparagine, to be associated with poor extrauterine growth in preterm infants (Dudzik et al., 2020; Wang et al., 2020). Both of these studies found higher asparagine levels in well-grown infants compared to infants with extrauterine growth restriction, which matches our data.

Detailed analysis of the relationship between nutrition and metabolites revealed that a majority of the analyzed amino acids in serum were negatively correlated with enteral energy intake (i.e., positively related to parenteral nutrition intake). This finding is expected and in line with previous reports showing an increase in infant blood amino acids after parenteral administration of amino acids (Clark et al., 2007; Blanco et al., 2011). Furthermore, glucose and glycerol levels were similarly related to parenteral nutrition intake, likely reflecting glucose and parenteral lipid administration.

Previous efforts have been made to detect disturbances in metabolic pathways relating to ROP and BPD development. However, the results of these studies have not been conclusive; for studies on ROP, differences likely relate to clinical characteristics of the subjects, timing of sample collection, and analysis platform (Yang et al., 2020; Zhou et al., 2020). In an animal model for ROP, oxygen-induced retinopathy, arginine and proline pathways were identified to be dysregulated and proposed as biomarkers

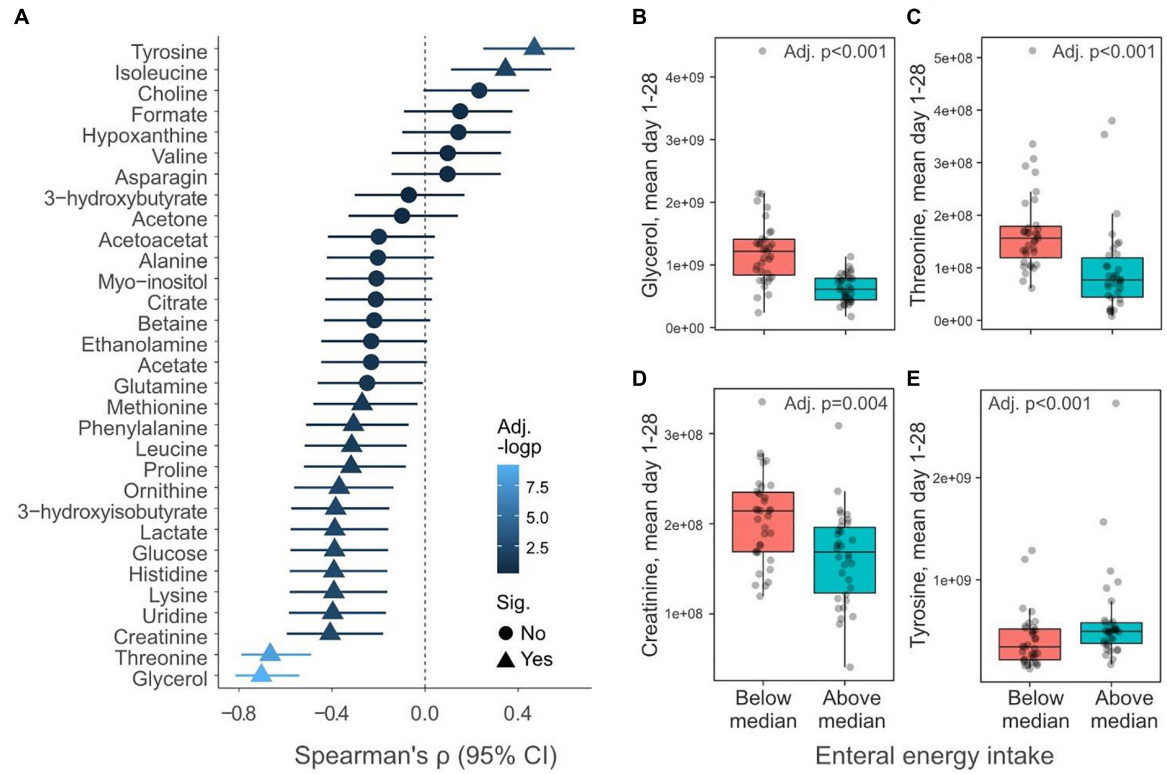

FIGURE 7 | Relationship between enteral nutrition and serum metabolites. **(A)** Spearman correlation (95% confidence interval) between energy provided as enteral nutrition day 1–28 and mean daily metabolite levels during the corresponding period ($n = 69$). Triangles indicate metabolites that significantly ($p < 0.05$) correlate with enteral energy intake and the color of the symbols reflect the negative logarithm of the p-value. **(B–E)** Boxplots show mean daily levels of selected metabolites that depend on the total energy provided as enteral energy. Infants have been dichotomously grouped if they received above ($n = 34$) or below ($n = 35$) the median amount of total energy as enteral energy day 1–28. Y-axis shows normalized NMR signal. p-values have been false discovery rate adjusted using the Benjamini–Hochberg method.

for human ROP (Paris et al., 2016; Lu et al., 2020). Blood, urine, and tracheal aspirate have been used as matrixes in search of metabolites relating to BPD (La Frano et al., 2018; Lal et al., 2018; Pintus et al., 2018; Piersigilli et al., 2019). As for ROP, the results from these studies have been inconclusive and several unrelated groups of metabolites have been pointed out as indicative for BPD development. We compared mean daily metabolite levels in the first 4 weeks of life with later development of severe ROP or BPD. While our analysis failed to identify metabolites related to ROP or BPD that could withstand false discovery rate correction, 10 of the analyzed metabolites were significantly associated with ROP outcome and three metabolites with BPD outcome before multiple testing corrections. We believe that these metabolites merit further discussion for hypothesis generation, keeping in mind the apparent risk of statistical Type 1 errors. There was considerable overlap between metabolites related to ROP outcome and enteral energy intake; metabolites associated with severe ROP tended to be negatively associated with enteral energy intake (3-hydroxyisobutyrate, glucose, glycerol, lactate, lysine, myoinositol, phenylalanine, and uridine). Moreover, several metabolites related to GA at PND 1 were also associated with severe ROP outcome (3-hydroxyisobutyrate, acetoacetate, glucose, lactate, and phenylalanine). We interpret this as a reflection of high parenteral nutrition intake as well as low GA in infants who develop severe ROP. Low energy intake *per se* in the 1st weeks of life is a known risk factor for ROP (Stoltz Sjöström et al., 2016; Klevebro et al., 2019). Metabolites associated with BPD severity (before adjusting for multiple testing) overlapped with those associated with ROP severity and included glucose, lactate, and uridine. In line with these results, severe BPD and severe ROP have been reported to be significantly related after adjustment for GA and other confounders (Podraza et al., 2018; Singh et al., 2019), and the two diseases share several pathogenic factors (Stark et al., 2018). As no metabolite was found to be significantly associated with ROP or BPD after correcting for multiple testing, we did not proceed to adjust for GA, nutritional intake, or other known confounders in our analyses. GA and parenteral nutrition are intimately linked: the transition to full enteral feeding proceeds slower in infants born at low GA. Thus, it is challenging to disentangle metabolomic alterations related to preterm disease and those that reflect GA-related nutritional management.

There are limitations to our study. Serum samples used in this study were subjected to one or a few freeze-thaw cycles before analysis, which is a known factor to impact the metabolome (Pinto et al., 2014). However, intra-individual

differences in metabolic profiles have been reported to be smaller than inter-individual differences, i.e., the variability between infants is more extensive than can be expected due to sample handling (Hirayama et al., 2015). Further, although we used an untargeted metabolomics approach, NMR analysis primarily identifies compounds in the micromolar range, introducing a bias to the type of metabolites that are quantified. Finally, this study included a limited number of infants, and larger prospective studies are needed to elucidate the intricate relationships between the metabolome, environmental factors, and prematurity-related disorders. One of the strengths of this study lies in its longitudinal design. Few, if any, studies have previously followed the metabolome of preterm infants over the neonatal period with comparable high temporal resolution.

CONCLUSION

We provide a comprehensive view of the evolution of the serum metabolome of extremely preterm infants from birth to term equivalent age. There was large interindividual variability in the metabolome that was partly explained by the GA at birth and by the amount of enteral and parenteral nutrition the infant received. The results from our and other studies imply that there is not a single metabolic biomarker that could satisfactorily distinguish those infants who are at the highest risk to develop ROP or BPD. Instead, enhanced diagnosis of ROP and BPD must likely rely on integrative and multiparameter biosignatures that encompass the complexity of these diseases.

DATA AVAILABILITY STATEMENT

The original contributions presented in the study are included in the article/**Supplementary Material**, further inquiries can be directed to the corresponding author.

ETHICS STATEMENT

The studies involving human participants were reviewed and approved by The Regional Ethical Review Board, Gothenburg. Written informed consent to participate in this study was provided by the participants' parents or legal guardians.

AUTHOR CONTRIBUTIONS

AN, GH, and AH contributed to the conception of the research. AP and DM contributed to the data acquisition. AN, AT, and DM contributed to the analysis of the data. AN drafted the manuscript. All authors critically revised the manuscript, agreed to be fully accountable for ensuring the integrity and accuracy of the work, read and approved the final manuscript, contributed to the design of the research, and contributed to the interpretation of the data.

FUNDING

This study was supported by grants provided by the Swedish Research Council (DNR# 2011–2432), Carmen och Bertil Regnérs Stiftelse för Forskning inom Ögonsjukdomar (DNR# 2016-00022), De blindas vänner foundation (DNR# 72/16), and Magnus Bergvalls Foundation (DNR# 2016-01492).

ACKNOWLEDGMENTS

The authors thank all participants and the study team led by Carola Pfeiffer–Mosesson.

SUPPLEMENTARY MATERIAL

The Supplementary Material for this article can be found online at: https://www.frontiersin.org/articles/10.3389/fnins.2022.830884/full#supplementary-material

REFERENCES

Blanco, C. L., Gong, A. K., Green, B. K., Falck, A., Schoolfield, J., and Liechty, E. A. (2011). Early changes in plasma amino acid concentrations during aggressive nutritional therapy in extremely low birth weight infants. *J. Pediatr.* 158, 543–548. doi: 10.1016/j.jpeds.2010.09.082

Brion, L. P., Phelps, D. L., Ward, R. M., Nolen, T. L., Hallman, N. M. K., Das, A., et al. (2021). Blood myo-inositol concentrations in preterm and term infants. *J. Perinatol.* 41, 247–254. doi: 10.1038/s41372-020-00799-5

Brosnan, J. T., Plumptre, L., Brosnan, M. E., Pongnopparat, T., Masih, S. P., Visentin, C. E., et al. (2019). Formate concentrations in maternal plasma during pregnancy and in cord blood in a cohort of pregnant Canadian women: relations to genetic polymorphisms and plasma metabolites. *Am. J. Clin. Nutr.* 110, 1131–1137. doi: 10.1093/ajcn/nqz152

Chisholm, J., Vincer, M., and Mitra, S. (2019). The association of postnatal growth velocity with retinopathy of prematurity and bronchopulmonary dysplasia in perterm infants: a population based retrospective cohort study. *Paediatr. Child Health* 24:e52. doi: 10.1093/pch/pxz066.132

Clark, R. H., Chace, D. H., and Spitzer, A. R. (2007). Effects of two different doses of amino acid supplementation on growth and blood amino acid levels in premature neonates admitted to the neonatal intensive care unit: a randomized, controlled trial. *Pediatrics* 120, 1286–1296. doi: 10.1542/peds.2007-0545

Clark, R. H., Kelleher, A. S., Chace, D. H., and Spitzer, A. R. (2014). Gestational Age and Age at Sampling Influence Metabolic Profiles in Premature Infants. *Pediatrics* 134, e37–46. doi: 10.1542/peds.2014-0329

Costeloe, L., Hennessy, E. M., Haider, S., Stacey, F., Marlow., N., and Draper, E. S. (2012). Short term outcomes after extreme preterm birth in England: comparison of two birth cohorts in 1995 and 2006 (the EPICure studies). *Br. Med. J.* 345:e7976. doi: 10.1136/bmj.e7976

Danielsson, H., Tebani, A., Zhong, W., Fagerberg, L., Brusselaers, N., Hård, A.-L., et al. (2021). Blood protein profiles related to preterm birth and retinopathy of prematurity. *Pediatr. Res.* [Epub online ahead of print]. doi: 10.1038/s41390-021-01528-0

Dudzik, D., Platas, I., Renau, M., Esponera, C., del, B., Hurtado de Mendoza, et al. (2020). Plasma Metabolome Alterations Associated with Extrauterine Growth Restriction. *Nutrients* 12:1188. doi: 10.3390/nu12041188

Ernst, M., Rogers, S., Lausten-Thomsen, U., Björkbom, A., Laursen, S. S., Courraud, J., et al. (2020). Gestational age-dependent development of the neonatal metabolome. *Pediatr. Res.* 89, 1396–1404. doi: 10.1038/s41390-020-01149-z

Fanos, V., Pintus, R., and Dessì, A. (2018). Clinical Metabolomics in Neonatology: from Metabolites to Diseases. *Neonatology* 113, 406–413. doi: 10.1159/000487620

Hallman, M., Bry, K., Hoppu, K., Lappi, M., and Pohjavuori, M. (1992). Inositol supplementation in premature infants with respiratory distress syndrome. *N. Engl. J. Med.* 326, 1233–1239. doi: 10.1056/NEJM199205073261901

Hård, A. L., Nilsson, A. K., Lund, A. M., Hansen-Pupp, I., Smith, L. E. H., and Hellström, A. (2019). Review shows that donor milk does not promote the growth and development of preterm infants as well as maternal milk. *Acta Paediatr.* 108, 998–1007. doi: 10.1111/apa.14702

Hellström, A., Ley, D., Hansen-Pupp, I., Niklasson, A., Smith, L., Löfqvist, C., et al. (2010). New insights into the development of retinopathy of prematurity–importance of early weight gain. *Acta Paediatr.* 99, 502–508. doi: 10.1111/j.1651-2227.2009.01568.x

Hellström, A., Nilsson, A. K., Wackernagel, D., Pivodic, A., Vanpee, M., and Sjöbom, U. (2021). Effect of Enteral Lipid Supplement on Severe Retinopathy of Prematurity: A Randomized Clinical Trial. *JAMA Pediatrics* 175, 359–367. doi: 10.1001/jamapediatrics.2020.5653

Hellström, A., Smith, L. E., and Dammann, O. (2013). Retinopathy of prematurity. *Lancet* 382, 1445–1457.

Hirayama, A., Sugimoto, M., Suzuki, A., Hatakeyama, Y., Enomoto, A., Harada, S., et al. (2015). Effects of processing and storage conditions on charged metabolomic profiles in blood. *Electrophoresis* 36, 2148–2155. doi: 10.1002/elps.201400600

Howlett, A., Ohlsson, A., and Plakkal, N. (2019). Inositol in preterm infants at risk for or having respiratory distress syndrome. *Cochrane Database Syst. Rev.* 7:Cd000366.

Kaufman, L., and Rousseeuw, P. J. (2009). *Finding Groups in Data: An Introduction to Cluster Analysis*. New Jersey, NJ: John Wiley & Sons.

Klevebro, S., Westin, V., Stoltz Sjöström, E., Norman, M., Domellöf, M., dstedt Bonamy, A. K. E., et al. (2019). Early energy and protein intakes and associations with growth, BPD, and ROP in extremely preterm infants. *Clin. Nutr.* 38, 1289–1295. doi: 10.1016/j.clnu.2018.05.012

Kume, H., Sasaki, H., and Kano-Sueoka, T. (2006). Serum ethanolamine and hepatocyte proliferation in perinatal and partially hepatectomized rats. *Life Sci.* 79, 1764–1772. doi: 10.1016/j.lfs.2006.06.036

La Frano, M. R., Fahrmann, J. F., Grapov, D., Pedersen, T. L., Newman, J. W., Fiehn, O., et al. (2018). Umbilical cord blood metabolomics reveal distinct signatures of dyslipidemia prior to bronchopulmonary dysplasia and pulmonary hypertension. *Am. J. Physiol. Lung Cell Mol. Physiol.* 315, L870–L881. doi: 10.1152/ajplung.00283.2017

Lal, C. V., Kandasamy, J., Dolma, K., Ramani, M., Kumar, R., Wilson, L., et al. (2018). Early airway microbial metagenomic and metabolomic signatures are associated with development of severe bronchopulmonary dysplasia. *Am. J. Physiol. Lung Cell Mol. Physiol.* 315, L810–L815. doi: 10.1152/ajplung.00085.2018

Löfqvist, C. A., Najm, S., Hellgren, G., Engström, E., Sävman, K., and Nilsson, A. K. (2018). Association of Retinopathy of Prematurity With Low Levels of Arachidonic Acid: A Secondary Analysis of a Randomized Clinical Trial. *JAMA Ophthalmol.* 136, 271–277. doi: 10.1001/jamaophthalmol.2017.6658

Lu, F., Liu, Y., Guo, Y., Gao, Y., Piao, Y., Tan, S., et al. (2020). Metabolomic changes of blood plasma associated with two phases of rat OIR. *Exp. Eye Res.* 190:107855. doi: 10.1016/j.exer.2019.107855

Lund, A. M., Löfqvist, C., Pivodic, A., Lundgren, P., Hård, A. L., Hellström, A., et al. (2020). Unpasteurised maternal breast milk is positively associated with growth outcomes in extremely preterm infants. *Acta Paediatr.* 109, 1138–1147. doi: 10.1111/apa.15102

Mathewson, K. J., Chow, C. H. T., Dobson, K. G., Pope, E. I., Schmidt, L. A., and Van Lieshout, R. J. (2017). Mental health of extremely low birth weight survivors: A systematic review and meta-analysis. *Psychol. Bull.* 143, 347–383. doi: 10.1037/bul0000091

Murtagh, F., and Legendre, P. (2014). Ward's Hierarchical Agglomerative Clustering Method: Which Algorithms Implement Ward's Criterion? *J. Classif.* 31, 274–295. doi: 10.1007/s00357-014-9161-z

Najm, S., Löfqvist, C., Hellgren, G., Engström, E., Lundgren, P., Hård, A.-L., et al. (2017). Effects of a lipid emulsion containing fish oil on polyunsaturated fatty acid profiles, growth and morbidities in extremely premature infants: A randomized controlled trial. *Clin. Nutr. ESPEN* 20, 17–23. doi: 10.1016/j.clnesp.2017.04.004

Niklasson, A., and Albertsson-Wikland, K. (2008). Continuous growth reference from 24th week of gestation to 24 months by gender. *BMC Pediatr.* 8:8. doi: 10.1186/1471-2431-8-8

Nilsson, A. K., Pedersen, A., Malmodin, D., Lund, A. M., Hellgren, G., Löfqvist, C., et al. (2020). Serum choline in extremely preterm infants declines with increasing parenteral nutrition. *Eur. J. Nutr.* 60, 1081–1089. doi: 10.1007/s00394-020-02312-2

Norman, M., Hallberg, B., Abrahamsson, T., Bjorklund, L. J., Domellof, M., Farooqi, A., et al. (2019). Association Between Year of Birth and 1-Year Survival Among Extremely Preterm Infants in Sweden During 2004-2007 and 2014-2016. *JAMA* 321, 1188–1199. doi: 10.1001/jama.2019.2021

Paris, L. P., Johnson, C. H., Aguilar, E., Usui, Y., Cho, K., Hoang, L. T., et al. (2016). Siuzdak, and M. Friedlander, Global metabolomics reveals metabolic dysregulation in ischemic retinopathy. *Metabolomics* 12:15. doi: 10.1007/s11306-015-0877-5

Pascal, A., Govaert, P., Oostra, A., Naulaers, G., Ortibus, E., and Van den Broeck, C. (2018). Neurodevelopmental outcome in very preterm and very-low-birthweight infants born over the past decade: a meta-analytic review. *Dev. Med. Child Neurol.* 60, 342–355. doi: 10.1111/dmcn.13675

Paterson, P., Sheath, J., Taft, P., and Wood, C. (1967). Maternal and foetal ketone concentrations in plasma and urine. *Lancet* 289, 862–865. doi: 10.1016/s0140-6736(67)91426-2

Phelps, D. L., Watterberg, K. L., Nolen, T. L., Cole, C. A., Cotten, C. M., Oh, W., et al. (2018). , Effects of Myo-inositol on Type 1 Retinopathy of Prematurity Among Preterm Infants < 28 Weeks'. *JAMA* 320, 1649–1658. doi: 10.1001/jama.2018.14996

Piersigilli, F., Lam, T. T., Vernocchi, P., Quagliariello, A., Putignani, L., Aghai, Z. H., et al. (2019). Identification of new biomarkers of bronchopulmonary dysplasia using metabolomics. *Metabolomics* 15:20. doi: 10.1007/s11306-019-1482-9

Pinto, J., Domingues, M. R., Galhano, E., Pita, C., Almeida Mdo, C. I, Carreira, M., et al. (2014). Human plasma stability during handling and storage: impact on NMR metabolomics. *Analyst* 139, 1168–1177. doi: 10.1039/c3an02188b

Pintus, M. C., Lussu, M., Dessì, R. Pintus, Noto, A., Masile, V., Marcialis, M. A., et al. (2018). Urinary (1)H-NMR Metabolomics in the First Week of Life Can Anticipate BPD Diagnosis. *Oxid. Med. Cell. Longev.* 2018:7620671. doi: 10.1155/2018/7620671

Podraza, W., Michalczuk, B., Jezierska, K., Domek, H., Kordek, A., Łoniewska, B., et al. (2018). Correlation of Retinopathy of Prematurity with Bronchopulmonary Dysplasia. *Open Med.* 13, 67–73. doi: 10.1515/med-2018-0012

Power, V. A., Spittle, A. J., Lee, K. J., Anderson, P. J., Thompson, D. K., Doyle, L. W., et al. (2019). Nutrition, Growth, Brain Volume, and Neurodevelopment in Very Preterm Children. *J. Pediatr.* 215, 50–55. doi: 10.1016/j.jpeds.2019.08.031

Roggero, P., Liotto, N., Menis, C., and Mosca, F. (2020). New Insights in Preterm Nutrition. *Nutrients* 12:1857. doi: 10.3390/nu12061857

Sasaki, H., Kume, H., Nemoto, A., Narisawa, S., and Takahashi, N. (1997). Ethanolamine modulates the rate of rat hepatocyte proliferation *in vitro* and *in vivo*. *Proc. Natl. Acad. Sci. U.S.A.* 94, 7320–7325.

Scalabre, A., Jobard, E., Demède, D., Gaillard, S., Pontoizeau, C., Mouriquand, P., et al. (2017). Evolution of Newborns' Urinary Metabolomic Profiles According to Age and Growth. *J. Proteome Res.* 16, 3732–3740. doi: 10.1021/acs.jproteome.7b00421

Siffel, C., Kistler, K. D., Lewis, J. F. M., and Sarda, S. P. (2021). Global incidence of bronchopulmonary dysplasia among extremely preterm infants: a systematic literature review. *J. Matern. Fetal Neonatal Med.* 34, 1721–1731. doi: 10.1080/14767058.2019.1646240

Singh, J. K., Wymore, E. M., Wagner, B. D., Thevarajah, T. S., Jung, J. L., Kinsella, J. P., et al. (2019). Relationship between severe bronchopulmonary dysplasia and severe retinopathy of prematurity in premature newborns. *J. Am. Assoc. Pediatr. Ophthalmol. Strab.* 23, e1–e209. doi: 10.1016/j.jaapos.2019.02.008

Stark, A., Dammann, C., Nielsen, H. C., and Volpe, M. V. (2018). A Pathogenic Relationship of Bronchopulmonary Dysplasia and Retinopathy of Prematurity? A Review of Angiogenic Mediators in Both Diseases. *Front. Pediatr.* 6, 125–125. doi: 10.3389/fped.2018.00125

Stoll, B. J., Hansen, N. I., Bell, E. F., Shankaran, S., Laptook, A. R., and Walsh, M. C. (2010). Neonatal outcomes of extremely preterm infants from the NICHD Neonatal Research Network. *Pediatrics* 126, 443–456. doi: 10.1542/peds.2009-2959

Stoltz Sjöström, E., Lundgren, P. I, Öhlund, G., Holmström, A., and Domellöf, M. (2016). Low energy intake during the first 4 weeks of life increases the risk for severe retinopathy of prematurity in extremely preterm infants. *Arch. Dis. Child. Fetal Neonatal Ed.* 101, F108–F113. doi: 10.1136/archdischild-2014-306816

The International Classification of Retinopathy of Prematurity (2005). International Committee for the Classification of Retinopathy of Prematurity. *Arch. Ophthalmol.* 123, 991–999.

Twilhaar, E. S., Wade, R. M., de Kieviet, J. F., van Goudoever, J. B., van Elburg, R. M., and Oosterlaan, J. (2018). Cognitive Outcomes of Children Born Extremely or Very Preterm Since the 1990s and Associated Risk Factors: A Meta-analysis and Meta-regression. *JAMA Pediatrics* 172, 361–367. doi: 10.1001/jamapediatrics.2017.5323

Wang, L., Liu, D., Shen, H., Wang, Y., Han, L., and He, Z. (2020). Analysis of Amino Acid Patterns With Nutrition Regimens in Preterm Infants With Extrauterine Growth Retardation. *Front. Pediatr.* 8:184.

Washburn, S. E., Caudill, M. A., Malysheva, O., MacFarlane, A. J., Behan, N. A., Harnett, B., et al. (2015). Formate metabolism in fetal and neonatal sheep. *Am. J. Physiol. Endocrinol. Metab.* 308, E921–E927. doi: 10.1152/ajpendo.00046.2015

Wilson, K., Hawken, S., Ducharme, R., Potter, B. K., Little, J., Thébaud, B., et al. (2014). Metabolomics of prematurity: analysis of patterns of amino acids, enzymes, and endocrine markers by categories of gestational age. *Pediatr. Res.* 75, 367–373. doi: 10.1038/pr.2013.212

Wishart, D. S., Feunang, Y. D., Marcu, A., Guo, A. C., Liang, K., Vazquez-Fresno, R., et al. (2018). HMDB 4.0: the human metabolome database for 2018. *Nucleic Acids Res.* 46, D608–D617. doi: 10.1093/nar/gkx1089

Yang, Y., Wu, Z., Li, S., Yang, M., Xiao, X., Lian, C., et al. (2020). Targeted Blood Metabolomic Study on Retinopathy of Prematurity. *Invest. Ophthalmol. Vis. Sci.* 61:12. doi: 10.1167/iovs.61.2.12

Zhou, Y., Xu, Y., Zhang, X., Zhao, P., Gong, X., He, M., et al. (2020). Plasma metabolites in treatment-requiring retinopathy of prematurity: Potential biomarkers identified by metabolomics. *Exp. Eye Res.* 199:108198. doi: 10.1016/j.exer.2020.108198

Conflict of Interest: The authors declare that the research was conducted in the absence of any commercial or financial relationships that could be construed as a potential conflict of interest.

Publisher's Note: All claims expressed in this article are solely those of the authors and do not necessarily represent those of their affiliated organizations, or those of the publisher, the editors and the reviewers. Any product that may be evaluated in this article, or claim that may be made by its manufacturer, is not guaranteed or endorsed by the publisher.

frontiers in Neuroscience

ORIGINAL RESEARCH
published: 25 February 2022
doi: 10.3389/fnins.2022.799739

Anti-inflammatory α-Melanocyte-Stimulating Hormone Protects Retina After Ischemia/Reperfusion Injury in Type I Diabetes

*Rajesh Kumar Goit[1], Andrew W. Taylor[2] and Amy C. Y. Lo[1]**

[1] Department of Ophthalmology, Li Ka Shing Faculty of Medicine, The University of Hong Kong, Pokfulam, Hong Kong SAR, China, [2] Department of Ophthalmology, Boston University School of Medicine, Boston, MA, United States

Retinal ischemia/reperfusion (I/R) injury is a major cause of vision loss in many ocular diseases. Retinal I/R injury is common in diabetic retinopathy, which as a result of hyperglycemia damages the retina and can cause blindness if left untreated. Inflammation is a major contributing factor in the pathogenesis of I/R injury. α-Melanocyte-stimulating hormone (α-MSH) is an anti-inflammatory peptide hormone that has displayed protective effects against I/R-induced organ damages. Here, we aimed to investigate the protective role of α-MSH on I/R-induced diabetic retinal damage using hyperglycemic C57BL/6J $Ins2^{Akita/+}$ mice. Experimental I/R injury was induced by blocking the right middle cerebral artery (MCA) for 2 h followed by 2 h or 22 h of reperfusion using the intraluminal method. Since ophthalmic artery originates proximal to the origin of the MCA, the filament also blocked blood supply to the retina. Upon treatment with α-MSH at 1 h after ischemia and 1 h after reperfusion, animals displayed significant improvement in amplitudes of b-wave and oscillatory potentials during electroretinography. α-MSH also prevented I/R-induced histological alterations and inhibited the development of retinal swelling. Loss of retinal ganglion cells as well as oxidative stress were significantly attenuated in the α-MSH-treated retinae. Level of interleukin 10 was significantly increased after α-MSH treatment. Moreover, gene expression of glutamate aspartate transporter 1, monocarboxylate transporter (MCT) 1 and MCT-2 were significantly higher after α-MSH administration. In conclusion, α-MSH mitigates the severity of I/R-induced retinal damage under hyperglycemic condition. These beneficial effects of α-MSH may have important therapeutic implications against retinal I/R injury under hyperglycemic condition.

Keywords: retina, ischemia, reperfusion, diabetes, inflammation, oxidative stress

OPEN ACCESS

Edited by:
Henri Leinonen,
University of Eastern Finland, Finland

Reviewed by:
Emma Lessieur,
University of California, Irvine, United States
Silke Becker,
The University of Utah, United States

***Correspondence:**
Amy C. Y. Lo
amylo@hku.hk
orcid.org/0000-0003-4239-6851

Specialty section:
This article was submitted to Neurodegeneration, a section of the journal Frontiers in Neuroscience

Received: *22 October 2021*
Accepted: *19 January 2022*
Published: *25 February 2022*

Citation:
Goit RK, Taylor AW and Lo ACY (2022) Anti-inflammatory α-Melanocyte-Stimulating Hormone Protects Retina After Ischemia/Reperfusion Injury in Type I Diabetes. Front. Neurosci. 16:799739. doi: 10.3389/fnins.2022.799739

INTRODUCTION

Retinal ischemia is a major cause of vision loss and blindness, and is a common feature in various retinal disorders such as glaucoma, diabetic retinopathy (DR), central retinal artery (CRA), or vein occlusion, carotid artery disease, blood hyperviscosity, and retinopathy of prematurity (Osborne et al., 2004). Retinal ischemia leads to depletion of oxygen and glucose, and in turn causes glutamate

excitotoxicity, increase in intracellular calcium and disruption of blood-retinal barrier (BRB). However, the degree of retinal damage during ischemia depends on the severity and duration of the obstruction to blood flow (D'Onofrio and Koeberle, 2013). Although immediate reperfusion could attenuate the retinal damage, it results in leukocyte infiltration, inflammation and production of reactive oxygen species (ROS) that alter the retinal structure and function.

DR is a common microvascular complication of diabetes, and remains the leading cause of vision loss and blindness in the working adult population (Wang and Lo, 2018). In diabetes, hyperglycemia leads to biochemical and cellular changes that trigger production of ROS as well as inflammatory cytokines and chemokines. These mediators are major pathogenic factors causing retinal neuronal dysfunction, BRB breakdown and vascular leakage in early DR (Wang and Lo, 2018). Also, pericytes that line retinal capillaries are damaged due to sustained increase in PKCδ level, which are not reversed with return of normoglycemia (Geraldes et al., 2009). As a result, these changes can lead to localized areas of ischemia, edema, and angiogenesis, all of which can impair vision (Caldwell et al., 2003) through hemorrhage and tractional retinal detachment (Cai and Boulton, 2002). One of the current treatment options for DR is targeting vascular endothelial growth factor (VEGF), an angiogenic factor that is upregulated. However, some patients do not respond to anti-VEGF therapy (Antonetti et al., 2021). Also, anti-VEGF mediators can cause systemic complications due to their ability to enter systemic circulation (Simo and Hernandez, 2008). This demonstrates the need to develop new therapeutic approaches.

α-Melanocyte-stimulating hormone (α-MSH) is a tridecapeptide derived from the precursor hormone pro-opiomelanocortin (POMC). Mainly synthesized in the hypothalamus and the brain stem as well as in the pituitary gland, POMC-derived peptides have a wide range of actions such as energy homeostasis, steroidogenesis, pigmentation, thermoregulation, and anti-inflammation. Several studies showed that α-MSH has protective effects against ischemia/reperfusion (I/R) organ damages such as brain (Huh et al., 1997; Huang and Tatro, 2002; Aronsson et al., 2006; Chen et al., 2008; Savos et al., 2011; Goit et al., 2021), eye (Varga et al., 2013), heart (Vecsernyes et al., 2003), kidney (Chiao et al., 1997; Gong et al., 2004), and gut (Hassoun et al., 2002; Zou et al., 2003). Indeed, α-MSH counteracts retinal degeneration during early diabetes, and it alleviates the pro-inflammatory microenvironment caused by hyperglycemia in diabetic retina (Cai et al., 2018). Since individuals with type 1 diabetes have an increased risk of DR (Fong et al., 2004; Jansson et al., 2018), this study aimed to investigate the protective role of α-MSH on I/R-induced retinal damage upon hyperglycemia using type 1 diabetic mouse.

MATERIALS AND METHODS

Animal

Twelve to fifteen weeks old C57BL/6J $Ins2^{Akita/+}$ ($Ins2^{Akita/+}$) mice were used as a model of type 1 diabetes in the present study. Since disease progression in female $Ins2^{Akita/+}$ mice is slower and less uniform (Yoshioka et al., 1997) while estrogen exerts powerful neuroprotective actions during reproductive age following ischemic stroke in female mice (Brann et al., 2007; Suzuki et al., 2009), only male mice were included in this study. They were kept under standard laboratory conditions with 12 h light-dark cycle at the Centre for Comparative Medicine Research at The University of Hong Kong. All animal experiments followed the Cap. 340 Animals (Control of Experiments) Ordinance and Regulations and were approved by the Committee on the Use of Live Animals in Teaching and Research (CULATR 4837-18) at The University of Hong Kong.

One day before the experiment, blood glucose level was measured by Contour XT blood glucose meter (ELITE XL, Bayer HealthCare) and test strip (ELITE, Bayer HealthCare). Only mice with high blood glucose level (>20 mM) were included and randomly assigned to various experimental conditions. They were challenged with either sham operation or I/R injury with (i) 2 h of ischemia and 2 h of reperfusion or (ii) 2 h of ischemia and 22 h of reperfusion.

Animal Model of Retinal Ischemia and Reperfusion

Retinal I/R injury was achieved by blocking blood flow into the middle cerebral artery (MCA) as previously described (Lo et al., 2005, 2007; Li et al., 2009, 2011, 2012; Goit et al., 2021). Briefly, animals were anesthetized with 2% isoflurane in 70% N_2O and 30% O_2 for induction and 1–1.5% isoflurane in 70% N_2O and 30% O_2 for maintenance during surgery. MCA occlusion (MCAO) was induced on the right side with a monofilament suture (Johnson and Johnson, Belgium) coated with vinyl polysiloxane impression material (3 M Dental Products, United States). The suture was introduced into the external carotid artery (ECA) and moved forward into the internal carotid artery (ICA) until the tip of the filament occluded the opening of MCA. The blockage was considered successful when a drop of more than 70% of baseline signal measured by the laser Doppler flowmeter (PeriFlux System 5000, Sweden) was observed. Since the origin of the ophthalmic artery (OA) is proximal to the origin of the MCA (Smith et al., 2002), the filament also blocked blood supply to the retina. Once the blockage was confirmed, the animals were transferred to an intensive care unit where they recovered from anesthesia. They were re-anesthetized for the removal of the filament and thus allowing reperfusion. The sham-operated animals underwent MCA exposure without occlusion. The core temperature during the surgery was maintained approximately at 37°C using a heating pad as described (Goit et al., 2021).

α-Melanocyte-Stimulating Hormone Treatment

Animals were injected with 2, 10, 20, 50, 70, or 100 μg/mouse of α-MSH (Bachem AG, Switzerland) in phosphate-buffer saline (PBS) intraperitoneally at 1 h after ischemia and 1 h after reperfusion. Since α-MSH at 50 μg/mouse showed

neuroprotective effects in cerebral I/R injury (Goit et al., 2021), this dosage was later used to further evaluate its protective effects in the I/R induced retinal damage. PBS was injected as a vehicle.

Electroretinography

Mice were dark-adapted before electroretinography (ERG). For general anesthesia, the animal was injected intraperitoneally with a mixture of Ketamine and Xylazine (100 and 10 mg/kg body weight, respectively) in PBS. The pupil was locally anesthetized with 0.5% proparacaine hydrochloride (Alcon, Belgium) and dilated with 1% Mydriacyl (Alcon, Belgium). Gold wire electrodes (Diagnosys, United States) were placed on the apex of the cornea. A reference electrode (Chalgren, United States) was attached subcutaneously on the forehead and a ground electrode (Chalgren, United States) was placed subcutaneously at the tail region. Tears naturale II (Alcon, Belgium) was used to lubricate the eye during the recording. White flash of 3 (p)cd.s/m^2 and 10 (p)cd.s/m^2 intensities were delivered from the ColorDome Ganzfeld System (Diagnosys, United States). a-wave, b-wave, and the ascending phase of the b-wave (oscillatory potentials, OPs) were recorded using the Espion ERG Diagnosys and analyzed by Epsion V5 System (Diagnosys software) as previously reported (Li et al., 2012; Yang et al., 2017; Wang et al., 2020).

Tissue Collection

After ERG recording, the animal was sacrificed by intraperitoneal injection of pentobarbital. Right eyeball was immediately enucleated and fixed with 4% paraformaldehyde (PFA) overnight at 4°C for histological and immunohistochemical staining. For Western blot and quantitative polymerase chain reaction (qPCR) techniques, the retina was snap frozen in liquid nitrogen immediately after collection.

Histological Evaluation

4% PFA fixed eyeball was first dehydrated with graded series of ethanol and then immersed in chloroform; and finally embedded in paraffin. 5 μm thick sections were obtained using a microtome (Microm HM 315R, Germany). After deparaffinization and rehydration, sections containing the optic nerve head were stained with hematoxylin and eosin. Subsequently, sections were dehydrated and mounted with Permount™ (Thermo Fisher Scientific, United States). Image of the whole retinal section was taken under 20× magnification with a microscope (Eclipse 80i; Nikon, Japan) equipped with a digital camera (Diagnostic Instruments, Inc., United States) using Spot Advanced software (SPOT Imaging Solutions, United States). ImageJ was used to count the total number of retinal ganglion cell (RGC) in the ganglion cell layer (GCL) as well as to measure thickness of GCL, inner plexiform layer (IPL), inner nuclear layer (INL), outer plexiform layer (OPL), outer nuclear layer (ONL), and the whole retina. The central (150 μm from the optic nerve head) and the mid-peripheral (middle area between the optic nerve and the most peripheral part of the retina) regions of the retina were selected for thickness measurement. Cells with pyknotic nuclei in the GCL were excluded in the counting. Pyknotic cells were identified by the presence of condensed and darkly stained or sometimes fragmented nuclei (Perry et al., 1983).

Immunohistochemistry

After deparaffinization and rehydration of sections containing the optic nerve head, antigen retrieval was achieved by incubation with proteinase K. Sections were blocked with 2% normal goat serum followed by overnight incubation with primary antibodies against glial fibrillary acidic protein (GFAP 1:500; Cat# ZO33429-2, Dako, Denmark), protein kinase C alpha (PKCα 1:1,000; Cat# sc-208, Santa Cruz Biotechnology, United States), calretinin (1:1,000; Cat# sc-11644, Santa Cruz Biotechnology, United States), and glutamine synthetase (GS 1:1,000; Cat# MAB302, Millipore, Germany). Subsequently, sections were incubated with the corresponding secondary antibodies (1:500; Molecular Probes, Invitrogen Corporation, United States) followed by incubation with 4′,6-diamidino-2-phenylindole (DAPI) and mounted for macroscopic analysis.

For DAB (3,3′-Diaminobenzidine) staining, 3% hydrogen peroxide was used to block endogenous peroxidase activity in sections after deparaffinization and rehydration. 10 mM sodium citrate was then used for antigen retrieval. Sections were blocked with 2% normal goat serum followed by overnight incubation with primary antibodies against poly-ADP-ribose (PAR 1:200; Cat# BML-SA216-0100, Enzo Life Sciences, United States) and nitrotyrosine (NT 1:200; Cat # 05-233, Merck KGaA, Germany). Subsequently, sections were incubated with the corresponding biotinylated secondary antibody (Vector Laboratories, United States) and avidin-biotin peroxidase complex (Vector Laboratories, United States). The immunoreactivity was developed with stable DAB (Invitrogen, United States) to generate the dark-brown color. After counterstaining with hematoxylin, sections were dehydrated and mounted for macroscopic analysis.

The immunohistochemical staining for each target antigen was performed in a single round including retinal sections from all experimental groups. The sections were then randomly coded and examined in a blinded approach. Photomicrographs were captured under 20× magnification. They were analyzed and scored according to the immunoreactivity intensity and distribution ranging from score 1 (absent or weak expression) to score 5 (strong expression) as previously reported (Li et al., 2009, 2011, 2012; Fu et al., 2012, 2015, 2017; Yang et al., 2017).

Western Blot

Retinal tissue lysates were obtained from snap frozen retina using the radio immunoprecipitation assay buffer. Total protein concentration of the sample was determined by bicinchoninic acid (BCA) protein assay (Thermo Fisher Scientific™ Pierce™ BCA Protein Assay Kit, Thermo Fisher, United States) using bovine serum albumin (Bio-Rad, United States) as a protein standard. Proteins were separated with SDS-PAGE and transferred to a polyvinylidene difluoride membrane (Merck KGaA, Germany). After blocking in 5% skim milk in TBST (Tris-buffered saline, 0.1% Tween 20), the membrane was incubated overnight at 4°C with primary antibodies against interleukin 10 (IL-10 1:1,000; Cat# sc-1783, Santa Cruz Biotechnology, United States) and B-cell lymphoma

2 (Bcl-2 1:1,000; Cat# 2876, Cell Signaling Technology, United States). Glyceraldehyde 3-phosphate dehydrogenase (GAPDH 1:1,000; Cat# sc-32233, Santa Cruz Biotechnology, United States) was used as an internal loading reference. After incubation with the corresponding horseradish peroxidase-labeled secondary antibody (Vector Laboratories, United States), protein bands on the membrane were detected by enhanced chemiluminescence using the ChemiDoc MP Imaging System (Bio-Rad Laboratories, Inc., United States). The intensities of bands were quantified with ImageJ.

Quantitative Polymerase Chain Reaction

RNA from snap frozen retina was extracted using TRIzol reagent (Invitrogen, United States). The concentration and quality of RNA were measured using a spectrophotometer (Hitachi Photodiode Array Bio-spectrophotometer U-0080D, Japan). Subsequently, 1 μg of total RNA was used as a template for cDNA synthesis using QunatiNova Reverse Transcription Kit (QIAGEN, Germany). cDNA equivalent to 50 ng of total RNA was subjected to qPCR using TB Green Master Mix (TaKaRa, Japan). The following sets of primers were used to determine the expression of glutamate and lactate related transporters in the retina: glutamate aspartate transporter (GLAST) 1 (Forward Primer 5′-GAATGGCGGCCCTAGATA GTA-3′; Reverse Primer 5′-CTTTCCGGGGTGGATGATGA-3′), monocarboxylate transporter (MCT) 1 (Forward Primer 5′-GGCTCCACTTAATCAGGCTTT-3′; Reverse Primer 5′-CAGGCCCTATTGGTCTCATCA-3′) and MCT-2 (Forward Primer 5′-GGGCTGGGTCGTAGTCTGT-3′; Reverse Primer 5′-ATCCAAGCGATCTGACTGGAG-3′). Beta-actin (Forward Primer 5′-GGCTGTATTCCCCTCCATCG-3′; Reverse Primer 5′-CCAGTTGGTAACAATGCCATGT-3′) was used as an internal reference. Each sample was tested in triplicate. The relative difference was expressed as the x-fold change of α-MSH-treated samples over vehicle-treated samples using the $2^{-\Delta\Delta CT}$ method.

Statistical Analysis

IBM SPSS Statistics Version 26 was used for statistical analysis. One-way ANOVA followed by Dunnett test was used to compare b-wave amplitude in ERG measurement. One-way ANOVA followed by Tukey's test was used to compare retinal layer thickness, RGC count and OPs. Immunoreactivity was compared using Mann-Whitney *U*-Test. Independent samples *t*-test was used to compare Western blot and qPCR results. The results are presented as mean ± standard deviation. $p < 0.05$ was considered statistically significant.

RESULTS

α-Melanocyte-Stimulating Hormone Improved b-Wave Amplitude and Oscillatory Potentials After I/R Injury

The a-wave in ERG recording is associated with photoreceptors and the b-wave reflects the combined activity of depolarizing bipolar, amacrine, ganglion, and Müller cells (Kolb et al., 1995). In this study, the amplitude of a-wave was comparable between vehicle-treated animals and α-MSH-treated animals with/without retinal I/R injury (data not shown). However, retinal I/R injury resulted in significantly decreased b-wave amplitude in animals treated with vehicle when compared with sham-operated vehicle treated animals at 2 h of reperfusion. After retinal I/R injury, the amplitudes of b-wave were significantly higher in animals treated with 10, 20, 50, or 70 μg of α-MSH when compared with vehicle treatment (**Figures 1A,C**). At 22 h of reperfusion, a non-significant trend of decrease in b-wave amplitude was observed in vehicle-treated I/R injury animals when compared with vehicle-treated sham-operated animals (**Figure 1D**). More importantly, α-MSH treatment at 10, 20, or 50 μg significantly increased b-wave amplitudes when compared with vehicle treatment after I/R injury (**Figures 1B,D**). In addition, the b-wave amplitude in each experimental group appeared to be higher at 22 h of reperfusion when compared with that at 2 h of reperfusion (**Figures 1A–D**). In this study, the b-wave implicit times were also analyzed and compared; yet, no difference could be found among vehicle-treated and α-MSH-treated groups.

The OPs in ERG recording were calculated as the sum of the amplitudes of OP1, OP2, OP3, and OP4. After retinal I/R injury, they were significantly higher in animals treated with 50 μg of α-MSH compared with vehicle-treated animals at both 2 h and 22 h of reperfusion (**Figures 1E,F**). Animals treated with other doses of α-MSH did not yield significant improvements in OPs (data not shown).

α-Melanocyte-Stimulating Hormone Preserved Retinal Structure After I/R Injury

Fifty microgram/mouse of α-MSH had been shown to be neuroprotective in cerebral I/R injury (Goit et al., 2021). It also yielded beneficial effects in recovering b-wave amplitude and OPs in ERG measurements as describe above. Therefore, we further evaluated its protective effects in retinal damage at this dosage. Firstly, thickness of various retinal layers was measured in the central and the mid-peripheral parts of the retina from sham/MCAO-challenged animals with/without α-MSH treatment. In the central retina, thickness of individual layer was comparable among all experimental groups except that of GCL and total retinal at 2 h of reperfusion. The thickness of GCL and total retina was significantly higher in vehicle-treated I/R injury animals when compared with sham-operated vehicle control or I/R injury α-MSH treated animals (**Figures 2A–D,I**), suggesting the presence of retinal swelling after I/R injury in vehicle-treated animals. Thus, α-MSH treatment resulted in preservation of retinal morphology and protection from swelling after I/R injury. However, thicknesses of various retinal layers were comparable between groups after retinal I/R injury at 22 h of reperfusion (**Figures 2E–H,J**). Thickness measurement was also performed in the mid-peripheral retina but no significant differences could be observed at 2 h as well as 22 h of reperfusion (data not shown).

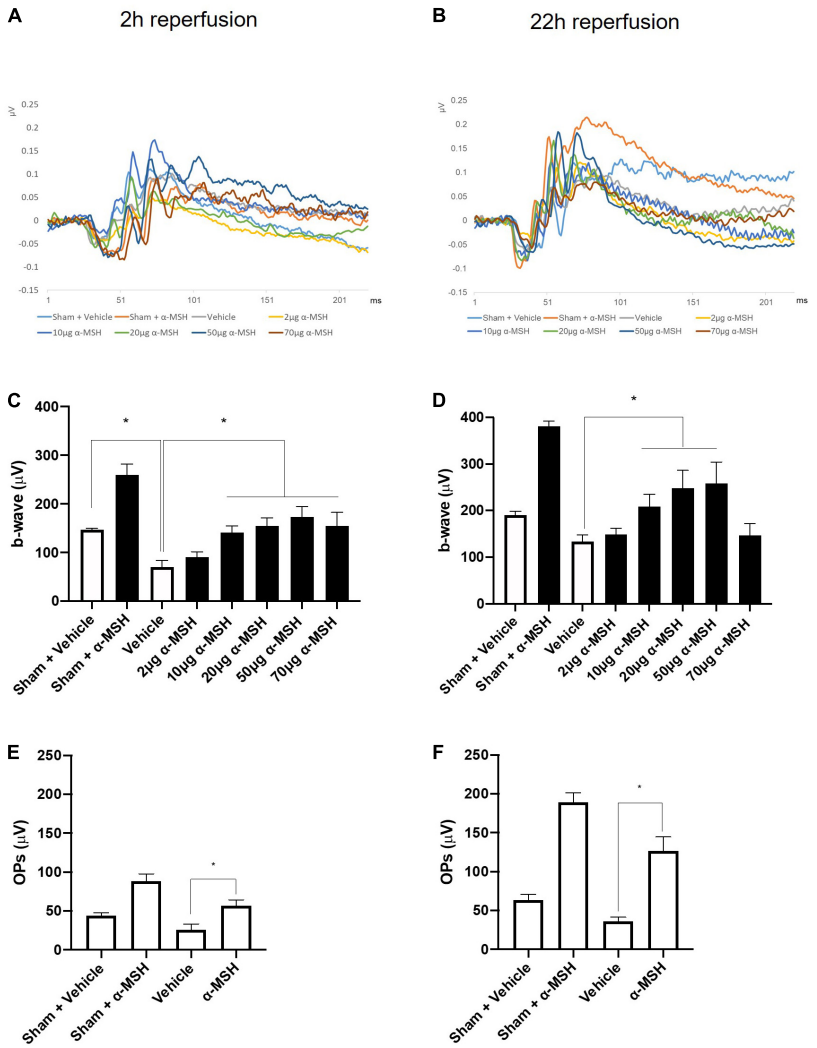

FIGURE 1 | α-MSH preserved the retinal function after I/R injury. **(A)** Representative ERG waves at 2 h of reperfusion. **(B)** Representative ERG waves at 22 h of reperfusion. **(C)** The amplitude of b-wave was significantly higher in animals treated with 10, 20, 50, and 70 μg of α-MSH at 2 h of reperfusion. **(D)** This amplitude was significantly higher in animals treated with 10, 20, and 50 μg of α-MSH at 22 h of reperfusion. One-way ANOVA followed by Dunnett test. **(E,F)** OPs were significantly higher in α-MSH (50 μg) treated animals in both experimental conditions. One-way ANOVA followed by Tukey's test. Flash 3 (P)cd.s/m^2. *$P < 0.05$, n = 5–6 for each group.

The number of viable RGC in GCL was counted. α-MSH treatment did not impose a change in RGC number with sham operation (**Figures 3A,B**). After I/R injury, the number of viable RGC was significantly decreased in vehicle-treated animals when compared with those in sham-operated animals at both 2 h and 22 h of reperfusion (**Figures 3A,B**). More importantly, α-MSH treatment significantly prevented decrease in the RGC count at both 2 h and 22 h of reperfusion, suggesting its ability in attenuating the damage upon retinal I/R injury.

Immunohistochemistry Analysis

The calcium binding protein calretinin is a known marker for amacrine cells in the retina (Fu et al., 2015). Normally, calretinin immunoreactivity can be observed in the INL and in three distinct strata in the IPL (**Figures 4A–D**). At 2 h of reperfusion, there was no difference in calretinin immunoreactivity between vehicle-treated and α-MSH-treated retinae (**Figures 4A,B,E**). However, higher calretinin expression was observed in α-MSH-treated animals at 22 h of reperfusion (**Figures 4C–E**). Meanwhile, PKC-α is abundantly expressed in retinal bipolar cells (Fu et al., 2015). There was a trend of increase in its expression in animals treated with α-MSH at 2 h of reperfusion (**Figures 4F,G,J**). However, this trend was not sustained at 22 h of reperfusion (**Figures 4H–J**).

Retinal glial activation was also assessed. GFAP, a well-known marker for astrocytes (Fu et al., 2015), was present mostly in the GCL. Its immunoreactivity was similar between vehicle-treated and α-MSH-treated groups in both experimental conditions (**Figures 4K–O**). Meanwhile, the expression of GS, a marker

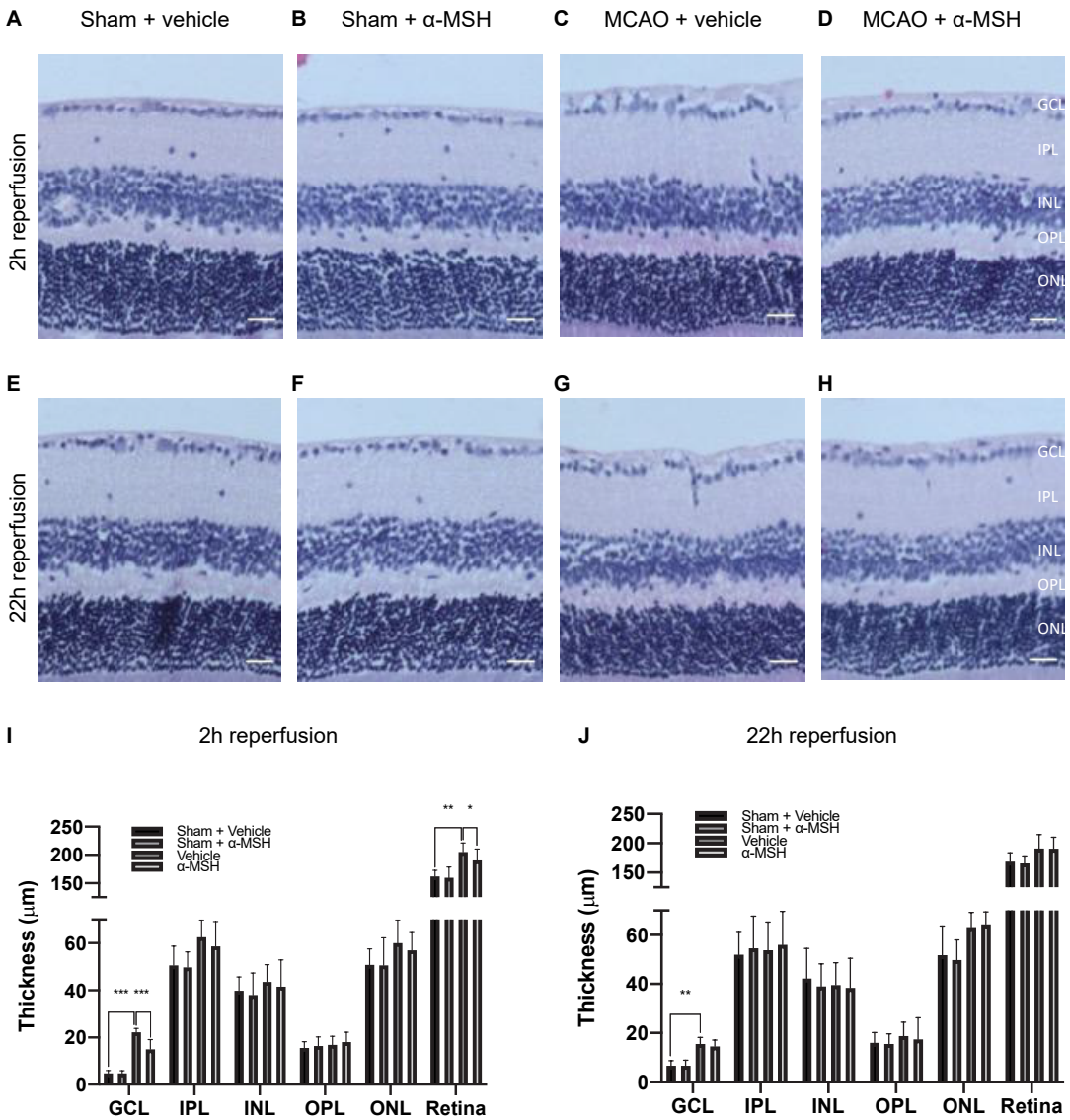

FIGURE 2 | α-MSH preserved morphological integrity of retina after I/R injury. **(A–D,I)** Thicknesses of GCL and total retina were significantly higher in animals treated with vehicle compared with α-MSH-treated animals or vehicle-treated sham animals at 2 h of reperfusion. **(E–H,J)** Only thickness of GCL was significantly higher in vehicle-treated animals compared to vehicle-treated sham animals at 22 h of reperfusion. $^{*}P < 0.05$, $^{**}P < 0.01$, $^{***}P < 0.001$, One-way ANOVA followed by Tukey's test, $n = 6$ for each group. Scale bar = 25 μm.

for Müller cells in the retina was also examined. At 2 h of reperfusion, GS expression appeared to be higher in vehicle-treated animals when compared with α-MSH-treated animals (**Figures 4P,Q,T**). GS level after vehicle treatment was decreased to a level similar to that in α-MSH-treated retinae at 22 h of reperfusion (**Figures 4R–T**).

Immunoreactivity of PAR, an indicator of nitric oxide-dependent DNA damage, was localized in the GCL and INL and was significantly higher in vehicle-treated animals compared with α-MSH-treated animals at 2 h of reperfusion (**Figures 5A,B,E**). Thus, α-MSH treatment was able to significantly decrease PAR immunoreactivity at 2 h of reperfusion. At 22 h of reperfusion, PAR immunoreactivity was comparable (**Figures 5C–E**). Immunoreactivity of NT, a marker of reactive nitrogen species-induced nitrative stress, showed a non-significant trend of decrease in animals treated with α-MSH when compared with vehicle-treated animals at 2 h as well as 22 h of reperfusion (**Figures 5F–J**).

α-Melanocyte-Stimulating Hormone Increased Expression of Anti-Inflammatory Protein After I/R Injury

The anti-inflammatory and anti-apoptotic properties of α-MSH was analyzed by Western blot. After I/R injury, IL-10 expression was significantly higher with α-MSH treatment at both 2 h

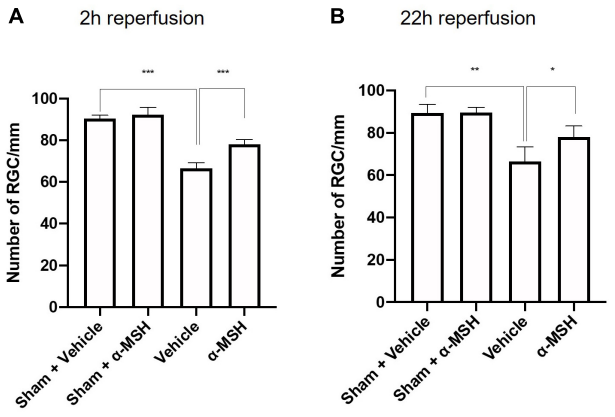

FIGURE 3 | α-MSH maintained the number of RGC in the GCL. **(A,B)** Significantly lower number of RGC was recorded in vehicle-treated animals compared with α-MSH-treated animals or vehicle-treated sham animals in both experimental conditions. $^{*}P < 0.05$, $^{**}P < 0.01$, $^{***}P < 0.001$, One-way ANOVA followed by Tukey's test, $n = 6$ for each group.

and 22 h of reperfusion (**Figures 6A,B**). On the other hand, expression of Bcl-2 was unchanged with/without α-MSH treatment in both experimental conditions (**Figures 6A,B**).

α-Melanocyte-Stimulating Hormone Increased Gene Expression of Glutamate and Lactate Transporters After I/R Injury

Glutamate release is a common phenomenon during/after ischemia. Glutamate uptake into Müller cells is a major mechanism in regulating extracellular glutamate concentration in the retina (Rauen et al., 1998). Therefore, the gene expression of GLAST-1, a glutamate transporter in Müller cells, was determined by qPCR. GLAST-1 gene expression was significantly increased in animals treated with α-MSH at 2 h of reperfusion but not 22 h of reperfusion (**Figure 7A**). Meanwhile, gene expressions of lactate transporters, MCT-1 and MCT-2, were also assessed. MCT-1 and MCT-2 gene expressions were significantly increased in animals treated with α-MSH at 22 h of reperfusion but not 2 h of reperfusion (**Figures 7B,C**).

DISCUSSION

Retinal ischemia induces a wide range of deleterious effects, including excitotoxicity, inflammation, and oxidative stress. These events finally contribute to the death of retinal neurons and several vision-threatening diseases. Similarly, DR is associated with reduced retinal blood flow, dysfunction of the retinal neurons, followed by breakdown of BRB and finally changes in visual function.

In the eye, α-MSH suppresses proinflammatory signals, promotes production of anti-inflammatory cytokines, transiently lowers intraocular pressure, protects neuronal cells from damage, and modulates immune response (Lee et al., 2009; Taylor and Lee, 2010; Clemson et al., 2017). Anti-oxidative and anti-apoptotic effects of α-MSH was also reported when it was administrated intravitreally in early DR (Zhang et al., 2014). Besides, this neuropeptide plays a role in inhibiting BRB breakdown and vascular leakage as well as improving electrophysiological functions and morphology of retina in early DR (Cai et al., 2018). More importantly, it has no known adverse effects (Clemson et al., 2017) and is already under clinical trial for advanced dry age-related macular degeneration (ClinicalTrials.gov, 2018). A melanocortin agonist, PL9643 as ophthalmic solution for subjects with dry eye is progressing into late-stage clinical trials after improvements in dry eye disease in a phase 2 study (ClinicalTrials.gov, 2020; Palatin, 2021). In addition, melanocortin receptor agonists are under investigation for their therapeutic potential in inflammatory ocular diseases such as non-infectious uveitis, DR, and diabetic macular edema (Palatin, 2021). All these results suggest the beneficial effects of α-MSH in DR. The microvascular changes in the diabetic retina often result in ischemia, after which retinal neurons die over a long period of time. Therefore, there is a possible therapeutic window to rescue these neurons destined to die (Antonetti et al., 2021). So, the possible protective role of α-MSH on I/R-induced retinal damage in type 1 diabetic mouse was investigated in this study.

The a-wave is considerably less affected by ischemia than the b-wave, and b-wave amplitude has been used as a quantitative marker of reduced retinal blood flow as well as experimental ischemic retinal injury despite normal retinal histology (Osborne et al., 2004). Among α-MSH-treated animals, b-wave amplitude was reduced in animals treated with either lower (2 μg) or higher (70 μg) concentrations of α-MSH. This suggests that α-MSH follows a bell-shaped dose-response curve (Holdeman and Lipton, 1985; Goit et al., 2021). The significantly decreased b-wave amplitude in vehicle-treated animals in both experimental conditions may be related to the level of GS expression proportional to the extracellular glutamate concentration (Shen et al., 2004), a sign of retinal stress and pathology (Bringmann et al., 2009). In darkness, photoreceptors release glutamate to activate receptors on bipolar and horizontal cells, and rapid clearance plus recycling of glutamate is critical for effective neurotransmission. In this study, animals were dark adapted before ERG recording; decreased b-wave amplitude in the vehicle-treated animals could be linked to a transient functional impairment of Müller cells in response to ischemia resulting in insufficient recycling of glutamate. High level of glutamate in the synaptic zones between photoreceptor cells and ON-bipolar cells saturates the glutamate receptors on the bipolar cells in darkness. This leads to a decline in the amplitude of b-wave in light (Winkler et al., 1999). Therefore, one possibility would be the inability of α-MSH to raise extracellular glutamate concentration to a level high enough to induce higher expression of GS. This may explain why reduced GS expression was observed with α-MSH treatment despite the beneficial effect of GS. Similarly, OPs indicate amacrine cells activity in the inner retina (Wachtmeister and Dowling, 1978) and OPs amplitude loss is a significant parameter of retinal ischemia (Jehle et al., 2008). Moreover, low expression of GLAST-1, a glutamate transporter, in vehicle-treated animals indicate the

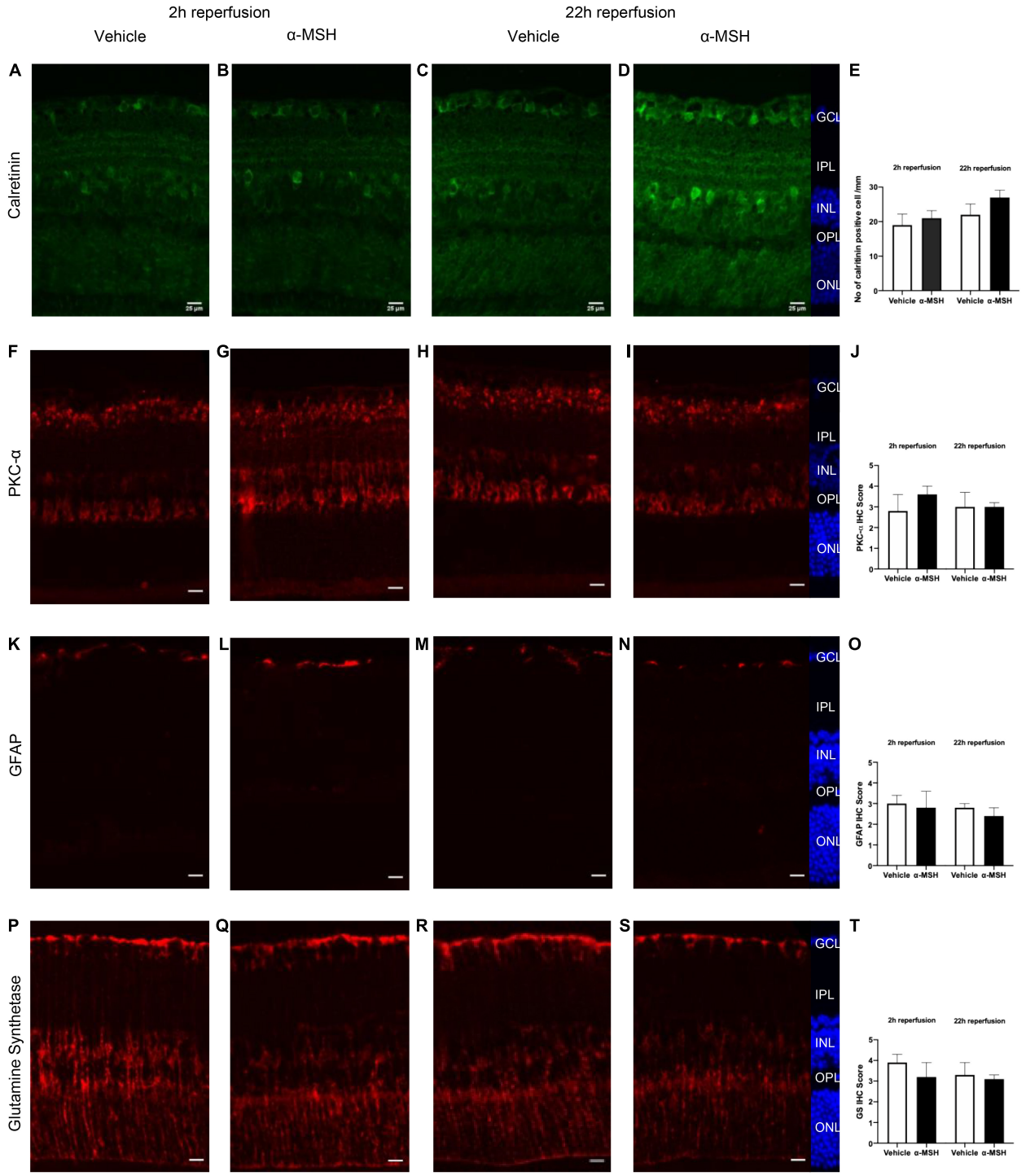

FIGURE 4 | Immunoreactivities of retinal neuronal and glial cells after I/R injury. **(A–D)** Calretinin expression was higher in α-MSH-treated animals at 22 h of reperfusion. **(E)** Number of calretinin positive cell/mm. **(F–I)** PKC-α expression was higher in α-MSH-treated animals at 2 h of reperfusion. **(J)** IHC scores for PKC-α.**(K–N)** GFAP expression was similar between the groups in both experimental conditions. **(O)** IHC scores for GFAP. **(P–S)** α-MSH reduced the GS expression at 2 h of reperfusion. **(T)** IHC scores for GS. Mann-Whitney *U*-Test, $n = 6$ for each group. Scale bar = 25 μm.

possibility of a temporary functional impairment of Müller cells after I/R injury with inadequate recycling of glutamate. The high intravitreal glutamate levels after suppression of glutamate transporter leads to elevated ganglion cell death (Vorwerk et al., 2000) and might affect impulse conduction. Treatment with α-MSH increased the gene expression of GLAST-1 as well as

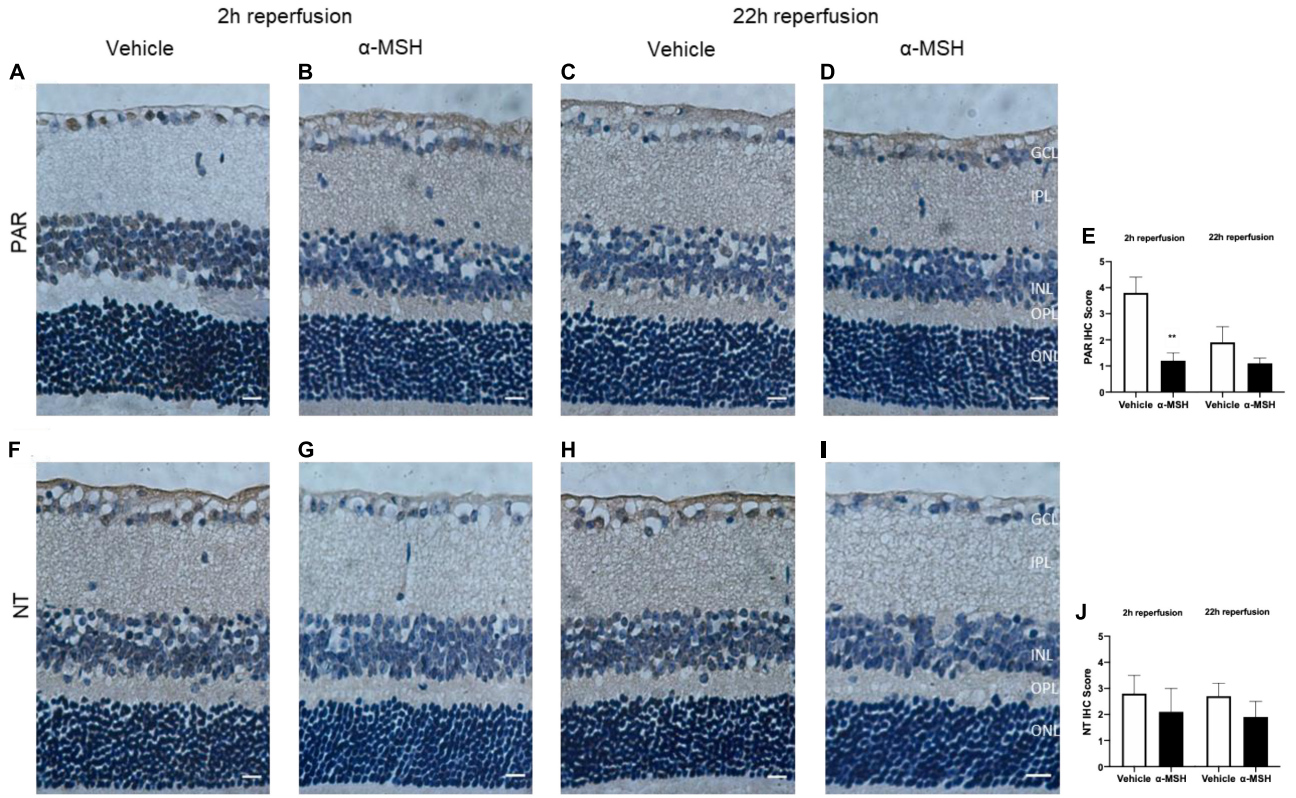

FIGURE 5 | α-MSH decreased the oxidative and nitrative stress after I/R injury. **(A–D)** Significantly weaker PAR immunoreactivity was observed in animals treated with α-MSH at 2 h of reperfusion. This immunoreactivity was comparable at 22 h of reperfusion. **(E)** IHC scores for PAR. **(F–I)** Weaker NT immunoreactivity was observed in α-MSH-treated animals in both experimental conditions. **(J)** IHC scores for NT. $^{**}P < 0.01$, Mann-Whitney *U*-Test, $n = 6$ for each group. Scale bar = 25 μm.

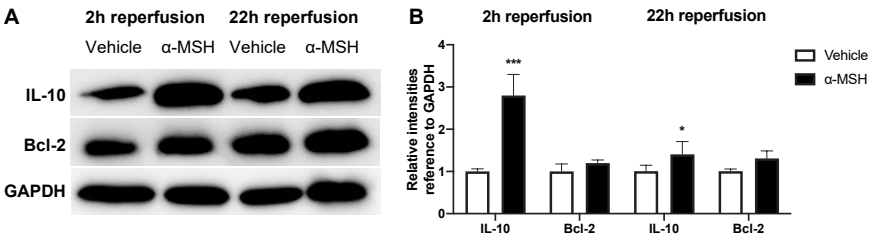

FIGURE 6 | α-MSH increased expressions of anti-inflammatory and pro-survival proteins after I/R injury. **(A,B)** Protein expressions of IL-10 was significantly higher in animals treated with α-MSH at 2 h and 22 h of reperfusion. **(A,B)** Although Bcl-2 expression was higher in animals treated with α-MSH in both experimental conditions, the expression was comparable. $^{*}P < 0.05$, $^{***}P < 0.001$, Independent samples *t*-test, $n = 5$–6 for each group.

increased immunoreactivities of PKC-α and calretinin, and in turn improved b-wave amplitude and OPs after I/R injury.

In sham operated animals, the amplitude of b-wave and OPs were higher in α-MSH treated animals compared to vehicle treated animals. It might be due to animals used in our study were dark adapted before ERG recording. More ATP is consumed in the dark due to Na^+/K^+ ATPase activity in the inner segment of rod photoreceptor. As lactate is produced, high photoreceptor metabolism may be maintained with lactate shuttles (Country, 2017). Lactate is taken up by Müller cells and oxidized to pyruvate to sustain oxidative metabolism (Lindsay et al., 2014). The lactate transporters, MCTs, are expressed in retinal cells and inhibition of MCTs causes reduction of b-wave and OPs (Bui et al., 2004). In addition, it has been suggested that hyperglycemia increases retinal metabolism and increases amplitudes of b-wave (Klemp et al., 2004) and OPs (Algvere and Gjotterberg, 1974) in diabetic patients without retinopathy compared to euglycemia. Both human and animal studies showed that α-MSH is involved in the management of glucose and slow progression of diabetes (Costa et al., 2006), suggesting its role in glucose metabolism. Interestingly, opposite effects have been observed in rodent studies. α-MSH when present in the central nervous system

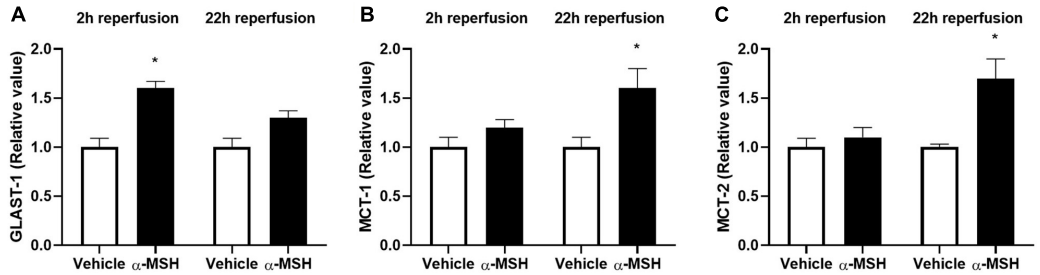

FIGURE 7 | α-MSH increased expression of glutamate and lactate related genes after I/R injury. **(A)** GLAST-1 expression was significantly higher in animals treated with α-MSH at 2 h of reperfusion. **(B,C)** MCT-1 and MCT-2 expressions were significantly higher in animals treated with α-MSH at 22 h of reperfusion. **(A–C)** GLAST-1 expression at 22 h of reperfusion and expressions of MCT-1 and MCT-2 at 2 h of reperfusion were comparable. *$P < 0.05$, Independent samples *t*-test, $n = 5$ for each group.

can increase insulin sensitivity but may contribute to insulin resistance when circulate in the periphery (Costa et al., 2006). At this point it is unclear which is the dominating effect in our investigations, although we cannot rule out the possibility that α-MSH's effect on ERG may be mediated *via* its influence on glucose metabolism.

The retina has a dual blood supply to sustain high metabolic function; the outer layers being supplied by the choroid capillaries and the inner layers being supplied by the CRA. Therefore, the severe effects of ocular ischemia are less frequently observed due to collateral vessels and retrograde blood flow in the retina (Shuaib et al., 2011). As a result, the blood flow to the retina is reduced but not completely blocked after MCAO (Kaja et al., 2003) and b-wave recovers after reperfusion (Osborne et al., 2004). Significantly higher amplitude of b-wave in animals treated with α-MSH compared to vehicle treated animals in both experimental conditions supported that α-MSH decreases the recovery time after retinal I/R injury. In this study, amplitude of b-wave and OPs were higher in 22 h of reperfusion groups compared to 2 h of reperfusion groups. This difference was due to short and long dark adaptation times. As the dark adaptation time increases, the amplitude of ERG waves increases gradually (Yu et al., 2007).

Inward movement of sodium, calcium and chloride ions along with water after ischemia can cause cell swelling and cytotoxic edema (Lipton, 1999). After retinal I/R injury, marked swelling of the ganglion cell bodies and their processes precede loss of these cells (Stevens et al., 2002). Indeed, there was an increase in the thickness of GCL and total retina in animals treated with vehicle after I/R injury, in agreement with the presence of retinal edema. Importantly, this increase in retinal thickness was ameliorated by α-MSH treatment, which supports the protective effects of α-MSH in preventing cell swelling and thus helps to maintain retinal structural integrity after I/R injury.

It has been shown that antioxidants play a role in the recovery of b-wave amplitude, preservation of retinal morphology and rescue of neurons in GCL (Li et al., 2009, 2011; Wang et al., 2020). Stronger PAR immunoreactivity in GCL and INL might be another possible reason for delayed recovery of b-wave amplitude and histological alternations in vehicle-treated animals after I/R injury. Despite the decreased amplitude of b-wave and number of damaged ganglion cells in vehicle-treated animals, we did not detect TUNEL-positive cells in retinal sections after I/R injury (data not shown). This agreed with our observation that Bcl-2 expression was comparable with/without α-MSH treatment in both experimental conditions. Bcl-2 is an anti-apoptotic protein which expression is important for retinal survival after ischemia (Martinou et al., 1994; Park et al., 2013). This suggests that ischemic damage may also occur by non-apoptotic mechanisms (Steele et al., 2008; Allen et al., 2014). It might also be due to the considerably longer survival of ischemic retina than the ischemic brain due to 100-time higher concentration of neuroglobin, a neuron-specific respiratory protein, in the mouse retina than in the mouse brain (Schmidt et al., 2003). Moreover, glucose concentration is higher in the retina when compared with the brain (Tang et al., 2000). This higher glucose concentration might likely fuel the retina during ischemia. In addition, vitreous humor bathes the retina and oxygen in the vitreous body makes it possible for the retina to tolerate ischemia (Hayreh and Weingeist, 1980). Besides, we only recorded laser-Doppler reading from the MCA but not from the OA. There is a possibility that the brain and the retina received different levels of occlusion. In addition, previous studies indicate that the amount of cell death is related to the method used to induce retinal ischemia. For example, occlusion of retinal vessels induces less severe consequence than increase of the intraocular pressure above systemic blood pressure (Hayreh and Weingeist, 1980).

Moreover, α-MSH has a role in anti-inflammation because retinal expression of IL-10 was upregulated in animals treated with α-MSH after I/R injury. IL-10 suppresses inflammation and angiogenesis in most ocular inflammations (Ghasemi et al., 2012). It modulates the expression of cytokines and chemokines that medicate inflammation as well as attenuates endothelial dysfunction and vasoconstriction mediated by oxidative stress after ischemia (Garcia et al., 2017). Importantly, higher IL-10 level correlates with its protective function against DR (Mysliwiec et al., 2006; Lee et al., 2008).

It has been shown that pre-existing hyperglycemic conditions including diabetes provide substantial structural and functional protection to the ischemic retina (Osborne et al., 2004). However, hyperglycemia-induced oxidative stress and inflammation are

primary pathogenic factors for DR. Also, degenerative changes in the ganglion cell and nerve fiber layers are prominent pathological features of DR. The reduction of oxidative stress and inflammatory effect are among the most important therapeutic strategies to slow down DR (Wang et al., 2020). In this study, α-MSH downregulated ROS production and upregulated expression of anti-inflammatory protein in addition to maintaining structural and functional integrities after I/R injury. Since neurodegenerative retinal disease such as DR alters expression of MCTs, these transporters may be important therapeutic targets (Kolko et al., 2016). Increased expressions of MCT-1 and MCT-2 in α-MSH-treated animals suggest a role for this neuropeptide in retinal metabolism through lactate signaling and transport. Thus, these beneficial effects of α-MSH may have important therapeutic implication against retinal I/R injury under hyperglycemic condition. As the present study was limited by inclusion of $Ins2^{Akita/+}$ mice only, further studies using non-diabetic mice are required to confirm whether α-MSH only acts on the retina or it also normalizes systemic changes due to hyperglycemia in order to restore normal structure and function of the retina.

DATA AVAILABILITY STATEMENT

The original contributions presented in the study are included in the article/supplementary material, further inquiries can be directed to the corresponding author/s.

ETHICS STATEMENT

The animals were handled according to the conditions of the Cap. 340 Animals (Control of Experiments) Ordinance and Regulations, and all relevant legislation and Codes of Practice in Hong Kong. All the animal handling and experimental methods were approved by the Committee on the Use of Live Animals in Teaching and Research (CULATR 4837-18) at The University of Hong Kong.

AUTHOR CONTRIBUTIONS

AL designed the idea and supervised the study. RG performed the experiments, analyzed the data, and wrote the manuscript. AL and AT revised the manuscript and approved the final manuscript. All authors contributed to the article and approved the submitted version.

FUNDING

This research was funded by the General Research Fund, Research Grants Council, The Government of the Hong Kong Special Administrative Region (17112919) and The University of Hong Kong Seed Funding Programme for Basic Research (201811159123) to AL; Boston University School of Medicine Wing Tat Lee Endowment to AT.

REFERENCES

Algvere, P., and Gjotterberg, M. (1974). The diagnostic value of the oscillatory potentials of the ERG and fluorescein angiography in diabetic proliferative retinopathy. *Ophthalmologica* 168, 97–108. doi: 10.1159/000307027

Allen, R. S., Sayeed, I., Cale, H. A., Morrison, K. C., Boatright, J. H., Pardue, M. T., et al. (2014). Severity of middle cerebral artery occlusion determines retinal deficits in rats. *Exp. Neurol.* 254, 206–215. doi: 10.1016/j.expneurol.2014.02.005

Antonetti, D. A., Silva, P. S., and Stitt, A. W. (2021). Current understanding of the molecular and cellular pathology of diabetic retinopathy. *Nat. Rev. Endocrinol.* 17, 195–206. doi: 10.1038/s41574-020-00451-4

Aronsson, A. F., Spulber, S., Popescu, L. M., Winblad, B., Post, C., Oprica, M., et al. (2006). alpha-melanocyte-stimulating hormone is neuroprotective in rat global cerebral ischemia. *Neuropeptides* 40, 65–75. doi: 10.1016/j.npep.2005.10.006

Brann, D. W., Dhandapani, K., Wakade, C., Mahesh, V. B., and Khan, M. M. (2007). Neurotrophic and neuroprotective actions of estrogen: basic mechanisms and clinical implications. *Steroids* 72, 381–405. doi: 10.1016/j.steroids.2007.02.003

Bringmann, A., Iandiev, I., Pannicke, T., Wurm, A., Hollborn, M., Wiedemann, P., et al. (2009). Cellular signaling and factors involved in Muller cell gliosis: neuroprotective and detrimental effects. *Prog. Retin Eye Res.* 28, 423–451. doi: 10.1016/j.preteyeres.2009.07.001

Bui, B. V., Kalloniatis, M., and Vingrys, A. J. (2004). Retinal function loss after monocarboxylate transport inhibition. *Invest. Ophthalmol. Vis. Sci.* 45, 584–593. doi: 10.1167/iovs.03-0695

Cai, J., and Boulton, M. (2002). The pathogenesis of diabetic retinopathy: old concepts and new questions. *Eye* 16, 242–260. doi: 10.1038/sj.eye.6700133

Cai, S., Yang, Q., Hou, M., Han, Q., Zhang, H., Wang, J., et al. (2018). Alpha-melanocyte-stimulating hormone protects early diabetic retina from blood-retinal barrier breakdown and vascular leakage via MC4R. *Cell Physiol. Biochem.* 45, 505–522. doi: 10.1159/000487029

Caldwell, R. B., Bartoli, M., Behzadian, M. A., El-Remessy, A. E., Al-Shabrawey, M., Platt, D. H., et al. (2003). Vascular endothelial growth factor and diabetic retinopathy: pathophysiological mechanisms and treatment perspectives. *Diabetes Metab. Res. Rev.* 19, 442–455. doi: 10.1002/dmrr.415

Chen, G., Frokiaer, J., Pedersen, M., Nielsen, S., Si, Z., Pang, Q., et al. (2008). Reduction of ischemic stroke in rat brain by alpha melanocyte stimulating hormone. *Neuropeptides* 42, 331–338. doi: 10.1016/j.npep.2008.01.004

Chiao, H., Kohda, Y., McLeroy, P., Craig, L., Housini, I., and Star, R. A. (1997). Alpha-melanocyte-stimulating hormone protects against renal injury after ischemia in mice and rats. *J. Clin. Invest.* 99, 1165–1172. doi: 10.1172/JCI119272

Clemson, C. M., Yost, J., and Taylor, A. W. (2017). The role of Alpha-MSH as a modulator of ocular immunobiology exemplifies mechanistic differences between melanocortins and steroids. *Ocul. Immunol. Inflamm.* 25, 179–189. doi: 10.3109/09273948.2015.1092560

ClinicalTrials.gov (2018). *Alpha MSH in Ocular Disease* [Online]. Available online at: https://clinicaltrials.gov/ct2/show/NCT03451578 (Accessed September 14, 2020).

ClinicalTrials.gov (2020). *Efficacy and Safety of PL9643 Ophthalmic Solution in Subjects With Dry Eye* [Online]. Available online at: https://clinicaltrials.gov/ct2/show/study/NCT04268069 (Accessed October 21, 2021).

Costa, J. L., Hochgeschwender, U., and Brennan, M. (2006). The role of melanocyte-stimulating hormone in insulin resistance and type 2 diabetes mellitus. *Treat Endocrinol.* 5, 7–13. doi: 10.2165/00024677-200605010-00002

Country, M. W. (2017). Retinal metabolism: a comparative look at energetics in the retina. *Brain Res.* 1672, 50–57. doi: 10.1016/j.brainres.2017.07.025

D'Onofrio, P. M., and Koeberle, P. D. (2013). What can we learn about stroke from retinal ischemia models? *Acta Pharmacol. Sin.* 34, 91–103. doi: 10.1038/aps.2012.165

Fong, D. S., Aiello, L., Gardner, T. W., King, G. L., Blankenship, G., Cavallerano, J. D., et al. (2004). Retinopathy in diabetes. *Diabetes Care* 27(Suppl. 1), S84–S87. doi: 10.2337/diacare.27.2007.s84

Fu, Z. J., Li, S. Y., Kociok, N., Wong, D., Chung, S. K., and Lo, A. C. (2012). Aldose reductase deficiency reduced vascular changes in neonatal mouse retina

in oxygen-induced retinopathy. *Invest. Ophthalmol. Vis. Sci.* 53, 5698–5712. doi: 10.1167/iovs.12-10122

Fu, Z., Meng, S. S., Burnim, S. B., Smith, L. E., and Lo, A. C. (2017). Lutein facilitates physiological revascularization in a mouse model of retinopathy of prematurity. *Clin. Exp. Ophthalmol.* 45, 529–538. doi: 10.1111/ceo.12908

Fu, Z., Nian, S., Li, S. Y., Wong, D., Chung, S. K., and Lo, A. C. (2015). Deficiency of aldose reductase attenuates inner retinal neuronal changes in a mouse model of retinopathy of prematurity. *Graefes Arch. Clin. Exp. Ophthalmol.* 253, 1503–1513. doi: 10.1007/s00417-015-3024-0

Garcia, J. M., Stillings, S. A., Leclerc, J. L., Phillips, H., Edwards, N. J., Robicsek, S. A., et al. (2017). Role of interleukin-10 in acute brain injuries. *Front. Neurol.* 8:244. doi: 10.3389/fneur.2017.00244

Geraldes, P., Hiraoka-Yamamoto, J., Matsumoto, M., Clermont, A., Leitges, M., Marette, A., et al. (2009). Activation of PKC-delta and SHP-1 by hyperglycemia causes vascular cell apoptosis and diabetic retinopathy. *Nat. Med.* 15, 1298–1306. doi: 10.1038/nm.2052

Ghasemi, H., Ghazanfari, T., Yaraee, R., Owlia, P., Hassan, Z. M., and Faghihzadeh, S. (2012). Roles of IL-10 in ocular inflammations: a review. *Ocul. Immunol. Inflamm.* 20, 406–418. doi: 10.3109/09273948.2012.723109

Goit, R. K., Ng, T. C., Tam, K. C., Tsang, J. K. W., Taylor, A. W., and Lo, A. C. Y. (2021). Neuropeptide alpha-melanocyte-stimulating hormone promotes neurological recovery and repairs cerebral ischemia/reperfusion injury in type 1 diabetes. *Neurochem Res.* Online ahead of print, doi: 10.1007/s11064-021-03453-4

Gong, H., Wang, W., Kwon, T. H., Jonassen, T., Li, C., Ring, T., et al. (2004). EPO and alpha-MSH prevent ischemia/reperfusion-induced down-regulation of AQPs and sodium transporters in rat kidney. *Kidney Int.* 66, 683–695. doi: 10.1111/j.1523-1755.2004.00791.x

Hassoun, H. T., Zou, L., Moore, F. A., Kozar, R. A., Weisbrodt, N. W., and Kone, B. C. (2002). Alpha-melanocyte-stimulating hormone protects against mesenteric ischemia-reperfusion injury. *Am. J. Physiol. Gastrointest. Liver Physiol.* 282, G1059–G1068. doi: 10.1152/ajpgi.00073.2001

Hayreh, S. S., and Weingeist, T. A. (1980). Experimental occlusion of the central artery of the retina. IV: retinal tolerance time to acute ischaemia. *Br. J. Ophthalmol.* 64, 818–825. doi: 10.1136/bjo.64.11.818

Holdeman, M., and Lipton, J. M. (1985). Effects of massive doses of alpha-MSH on thermoregulation in the rabbit. *Brain Res. Bull.* 14, 327–330. doi: 10.1016/0361-9230(85)90193-5

Huang, Q., and Tatro, J. B. (2002). Alpha-melanocyte stimulating hormone suppresses intracerebral tumor necrosis factor-alpha and interleukin-1beta gene expression following transient cerebral ischemia in mice. *Neurosci. Lett.* 334, 186–190. doi: 10.1016/s0304-3940(02)01088-1

Huh, S. K., Lipton, J. M., and Batjer, H. H. (1997). The protective effects of alpha-melanocyte stimulating hormone on canine brain stem ischemia. *Neurosurgery* 40, 132–139;discussion 139–140. doi: 10.1097/00006123-199701000-00030

Jansson, R. W., Hufthammer, K. O., and Krohn, J. (2018). Diabetic retinopathy in type 1 diabetes patients in Western Norway. *Acta Ophthalmol.* 96, 465–474. doi: 10.1111/aos.13654

Jehle, T., Wingert, K., Dimitriu, C., Meschede, W., Lasseck, J., Bach, M., et al. (2008). Quantification of ischemic damage in the rat retina: a comparative study using evoked potentials, electroretinography, and histology. *Invest. Ophthalmol. Vis. Sci.* 49, 1056–1064. doi: 10.1167/iovs.07-1050

Kaja, S., Yang, S. H., Wei, J., Fujitani, K., Liu, R., Brun-Zinkernagel, A. M., et al. (2003). Estrogen protects the inner retina from apoptosis and ischemia-induced loss of Vesl-1L/Homer 1c immunoreactive synaptic connections. *Invest. Ophthalmol. Vis. Sci.* 44, 3155–3162. doi: 10.1167/iovs.02-1204

Klemp, K., Larsen, M., Sander, B., Vaag, A., Brockhoff, P. B., and Lund-Andersen, H. (2004). Effect of short-term hyperglycemia on multifocal electroretinogram in diabetic patients without retinopathy. *Invest. Ophthalmol. Vis. Sci.* 45, 3812–3819. doi: 10.1167/iovs.03-1260

Kolb, H., Fernandez, E., and Nelson, R. (Eds.). (1995). *Webvision: The Organization of the Retina and Visual System.* University of Utah Health Sciences Center.

Kolko, M., Vosborg, F., Henriksen, U. L., Hasan-Olive, M. M., Diget, E. H., Vohra, R., et al. (2016). Lactate transport and receptor actions in retina: potential roles in retinal function and disease. *Neurochem. Res.* 41, 1229–1236. doi: 10.1007/s11064-015-1792-x

Lee, D. J., Biros, D. J., and Taylor, A. W. (2009). Injection of an alpha-melanocyte stimulating hormone expression plasmid is effective in suppressing experimental autoimmune uveitis. *Int. Immunopharmacol.* 9, 1079–1086. doi: 10.1016/j.intimp.2009.05.001

Lee, J. H., Lee, W., Kwon, O. H., Kim, J. H., Kwon, O. W., Kim, K. H., et al. (2008). Cytokine profile of peripheral blood in type 2 diabetes mellitus patients with diabetic retinopathy. *Ann. Clin. Lab. Sci.* 38, 361–367.

Li, S. Y., Fu, Z. J., Ma, H., Jang, W. C., So, K. F., Wong, D., et al. (2009). Effect of lutein on retinal neurons and oxidative stress in a model of acute retinal ischemia/reperfusion. *Invest. Ophthalmol. Vis. Sci.* 50, 836–843. doi: 10.1167/iovs.08-2310

Li, S. Y., Fung, F. K., Fu, Z. J., Wong, D., Chan, H. H., and Lo, A. C. (2012). Anti-inflammatory effects of lutein in retinal ischemic/hypoxic injury: *in vivo* and *in vitro* studies. *Invest. Ophthalmol. Vis. Sci.* 53, 5976–5984. doi: 10.1167/iovs.12-10007

Li, S. Y., Yang, D., Yeung, C. M., Yu, W. Y., Chang, R. C., So, K. F., et al. (2011). Lycium barbarum polysaccharides reduce neuronal damage, blood-retinal barrier disruption and oxidative stress in retinal ischemia/reperfusion injury. *PLoS One* 6:e16380. doi: 10.1371/journal.pone.0016380

Lindsay, K. J., Du, J., Sloat, S. R., Contreras, L., Linton, J. D., Turner, S. J., et al. (2014). Pyruvate kinase and aspartate-glutamate carrier distributions reveal key metabolic links between neurons and glia in retina. *Proc. Natl. Acad. Sci. U.S.A.* 111, 15579–15584. doi: 10.1073/pnas.1412441111

Lipton, P. (1999). Ischemic cell death in brain neurons. *Physiol Rev* 79, 1431–1568. doi: 10.1152/physrev.1999.79.4.1431

Lo, A. C., Chen, A. Y., Hung, V. K., Yaw, L. P., Fung, M. K., Ho, M. C., et al. (2005). Endothelin-1 overexpression leads to further water accumulation and brain edema after middle cerebral artery occlusion via aquaporin 4 expression in astrocytic end-feet. *J. Cereb. Blood Flow Metab.* 25, 998–1011. doi: 10.1038/sj.jcbfm.9600108

Lo, A. C., Cheung, A. K., Hung, V. K., Yeung, C. M., He, Q. Y., Chiu, J. F., et al. (2007). Deletion of aldose reductase leads to protection against cerebral ischemic injury. *J. Cereb. Blood Flow Metab.* 27, 1496–1509. doi: 10.1038/sj.jcbfm.9600452

Martinou, J. C., Dubois-Dauphin, M., Staple, J. K., Rodriguez, I., Frankowski, H., Missotten, M., et al. (1994). Overexpression of BCL-2 in transgenic mice protects neurons from naturally occurring cell death and experimental ischemia. *Neuron* 13, 1017–1030. doi: 10.1016/0896-6273(94)90266-6

Mysliwiec, M., Zorena, K., Balcerska, A., Mysliwska, J., Lipowski, P., and Raczynska, K. (2006). The activity of N-acetyl-beta-D-glucosaminidase and tumor necrosis factor-alpha at early stage of diabetic retinopathy development in type 1 diabetes mellitus children. *Clin. Biochem.* 39, 851–856. doi: 10.1016/j.clinbiochem.2006.03.013

Osborne, N. N., Casson, R. J., Wood, J. P., Chidlow, G., Graham, M., and Melena, J. (2004). Retinal ischemia: mechanisms of damage and potential therapeutic strategies. *Prog. Retin. Eye Res.* 23, 91–147. doi: 10.1016/j.preteyeres.2003.12.001

Palatin (2021). *Demonstrated Leader in the Discovery and Development of Melanocortin Agonist Treatments* [Online]. Available online at: https://palatin.com/pipeline/ (Accessed October 21, 2021).

Park, M. H., Kim, S. Y., Moon, C., Bae, Y. C., Moon, J. I., and Moon, C. (2013). Differential cell death and Bcl-2 expression in the mouse retina after glutathione decrease by systemic D,L-buthionine sulphoximine administration. *Mol. Cells* 35, 235–242. doi: 10.1007/s10059-013-2276-y

Perry, V. H., Henderson, Z., and Linden, R. (1983). Postnatal changes in retinal ganglion cell and optic axon populations in the pigmented rat. *J. Comp. Neurol.* 219, 356–368. doi: 10.1002/cne.902190309

Rauen, T., Taylor, W. R., Kuhlbrodt, K., and Wiessner, M. (1998). High-affinity glutamate transporters in the rat retina: a major role of the glial glutamate transporter GLAST-1 in transmitter clearance. *Cell Tissue Res.* 291, 19–31. doi: 10.1007/s004410050976

Savos, A. V., Gee, J. M., Zierath, D., and Becker, K. J. (2011). alpha-MSH: a potential neuroprotective and immunomodulatory agent for the treatment of stroke. *J. Cereb. Blood Flow Metab.* 31, 606–613. doi: 10.1038/jcbfm.2010.130

Schmidt, M., Giessl, A., Laufs, T., Hankeln, T., Wolfrum, U., and Burmester, T. (2003). How does the eye breathe? Evidence for neuroglobin-mediated oxygen supply in the mammalian retina. *J. Biol. Chem.* 278, 1932–1935. doi: 10.1074/jbc.M209909200

Shen, F., Chen, B., Danias, J., Lee, K. C., Lee, H., Su, Y., et al. (2004). Glutamate-induced glutamine synthetase expression in retinal Muller cells after short-term ocular hypertension in the rat. *Invest. Ophthalmol. Vis. Sci.* 45, 3107–3112. doi: 10.1167/iovs.03-0948

Shuaib, A., Butcher, K., Mohammad, A. A., Saqqur, M., and Liebeskind, D. S. (2011). Collateral blood vessels in acute ischaemic stroke: a potential therapeutic target. *Lancet Neurol.* 10, 909–921. doi: 10.1016/S1474-4422(11)70195-8

Simo, R., and Hernandez, C. (2008). Intravitreous anti-VEGF for diabetic retinopathy: hopes and fears for a new therapeutic strategy. *Diabetologia* 51, 1574–1580. doi: 10.1007/s00125-008-0989-9

Smith, R. S., John, S. W. M., and Nishina, P. M. (2002). "Posterior segment and orbit," in *Systematic Evaluation of the Mouse Eye: Anatomy, Pathology, and Biomethods*, eds R. S. Smith, S. W. M. John, P. M. Nishina, and J. P. Sundberg (Boca Raton, FL: CRC Press), 25–44. doi: 10.1016/j.cvsm.2003.12.010

Steele, E. C. Jr., Guo, Q., and Namura, S. (2008). Filamentous middle cerebral artery occlusion causes ischemic damage to the retina in mice. *Stroke* 39, 2099–2104. doi: 10.1161/STROKEAHA.107.504357

Stevens, W. D., Fortin, T., and Pappas, B. A. (2002). Retinal and optic nerve degeneration after chronic carotid ligation: time course and role of light exposure. *Stroke* 33, 1107–1112. doi: 10.1161/01.str.0000014204.05597.0c

Suzuki, S., Brown, C. M., and Wise, P. M. (2009). Neuroprotective effects of estrogens following ischemic stroke. *Front. Neuroendocrinol.* 30:201–211. doi: 10.1016/j.yfrne.2009.04.007

Tang, J., Zhu, X. W., Lust, W. D., and Kern, T. S. (2000). Retina accumulates more glucose than does the embryologically similar cerebral cortex in diabetic rats. *Diabetologia* 43, 1417–1423. doi: 10.1007/s001250051548

Taylor, A. W., and Lee, D. (2010). Applications of the role of alpha-MSH in ocular immune privilege. *Adv. Exp. Med. Biol.* 681, 143–149. doi: 10.1007/978-1-4419-6354-3_12

Varga, B., Gesztelyi, R., Bombicz, M., Haines, D., Szabo, A. M., Kemeny-Beke, A., et al. (2013). Protective effect of alpha-melanocyte-stimulating hormone (alpha-MSH) on the recovery of ischemia/reperfusion (I/R)-induced retinal damage in a rat model. *J. Mol. Neurosci.* 50, 558–570. doi: 10.1007/s12031-013-9998-3

Vecsernyes, M., Juhasz, B., Der, P., Kocsan, R., Feher, P., Bacskay, I., et al. (2003). The administration of alpha-melanocyte-stimulating hormone protects the ischemic/reperfused myocardium. *Eur. J. Pharmacol.* 470, 177–183. doi: 10.1016/s0014-2999(03)01780-1

Vorwerk, C. K., Naskar, R., Schuettauf, F., Quinto, K., Zurakowski, D., Gochenauer, G., et al. (2000). Depression of retinal glutamate transporter function leads to elevated intravitreal glutamate levels and ganglion cell death. *Invest. Ophthalmol. Vis. Sci.* 41, 3615–3621.

Wachtmeister, L., and Dowling, J. E. (1978). The oscillatory potentials of the mudpuppy retina. *Invest. Ophthalmol. Vis. Sci.* 17, 1176–1188.

Wang, W., and Lo, A. C. Y. (2018). Diabetic retinopathy: pathophysiology and treatments. *Int. J. Mol. Sci.* 19:1816. doi: 10.3390/ijms19061816

Wang, W., Tam, K. C., Ng, T. C., Goit, R. K., Chan, K. L. S., and Lo, A. C. Y. (2020). Long-term lutein administration attenuates retinal inflammation and functional deficits in early diabetic retinopathy using the Ins2(Akita/+) mice. *BMJ Open Diabetes Res. Care* 8:e001519. doi: 10.1136/bmjdrc-2020-001519

Winkler, B. S., Kapousta-Bruneau, N., Arnold, M. J., and Green, D. G. (1999). Effects of inhibiting glutamine synthetase and blocking glutamate uptake on b-wave generation in the isolated rat retina. *Vis. Neurosci.* 16, 345–353. doi: 10.1017/s095252389916214x

Yang, D., So, K. F., and Lo, A. C. (2017). Lycium barbarum polysaccharide extracts preserve retinal function and attenuate inner retinal neuronal damage in a mouse model of transient retinal ischaemia. *Clin. Exp. Ophthalmol.* 45, 717–729. doi: 10.1111/ceo.12950

Yoshioka, M., Kayo, T., Ikeda, T., and Koizumi, A. (1997). A novel locus, Mody4, distal to D7Mit189 on chromosome 7 determines early-onset NIDDM in nonobese C57BL/6 (Akita) mutant mice. *Diabetes* 46, 887–894. doi: 10.2337/diab.46.5.887

Yu, H. A., Jeong, M. B., Park, S. A., Kim, W. T., Kim, S. E., Chae, J. M., et al. (2007). The determination of dark adaptation time using electroretinography in conscious miniature Schnauzer dogs. *J. Vet. Sci.* 8, 409–414. doi: 10.4142/jvs.2007.8.4.409

Zhang, L., Dong, L., Liu, X., Jiang, Y., Zhang, L., Zhang, X., et al. (2014). alpha-Melanocyte-stimulating hormone protects retinal vascular endothelial cells from oxidative stress and apoptosis in a rat model of diabetes. *PLoS One* 9:e93433. doi: 10.1371/journal.pone.0093433

Zou, L., Sato, N., Attuwaybi, B. O., and Kone, B. C. (2003). Delayed administration of alpha-melanocyte-stimulating hormone or combined therapy with BAY 11-7085 protects against gut ischemia-reperfusion injury. *Shock* 20, 469–475. doi: 10.1097/01.shk.0000091205.08003.fd

Conflict of Interest: The authors declare that the research was conducted in the absence of any commercial or financial relationships that could be construed as a potential conflict of interest.

Publisher's Note: All claims expressed in this article are solely those of the authors and do not necessarily represent those of their affiliated organizations, or those of the publisher, the editors and the reviewers. Any product that may be evaluated in this article, or claim that may be made by its manufacturer, is not guaranteed or endorsed by the publisher.

frontiers | Frontiers in Molecular Neuroscience

ORIGINAL RESEARCH
published: 23 June 2022
doi: 10.3389/fnmol.2022.896786

Dimethyl Fumarate Blocks Tumor Necrosis Factor-Alpha-Driven Inflammation and Metabolic Rewiring in the Retinal Pigment Epithelium

*Daisy Y. Shu[1,2], Scott I. Frank[1], Tessa C. Fitch[1], Margarete M. Karg[1,2], Erik R. Butcher[1], Emmanuella Nnuji-John[1,3], Leo A. Kim[1,2] and Magali Saint-Geniez[1,2]**

[1] Schepens Eye Research Institute of Massachusetts Eye and Ear, Boston, MA, United States, [2] Department of Ophthalmology, Harvard Medical School, Boston, MA, United States, [3] Cold Spring Harbor Laboratory, School of Biological Sciences, Cold Spring Harbor, NY, United States

OPEN ACCESS

Edited by:
Henri Leinonen,
University of Eastern Finland, Finland

Reviewed by:
Kai Kaarniranta,
University of Eastern Finland, Finland
Dorota Skowronska-Krawczyk,
UCI Health, United States

***Correspondence:**
Magali Saint-Geniez
msaintgeniez@gmail.com

Specialty section:
This article was submitted to Brain Disease Mechanisms, a section of the journal Frontiers in Molecular Neuroscience

Received: 15 March 2022
Accepted: 25 May 2022
Published: 23 June 2022

Citation:
Shu DY, Frank SI, Fitch TC, Karg MM, Butcher ER, Nnuji-John E, Kim LA and Saint-Geniez M (2022) Dimethyl Fumarate Blocks Tumor Necrosis Factor-Alpha-Driven Inflammation and Metabolic Rewiring in the Retinal Pigment Epithelium. Front. Mol. Neurosci. 15:896786. doi: 10.3389/fnmol.2022.896786

The retinal pigment epithelium (RPE) acts as a metabolic gatekeeper between photoreceptors and the choroidal vasculature to maintain retinal function. RPE dysfunction is a key feature of age-related macular degeneration (AMD), the leading cause of blindness in developed countries. Inflammation is a key pathogenic mechanism in AMD and tumor necrosis factor-alpha (TNFα) has been implicated as a pro-inflammatory cytokine involved in AMD. While mitochondrial dysfunction has been implicated in AMD pathogenesis, the interplay between inflammation and cellular metabolism remains elusive. The present study explores how the pro-inflammatory cytokine, TNFα, impacts mitochondrial morphology and metabolic function in RPE. Matured human primary RPE (H-RPE) were treated with TNFα (10 ng/ml) for up to 5 days. TNFα-induced upregulation of IL-6 secretion and inflammatory genes (IL-6, IL-8, MCP-1) was accompanied by increased oxidative phosphorylation (OXPHOS) and reduced glycolysis, leading to an increase in cellular adenosine triphosphate (ATP) content. Transmission electron microscopy (TEM) revealed defects in mitochondrial morphology with engorged mitochondria and loss of cristae integrity following TNFα treatment. Pre-treatment with the anti-inflammatory drug, 80 μM dimethyl fumarate (DMFu), blocked TNFα-induced inflammatory activation of RPE (IL-6, IL-8, MCP-1, CFH, CFB, C3) and normalized their bioenergetic profile to control levels by regulating PFKFB3 and PKM2 gene expression. Furthermore, DMFu prevented TNFα-induced mitochondrial dysfunction and morphological anomalies. Thus, our results indicate that DMFu serves as a novel therapeutic avenue for combating inflammatory activation and metabolic dysfunction of RPE in AMD.

Keywords: inflammation, metabolism, mitochondria, retinal pigment epithelium, tumor necrosis factor-alpha, oxidative phosphorylation, glycolysis, age-related macular degeneration

INTRODUCTION

Dysfunction of retinal pigment epithelial cells (RPE) is an early sign of AMD and loss of RPE integrity increases as AMD progresses (Bonilha, 2008; Ao et al., 2018). Inflammation is a key pathogenic mechanism in AMD (Datta et al., 2017) through complement system activation, upregulation of inflammatory cytokines and recruitment of macrophages to the outer surface of the RPE-Bruch's membrane interface in AMD eyes (Hageman et al., 2001) that facilitates drusen growth (Levy et al., 2015). A critical cytokine mediating inflammatory responses throughout the body is tumor necrosis factor-alpha (TNFα), which has been implicated in the pathogenesis of AMD (Oh et al., 1999; Wan et al., 2010; Kutty et al., 2016). Single nucleotide polymorphisms (SNPs) have been detected in the TNFα gene in AMD patients (Wan et al., 2010; Chernykh et al., 2019) and TNFα decreases the expression of genes regulating RPE function, including RPE65 (Kutty et al., 2016). Further, lower serum levels of TNFα have been associated with improved visual acuity after anti-VEGF therapy in wet AMD patients (Khan et al., 2021), highlighting TNFα as a pathogenic driver of wet AMD.

Defects in RPE mitochondria and metabolism drive AMD pathogenesis (Fisher and Ferrington, 2018; Kaarniranta et al., 2020; Zhang et al., 2020). Work in our laboratory has further implicated metabolic and mitochondrial dysfunction of RPE in AMD (Iacovelli et al., 2016; Satish et al., 2018; Rosales et al., 2019; Shu et al., 2020, 2021). Despite evidence for both inflammation and metabolic dysfunction in AMD, there is a paucity of literature dissecting the crosstalk between these two mechanisms in the AMD field. Hence, this study sought to examine whether TNFα-driven inflammation in RPE is accompanied by changes in mitochondria and metabolism. Further, we investigated the efficacy of the fumaric acid ester, dimethyl fumarate (DMFu), in blocking TNFα-driven inflammation and metabolic changes in RPE.

Fumaric acid esters have been used as anti-inflammatory treatments for the autoimmune disease, psoriasis, for over 20 years (Blair, 2018). DMFu is FDA-approved for the treatment of relapsing multiple sclerosis in the form of delay-release capsules for oral use (Cada et al., 2013). DMFu is rapidly hydrolyzed to its active metabolite, monomethyl fumarate (MMF), which has a terminal half-life of 1 h. MMF is then metabolized by the TCA cycle to fumaric acid, citric acid, glucose, and carbon dioxide. The potent anti-inflammatory effect of DMFu is linked to its ability to block the NF-κB pathway (Borgers et al., 2001), a downstream target of TNFα activation.

Here, we bridge the gap between inflammation and metabolic dysfunction in RPE showing that the pro-inflammatory effects of TNFα are associated with a dramatic change in mitochondrial morphology, function, and rewiring of the metabolic pathways. We reveal that pre-treatment of primary human RPE with the metabolic drug, DMFu, blocks the pro-inflammatory effects of TNFα, further highlighting the intertwined link between inflammation and metabolism.

MATERIALS AND METHODS

Cell Culture

Primary human fetal retinal pigment epithelial cells (H-RPE, Lonza Cat #00194987) were cultured in RtEGM Retinal Pigment Epithelial Cell Growth Medium supplemented with RtEGM SingleQuots (Lonza, Walkersville, MD, United States) as described previously (Shu et al., 2021). H-RPE were maintained at 37°C and 5% CO_2 in a humidified incubator and passaged 1:3 at a maximum of 5 passages. Half media changes for H-RPE were performed every 2–4 days for a month to ensure proper RPE maturation and pigment accumulation. Cells were serum starved for 2–3 days before treatment for up to 5 days with recombinant human TNFα (Peprotech, Rocky Hill, NJ, United States) at 10 ng/mL and/or 80 μM dimethyl fumarate (242926, Sigma, St Louis, MO, United States) dissolved in the vehicle control, DMSO at the equivalent concentration of 0.04% (D4540, Sigma, St Louis, MO, United States). Brightfield images were captured on the EVOS M7000 Imaging System (Invitrogen, ThermoFisher, Waltham, MA, United States). Cells were tested monthly for mycoplasma contamination using the Mycoplasma PCR test (Applied Biological Materials, Cat #G238).

Quantitative PCR

Quantitative PCR (qPCR) assays were performed as previously described (Shu et al., 2021). Briefly, the E.Z.N.A. total RNA Kit I (Omega BioTek, Norcross, GA, United States) was used to extract total RNA and concentrations were determined using the NanoDrop Spectrophotometer ND-1000 (ThermoFisher Scientific, San Jose, CA, United States). cDNA synthesis was performed using the SuperScript IV VILO MasterMix and the Techne TC-512 Thermal Cycler at 25°C, 10 min; 50°C, 10 min; 85°C, 5 min (ThermoFisher Scientific, San Jose, CA, United States) and amplified by real-time PCR using the PowerUp SYBR Green Master Mix (ThermoFisher Scientific, San Jose, CA, United States) in a LightCycler 480 (Roche, Basel, Switzerland). Reactions were run in duplicate under the following thermal cycling conditions: 50°C, 2 min; 95°C, 2 min, followed by 40 cycles of 95°C for 15 s and 60°C for 1 min. Melt curve analysis was performed to confirm amplification specificity. *Ct* values were normalized to the housekeeping gene, TATA-binding protein (TBP), using the second derivative maximum method. Primer sequences are listed in **Table 1**.

High-Resolution Respirometry

The Seahorse XFe96 Analyzer (Agilent Technologies, Santa Clara, CA, United States) was used to determine real-time bioenergetic profiles. 20,000 H-RPE cells were seeded per well according to the manufacturer's instructions. For the Mito Stress Test, the medium was replaced with the assay medium (Seahorse XF Base Medium without Phenol Red, Agilent) supplemented with 2 mM GlutaMAX (ThermoFisher), 1 mM pyruvate (Gibco, Carlsbad, CA, United States) and 25 mM glucose (Sigma, St.

TABLE 1 | Primer sequences for qPCR.

Gene symbol	Gene name	Forward sequence (5′-3′)	Reverse sequence (5′-3′)
ATP5O	ATP synthase subunit O	TTTGAATCCCTATGTGAAGCGTT	CCTTGGGTATTGCTTAATCGACC
C3	Complement component 3	ACGGCCTTTGTTCTCATCTC	CAAGGAAGTCTCCTGCTTTAGT
CFB	Complement factor B	GCTGTGAGAGAGATGCTCAATA	GACTCACTCCAGTACAAAG
CFH	Complement factor H	CTGATCGCAAGAAAGACCAGTA	TGGTAGCACTGAACGGAATTAG
IL-6	Interleukin-6	ACTCACCTCTTCAGAACGAATTG	CCATCTTTGGAAGGTTCAGGTTG
IL-8	Interleukin-8	TTTTGCCAAGGAGTGCTAAAGA	AACCCTCTGCACCCAGTTTTC
MCP-1	Monocyte chemoattractant protein-1	CAGCCAGATGCAATCAATGCC	TGGAATCCTGAACCCACTTCT
PFKFB3	6-phosphofructo-2-kinase/fructose-2,6-biphosphatase 3	CAGTTGTGCCTCCAATATC	GGCTTCATAGCAACTGATCC
PGC-1A	Peroxisome proliferator-activated receptor gamma, coactivator 1 alpha (PPARGC1A)	GTCACCACCCAAATCCTTAT	ATCTACTGCCTGGAGACCTT
PKM2	Pyruvate kinase muscle isozyme M2	CAAAGGACCTCAGCAGCCATGTC	GGGAAGCTGGGCCAATGGTACAGA
VEGFA	Vascular endothelial growth factor A	GGGCAGAATCATCACGAAGTG	ATTGGATGGCAGTAGCTGCG
VEGFC	Vascular endothelial growth factor C	GCCAATCACACTTCCTGCCGAT	AGGTCTTGTTCGCTGCCTGACA
TBP	TATA-binding protein	TGCACAGGAGCCAAGAGTGAA	CACATCACAGCTCCCCACCA

Louis, MO, United States), pH 7.4 and placed in a 37°C, CO_2-free, humidified incubator for 1 h. The drug injections were oligomycin (2.5 μM), BAM15 (10 μM) and a combination of rotenone and antimycin A (both at 2 μM). The same reagents were used for the ATP Rate Assay with the BAM15 drug injection excluded. For the Glycolytic Stress Test, the medium was replaced with the assay medium (Seahorse XF Base Medium without Phenol Red, Agilent) supplemented with 1 mM GlutaMAX (ThermoFisher), pH 7.4, and placed in a 37°C, CO_2-free, humidified incubator for 1 h. The drug injections were glucose (10 mM), oligomycin (2 μM), and 2DG (50 mM). On completion of the Seahorse assays, cells were lysed in cold 1× Cell Lysis Buffer (Cell Signaling Technology, Beverly, MA, United States) supplemented with 1 mM PMSF (Sigma, St Louis, MO, United States) and stored at −80°C. Protein concentration was quantified using the Pierce BCA Assay kit (ThermoFisher, Waltham, MA, United States). Data were normalized to protein content using the XF Wave software by exporting the XF Mito Stress Test, XF Glycolytic Stress Test and XF ATP Rate Assay Test Report Generators to Excel and GraphPad Prism.

Oxygen Consumption Rate (OCR) was also measured using the Resipher (Lucid Scientific, Atlanta, GA, United States). 50,000 H-RPE cells were seeded into the Falcon flat-bottom 96-well microplate (Corning #353072) in H-RPE culture medium with the Resipher oxygen sensing lid. Cells were serum starved for 2 days before treatment with TNFα at 10 ng/ml. Real-time continuous OCR measurements were monitored in the incubator for a week. Data were analyzed using the Resipher web application and Python.

Measurement of Intracellular ATP Content

ATP content was measured using the ATP bioluminescence assay kit CLS II (Roche, Heidelberg, Germany) as previously described (Shu et al., 2021). Protein content was measured using the Pierce BCA Assay kit. 20 μg of protein was run in duplicate in a white, flat-bottom 96-well microplate. Determination of free ATP was performed against an ATP standard curve. Luminescence was determined at 60 ms integration using a Synergy H1 Plate Reader (BioTek, Winooski, VT, United States).

Quantification of Mitochondrial Copy Number

Genomic DNA (gDNA) was isolated using the Universal Genomic DNA Kit (CWBio #CW2298S). DNA concentration and purity was measured using the NanoDrop Spectrophotometer ND-1000. 10 ng of gDNA was used for the qPCR reactions and performed as previously described (Shu et al., 2021) using the Clontech Human Mitochondrial DNA (mtDNA) Monitoring Primer Set (Takara Bio Inc., Kusatsu, Shiga, Japan). mtDNA copy number was calculated as the average of the ratio of mtDNA to nuclear DNA using the two pairs of genes mt-*ND5* with *SERPINA1* and *ND1* with *SLCO2B1*.

Transmission Electron Microscopy

Cells were fixed with quarter strength Karnovsky's fixative (1% formaldehyde + 1.25% glutaraldehyde, in 0.1 M sodium cacodylate buffer, pH 7.4) for 6 h at room temperature, then transferred into 0.1 M sodium cacodylate buffer, post-fixed with 1% osmium tetroxide in 0.1 M sodium cacodylate buffer for 1 h, en bloc stained with 1% gadolinium triacetate in 0.05 M sodium maleate buffer, 4–6°C, pH 6 for 30 min. Samples were dehydrated with graded ethyl alcohol solutions, transitioned with propylene oxide and infiltrated in tEPON-812 epoxy resin (Tousimis, Rockville, MD, United States) utilizing an automated EMS Lynx 2 EM tissue processor (Electron Microscopy Sciences, Hatfield, PA, United States). The processed samples were oriented into tEPON-812 epoxy resin inside flat molds and polymerized using an oven set at 60°C. The polymerized blocks were cleaved from the coverglass through brief exposure in liquid nitrogen. Semi-thin sections were cut at 1 μm thickness and stained with 1% toluidine blue in 1% sodium tetraborate aqueous solution for assessment by light microscopy. A region containing a monolayer of cells was selected from each sample from the semi-thin toluidine blue stained sections and block face trimmed

to <1 mm × 0.5 mm for ultramicrotomy. Ultrathin sections (80 nm) were cut from each block face using a Leica EM UC7 ultramicrotome (Leica Microsystems, Buffalo Grove, IL, United States) and diamond knives (Diatome, Hatfield, PA, United States), to collect onto 2 × 1 mm, single slot formvar-carbon coated grids and 200 mesh copper/rhodium uncoated grids (Electron Microscopy Sciences, Hatfield, PA, United States). The ultrathin sections on grids were stained with aqueous 2.5% gadolinium triacetate and modified Sato's lead citrate using a modified Hiraoka grid staining system (Seifert, 2017). Grids were imaged using a FEI Tecnai G2 Spirit transmission electron microscope (FEI, Hillsboro, OR, United States) at 80 kV interfaced with an AMT XR41 digital CCD camera (Advanced Microscopy Techniques, Woburn, MA, United States) for digital TIFF file image acquisition. All TEM digital images were captured at 2k × 2k pixels at 16-bit resolution with the same magnification. Images were processed using Contrast Limited AHE (CLAHE) on ImageJ to reduce background noise and amplify mitochondrial ultrastructural features. Images were further analyzed on ImageJ using the hand-trace tool to obtain the area of the mitochondria.

Statistical Analysis

Statistical analyses were performed using GraphPad Prism 9.1.1. Parametric data were analyzed by one-way ANOVA with Tukey's *post hoc* analysis or unpaired Student's *t*-test. Statistical significance was considered when $p \leq 0.05$ and all data are shown as mean ± SEM. * $p \leq 0.05$, ** $p \leq 0.01$, *** $p \leq 0.001$, and **** $p \leq 0.0001$.

RESULTS

Tumor Necrosis Factor-Alpha-Induced Inflammation in Retinal Pigment Epithelial Cells Is Accompanied by Mitochondrial Dysfunction

TNFα induced H-RPE elongation after 5 days of treatment (**Figure 1A**) while triggering a rapid inflammatory response with increased IL-6 secretion (**Figure 1B**) and increased gene expression of pro-inflammatory cytokines (IL-6, IL-8, and MCP-1) at 24 h (**Figure 1C**). This pro-inflammatory activation of RPE by TNFα was accompanied by the repression of PGC-1α, a master regulator of RPE mitochondrial function and homeostasis, at 24 h (**Figure 1D**). Ultrastructural analysis showed that TNFα induced a dramatic enlargement of mitochondria and cristae sparsity at 5 days as observed by TEM imaging (**Figure 1E**). Quantification of mitochondrial area showed that TNFα-treated cells displayed a higher frequency of larger mitochondria (**Figure 1F**) and a significantly larger average mitochondrial area (**Figure 1G**).

Tumor Necrosis Factor-Alpha Increased Mitochondrial Respiration and Reduced Glycolysis in Retinal Pigment Epithelial Cells

Given the aberrant mitochondrial morphology observed, we next investigated whether TNFα induced any changes in mitochondrial function by assessing RPE bioenergetics on the Seahorse XFe96 Mito Stress Test. Enlarged mitochondrial size typically confers enhanced bioenergetic capacity (Westermann, 2012). Accordingly, the larger mitochondria observed with TNFα was associated with a significantly increased basal respiration, maximal respiration, ATP production, and spare respiratory capacity (SRC) at 5 days (**Figures 2A,B**). TNFα also significantly increased coupling efficiency (**Figure 2C**). In contrast, TNFα reduced glycolysis and glycolytic capacity with a slight elevation of glycolytic reserve (**Figures 2D,E**). Consistent with the fact that OXPHOS is far more efficient at generating ATP compared to glycolysis, the increased mitochondrial respiration with TNFα was accompanied by a significant increase in intracellular ATP content at 5 days (**Figure 2F**). Furthermore, the Seahorse ATP rate assay confirmed the enhanced OXPHOS with TNFα, highlighting that a higher proportion of ATP generation was derived from mitochondrial respiration than glycolysis (**Figures 2G,H**), further indicated by the significantly higher ATP rate index (**Figures 2I,J**). Continuous monitoring of oxygen flux of H-RPE in the incubator using the Resipher confirmed the elevated OCR with TNFα (**Figure 2K**) with increasingly significant OCR elevations over time from 24 to 96 h (**Figure 2L**).

Pre-treatment With Dimethyl Fumarate Blocks Tumor Necrosis Factor-Alpha-Induced Inflammation and Restores Mitochondrial Health

Pre-treatment with DMFu for 2 h prior to TNFα exposure blocked TNFα-induced cellular elongation, maintaining the regular cobblestone-like epithelial morphology (**Figure 3A**). DMFu alone did not affect cellular morphology (**Figure 3A**). DMFu significantly suppressed TNFα-induced IL-6 secretion at both 24 h (**Figure 3B**) and 5 days (**Figure 3C**). Moreover, DMFu reduced gene expression of inflammatory cytokines including IL-6 (**Figure 3D**), IL-8 (**Figure 3E**), and MCP-1 (**Figure 3F**) at 24 h and 5 days.

Local activation and induction of the alternative complement cascade, an integral part of innate immunity, has been implicated in AMD pathogenesis (Johnson et al., 2001). At 24 h, TNFα robustly enhanced the gene expression of key components of the alternative complement cascade including complement factor H (CFH, **Figure 4A**), complement factor B (CFB, **Figure 4B**), and complement component 3 (C3, **Figure 4C**), which were all significantly suppressed with DMFu pre-treatment. There were no significant changes observed for complement factor I (CFI, **Figure 4D**).

A critical driver of late-stage neovascular AMD is the pro-angiogenic factor, vascular endothelial growth factor (VEGF) (Rosenfeld et al., 2006). Polarized VEGF expression is important for RPE homeostasis and survival (Ford et al., 2011). Specifically, VEGF-A expression by RPE is essential for choriocapillaris maintenance, and RPE dedifferentiation is associated with loss of VEGF secretion and choriocapillaris dropout (Blaauwgeers et al., 1999; Saint-Geniez et al., 2009). TNFα significantly reduced VEGF-A gene expression at 5 days while pre-treatment with DMFu maintained basal VEGF-A levels (**Figure 4E**). No

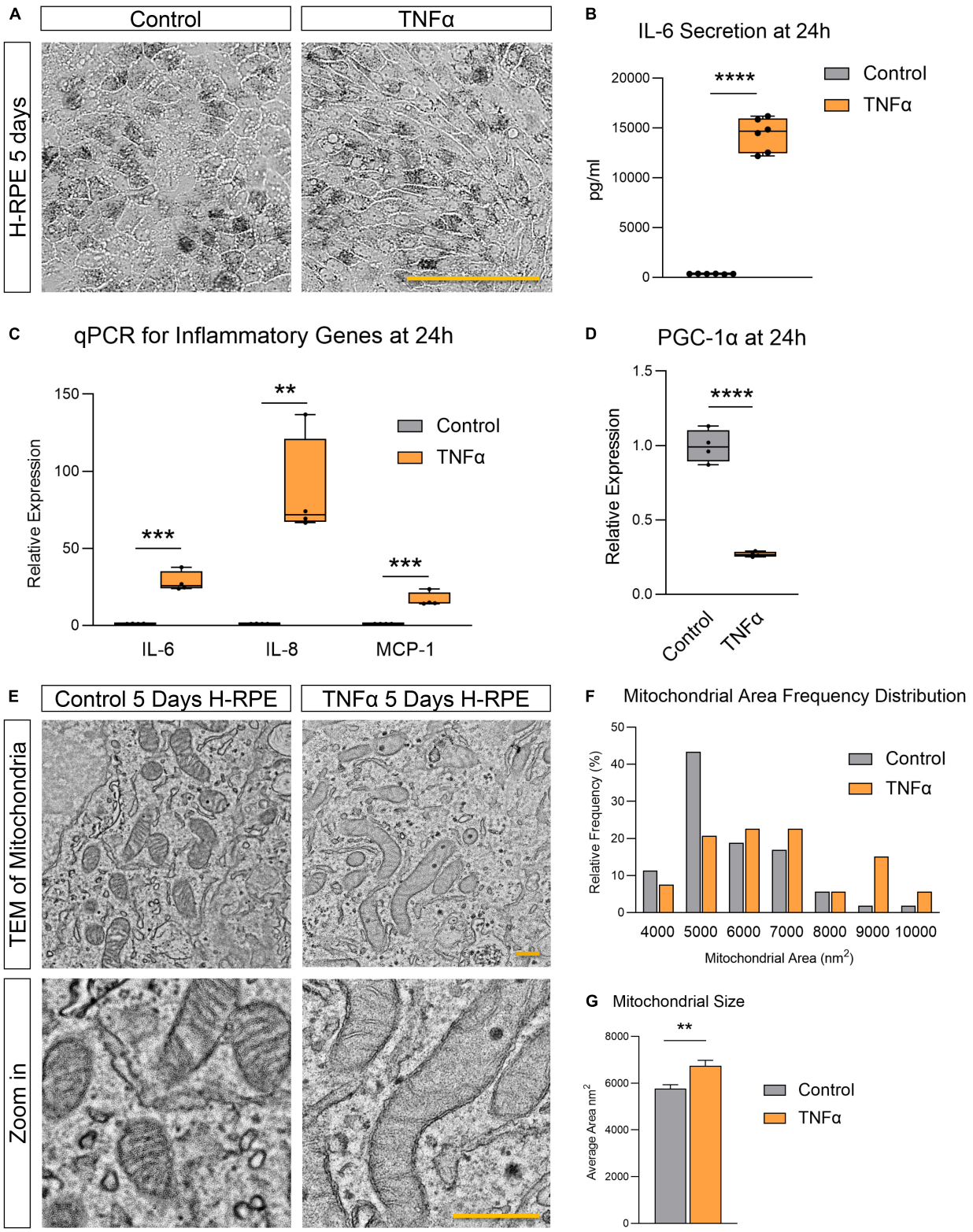

FIGURE 1 | Tumor necrosis factor-alpha-induced inflammation in H-RPE is accompanied by mitochondrial dysfunction. **(A)** Brightfield images of H-RPE cells with and without TNFα treatment. **(B)** IL-6 secretion at 24 h measured using ELISA for H-RPE. **(C,D)** qPCR analysis of inflammatory **(C)** and PGC-1α **(D)** gene expression in H-RPE following 24 h treatment with TNFα. **(E)** TEM images of H-RPE comparing untreated control and TNFα-treatment for 5 days. **(F)** Quantification of mitochondrial size from TEM images presented as a frequency distribution histogram, and **(G)** quantification of average mitochondrial size (unpaired *t*-test). Error bars are means ± SEM. ** $p \leq 0.01$; *** $p \leq 0.001$; **** $p \leq 0.0001$; ns, not significant. Scale bar for panel **(A)** is 100 μm and panel **(E)** is 500 nm.

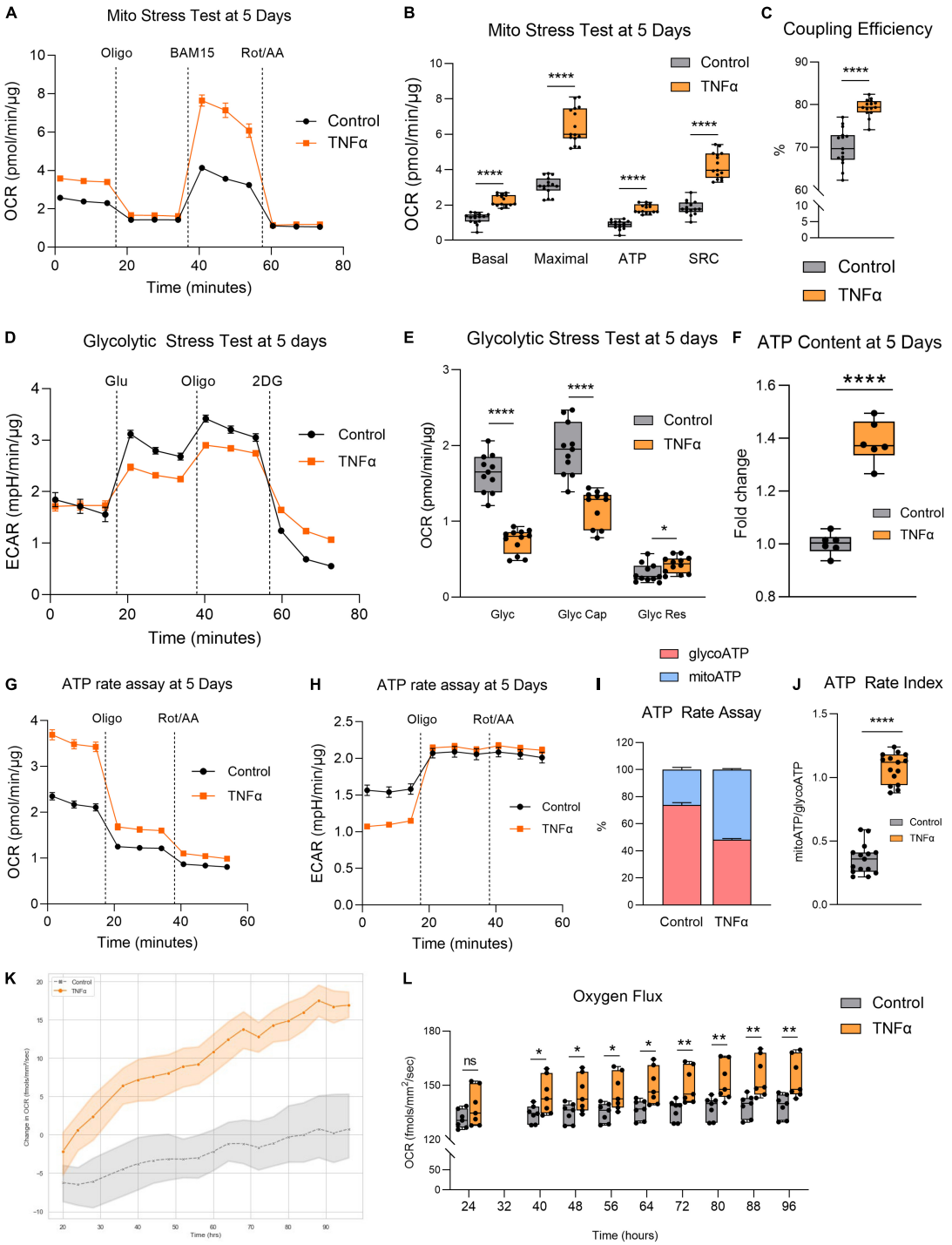

FIGURE 2 | Tumor necrosis factor-alpha increased mitochondrial respiration and reduced glycolysis in RPE. **(A)** Real-time measurement of oxygen consumption rate (OCR) using the Seahorse XFe96 BioAnalyzer to assess **(B)** OXPHOS parameters: basal respiration, ATP-linked respiration, proton leak, spare respiratory capacity (SRC), and maximal respiration based on responses to drug injections of oligomycin (Oligo), BAM15, and rotenone and antimycin A (Rot/AA) at 5 days with and without TNFα (n = 10–12, unpaired t-test) and **(C)** coupling efficiency. **(D)** Real-time measurement of extracellular acidification rate (ECAR) using the Seahorse XFe96 BioAnalyzer to assess glycolytic function parameters: **(E)** glycolysis, glycolytic capacity, and glycolytic reserve based on responses to drug injections of glucose (Glu), oligomycin (Oligo), and 2-deoxyglucose (2DG) at 5 days of treatment with and without TNFα (n = 10–12, unpaired t-test). **(F)** Intracellular ATP content at 5 days with or without TNFα (n = 6, unpaired t-test). **(G)** OCR curves and **(H)** ECAR curves for the Seahorse ATP rate assay at 5 days with TNFα. **(I)** Proportion of mitochondria-derived ATP production and glycolysis-derived ATP production and **(J)** increased ATP Rate Index representing a more oxidative and less glycolytic phenotype with TNFα treatment. **(K)** Real-time monitoring of OCR using the Resipher technology over 96 h following treatment with TNFα and **(L)** quantification of OCR over time (n = 7, unpaired t-test). Error bars are means ± SEM. * $p \leq 0.05$; ** $p \leq 0.01$; **** $p \leq 0.0001$; ns, not significant.

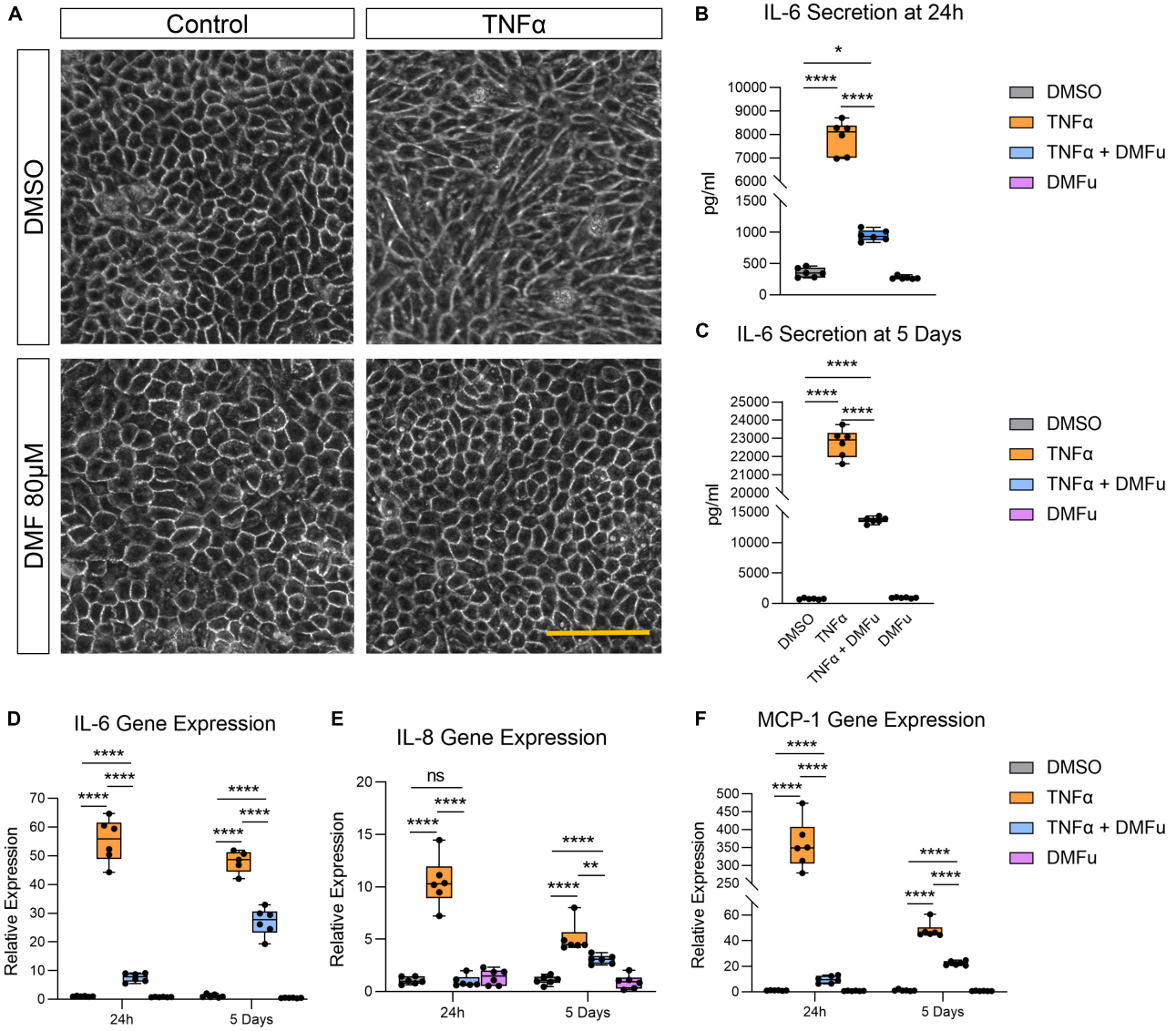

FIGURE 3 | Pre-treatment with dimethyl fumarate (DMFu) blocks TNFα-induced inflammation. **(A)** Brightfield images of H-RPE cells treated with TNFα (10 ng/ml) and/or DMFu (80 μM) or vehicle control (DMSO). **(B,C)** Quantification of secreted IL-6 following TNFα and/or DMFu treatment for **(B)** 24 h and **(C)** 5 days. **(D–F)** qPCR analysis of inflammatory gene expression following treatments on H-RPE for **(D)** IL-6, **(E)** IL-8, and **(F)** MCP-1. $n = 6$, one-way ANOVA with Tukey's *post hoc* analysis. Error bars are means ± SEM. * $p \leq 0.05$; ** $p \leq 0.01$; **** $p \leq 0.0001$; ns, not significant. Scale bar is 100 μm.

significant changes for VEGF-A occurred at 24 h (**Figure 4E**). VEGF-C is a potent enhancer of vascular permeability and has been identified in RPE derived from choroidal neovascular (CNV) specimens from patients (Martin et al., 2004). VEGF-C gene expression was increased with TNFα at both 24 h and 5 days and appeared to be further increased in the presence of DMFu (**Figure 4F**).

The anti-inflammatory activity of DMFu was accompanied by a shift toward normalized mitochondrial function. While TNFα increased mtDNA copy number, co-treatment with TNFα and DMFu reduced mtDNA copy number down to basal levels (**Figure 5A**). Similarly, co-treatment with TNFα and DMFu significantly enhanced PGC-1α levels compared to TNFα alone; however, this was not sufficient to maintain basal levels of PGC-1α (**Figure 5B**). On an ultrastructural level, DMFu blocked TNFα-induced loss of cristae architecture and maintained normal mitochondrial size (**Figure 5C**).

Pre-treatment With Dimethyl Fumarate Blocks Tumor Necrosis Factor-Alpha-Induced Metabolic Reprogramming

On the Seahorse Mito Stress Test, DMFu blocked the elevated mitochondrial respiration induced by TNFα (**Figure 6A**). Specifically, DMFu blocked TNFα-dependent elevation of basal

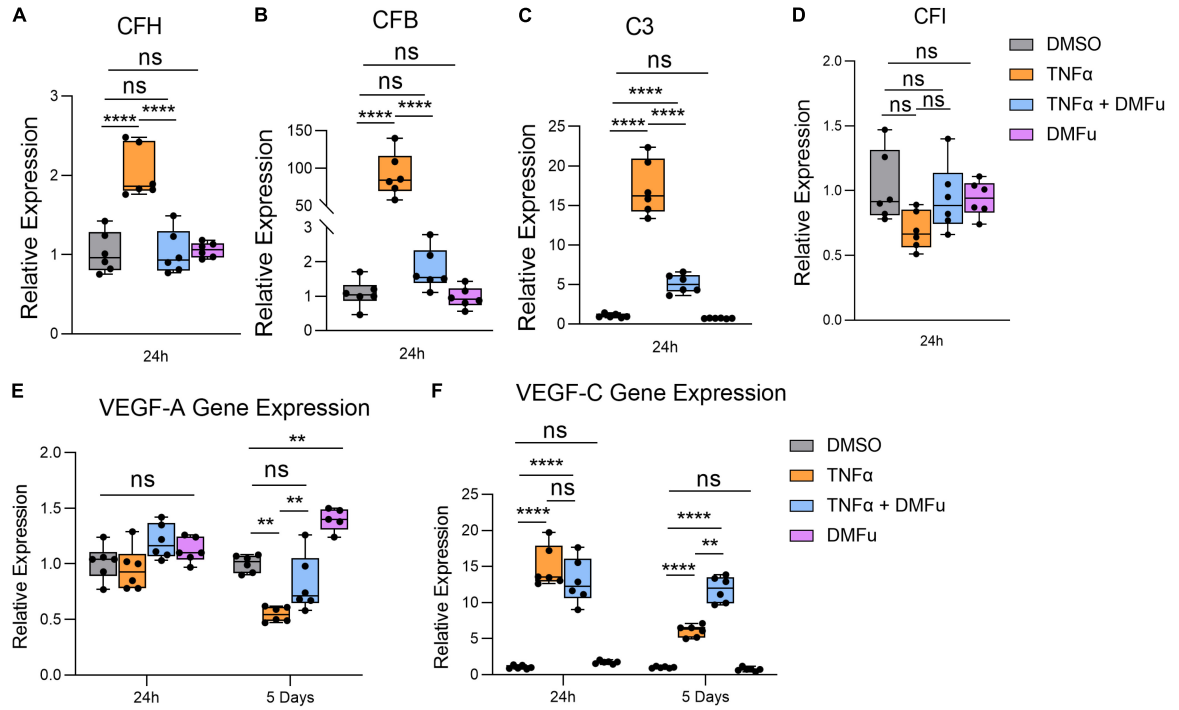

FIGURE 4 | Pre-treatment with dimethyl fumarate (DMFu) blocks TNFα-induced complement activation. qPCR analysis of gene expression of the complement cascade following treatments on H-RPE for **(A)** complement factor H, **(B)** complement factor B, **(C)** complement component 3, **(D)** complement factor I at 24 h. qPCR analysis of gene expression of **(E)** VEGF-A and **(F)** VEGF-C n = 5–6, one-way ANOVA with Tukey's *post hoc* analysis. Error bars are means ± SEM. ** $p \leq 0.01$; **** $p \leq 0.0001$; ns, not significant.

respiration (**Figure 6B**), maximal respiration (**Figure 6C**), ATP production (**Figure 6D**), spare respiratory capacity (**Figure 6E**), and coupling efficiency (**Figure 6F**). This blockade was accompanied by a reduction in gene expression of ATP5O, a key component of ATP synthase in the electron transport chain (**Figure 6G**). The Seahorse Glycolytic Stress Test showed that DMFu restored the suppression of glycolysis induced by TNFα (**Figure 6H**) with a statistically significant increase in glycolysis (**Figure 6I**), but no changes in glycolytic capacity (**Figure 6J**) and a reduction in glycolytic reserve (**Figure 6K**). The enhanced glycolysis with co-treatment of DMFu and TNFα is supported by the enhanced gene expression of glycolytic enzymes, namely, PFKFB3 (**Figure 6L**) and PKM2 (**Figure 6M**).

DISCUSSION

TNFα-induced inflammation in H-RPE is accompanied by a dramatic disruption in normal mitochondrial morphology and metabolic function. We show that TNFα induces the accumulation of engorged mitochondria with loss of cristae integrity and overactive metabolic function, promoting increased mitochondrial respiration, ATP production and reduced glycolysis in H-RPE. Pre-treatment of H-RPE with DMFu blocked TNFα-induced inflammation and normalized metabolic function and mitochondrial ultrastructural morphology.

An intricate interplay exists between inflammation and metabolic dysfunction at sites of ongoing inflammation (Kominsky et al., 2010). The enhanced OXPHOS and increased ATP production induced by TNFα in our study highlights the substantial bioenergetic challenge required to mount an inflammatory response in RPE. Intriguingly, our previous work showed that TGFβ2, an important cytokine in AMD pathogenesis, induces the opposite metabolic changes in RPE with reduced OXPHOS and enhanced glycolysis, leading to an overall reduction in ATP content (Shu et al., 2021). Since TGFβ2 itself does not induce inflammation, it is possible that the enhanced OXPHOS induced by TNFα may facilitate its pro-inflammatory activity. The capacity of RPE to switch between different bioenergetic profiles depending on cytokine stimulation shows the metabolic flexibility of RPE. Despite the capacity of both TGFβ2 and TNFα to induce robust EMT responses in RPE, a key component of pathogenic subretinal fibrosis in AMD (Shu et al., 2020, 2021), their divergent impact on metabolic reprogramming highlights the complexity of targeting metabolism as a therapeutic avenue for AMD. Future studies will continue to dissect the extensive crosstalk that exists between metabolism and EMT (Jia et al., 2021), examining how other metabolic pathways such as fatty acid oxidation and glutamine metabolism are impacted by TGFβ2 and TNFα in RPE.

Metabolic reprograming of immune cells during activation is highly cell-type and context dependent. Divergent metabolic profiles have been observed with B and T lymphocytes with

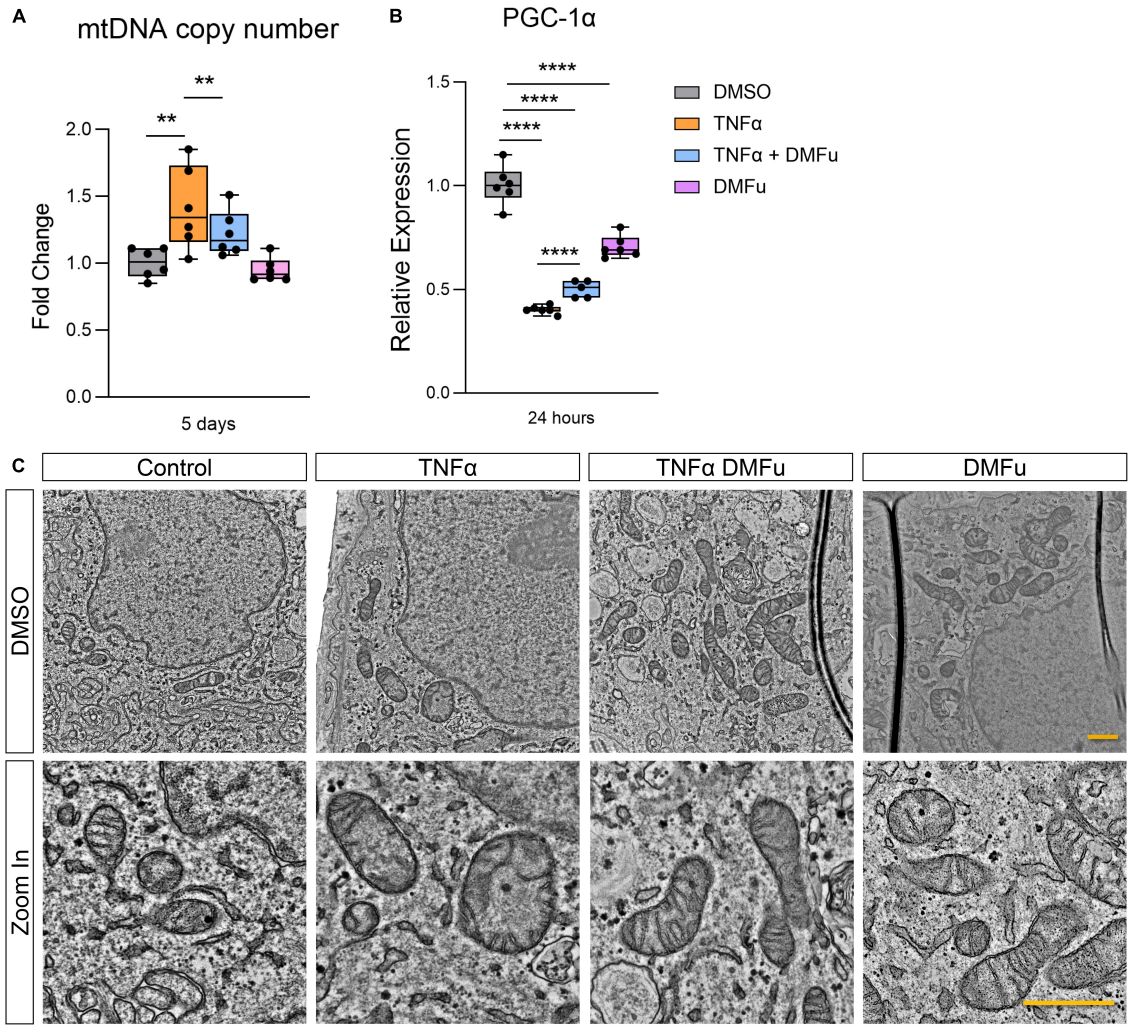

FIGURE 5 | Pre-treatment with dimethyl fumarate (DMFu) blocks TNFα-induced mitochondrial dysfunction. **(A)** Quantification of mtDNA copy number following treatments with TNFα and/or DMFu or the vehicle control (DMSO). **(B)** qPCR analysis of gene expression of PGC-1α on H-RPE following treatments. $n = 6$, one-way ANOVA with Tukey's *post hoc* analysis. Error bars are means ± SEM. ** $p \leq 0.01$; **** $p \leq 0.0001$. **(C)** TEM images of H-RPE treated with DMSO, TNFα 10 ng/ml, TNFα with DMFu, and DMFu alone and magnified images. Scale bar is 1 μm.

B cells relying more on OXPHOS, while T cells rely more on aerobic glycolysis (Khalsa et al., 2019). Activation of B cells is bioenergetically demanding and consequently induces a progressive upregulation of OXPHOS to fulfill their new energy requirements (Price et al., 2018). Treatment of RPE with TNFα appears to mimic the metabolic changes observed in activated B cells. Indeed, activated B cells are known to secrete pro-inflammatory cytokines including TNFα and IL-6 (Gupta et al., 2013), which may, in turn, further potentiate inflammation and mitochondrial respiration. Our finding that TNFα increases OXPHOS in RPE has also been reported in platelets of aged mice where the pro-inflammatory activity of TNFα was linked to mitochondrial dysfunction, increased mitochondrial mass and metabolite rewiring to favor elevated pentose phosphate pathway intermediates (Davizon-Castillo et al., 2019). Future studies on comprehensive metabolomics analysis of TNFα-treated H-RPE will determine the precise metabolic pathway reconfigurations, further unraveling the complex interplay between inflammation and the RPE metabolome.

Activation of the alternative pathway of the complement cascade has been implicated in the pathogenesis of AMD and in particular, geographic atrophy (Desai and Dugel, 2022). Our study shows that TNFα robustly upregulates critical components of the complement cascade and that DMFu is able to suppress TNFα-induced complement activation. Intriguingly, the ability of DMFu to suppress complement activation is accompanied by enhanced angiogenic gene expression. VEGF-C, an established pro-angiogenic factor and enhancer of vascular permeability, was strongly induced by TNFα and further upregulated in the presence of DMFu, indicating a potential risk for promoting an angiogenic response as observed in neovascular AMD. Complement inhibition is believed to induce a shift in

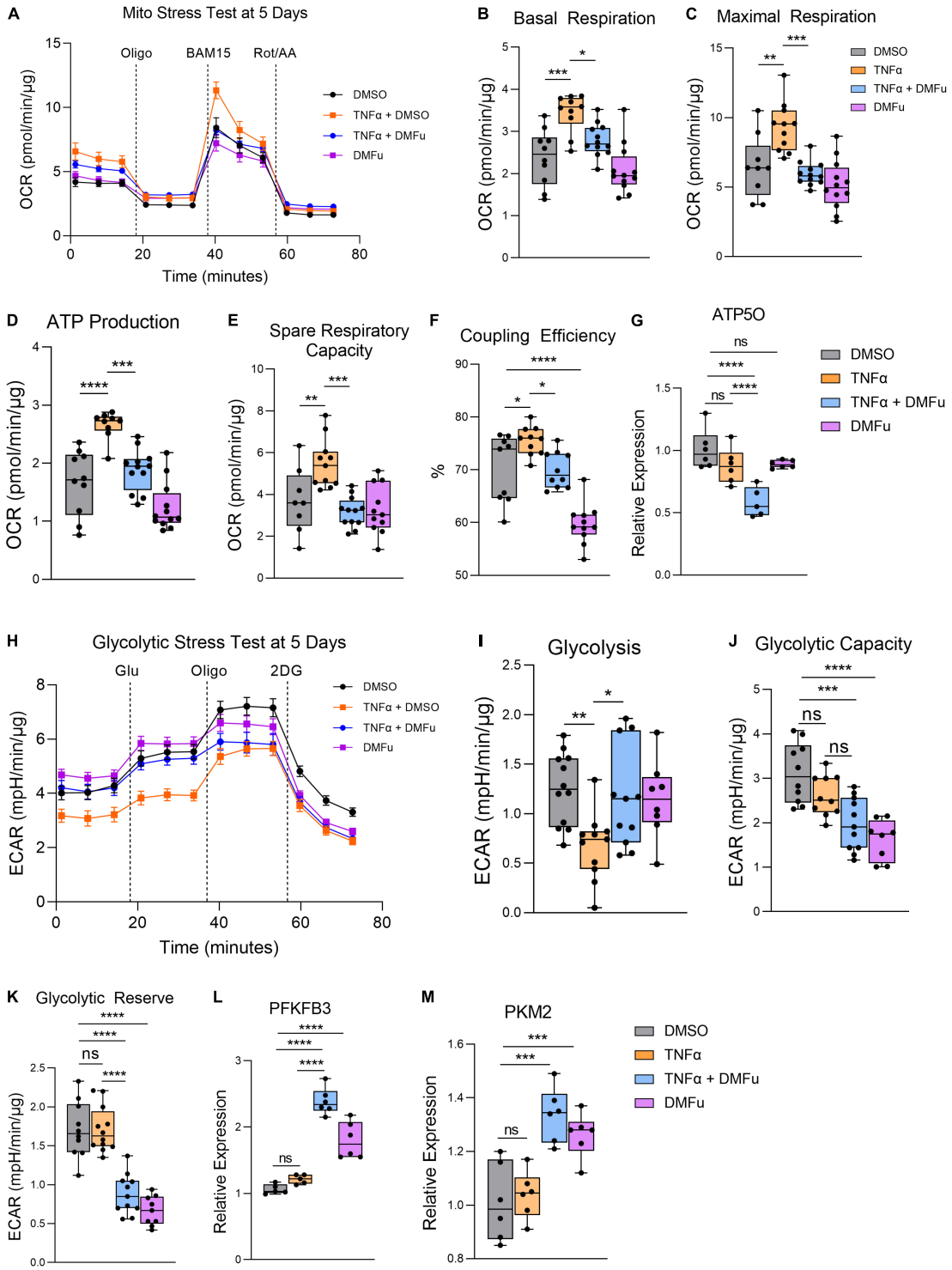

FIGURE 6 | Pre-treatment with dimethyl fumarate (DMFu) blocks TNFα-induced metabolic reprogramming. **(A)** Real-time measurement of oxygen consumption rate (OCR) using the Seahorse XFe96 BioAnalyzer to assess OXPHOS parameters: **(B)** basal respiration, **(C)** maximal respiration, **(D)** ATP-linked respiration, **(E)** spare respiratory capacity, and **(F)** coupling efficiency based on responses to drug injections of oligomycin (Oligo), BAM15 and rotenone and antimycin A (Rot/AA) at 5 days with and without TNFα and/or DMFu or the vehicle control (DMSO) (n = 10–12, unpaired t-test). qPCR gene expression of **(G)** ATP5O following 24 h of treatments. **(H)** Real-time measurement of extracellular acidification rate (ECAR) using the Seahorse XFe96 BioAnalyzer to assess glycolytic function parameters including **(I)** glycolysis, **(J)** glycolytic capacity, and **(K)** glycolytic reserve based on responses to drug injections of glucose (Glu), oligomycin (Oligo), and 2-deoxyglucose (2DG) at 5 days of treatments (n = 10–12, unpaired t-test). qPCR gene expression of **(L)** PFKFB3 and **(M)** PKM2 following 24 h of treatments. n = 6 for gene expression, one-way ANOVA with Tukey's *post hoc* analysis. Error bars are means ± SEM. * $p \leq 0.05$; ** $p \leq 0.01$; *** $p \leq 0.001$; **** $p \leq 0.0001$; ns, not significant.

macrophage polarization from the pro-inflammatory M1 to the pro-angiogenic M2 macrophages (Cao et al., 2011). Indeed, in the clinical trial for the C3 inhibitor, APL-2, 18% of patients on monthly injections showed conversion to neovascular AMD, highlighting a critical link between complement inhibition and the risk of increased angiogenic potential (Park et al., 2019).

Our study highlights DMFu as a novel immunometabolic regulator of RPE. We show that the anti-inflammatory effect of DMFu was accompanied by a normalization of RPE metabolic function, blocking TNFα-induced elevated OCR and maintaining glycolysis at basal levels. The anti-inflammatory capacity of DMFu showed beneficial effects in an autoimmune uveitis rat model (Labsi et al., 2021) and optic neuritis murine model (Zyla et al., 2019). Further, DMFu promotes the survival of retinal ganglion cells (RGCs) after optic nerve crush (Mori et al., 2020) and protects against retinal degeneration in a light-induced photoreceptor loss mouse model (Dietrich et al., 2020). Mechanistically, studies have shown that DMFu activates Nrf2/heme oxygenase-1 (HO-1) (Zyla et al., 2019; Mori et al., 2020) and increases glutathione (Nelson et al., 1999; Dietrich et al., 2020) to mediate its anti-inflammatory and anti-oxidative effects. Intriguingly, in this study, DMFu alone induces significant metabolic changes compared to DMSO-treated control cells. For example, DMFu slightly reduces basal levels of PGC-1α gene expression and increases the gene expression of glycolytic enzymes, PFKFB3 and PKM2, despite reducing glycolytic capacity and reserve. These metabolic changes do not impinge on the potent anti-inflammatory activity of DMFu against TNFα in RPE. The favorable efficacy and safety profiles of oral administration of DMFu for psoriasis and multiple sclerosis highlights its promise as a therapeutic avenue for immunomodulation of retinal diseases, including AMD. Furthermore, DMFu will only be considered as a treatment against active pathology rather than as a prophylactic therapy.

Ultrastructural mitochondrial imaging on TEM revealed dramatic mitochondrial defects following TNFα treatment of H-RPE, which was prevented by co-treatment with DMFu. Typically, long fused mitochondria are associated with enhanced OXPHOS capacity compared to smaller, fragmented mitochondria with reduced OXPHOS (Galloway et al., 2012). Indeed, our data shows that TNFα-induced elevated OXPHOS is associated with enlarged mitochondrial size, highlighting the morphological plasticity of RPE and reciprocal relationship between bioenergetic status and mitochondrial morphology. Elevated OXPHOS levels may generate more reactive oxygen species (ROS) byproducts that can cause further oxidative damage to mitochondrial morphology (Jassim et al., 2021). It is hypothesized that increased oxidative damage to mitochondria may lead to increased mtDNA copy number as an initial compensatory mechanism (Wang et al., 2014). Our data shows that TNFα increases mtDNA copy number in RPE, which can be blocked by co-treatment with DMFu. Similar results were observed in a clinical study of obese diabetic participants where increased body mass index (BMI) was associated with increased TNFα production, inflammation and mtDNA copy number (Skuratovskaia et al., 2019).

Our study reveals the dynamic interplay between inflammation and metabolic function in RPE, highlighting the morphological and bioenergetic alterations in mitochondria following TNFα stimulation. TNFα-driven inflammation causes a dramatic increase in energy demands in RPE, leading to increased oxygen consumption and ATP production at the expense of mitochondrial health. Such pro-inflammatory activation of RPE *in vivo* would undoubtedly cause an imbalance in the tightly regulated metabolic ecosystem of the retina (Kanow et al., 2017) through altered nutrient and oxygen availability for neighboring retinal cells. DMFu effectively abolished the drastic mitochondrial changes induced by TNFα, maintaining normal mitochondrial morphology and bioenergetic profiles and thus serves as a promising therapeutic avenue for combating inflammation in AMD.

DATA AVAILABILITY STATEMENT

The original contributions presented in this study are included in the article/supplementary material, further inquiries can be directed to the corresponding author.

AUTHOR CONTRIBUTIONS

DYS and MS-G: conceptualization and design. DYS, MS-G, SIF, and TCF: methodology. DYS, SIF, and MMK: writing–original draft preparation. DYS, SIF, TCF, ERB, and EN-J: formal analysis and investigation. DYS, SIF, TCF, MMK, ERB, EN-J, LAK, and MS-G: writing–review and editing. DYS, MS-G, and LAK: project administration and funding acquisition. All authors contributed to the article and approved the submitted version.

FUNDING

This study was supported in part by grants from the Fight for Sight Leonard & Robert Weintraub Postdoctoral Fellowship (DYS); BrightFocus Foundation Postdoctoral Fellowship Program in Macular Degeneration Research (M2021010F, DYS); Department of Defense, Spinal Vision Research Program under Award no. VR180132 (MS-G and LAK); National Eye Institute of the National Institutes of Health under Award no. R01EY027739 (LAK); the Grimshaw-Gudewicz Charitable Foundation (MS-G); The Iraty Award (MS-G); and the NEI Core Grant P30EYE003790.

ACKNOWLEDGMENTS

Acknowledgment is made to the donors of the Macular Degeneration Research M2021010F, a program of the BrightFocus Foundation, for support of this research. We thank Richard Bryan and Kin Lo for their assistance with the Resipher technology and data analysis. We also thank Philip Seifert at the Schepens Eye Research Institute (SERI) Morphology Core for electron microscopy assistance.

REFERENCES

Ao, J., Wood, J. P., Chidlow, G., Gillies, M. C., and Casson, R. J. (2018). Retinal pigment epithelium in the pathogenesis of age-related macular degeneration and photobiomodulation as a potential therapy? *Clin. Exp. Ophthalmol.* 46, 670–686. doi: 10.1111/ceo.13121

Blaauwgeers, H. G., Holtkamp, G. M., Rutten, H., Witmer, A. N., Koolwijk, P., Partanen, T. A., et al. (1999). Polarized vascular endothelial growth factor secretion by human retinal pigment epithelium and localization of vascular endothelial growth factor receptors on the inner choriocapillaris. evidence for a trophic paracrine relation. *Am. J. Pathol.* 155, 421–428. doi: 10.1016/S0002-9440(10)65138-3

Blair, H. A. (2018). Dimethyl Fumarate: a review in moderate to severe plaque psoriasis. *Drugs* 78, 123–130. doi: 10.1007/s40265-017-0854-6

Bonilha, V. L. (2008). Age and disease-related structural changes in the retinal pigment epithelium. *Clin. Ophthalmol.* 2, 413–424. doi: 10.2147/opth.s2151

Borgers, M., Beyaert, R., Borghmans, I., Vandermeeren, M., Geysen, J., Wouters, H., et al. (2001). Dimethylfumarate is an inhibitor of cytokine-induced nuclear translocation of NF-κB1, but not RelA in normal human dermal fibroblast cells. *J. Investig. Dermatol.* 116, 124–130. doi: 10.1046/j.1523-1747.2001.00211.x

Cada, D. J., Levien, T. L., and Baker, D. E. (2013). Dimethyl fumarate. *Hosp. Pharm.* 48, 668–679.

Cao, X., Shen, D., Patel, M. M., Tuo, J., Johnson, T. M., Olsen, T. W., et al. (2011). Macrophage polarization in the maculae of age-related macular degeneration: a pilot study. *Pathol. Int.* 61, 528–535. doi: 10.1111/j.1440-1827.2011.02695.x

Chernykh, V., Shevchenko, A., Konenkov, V., Prokofiev, V., Eremina, A., and Trunov, A. (2019). TNF-alpha gene polymorphisms: association with age-related macular degeneration in Russian population. *Int. J. Ophthalmol.* 12, 25–29. doi: 10.18240/ijo.2019.01.04

Datta, S., Cano, M., Ebrahimi, K., Wang, L., and Handa, J. T. (2017). The impact of oxidative stress and inflammation on RPE degeneration in non-neovascular AMD. *Prog. Retin. Eye Res.* 60, 201–218. doi: 10.1016/j.preteyeres.2017.03.002

Davizon-Castillo, P., Mcmahon, B., Aguila, S., Bark, D., Ashworth, K., Allawzi, A., et al. (2019). TNF-alpha-driven inflammation and mitochondrial dysfunction define the platelet hyperreactivity of aging. *Blood* 134, 727–740. doi: 10.1182/blood.2019000200

Desai, D., and Dugel, P. U. (2022). Complement cascade inhibition in geographic atrophy: a review. *Eye* 36, 294–302. doi: 10.1038/s41433-021-01765-x

Dietrich, M., Hecker, C., Nasiri, M., Samsam, S., Issberner, A., Kohne, Z., et al. (2020). Neuroprotective properties of dimethyl fumarate measured by optical coherence tomography in non-inflammatory animal models. *Front. Neurol.* 11:601628. doi: 10.3389/fneur.2020.601628

Fisher, C. R., and Ferrington, D. A. (2018). Perspective on AMD pathobiology: a bioenergetic crisis in the RPE. *Invest. Ophthalmol. Vis. Sci.* 59, AMD41–AMD47. doi: 10.1167/iovs.18-24289

Ford, K. M., Saint-Geniez, M., Walshe, T., Zahr, A., and D'amore, P. A. (2011). Expression and role of VEGF in the adult retinal pigment epithelium. *Invest. Ophthalmol. Vis. Sci.* 52, 9478–9487. doi: 10.1167/iovs.11-8353

Galloway, C. A., Lee, H., and Yoon, Y. (2012). Mitochondrial morphology-emerging role in bioenergetics. *Free Radic. Biol. Med.* 53, 2218–2228. doi: 10.1016/j.freeradbiomed.2012.09.035

Gupta, S., Agrawal, S., and Gollapudi, S. (2013). Increased activation and cytokine secretion in B cells stimulated with leptin in aged humans. *Immun. Ageing* 10:3. doi: 10.1186/1742-4933-10-3

Hageman, G. S., Luthert, P. J., Victor Chong, N. H., Johnson, L. V., Anderson, D. H., and Mullins, R. F. (2001). An integrated hypothesis that considers drusen as biomarkers of immune-mediated processes at the RPE-Bruch's membrane interface in aging and age-related macular degeneration. *Prog. Retin Eye Res.* 20, 705–732. doi: 10.1016/s1350-9462(01)00010-6

Iacovelli, J., Rowe, G. C., Khadka, A., Diaz-Aguilar, D., Spencer, C., Arany, Z., et al. (2016). PGC-1alpha induces human RPE oxidative metabolism and antioxidant capacity. *Invest. Ophthalmol. Vis. Sci.* 57, 1038–1051. doi: 10.1167/iovs.15-17758

Jassim, A. H., Inman, D. M., and Mitchell, C. H. (2021). Crosstalk between dysfunctional mitochondria and inflammation in glaucomatous neurodegeneration. *Front. Pharmacol.* 12:699623. doi: 10.3389/fphar.2021.699623

Jia, D., Park, J. H., Kaur, H., Jung, K. H., Yang, S., Tripathi, S., et al. (2021). Towards decoding the coupled decision-making of metabolism and epithelial-to-mesenchymal transition in cancer. *Br. J. Cancer* 124, 1902–1911. doi: 10.1038/s41416-021-01385-y

Johnson, L. V., Leitner, W. P., Staples, M. K., and Anderson, D. H. (2001). Complement activation and inflammatory processes in drusen formation and age related macular degeneration. *Exp. Eye Res.* 73, 887–896. doi: 10.1006/exer.2001.1094

Kaarniranta, K., Uusitalo, H., Blasiak, J., Felszeghy, S., Kannan, R., Kauppinen, A., et al. (2020). Mechanisms of mitochondrial dysfunction and their impact on age-related macular degeneration. *Prog. Retin. Eye Res.* 79:100858. doi: 10.1016/j.preteyeres.2020.100858

Kanow, M. A., Giarmarco, M. M., Jankowski, C. S., Tsantilas, K., Engel, A. L., Du, J., et al. (2017). Biochemical adaptations of the retina and retinal pigment epithelium support a metabolic ecosystem in the vertebrate eye. *Elife* 6:e28899. doi: 10.7554/eLife.28899

Khalsa, J. K., Chawla, A. S., Prabhu, S. B., Vats, M., Dhar, A., Dev, G., et al. (2019). Functionally significant metabolic differences between B and T lymphocyte lineages. *Immunology* 158, 104–120. doi: 10.1111/imm.13098

Khan, A. H., Pierce, C. O., De Salvo, G., Griffiths, H., Nelson, M., Cree, A. J., et al. (2021). The effect of systemic levels of TNF-alpha and complement pathway activity on outcomes of VEGF inhibition in neovascular. *AMD. Eye* 8. doi: 10.1038/s41433-021-01824-3 [Epub ahead of print].

Kominsky, D. J., Campbell, E. L., and Colgan, S. P. (2010). Metabolic shifts in immunity and inflammation. *J. Immunol.* 184, 4062–4068. doi: 10.4049/jimmunol.0903002

Kutty, R. K., Samuel, W., Boyce, K., Cherukuri, A., Duncan, T., Jaworski, C., et al. (2016). Proinflammatory cytokines decrease the expression of genes critical for RPE function. *Mol. Vis.* 22, 1156–1168.

Labsi, M., Soufli, I., Belguendouz, H., Djebbara, S., Hannachi, L., Amir, Z. C., et al. (2021). Beneficial effect of dimethyl fumarate on experimental autoimmune uveitis is dependent of pro-inflammatory markers immunomodulation. *Inflammopharmacology* 29, 1389–1398. doi: 10.1007/s10787-021-00864-1

Levy, O., Calippe, B., Lavalette, S., Hu, S. J., Raoul, W., Dominguez, E., et al. (2015). Apolipoprotein E promotes subretinal mononuclear phagocyte survival and chronic inflammation in age-related macular degeneration. *EMBO Mol. Med.* 7, 211–226. doi: 10.15252/emmm.201404524

Martin, G., Schlunck, G., Hansen, L. L., and Agostini, H. T. (2004). Differential expression of angioregulatory factors in normal and CNV-derived human retinal pigment epithelium. *Graefes Arch. Clin. Exp. Ophthalmol.* 242, 321–326. doi: 10.1007/s00417-003-0838-y

Mori, S., Kurimoto, T., Maeda, H., and Nakamura, M. (2020). Dimethyl fumarate promotes the survival of retinal ganglion cells after optic nerve injury, possibly through the Nrf2/HO-1 pathway. *Int. J. Mol. Sci.* 22, 297. doi: 10.3390/ijms22010297

Nelson, K. C., Carlson, J. L., Newman, M. L., Sternberg, P. Jr., Jones, D. P., Kavanagh, T. J., et al. (1999). Effect of dietary inducer dimethylfumarate on glutathione in cultured human retinal pigment epithelial cells. *Invest. Ophthalmol. Vis. Sci.* 40, 1927–1935.

Oh, H., Takagi, H., Takagi, C., Suzuma, K., Otani, A., Ishida, K., et al. (1999). The potential angiogenic role of macrophages in the formation of choroidal neovascular membranes. *Invest. Ophthalmol. Vis. Sci.* 40, 1891–1898.

Park, D. H., Connor, K. M., and Lambris, J. D. (2019). The challenges and promise of complement therapeutics for ocular diseases. *Front. Immunol.* 10:1007. doi: 10.3389/fimmu.2019.01007

Price, M. J., Patterson, D. G., Scharer, C. D., and Boss, J. M. (2018). Progressive upregulation of oxidative metabolism facilitates plasmablast differentiation to a T-Independent antigen. *Cell. Rep.* 23, 3152–3159. doi: 10.1016/j.celrep.2018.05.053

Rosales, M. A. B., Shu, D. Y., Iacovelli, J., and Saint-Geniez, M. (2019). Loss of PGC-1alpha in RPE induces mesenchymal transition and promotes retinal degeneration. *Life Sci. Alliance* 2:e201800212.

Rosenfeld, P. J., Brown, D. M., Heier, J. S., Boyer, D. S., Kaiser, P. K., Chung, C. Y., et al. (2006). Ranibizumab for neovascular age-related macular degeneration. *N. Engl. J. Med.* 355, 1419–1431.

Saint-Geniez, M., Kurihara, T., Sekiyama, E., Maldonado, A. E., and D'amore, P. A. (2009). An essential role for RPE-derived soluble VEGF in the maintenance

of the choriocapillaris. *Proc. Natl. Acad. Sci. U.S.A* 106, 18751–18756. doi: 10.1073/pnas.0905010106

Satish, S., Philipose, H., Rosales, M. A. B., and Saint-Geniez, M. (2018). Pharmaceutical induction of PGC-1alpha promotes retinal pigment epithelial cell metabolism and protects against oxidative damage. *Oxid. Med. Cell Longev* 2018:9248640. doi: 10.1155/2018/9248640

Seifert, P. (2017). Modified hiraoka TEM grid staining apparatus and technique using 3D printed materials and gadolinium triacetate tetrahydrate, a non-radioactive uranyl acetate substitute. *J. Histotechnol.* 40, 130–135. doi: 10.1080/01478885.2017.1361117

Shu, D. Y., Butcher, E., and Saint-Geniez, M. (2020). EMT and EndMT: emerging roles in age-related macular degeneration. *Int. J. Mol. Sci.* 21:4271. doi: 10.3390/ijms21124271

Shu, D. Y., Butcher, E. R., and Saint-Geniez, M. (2021). Suppression of PGC-1alpha drives metabolic dysfunction in TGFbeta2-induced EMT of retinal pigment epithelial cells. *Int. J. Mol. Sci.* 22:4701. doi: 10.3390/ijms22094701

Skuratovskaia, D., Zatolokin, P., Vulf, M., Mazunin, I., and Litvinova, L. (2019). Interrelation of chemerin and TNF-α with mtDNA copy number in adipose tissues and blood cells in obese patients with and without type 2 diabetes. *BMC Med. Genomics* 12:40. doi: 10.1186/s12920-019-0485-8

Wan, L., Lin, H. J., Tsai, Y., Lee, C. C., Tsai, C. H., Tsai, F. J., et al. (2010). Tumor necrosis factor-alpha gene polymorphisms in age-related macular degeneration. *Retina* 30, 1595–1600. doi: 10.1097/IAE.0b013e3181dc58a6

Wang, P. W., Kuo, H. M., Huang, H. T., Chang, A. Y., Weng, S. W., Tai, M. H., et al. (2014). Biphasic response of mitochondrial biogenesis to oxidative stress in visceral fat of diet-induced obesity mice. *Antioxid. Redox. Signal* 20, 2572–2588. doi: 10.1089/ars.2013.5334

Westermann, B. (2012). Bioenergetic role of mitochondrial fusion and fission. *Biochim. Biophys. Acta* 1817, 1833–1838. doi: 10.1016/j.bbabio.2012.02.033

Zhang, M., Jiang, N., Chu, Y., Postnikova, O., Varghese, R., Horvath, A., et al. (2020). Dysregulated metabolic pathways in age-related macular degeneration. *Sci. Rep.* 10:2464. doi: 10.1038/s41598-020-59244-4

Zyla, K., Larabee, C. M., Georgescu, C., Berkley, C., Reyna, T., and Plafker, S. M. (2019). Dimethyl fumarate mitigates optic neuritis. *Mol. Vis.* 25, 446–461.

Conflict of Interest: The authors declare that the research was conducted in the absence of any commercial or financial relationships that could be construed as a potential conflict of interest.

Publisher's Note: All claims expressed in this article are solely those of the authors and do not necessarily represent those of their affiliated organizations, or those of the publisher, the editors and the reviewers. Any product that may be evaluated in this article, or claim that may be made by its manufacturer, is not guaranteed or endorsed by the publisher.

frontiers | Frontiers in Neuroscience

REVIEW
published: 29 June 2022
doi: 10.3389/fnins.2022.911430

Necroptosis and Neuroinflammation in Retinal Degeneration

Yan Tao[1], *Yusuke Murakami*[1]*, *Demetrios G. Vavvas*[2] *and Koh-Hei Sonoda*[1]

[1] *Department of Ophthalmology, Graduate School of Medical Sciences, Kyushu University, Fukuoka, Japan,* [2] *Ines and Frederick Yeatts Retinal Research Laboratory, Retina Service, Department of Ophthalmology, Massachusetts Eye and Ear, Harvard Medical School, Boston, MA, United States*

Necroptosis mediates the chronic inflammatory phenotype in neurodegeneration. Receptor-interacting protein kinase (RIPK) plays a pivotal role in the induction of necroptosis in various cell types, including microglia, and it is implicated in diverse neurodegenerative diseases in the central nervous system and the retina. Targeting RIPK has been proven beneficial for alleviating both neuroinflammation and degeneration in basic/preclinical studies. In this review, we discuss the role of necroptosis in retinal degeneration, including (1) the molecular pathways involving RIPK, (2) RIPK-dependent microglial activation and necroptosis, and (3) the interactions between necroptosis and retinal neuroinflammation/degeneration. This review will contribute to a renewed focus on neuroinflammation induced by necroptosis and to the development of anti-RIPK drugs against retinal degeneration.

Keywords: necroptosis, neuroinflammation, microglia, retinal degeneration, RIPK

OPEN ACCESS

Edited by:
Henri Leinonen,
University of Eastern Finland, Finland

Reviewed by:
Yi Dai,
Fudan University, China
Lian Zhao,
National Eye Institute (NIH), United States

***Correspondence:**
Yusuke Murakami
murakami.yusuke.407@m.kyushu-u.ac.jp

Specialty section:
This article was submitted to Neurodegeneration, a section of the journal Frontiers in Neuroscience

Received: *02 April 2022*
Accepted: *23 May 2022*
Published: *29 June 2022*

Citation:
Tao Y, Murakami Y, Vavvas DG and Sonoda K-H (2022) Necroptosis and Neuroinflammation in Retinal Degeneration. Front. Neurosci. 16:911430. doi: 10.3389/fnins.2022.911430

INTRODUCTION

Neurodegenerative diseases are a complex group of disorders involving the processes of cell death and inflammation cell death inflammation, and include Alzheimer's and Parkinson's disease, amyotrophic lateral sclerosis (ALS) and retinal degeneration (Tansey and Goldberg, 2010; Heneka et al., 2015; Ito et al., 2016; Kauppinen et al., 2016). Inflammation is a multicellular process by which immune cells defend against pathogens and repair injury through a series of molecular and cellular changes, including the release of pro-inflammatory cytokines, apoptosis, and necroptosis (Wallach et al., 2014). Inflammation is strongly associated with cell death, especially that in a necrotic form (Wallach et al., 2014). Damage associated molecular patterns (DAMPs) generated by necrotic cells, such as interleukin-1α (IL-1α), tumor necrosis factor α (TNF-α), and high-mobility group box 1 protein (HMGB1) (Rock and Kono, 2008; Yanai et al., 2009; Wallach et al., 2014), strongly exacerbate inflammation.

Microglia are the first line of defense in the central nervous system (CNS), and exert both cytotoxic and cytoprotective effects at the crossroads between homeostasis and disease (Cherry et al., 2014; Lloyd et al., 2019; Rodríguez-Gómez et al., 2020). Persistent activation of microglia can trigger necroptosis, a type of necrosis induced by the activation of receptor-interacting protein kinase 1 (RIPK1)/RIPK3 (Weinlich et al., 2017; Galluzzi et al., 2018), and necroptosis in turn induces secretion of proinflammatory DAMPs and mediates chronic inflammation (Rodríguez-Gómez et al., 2020). It has been shown that microglial necroptosis executed by RIPK1/3 contributes to neuronal damage as well as brain regeneration (Welser et al., 2010; Ofengeim et al., 2017; He et al., 2021).

This review focuses on RIPK-dependent necroptosis which orchestrates neuroinflammation and degeneration in the CNS and retina. We also discuss the potency of anti-necroptosis therapy, which may inhibit excessive neuroinflammation and promote neuronal survival and regeneration.

NECROPTOSIS AND RIPK SIGNALING

Necroptosis—A Programmed Necrotic Cell Death

Necrosis is a type of cell death that has morphologic features of cellular swelling, cell membrane rupture and the release of intracellular molecules including DAMPs (Kaczmarek et al., 2013; Galluzzi et al., 2018; Yuan et al., 2019). Although necrosis was traditionally deemed as a passive process of cell death, it is now known that some necrosis is molecularly regulated, and differential mechanisms that underlie programmed necrosis have been identified (e.g., necroptosis, pyroptosis, and ferroptosis). Necroptosis was originally described in 2005 as necrotic cell death mediated by the activation of RIPK1 (Degterev et al., 2005). The stimuli that induce necroptosis include TNF-α (Degterev et al., 2008), Fas ligand (FasL) (Holler et al., 2000), TNF-related apoptosis-inducing ligand (TRAIL) (Holler et al., 2000), the interferons (IFNs) (Thapa et al., 2013; Dillon et al., 2014), and ligands for pathogen recognition receptors (PRRs), such as toll-like receptor 3 (TLR3) (Bermejo and Rey-Bellet, 1975), TLR4 and DNA-dependent activator of interferon regulatory factors (DAI) (Upton et al., 2012; Wang et al., 2014; Huang et al., 2015).

Structure and Function of RIPK

RIPK1 is a multi-functional protein that regulates cell survival, inflammation, and cell death. It is composed of three domains, an N-terminal kinase domain for phosphorylation, an intermediate domain containing an RIP homotypic interaction motif (RHIM) for RIPK1/RIPK3 interaction and pro-inflammatory action, and a C-terminal death domain (DD) for recruiting TNFα receptor 1 (TNFR1) and the TNFR1-associated death domain (TRADD) protein (**Figure 1**) (Yuan et al., 2019). RIPK3, a key molecule for RIPK1/RIPK3 phosphorylation, also has an N-terminal kinase domain and RHIM domain, but lacks the DD in its C-terminus (**Figure 1**) (Wu et al., 2014). Mixed lineage kinase domain-like protein (MLKL) consists of an N-terminal 4-helix bundle (4HB) for interacting with the membrane and the first brace helix, an intermediate brace region with two helices involved in MLKL oligomerization, and a C-terminal pseudokinase domain (PsKD) for interaction with phosphorylated RIPK3 kinase domains (**Figure 1**) (Murphy et al., 2013; Quarato et al., 2016; Petrie et al., 2018, 2019). MLKL forms oligomers and the 4HB insert into the plasma membrane through phosphatidylinositol phosphate (PIP)-binding sites, resulting in membrane disruption and necroptosis induction (Dondelinger et al., 2014; Su et al., 2014; Quarato et al., 2016; Petrie et al., 2019). Therefore, the phosphorylation of MLKL and the membrane translocation of MLKL oligomers are the optimal markers for necroptosis (Fricker et al., 2018).

Among several stimuli for necroptosis, TNFR1 signaling is the most thoroughly investigated and proceeds as follows (**Figure 2**) (Seo et al., 2019). First, TNF binding to its receptor initiates the formation of complex I at the cell membrane. TNFR1 recruits RIPK1, TRADD, TNF receptor associated factor 2 (TRAF2) and cellular inhibitor of apoptosis 1/2 (cIAP1/2). cIAP1/2 initiates the ubiquitination process on the complex I (Bertrand et al., 2008; Varfolomeev et al., 2008; Annibaldi et al., 2018; Seo et al., 2019), and K63 poly-ubiquitination (Ub) of RIPK1 links many molecules, thereby forming a larger complex I. The TGF-β activated kinase 1 (TAK1) complex phosphorylates inhibitor of NF-κB kinase β (IKKβ) to activate the nuclear factor-κB (NF-κB) pathway (Jha et al., 2019; Seo et al., 2019). The NF-κB-dependent production of pro-survival genes, such as cIAP1, A20 and caspase-8-like inhibitory protein (c-FLIP$_L$), protects cells from RIPK1-independent death. A20 is a deubiquitinating enzyme that prevents NF-κB activation and restricts TNF-induced apoptosis (Onizawa et al., 2015). cIAP1 and c-FLIP$_L$ facilitate NF-κB activation and inhibit necroptosis. NF-κB activation also modulates immune response *via* the production of proinflammatory molecules (Jha et al., 2019; Jensen et al., 2020).

The TNFR1-mediated signaling pathway can induce apoptosis. Once the NF-κB pathway or complex I is inhibited by cIAP1/2 or by the linear ubiquitination assembly complex (LUBAC), TAK1, or TANK binding kinase 1 (TBK1), the membrane-bound complex I is dissociated and cytosolic complex IIa and IIb are formed. TRADD, FADD and caspase-8 form complex IIa and mediate RIPK1-independent apoptosis (Dondelinger et al., 2016; Annibaldi and Meier, 2018). Complex

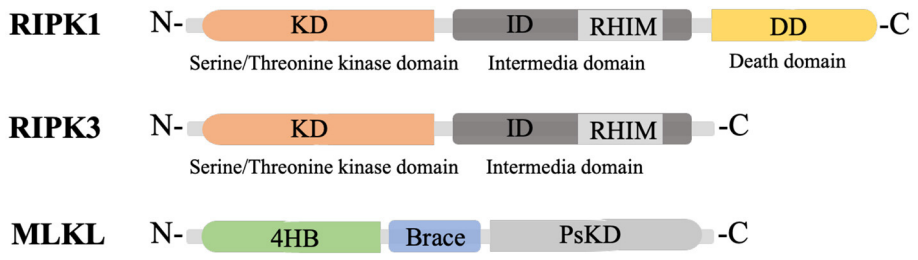

FIGURE 1 | Structure of RIPK1, RIPK3 and MLKL. KD, N-terminal kinase domain; ID, intermediate domain; RHIM, RIP homotypic interaction motif; DD, death domain; 4HB, 4-helix bundle; PsKD, pseudokinase domain.

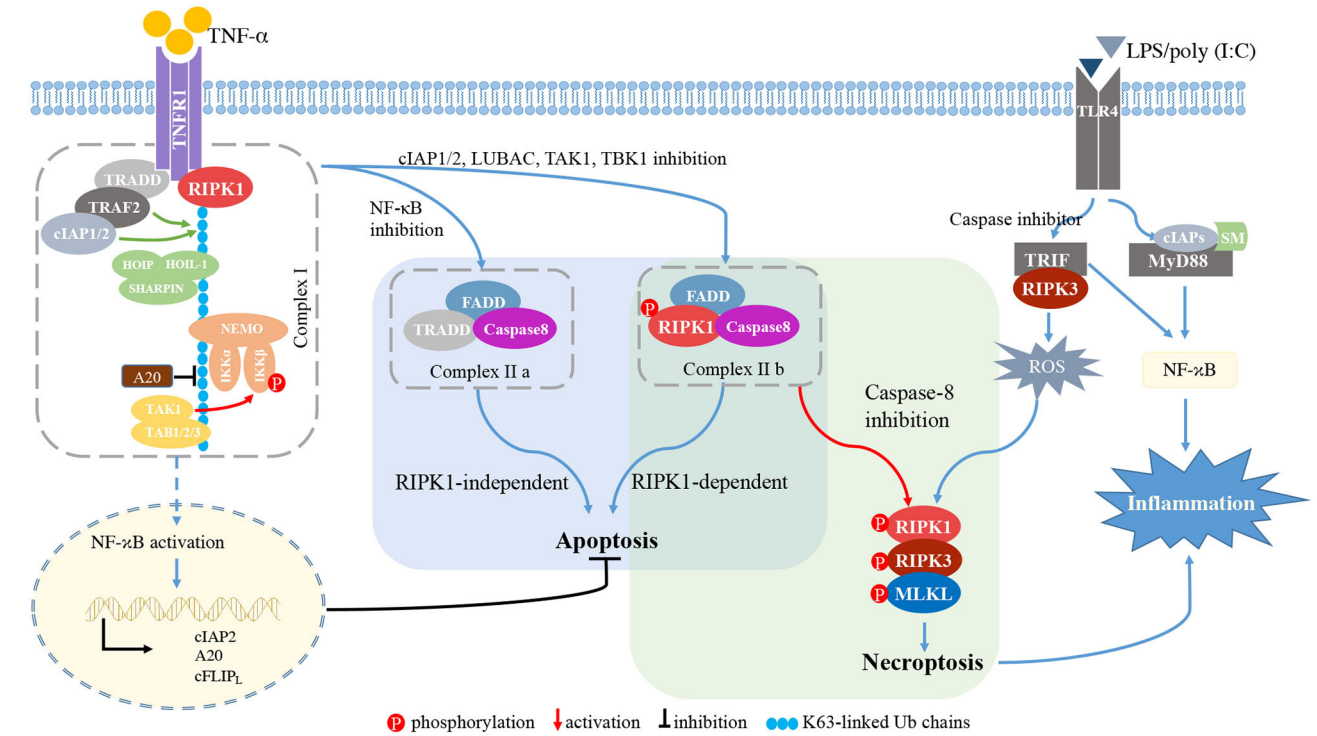

FIGURE 2 | RIPK signaling. TNFR1 recruits RIPK1, TRADD, TRAF2, and cIAP1/2. cIAP1/2 initiates the ubiquitination process on complex I. The K63 Ub chain of RIPK1 links molecules in the large TNF complex I. The TAK1 complex phosphorylates IKKβ to induce NF-κB activation. When NF-κB, the complex of cIAP1/2, or LUBAC, TAK1, or TBK1 is inhibited, membrane-bound complex I is dissociated and complex II is formed. If NF-κB is inhibited, TRADD, FADD and caspase-8 form complex IIa, inducing RIPK1-independent apoptosis. When inhibition of cIAP1/2, TAK1, TBK1, or LUBAC occurs, RIPK1, FADD, caspase-8, and c-FLIPL form complex IIb, inducing RIPK1-dependent apoptosis. Procaspase-8/cFLIPL heterodimers prevent necroptosis. Upon caspase-8 inhibition, complex IIb initiates RIPK1- and RIPK3-dependent necroptosis. Activated RIPK1 heterodimerizes with RIPK3 and RIPK3 phosphorylates MLKL, thereby driving the polymerization of RIPK1, RIPK3 and MLKL. This RIPK1-RIPK3-MLKL complex is called a "necrosome." In macrophages/microglia, LPS or poly(I:C) is recognized by TLR4 and mediates the interaction between TRIF and RIPK3. In the presence of caspase inhibitor, the TRIF/RIPK3 complex induces ROS accumulation, and subsequently triggers necroptosis independent of NF-κB activation. TLR4 also recruits MyD88 and cIAPs to activate the NF-κB pathway, thereby inducing pro-inflammatory cytokines. TNF-α, tumor necrosis factor-α; TNFR1, TNFα receptor 1; RIPK1/3, receptor-interacting protein kinases 1/3; TRADD, TNFR1-associated death domain protein; TRAF2, TNF receptor associated factor 2; cIAP1/2, cellular inhibitor of apoptosis 1/2; HOIL-1, haem-oxidized iron-regulatory protein 2 ubiquitin ligase-1; HOIP, HOIL-1 interacting protein; SHARPIN, SHANK-associated RH domain-interacting protein; NF-κB, nuclear factor-κB; NEMO, cell death-protective nuclear factor-κB essential modulator; IKKα/β, inhibitor of NF-κB kinase α/β; TAB2/3, TAK1-binding protein 2 and 3; FADD, Fas associated *via* death domain; cFLIP$_L$, the long isoform of cellular FLICE-like inhibitory protein; MLKL, mixed lineage kinase domain-like protein; TIRF, TIR-domain containing adapter-inducing interferon-b; MYD88, myeloid differentiation primary response gene 88; SMs, SMAC mimetics; ROS, reactive oxygen species.

IIb is composed of RIPK1, FADD, caspase-8 and c-FLIP$_L$, and initiates RIPK1-dependent apoptosis (Cho et al., 2009; Oberst et al., 2011; Sun et al., 2012).

Upon caspase-8 inhibition, complex IIa contributes to necroptotic induction by recruiting RIPK1, and complex IIb initiates RIPK1- and RIPK3-dependent necroptosis. Activated RIPK1 heterodimerizes with RIPK3 and RIPK3 phosphorylates MLKL, thereby polymerizing RIPK1, RIPK3 and MLKL (Sun et al., 2012; Zhao et al., 2012). This RIPK1-RIPK3-MLKL complex, called a "necrosome," triggers the subsequent cell lysis. A20 inhibits formation of the RIPK1-RIPK3 complexes by deubiquitinating RIPK3 (Onizawa et al., 2015; Galluzzi et al., 2018).

The PRR family can also initiate necroptosis. TLR4 recruits the adaptor molecules myeloid differentiation primary response gene 88 (MyD88) and TIR-domain containing adapter-inducing interferon-b (TRIF), while TRIF is the sole adaptor molecule for TLR3 (Kawai and Akira, 2010). Stimulation of TLR4/TLR3 *via* LPS or poly(I:C) induces the formation of the TRIF-RIPK3 complex (Kaiser and Offermann, 2005; He et al., 2011). In the presence of caspase-8 inhibitor, reactive oxygen species (ROS) accumulation occurs downstream of the TRIF-RIPK3 complex, and the subsequent c-jun N-terminal kinase (JNK) activation forms the RIPK1-RIPK3-MLKL complex and induces necroptosis independent of NF-κB activation (He et al., 2011; Kim and Li, 2013). TLR4 also recruits the adaptor molecules MyD88 and cIAPs to induce the NF-κB pathway activation and release of pro-inflammatory cytokines (**Figure 2**).

INTERACTIONS BETWEEN NECROPTOSIS AND NEUROINFLAMMATION

Necroptosis can trigger inflammation. Activated microglia/macrophages also induce necroptosis at the chronic

inflammatory site, thereby forming a positive feedback loop. In neurodegenerative diseases, dying or dead neuronal cells release DAMPs and activate PRRs (Wallach et al., 2014). PRR signaling activates microglia and transforms them to a pro-inflammatory phenotype that produces abundant pro-inflammatory cytokines (Fernández-Velasco et al., 2014). TNF-α and PRPs-mediated signals activate intracellular pathways, such as the NF-κB activation pathway, which leads to the transcription of various pro-inflammatory molecules, and the RIPK pathway, which mediates microglial activation and necroptosis (Granger and Kolb, 1968; Liu et al., 2017).

Characteristics of Microglial Activation in Neurodegeneration

Microglia are resident macrophages in the CNS and retina that surveil the surrounding environment and maintain tissue homeostasis (Nimmerjahn et al., 2005). Microglia can dynamically change their morphology and function in response to microenvironmental alterations (Choi et al., 2021). Although, in healthy individuals, blood circulating monocytes cannot enter the CNS and retina due to the healthy blood-brain and retina-barrier, under disease conditions they can infiltrate and differentiate into macrophages.

Microglia exhibit diverse functional phenotypes depending on the disease context (Ransohoff, 2016). In the same way that peripheral macrophages are traditionally classified into two major phenotypes (Martinez and Gordon, 2014) (i.e., M1 and M2), microglia can also polarize into both pro- and anti-inflammatory states at the diseased loci. Once microglia and/or macrophages detect DAMPs, they convert to the pro-inflammatory M1-like phenotype and form a high motility amoeboid shape (Chen and Xu, 2015). Activated microglia translocate to the damage site and secrete pro-inflammatory cytokines (IL-1β, IL-6, IL-8, TNF-α, iNOS) (Kalkman and Feuerbach, 2016; Aguzzi and Zhu, 2017). After the damaging molecules are diminished, the microglia change their polarity to an anti-inflammatory M2-like phenotype, improving their phagocytotic function, secreting IL-4, IL-10, IL-13, TGF-β, and arginase 1 and clearing the cellular debris to promote recovery (Cherry et al., 2014; Park et al., 2016). Triggering-receptors-expressed-on-myeloid-cells 2 (TREM2) is one kind of microglial receptor that is highly expressed in anti-inflammatory or pro-regenerative microglia and involved in phagocytosis and immune regulation (Paloneva et al., 2002; Hickman and El Khoury, 2014; Hickman et al., 2018). Overexpression of TREM2 enhances phagocytic activity and down-regulates pro-inflammatory responses (Han et al., 2017). In contrast, deletion of TREM2 or the adaptor tyrosine kinase-binding protein (TyroBP or DAP12), which binds to TREM2, leads to an excess of the pro-inflammatory phenotype, which decreases microglial survival and causes amyloid plaque deposition in experimental models of Alzheimer's disease (AD) (Ito and Hamerman, 2012). Therefore, these findings suggest that TREM2 is a key immune regulator that mediates the homeostatic function of microglia. However, it should be noted that there are more diverse and complex phenotypes in microglia and macrophages, and their plasticity (reaction states) and diversity (subtypes) should both be considered rather than merely the two commonly phenotypes (Stratoulias et al., 2019). Single-cell level analyses will help further clarify the microglia/macrophage subsets that regulate CNS health and diseases (Ransohoff, 2016; Hammond et al., 2019; Masuda et al., 2019; Stratoulias et al., 2019).

RIPK Modulates Microglial Activation and Necroptosis in Neuroinflammation

Microglia recognize the DAMPs through pattern recognition proteins (PRPs) such as TLRs. As shown in Section 2.2, TLR signaling mediates microglial activation (i.e., M1-like polarization) as well as apoptosis/necroptosis through RIPK recruitment into the cell death complex. TNF-α released from microglia may also activate RIPK pathways in the surrounding neuronal cells as well as microglia themselves.

Soluble oligomeric amyloid β (Aβ) has been shown to stimulate TNF-α release from activated microglia, leading to the induction of neuronal necroptosis in an *in vitro* model of AD (Salvadores et al., 2021). *Ripk3*$^{-/-}$ and *Mlkl*$^{-/-}$ mice favor pro- to anti-inflammatory phenotype transformation of microglia in response to ischemic cortex injury (Yang et al., 2018). Therefore, RIPK may regulate necroptosis and microglia/macrophage polarization in neurodegeneration (**Table 1**).

RIPK may contribute to microglia/macrophage polarization *via* a mechanism that is at least partly independent of necroptosis (Ofengeim and Yuan, 2013; Ofengeim et al., 2015, 2017; Kondylis et al., 2017; Ueta et al., 2019). Our previous study showed that RIPK inhibition suppresses M2-like polarization through caspase activation and attenuates the formation of laser-induced choroidal neovascularization (CNV) (Ueta et al., 2019). Both *in vivo* and *in vitro* experiments have shown that infiltrating macrophages, rather than vascular endothelial cells, are the main target for catalytic inhibition of RIPK. These findings suggest that RIPK has a non-necrotic function in angiogenesis *via* regulation of the macrophage phenotype. Ofengeim et al. reported a non-cell death function of RIPK1—namely, mediation of the disease-associated microglia (DAM) phenotype—in AD pathology (Ofengeim et al., 2017). They showed that RIPK1 is highly expressed in the cerebral microglia of patients with AD. In a mouse model of AD and *in vitro* cultured microglia, RIPK1 inhibition was shown to attenuate the DAM response and to enhance phagocyte activity to clear Aβ (Ofengeim et al., 2017). Transcriptional analysis found that RIPK1 induces Cst7 expression, which regulates the lysosomal function of microglia, suggesting that RIPK1-dependent transcription disturbs the homeostatic function of microglia and leads to Aβ accumulation in AD (Ofengeim et al., 2017). Alternatively, Vince et al. demonstrated that RIPK3 directly regulates NLRP3 inflammasome activation and IL-1β secretion in macrophages (Vince et al., 2012). They showed that RIPK3 mediates IAP-antagonist-induced IL-1β secretion prior to inducing necrotic changes (Vince et al., 2012).

TABLE 1 | Pharmacological and genetic interventions that manage cell death and inflammation in RIPK-related pathways in CNS diseases.

Role of the RIPK/related pathway	Disease and model	Mode of RIPK inhibition	Outcome	References
Mediates DAM response and reduces the lysosomal function of microglia	AD (APP/PS1)	RIPK1 inhibitor; *Ripk1-D138N* double mutant mice	• Attenuated DAM response • Enhanced phagocytosis of Aβ	Ofengeim et al., 2017
Activates the NLRP3 inflammasome	Bacterial encephalitis (LPS treatment in macrophages)	*Ripk3* knockout	• Inhibited the IL-1 secretion induced by LPS and IAP antagonist	Vince et al., 2012
Induces microglial necroptosis	ICH (injection of autologous blood from the femoral artery into the right basal ganglia)	Melatonin (upregulation of deubiquitinating enzyme A20)	• Reduced microglial necroptosis and TNF secretion • Suppressed neuronal necroptosis	Lu et al., 2019
Induces necroptosis and age-related neuroinflammation	Aging (old WT mice)	RIPK1 inhibitor; *Mlkl* knockout; *Ripk3* knockout	• Reduced age-associated neuroinflammation	Thadathil et al., 2021
Promotes axonal degeneration and neuroinflammation	ALS (Optn-deficient mice, SOD1 transgenic mice)	RIPK1 inhibitor; *Ripk1*-D138N mutant	• Suppressed neuronal cell death • Reduced microglial response	Ito et al., 2016

DAM, disease-associated microglia; AD, Alzheimer's disease; APP/PS1, amyloid precursor protein/presenilin 1; Aβ, amyloid-β; ALS, amyotrophic lateral sclerosis; ICH, intracerebral hemorrhage.

Ubiquitination in Microglia-Related Inflammation

Ubiquitin participates in various biological processes, including protein degradation, transcription, DNA and immune regulation (Husnjak and Dikic, 2012; Zinngrebe et al., 2014). Several E3 ubiquitin ligases are involved in the regulation of MyD88- and TRIF-dependent signaling from TLRs (Wertz and Dixit, 2010). TRAF6, one of the ubiquitin E3 ligases, mediates K63-linked ubiquitination of the IKK complex subunit, IKKγ, and activates MyD88- and TRIF-dependent NF-κB signaling (Walsh et al., 2008). A20 can modulate ubiquitination and remove K63 polyubiquitin chains from target proteins to terminate signaling, as shown in **Figure 2** (Komander et al., 2009; Mohebiany et al., 2020).

Kinsella et al. (2016) identified that the Bcl-2 family protein BH3-interacting domain death agonist (Bid) strengthens the TLR4-NF-κB pro-inflammatory response by promoting K63-linked polyubiquitination of TRAF6 in microglia. In a subsequent study, they demonstrated that Bid modulates MyD88- and TRIF-dependent signaling by attenuating the cleavage of polyubiquitin chains, thereby enhancing the inflammatory response (Kinsella et al., 2018).

A study on AD demonstrated that the E3 ubiquitin ligase COP1 inhibits the activation of microglia and the release of pro-inflammatory factors by degrading the transcription factor CCAAT/enhancer binding protein beta (c/EBPβ) (Ndoja et al., 2020). These transcription factors promote gene expressions related to microglial activation and inflammation. Increased secretion of pro-inflammatory factors and neurotoxicity in COP1-deficient microglia were observed in a mouse model of tau-mediated neurodegeneration and microglia-neuronal co-cultures. Thus, COP1 is important for suppression of the pathogenic c/EBPβ-dependent gene expression process in microglia.

RIPK is also involved in K63-linked Ub. IAPs are the key E3 ubiquitin ligases that ubiquitinate RIPK1/2 and cause NF-κB activation (**Figure 2**) (Jensen et al., 2020). Several studies have shown that RIPK1-mediated inflammatory signaling can be inhibited by second mitochondria-derived activator of caspases (SMAC), a small-molecule antagonist of IAPs (Busca et al., 2018; Goncharov et al., 2018). SMAC mimetics can also suppress the pro-inflammatory response in TLR signaling (**Figure 2**) (Tseng et al., 2010). Deubiquitinating enzyme is an alternative target to modulate RIPK activation. Lu et al. recently demonstrated that microglial necroptosis is suppressed by melatonin *via* the regulation of A20 in a model of intracerebral hemorrhage (Lu et al., 2019). Therefore, targeting ubiquitination may be a promising anti-inflammatory strategy.

The Role of Microglial Necroptosis in Neuroinflammation

Necroptosis can occur in neurons as well as microglial cells in CNS diseases. Thadathil et al. investigated the expression of p-MLKL, a marker of necroptosis, in the brains of young and aged mice and showed that nearly 70–80% of p-MLKL immunoreactivity is observed in neurons and <10% in microglia (Thadathil et al., 2021). Blocking or inhibiting necroptosis resulted in a significant reduction in neuroinflammation in aged mice (Thadathil et al., 2021). Therefore, necroptosis may be critically important in age-associated neuroinflammation and neurodegeneration.

Ito et al. investigated the functional roles of RIPK in an amyotrophic lateral sclerosis (ALS) model. Mutations in the optineurin *OPTN* gene have been implicated in patients with ALS (Ito et al., 2016). Using an ALS model of *optineurin* (*Optn*)-deficient mice, they reported that RIPK1 inhibition reduces the levels of proinflammatory cytokines, including IL-1α, IL-1β, interferon-γ (IFNγ), and TNF-α, in the spinal cord (Ito et al., 2016). RNA-sequencing analysis of $Optn^{-/-}$, and $Optn^{-/-}$;

Ripk1$^{D138N/D138N}$ microglia revealed that the M1-like phenotype in *Optn*$^{-/-}$ microglia is suppressed by RIPK1 inhibition (Kigerl et al., 2009; Ito et al., 2016). In addition, necrotic cell death in the spinal cord of *Optn*$^{-/-}$ mice was rescued by RIPK inhibition, which led to improved motor function (Ito et al., 2016). In pathological spinal cord sections from patients with ALS, increased co-immunostainings of RIPK1, RIPK3, MLKL, RIPK1 p-Ser14/15, p-MLKL, and microglia were observed (Ito et al., 2016). Therefore, RIPK1 may be a critical mediator of microglial activation as well as necroptosis in the axonal pathology of ALS.

THE ROLE OF RIPK IN RETINAL DEGENERATION AND NEUROINFLAMMATION

Given the significant roles of the RIPK pathway in necroptosis induction and microglial activation in CNS disorders, it would be natural to expect that RIPK is involved in retinal necroptosis and inflammation. Indeed, although it was traditionally considered that apoptosis is the main form of cell death in retinal degeneration, our group revealed that RIPK-dependent necroptosis is redundantly activated when caspases are inhibited in experimental retinal detachment (RD) (Trichonas et al., 2010). Rosenbaum et al. also demonstrated that treatment with Nec-1 prevents retinal cell death in a rat model of retinal ischemia (Rosenbaum et al., 2010). It is now known that RIPK plays pivotal roles in various retinal and optic nerve disorders, including inherited retinal diseases (IRDs), age-related macular degeneration (AMD), and glaucoma, even in the absence of caspase inhibition (Trichonas et al., 2010; Murakami et al., 2012, 2014; Kataoka et al., 2015; Do et al., 2017; Kayama et al., 2018). In the discussion below, we introduce studies addressing the RIPK function in necroptosis, microglial activation, and neuroinflammation in retinal degeneration (**Figure 3**; **Table 2**).

Role of RIPK in Retinal Detachment

Photoreceptor cells receive metabolic support from the underlying retinal pigment epithelium (RPE) and choroidal vessels, and when the neuroretina is physically detached from the RPE, photoreceptor cells start to die. Experimental models of RD induced by the subretinal injection of sodium hyaluronate and human samples with RD have shown that photoreceptor cell death is induced as early as 12 h and peaks at around 2–3 days after RD (Cook et al., 1995; Hisatomi et al., 2001; Arroyo et al., 2005). Hypoxia plays an important role in this process, because oxygen therapy substantially prevents photoreceptor cell loss in a cat model of RD (Lewis et al., 2004). Neuroinflammation also contributes to RD-induced retinal degeneration. Multiple cytokines/chemokines, including TNF-α, IL-1β, and MCP-1, are substantially elevated in the eyes in both experimental and human RD (Nakazawa et al., 2006a; Yoshimura et al., 2009). Moreover, genetic knockout of *Mcp-1* attenuates macrophage infiltration and prevents photoreceptor cell death in a rodent model of RD (Nakazawa et al., 2007). Sweigard et al. suggested that hypoxia mediates the activation of the alternative complement pathway in the detached mouse retina, indicating a molecular link between hypoxia and neuroinflammation (Sweigard et al., 2015).

Apoptosis is the main form of photoreceptor cell death after RD (Cook et al., 1995; Hisatomi et al., 2001; Arroyo et al., 2005). Consistent with the apoptotic morphological changes, such as pyknosis, both caspase activation in intrinsic and extrinsic pathways and upregulated expression of death receptor ligands (e.g., TNF-α and Fas-L) are observed in the rat retina after RD (Zacks et al., 2003, 2004). Paradoxically, however, caspase inhibition *via* intravitreal injection of pan-caspase inhibitor did not lead to protection against RD-induced retinal degeneration, suggesting the presence of other or redundant effectors for the photoreceptor cell death after RD.

As described above, caspases and RIPK redundantly function as cell death effectors in TNF-α signaling. Given the evidence that RIPK-dependent necrosis is strongly induced when the caspase pathway is blocked under various physiological and pathological conditions, we hypothesized that RIPK may mediate photoreceptor cell death after RD in concert with caspases. Indeed, we found that caspase inhibition in rodent models of RD substantially reduced apoptosis of photoreceptor cells while simultaneously increasing necrotic cell death in the detached retina. This necrotic change was rescued by additional treatment with Nec-1 or *Ripk3* deficiency, indicating that photoreceptor cell death after RD is redundantly regulated by at least two cell death pathways, i.e., caspase-dependent apoptosis and RIPK-dependent necroptosis (Trichonas et al., 2010). Consistent with our findings, Dong et al. demonstrated that Nec-1 inhibits RIPK phosphorylation and prevents necrotic photoreceptor cells after experimental RD (Dong et al., 2012).

RIPK inhibition in experimental RD prevents photoreceptor cell death, in addition to attenuating the infiltration of CD11b-positive microglia/macrophages in the detached retina (Trichonas et al., 2010). Kataoka et al. further investigated the roles of RIPK in inducing neuroinflammation after mouse experimental and human RD and showed that RIPK regulates NLRP3/caspase-1 inflammasome activation and prevents IL-1β secretion from subretinal microglia/macrophages (Kataoka et al., 2015). Because Vince et al. (2012) demonstrated that RIPK3 directly promotes IL-1β secretion in macrophages *via* inflammasome-dependent and -independent mechanisms, it may be possible that RIPK directly modulates microglia/macrophage activation after RD, in addition to indirectly activating neuroinflammation through the release of necrotic DAMPs.

Role of RIPK in Retinitis Pigmentosa

Retinitis pigmentosa (RP) is a set of hereditary retinal diseases characterized by the degeneration of rod and cone photoreceptors with genetic defects (Hartong et al., 2006). The typical progression in patients with RP begins with night blindness and loss of mid-peripheral visual field due to rod cell dysfunction and death, followed by loss of peripheral and central vision due to cone cell death (Hartong et al., 2006; Murakami et al., 2015). Many studies have shown that multiple signaling pathways lead to photoreceptor death, including apoptosis,

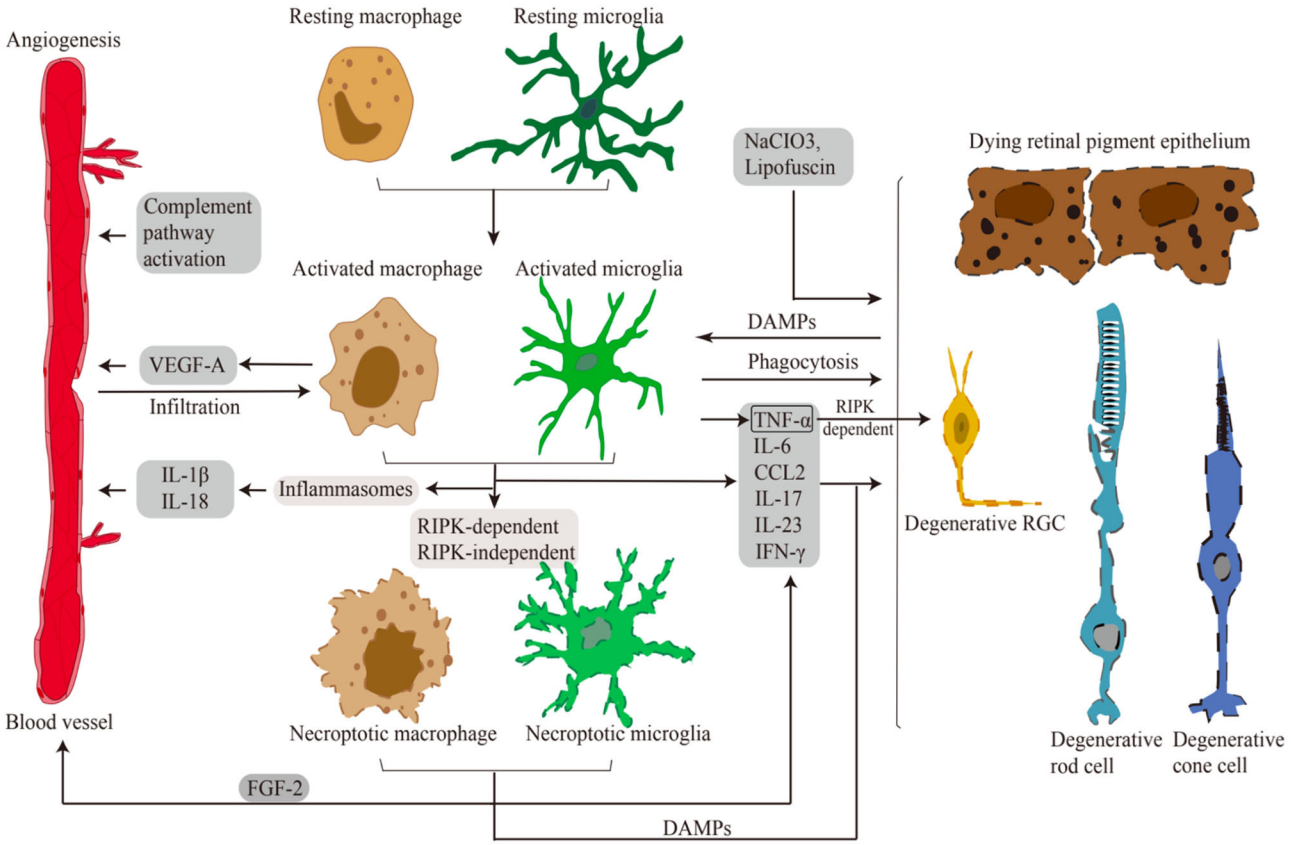

FIGURE 3 | Microglia/Macrophages in retinal disorders. Schematic representation of necroptotic and activated microglia/macrophages in retinal necroptosis and inflammation. Various damages and DAMPs activate innate immune cells. Activated and necroptotic microglia/macrophages *via* inflammasome-dependent/-independent mechanisms secrete inflammatory and angiogenic mediators. These pro-inflammatory and angiogenic factors induce choroidal neovascularization. Pro-inflammatory factors and DAMPs also lead to necrotic cell death of RGCs, RPE cells and photoreceptors. Moreover, activated microglia/macrophages infiltrate to the outer retina to phagocytose dead cells and modulate inflammation.

autophagy and necroptosis (Murakami et al., 2012, 2015; Sizova et al., 2014; Athanasiou et al., 2018; Viringipurampeer et al., 2019). However, the specific mechanisms predominating in each of rod and cone photoreceptor cell death in RP remain elusive.

Rod cell death in RP is induced by mutations in the causal genes, most of which are related to rod function, structure or homeostasis, and the dead cells exhibit apoptotic morphology. In contrast, cone cells, which do not express deleterious genes, remain healthy in the early stage of disease, but also degenerate after rod cell death. The mechanisms of this secondary cone cell death have not been fully understood; however, accumulating evidence suggests that microenvironmental alterations such as neuroinflammation, oxidation and metabolic imbalance contribute to the cone cell death in RP (Yoshida et al., 2013; Olivares-González et al., 2018, 2021; Newton and Megaw, 2020). Interestingly, morphological analyses of the postmortem eyes of RP patients demonstrated some necrotic features, such as swollen cytoplasm and membrane rupture in remaining cones (To et al., 2004). Consistent with these anatomical features, our group demonstrated that RIPK is essential for induction of cone necroptosis and microglia activation in rd10 mice, a mouse model of RP induced by a missense mutation in the *Pde6β* gene, and both effects could be suppressed by *Ripk3* deletion (Murakami et al., 2012). Subsequently, we found significantly enlarged cone cells in the macula of human RP patients using adaptive optics technology, and observed higher levels of HMGB1, a DAMP released from necrotic cells, in the vitreous of RP patients (Scaffidi et al., 2002; Murakami et al., 2015).

Consistent with our findings, Viringipurampeer et al. (2014) identified that cones expressed high levels of RIPK1 and RIPK3, and that the dying cones could be rescued by knockdown of *Ripk3* in *pde6c*^{w59} mutant zebrafish. Yang et al. (2017) also revealed that RIPK1 and RIPK3 were markedly upregulated in the retinas of sigma-1 receptor (S1R)-deficient rd10 mice, accompanied with a deteriorated loss of cones. A recent study reported that the necroptosis pathway is highly activated during photoreceptor death in Pro23His (P23H) transgenic albino rats, and P23H is also the most common mutation in autosomal dominant RP (Kakavand et al., 2020). Increased phospho-MLKL has been observed in the inner and outer segments of the P23H-3

TABLE 2 | Pharmacological and genetic interventions that manage cell death and inflammation in RIPK-related pathways in retinal diseases.

Role of the RIPK-related pathways	Disease and model	Mode of RIPK inhibition	Outcome	References
Mediates photoreceptor necroptosis and neuroinflammation	RD (subretinal injection of sodium hyaluronate), RP (rd10, rd1), acute retinal neural injury (NMDA-damaged mice), achromatopsia (*pde6c*^{w59} mutant zebrafish)	RIPK inhibitors; *Ripk3* knockout; *Ripk3* knockdown	• Rescued photoreceptor cells • Reduced Iba1^{+} or CD11b$^{+\cdot}$ microglia/macrophages	Trichonas et al., 2010; Murakami et al., 2012; Viringipurampeer et al., 2014; Huang et al., 2018
Activates the NLRP3 inflammasome	RD (subretinal injection of sodium hyaluronate)	*Ripk3* knockout	• Inhibited NLRP3/ IL-1β secretion • Rescued photoreceptor cell death	Kataoka et al., 2015
Mediates RPE necroptosis and DAMPs-mediated neuroinflammation	Dry AMD (dsRNA-induced retinal degeneration)	RIPK1 inhibitor; *Ripk3* knockout	• Rescued RPE and photoreceptor cell death • Reduced release of DAMPs and attenuated microglia/macrophages activation	Murakami et al., 2014
Induces microglial necroptosis	RP (rd1), acute retinal neural injury (NMDA-damaged mice)	RIPK1 inhibitor	• Decreased cytokine production • Rescued photoreceptor and retinal ganglion cell death	Huang et al., 2018
Induces microglial necroptosis	Retinal neovascularization (OIR)	RIPK1 inhibitor; Microglia-specific *Ripk3* knockout	• Decreased FGF2 release • Suppressed angiogenic retinopathy	He et al., 2021
Activates macrophages (M2 polarization)	Wet AMD (laser CNV)	RIPK1 inhibitor; *Ripk1* K45A mutant	• Suppressed M2-like polarization of macrophages • Attenuated pathological angiogenesis	Ueta et al., 2019
Induces necroptosis and neuroinflammation	Glaucoma (IR, acute high intraocular pressure)	RIPK1 inhibitor	• Reduced retinal damage and neuroinflammation	Rosenbaum et al., 2010; Dvoriantchikova et al., 2014
Induces RGCs necroptosis	Glaucoma (ON, optic nerve crush model)	RIPK1 inhibitor; *Ripk3* knockout	• Promoted RGC survival and axon regeneration	Kayama et al., 2018

RD, retinal detachment; AIF, apoptosis-inducing factor; RP, retinitis pigmentosa; DR, diabetic retinopathy; AMD, age-related macular degeneration; OIR, oxygen-induced retinopathy model; RGCs, retinal ganglion cells; IR, ischemia–reperfusion.

mouse retina (Kakavand et al., 2020). Furthermore, Sato et al. (2013) observed TNF-induced rod and cone necroptosis in *Irbp*-deficient mice. Interphotoreceptor retinoid-binding protein (IRBP) secreted by photoreceptors is important for photoreceptor survival, and *IRBP* mutation is associated with human RP.

Therefore, RIPK-mediated necroptosis may be a common mechanism for cone cell death in RP, and RIPK-mediated necroptosis may be a novel target to prevent the death of photoreceptors in RP patients.

Cell death and inflammation are interconnected. Indeed, we previously demonstrated that microglial activation is suppressed by *Ripk3* deficiency in rd10 mice. This anti-inflammatory effect of RIPK inhibition may be explained by the reduced release of DAMPs from necrotic cone cells as well as by the attenuation of microglial activation/necroptosis.

To our knowledge, only a single report has described the implications of microglial necroptosis in both *in vitro* and *in vivo* (rd1 mice, pde6β^{rd1} and NMDA-damaged mice) models of retinal degeneration (Huang et al., 2018). TLR4 is involved in the activation of microglia in these models, in association with infiltration of Iba-1^{+}/RIPK3^{+} necroptotic microglia at the site of degeneration. These necroptotic microglia secrete inflammation mediators, e.g., TNF-α, chemokine (C-C motif) ligand 2 (CCL2), IL-17, IL-23 and IFN-γ. Pharmacological blockade of RIPK1 has been shown to ameliorate microglial activation and retinal degeneration in both an NMDA-induced retinal neural injury model and murine BV2 microglial cells (Huang et al., 2018). These findings suggest that microglial necroptosis may regulate neuroinflammation in RP, at least in part.

Role of RIPK in Dry Age-Related Macular Degeneration

AMD is a primary cause of central visual loss in developed countries and affects primarily the elderly (Smith et al., 2001). Early AMD is characterized by pathological deposits (drusen) between the RPE and the Bruch's membrane (Al-Zamil and Yassin, 2017; Handa et al., 2019). RPE are monolayer cells maintaining the functionality of overlying photoreceptors (Boulton and Dayhaw-Barker, 2001). Widespread drusen, various pathologies such as inflammation, and various genetic and environmental factors promote RPE dysfunction and photoreceptor death (Handa et al., 2019; Miller et al., 2021). Advanced late-stage dry AMD, also known as geographic atrophy (GA), is associated with the degradation of RPE cells in a non-neovascular form (Handa et al., 2019; Miller et al., 2021). Oxidative stress is implicated in the pathogenesis of both wet and

dry AMD, and it can cause blood-retinal barrier breakdown that triggers chronic inflammation (Barnett and Handa, 2013).

Alterations of many inflammatory cytokines have been detected in plasma, serum or intraocular fluid in patients with AMD, but regrettably there is no stable trend or consistency in the reported findings (Tan et al., 2020).

Infiltration of macrophages has been detected in late advanced dry AMD and neovascular AMD (Penfold et al., 1985; Lad et al., 2015). Activated immune cells such as microglia/macrophages can migrate or infiltrate to the outer nuclear layer and remove photoreceptor debris, which is believed to be related to atrophic AMD (Killingsworth et al., 1990; Gupta et al., 2003). Analysis of a single-cell transcriptomic atlas of human retinas indicated that microglia are one of the factors most predictive of AMD, which highlights the importance of microglia in AMD pathogenesis (Menon et al., 2019). A histological study of the human eyes revealed that higher numbers of macrophages are concentrated in the choroid in late dry AMD than in normal AMD (Wang et al., 2022). Taken together, these data indicate a pathogenetic role of inflammation and immune response in AMD. Yet there is still controversy and debate regarding the origin of the cells reported in histopathology as macrophages, with some studies supporting the notion that some of these cells may not be bona-fide immune cells but rather transdifferentiated RPE cells (Lad et al., 2015; Curcio and Ach, 2016).

The RIPK-dependent necrotic pathway is crucial in RPE and photoreceptor cell death in AMD. Our previous study identified that programmed necroptosis is the main mechanism for cell death of RPE in dsRNA-induced retinal degeneration, a model of dry AMD (Murakami et al., 2014). *Ripk3* deficiency in this model reduced the release of DAMPs and suppressed the inflammatory response in the retina (Murakami et al., 2014). These findings suggest that RIPK-dependent necroptosis amplifies neuroinflammation by regulating the release of intracellular DAMPs (Murakami et al., 2014). Oxidative stress is one important component of AMD pathogenesis. Hanus et al. (2015) confirmed that RPE necroptosis is the predominant mechanism of $NaIO_3$-induced RPE cell death, a model of dry AMD induced by oxidative injury. Because caspase-8 is severely downregulated in the mature RPE (Yang et al., 2007), RPE cells may be predisposed to undergo necroptosis under a stressed condition.

A study by Pan et al. (2021) reported that retinal lipofuscin activates an atypical necroptosis in RPE cells as well as macrophages/microglia. That study provided new insights into necroptosis activation in aged human retinas with AMD. Interestingly, its authors demonstrated an atypical RPE necroptotic mechanism that involves neither RIPK1 nor RIPK3, but rather is mediated by lysosomal membrane permeabilization (LMP) and subsequent MLKL phosphorylation (Pan et al., 2021). In addition to RPE cells, phospho-MLKL staining was also observed in microglia/macrophages, which phagocytosed the sloughed RPE fragments (Pan et al., 2021). These findings suggest the intimate interactions between necroptosis and neuroinflammation in the pathology of dry AMD. They also show that anti-necroptosis agents that target MLKL phosphorylation (Nec-7) and oligomerization (NSA) prevent light-independent lipofuscin-elicited necroptosis. Thus, targeting lipofuscin-induced necroptosis may be a new therapeutic strategy for dry AMD.

Role of RIPK in Wet Age-Related Macular Degeneration

CNV is the end stage of the wet form of AMD, with growth of new blood vessels between Bruch's membrane and the RPE (Hobbs and Pierce, 2021). After CNV, extravasations, hemorrhage and fibrovascular scar formation occur in the subretinal space, leading to the death of the neurosensory retina and vision loss (Al-Zamil and Yassin, 2017; Hobbs and Pierce, 2021). How does the accumulated drusen induce neovascularization? Although vascular endothelial growth factor (VEGF) has been established as the key factor that initiates and promotes CNV, neuroinflammation also modulates CNV formation (Balser et al., 2019; Uemura et al., 2021). Activated microglia/macrophages release angiogenic and anti-angiogenic factors and work with VEGF to regulate retinal and choroidal angiogenesis (Pollard, 2009; Welser et al., 2010).

Doyle et al. (2012) showed that isolated drusen from AMD donor eyes can activate the NLRP3 inflammasome and secretion of IL-1b and IL-18. In a model of wet AMD with laser-induced CNV, IL-18 activation inhibited CNV development in *Nlrp3*$^{-/-}$ mice (Doyle et al., 2012). This study indicates that NLRP3 and IL-18 play a protective role in angiogenesis. Some *in vitro* studies have suggested that IL-18 may inhibit vascular endothelial cell proliferation (Park et al., 2001; Kim et al., 2005, 2006). The results of numerous studies are consistent with those of Doyle et al. (2012) that IL-18 has an antiangiogenic effect (Kim et al., 2005, 2006). The findings of Qiao et al. support the notion that IL-18 plays a role in suppressing angiogenesis by promoting the regression of pathologic neovascularization (NV), and the work of Cao et al. revealed an inhibitory effect of IL-18 on FGF-induced NV (Cao et al., 1999; Qiao et al., 2007). Therefore, IL-18 neuroinflammation may function in part to repress CNV formation in AMD, though other studies have failed to observe a significant contribution of IL-18 deficiency to spontaneous CNVM formation in *Vegfa*^{hyper} mice (Malsy et al., 2020; Marneros, 2021).

RIPK-dependent microglial necroptosis is also involved in retinal angiogenesis. He et al. argued that microglial necroptosis may be an important biological process in the etiology of retinal angiogenesis. They identified a subpopulation of microglia that highly express RIPK3 and MLKL through single-cell RNA sequencing in an oxygen-induced retinopathy (OIR) model (He et al., 2021). This necroptotic subpopulation of microglia promoted angiogenesis by releasing intracellular FGF2 (an angiogenic factor). The extracellular release of FGF2 was reduced by Nec1 treatment or conditional deletion of *Ripk3*. Moreover, combined treatment with anti-RIPK1 and anti-VEGF drugs has been shown to remarkably suppress angiogenesis in an OIR model (He et al., 2021). Collectively, this evidence reveals a new mechanism by which microglial necroptosis contributes to angiogenic retinopathy.

RIPK also regulates angiogenesis *via* non-necroptotic modulation of macrophages. Ueta et al. demonstrated that RIPK1 inhibition suppressed angiogenesis by modulating macrophage polarization in a mouse model of laser-induced CNV and alkali injury-induced corneal neovascularization (Ueta et al., 2019). Mechanistically, we revealed that RIPK1 inhibition mediates caspase activation and suppresses the pro-angiogenic M2-like phenotype in infiltrating macrophages. Therefore, RIPK may be a potential therapeutic target of pathological angiogenesis that could both inhibit necroptosis and modulate microglia/macrophage polarization.

Role of RIPK in Glaucoma

Glaucoma is characterized by the progressive loss of retinal ganglion cells (RGCs) and is a leading cause of irreversible blindness (Quigley and Broman, 2006). Glaucomatous neurodegeneration is attributed to various pathologies, such as mechanical pressure, vascular deficiency, inflammation, oxidative stress and metabolic dysregulation (Tezel, 2021). Elevated intraocular pressure (IOP) is the major risk factor for the progression of glaucoma, and pressure-induced retinal ischemia aggravates the death of RGCs (Sellés-Navarro et al., 1996).

While apoptosis has traditionally been considered the major type of RGC death in glaucoma, attempts to rescue RGCs by regulating apoptosis in glaucoma have been unsuccessful. Accumulating evidence indicates that both apoptosis and necroptosis participate in glaucomatous RGC death, and RIPK also plays a crucial role (Lee et al., 2013; Dvoriantchikova et al., 2014; Do et al., 2017; Wang et al., 2020). Dvoriantchikova et al. demonstrated that RIPK inhibition prevented RGC necroptosis in both an *in vitro* and an *in vivo* model of ischemic injury (Dvoriantchikova et al., 2014). Do et al. reported that RIPK1 was activated in a rat model of high IOP-induced ischemic injury, and a novel RIPK1-inhibitory compound significantly attenuated RGC death in a dose-dependent manner (Do et al., 2017). Consistent with these *in vivo* findings, Xiong et al. revealed that RIPK-mediated necroptosis is induced by oxygen-glucose deprivation in retinal ganglion cell line 5 (RGC-5) (Liao et al., 2017). Subsequently, they found that p90 ribosomal protein S6 kinase 3 (RSK3) is an upstream regulator of RIPK3 phosphorylation, and that an RSK3 inhibitor conferred RGC protection and functional recovery in rat with high IOP-induced ischemic injury (Wang et al., 2020). Our previous study also revealed that the expression of RIPK was increased in an optic nerve (ON) crush model, and necrosis inhibitors promoted a moderate level of axonal regeneration (Kayama et al., 2018). Collectively, these findings suggest that RIP kinase-dependent necroptosis is both a novel mechanism of RGC death and a suitable therapeutic target.

As described above, neuroinflammation is one of the pathogenic mechanisms of RGC degeneration in glaucoma (Weinreb et al., 2014). TNF-α is elevated in the aqueous humor, retina and optic nerve of glaucoma patients (Yan et al., 2000; Tezel, 2008; Sawada et al., 2010) as well as in a glaucoma mouse model induced by chronic ocular hypertension (Nakazawa et al., 2006b). In the latter study in mice (Nakazawa et al., 2006b) further showed that increased IOP induces TNF-α production in the retina and optic nerve, and ultimately causes RGC loss *via* microglia activation (**Figure 3**). Moreover, they found that intravitreal TNF-α injection induced RGC death that mimics that the glaucoma, and blockade of microglial activation rescued this RGC death induced by TNF-α (Nakazawa et al., 2006b). Collectively, these findings of Nakazawa et al. (2006b) highlight the importance of TNF-α and microglial neuroinflammation in the pathology of glaucoma. Other authors similarly showed that microglia are highly activated in the optic nerve head in human eyes with glaucoma, in association with the abundant expression of TNF-α, TGF-β and matrix metalloproteinases (Neufeld, 1999; Yuan and Neufeld, 2001).

The roles of RIPK and necroptosis in the neuroinflammation of glaucoma are still elusive. Dvoriantchikova et al. demonstrated that RIPK inhibition attenuates the expression of pro-inflammatory genes such as Il-1b, Ccl5, Cxcl10, Nos2, and Cybb in a high-IOP induced ischemic injury model, suggesting that RIPK may also mediate neuroinflammation in glaucoma (Dvoriantchikova et al., 2014).

Using a neuroinflammatory model of glaucoma (TNF-α induced RGC degeneration), Ko et al. revealed that a non-canonical form of necroptosis is critical for axonal degeneration of RGCs. They showed that sterile alpha and TIR motif 1 (SARM1), an inducible NAD+ cleavage enzyme, act downstream of TNF-α and activate MLKL. In this model, MLKL does not directly induce necroptosis but rather mediates the loss of axon survival factors NMNAT2 and SCG10/STMN2, which leads to axon degeneration. Therefore, inhibition of TNF-α and/or SARM1 may suppress axon necroptosis, and these pathways may serve as alternative targets for glaucomatous neurodegeneration.

PROSPECTS FOR ANTI-RIPK/NECROPTOSIS TREATMENT IN RETINAL DISORDERS

RIPK-dependent necroptosis has been proposed as a promising target for a variety of neurodegenerative diseases that involve both neuronal cell death and neuroinflammation. Inhibition of the RIPK pathway has been proven effective in blocking necroptosis and suppressing neuroinflammation in many of the basic experiments mentioned above, and therefore, strategies to translate these studies into clinical trials should be explored.

In preclinical studies, RIPK1 inhibitors have been the agents most studied for the treatment of CNS diseases. Such research has shown that Nec-1 administration controls the neuronal cell death induced by acute neuronal injury and improves motor and spatial memory (You et al., 2008). Nec-1 also promotes the ability of microglia to degrade Aβ in APP/PS1 mice (Ofengeim et al., 2017). The RIPK1 inhibitor GSK′547 ameliorated the aggregation of

lipofuscin-like lysosomal inclusions in microglia and improved survival in a model of lysosomal storage disorder (Safaiyan et al., 2016; Cougnoux et al., 2018). RIPK is activated under various necrotic or non-necrotic pathological inflammatory conditions, and thus well-designed drugs that target certain RIPK regulation points are critical for the treatment of human CNS and peripheral pathologies.

Indeed, Nec-1s and other RIPK1 inhibitors (e.g., GSK2982772, DNL104, DNL747, and DNL788) are presently being assessed in clinical trials for neurodegenerative and autoimmune diseases (Degterev et al., 2019; Mifflin et al., 2020). A phase II study of GSK2982772 for the treatment of psoriasis and ulcerative colitis (UC) was completed. The authors reported that GSK2982772 was safe and well-tolerated when dosed at 60 mg t.i.d., and that it may have ameliorated inflammation in 65 psoriasis patients (Weisel et al., 2020). They then assessed the potential effects at higher dosages and in patients with more active disease (Weisel et al., 2020). However, GSK2982772 showed no significant difference in clinical efficacy between the treatment and placebo groups in UC patients (Weisel et al., 2021). A phase I clinical trial of DNL747 for the treatment of AD has been completed, but the results have not been disclosed. RIPK3 inhibitors have not yet entered clinical trials, but studies on these agents are developing rapidly (Jensen et al., 2020).

Although the existing results of these clinical trials show the safety of anti-RIPK drugs with currently unknown efficacy, it will be critical to develop more secure, sustained, and effective inhibitors of RIPK to combat chronic neurodegeneration. Therefore, medicines with better pharmacological designs and sustained local delivery may be required for the further development of anti-RIPK therapy to prevent blindness in patients with currently incurable retinal degeneration.

AUTHOR CONTRIBUTIONS

YM proposed and guided the direction of the manuscript. YT and YM wrote the main body of this manuscript. K-HS and DV provided supervision of the review. All authors contributed to the article and approved the submitted version.

FUNDING

This work was supported by Grants-in-Aid for Scientific Research, #JP19K09952 and #JP22H03242 (to YM), a Uehara Memorial Foundation grant (to YM), a Charitable Trust Fund for Ophthalmic Research in Commemoration of Santen Pharmaceutical's Founder grant (to YM), and a Bayer Retina Award (to YM).

REFERENCES

Aguzzi, A., and Zhu, C. (2017). Microglia in prion diseases. *J. Clin. Invest.* 127, 3230–3239. doi: 10.1172/jci90605

Al-Zamil, W. M., and Yassin, S. A. (2017). Recent developments in age-related macular degeneration: a review. *Clin. Interv. Aging* 12, 1313–1330. doi: 10.2147/cia.S143508

Annibaldi, A., and Meier, P. (2018). Checkpoints in TNF-induced cell death: implications in inflammation and cancer. *Trends Mol. Med.* 24, 49–65. doi: 10.1016/j.molmed.2017.11.002

Annibaldi, A., Wicky John, S., Vanden Berghe, T., Swatek, K. N., Ruan, J., Liccardi, G., et al. (2018). Ubiquitin-mediated regulation of RIPK1 kinase activity independent of IKK and MK2. *Mol. Cell* 69, 566–580.e565. doi: 10.1016/j.molcel.2018.01.027

Arroyo, J. G., Yang, L., Bula, D., and Chen, D. F. (2005). Photoreceptor apoptosis in human retinal detachment. *Am. J. Ophthalmol.* 139, 605–610. doi: 10.1016/j.ajo.2004.11.046

Athanasiou, D., Aguila, M., Bellingham, J., Li, W., McCulley, C., Reeves, P. J., et al. (2018). The molecular and cellular basis of rhodopsin retinitis pigmentosa reveals potential strategies for therapy. *Prog. Retin. Eye Res.* 62, 1–23. doi: 10.1016/j.preteyeres.2017.10.002

Balser, C., Wolf, A., Herb, M., and Langmann, T. (2019). Co-inhibition of PGF and VEGF blocks their expression in mononuclear phagocytes and limits neovascularization and leakage in the murine retina. *J. Neuroinflamm.* 16, 26. doi: 10.1186/s12974-019-1419-2

Barnett, B. P., and Handa, J. T. (2013). Retinal microenvironment imbalance in dry age-related macular degeneration: a mini-review. *Gerontology* 59, 297–306. doi: 10.1159/000346169

Bermejo, E., and Rey-Bellet, J. (1975). Comparative study on the hypnotic effect of flurazepam and heptabarbital. *Rev. Med. Suisse Romande* 95, 635–641.

Bertrand, M. J., Milutinovic, S., Dickson, K. M., Ho, W. C., Boudreault, A., Durkin, J., et al. (2008). cIAP1 and cIAP2 facilitate cancer cell survival by functioning as E3 ligases that promote RIP1 ubiquitination. *Mol. Cell* 30, 689–700. doi: 10.1016/j.molcel.2008.05.014

Boulton, M., and Dayhaw-Barker, P. (2001). The role of the retinal pigment epithelium: topographical variation and ageing changes. *Eye* 15(Pt 3), 384–389. doi: 10.1038/eye.2001.141

Busca, A., Konarski, Y., Gajanayaka, N., O'Hara, S., Angel, J., Kozlowski, M., et al. (2018). cIAP1/2-TRAF2-SHP-1-Src-MyD88 complex regulates lipopolysaccharide-induced IL-27 production through NF-κB activation in human macrophages. *J. Immunol.* 200, 1593–1606. doi: 10.4049/jimmunol.1700199

Cao, R., Farnebo, J., Kurimoto, M., and Cao, Y. (1999). Interleukin-18 acts as an angiogenesis and tumor suppressor. *FASEB J.* 13, 2195–2202. doi: 10.1096/fasebj.13.15.2195

Chen, M., and Xu, H. (2015). Parainflammation, chronic inflammation, and age-related macular degeneration. *J. Leukoc. Biol.* 98, 713–725. doi: 10.1189/jlb.3RI0615-239R

Cherry, J. D., Olschowka, J. A., and O'Banion, M. K. (2014). Neuroinflammation and M2 microglia: the good, the bad, and the inflamed. *J. Neuroinflamm.* 11, 98. doi: 10.1186/1742-2094-11-98

Cho, Y. S., Challa, S., Moquin, D., Genga, R., Ray, T. D., Guildford, M., et al. (2009). Phosphorylation-driven assembly of the RIP1-RIP3 complex regulates programmed necrosis and virus-induced inflammation. *Cell* 137, 1112–1123. doi: 10.1016/j.cell.2009.05.037

Choi, S., Guo, L., and Cordeiro, M. F. (2021). Retinal and brain microglia in multiple sclerosis and neurodegeneration. *Cells* 10, 1507. doi: 10.3390/cells10061507

Cook, B., Lewis, G. P., Fisher, S. K., and Adler, R. (1995). Apoptotic photoreceptor degeneration in experimental retinal detachment. *Invest. Ophthalmol. Vis. Sci.* 36, 990–996.

Cougnoux, A., Clifford, S., Salman, A., Ng, S. L., Bertin, J., and Porter, F. D. (2018). Necroptosis inhibition as a therapy for Niemann-Pick disease, type C1: Inhibition of RIP kinases and combination therapy with 2-hydroxypropyl-β-cyclodextrin. *Mol. Genet. Metab.* 125, 345–350. doi: 10.1016/j.ymgme.2018.10.009

Curcio, C. A., and Ach, T. (2016). Macrophages or retinal pigment epithelium expressing macrophage markers in age-related macular degeneration? Comment on Lad et al. 2015. *Graefes Arch. Clin. Exp. Ophthalmol.* 254, 1237–1238. doi: 10.1007/s00417-016-3300-7

Degterev, A., Hitomi, J., Germscheid, M., Ch'en, I. L., Korkina, O., Teng, X., et al. (2008). Identification of RIP1 kinase as a specific cellular target of necrostatins. *Nat. Chem. Biol.* 4, 313–321. doi: 10.1038/nchembio.83

Degterev, A., Huang, Z., Boyce, M., Li, Y., Jagtap, P., Mizushima, N., et al. (2005). Chemical inhibitor of nonapoptotic cell death with therapeutic potential for ischemic brain injury. *Nat. Chem. Biol.* 1, 112–119. doi: 10.1038/nchembio711

Degterev, A., Ofengeim, D., and Yuan, J. (2019). Targeting RIPK1 for the treatment of human diseases. *Proc. Natl. Acad. Sci. U.S.A.* 116, 9714–9722. doi: 10.1073/pnas.1901179116

Dillon, C. P., Weinlich, R., Rodriguez, D. A., Cripps, J. G., Quarato, G., Gurung, P., et al. (2014). RIPK1 blocks early postnatal lethality mediated by caspase-8 and RIPK3. *Cell* 157, 1189–1202. doi: 10.1016/j.cell.2014.04.018

Do, Y. J., Sul, J. W., Jang, K. H., Kang, N. S., Kim, Y. H., Kim, Y. G., et al. (2017). A novel RIPK1 inhibitor that prevents retinal degeneration in a rat glaucoma model. *Exp. Cell Res.* 359, 30–38. doi: 10.1016/j.yexcr.2017.08.012

Dondelinger, Y., Darding, M., Bertrand, M. J., and Walczak, H. (2016). Poly-ubiquitination in TNFR1-mediated necroptosis. *Cell. Mol. Life Sci.* 73, 2165–2176. doi: 10.1007/s00018-016-2191-4

Dondelinger, Y., Declercq, W., Montessuit, S., Roelandt, R., Goncalves, A., Bruggeman, I., et al. (2014). MLKL compromises plasma membrane integrity by binding to phosphatidylinositol phosphates. *Cell Rep.* 7, 971–981. doi: 10.1016/j.celrep.2014.04.026

Dong, K., Zhu, H., Song, Z., Gong, Y., Wang, F., Wang, W., et al. (2012). Necrostatin-1 protects photoreceptors from cell death and improves functional outcome after experimental retinal detachment. *Am. J. Pathol.* 181, 1634–1641. doi: 10.1016/j.ajpath.2012.07.029

Doyle, S. L., Campbell, M., Ozaki, E., Salomon, R. G., Mori, A., Kenna, P. F., et al. (2012). NLRP3 has a protective role in age-related macular degeneration through the induction of IL-18 by drusen components. *Nat. Med.* 18, 791–798. doi: 10.1038/nm.2717

Dvoriantchikova, G., Degterev, A., and Ivanov, D. (2014). Retinal ganglion cell (RGC) programmed necrosis contributes to ischemia-reperfusion-induced retinal damage. *Exp. Eye Res.* 123, 1–7. doi: 10.1016/j.exer.2014.04.009

Fernández-Velasco, M., González-Ramos, S., and Boscá, L. (2014). Involvement of monocytes/macrophages as key factors in the development and progression of cardiovascular diseases. *Biochem. J.* 458, 187–193. doi: 10.1042/bj20131501

Fricker, M., Tolkovsky, A. M., Borutaite, V., Coleman, M., and Brown, G. C. (2018). Neuronal cell death. *Physiol. Rev.* 98, 813–880. doi: 10.1152/physrev.00011.2017

Galluzzi, L., Vitale, I., Aaronson, S. A., Abrams, J. M., Adam, D., Agostinis, P., et al. (2018). Molecular mechanisms of cell death: recommendations of the Nomenclature Committee on Cell Death 2018. *Cell Death Differ.* 25, 486–541. doi: 10.1038/s41418-017-0012-4

Goncharov, T., Hedayati, S., Mulvihill, M. M., Izrael-Tomasevic, A., Zobel, K., Jeet, S., et al. (2018). Disruption of XIAP-RIP2 association blocks NOD2-mediated inflammatory signaling. *Mol. Cell* 69, 551–565.e557. doi: 10.1016/j.molcel.2018.01.016

Granger, G. A., and Kolb, W. P. (1968). Lymphocyte *in vitro* cytotoxicity: mechanisms of immune and non-immune small lymphocyte mediated target L cell destruction. *J. Immunol.* 101, 111–120.

Gupta, N., Brown, K. E., and Milam, A. H. (2003). Activated microglia in human retinitis pigmentosa, late-onset retinal degeneration, and age-related macular degeneration. *Exp. Eye Res.* 76, 463–471. doi: 10.1016/s0014-4835(02)00332-9

Hammond, T. R., Dufort, C., Dissing-Olesen, L., Giera, S., Young, A., Wysoker, A., et al. (2019). Single-cell RNA sequencing of microglia throughout the mouse lifespan and in the injured brain reveals complex cell-state changes. *Immunity* 50, 253–271.e256. doi: 10.1016/j.immuni.2018.11.004

Han, J., Wang, M., Ren, M., and Lou, H. (2017). Contributions of triggering-receptor-expressed-on-myeloid-cells-2 to neurological diseases. *Int. J. Neurosci.* 127, 368–375. doi: 10.1080/00207454.2016.1264072

Handa, J. T., Bowes Rickman, C., Dick, A. D., Gorin, M. B., Miller, J. W., Toth, C. A., et al. (2019). A systems biology approach towards understanding and treating non-neovascular age-related macular degeneration. *Nat. Commun.* 10, 3347. doi: 10.1038/s41467-019-11262-1

Hanus, J., Anderson, C., and Wang, S. (2015). RPE necroptosis in response to oxidative stress and in AMD. *Ageing Res. Rev.* 24(Pt B), 286–298. doi: 10.1016/j.arr.2015.09.002

Hartong, D. T., Berson, E. L., and Dryja, T. P. (2006). Retinitis pigmentosa. *Lancet* 368, 1795–1809. doi: 10.1016/s0140-6736(06)69740-7

He, C., Liu, Y., Huang, Z., Yang, Z., Zhou, T., Liu, S., et al. (2021). A specific RIP3(+) subpopulation of microglia promotes retinopathy through a hypoxia-triggered necroptotic mechanism. *Proc. Natl. Acad. Sci. U. S. A.* 118, 1–10. doi: 10.1073/pnas.2023290118

He, S., Liang, Y., Shao, F., and Wang, X. (2011). Toll-like receptors activate programmed necrosis in macrophages through a receptor-interacting kinase-3-mediated pathway. *Proc. Natl. Acad. Sci. U.S.A.* 108, 20054–20059. doi: 10.1073/pnas.1116302108

Heneka, M. T., Carson, M. J., El Khoury, J., Landreth, G. E., Brosseron, F., Feinstein, D. L., et al. (2015). Neuroinflammation in Alzheimer's disease. *Lancet Neurol.* 14, 388–405. doi: 10.1016/s1474-4422(15)70016-5

Hickman, S., Izzy, S., Sen, P., Morsett, L., and El Khoury, J. (2018). Microglia in neurodegeneration. *Nat. Neurosci.* 21, 1359–1369. doi: 10.1038/s41593-018-0242-x

Hickman, S. E., and El Khoury, J. (2014). TREM2 and the neuroimmunology of Alzheimer's disease. *Biochem. Pharmacol.* 88, 495–498. doi: 10.1016/j.bcp.2013.11.021

Hisatomi, T., Sakamoto, T., Murata, T., Yamanaka, I., Oshima, Y., Hata, Y., et al. (2001). Relocalization of apoptosis-inducing factor in photoreceptor apoptosis induced by retinal detachment *in vivo*. *Am. J. Pathol.* 158, 1271–1278. doi: 10.1016/s0002-9440(10)64078-3

Hobbs, S. D., and Pierce, K. (2021). "Wet age-related macular degeneration (Wet AMD)," in *StatPearls* (Treasure Island, FL: StatPearls Publishing).

Holler, N., Zaru, R., Micheau, O., Thome, M., Attinger, A., Valitutti, S., et al. (2000). Fas triggers an alternative, caspase-8-independent cell death pathway using the kinase RIP as effector molecule. *Nat. Immunol.* 1, 489–495. doi: 10.1038/82732

Huang, Z., Wu, S. Q., Liang, Y., Zhou, X., Chen, W., Li, L., et al. (2015). RIP1/RIP3 binding to HSV-1 ICP6 initiates necroptosis to restrict virus propagation in mice. *Cell Host Microbe* 17, 229–242. doi: 10.1016/j.chom.2015.01.002

Huang, Z., Zhou, T., Sun, X., Zheng, Y., Cheng, B., Li, M., et al. (2018). Necroptosis in microglia contributes to neuroinflammation and retinal degeneration through TLR4 activation. *Cell Death Differ.* 25, 180–189. doi: 10.1038/cdd.2017.141

Husnjak, K., and Dikic, I. (2012). Ubiquitin-binding proteins: decoders of ubiquitin-mediated cellular functions. *Annu. Rev. Biochem.* 81, 291–322. doi: 10.1146/annurev-biochem-051810-094654

Ito, H., and Hamerman, J. A. (2012). TREM-2, triggering receptor expressed on myeloid cell-2, negatively regulates TLR responses in dendritic cells. *Eur. J. Immunol.* 42, 176–185. doi: 10.1002/eji.201141679

Ito, Y., Ofengeim, D., Najafov, A., Das, S., Saberi, S., Li, Y., et al. (2016). RIPK1 mediates axonal degeneration by promoting inflammation and necroptosis in ALS. *Science* 353, 603–608. doi: 10.1126/science.aaf6803

Jensen, S., Seidelin, J. B., LaCasse, E. C., and Nielsen, O. H. (2020). SMAC mimetics and RIPK inhibitors as therapeutics for chronic inflammatory diseases. *Sci. Signal.* 13. doi: 10.1126/scisignal.aax8295

Jha, N. K., Jha, S. K., Kar, R., Nand, P., Swati, K., and Goswami, V. K. (2019). Nuclear factor-kappa β as a therapeutic target for Alzheimer's disease. *J. Neurochem.* 150, 113–137. doi: 10.1111/jnc.14687

Kaczmarek, A., Vandenabeele, P., and Krysko, D. V. (2013). Necroptosis: the release of damage-associated molecular patterns and its physiological relevance. *Immunity* 38, 209–223. doi: 10.1016/j.immuni.2013.02.003

Kaiser, W. J., and Offermann, M. K. (2005). Apoptosis induced by the toll-like receptor adaptor TRIF is dependent on its receptor interacting protein homotypic interaction motif. *J. Immunol.* 174, 4942–4952. doi: 10.4049/jimmunol.174.8.4942

Kakavand, K., Jobling, A. I., Greferath, U., Vessey, K. A., de Iongh, R. U., and Fletcher, E. L. (2020). Photoreceptor degeneration in Pro23His transgenic rats (line 3) involves autophagic and necroptotic mechanisms. *Front. Neurosci.* 14, 581579. doi: 10.3389/fnins.2020.581579

Kalkman, H. O., and Feuerbach, D. (2016). Antidepressant therapies inhibit inflammation and microglial M1-polarization. *Pharmacol. Ther.* 163, 82–93. doi: 10.1016/j.pharmthera.2016.04.001

Kataoka, K., Matsumoto, H., Kaneko, H., Notomi, S., Takeuchi, K., Sweigard, J. H., et al. (2015). Macrophage- and RIP3-dependent inflammasome activation exacerbates retinal detachment-induced photoreceptor cell death. *Cell Death Dis.* 6, e1731. doi: 10.1038/cddis.2015.73

Kauppinen, A., Paterno, J. J., Blasiak, J., Salminen, A., and Kaarniranta, K. (2016). Inflammation and its role in age-related macular degeneration. *Cell. Mol. Life Sci.* 73, 1765–1786. doi: 10.1007/s00018-016-2147-8

Kawai, T., and Akira, S. (2010). The role of pattern-recognition receptors in innate immunity: update on Toll-like receptors. *Nat. Immunol.* 11, 373–384. doi: 10.1038/ni.1863

Kayama, M., Omura, K., Murakami, Y., Reshef, E., Thanos, A., Morizane, Y., et al. (2018). Combined inhibition of apoptosis and necrosis promotes transientneuroprotection of retinal ganglion cells and partial-axon regeneration after optic nerve damage. *bioRxiv. [Preprint]*. doi: 10.1101/357566

Kigerl, K. A., Gensel, J. C., Ankeny, D. P., Alexander, J. K., Donnelly, D. J., and Popovich, P. G. (2009). Identification of two distinct macrophage subsets with divergent effects causing either neurotoxicity or regeneration in the injured mouse spinal cord. *J. Neurosci.* 29, 13435–13444. doi: 10.1523/jneurosci.3257-09.2009

Killingsworth, M. C., Sarks, J. P., and Sarks, S. H. (1990). Macrophages related to Bruch's membrane in age-related macular degeneration. *Eye* 4 (Pt 4), 613–621. doi: 10.1038/eye.1990.86

Kim, B., Lee, S., Suvas, S., and Rouse, B. T. (2005). Application of plasmid DNA encoding IL-18 diminishes development of herpetic stromal keratitis by antiangiogenic effects. *J. Immunol.* 175, 509–516. doi: 10.4049/jimmunol.175.1.509

Kim, J., Kim, C., Kim, T. S., Bang, S. I., Yang, Y., Park, H., et al. (2006). IL-18 enhances thrombospondin-1 production in human gastric cancer via JNK pathway. *Biochem. Biophys. Res. Commun.* 344, 1284–1289. doi: 10.1016/j.bbrc.2006.04.016

Kim, S. J., and Li, J. (2013). Caspase blockade induces RIP3-mediated programmed necrosis in Toll-like receptor-activated microglia. *Cell Death Dis.* 4, e716. doi: 10.1038/cddis.2013.238

Kinsella, S., Fichtner, M., Watters, O., König, H. G., and Prehn, J. H. M. (2018). Increased A20-E3 ubiquitin ligase interactions in bid-deficient glia attenuate TLR3- and TLR4-induced inflammation. *J. Neuroinflamm.* 15, 130. doi: 10.1186/s12974-018-1143-3

Kinsella, S., König, H. G., and Prehn, J. H. (2016). Bid promotes K63-linked polyubiquitination of tumor necrosis factor receptor associated factor 6 (TRAF6) and sensitizes to mutant SOD1-induced proinflammatory signaling in microglia. *eNeuro* 3. doi: 10.1523/eneuro.0099-15.2016

Komander, D., Clague, M. J., and Urbé, S. (2009). Breaking the chains: structure and function of the deubiquitinases. *Nat. Rev. Mol. Cell Biol.* 10, 550–563. doi: 10.1038/nrm2731

Kondylis, V., Kumari, S., Vlantis, K., and Pasparakis, M. (2017). The interplay of IKK, NF-κB and RIPK1 signaling in the regulation of cell death, tissue homeostasis and inflammation. *Immunol. Rev.* 277, 113–127. doi: 10.1111/imr.12550

Lad, E. M., Cousins, S. W., Van Arnam, J. S., and Proia, A. D. (2015). Abundance of infiltrating CD163+ cells in the retina of postmortem eyes with dry and neovascular age-related macular degeneration. *Graefes Arch. Clin. Exp. Ophthalmol.* 253, 1941–1945. doi: 10.1007/s00417-015-3094-z

Lee, Y. S., Dayma, Y., Park, M. Y., Kim, K. I., Yoo, S. E., and Kim, E. (2013). Daxx is a key downstream component of receptor interacting protein kinase 3 mediating retinal ischemic cell death. *FEBS Lett.* 587, 266–271. doi: 10.1016/j.febslet.2012.12.004

Lewis, G. P., Talaga, K. C., Linberg, K. A., Avery, R. L., and Fisher, S. K. (2004). The efficacy of delayed oxygen therapy in the treatment of experimental retinal detachment. *Am. J. Ophthalmol.* 137, 1085–1095. doi: 10.1016/j.ajo.2004.01.045

Liao, L., Shang, L., Li, N., Wang, S., Wang, M., Huang, Y., et al. (2017). Mixed lineage kinase domain-like protein induces RGC-5 necroptosis following elevated hydrostatic pressure. *Acta Biochim. Biophys. Sin.* 49, 879–889. doi: 10.1093/abbs/gmx088

Liu, T., Zhang, L., Joo, D., and Sun, S. C. (2017). NF-κB signaling in inflammation. *Signal. Transduct. Target Ther.* 2, 17023. doi: 10.1038/sigtrans.2017.23

Lloyd, A. F., Davies, C. L., Holloway, R. K., Labrak, Y., Ireland, G., Carradori, D., et al. (2019). Central nervous system regeneration is driven by microglia necroptosis and repopulation. *Nat. Neurosci.* 22, 1046–1052. doi: 10.1038/s41593-019-0418-z

Lu, J., Sun, Z., Fang, Y., Zheng, J., Xu, S., Xu, W., et al. (2019). Melatonin suppresses microglial necroptosis by regulating deubiquitinating enzyme A20 after intracerebral hemorrhage. *Front. Immunol.* 10, 1360. doi: 10.3389/fimmu.2019.01360

Malsy, J., Alvarado, A. C., Lamontagne, J. O., Strittmatter, K., and Marneros, A. G. (2020). Distinct effects of complement and of NLRP3- and non-NLRP3 inflammasomes for choroidal neovascularization. *Elife* 9. doi: 10.7554/eLife.60194

Marneros, A. G. (2021). Role of inflammasome activation in neovascular age-related macular degeneration. *FEBS J.* doi: 10.1111/febs.16278

Martinez, F., and Gordon, S. (2014). Martinez, FO & Gordon, S. The M1 and M2 paradigm of macrophage activation: time for reassessment. *F1000Prime Rep.* 6, 13. doi: 10.12703/P6-13

Masuda, T., Sankowski, R., Staszewski, O., Böttcher, C., and Amann, L., Sagar, et al. (2019). Spatial and temporal heterogeneity of mouse and human microglia at single-cell resolution. *Nature* 566, 388–392. doi: 10.1038/s41586-019-0924-x

Menon, M., Mohammadi, S., Davila-Velderrain, J., Goods, B. A., Cadwell, T. D., Xing, Y., et al. (2019). Single-cell transcriptomic atlas of the human retina identifies cell types associated with age-related macular degeneration. *Nat. Commun.* 10, 4902. doi: 10.1038/s41467-019-12780-8

Mifflin, L., Ofengeim, D., and Yuan, J. (2020). Receptor-interacting protein kinase 1 (RIPK1) as a therapeutic target. *Nat. Rev. Drug Discov.* 19, 553–571. doi: 10.1038/s41573-020-0071-y

Miller, J. W., D'Anieri, L. L., Husain, D., Miller, J. B., and Vavvas, D. G. (2021). Age-related macular degeneration (AMD): a view to the future. *J. Clin. Med.* 10, 1124–1127. doi: 10.3390/jcm10051124

Mohebiany, A. N., Ramphal, N. S., Karram, K., Di Liberto, G., Novkovic, T., Klein, M., et al. (2020). Microglial A20 protects the brain from CD8 T-cell-mediated immunopathology. *Cell Rep.* 30, 1585–1597.e1586. doi: 10.1016/j.celrep.2019.12.097

Murakami, Y., Ikeda, Y., Nakatake, S., Tachibana, T., Fujiwara, K., Yoshida, N., et al. (2015). Necrotic enlargement of cone photoreceptor cells and the release of high-mobility group box-1 in retinitis pigmentosa. *Cell Death Discov.* 1, 15058. doi: 10.1038/cddiscovery.2015.58

Murakami, Y., Matsumoto, H., Roh, M., Giani, A., Kataoka, K., Morizane, Y., et al. (2014). Programmed necrosis, not apoptosis, is a key mediator of cell loss and DAMP-mediated inflammation in dsRNA-induced retinal degeneration. *Cell Death Differ.* 21, 270–277. doi: 10.1038/cdd.2013.109

Murakami, Y., Matsumoto, H., Roh, M., Suzuki, J., Hisatomi, T., Ikeda, Y., et al. (2012). Receptor interacting protein kinase mediates necrotic cone but not rod cell death in a mouse model of inherited degeneration. *Proc. Natl. Acad. Sci. U.S.A.* 109, 14598–14603. doi: 10.1073/pnas.1206937109

Murphy, J. M., Czabotar, P. E., Hildebrand, J. M., Lucet, I. S., Zhang, J. G., Alvarez-Diaz, S., et al. (2013). The pseudokinase MLKL mediates necroptosis via a molecular switch mechanism. *Immunity* 39, 443–453. doi: 10.1016/j.immuni.2013.06.018

Nakazawa, T., Hisatomi, T., Nakazawa, C., Noda, K., Maruyama, K., She, H., et al. (2007). Monocyte chemoattractant protein 1 mediates retinal detachment-induced photoreceptor apoptosis. *Proc. Natl. Acad. Sci. U.S.A.* 104, 2425–2430. doi: 10.1073/pnas.0608167104

Nakazawa, T., Matsubara, A., Noda, K., Hisatomi, T., She, H., Skondra, D., et al. (2006a). Characterization of cytokine responses to retinal detachment in rats. *Mol. Vis.* 12, 867–878. doi: 10.1017/S0952523806230219

Nakazawa, T., Nakazawa, C., Matsubara, A., Noda, K., Hisatomi, T., She, H., et al. (2006b). Tumor necrosis factor-alpha mediates oligodendrocyte death and delayed retinal ganglion cell loss in a mouse model of glaucoma. *J. Neurosci.* 26, 12633–12641. doi: 10.1523/jneurosci.2801-06.2006

Ndoja, A., Reja, R., Lee, S. H., Webster, J. D., Ngu, H., Rose, C. M., et al. (2020). Ubiquitin ligase COP1 suppresses neuroinflammation by degrading c/EBPβ in microglia. *Cell* 182, 1156–1169.e1112. doi: 10.1016/j.cell.2020.07.011

Neufeld, A. H. (1999). Microglia in the optic nerve head and the region of parapapillary chorioretinal atrophy in glaucoma. *Arch. Ophthalmol.* 117, 1050–1056. doi: 10.1001/archopht.117.8.1050

Newton, F., and Megaw, R. (2020). Mechanisms of photoreceptor death in retinitis pigmentosa. *Genes.* 11, 1120–1148. doi: 10.3390/genes11101120

Nimmerjahn, A., Kirchhoff, F., and Helmchen, F. (2005). Resting microglial cells are highly dynamic surveillants of brain parenchyma *in vivo*. *Science* 308, 1314–1318. doi: 10.1126/science.1110647

Oberst, A., Dillon, C. P., Weinlich, R., McCormick, L. L., Fitzgerald, P., Pop, C., et al. (2011). Catalytic activity of the caspase-8-FLIP(L) complex inhibits RIPK3-dependent necrosis. *Nature* 471, 363–367. doi: 10.1038/nature09852

Ofengeim, D., Ito, Y., Najafov, A., Zhang, Y., Shan, B., DeWitt, J. P., et al. (2015). Activation of necroptosis in multiple sclerosis. *Cell Rep.* 10, 1836–1849. doi: 10.1016/j.celrep.2015.02.051

Ofengeim, D., Mazzitelli, S., Ito, Y., DeWitt, J. P., Mifflin, L., Zou, C., et al. (2017). RIPK1 mediates a disease-associated microglial response in Alzheimer's disease. *Proc. Natl. Acad. Sci. U.S.A.* 114, E8788–e8797. doi: 10.1073/pnas.1714175114

Ofengeim, D., and Yuan, J. (2013). Regulation of RIP1 kinase signalling at the crossroads of inflammation and cell death. *Nat. Rev. Mol. Cell Biol.* 14, 727–736. doi: 10.1038/nrm3683

Olivares-González, L., Martínez-Fernández de la Cámara, C., Hervás, D., Millán, J. M., and Rodrigo, R. (2018). HIF-1α stabilization reduces retinal degeneration in a mouse model of retinitis pigmentosa. *FASEB J.* 32, 2438–2451. doi: 10.1096/fj.201700985R

Olivares-González, L., Velasco, S., Campillo, I., and Rodrigo, R. (2021). Retinal inflammation, cell death and inherited retinal dystrophies. *Int. J. Mol. Sci.* 22, 2096–2113. doi: 10.3390/ijms22042096

Onizawa, M., Oshima, S., Schulze-Topphoff, U., Oses-Prieto, J. A., Lu, T., Tavares, R., et al. (2015). The ubiquitin-modifying enzyme A20 restricts ubiquitination of the kinase RIPK3 and protects cells from necroptosis. *Nat. Immunol.* 16, 618–627. doi: 10.1038/ni.3172

Paloneva, J., Manninen, T., Christman, G., Hovanes, K., Mandelin, J., Adolfsson, R., et al. (2002). Mutations in two genes encoding different subunits of a receptor signaling complex result in an identical disease phenotype. *Am. J. Hum. Genet.* 71, 656–662. doi: 10.1086/342259

Pan, C., Banerjee, K., Lehmann, G. L., Almeida, D., Hajjar, K. A., Benedicto, I., et al. (2021). Lipofuscin causes atypical necroptosis through lysosomal membrane permeabilization. *Proc. Natl. Acad. Sci. U.S.A.* 118. doi: 10.1073/pnas.2100122118

Park, H., Byun, D., Kim, T. S., Kim, Y. I., Kang, J. S., Hahm, E. S., et al. (2001). Enhanced IL-18 expression in common skin tumors. *Immunol. Lett.* 79, 215–219. doi: 10.1016/s0165-2478(01)00278-4

Park, H. J., Oh, S. H., Kim, H. N., Jung, Y. J., and Lee, P. H. (2016). Mesenchymal stem cells enhance α-synuclein clearance via M2 microglia polarization in experimental and human parkinsonian disorder. *Acta Neuropathol.* 132, 685–701. doi: 10.1007/s00401-016-1605-6

Penfold, P. L., Killingsworth, M. C., and Sarks, S. H. (1985). Senile macular degeneration: the involvement of immunocompetent cells. *Graefes Arch. Clin. Exp. Ophthalmol.* 223, 69–76. doi: 10.1007/bf02150948

Petrie, E. J., Czabotar, P. E., and Murphy, J. M. (2019). The structural basis of necroptotic cell death signaling. *Trends Biochem. Sci.* 44, 53–63. doi: 10.1016/j.tibs.2018.11.002

Petrie, E. J., Sandow, J. J., Jacobsen, A. V., Smith, B. J., Griffin, M. D. W., Lucet, I. S., et al. (2018). Conformational switching of the pseudokinase domain promotes human MLKL tetramerization and cell death by necroptosis. *Nat. Commun.* 9, 2422. doi: 10.1038/s41467-018-04714-7

Pollard, J. W. (2009). Trophic macrophages in development and disease. *Nat. Rev. Immunol.* 9, 259–270. doi: 10.1038/nri2528

Qiao, H., Sonoda, K. H., Ikeda, Y., Yoshimura, T., Hijioka, K., Jo, Y. J., et al. (2007). Interleukin-18 regulates pathological intraocular neovascularization. *J. Leukoc. Biol.* 81, 1012–1021. doi: 10.1189/jlb.0506342

Quarato, G., Guy, C. S., Grace, C. R., Llambi, F., Nourse, A., Rodriguez, D. A., et al. (2016). Sequential engagement of distinct MLKL phosphatidylinositol-binding sites executes necroptosis. *Mol. Cell* 61, 589–601. doi: 10.1016/j.molcel.2016.01.011

Quigley, H. A., and Broman, A. T. (2006). The number of people with glaucoma worldwide in 2010 and 2020. *Br. J. Ophthalmol.* 90, 262–267. doi: 10.1136/bjo.2005.081224

Ransohoff, R. M. (2016). A polarizing question: do M1 and M2 microglia exist? *Nat. Neurosci.* 19, 987–991. doi: 10.1038/nn.4338

Rock, K. L., and Kono, H. (2008). The inflammatory response to cell death. *Annu. Rev. Pathol.* 3, 99–126. doi: 10.1146/annurev.pathmechdis.3.121806.151456

Rodríguez-Gómez, J. A., Kavanagh, E., Engskog-Vlachos, P., Engskog, M. K. R., Herrera, A. J., Espinosa-Oliva, A. M., et al. (2020). Microglia: agents of the CNS pro-inflammatory response. *Cells*. 9, 1717–1762. doi: 10.3390/cells9071717

Rosenbaum, D. M., Degterev, A., David, J., Rosenbaum, P. S., Roth, S., Grotta, J. C., et al. (2010). Necroptosis, a novel form of caspase-independent cell death, contributes to neuronal damage in a retinal ischemia-reperfusion injury model. *J. Neurosci. Res.* 88, 1569–1576. doi: 10.1002/jnr.22314

Safaiyan, S., Kannaiyan, N., Snaidero, N., Brioschi, S., Biber, K., Yona, S., et al. (2016). Age-related myelin degradation burdens the clearance function of microglia during aging. *Nat. Neurosci.* 19, 995–998. doi: 10.1038/nn.4325

Salvadores, N., Moreno-Gonzalez, I., Ruiz, N. G., Quiroz, G., Vegas, L., Escandón, M., et al. (2021). Aβ oligomers trigger necroptosis-mediated neurodegeneration via microglia activation in Alzheimer's disease. *bioRxiv.* 10, 31–48. doi: 10.1101/2021.08.27.457960

Sato, K., Li, S., Gordon, W. C., He, J., Liou, G. I., Hill, J. M., et al. (2013). Receptor interacting protein kinase-mediated necrosis contributes to cone and rod photoreceptor degeneration in the retina lacking interphotoreceptor retinoid-binding protein. *J. Neurosci.* 33, 17458–17468. doi: 10.1523/jneurosci.1380-13.2013

Sawada, H., Fukuchi, T., Tanaka, T., and Abe, H. (2010). Tumor necrosis factor-alpha concentrations in the aqueous humor of patients with glaucoma. *Invest. Ophthalmol. Vis. Sci.* 51, 903–906. doi: 10.1167/iovs.09-4247

Scaffidi, P., Misteli, T., and Bianchi, M. E. (2002). Release of chromatin protein HMGB1 by necrotic cells triggers inflammation. *Nature* 418, 191–195. doi: 10.1038/nature00858

Sellés-Navarro, I., Villegas-Pérez, M. P., Salvador-Silva, M., Ruiz-Gómez, J. M., and Vidal-Sanz, M. (1996). Retinal ganglion cell death after different transient periods of pressure-induced ischemia and survival intervals. A quantitative *in vivo* study. *Invest. Ophthalmol. Vis. Sci.* 37, 2002–2014.

Seo, J., Kim, M. W., Bae, K. H., Lee, S. C., Song, J., and Lee, E. W. (2019). The roles of ubiquitination in extrinsic cell death pathways and its implications for therapeutics. *Biochem. Pharmacol.* 162, 21–40. doi: 10.1016/j.bcp.2018.11.012

Sizova, O. S., Shinde, V. M., Lenox, A. R., and Gorbatyuk, M. S. (2014). Modulation of cellular signaling pathways in P23H rhodopsin photoreceptors. *Cell. Signal.* 26, 665–672. doi: 10.1016/j.cellsig.2013.12.008

Smith, W., Assink, J., Klein, R., Mitchell, P., Klaver, C. C., Klein, B. E., et al. (2001). Risk factors for age-related macular degeneration: pooled findings from three continents. *Ophthalmology* 108, 697–704. doi: 10.1016/s0161-6420(00)00580-7

Stratoulias, V., Venero, J. L., Tremblay, M., and Joseph, B. (2019). Microglial subtypes: diversity within the microglial community. *EMBO J.* 38, e101997. doi: 10.15252/embj.2019101997

Su, L., Quade, B., Wang, H., Sun, L., Wang, X., and Rizo, J. (2014). A plug release mechanism for membrane permeation by MLKL. *Structure* 22, 1489–1500. doi: 10.1016/j.str.2014.07.014

Sun, L., Wang, H., Wang, Z., He, S., Chen, S., Liao, D., et al. (2012). Mixed lineage kinase domain-like protein mediates necrosis signaling downstream of RIP3 kinase. *Cell* 148, 213–227. doi: 10.1016/j.cell.2011.11.031

Sweigard, J. H., Matsumoto, H., Smith, K. E., Kim, L. A., Paschalis, E. I., Okonuki, Y., et al. (2015). Inhibition of the alternative complement pathway preserves photoreceptors after retinal injury. *Sci. Transl. Med.* 7, 297ra116. doi: 10.1126/scitranslmed.aab1482

Tan, W., Zou, J., Yoshida, S., Jiang, B., and Zhou, Y. (2020). The role of inflammation in age-related macular degeneration. *Int. J. Biol. Sci.* 16, 2989–3001. doi: 10.7150/ijbs.49890

Tansey, M. G., and Goldberg, M. S. (2010). Neuroinflammation in Parkinson's disease: its role in neuronal death and implications for therapeutic intervention. *Neurobiol. Dis.* 37, 510–518. doi: 10.1016/j.nbd.2009.11.004

Tezel, G. (2008). TNF-alpha signaling in glaucomatous neurodegeneration. *Prog. Brain Res.* 173, 409–421. doi: 10.1016/s0079-6123(08)01128-x

Tezel, G. (2021). Multifactorial pathogenic processes of retinal ganglion cell degeneration in glaucoma towards multi-target strategies for broader treatment effects. *Cells*. 10, 1372–1398. doi: 10.3390/cells10061372

Thadathil, N., Nicklas, E. H., Mohammed, S., Lewis, T. L. Jr., Richardson, A., and Deepa, S. S. (2021). Necroptosis increases with age in the brain and contributes to age-related neuroinflammation. *Geroscience*. 43, 2345–2361. doi: 10.1007/s11357-021-00448-5

Thapa, R. J., Nogusa, S., Chen, P., Maki, J. L., Lerro, A., Andrake, M., et al. (2013). Interferon-induced RIP1/RIP3-mediated necrosis requires PKR and is

licensed by FADD and caspases. *Proc. Natl. Acad. Sci. U.S.A.* 110, E3109–3118. doi: 10.1073/pnas.1301218110

To, K., Adamian, M., and Berson, E. L. (2004). Histologic study of retinitis pigmentosa due to a mutation in the RP13 gene (PRPC8): comparison with rhodopsin Pro23His, Cys110Arg, and Glu181Lys. *Am. J. Ophthalmol.* 137, 946–948. doi: 10.1016/j.ajo.2003.10.047

Trichonas, G., Murakami, Y., Thanos, A., Morizane, Y., Kayama, M., Debouck, C. M., et al. (2010). Receptor interacting protein kinases mediate retinal detachment-induced photoreceptor necrosis and compensate for inhibition of apoptosis. *Proc. Natl. Acad. Sci. U.S.A.* 107, 21695–21700. doi: 10.1073/pnas.1009179107

Tseng, P. H., Matsuzawa, A., Zhang, W., Mino, T., Vignali, D. A., and Karin, M. (2010). Different modes of ubiquitination of the adaptor TRAF3 selectively activate the expression of type I interferons and proinflammatory cytokines. *Nat. Immunol.* 11, 70–75. doi: 10.1038/ni.1819

Uemura, A., Fruttiger, M., D'Amore, P. A., De Falco, S., Joussen, A. M., Sennlaub, F., et al. (2021). VEGFR1 signaling in retinal angiogenesis and microinflammation. *Prog. Retin. Eye Res.* 84, 100954. doi: 10.1016/j.preteyeres.2021.100954

Ueta, T., Ishihara, K., Notomi, S., Lee, J. J., Maidana, D. E., Efstathiou, N. E., et al. (2019). RIP1 kinase mediates angiogenesis by modulating macrophages in experimental neovascularization. *Proc. Natl. Acad. Sci. U.S.A.* 116, 23705–23713. doi: 10.1073/pnas.1908355116

Upton, J. W., Kaiser, W. J., and Mocarski, E. S. (2012). DAI/ZBP1/DLM-1 complexes with RIP3 to mediate virus-induced programmed necrosis that is targeted by murine cytomegalovirus vIRA. *Cell Host Microbe* 11, 290–297. doi: 10.1016/j.chom.2012.01.016

Varfolomeev, E., Goncharov, T., Fedorova, A. V., Dynek, J. N., Zobel, K., Deshayes, K., et al. (2008). c-IAP1 and c-IAP2 are critical mediators of tumor necrosis factor alpha (TNFalpha)-induced NF-kappaB activation. *J. Biol. Chem.* 283, 24295–24299. doi: 10.1074/jbc.C800128200

Vince, J. E., Wong, W. W., Gentle, I., Lawlor, K. E., Allam, R., O'Reilly, L., et al. (2012). Inhibitor of apoptosis proteins limit RIP3 kinase-dependent interleukin-1 activation. *Immunity* 36, 215–227. doi: 10.1016/j.immuni.2012.01.012

Viringipurampeer, I. A., Gregory-Evans, C. Y., Metcalfe, A. L., Bashar, E., Moritz, O. L., and Gregory-Evans, K. (2019). Cell death pathways in mutant rhodopsin rat models identifies genotype-specific targets controlling retinal degeneration. *Mol. Neurobiol.* 56, 1637–1652. doi: 10.1007/s12035-018-1192-8

Viringipurampeer, I. A., Shan, X., Gregory-Evans, K., Zhang, J. P., Mohammadi, Z., and Gregory-Evans, C. Y. (2014). Rip3 knockdown rescues photoreceptor cell death in blind pde6c zebrafish. *Cell Death Differ.* 21, 665–675. doi: 10.1038/cdd.2013.191

Wallach, D., Kang, T. B., and Kovalenko, A. (2014). Concepts of tissue injury and cell death in inflammation: a historical perspective. *Nat. Rev. Immunol.* 14, 51–59. doi: 10.1038/nri3561

Walsh, M. C., Kim, G. K., Maurizio, P. L., Molnar, E. E., and Choi, Y. (2008). TRAF6 autoubiquitination-independent activation of the NFkappaB and MAPK pathways in response to IL-1 and RANKL. *PLoS ONE* 3, e4064. doi: 10.1371/journal.pone.0004064

Wang, J., Zhang, H., Ji, J., Wang, L., Lv, W., He, Y., et al. (2022). A histological study of atherosclerotic characteristics in age-related macular degeneration. *Heliyon* 8, e08973. doi: 10.1016/j.heliyon.2022.e08973

Wang, M., Wan, H., Wang, S., Liao, L., Huang, Y., Guo, L., et al. (2020). RSK3 mediates necroptosis by regulating phosphorylation of RIP3 in rat retinal ganglion cells. *J. Anat.* 237, 29–47. doi: 10.1111/joa.13185

Wang, X., Li, Y., Liu, S., Yu, X., Li, L., Shi, C., et al. (2014). Direct activation of RIP3/MLKL-dependent necrosis by herpes simplex virus 1 (HSV-1) protein ICP6 triggers host antiviral defense. *Proc. Natl. Acad. Sci. U.S.A.* 111, 15438–15443. doi: 10.1073/pnas.1412767111

Weinlich, R., Oberst, A., Beere, H. M., and Green, D. R. (2017). Necroptosis in development, inflammation and disease. *Nat. Rev. Mol. Cell Biol.* 18, 127–136. doi: 10.1038/nrm.2016.149

Weinreb, R. N., Aung, T., and Medeiros, F. A. (2014). The pathophysiology and treatment of glaucoma: a review. *JAMA* 311, 1901–1911. doi: 10.1001/jama.2014.3192

Weisel, K., Berger, S., Papp, K., Maari, C., Krueger, J. G., Scott, N., et al. (2020). Response to inhibition of receptor-interacting protein kinase 1 (RIPK1) in active plaque psoriasis: a randomized placebo-controlled study. *Clin. Pharmacol. Ther.* 108, 808–816. doi: 10.1002/cpt.1852

Weisel, K., Scott, N., Berger, S., Wang, S., Brown, K., Powell, M., et al. (2021). A randomised, placebo-controlled study of RIPK1 inhibitor GSK2982772 in patients with active ulcerative colitis. *BMJ Open Gastroenterol.* 8. doi: 10.1136/bmjgast-2021-000680

Welser, J. V., Li, L., and Milner, R. (2010). Microglial activation state exerts a biphasic influence on brain endothelial cell proliferation by regulating the balance of TNF and TGF-β1. *J. Neuroinflamm.* 7, 89. doi: 10.1186/1742-2094-7-89

Wertz, I. E., and Dixit, V. M. (2010). Signaling to NF-kappaB: regulation by ubiquitination. *Cold Spring Harb. Perspect. Biol.* 2, a003350. doi: 10.1101/cshperspect.a003350

Wu, X. N., Yang, Z. H., Wang, X. K., Zhang, Y., Wan, H., Song, Y., et al. (2014). Distinct roles of RIP1-RIP3 hetero- and RIP3-RIP3 homo-interaction in mediating necroptosis. *Cell Death Differ.* 21, 1709–1720. doi: 10.1038/cdd.2014.77

Yan, X., Tezel, G., Wax, M. B., and Edward, D. P. (2000). Matrix metalloproteinases and tumor necrosis factor alpha in glaucomatous optic nerve head. *Arch. Ophthalmol.* 118, 666–673. doi: 10.1001/archopht.118.5.666

Yanai, H., Ban, T., Wang, Z., Choi, M. K., Kawamura, T., Negishi, H., et al. (2009). HMGB proteins function as universal sentinels for nucleic-acid-mediated innate immune responses. *Nature* 462, 99–103. doi: 10.1038/nature08512

Yang, H., Fu, Y., Liu, X., Shahi, P. K., Mavlyutov, T. A., Li, J., et al. (2017). Role of the sigma-1 receptor chaperone in rod and cone photoreceptor degenerations in a mouse model of retinitis pigmentosa. *Mol. Neurodegener.* 12, 68. doi: 10.1186/s13024-017-0202-z

Yang, J., Zhao, Y., Zhang, L., Fan, H., Qi, C., Zhang, K., et al. (2018). RIPK3/MLKL-mediated neuronal necroptosis modulates the M1/M2 polarization of microglia/macrophages in the ischemic cortex. *Cereb. Cortex* 28, 2622–2635. doi: 10.1093/cercor/bhy089

Yang, P., Peairs, J. J., Tano, R., Zhang, N., Tyrell, J., and Jaffe, G. J. (2007). Caspase-8-mediated apoptosis in human RPE cells. *Invest. Ophthalmol. Vis. Sci.* 48, 3341–3349. doi: 10.1167/iovs.06-1340

Yoshida, N., Ikeda, Y., Notomi, S., Ishikawa, K., Murakami, Y., Hisatomi, T., et al. (2013). Clinical evidence of sustained chronic inflammatory reaction in retinitis pigmentosa. *Ophthalmology* 120, 100–105. doi: 10.1016/j.ophtha.2012.07.006

Yoshimura, T., Sonoda, K. H., Sugahara, M., Mochizuki, Y., Enaida, H., Oshima, Y., et al. (2009). Comprehensive analysis of inflammatory immune mediators in vitreoretinal diseases. *PLoS ONE* 4, e8158. doi: 10.1371/journal.pone.0008158

You, Z., Savitz, S. I., Yang, J., Degterev, A., Yuan, J., Cuny, G. D., et al. (2008). Necrostatin-1 reduces histopathology and improves functional outcome after controlled cortical impact in mice. *J. Cereb. Blood Flow Metab.* 28, 1564–1573. doi: 10.1038/jcbfm.2008.44

Yuan, J., Amin, P., and Ofengeim, D. (2019). Necroptosis and RIPK1-mediated neuroinflammation in CNS diseases. *Nat. Rev. Neurosci.* 20, 19–33. doi: 10.1038/s41583-018-0093-1

Yuan, L., and Neufeld, A. H. (2001). Activated microglia in the human glaucomatous optic nerve head. *J. Neurosci. Res.* 64, 523–532. doi: 10.1002/jnr.1104

Zacks, D. N., Hänninen, V., Pantcheva, M., Ezra, E., Grosskreutz, C., and Miller, J. W. (2003). Caspase activation in an experimental model of retinal detachment. *Invest. Ophthalmol. Vis. Sci.* 44, 1262–1267. doi: 10.1167/iovs.02-0492

Zacks, D. N., Zheng, Q. D., Han, Y., Bakhru, R., and Miller, J. W. (2004). FAS-mediated apoptosis and its relation to intrinsic pathway activation in an experimental model of retinal detachment. *Invest. Ophthalmol. Vis. Sci.* 45, 4563–4569. doi: 10.1167/iovs.04-0598

Zhao, J., Jitkaew, S., Cai, Z., Choksi, S., Li, Q., Luo, J., et al. (2012). Mixed lineage kinase domain-like is a key receptor interacting protein 3 downstream component of TNF-induced necrosis. *Proc. Natl. Acad. Sci. U.S.A.* 109, 5322–5327. doi: 10.1073/pnas.1200012109

Zinngrebe, J., Montinaro, A., Peltzer, N., and Walczak, H. (2014). Ubiquitin in the immune system. *EMBO Rep.* 15, 28–45. doi: 10.1002/embr.201338025

Conflict of Interest: The authors declare that the research was conducted in the absence of any commercial or financial relationships that could be construed as a potential conflict of interest.

Publisher's Note: All claims expressed in this article are solely those of the authors and do not necessarily represent those of their affiliated organizations, or those of the publisher, the editors and the reviewers. Any product that may be evaluated in this article, or claim that may be made by its manufacturer, is not guaranteed or endorsed by the publisher.

frontiers | Frontiers in Neuroscience

TYPE Original Research
PUBLISHED 05 August 2022
DOI 10.3389/fnins.2022.957034

OPEN ACCESS

EDITED BY
Zhongjie Fu,
Boston Children's Hospital and
Harvard Medical School, United States

REVIEWED BY
Michael Risner,
Vanderbilt University, United States
Haiyan Li,
Upstate Medical University,
United States

*CORRESPONDENCE
Denise M. Inman
denise.inman@unthsc.edu

SPECIALTY SECTION
This article was submitted to
Neurodegeneration,
a section of the journal
Frontiers in Neuroscience

RECEIVED 30 May 2022
ACCEPTED 12 July 2022
PUBLISHED 05 August 2022

CITATION
Pappenhagen N, Yin E, Morgan AB,
Kiehlbauch CC and Inman DM (2022)
Stretch stress propels glutamine
dependency and glycolysis in optic
nerve head astrocytes.
Front. Neurosci. 16:957034.
doi: 10.3389/fnins.2022.957034

Stretch stress propels glutamine dependency and glycolysis in optic nerve head astrocytes

Nathaniel Pappenhagen[1], Eric Yin[2], Autumn B. Morgan[1], Charles C. Kiehlbauch[1] and Denise M. Inman[1]*

[1]Department of Pharmaceutical Sciences, North Texas Eye Research Institute, University of North Texas Health Science Center, Fort Worth, TX, United States, [2]Texas College of Osteopathic Medicine, University of North Texas Health Science Center, Fort Worth, TX, United States

Glaucoma is an optic neuropathy that leads to irreversible blindness, the most common subtype of which is typified by a chronic increase in intraocular pressure that promotes a stretch injury to the optic nerve head. In rodents, the predominant glial cell in this region is the optic nerve head astrocyte that provides axons with metabolic support, likely by releasing lactate produced through astrocytic glycolysis. Our primary hypothesis is that stretching of the optic nerve head astrocytes alters their metabolic activity, thereby advancing glaucoma-associated degeneration by compromising the metabolic support that the astrocytes provide to the axons in the optic nerve head. Metabolic changes in optic nerve head astrocytes were investigated by subjecting them to 24 h of 12% biaxial stretch at 1 Hz then measuring the cells' bioenergetics using a Seahorse XFe24 Analyzer. We observed significant glycolytic and respiratory activity differences between control and stretched cells, including greater extracellular acidification and lower ATP-linked respiration, yet higher maximal respiration and spare capacity in stretched optic nerve head astrocytes. We also determined that both control and stretched optic nerve head astrocytes displayed a dependency for glutamine over pyruvate or long-chain fatty acids for fuel. The increased use of glycolysis as indicated by the extracellular acidification rate, concomitant with a dependency on glutamine, suggests the need to replenish NAD + for continued glycolysis and provision of carbon for TCA cycle intermediates. Stretch alters optic nerve astrocyte bioenergetics to support an increased demand for internal and external energy.

KEYWORDS

astrocyte, glaucoma, optic nerve head, metabolism, glycolysis

Introduction

Glaucoma is an optic neuropathy that is the largest cause of irreversible blindness in the world (Weinreb et al., 2014). The optic nerve head (ONH) is the initial site of degeneration in glaucoma as demonstrated in human glaucomic patients (Quigley et al., 1981), as well as rodent glaucoma models (Howell et al., 2007; Chidlow et al., 2011). Loss of axon transport and axonal loss at the ONH is present in many *in vivo* models of glaucoma (Guo et al., 2005; Chidlow et al., 2011; Wilson et al., 2016; Maddineni et al., 2020), indicating that the ONH is an important region for understanding glaucoma. The distension of the eye through the lamina cribrosa causes the optic disk to press back through the lamina cribrosa of the ONH, leading to an estimated chronic 9% stretch (Girard et al., 2016). This optic cupping accompanies RGC loss, axonal transport loss, and visual field loss. Optic nerve head astrocytes (ONHAs) react to this stretch in glaucoma by entering a state of reactivity and hypertrophy (Hernandez, 2000a; Sun et al., 2013) that impacts the health of the retinal ganglion cells (RGCs) and their axons (Schneider and Fuchshofer, 2015). Reactive astrocytes negatively impact neurons through the generation of pro-inflammatory molecules (Neufeld and Liu, 2003; Oikawa et al., 2020), deposition of extracellular matrix (Morgan, 2000), and changes in metabolic support that can impact axonal transport, mismanage metabolism, and lead to degeneration (Chung et al., 2009; Vohra et al., 2013; Iglesias et al., 2017).

We have demonstrated changes in metabolic transporter profiles in retina and optic nerve from glaucoma subjects (Harun-or-Rashid et al., 2018). Glucose transporter 1 (GLUT1), the primary glucose transporter found on epithelial cells and astrocytes (Morgello et al., 1995), is decreased in the optic nerve (ON) in a chronic mouse model of glaucoma (Harun-or-Rashid et al., 2018). Additionally, monocarboxylate transporters that move lactate, pyruvate, and ketone bodies (Halestrap, 2012) across membranes, are decreased in glaucomic ON. Downregulation of transporter proteins suggest metabolic shifts accompany glaucomic degeneration because glial cells and RGCs form a metabolic unit of cells that operate as a mutually supportive entity to meet energy needs (Tsacopoulos and Magistretti, 1996). The lactate shuttle hypothesis proposes that glial glycolysis produces lactate to be exported to neighboring neurons for conversion to pyruvate and as fuel for mitochondrial respiration (Pellerin et al., 1998; Volkenhoff et al., 2015; Saab et al., 2016; Muraleedharan et al., 2020). Glucose entry to this metabolic unit would be decreased by the loss of GLUT1, and loss of MCT-1, -2, or -4 would ultimately limit the energy availability in the RGC axons in the ON, which is detrimental for the health of the glaucomic nerve.

Altering metabolic activity in mouse models of glaucoma has had protective effects for RGCs, suggesting that provision of adequate sources of energy can sustain RGC survival (Harun-Or-Rashid et al., 2020b; Tribble et al., 2021). We have increased metabolic activity in glaucomic animals by using a ketogenic diet to increase mitochondrial activity and by using an adeno-associated virus to increase MCT-2 expression, thereby increasing metabolic substrate availability in glaucomic tissues (Harun-or-Rashid et al., 2018; Harun-Or-Rashid et al., 2020a). Additionally, restoration of nicotinamide adenine dinucleotide (NAD^+), a critical electron carrying molecule for the citric acid cycle and glycolysis, to glaucomatous retina with administration of vitamin B_3 protects RGCs (Williams et al., 2017). Providing pyruvate or nicotinamide directly in the drinking water preserved RGC number and positively impacted inner retina function in the DBA/2J model of glaucoma (Harder et al., 2020). Promisingly, treatment of glaucoma patients with a nicotinamide supplement increased inner retina function (Hui et al., 2020). Our lab has shown that glaucomic ON has a higher glycolytic rate and impaired glycolytic responsiveness than control ON by measuring the extracellular acidification rate (ECAR) as well as measuring glycolytic increase after inhibiting mitochondrial ATP production in *ex vivo* ON (Jassim et al., 2019). In this study, we move from the ON to the ONH to evaluate the metabolic changes in ONHAs that have been subjected to a glaucoma-associated stretch injury. Previous investigation of basic ONH metabolism has been limited to human lamina cribrosa cells, which were observed to increase glycolysis concomitant with reduced oxidative phosphorylation in glaucoma patients (Kamel et al., 2020). Our findings in ONH astrocytes show greater capacity for oxidative phosphorylation when cells are placed under stretch. We also observe increases in glycolysis in stretched cells, and find that ONH astrocytes have a preference for glutamine to meet their energy needs.

Materials and methods

Primary optic nerve head astrocyte isolation

Primary optic nerve head astrocytes (ONHAs) were isolated from postnatal day (P) 5-7 rat pups (CD (Sprague Dawley) IGS rats from Charles River Laboratories, Wilmington, MA, United States) using modified methods (Kaja et al., 2015). P5-7 rat pups were sacrificed by decapitation and their eyes and ON were harvested. All procedures were approved by the Institutional Animal Care and Use Committee and performed in accordance with the ARVO Statement for the Use of Animals in Ophthalmic and Vision Research. Individual optic nerve head explants were placed into a 24-well plate, and allowed to adhere before 1 mL of astrocyte growth media (DMEM with 4.5 mg/mL glucose (Gibco through Fisher Scientific, Cat. No. 11995073), 2 mM glutamine, 1 mM sodium pyruvate, 1x penicillin/streptomycin and 10% heat inactivated-fetal bovine serum, [ThermoFisher Scientific, Cat. No. 16140063)] was added to the explants. Astrocytes grew out from the explants

for 5–7 days before they were passaged using TrypLE (Gibco through Fisher Scientific, Cat. No. 50-591-419), with additional filtration through a sterile 100 μm filter before centrifugation, TrypLE removal, then plating in T75 flasks. In the flasks, primary astrocytes were grown to 75% confluence then shaken at 200 RPM for 30 min at room temperature to remove any non-astrocytic cells. ONH astrocytes (150,000 per well) were then seeded on 6-well FlexCell culture plates coated with 200 μg/mL type 1 collagen for the stretch experiments (FlexCell International, Cat. No. BF-3001C).

Stretch experiments

Primary cells grown to 75% confluency were stretched in a manner similar to that experienced in the optic nerve head (ONH) in glaucoma (Downs et al., 2008; Girard et al., 2016) using the FlexCell 6000T which uses vacuum to pull the membrane on which the cells are seeded over a plastic post, thus stretching them biaxially. We used a 12% sinusoidal stretch protocol with a 1 Hz frequency for 24 h to imitate glaucomic stretch in the cultured ONH astrocytes, and emulate other published research done on mechanical stretch in primary ONH cells and astrocytes (Rogers et al., 2012a,b; Albalawi et al., 2017). Control primary cells were grown on 6-well FlexCell plates coated with 200 μg/mL type 1 collagen until 75% confluency before being collected for the Seahorse experiments.

Seahorse XFe 24 analyzer experiments

The Seahorse XFe24 Analyzer (Agilent Technologies, Santa Clara, CA, United States) measures oxygen and pH in mitochondria, cells or tissue using fiber optic sensors. Oxygen consumption rate allows the user to estimate mitochondrial respiration while released protons can be used to estimate lactate release, a measure of glycolytic activity. Injection ports for each culture well enable challenges of cellular metabolic processes through the addition of inhibitors of electron transport chain complexes. We used the glycolytic rate assay, the mitochondrial fuel flex test, and the mitochondrial stress test protocols to measure the metabolic changes in ONHAs following glaucoma-like stretch. Seeding optimization for the initial Seahorse experiments proceeded by seeding at densities from 10,000 to 50,000 cells per well, then evaluating baseline oxygen consumption rate. The most reliable oxygen consumption rate was obtained with 50,000 cells per well, so that is the cell density used throughout these experiments. Data points in all graphs represent data from individual wells in the Seahorse plate. The experiments were repeated 5-6 times using biological replicates (separate ONH astrocyte isolations from different rat litters).

CellTak-coated Seahorse plates were prepared prior to the addition of the ONH astrocytes by incubating the plates with 22.4 μg/mL CellTak (Corning, through Fisher Scientific, Cat. No. 354240) for 20 min before rinsing twice with sterile ddH_2O. Once the FlexCell stretch protocol was complete, ONH astrocytes were removed from the membranes with TrypLE, resuspended in 1 mL of the appropriate Seahorse assay media (DMEM with 2 mM glutamine for the glycolytic stress test, or DMEM with 2 mM Glutamine, 1 mM sodium pyruvate, and 1 mM glucose for the mitochondrial stress test, mitochondrial fuel dependency test, or mitochondrial fuel flexibility test), and seeded at 50,000 cells per well on the CellTak-coated Seahorse culture plates. The plates were spun at 200 g for 1 min with no braking then incubated without CO_2 at 37°C for 25 min before the final 400 μL of Seahorse assay media was added to each well in preparation for the Seahorse experiment.

Glycolytic stress test

For the modified glycolytic stress test, cells were assayed in DMEM media with only 2 mM glutamine, depriving the cells of glucose to allow for a baseline measurement of the extracellular acidification rate (ECAR). Once glucose is added, the difference between baseline and post-glucose injection is the ECAR associated with glycolysis. All inhibitor compounds are from Sigma-Aldrich, St. Louis, MO, United States, unless otherwise specified. With the injection of 0.5 μM rotenone (Cat. No. R8875) and 0.5 μM antimycin-a (Cat. No. A8674), Complex I and Complex III inhibitors, respectively, mitochondrial respiration in the cells ceases while glycolytic activity and ECAR increase due to metabolic shift from the loss of mitochondrial adenosine triphosphate (ATP) production. Finally, addition of excess 2-deoxyglucose (2-DG, 50 mM, Cat. No. D8375), a non-hydrolyzable form of glucose, competitively inhibits hexokinase, thereby stopping glycolysis and restoring cells to baseline ECAR. The maximal glycolytic rate is defined as the maximal ECAR minus the baseline ECAR, and the glycolytic reserve is the maximal ECAR minus the glycolytic ECAR.

Cells were removed following the glycolytic rate assay, fixed for 15 min at 37°C with 2% formaldehyde, labeled with 4′,6-diamidino-2-phenylindole (DAPI, Cat. No. D9542) in Tris-buffered saline (TBS) for 10 min, then rinsed with PBS with 0.1% sodium azide until the cells were counted for assay data normalization.

Mitochondrial stress test

The mitochondrial stress test measures oxygen consumption rate (OCR) in response to serial injection of an inhibitor of ATP synthase (oligomycin-a, Cat. No. 75351), a protonophore (trifluoromethoxy carbonylcyanide phenylhydrazone, FCCP, Cat. No. C2920), and electron transport chain Complex I and III inhibitors (rotenone and antimycin-a). The media used

was DMEM with 1 mM glucose, 1 mM sodium pyruvate, and 2 mM glutamine. After baseline OCR measures, an injection of oligomycin (1 mM) typically halts mitochondrial respiration-associated ATP production and the OCR falls; the difference between baseline OCR and OCR during oligomycin-a exposure is considered the oxygen consumption attributable to ATP production. The protonophore FCCP (2 mM), by uncoupling the mitochondrial membrane potential from ATP production, leads to an increase in oxygen consumption (maximal respiration) as the electron transport chain (ETC) tries to maintain the proton gradient. Finally, rotenone and antimycin-a (0.5 μM each) inhibit Complexes I and III, respectively, thereby completely shutting down respiration-associated OCR. Following the mitochondrial stress test, cells were fixed and labeled with DAPI as previously described.

Mitochondrial fuel dependency

The mitochondrial fuel dependency test was used to test the reliance of the mitochondria on three of the most common mitochondrial substrates; pyruvate, glutamine, and long chain fatty acids. The assay was run in triplicate on a single plate, with 6-7 wells dedicated to each fuel dependency. All compounds for the dependency tests were obtained from Sigma-Aldrich (St. Louis, MO, United States). The assay used the mitochondrial pyruvate carrier inhibitor 2-cyano-3-(1-phenyl-1H-indol-3-yl)-2-propenoic acid (UK5099, Cat. No. PZ0160); an allosteric inhibitor of glutaminase, bis-2-(5-phenylacetamido-1,3,4-thiadiazol-2-yl)ethyl sulfide (BPTES, Cat. No. SML0601); and the carnitine palmitoyl-transferase 1A inhibitor etomoxir (Cat. No. 236020) to inhibit long chain fatty acid transport into the mitochondria. To determine the mitochondrial dependency on each fuel source, we followed instructions as outlined in the Agilent Seahorse XF Mito Fuel Flex Test Kit. To summarize, changes in OCR are measured after addition of a pathway inhibitor followed by the addition of the other inhibitors. For example, to measure pyruvate dependence, baseline OCR is measured then UK5099 is added; OCR change is recorded, then BPTES and etomoxir (inhibitors of the glutamine and long chain fatty acid pathways, respectively) are added. The difference in the UK5099 OCR from baseline divided by and the other inhibitors' OCR compared to baseline yields the dependency measure; the equation used: Dependency% = [Baseline OCR – Target Inhibitor OCR/Baseline OCR – All Inhibitors OCR] *100.

Protein isolation and analysis

Optic nerve head astrocyte (ONHA) protein was isolated from control and stretched primary cells after removal from FlexCell plates using TrypLE followed by lysis in tissue protein extraction reagent (T-PER, ThermoFisher, Waltham, MA, United States, Cat. No. PI78510) containing HALT protease and phosphatase inhibitors (ThermoFisher, Cat. No. 78442). Protein lysates collected from four separate experiments were subjected to three pulses of sonication (10% amplitude), with a few minutes rest between pulses, then centrifugation at 10,000 *g* for 10 min. Supernatants were collected and protein concentration determined through BCA assay (Pierce through ThermoFisher, Cat. No. PI23225). Proteins were quantified using the Jess capillary electrophoresis instrument from ProteinSimple (San Jose, CA, United States), and normalized to total protein. For each ONH astrocyte sample, a "no primary antibody" negative control was included, as well as a positive control consisting of mouse retinal protein. Protein-antibody interactions were optimized by varying the protein and antibody concentrations until clear, strong, specific binding was observed as denoted by a single peak at the correct molecular weight for the protein in question. All antibodies were tested at 1:25, 1:50, and 1:100 concentrations across protein concentrations of 0.2, 0.4, 0.8, and 1.2 μg/μL. Chemiluminescence plots with the highest peaks were identified and the antibody-protein concentrations from those combinations were used. Antibodies used were LDH-A (Novus Biologicals, Centennial, CO, United States, NBP1-48336, RRID:AB_10011099), GFAP (Abcam, Cambridge, MA, United States, Cat# ab53554, RRID:AB_880202), GFAP (Millipore, Burlington, MA, United States, Cat# MAB3402, RRID:AB_94844), GLUT-1 (Novus Biologicals, Centennial, CO, United States, NB110-39113, RRID:AB_1851003), Glutamine synthetase (Santa Cruz Biotechnology, Dallas, TX, United States, sc-74430, RRID:AB_1127501), GLAST (Novus Biologicals, NB100-1869, RRID:AB_531518), S100β (Sigma-Aldrich Cat# S2644, RRID:AB_477501), glucose-6-phosphate dehydrogenase (Cell Signaling Technology, Danvers, MA, United States, 8866, RRID:AB_10827744), Iba1 (FUJIFILM Wako Shibayagi, Richmond, VA, United States, Cat# 019-19741, RRID:AB_839504), and β-tubulin (Covance Cat# PRB-435P-100, RRID:AB_291637).

mRNA isolation and analysis

All reagents for mRNA isolation and analysis were obtained from ThermoFisher Scientific (Waltham, MA, United States) unless otherwise specified. ONH astrocytes were grown to confluence, media was removed and Trizol (Invitrogen through ThermoFisher Scientific, Cat. No. 15596026) added to the flask. Cells in Trizol were scraped together and collected into a 2 mL tube. Isolation of mRNA proceeded according to the manufacturer's instructions for Trizol. Briefly, the cells were pipetted up and down to shear, then rested for 5 min for nucleoprotein complex dissociation before addition of chloroform. After 3 min incubation, samples were centrifuged for 15 min at 14,000× *g* at 4°C. The resultant upper aqueous

phase was transferred to a new tube and isopropanol was added to precipitate the RNA. The samples were incubated for 10 min then centrifuged for 10 min at 14,000× *g* at 4°C. The pellet was washed 2× in 75% ethanol then resuspended in 20 uL RNase-free water (Cat. No. AM9937). Isolated mRNA was converted to cDNA using the Verso cDNA Synthesis Kit (Cat. No. AB1453B). For qPCR, cDNA was diluted to 5 ng/uL, combined with TaqMan Universal PCR Master Mix (Cat. No. 4440040) and one of the following TaqMan assays (Cat. No. 4331182, see below) then loaded onto a QuantStudio-5 384-well real-time PCR system (Applied Biosystems through ThermoFisher Scientific, Cat. No. A28575). Samples were run in triplicate. The housekeeping gene was β-actin. The endogenous control was cDNA from a 2 month-old mouse retina. Fully validated TaqMan assays used in this analysis: *Actb* (Mm02619580_g1), *Gfap* (Mm01253033_m1), *Glud1* (Mm00492353_m1), *Glul* (Mm00725701_s1), *Slc1a3* (Mm00600697_m1), *Rbpms* (Mm00803908_m1), *Mbp* (Mm01262037_m1), *Iba1* (Mm00479862_g1), *Gja1* (Mm00439105_m1).

Immunolabeling of cells and tissue

Optic nerve head (ONH) astrocytes grown on coverslips were fixed in pre-warmed 3% paraformaldehyde in minimal media for 15 min at 37°C. Coverslips were rinsed 2× in 0.1M phosphate buffered saline (PBS) before aldehydes were quenched during 30 min incubation with 50mM ammonium chloride. Cells were permeabilized for 10 min with 0.1% Triton X-100 in 0.1M PBS, then rinsed 2× in 0.1M PBS. Cells were blocked in 5% bovine serum albumin + 5% donkey serum in 0.1M PBS for 2 h at room temperature. Block was removed and primary antibodies added for 2 h at RT. Primary antibody information is listed above in the section on Protein Isolation and Analysis. Cells were rinsed 1× in block solution prior to addition of secondary antibodies for 1h at RT. Secondary antibodies were species-specific secondary antibodies conjugated to AlexaFluor-488 or -594, or -647 (Jackson ImmunoResearch, Cat. No.s 711-545-152, 703-585-155, and 715-605-151). Cells were rinsed 3x in 0.1M PBS then coverslipped with DAPI-Fluoromount-G (SouthernBiotech, Cat. No. 0100-20).

Eye globes with attached optic nerves were obtained from a 2 month-old mouse that had been trans-caridally perfused with 4% paraformaldehyde. After cryoprotection in 30% sucrose for 24 h, the lens and cornea were removed from the globes and then they were frozen using isopentane-cooled liquid nitrogen in Tissue-Tek OCT Compound (Sakura Finetek, Torrance, CA, United States, Cat. No. 4583). Globes were sectioned at 20 μm using a Leica CM-1510 cryostat and collected on SuperFrost charged glass slides (Fisher Scientific, Cat. No. 12-550-15). Immunolabeling proceeded after frozen tissue was thawed for 20 min at RT, followed by 3 × 10 min rinses in 0.1M PBS. Slides were blocked for 1 h in 5% donkey serum and 0.4% Triton X-100 in 0.1M PBS then incubated in primary antibodies (see above) overnight at 4°C. After washing 3× for 10 min each with 0.1M PBS, slides were incubated in block for 30 min then incubated for 2 h in secondary antibodies (described above). A final series of 0.1M PBS washes were followed by coverslipping the slides in DAPI-Fluoromount-G.

Cells and tissue were imaged using a Leica DMi8 confocal microscope. Laser intensity and exposure settings were kept consistent across groups within cell or tissue imaging sessions.

Data normalization

Oxygen consumption rate (OCR) and ECAR values were normalized to DAPI-labeled cell number in each well as quantified using the Cytation 5 (Biotek) cell imaging multi-mode reader and its automated counting feature. Five images at 4× were taken per well, and images were examined to exclude aberrations such as cell clusters in which individual nuclei could not be resolved. Average cell density of each image was used to calculate the number of cells present in each well. Normalized OCR and ECAR data were analyzed in GraphPad Prism v. 9.

Statistical analysis

Unpaired two-tailed student's *t*-tests were used to compare control and stretched ONH astrocytes, with Mann-Whitney rank comparisons when necessary for data that was not normally distributed. Fuel dependency data (**Figure 4**) was analyzed by one-way ANOVA with Tukey's multiple comparisons test to compare individual groups. Comparisons for which $p < 0.05$ were considered statistically significant. Statistical analysis was done using GraphPad Prism 9. Data points in all bioenergetic analysis graphs represent data from individual wells in the Seahorse plate. Experiments were repeated 5-6 times using biological replicates (separate ONH astrocyte isolations from different rat litters).

Results

Optic nerve head astrocyte characterization

Optic nerve head astrocytes from the initial cell isolations were grown on coverslips to facilitate characterization by immunocytochemistry, protein analysis by capillary electrophoresis, and by quantitative PCR. **Figure 1A** shows the ONH astrocytes fully confluent and immunolabeled with astrocyte marker GFAP, neuronal marker β-tubulin, and

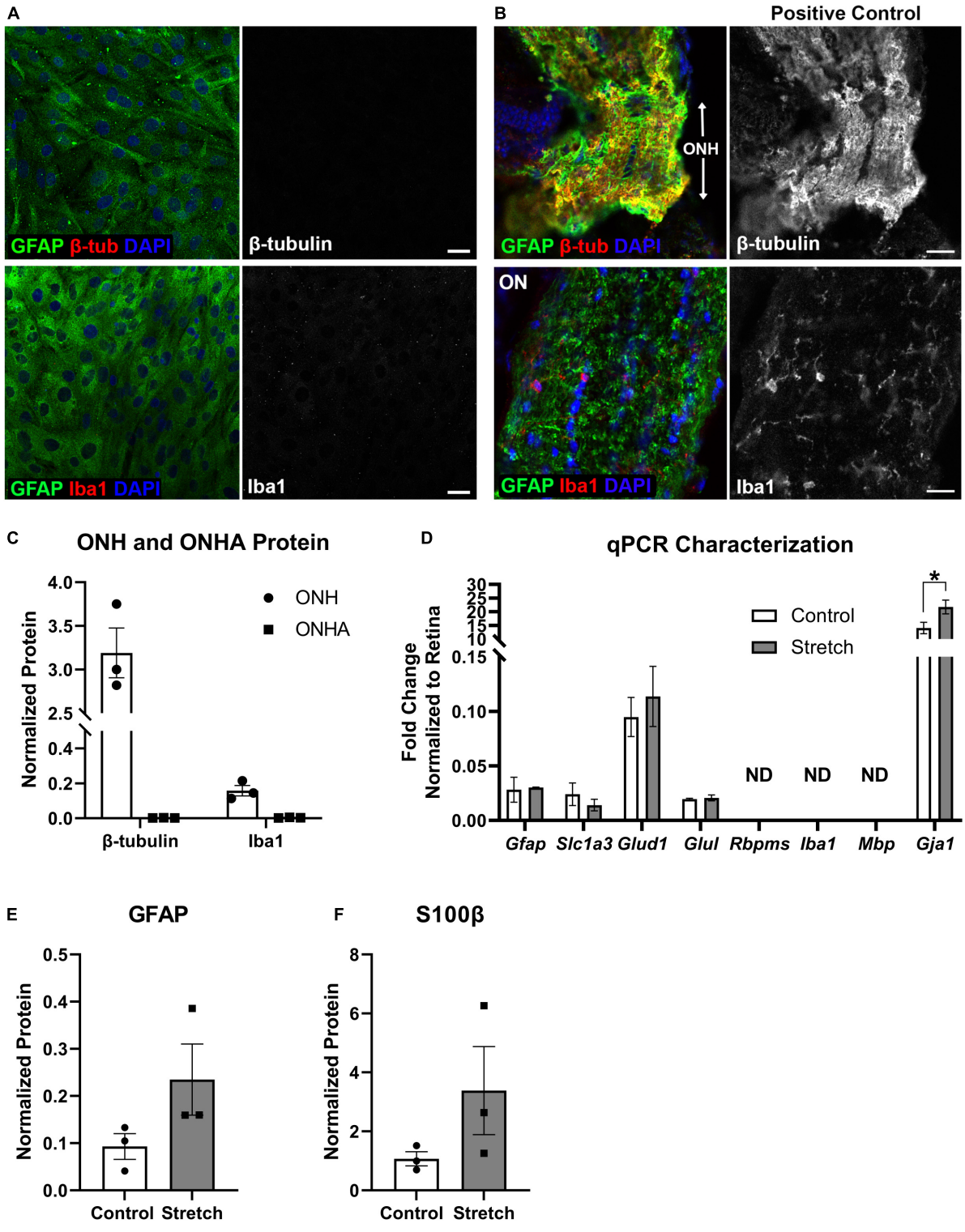

FIGURE 1

Optic nerve head astrocyte characterization. **(A)** Isolated optic nerve head (ONH) astrocytes were immunolabeled using antibodies against GFAP (green), β-tubulin (red, upper panels), and Iba1 (red, lower panels) to determine the purity of the cell cultures. DAPI was used to stain cell nuclei (blue). Neither β-tubulin nor Iba1 was detected in the cultures. Scale bar = 10 μm. **(B)** Sections of retina with ONH and optic nerve attached served as positive controls for the immunolabeling in **(A)**. Both β-tubulin and Iba1 were observed in the mouse ONH and optic nerve. Scale bar = 25 μm. **(C)** Quantification of β-tubulin and Iba1 protein in the optic nerve head (ONH) and isolated ONH astrocytes using capillary electrophoresis. Neither β-tubulin nor Iba1 was detected in the ONH astrocyte cultures (square symbols); *n* = 3 biological replicates per group.

(Continued)

FIGURE 1
(D) Quantitative PCR for a number of glial transcripts and transcripts for retinal ganglion cells (*Rbpms*), microglia (*Iba1*), and oligodendrocytes (*Mbp*) was used to further characterize the ONH astrocytes. *Rbpms*, *Iba1*, and *Mbp* were not detected in mRNA isolated from control or stretched ONH astrocytes (ND). There were no differences in transcripts for *Gfap*, *Slc1a3* (glutamate-aspartate transporter), *Glud1* (glutamate dehydrogenase-1), and *Glul* (glutamine synthetase). There were significant differences in the *Gja1* transcript levels, with stretched ONH astrocytes showing greater fold change as compared to control (*$p = 0.0152$, $n = 3$). *Gja1* encodes Connexin-43; $n = 3$ biological replicates per group. **(E)** GFAP protein, increased when astrocytes undergo hypertrophic reactivity, did not statistically differ between control and stretched ONH astrocytes; $n = 3$ biological replicates per group. **(F)** S100β protein, also upregulated in reactive astrocytes, did not statistically differ between control and stretched ONH astrocytes; $n = 3$ biological replicates per group.

microglial marker Iba1. No cells were observed to express either β-tubulin or Iba1. Tissue from mouse optic nerve head and optic nerve were also immunolabeled with GFAP, β-tubulin, and Iba1 for use as a positive control (**Figure 1B**). Quantification of β-tubulin and Iba1 in the optic nerve head (positive control) and ONH astrocytes also showed no measurable β-tubulin or Iba1 in the ONH astrocytes (ONHA), **Figure 1C**. We used isolated mRNA from the control and stretched ONH astrocytes to characterize culture purity, finding that transcripts such as *Rbpms* (a retinal ganglion cell gene), *Iba1* (specifically found in microglia), and *Mbp* (myelin basic protein found in oligodendrocytes) were not detected in the control and stretched ONH astrocyte cultures (**Figure 1D**). There were no statistically significant differences in transcripts between the control and stretch ONH astrocytes with the exception of *Gja1*, the gene that encodes Connexin-43. Stretched ONH astrocytes had significantly higher *Gja1* transcript levels as compared to control ($p = 0.0152$, $n = 3$).

Biaxial stretch (12% stretch for 24 h, see Methods for more detail) of the ONH astrocytes resulted in increased GFAP and S100β protein in the stretched ONH astrocytes, though these changes were not statistically significant (**Figures 1E,F**), likely a reflection of the relatively short duration of stretch injury. Both GFAP and S100β are upregulated in reactive astrocytes (Cerutti and Chadi, 2000; Sofroniew, 2005).

Glycolytic rate assay

We first exposed stretched and control ONH astrocytes to a glycolytic stress test in order to compare the glycolytic rate, as measured by extracellular acidification rate (ECAR) following exposure to electron transport chain (ETC) inhibitors rotenone (Complex I) and antimycin-A (Complex III). ECAR data normalized to cell number showed no difference in baseline ECAR between stretched and control ONH astrocytes (**Figure 2A**; $p = 0.770$, $n = 20$). Due to the absence of glucose in the media, this extracellular acidification comes from cell processes other than glycolysis, mainly oxidative respiration (Wu et al., 2007; Mookerjee et al., 2015). Once glucose was added, stretched ONH astrocytes had higher glycolytic ECAR values compared to control (**Figure 2B**, $p = 0.0037$, $n = 20$), suggesting that the stretched ONH astrocytes are more glycolytically active than control astrocytes. Maximal ECAR, the degree to which the cells can increase their glycolytic activity to produce ATP when mitochondrial respiration is inhibited, was significantly higher in stretched compared to control ONH astrocytes (**Figure 2C**, $p = 0.0039$, $n = 20$). Stretched ONH astrocytes also had a higher glycolytic reserve than control ONH astrocytes, as determined by the difference between maximal and glycolytic ECAR (**Figure 2D**, $p = 0.0136$, $n = 20$). These data indicate the stress caused by biaxial stretch of the ONH astrocytes expanded energy utilizing processes.

Mitochondrial stress test

To determine to what degree the stretched ONH astrocytes utilized their mitochondria, we exposed ONH astrocytes to the mitochondrial stress test, and assay that uses electron transport chain complex inhibitors to challenge mitochondrial respiration as measured by oxygen consumption rate (OCR) in the Seahorse Analyzer. Stretched ONH astrocytes had no difference in their basal respiration compared to control ONH astrocytes (**Figure 3A**). Inhibition of the ATP synthase using oligomycin-A showed that stretched ONH astrocytes had lower ATP-linked respiration compared to control ONH astrocytes (**Figure 3B**, $p = 0.0009$, $n = 27$). Despite this difference in ATP-linked respiration, stretched ONH astrocytes had higher maximal respiration (**Figure 3C**, $p = 0.0157$, $n = 27$) and higher spare capacity (**Figure 3D**, $p = 0.0010$, $n = 27$), than control ONH astrocytes. This suggests that the stretched ONH astrocytes have the capacity to be more responsive to metabolic challenges than control ONH astrocytes.

Mitochondrial fuel dependency test

Cells under stress may be inclined to shift their ability to use energy substrates for fuel, including expanding their capacity to use certain substrates. To test this hypothesis, we used the mitochondrial fuel dependency test on three possible fuel sources, pyruvate, glutamine, and long chain fatty acids. Compounds that can block transport or conversion of each of these fuel sources are used to observe how OCR changes under their influence. A large decrease in OCR after

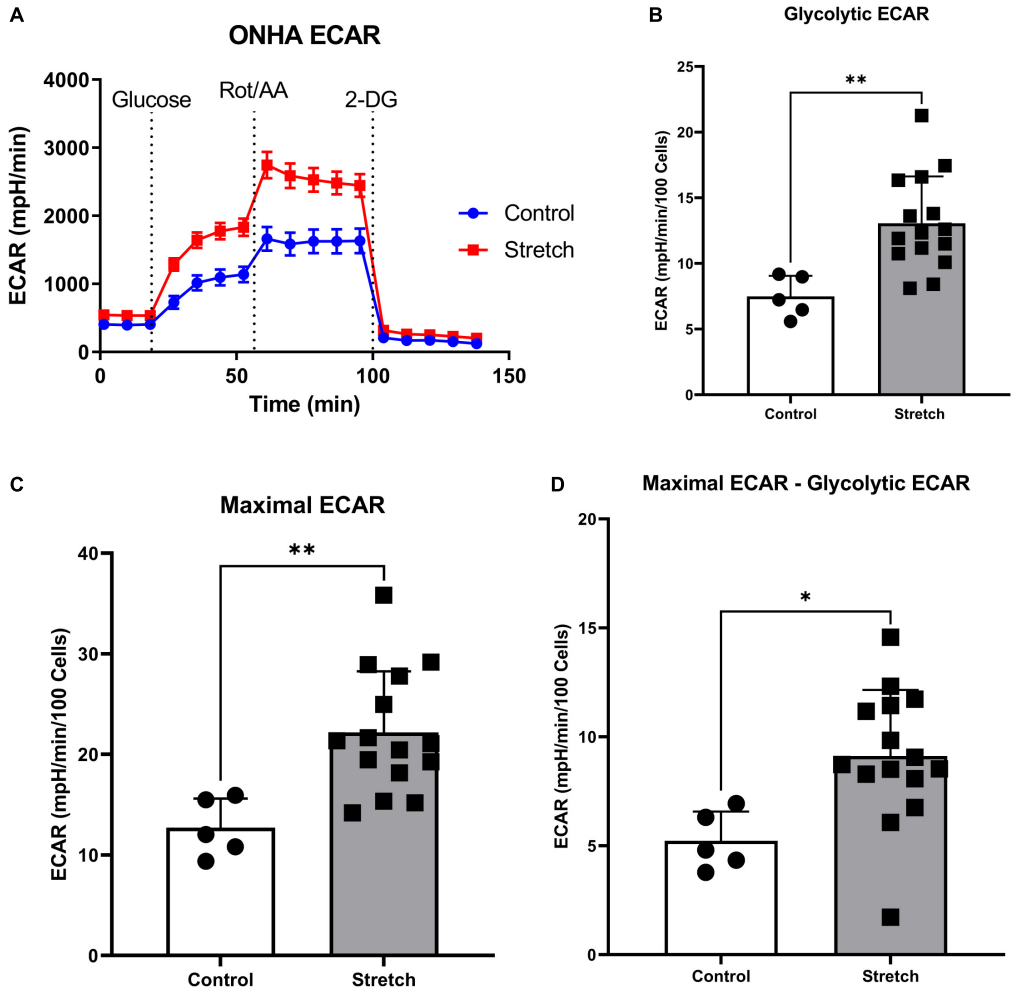

FIGURE 2
Glaucoma-like stretch causes an increase in glycolytic activity in primary optic nerve head astrocytes (ONHAs). **(A)** Stretch increases the extracellular acidification rate (ECAR) of primary ONH astrocytes. Measurements were taken every 9 min for baseline OCR, then addition of glucose, rotenone with Antimycin-A, and 2-deoxyglucose (2-DG). **(B)** Following the addition of glucose, stretched ONH astrocytes have a significantly higher ECAR than control ONH astrocytes (**p = 0.0037, n = 20). **(C)** Stretched ONH astrocytes have a significantly higher maximal ECAR than control ONH astrocytes (**p = 0.0039, n = 20). **(D)** Stretched ONH astrocytes have a significantly higher ECAR upregulation following the addition of rotenone and Antimycin-A compared to control ONH astrocytes (*p = 0.0136, n = 20). Values for panels **(B–D)** are normalized to cell number.

application of UK5099, an inhibitor of the mitochondrial pyruvate carrier, for example, suggests pyruvate as an important source of mitochondrial fuel for ONH astrocytes. Inhibitors of glutaminase for glutamine conversion to glutamate (BPTES), and carnitine palmitoyl-transferase 1A for long chain fatty acid translocation into the mitochondria for β-oxidation (Etomoxir) were used to evaluate dependence on glutamine and long chain fatty acids, respectively (Figures 4A–C). Representative OCR plots for pyruvate, glutamine, and long chain fatty acids are shown (Figures 4A–C). Stretched ONH astrocytes significantly increased their dependence on pyruvate compared to control (p = 0.0347, n = 12), Figure 4B. Dependence on glutamine decreased significantly in the stretched ONH astrocytes compared to control (p = 0.0052, n = 16), Figure 4D. Stretched ONH astrocytes significantly increased their reliance on fatty acids, as shown in Figures 4E,F (p = 0.0071, n = 9).

Interestingly, the stretched ONH astrocytes increased their dependency on pyruvate and fatty acids compared to control ONH astrocytes, but the relative dependence of specific substrates within groups remained equivalent. For example, both control and stretched ONH astrocytes were dependent upon glutamine to degree that was significantly greater than either long chain fatty acid or pyruvate (Figures 4G,H; p < 0.0001 for glutamine comparisons to either long chain fatty acid or pyruvate). There was no difference in dependence on long chain fatty acid or pyruvate within the control or stretched ONHA groups. These data indicate that dependency on pyruvate and fatty acids expanded, making

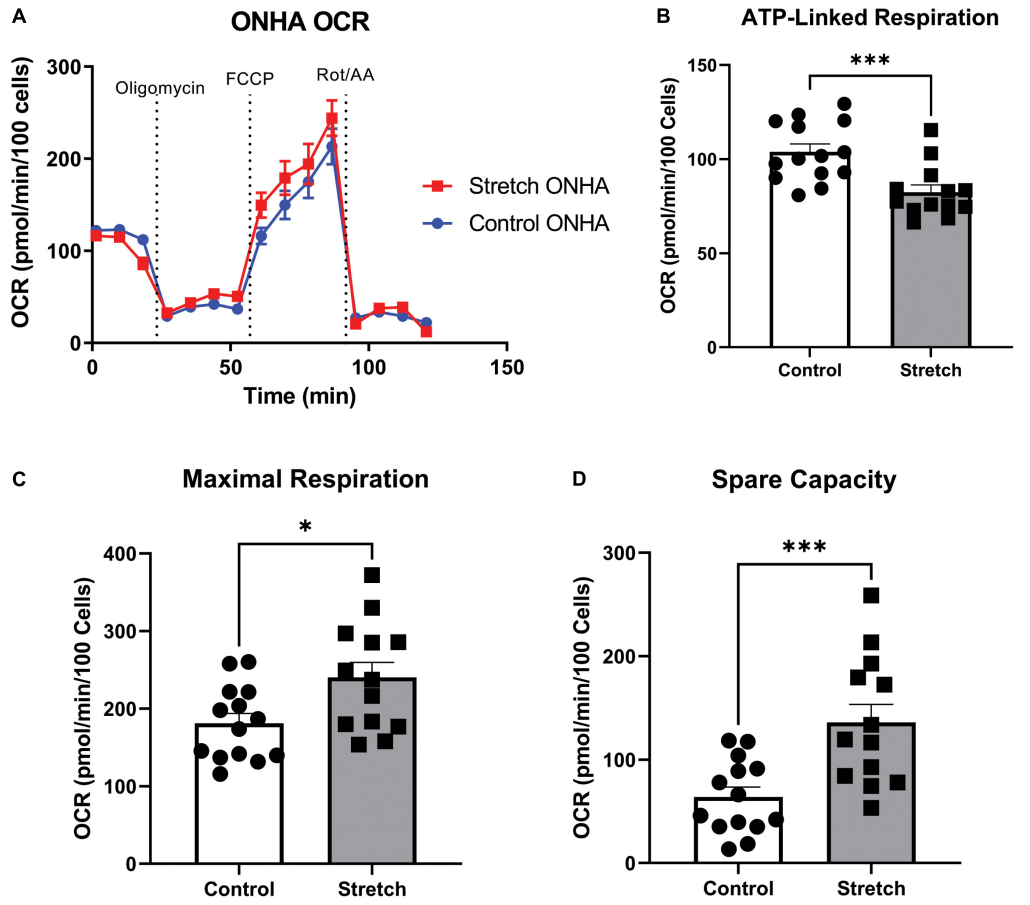

FIGURE 3
Optic Nerve Head Astrocytes (ONHAs) stretched as in glaucoma have altered mitochondrial respiration compared to control ONHAs. **(A)** Stretched ONH astrocytes have no difference in basal oxygen consumption rate (OCR) when compared to Control. Graph shows one representative example of OCR taken from the three biological replicates analyzed over 20–30 wells. **(B)** Stretched ONH astrocytes have a significantly lower ATP-linked mitochondrial OCR than control ONH astrocytes (***p = 0.0009, n = 27). **(C,D)** Stretched ONH astrocytes have a higher maximal respiration and spare capacity than control ONH astrocytes (*p = 0.0157, n = 27; ***p = 0.0010, n = 27).

up the share of fuel that was not coming from glutamine in stretched ONH astrocytes.

Optic nerve head astrocyte protein analysis

The metabolic alterations we observed in ONHA function after stretch suggest we might also identify corresponding changes in metabolism-associated proteins in these cells. For example, glutamine dependency might suggest potential changes in glutamate-aspartate transporter (GLAST), or glutamine synthetase. There was a significant increase in the protein levels of glucose transporter-1 (GLUT1) in the stretched ONH astrocytes as compared to control; the difference was noted in the astrocyte-specific 45kDa isoform of the transporter (p = 0.0225, Figure 5A). This suggests that stretched astrocytes had an increased capacity for the uptake of glucose. There was no difference in protein levels for the astrocyte-specific lactate dehydrogenase (Figure 5B); glucose-6-phosphate-dehydrogenase (Figure 5C), the enzyme that shunts glucose into the pentose-phosphate pathway; or glutamine synthetase (Figure 5D), the enzyme that converts glutamate to glutamine. However, the glutamate-aspartate transporter (GLAST) protein in monomeric form was significantly increased in the Stretch group (p = 0.020). GLAST dimers were prominent in the analyzed proteins, but did not differ across the Control and Stretch groups.

Discussion

Isolating ONH astrocytes, subjecting them to biaxial stretch then evaluating their bioenergetics using the Seahorse Analyzer has yielded insight into astrocytic metabolic changes as a result of mechanical stress. To the degree that these

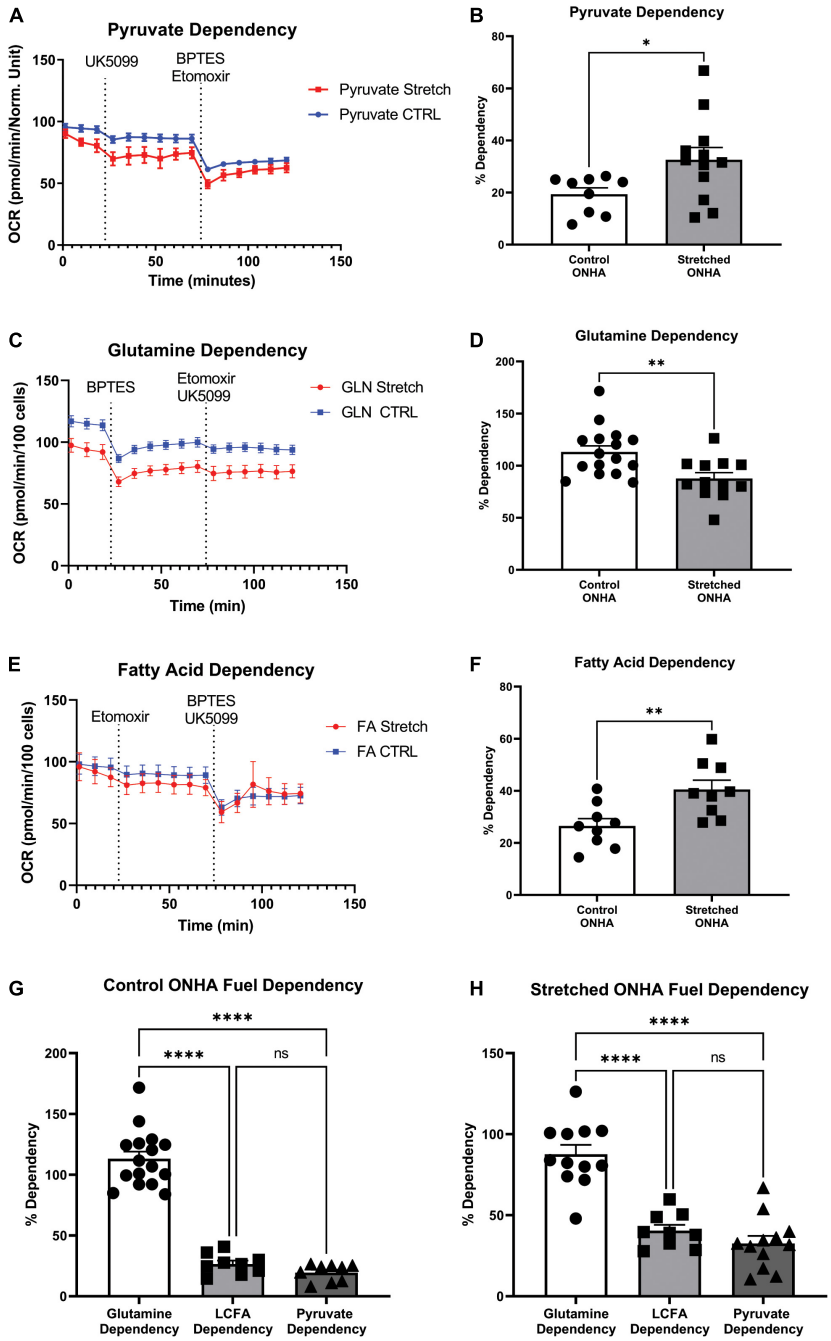

FIGURE 4
Mitochondrial substrate dependency of optic nerve head astrocytes (ONHAs) is changed by glaucomic stretch. **(A)** Representative oxygen consumption rate (OCR) output for the pyruvate dependency test. Cells are exposed to the mitochondrial pyruvate carrier inhibitor UK5099 followed by the glutamine and fatty acid oxidation pathway inhibitors BPTES and Etomoxir, respectively. **(B)** OCR for pyruvate dependency is significantly higher for stretched ONH astrocytes compared to Control (*$p = 0.0347$, $n = 20$). **(C)** Representative oxygen consumption rate (OCR) output for the glutamine dependency test. Cells are exposed to the glutaminase inhibitor BPTES followed by the fatty acid oxidation and pyruvate pathway inhibitors Etomoxir and UK5099, respectively. **(D)** Glutamine dependency is significantly lower in Stretched ONH astrocytes compared to Control (**$p = 0.0052$, $n = 27$). **(E)** Representative OCR output for the fatty acid dependency test. Cells are exposed to the carnitine palmitoyl-transferase 1a inhibitor Etomoxir followed by the glutamine and pyruvate pathway inhibitors BPTES and UK5099, respectively. **(F)** Fatty acid metabolic dependency is significantly higher in Stretched compared to Control ONH astrocytes (**$p = 0.0071$, $n = 17$). **(G)** Control ONHA fuel dependency is significantly different by one-way ANOVA ($p < 0.0001$). Control ONH astrocytes are significantly more dependent on glutamine as compared to fatty acids (****$p < 0.0001$) or pyruvate (****$p < 0.0001$) for fuel. These control ONH astrocyte data are the same as in panels **(B–F)**, collected together for ease of comparison. **(H)** Stretch ONHA fuel dependency is significantly different by one-way ANOVA ($p < 0.0001$). Stretched ONH astrocytes are also significantly more dependent on glutamine as compared to fatty acids (****$p < 0.0001$) or pyruvate (****$p < 0.0001$) for fuel. These stretch ONH astrocyte data are the same as in panels **(B–F)**, collected together for ease of comparison.

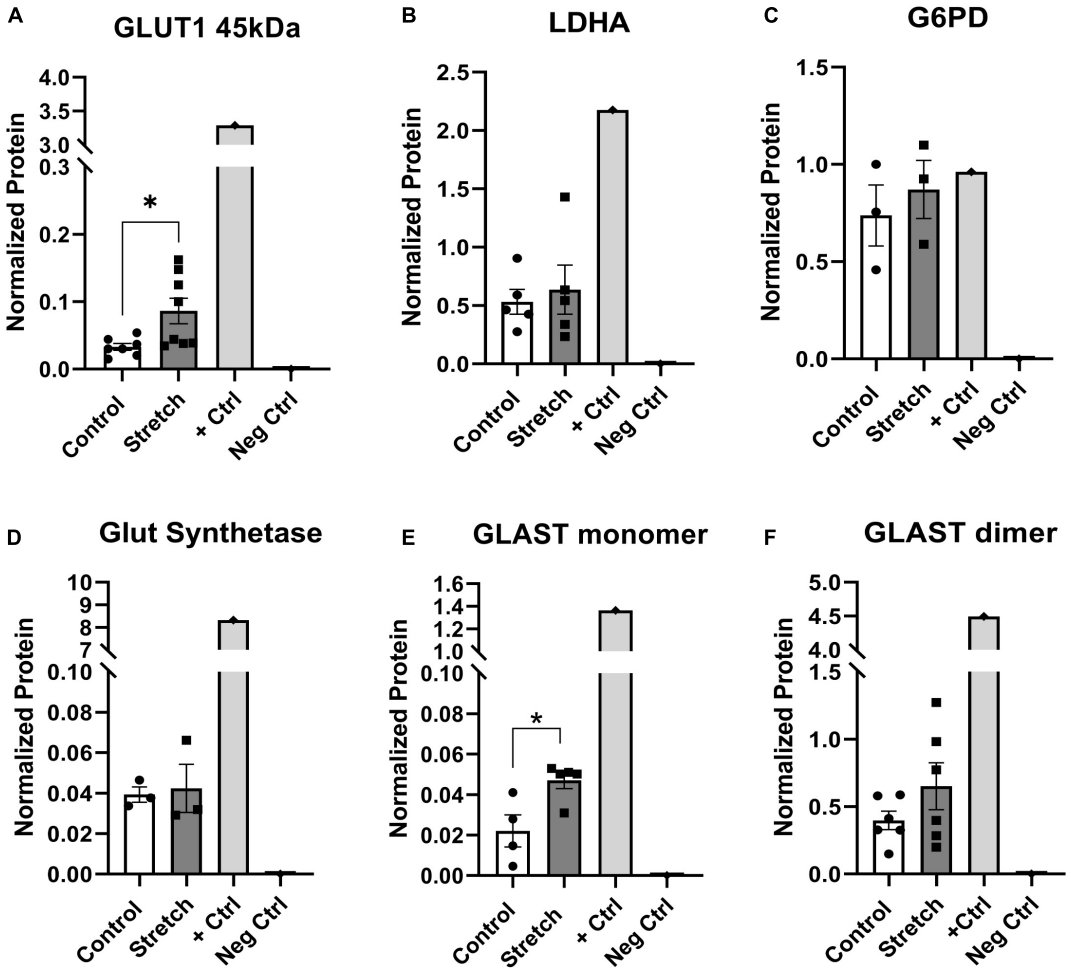

FIGURE 5
Protein changes in ONHAs corroborate bioenergetics data. **(A)** Glucose transporter-1 protein levels in Stretched ONH astrocytes are significantly higher than Control (*p = 0.0225, n = 7 Control, n = 8 Stretch). Retinal lysate from a 2 month-old mouse was used as a positive control for each protein analyzed, while negative control was the signal obtained when no primary antibody was included in the capillary. **(B)** Lactate dehydrogenase-A, the astrocyte-specific isoform of the enzyme that catalyzes the interconversion of pyruvate and lactate, has equivalent protein levels in Control and Stretch ONH astrocytes. **(C)** Glucose-6-phosphate dehydrogenase, the enzyme that shunts glucose into the pentose phosphate pathway, is no different in Control and Stretch ONH astrocytes. **(D)** Glutamine synthetase, the enzyme that synthesizes glutamine from glutamate, is no different in Control and Stretch ONH astrocytes. **(E)** The monomeric form of glutamate-aspartate transporter (GLAST) has significantly higher protein levels in the Stretch as compared to the Control ONH astrocytes (p = 0.020; n = 4 Control, n = 5 Stretch). **(F)** GLAST dimer protein levels are no different in Control and Stretch ONH astrocytes.

mechanical stresses recapitulate the strain experienced by the cells of the ONH during ocular hypertension, we have gained insight into the metabolic shifts and fuel preferences of ONH astrocytes in glaucoma.

Optic nerve head astrocytes subjected to stretch increase their extracellular acidification when glucose is made available, but also after electron transport chain (ETC) disruption. This likely reflects an overall increase in metabolic demand as a result of mechanical stress. Interestingly, stretched ONH astrocytes had higher maximal respiration and spare capacity compared to control cells, but lower ATP-linked respiration. Finally, we showed that stretched ONH astrocytes were more dependent on pyruvate and fatty acids as fuel compared to control ONH astrocytes, but this did not significantly alter their significant reliance on glutamine. Both control and stretched ONH astrocytes exhibit a preference for glutamine.

Despite having extensive mitochondrial networks, astrocytes are primarily reliant on glycolysis (Rahman and Suk, 2020) for their ATP production than on mitochondrial respiration (Dienel and Hertz, 2001; Turner and Adamson, 2011). Consistent with this, extracellular acidification rate (ECAR) in the stretched and control ONH astrocytes was robust. The stretched ONH astrocytes exhibited significantly greater ECAR than control in the presence of glucose and after inhibition of Complexes I and III of the electron transport chain (ETC). Our interpretation of these data is that the

stretched ONH astrocytes were much more metabolically active than control cells. Our ECAR data does not distinguish between proton release from lactate extrusion versus from the tricarboxylic acid cycle, though with glucose as the primary substrate, the contribution of ECAR from glycolysis often outpaces that from the TCA cycle (Mookerjee et al., 2015). Lamina cribrosa cells isolated from ONHs of patients with glaucoma showed increased lactate-associated extracellular acidification compared to control patient lamina cribrosa (LC) cells, suggesting increased glycolytic flux with glaucoma (Kamel et al., 2020). Our findings are consistent with the LC observations. Whereas the human LC cells are not astrocytes, the two cell types have overlapping roles in the ONH since rodents possess a glial lamina composed of astrocytes (Hernandez, 2000b; Sun et al., 2009).

The increased ECAR after glucose addition in the stretched ONH astrocytes might have been anticipated to accompany an increase in lactate dehydrogenase (LDH) since ECAR is primarily a result of lactate release, which co-transports a proton, thereby acidifying the extracellular milieu. In many contexts, astrocytes are a source of lactate to fuel/support the neurons in their vicinity (Pellerin et al., 1998; Volkenhoff et al., 2015; Muraleedharan et al., 2020). However, we observed no changes in the LDH protein when comparing control and stretched ONH astrocytes. One possible explanation is that the dual role of LDH, the interconversion of pyruvate and lactate, precludes a linear relationship between lactate production and LDH protein levels. We specifically probed for LDHA, the isoform that preferentially converts pyruvate into lactate (O'Brien et al., 2007). Another possibility is that LDH enzymatic activity might have been increased in stretched ONH astrocytes without a change in the overall protein. ECAR was not different between control and stretched ONH astrocytes prior to the addition of glucose, so LDH stability is consistent with the data indicating stretched ONH astrocytes are more dependent on glutamine than pyruvate. Proteomics undertaken on human ONH astrocytes subjected to 2h of 3% stretch showed a downregulation of lactate dehydrogenase A-like 6B protein (Rogers et al., 2012a), but this change was not observed when the degree of stretch and length of time at stretch were increased to values that matched our own experiment.

Stretched optic nerve head astrocyte mitochondria are more responsive than control

Stretched ONH astrocytes showed increased maximal respiratory rate and spare capacity compared to control ONH astrocytes. We observed no difference in the baseline mitochondrial OCR in stretch and control ONHA groups. These observations differ from those made of glaucoma patient LC cells, which showed significantly lower basal OCR and spare capacity compared to control patient LC cells (Kamel et al., 2020). A key difference is that LC cells from glaucoma patients are likely to have had chronic exposure to strain, while our ONH astrocytes were under biaxial strain for 24 h only. In microarray analysis of human glaucomatous ONHA, genes associated with ATP metabolism were downregulated (Nikolskaya et al., 2009). Though not detailed enough to indicate which metabolic genes in particular were affected, the ATP metabolism gene downregulation could be consistent with the significantly lower ATP-linked respiration we observed in stretched ONH astrocytes compared to control. Since ECAR data indicates greater metabolic activity in the stretched cells, these observations indicate the stretched cells obtained slightly greater metabolic support from glycolysis than the control ONH astrocytes. This is corroborated by the increased pyruvate dependency demonstrated by the stretched ONH astrocytes. The stretched ONH astrocytes had greater maximal respiration and spare capacity than control, indicating that the biaxial strain has promoted a metabolic resilience or responsiveness in the cells such that they should be able to meet additional energy demand when called upon to do so. The increased dependency on fatty acids for energy by the stretched cells is consistent with studies showing that reactive astrocytes increase their fatty acid metabolism (Zamanian et al., 2012; Liddelow et al., 2017). The ability to utilize fatty acids contributes to the metabolic resilience. Fuel flexibility and resilience are positive, though *in vivo* would be limited by the eventual structural breakdown of ONH astrocytes that has been observed in rat (Dai et al., 2012) and mouse (Lye-Barthel et al., 2013) ONH in the course of glaucoma pathogenesis.

Stretched optic nerve head astrocytes had altered mitochondrial fuel dependency

The dependency of ONH astrocytes for each of the three fuel sources we tested differed across stretched and control ONH astrocytes. Stretched ONH astrocytes had significantly greater dependency on pyruvate and fatty acids than controls ONH astrocytes. Dependence of stretched ONH astrocytes on glutamine decreased compared to control. However, since the dependence of both stretched and control ONH astrocytes was nevertheless overwhelmingly for glutamine, we interpret the shift toward pyruvate and fatty acid for the stretched ONH astrocytes as revealing an expansion of their possible means by which to meet their increased metabolic needs.

Optic nerve head astrocyte dependence on glutamine over fatty acids or pyruvate was somewhat unexpected given the emphasis on astrocyte glycolysis as opposed to respiration to meet metabolic needs (Dienel and Hertz, 2001; Turner and Adamson, 2011). Our data suggest the glutamate-glutamine cycle plays a much larger role in ONHA metabolism than

previously appreciated. Astrocytes transport glutamate from the extracellular space using GLAST and GLT-1, a critical management of excitatory neurotransmitters (Robinson and Jackson, 2016). Glutamate is converted to glutamine through the activity of glutamine synthetase. We observed no difference in glutamine synthetase (GS) protein in control versus stretched ONH astrocytes. At first glance, this could suggest that imported glutamate may not be the source of glutamine for these ONH astrocytes; glutamine was available directly from the cell media. However, we observed significant upregulation of GLAST in the stretched ONH astrocytes. The capacity for glutamate import increased in stretched ONH astrocytes, and it may be the case that GS activity increased to address the greater concentrations of glutamate without altering overall GS protein. Alternatively, the dependency on glutamine may be masking a use of glutamate by the ONH astrocytes. Glutamate can be oxidized via glutamate dehydrogenase, or oxidized to α-ketoglutarate for the TCA cycle via aspartate aminotransferase (Daikhin and Yudkoff, 2000). In fact, glutamate could theoretically substitute for glucose for fuel. In human LC cells from glaucoma patients, there was a significant upregulation of glutaminase-2 (Kamel et al., 2020), an enzyme that converts glutamine to glutamate. We did not measure glutaminase-2, but anticipate that it may be increased in stretched ONH astrocytes. If ONH astrocytes are using glutamine to generate glutamate that supplies the TCA cycle with carbon, then we would anticipate that these cells would not be exporting glutamine for uptake by neurons. This is testable by measuring amino acid transporter Slc38a1 protein or activity (Bröer and Brookes, 2001). Interestingly, fatty acids are critical for the success of the glutamate-glutamine cycle because the amino groups provide the nitrogen for the production of glutamine from glutamate (Daikhin and Yudkoff, 2000). This may explain the increased metabolic dependency of stretched ONH astrocytes on fatty acids we observe.

Might the ONH astrocytes generate glutamine only to convert it to glutamate for fuel when it is not taken up by neurons? At high external concentrations of glutamate, the entry of glutamate into the TCA cycle in astrocytes is favored over conversion to glutamine (McKenna et al., 1996). What is unclear for our experiments is the source of glutamate since these cultures did not include cells other than the ONH astrocytes. Relatedly, the dependence of ONH astrocytes in general on glutamine in our experiments raises the issue of whether their metabolic choices are governed by being a monoculture. It would not be surprising if ONH astrocytes do not prefer glucose for fuel as a result of not having neurons to which they can easily pass lactate. Future experiments that co-culture ONH astrocytes with neurons could resolve this question. The upregulation in GLAST and the distinct reliance of ONH astrocytes on glutamine metabolism also indicates a larger role for mitochondrial respiration in the stretched ONH astrocytes. The astrocytic preference for glutamine over pyruvate as a mitochondrial fuel source reinforces the lactate-shuttle hypothesis (Pellerin et al., 1998) since not relying on pyruvate for mitochondrial respiration allows them to export lactate.

In our protein analysis to corroborate our bioenergetic findings, we observed no increase in glucose-6-phosphate-dehydrogenase, the enzyme that shunts glucose into the pentose phosphate pathway. This suggests that there is no change in the management of metabolites into the pentose phosphate pathway, which may also be consistent with the emphasis of these ONH astrocytes on utilizing glutamine for fuel. The absence of this shunting could ultimately be deleterious for the stretched ONH astrocytes since NADPH from the pentose phosphate pathway is used for the production of glutathione (Grant, 2008), an antioxidant effective at limiting reactive oxygen species (ROS). ROS production is upregulated in reactive astrocytes (Sheng et al., 2013; Vicente-Gutiérrez et al., 2021), so one might expect increased glutathione from the pentose phosphate pathway could assist in ROS management. In future experiments, we will evaluate antioxidant production in stretched ONH astrocytes.

We observed a significant increase in GLUT1 protein, the primary means by which astrocytes take up glucose from the vasculature and the parenchyma. In past studies, we have reported a significant decline in GLUT1 protein in the optic nerve (ON) of glaucomatous mice (Harun-or-Rashid et al., 2018). Timing is a consideration here, as we cannot easily compare ONH astrocytes exposed to 24 h of stretch to ONs from mice with 6 + months of increased IOP. Perhaps the difference between GLUT1 protein in the ON and ONH is one that requires a metabolic perspective and not just a structural one. GLUT1 upregulation serves the stretched ONH astrocytes well by importing more glucose. Our data indicates the stretched ONH astrocytes become more dependent on pyruvate, a situation that would be enabled by increased glucose transport. We have little reason to think that ON and ONH astrocytes are homogeneous. The glia lamina of the ONH is a unique structure with astrocytes oriented differently than those in the ON (Sun et al., 2009). While it has been shown that ONH astrocytes are connected by gap junctions (Quigley, 1977), it remains to be determined if the two populations of ON and ONH astrocytes are connected by gap junctions. *In vitro* experiments have shown that both hydrostatic pressure and oxygen-glucose deprivation and reperfusion led to decreases and relocation of connexin-43 intracellularly (Malone et al., 2007; Xie et al., 2017), potentially reducing the availability of glucose among astrocytes. We did not evaluate astrocyte coupling, but recognize the need to determine whether ON and ONH astrocytes form a network. The alternate roles and morphologies across the ON and ONH argue for heterogeneous populations of astrocytes. Increased GLUT1 protein in the stretched ONH astrocytes enables greater metabolic activity, likely to support the cellular alterations in cytoskeleton and function prompted by the strain experienced by the cells.

Stretched ONH astrocytes demonstrate metabolic changes that indicate the expansion of metabolic substrate utilization to support the increased metabolic activity noted in these cells. Future work will investigate the implications of these ONHA changes on retinal ganglion cells axon function.

Data availability statement

The original contributions presented in this study are included in the article/**Supplementary material**, further inquiries can be directed to the corresponding author.

Ethics statement

The animal study was reviewed and approved by The Institutional Animal Care and Use Committee of UNTHSC.

Author contributions

NP designed and performed experiments, analyzed data, created figures, and wrote the initial draft of the manuscript. EY, ABM, and CCK performed experiments and analyzed data. DMI designed experiments, analyzed data, created figures, edited the manuscript, and funded the research. All authors contributed to the article and approved the submitted version.

Funding

This study was funded by the National Eye Institute, R01 EY026662 to DMI.

Conflict of interest

The authors declare that the research was conducted in the absence of any commercial or financial relationships that could be construed as a potential conflict of interest.

Publisher's note

Supplementary material

The Supplementary Material for this article can be found online at: https://www.frontiersin.org/articles/10.3389/fnins.2022.957034/full#supplementary-material

References

Albalawi, F., Lu, W., Beckel, J. M., Lim, J. C., McCaughey, S. A., and Mitchell, C. H. (2017). The P2X7 receptor primes IL-1β and the NLRP3 inflammasome in astrocytes exposed to mechanical strain. *Front. Cell. Neurosci.* 11:227. doi: 10.3389/fncel.2017.00227

Bröer, S., and Brookes, N. (2001). Transfer of glutamine between astrocytes and neurons. *J. Neurochem.* 77, 705–719. doi: 10.1046/j.1471-4159.2001.00322.x

Cerutti, S. M., and Chadi, G. (2000). S100 immunoreactivity is increased in reactive astrocytes of the visual pathways following a mechanical lesion of the rat occipital cortex. *Cell Biol.* 24, 35–49.

Chidlow, G., Ebneter, A., Wood, J. P. M., and Casson, R. J. (2011). The optic nerve head is the site of axonal transport disruption, axonal cytoskeleton damage and putative axonal regeneration failure in a rat model of glaucoma. *Acta Neuropathol.* 121, 737–751. doi: 10.1007/s00401-011-0807-1

Chung, C. Y., Koprich, J. B., Siddiqi, H., and Isacson, O. (2009). Dynamic changes in presynaptic and axonal transport proteins combined with striatal neuroinflammation precede dopaminergic neuronal loss in a rat model of AAV α-synucleinopathy. *J. Neurosci.* 29, 3365–3373. doi: 10.1523/JNEUROSCI.5427-08.2009

Dai, C., Khaw, P. T., Yin, Z. Q., Li, D., Raisman, G., and Li, Y. (2012). Structural basis of glaucoma: the fortified astrocytes of the optic nerve head are the target of raised intraocular pressure. *Glia* 60, 13–28. doi: 10.1002/glia.21242

Daikhin, Y., and Yudkoff, M. (2000). Compartmentation of brain glutamate metabolism in neurons and glia. *J. Nutr.* 130, 1026–1031. doi: 10.1093/jn/130.4.1026s

Dienel, G. A., and Hertz, L. (2001). Glucose and lactate metabolism during brain activation. *J. Neurosci. Res.* 66, 824–838. doi: 10.1002/jnr.10079

Downs, J. C., Roberts, M. D., and Burgoyne, C. F. (2008). Mechanical environment of the optic nerve head in glaucoma. *Optom. Vis. Sci.* 85, 425–435. doi: 10.1097/OPX.0b013e31817841cb

Girard, M. J. A., Beotra, M. R., Chin, K. S., Sandhu, A., Clemo, M., Nikita, E., et al. (2016). In vivo 3-dimensional strain mapping of the optic nerve head following intraocular pressure lowering by trabeculectomy. *Opthamology* 123, 1190–1200.

Grant, C. M. (2008). Metabolic reconfiguration is a regulated response to oxidative stress. *J. Biol.* 7, 1. doi: 10.1186/jbiol63

Guo, L., Tsatourian, V., Luong, V., Podolean, A. G., Jackson, D. A., Fitzke, F. W., et al. (2005). En face optical coherence tomography: a new method to analyse structural changes of the optic nerve head in rat glaucoma. *Br. J. Ophthalmol.* 89, 1210–1216. doi: 10.1136/bjo.2004.058941

Halestrap, A. P. (2012). The monocarboxylate transporter family-structure and functional characterization. *IUBMB Life* 64, 1–9. doi: 10.1002/iub.573

Harder, J. M., Guymer, C., Wood, J. P. M., Daskalaki, E., Chidlow, G., Zhang, C., et al. (2020). Disturbed glucose and pyruvate metabolism in glaucoma with neuroprotection by pyruvate or rapamycin. *Proc. Natl. Acad. Sci. U.S.A.* 117, 33619–33627. doi: 10.1073/pnas.2014213117

Harun-or-Rashid, M., Pappenhagen, N., Palmer, P. G., Smith, M. A., Gevorgyan, V., Wilson, G. N., et al. (2018). Structural and functional rescue of chronic metabolically stressed optic nerves through respiration. *J. Neurosci.* 38, 5122–5139. doi: 10.1523/JNEUROSCI.3652-17.2018

Harun-Or-Rashid, M., Pappenhagen, N., Zubricky, R., Coughlin, L., Jassim, A. H., and Inman, D. M. (2020b). MCT2 overexpression rescues

metabolic vulnerability and protects retinal ganglion cells in two models of glaucoma. *Neurobiol. Dis.* 141:104944. doi: 10.1016/j.nbd.2020.104944

Harun-Or-Rashid, M., Pappenhagen, N., Zubricky, R., Coughlin, L., Jassim, A. H., and Inman, D. M. (2020a). MCT2 overexpression rescues metabolic vulnerability and protects retinal ganglion cells in two glaucoma models. *BioRXiv* [Preprint]. doi: 10.1101/2020.02.14.950097

Hernandez, M. R. (2000a). The optic nerve head in glaucoma: role of astrocytes in tissue remodeling. *Prog. Retin. Eye Res.* 19, 297–321.

Hernandez, M. R. (2000b). The optic nerve head in glaucoma: role of astrocytes in tissue remodeling. *Prog. Retin. Eye Res.* 19, 297–321.

Howell, G. R., Libby, R. T., Jakobs, T. C., Smith, R. S., Phalan, F. C., Barter, J. W., et al. (2007). Axons of retinal ganglion cells are insulted in the optic nerve early in DBA/2J glaucoma. *J. Cell Biol.* 179, 1523–1537. doi: 10.1083/jcb.200706181

Hui, F., Tang, J., Williams, P. A., McGuinness, M. B., Hadoux, X., Casson, R. J., et al. (2020). Improvement in inner retinal function in glaucoma with nicotinamide (vitamin B3) supplementation: a crossover randomized clinical trial. *Clin. Exp. Ophthalmol.* 48, 903–914. doi: 10.1111/ceo.13818

Iglesias, J., Morales, L., and Barreto, G. E. (2017). Metabolic and inflammatory adaptation of reactive astrocytes: role of PPARs. *Mol. Neurobiol.* 54, 2518–2538. doi: 10.1007/s12035-016-9833-2

Jassim, A. H., Coughlin, L., Harun-or-rashid, M., Kang, P. T., Chen, Y., and Inman, D. M. (2019). Higher reliance on glycolysis limits glycolytic responsiveness in degenerating glaucomatous optic nerve. *Mol. Neurobiol.* 56, 7097–7112.

Kaja, S., Payne, A. J., Patel, K. R., Naumchuk, Y., and Koulen, P. (2015). Differential subcellular Ca^{2+} signaling in a highly specialized subpopulation of astrocytes. *Exp. Neurol.* 265, 59–68. doi: 10.1016/j.expneurol.2014.12.014

Kamel, K., O'Brien, C. J., Zhdanov, A. V., Papkovsky, D. B., Clark, A. F., Stamer, D., et al. (2020). Reduced oxidative phosphorylation and increased glycolysis in human glaucoma lamina cribrosa cells. *Invest. Ophthalmol. Vis. Sci.* 61:4. doi: 10.1167/IOVS.61.13.4

Liddelow, S. A., Guttenplan, K. A., Clarke, L. E., Bennett, F. C., Bohlen, C. J., Schirmer, L., et al. (2017). Neurotoxic reactive astrocytes are induced by activated microglia. *Nature* 541, 481–487. doi: 10.1038/nature21029

Lye-Barthel, M., Sun, D., and Jakobs, T. C. (2013). Morphology of astrocytes in a glaucomatous optic nerve. *Invest. Ophthalmol. Vis. Sci.* 54, 909–917. doi: 10.1167/iovs.12-10109

Maddineni, P., Kasetti, R. B., Patel, P. D., Millar, J. C., Kiehlbauch, C., Clark, A. F., et al. (2020). CNS axonal degeneration and transport deficits at the optic nerve head precede structural and functional loss of retinal ganglion cells in a mouse model of glaucoma. *Mol. Neurodegener.* 15:48. doi: 10.1186/s13024-020-00400-9

Malone, P., Miao, H., Parker, A., Juarez, S., and Hernandez, M. R. (2007). Pressure induces loss of gap junction communication and redistribution of connexin 43 in astrocytes. *Glia* 55, 1085–1098. doi: 10.1002/glia.20527

McKenna, M. C., Sonnewald, U., Huang, X., Stevenson, J., and Zielke, H. R. (1996). Exogenous glutamate concentration regulates the metabolic fate of glutamate in astrocytes. *J. Neurochem.* 66, 386–393.

Mookerjee, S. A., Goncalves, R. L. S., Gerencser, A. A., Nicholls, D. G., and Brand, M. D. (2015). The contributions of respiration and glycolysis to extracellular acid production. *Biochim. Biophys. Acta* 1847, 171–181. doi: 10.1016/j.bbabio.2014.10.005

Morgan, J. E. (2000). Optic nerve head structure in glaucoma: astrocytes as mediators of axonal damage. *Eye* 14, 437–444. doi: 10.1038/eye.2000.128

Morgello, S., Uson, R. R., Schwartz, E. J., and Haber, R. S. (1995). The human blood–brain barrier glucose transporter (GLUT1) is a glucose transporter of gray matter astrocytes. *Glia* 14, 43–54. doi: 10.1002/glia.440140107

Muraleedharan, R., Gawali, M. V., Tiwari, D., Sukumaran, A., Oatman, N., Anderson, J., et al. (2020). AMPK-regulated astrocytic lactate shuttle plays a non-cell-autonomous role in neuronal survival. *Cell Rep.* 32:108092. doi: 10.1016/j.celrep.2020.108092

Neufeld, A. H., and Liu, B. (2003). Glaucomatous optic neuropathy: when glia misbehave. *Neuroscientist* 9, 485–495.

Nikolskaya, T., Nikolsky, Y., Serebryiskaya, T., Zvereva, S., Sviridov, E., Dezso, Z., et al. (2009). Network analysis of human glaucomatous optic nerve head astrocytes. *BMC Med. Genomics* 2:24. doi: 10.1186/1755-8794-2-24

O'Brien, J., Kla, K. M., Hopkins, I. B., Malecki, E. A., and McKenna, M. C. (2007). Kinetic parameters and lactate dehydrogenase isozyme activities support possible lactate utilization by neurons. *Neurochem. Res.* 32, 597–607. doi: 10.1007/s11064-006-9132-9

Oikawa, K., Ver Hoeve, J. N., Teixeira, L. B. C., Snyder, K. C., Kiland, J. A., Ellinwood, N. M., et al. (2020). Sub-region-specific optic nerve head glial activation in glaucoma. *Mol. Neurobiol.* 57, 2620–2638. doi: 10.1007/s12035-020-01910-9

Pellerin, L., Pellegri, G., Bittar, P., Charnay, Y., Bouras, C., Martin, J., et al. (1998). Evidence supporting the existence of an activity-dependent astrocyte-neuron lactate shuttle. *Dev. Neurosci.* 20, 291–299.

Quigley, H. A. (1977). Gap junctions between optic nerve head astrocytes. *Invest. Ophthalmol. Vis. Sci.* 16, 582–585.

Quigley, H. A., Addicks, E. M., Green, W. R., and Maumenee, A. E. (1981). Optic nerve damage in human glaucomaII. The site of injury and susceptibility to damage. *Arch. Ophthalmol.* 99, 635–649.

Rahman, M. H., and Suk, K. (2020). Mitochondrial dynamics and bioenergetic alteration during inflammatory activation of astrocytes. *Front. Aging Neurosci.* 12:459. doi: 10.3389/fnagi.2020.614410

Robinson, M. B., and Jackson, J. G. (2016). Astroglial glutamate transporters coordinate excitatory signaling and brain energetics. *Neurochem. Int.* 98, 56–71.

Rogers, R. S., Dharsee, M., Ackloo, S., Sivak, J. M., and Flanagan, J. G. (2012b). Proteomics analyses of human optic nerve head astrocytes following biomechanical. *Mol. Cell Proteomics* 11:M111.012302. doi: 10.1074/mcp.M111.012302

Rogers, R., Dharsee, M., Ackloo, S., and Flanagan, J. G. (2012a). Proteomics analyses of activated human optic nerve head lamina cribrosa cells following biomechanical strain. *Invest. Opthalmol. Vis. Sci.* 53:3806. doi: 10.1167/iovs.11-8480

Saab, A. S., Tzvetavona, I. D., Trevisiol, A., Baltan, S., Dibaj, P., Kusch, K., et al. (2016). Oligodendroglial NMDA receptors regulate glucose import and axonal energy metabolism. *Neuron* 91, 119–132. doi: 10.1016/j.neuron.2016.05.016

Schneider, M., and Fuchshofer, R. (2015). The role of astrocytes in optic nerve head fibrosis in glaucoma. *Exp. Eye Res.* 142, 49–55. doi: 10.1016/j.exer.2015.08.014

Sheng, W. S., Hu, S., Feng, A., and Rock, R. B. (2013). Reactive oxygen species from human astrocytes induced functional impairment and oxidative damage. *Neurochem. Res.* 38, 2148–2159. doi: 10.1007/s11064-013-1123-z

Sofroniew, M. V. (2005). Reactive astrocytes in neural repair and protection. *Neuroscientist* 11, 400–407. doi: 10.1177/1073858405278321

Sun, D., Lye-Barthel, M., Masland, R. H., and Jakobs, T. C. (2009). The morphology and spatial arrangement of astrocytes in the optic nerve head of the mouse. *J. Comp. Neurol.* 516, 1–19. doi: 10.1002/cne.22058

Sun, D., Qu, J., and Jakobs, T. C. (2013). Reversible reactivity by optic nerve astrocytes. *Glia* 61, 1218–1235. doi: 10.1002/glia.22507

Tribble, J. R., Otmani, A., Sun, S., Ellis, S. A., Cimaglia, G., Vohra, R., et al. (2021). Nicotinamide provides neuroprotection in glaucoma by protecting against mitochondrial and metabolic dysfunction. *Redox Biol.* 43:101988. doi: 10.1016/j.redox.2021.101988

Tsacopoulos, M., and Magistretti, P. J. (1996). Metabolic Coupling Glia and Neurons. *J. Neurosci.* 16, 877–885.

Turner, D. A., and Adamson, D. C. (2011). Neuronal-astrocyte metabolic interactions: understanding the transition into abnormal astrocytoma metabolism. *J. Neuropathol. Exp. Neurol.* 70, 167–176. doi: 10.1097/NEN.0b013e31820e1152

Vicente-Gutiérrez, C., Jiménez-Blasco, D., and Quintana-Cabrera, R. (2021). Intertwined ROS and metabolic signaling at the neuron-astrocyte interface. *Neurochem. Res.* 46, 23–33. doi: 10.1007/s11064-020-02965-9

Vohra, R., Tsai, J. C., and Kolko, M. (2013). The role of inflammation in the pathogenesis of glaucoma. *Surv. Ophthalmol.* 58, 311–320. doi: 10.1016/J.SURVOPHTHAL.2012.08.010

Volkenhoff, A., Weiler, A., Letzel, M., Stehling, M., Klämbt, C., and Schirmeier, S. (2015). Glial glycolysis is essential for neuronal survival in drosophila. *Cell Metab.* 22, 437–447. doi: 10.1016/j.cmet.2015.07.006

Weinreb, R. N., Aung, T., and Medeiros, F. A. (2014). The pathophysiology and treatment of glaucoma: a review. *JAMA* 311, 1901–1911. doi: 10.1001/jama.2014.3192

Williams, P. A., Harder, J. M., Foxworth, N. E., Cochran, K. E., Philip, V. M., Porciatti, V., et al. (2017). Vitamin B3 modulates mitochondrial vulnerability and prevents glaucoma in aged mice. *Science* 760, 756–760. doi: 10.1120/science.aal0092

Wilson, G. N., Smith, M. A., Inman, D. M., Dengler-Crish, C. M., and Crish, S. D. (2016). Early cytoskeletal protein modifications precede overt structural

degeneration in the DBA/2J mouse model of glaucoma. *Front. Neurosci.* 10:494. doi: 10.3389/fnins.2016.00494

Wu, M., Neilson, A., Swift, A. L., Moran, R., Tamagnine, J., Parslow, D., et al. (2007). Multiparameter metabolic analysis reveals a close link between attenuated mitochondrial bioenergetic function and enhanced glycolysis dependency in human tumor cells. *Am. J. Physiol. Cell Physiol.* 292, C125–C136. doi: 10.1152/ajpcell.00247.2006

Xie, H., Cui, Y., Hou, S., Wang, J., Miao, J., Deng, F., et al. (2017). Evaluation of connexin 43 redistribution and endocytosis in astrocytes subjected to ischemia/reperfusion or oxygen-glucose deprivation and reoxygenation. *Biomed Res. Int.* 2017:5064683. doi: 10.1155/2017/5064683

Zamanian, J. L., Xu, L., Foo, L. C., Nouri, N., Zhou, L., Giffard, R. G., et al. (2012). Genomic analysis of reactive astrogliosis. *J. Neurosci.* 32, 6391–6410. doi: 10.1523/JNEUROSCI.6221-11.2012

frontiers | Frontiers in Neuroscience

TYPE Review
PUBLISHED 03 November 2022
DOI 10.3389/fnins.2022.1009599

OPEN ACCESS

EDITED BY
Anu Kauppinen,
University of Eastern Finland, Finland

REVIEWED BY
Ana Isabel Arroba,
Fundación para la gestión de la Investigación Biomédica de Cádiz, Spain
Wai Wong,
Janssen Research & Development, LLC, United States

*CORRESPONDENCE
Kirstan A. Vessey
k.vessey@unimelb.edu.au

†These authors have contributed equally to this work and share first authorship

SPECIALTY SECTION
This article was submitted to Neurodegeneration, a section of the journal Frontiers in Neuroscience

RECEIVED 02 August 2022
ACCEPTED 12 October 2022
PUBLISHED 03 November 2022

CITATION
Wong JHC, Ma JYW, Jobling AI, Brandli A, Greferath U, Fletcher EL and Vessey KA (2022) Exploring the pathogenesis of age-related macular degeneration: A review of the interplay between retinal pigment epithelium dysfunction and the innate immune system. *Front. Neurosci.* 16:1009599. doi: 10.3389/fnins.2022.1009599

Exploring the pathogenesis of age-related macular degeneration: A review of the interplay between retinal pigment epithelium dysfunction and the innate immune system

Josephine H. C. Wong†, Jessica Y. W. Ma†, Andrew I. Jobling, Alice Brandli, Ursula Greferath, Erica L. Fletcher and Kirstan A. Vessey*

Department of Anatomy and Physiology, The University of Melbourne, Melbourne, VIC, Australia

Age-related macular degeneration (AMD) is a leading cause of irreversible vision loss in the older population. Classical hallmarks of early and intermediate AMD are accumulation of drusen, a waste deposit formed under the retina, and pigmentary abnormalities in the retinal pigment epithelium (RPE). When the disease progresses into late AMD, vision is affected due to death of the RPE and the light-sensitive photoreceptors. The RPE is essential to the health of the retina as it forms the outer blood retinal barrier, which establishes ocular immune regulation, and provides support for the photoreceptors. Due to its unique anatomical position, the RPE can communicate with the retinal environment and the systemic immune environment. In AMD, RPE dysfunction and the accumulation of drusen drive the infiltration of retinal and systemic innate immune cells into the outer retina. While recruited endogenous or systemic mononuclear phagocytes (MPs) contribute to the removal of noxious debris, the accumulation of MPs can also result in chronic inflammation and contribute to AMD progression. In addition, direct communication and indirect molecular signaling between MPs and the RPE may promote RPE cell death, choroidal neovascularization and fibrotic scarring that occur in late AMD. In this review, we explore how the RPE and innate immune cells maintain retinal homeostasis, and detail how RPE dysfunction and aberrant immune cell recruitment contribute to AMD pathogenesis. Evidence from AMD patients will be discussed in conjunction with data from preclinical models, to shed light on future therapeutic targets for the treatment of AMD.

KEYWORDS

age related macular degeneration (AMD), retinal pigment epithelium (RPE), mononuclear phagocyte (MP), microglia, dendritic cell, macrophage, para-inflammation, inflammation

Introduction

Age-related macular degeneration (AMD) is a leading cause of irreversible blindness in people over 50 years of age. Patients initially present with distortions in fine visual perception, and as the disease develops, vision symptoms progress to loss of central vision impacting abilities such as reading, face recognition and driving (Hassell et al., 2006; Rattner and Nathans, 2006). In severe cases, vision loss can progress to complete legal blindness impacting an affected individual's independence and quality of life (Hassell et al., 2006; Rattner and Nathans, 2006). AMD is characterized by chronic and progressive degeneration of the light sensitive neurons of the retina, the photoreceptors, and their support cells, the retinal pigment epithelium (RPE) (Miller, 2013). In the early and intermediate stages, AMD is diagnosed based on the presence and size of extracellular deposits, called drusen, which accumulate between the RPE and choroidal blood supply, and also by the presence of pigmentary abnormalities in the RPE. Abnormal waste deposits within RPE cells, called lipofuscin, and extracellular deposits between the photoreceptor and the RPE, called reticular pseudodrusen (RPD) are also manifestations of the disease (Holz et al., 2001; Greferath et al., 2016). Late AMD is generally classified into two groups: dry AMD or geographic atrophy (GA), and wet or neovascular AMD (nAMD) (**Figure 1**). Around 80–90% of AMD cases including intermediate and late-stage GA are the dry, atrophic form, which is generally a slowly progressing disease, where over time the atrophic areas become larger and confluent (Ferris et al., 1984). nAMD occurs when abnormal choroidal vessels grow under the RPE or when retinal blood vessels sprout within the retina. Vision loss in nAMD is accelerated as these abnormal vessels leak and bleed into the macula, leading to sudden vision loss due to macular edema and direct damage to the photoreceptors, and over time this leads to fibrous scarring (Ciulla et al., 2001; Lim et al., 2012; Little et al., 2018). At present, there are no effective treatments to slow progression from early and intermediate AMD to late stages of the disease (GA and nAMD). While there are no treatments for GA, nAMD is treated with anti-vascular endothelial growth factor (VEGF) drugs (Solomon et al., 2019) and while short-term visual acuity improvement is often observed, vision loss over the longer term occurs despite treatment in most cases (Rofagha et al., 2013). Effective treatments for slowing progression of early AMD to the late stages are urgently required.

In AMD, RPE and photoreceptor dysfunction occur alongside accumulation of waste materials in the subretinal space (RPD) and between the RPE and choroid (drusen), initiating recruitment of resident and systemic immune cells. The dominant immune cell type observed is mononuclear phagocytes (MPs) and these are rarely seen in the outer retina and RPE-Bruch's membrane complex in age-matched, non-diseased eyes, which implicates MPs in the pathology of AMD. MPs play a primary role in phagocytosis of pathological material in AMD. Resident MPs in the retina are called microglia and are postulated to remove cell debris in the subretinal space to protect photoreceptors and the RPE against injury and death (Langmann, 2007; Ambati et al., 2013). Additionally, drusen deposition between the RPE and choroid and failure of the RPE can cause breakdown of the blood retinal barrier, which can lead to recruitment and infiltration of systemic circulating MPs, the myeloid cells in the peripheral blood circulation comprising monocytes, macrophages and dendritic cells (Ransohoff and Cardona, 2010; Luhmann and Ali, 2012). In the early stages, AMD presents as a disease of low-grade chronic inflammation, called para-inflammation, which is denoted by the perpetual recruitment and non-resolving presence of MPs (Xu et al., 2009; Leveillard et al., 2019). Indeed, RPE dysfunction and non-resolving inflammation remain two prominent hypotheses for the pathogenesis of AMD (Xu et al., 2009; Guillonneau et al., 2017). In this review, we explore how the RPE and innate immune cells maintain retinal homeostasis, and consider the role of RPE dysfunction and aberrant immune cell recruitment in AMD pathogenesis.

Clinical definitions and treatment of age-related macular degeneration

Early and intermediate age-related macular degeneration

Diagnosis of AMD is made based on clinical fundus examination or assessment of color fundus photographs usually in conjunction with imaging for pigmentary changes and changes in the structure of the retina. Several classification systems for AMD are available. The Beckman classification suggests small drusen with a size of $\leq$63 μm are considered as a sign of normal aging and are associated with a low risk of progressing to AMD, with around 1% of population having small drusen that may progress to late AMD in 10 years (Ferris et al., 2013). Medium drusen between >63 and $\leq$125 μm are considered as an early sign of AMD and suggest an increased risk of progressing to large drusen and late AMD (Ferris et al., 2013). Other phenotypes that are associated with early to intermediate AMD include RPE pigmentary changes and the formation of RPD deposits in the subretinal space. There are no treatments for early or intermediate AMD to markedly slow or completely arrest development to late stages of the disease.

Geographic atrophy

Patients with early or intermediate AMD may develop either of the two advanced forms of the disease: GA or nAMD. In GA

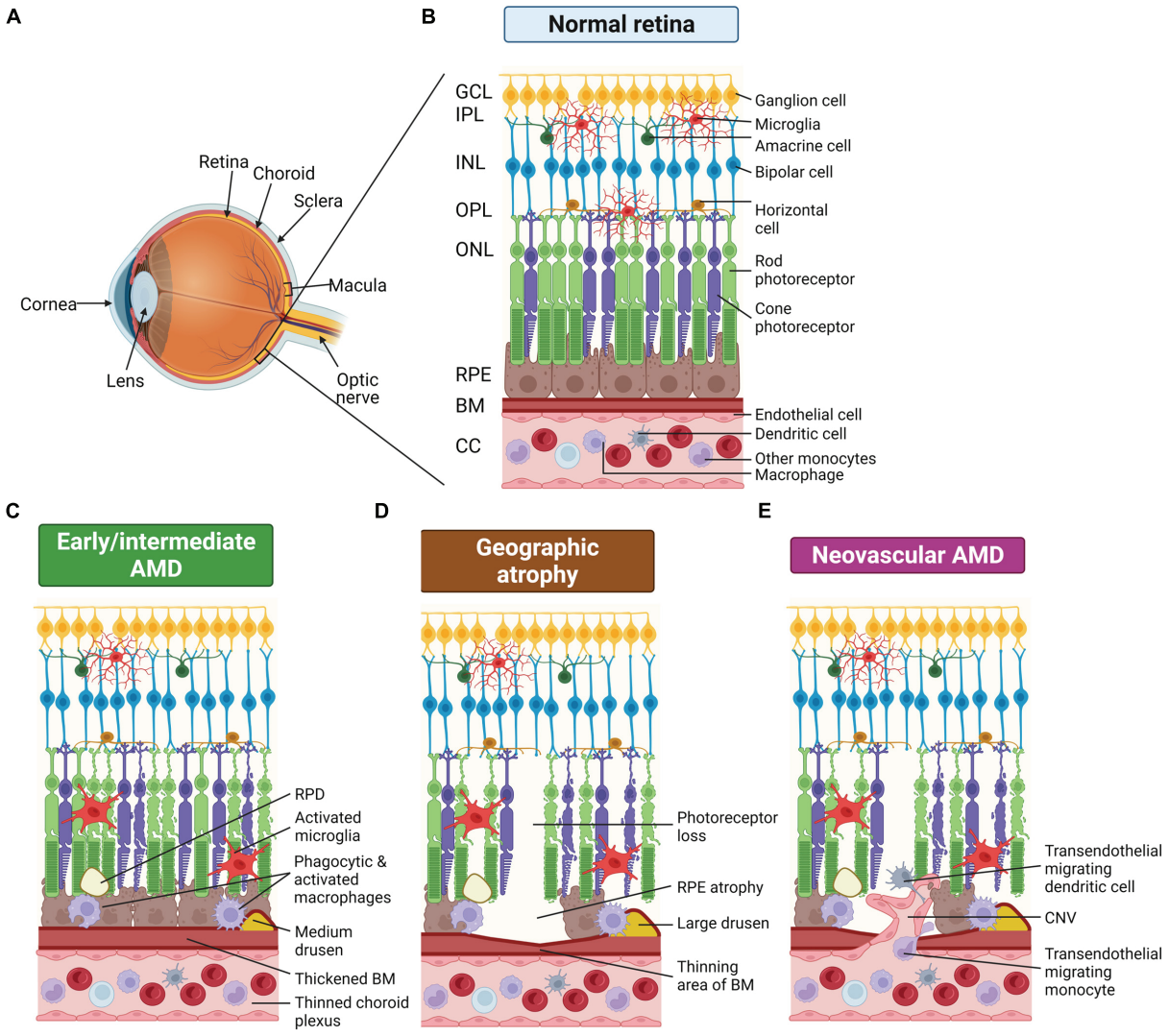

FIGURE 1
Schematic of changes that occur in the eye of age-related macular degeneration (AMD) patients. **(A)** Schematic render of the eye showing posterior ocular tissues affected in AMD, expanded in subsequent panels. **(B)** Healthy posterior eye, showing transverse section of the retinal layers, the retinal pigment epithelium (RPE), Bruch's membrane (BM), and vascular supply (the choriocapillaris, CC). The location of the mononuclear phagocytes (MPs) is indicated including retinal tissue resident microglia associated with the neuronal synaptic layers (nerve fiber layer MPs not shown) and MPs in the choroid, including dendritic cells, macrophages and other monocytes. **(C)** Schematic of early/intermediate AMD showing thickening of BM, deposition of extracellular waste around the RPE (drusen and reticular pseudodrusen, RPD), thinned choroid, and changes in MPs, including activation of microglia within the retina. **(D)** Schematic of late-stage AMD, geographic atrophy, showing loss of photoreceptors and RPE cells, thinning of BM in regions of cell loss, and deposition of large drusen. Microglia within the retina are activated and activated macrophages on the choroidal side are associated with the damaged basal RPE/BM. **(E)** Schematic of late-stage neovascular AMD showing choroidal neovascularization (CNV), loss of photoreceptors and RPE cells, thinning of BM in regions of cell loss and deposition of large drusen. Microglia within the retina are activated and peripheral circulating monocytes and dendritic cells are activated and associated with damaged RPE and are also able to enter the retina via new leaky vessels. This illustration was started from a BioRender Template and content and stylistic modifications were made.

there is a sharply demarcated area of RPE hypo-pigmentation with a diameter of at least 175 μm and visible choroidal vessels on fundus examination (Bird et al., 1995). GA usually originates in a region around the perimeter of the fovea and expands across other parts of the parafovea (Sarks et al., 1988; Sunness, 1999; Wolf-Schnurrbusch et al., 2008). The hypo-pigmentary abnormalities of the RPE correlate with RPE atrophy and photoreceptor deterioration, involving the disorganization and loss of photoreceptor inner and outer segments and eventually photoreceptor death (Young, 1987; Sarks et al., 1988; Kim et al., 2002). Additionally, age-dependent accumulations of autofluorescent lipofuscin, which are hyperfluorescent waste deposits within the RPE, is another characteristic of AMD (Hogan, 1972; Sarks, 1976; Young, 1987). Diagnosis of GA

can be aided by examination of fundus autofluorescence (FAF). Regions of hyper-autofluorescence correlate with increased deposition of autofluorescent lipofuscin, subretinal autofluorescent material including RPD, and changes in the photoreceptor photopigment. Large regions of hypo-autofluorescence correlate with decreased lipofuscin due to loss of RPE cells, generally indicating regions of late-stage AMD. There are no approved therapies for atrophic AMD.

Neovascular age-related macular degeneration

The hallmark of nAMD is the pathological proliferation of new blood vessels into the macula, with subsequent macular edema, subretinal hemorrhage and end-stage fibrous scarring. Based on the origin of the abnormal vessel growth, nAMD can be classified into three subtypes: types I and II choroidal neovascularization (CNV), and type III which occurs in the retina, retinal angiomatous proliferation (RAP) (Sarks et al., 1997; Yannuzzi et al., 2008). CNV is the aberrant extension of vessels from the choroid passing into either the sub-RPE space (occult CNV; type I), or further anteriorly into the subretinal space following loss of the RPE (classic CNV; type II) (Sarks et al., 1997). RAP refers to the growth of blood vessels originating from the inner retinal circulation, which continues into the subretinal space, and merges with the choroidal circulation to form an anastomosis between the retinal and the choroidal vessels (Yannuzzi et al., 2001, 2008). Regardless of the nAMD subtypes, the new blood vessels can be leaky, causing serous fluid and blood to accumulate in the subretinal space and the neural retina, often leading to rapid and severe vision impairment and potential detachment of the retina. Furthermore, fibrotic changes occur in late stages of nAMD and this is denoted by a well-circumscribed fibrotic white or yellow scar on fundus examination (Stevens et al., 1997; Rogers et al., 2002; Bloch et al., 2013). Fibrosis may cause dysfunction and degeneration of the photoreceptors, through hindering vascular supply and provoking RPE degeneration (Bloch et al., 2013).

Therapeutic approaches currently approved by the United States Food and Drug Administration and the Australian Therapeutic Goods Administration for arresting nAMD are intravitreal injections of drugs that block VEGF, a growth factor which induces proliferation of vascular endothelial cells and angiogenesis (Solomon et al., 2019). Whilst this treatment enables short-term visual improvement in the majority of treated patients, one-third of nAMD patients, especially those with classic CNV, do not show any arrest of vision loss or improvement in visual acuity after receiving anti-VEGF therapy (Bloch et al., 2013; Rofagha et al., 2013). Moreover, patients with RAP frequently develop GA following anti-VEGF treatment (McBain et al., 2011). These poor visual outcomes are associated with subfoveal fibrosis development, which remains untreatable (Rofagha et al., 2013).

The role of the retinal pigment epithelium in retinal homeostasis and retinal pigment epithelium changes in aging and age-related macular degeneration

Retinal pigment epithelium cellular morphology

Dysfunction and degeneration of the RPE is one of the key features of AMD. In the following sections the function of the RPE in maintaining retinal homeostasis and how it changes in normal aging vs. in AMD will be considered (**Figure 2**). The RPE is a continuous monolayer of terminally differentiated epithelial cells that lies between the neural retina and choroidal blood supply (Boulton and Dayhaw-Barker, 2001; Strauss, 2005 for general reviews of RPE structure and function). The RPE apical surface has long and thin microvilli that interface with the photoreceptor outer segments. The basal surface of the RPE has numerous infoldings and the basolateral membrane forms a part of Bruch's membrane, comprising the inner wall of the choroid. The RPE nucleus is located basally and a number of unique organelles are present inside the cells to support function (Boulton and Dayhaw-Barker, 2001; Strauss, 2005). These organelles include mitochondria, phagosomes and lysosomes which are associated with renewal of the photoreceptor outer segments and are found at the basal side of the cell. Additionally, the RPE contains melanosomes, which are located either at the base of or within the apical process of the RPE depending on diurnal phase, and these are important in absorbing stray light to improve visual acuity (Boulton and Dayhaw-Barker, 2001; Strauss, 2005). The size and phenotype of the RPE cells vary with retinal eccentricity in human eyes. The cells at the macula are smaller, with a diameter varying from 7 to 11 μm. They become larger and irregular away from the macula, reaching 60 μm or more in the peripheral retina (Salzmann and Brown, 1912; Ach et al., 2014).

When eyes age normally, there is a decrease in the density of RPE cells representing cell loss (Gao and Hollyfield, 1992; Bhatia et al., 2016). In addition, some RPE cells become multinucleated with age particularly in the periphery, representing either cell fusion or failed attempts at cell division (Ts'o and Friedman, 1967). Changes in the RPE cytoskeleton are also associated with aging. RPE cells lose their hexagonal shape and become larger, elongated and more irregular with aging (Tarau et al., 2019). This is particularly evident in the macula and far peripheral retina (Rashid et al., 2016), while in the far periphery, RPE cells become thinner and more irregular with

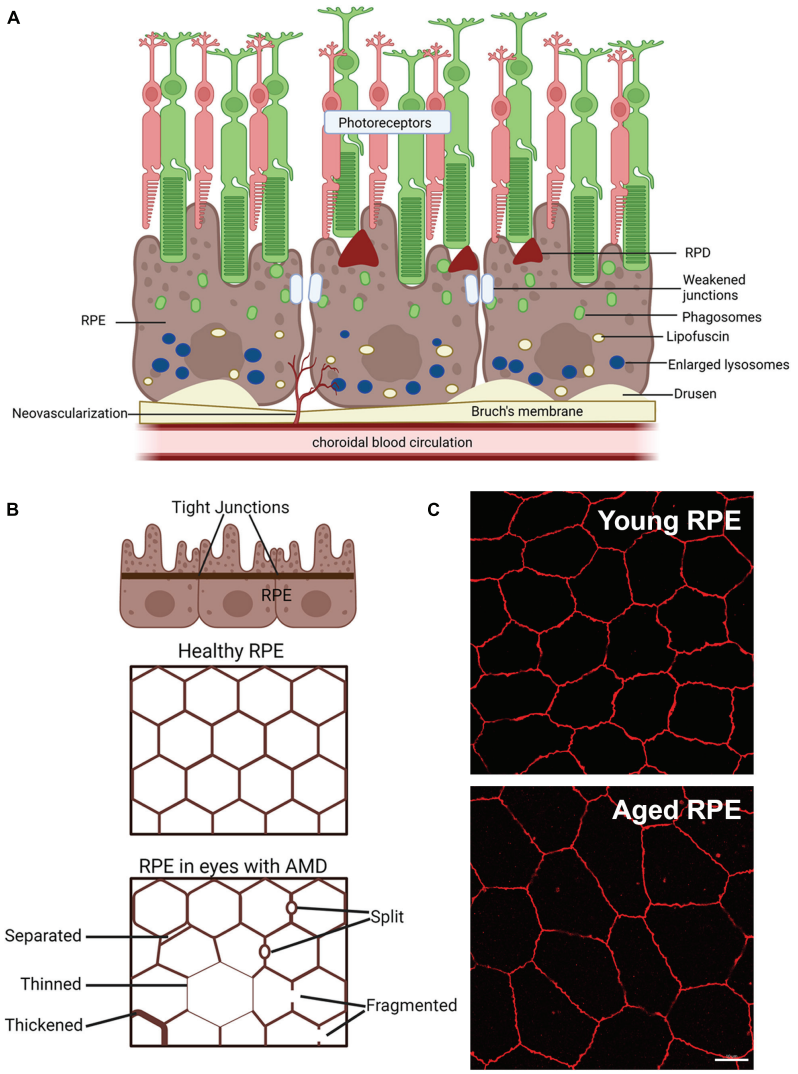

FIGURE 2
Schematic of changes that occur in the retinal pigment epithelium (RPE) of age-related macular degeneration (AMD) patients. **(A)** Schematic of changes within the RPE in late-stage AMD, including weakening of tight junctions that form the blood retinal barrier, deposition of lipofuscin and enlarged failed lysosomes. Deposition of extracellular waste around the RPE, large drusen on the basal side of the RPE are apparent and reticular pseudodrusen (RPD) on the apical side may also manifest. **(B)** Schematic showing changes in the tight junctions of the RPE in AMD in flat mount view. Healthy RPE are hexagonal in shape and tight junctions form a continuous connection around each RPE cell. In AMD, RPE cells may be larger due to cell loss and tight junctions may be separated, thinned, thickened, split or fragmented, modified from Ach et al. (2015). **(C)** Example of the effects of aging on the mouse RPE. Tight junction ZO-1 labeling of young (3 month) and old (22 month) mouse RPE, shows increased RPE cell size in the aged tissue, suggesting cell loss with age. Some of this illustration was started from a BioRender Template and content and stylistic modifications were made.

age (Bhatia et al., 2016; Rashid et al., 2016). Despite the change in geometry and decreased cell density, the intact monolayer is maintained during normal aging.

In eyes with AMD, in addition to regions of RPE cell loss, additional RPE structural changes occur that are different from those seen in normal aging. Prior to cell loss, the RPE cells in the context of AMD lesions show morphological changes, becoming concave and round (Ach et al., 2015). Uneven thinning, thickening, separation, and splitting are observed along with fragmentation of the cytoskeletal component, F-actin (Tarau et al., 2019). The separation and fragmentation of F-actin suggests RPE-regulated outer blood-retinal barrier (discussed later) may be weakened in AMD.

Bruch's membrane

As mentioned above, the RPE contributes to Bruch's membrane, a layered semi-permeable extracellular matrix tissue delineated by and including the choriocapillaris and RPE

basement membranes (Hogan and Alvarado, 1967; Sarks, 1976; Kliffen et al., 1997; Curcio and Millican, 1999). Bruch's membrane consists of five layers: the basement membrane of the RPE, the inner collagenous zone, a central band of elastic fibers, the outer collagenous zone and finally the basement membrane of the choriocapillaris (Nakaizumi et al., 1964). Nutrients and oxygen from the choroid and waste from the RPE must be transported across Bruch's membrane to maintain retinal homeostasis. It also acts as a support for RPE physical adhesion and restricts RPE and choroidal vessel migration (Bhutto and Lutty, 2012).

During normal aging, Bruch's membrane thickens. In the early stages of AMD, Bruch's membrane thickness increases above that seen in normal aging. Further analysis of Bruch's membrane using electron microscopy shows that abnormal deposits appear above and below the RPE basement membrane, called basal laminar and basal linear deposits respectively, in early/intermediate AMD (Hogan and Alvarado, 1967; Sarks, 1976; Kliffen et al., 1997; Curcio and Millican, 1999). The appearance of basal linear deposits correlates with large drusen observed in early/intermediate AMD and may constitute an early form of drusen (Curcio and Millican, 1999). This thickening process has been suggested to reduce nutrient and waste exchange between the RPE and the choroid, contributing to RPE and photoreceptor dysfunction in AMD. As AMD progresses to the late stages of the disease, Bruch's membrane thins in areas where the choroid, RPE and photoreceptors are lost (McLeod et al., 2009).

The blood retinal barrier

One of the primary functions of the RPE is providing nutrients and oxygen from the choroidal blood supply to the neural retina and in exchange, removing and recycling waste products from the retina, some of which are returned to the choroid (O'Leary and Campbell, 2021). To ensure controlled movement of molecules between the retina and fenestrated choroid, the RPE layer forms the blood retinal barrier in the outer retina, while endothelial cells, glia and pericytes contribute to the blood retinal barrier in the inner retina (O'Leary and Campbell, 2021). Tight junctions between neighboring RPE cells provide this dynamic barrier that controls the movement of crucial nutrients and waste between the neural retina and the choroid (Marmorstein, 2001; Rizzolo, 2014). The tight junctions predominantly include claudin family proteins, MARVEL family transmembrane proteins and junctional adhesion molecules (O'Leary and Campbell, 2021). These tight junctions prevent the infiltration of large molecules, pathogens and active immune cells from the peripheral blood circulation into the neural retina. The presence of Bruch's membrane and an intact outer blood retinal barrier together with the anti-inflammatory and immunosuppressive factors released by the RPE cells, maintain the immune privilege of the outer retina (Sugita, 2009).

During healthy aging, tight junctions between the RPE remain intact, maintaining a continuous barrier between the choroid and the neural retina, however, the choroidal plexus does thin with age (Wakatsuki et al., 2015). In intermediate AMD, toxic plasma components, that should be excluded from the retina and are absent in healthy aged tissue become apparent, suggesting the blood retinal barrier is compromised prior to late-stage disease (Schultz et al., 2019). Specifically, plasma proteins: albumin, fibrinogen, immunoglobulin G (IgG), and complement component 9 (C9) are present in the retina of intermediate AMD patients (Schultz et al., 2019). In GA, the choroid plexus becomes thinner than observed in normal aging (Adhi et al., 2014) and even when there is no overt sign of exudative change, the blood retinal barrier is compromised with plasma proteins apparent in the retina (Schultz et al., 2019). A compromised blood retinal barrier is also observed in nAMD, evidenced by the pathological proliferation of leaky, new blood vessels. A recent study suggests altered granzyme B expression, which is produced by the RPE and choroidal mast cells, contributes to the breakdown of RPE tight junctions and the extracellular matrix in nAMD (Matsubara et al., 2020). Indeed, deterioration of RPE tight junctions and the blood retinal barrier is required for neovascular changes, as animal studies indicate upregulation of expression of angiogenic factors such as VEGF or angiopoietin 2 are not enough to induce new vessel growth and that loss of tight junctions is required (Oshima et al., 2004). Together these results suggest that deterioration of the RPE and the blood retinal barrier is an important pathological occurrence in intermediate and late-stage AMD, which is required for the formation of new blood vessels in nAMD.

Retinal pigment epithelium immune regulation

The RPE contributes to immune regulation of the retina in several ways: generation of the outer blood retinal barrier, production of an immunosuppressive and anti-inflammatory microenvironment, and ability to sense and respond to pathogens. The RPE expresses a range of factors and receptors that play a role in protecting the retina from pathogens that may be present in the circulatory system. The RPE expresses pattern recognition receptors such as toll-like receptors (TLR), which sense molecular patterns associated with microbe pathogens (e.g., bacteria, viruses, and fungi) that may be present in the circulatory system (Kumar et al., 2004). To date 10 mammalian TLRs have been identified with 9 identified in human RPE cells (TLR 1-7 and 9 and 10) (Kumar et al., 2004). In addition to the TLRs, the RPE also expresses other pattern recognition receptors (e.g., Nucleotide-binding oligomerization domain,

Leucine rich Repeat and Pyrin domain containing proteins; NLRP), complement components, and a range of cytokines, chemokines and growth factors which limit pathological insult (Detrick and Hooks, 2020). In response to pathogens and the presence of systemic immune cells, the RPE expresses antigen presenting receptors (e.g., major histocompatibility complex class I and II molecules; MHC 1 and II) (Liversidge et al., 1988; Osusky et al., 1997; Detrick and Hooks, 2020). However, the healthy RPE favors an immunosuppressive state. For example, RPE cells induce Fas ligand expression when in contact with either activated T-cells or MPs such as monocytes that induces apoptosis of these inflammatory cells (Jorgensen et al., 1998; Hettich et al., 2014). It is likely that the RPE produces a unique balance between an anti-inflammatory and pro-inflammatory environment to maintain optimal retinal function.

With age, changes in the immune response of the RPE occur, however, few studies have been completed on human samples. In RPE culture, aged cells show significantly increased production of cytokines, interferon (IFN)-γ, tumor necrosis factor (TNF)-α, interleukin (IL)-1α, IL-1β, IL-6, IL-8, IL-10 (Sreekumar et al., 2022) suggesting with age there is a shift toward to a more inflammatory environment. In AMD, there have been reported changes in RPE production of cytokines and chemokines that would likely alter the immunosuppressive environment of the outer retina. In AMD, transcriptome analysis of RNA sequencing (RNA-seq) data from human RPE of healthy control and AMD samples indicates changes in expression in a range of immune factors occur in late-stage disease (Saddala et al., 2019). Upregulation in TLR receptors, and their receptor cascades, complement receptors and a range of cytokines and chemokines and their receptors were identified in RPE from AMD patients (Saddala et al., 2019). Chemokines and their receptors have key roles in the movement of immune cells and altered expression of these factors are implicated in a wide range of inflammatory diseases including AMD. Chemokine ligands such as C-C motif chemokine ligand (CCL) 2 (CCL2), CCL3, CCL4, CCL13, CCL19, CCL21, chemokine C-X-C motif ligand (CXCL) 9 (CXCL9), CXCL10, CXCL16 and receptors C-C motif chemokine receptor (CCR) 1 (CCR1), CCR5, and CXCR6 were all identified as changing in the RPE of AMD patients (Saddala et al., 2019). Additionally, the alternative and classical complement pathways complement component 3 (C3), complement factor B (CFB), complement factor H (CFH), complement factor I (CFI), complement C1q A chain (C1QA) have been identified by RNAscope to change in GA (Demirs et al., 2021). The upregulation of complement factors and chemokines and associated receptors in the RPE suggests the RPE is generating a pro-inflammatory environment in late-stage AMD. The change in RPE expression of these immunogenic components would contribute to the recruitment of MPs between the RPE and choroid and to the subretinal space in AMD and this interaction will be considered in more detail below under the sections on MPs.

Phagocytosis

Retinal pigment epithelium cells are one of the most phagocytic post-mitotic cells found in the body (Young, 1967, 1987). One RPE cell is in contact with 30–50 photoreceptors, that shed around 10% of their photoreceptor outer segment mass daily (Zinn and Benjamin-Henkind, 1979). The RPE carries out diurnal phagocytosis of these shed photoreceptor outer segments, and this process is required for maintaining optimal photoreceptor function (Strauss, 2005). Phagocytosis of the photoreceptor outer segment involves RPE binding, engulfment and phagocytosis, allowing recycling of vitamin A and fatty acids through the visual cycle and lipid cycling, respectively (Baehr et al., 2003). Following engulfment, the phagosomes bind with lysosomes, which contain enzymes allowing effective degradation of the photoreceptor outer segments.

The phagocytic ability of the RPE declines moderately with age, but it is greatly decreased in eyes with AMD when compared to age-matched normal RPE from human donors (Inana et al., 2018). Following binding and engulfment, RPE phagosomes of photoreceptor outer segments fuse with lysosomes to effectively recycle vitamin A derivatives and lipids. Failure in this process lead to lysosomal accumulations with age, which are greatly increased in AMD (Inana et al., 2018). These enlarged lysosomes contain undigested waste that accumulate as residual bodies, which are autofluroescent waste in the RPE, known as lipofuscin (discussed in more detail below in intracellular waste accumulations).

In animal models of AMD also, the RPE shows a similar decrease in phagocytic ability. This has been attributed in part to increased iron levels, as mRNA and protein expressions of several iron-regulatory molecules are significantly increased with age leading to iron accumulation. Excess iron is toxic to the RPE cells and impairs phagocytosis and lysosomal function (Chen et al., 2009). However, other processes, including changes in autophagy, have been implicated in slowing the phagocytosis process (Yu et al., 2018). The phagocytosis process and autophagy pathways share similar intracellular protein pathways and slowing of autophagy in the RPE with age may contribute to the slowing of processing of outer segment renewal by phagocytosis (Mitter et al., 2014; Yu et al., 2018).

Autophagy

In addition to phagocytosis, the RPE carries out autophagy, a process by which cell components such as old mitochondria and waste products such as lipids and proteins are renewed by intracellular recycling (Kunchithapautham and Rohrer, 2007). Like the recycling of photoreceptor outer segments, this process also involves compartmentalizing intracellular waste within an autophagosome and binding with a lysosome to complete the

degradation process. In general, autophagy becomes insufficient with age, either because autophagic flux is reduced or because there are too many cellular components that need to be removed from chronic cellular damage (Kroemer, 2015). Examination of control human donor specimens shows there is an age-related increase in autophagosome numbers and expression of autophagy proteins in the RPE (Mitter et al., 2014). RPE cells upregulate autophagy to enhance the renewal of different cellular components in response to a variety of insults with age. Yet, when the insult is prolonged and there are too many cellular components that need to be removed, autophagy becomes impaired. In line with this, autophagy proteins and autophagy flux are significantly reduced in RPE from human donors with AMD (Mitter et al., 2014; Golestaneh et al., 2017). Additionally, there is an accumulation of cytoplasmic debris, lipid and undigested protein aggregates tagged for autophagic degradation, confirming dysregulated autophagy in the RPE of eyes with AMD (Golestaneh et al., 2017).

Mice with impaired autophagy demonstrate age-dependent degeneration of the RPE with RPE pigmentation defects and RPE atrophy, hallmarks of late-stage AMD, observed. Furthermore, mice in which the autophagy pathway genes *ATG5* and 7 have been conditionally deleted from the RPE, show defects consistent with early AMD (Zhang et al., 2017), while other rodent models of AMD [apolipoprotein E4 (ApoE4) mice fed a high fat diet and apolipoprotein E (ApoE) null animals] show impaired autophagy in aged animals and RPE change consistent with early AMD (Mitter et al., 2014; Vessey et al., 2022). Failure in the autophagy pathways would lead to intracellular waste accumulation, which would contribute to RPE cell damage in AMD.

Impaired autophagy in the RPE has also been reported to promote inflammation. In RPE culture, mouse RPE cells with dysfunctional autophagy significantly increase secretion of inflammatory caspase-1, a marker for NLRP3 inflammasome activation, and cytokine IL-1β following co-culture with bone marrow derived macrophages (Liu et al., 2016). This indicates inflammasome activation in MPs follows defective autophagy in the RPE. Accumulation of macrophages with caspase-1 activation in the subretinal space was also detected after RPE and photoreceptor death in mice with impaired autophagy in the RPE (Liu et al., 2016). These data suggest that autophagy dysfunction in RPE cells can potentially trigger a series of inflammatory responses, including the influx of MPs and the activation of the inflammasome cascade, which may contribute to cell death in AMD.

Lipid cycling

The photoreceptors require high levels of lipids, fatty acids and unesterified cholesterol and these are actively transported between the photoreceptors, RPE and choroidal blood supply (Tserentsoodol et al., 2006). For example, the RPE recycles phospholipid-esterified docosahexaenoic acid (DHA), which is otherwise primarily acquired from the diet, from shed rod outer segment disks to renew the function of the photoreceptors (Fu et al., 2021). In addition, fatty acids are used by photoreceptors to supplement their energy needs (Heckenlively et al., 2003; Joyal et al., 2016). Very low-density lipoprotein receptor (VLDLR) expressed by the RPE and photoreceptors, is critical for transport of lipids into the cell by anchoring ApoE triglyceride-rich lipoproteins. The fatty acid, palmitate, has been shown to be an energy source for photoreceptor mitochondria, likely as it yields three times the number of adenosine triphosphate (ATP) molecules than a single glucose molecule (Fu et al., 2021). To maintain the health of the retina, these lipids need to be recycled or transported from the RPE to the photoreceptors.

In AMD, abnormal lipid cycling has been suggested as a driver of AMD progression due to changes in lipid levels either through lifestyle factors or genetic mutations. In AMD eyes, accumulations of lipid droplets and lipid-derived components occur within the RPE cell (Curcio et al., 2009). Also, lipid pools develop as basal linear deposits, between the RPE basement membrane and the inner collagenous layer of Bruch's membrane, occasionally form a "lipid wall" (Curcio et al., 2009). The presence of a "lipid wall" basal linear deposit would significantly reduce nutrient and oxygen transfer from the choroid to the RPE, impairing RPE function. The location and content of these basal linear deposits is suggested to represent soft drusen and highlights the importance of lipid cycling in the RPE in AMD.

Systemic changes in circulating lipids, genetic alterations in lipid processing and body mass have been found to have variable associations with risk of AMD development. A higher body mass index is an established risk factor for AMD development (Seddon et al., 2011). Interestingly evidences for systemic lipid changes as being associated with an increased risk of AMD are still not clear (Semba et al., 2019). A study of 177 serum lipids found no association to AMD status (Semba et al., 2019). It may even be those classic markers of "healthy" lipid levels in the serum, such as high density lipoprotein (HDL), low density lipoprotein (LDL) and low triglycerides may even incur increased risk of developing AMD (Grassmann et al., 2017). However, genetic association of increased risk of AMD with lipid transporters such as ApoE (Klaver et al., 1998) and changes in lipid processing within the RPE itself, may contribute to disease progression. Additionally, systemic changes in the carnitine shuttle, which is essential for mitochondrial β-oxidation of fatty acids, indicate that progressive dysfunction of mitochondrial fatty acid metabolism could be a key contributing factor to AMD progression (Mitchell et al., 2021).

Intracellular waste accumulation: Lipofuscin and melanolipofuscin

Intracellular deposition of autofluorescent waste called lipofuscin occurs normally with age (Bianchi et al., 2013). It is believed to accumulate due to incomplete degradation of photoreceptor outer segments and slowing of autophagy resulting in accumulation of waste proteins and lipids contained within lysosomes and also failed lysosomes (residual bodies). Melanolipofuscin is lipofuscin that is associated with melanosomes present within the RPE and like lipofuscin, accumulates normally with age contributing to autofluorescence on FAF imaging (Ach et al., 2015). Excess accumulation of lipofuscin and melanolipofuscin occurs with age and in AMD and has been suggested to interfere with RPE function (Haralampus-Grynaviski et al., 2003; Rozanowska et al., 2004; Bianchi et al., 2013). In eyes with AMD, lipofuscin and melanolipofuscin redistribute within the RPE, sometimes forming large deposits or granulations within the cell, leaving other regions free from these accumulations (Ach et al., 2015). These deposits can result in cellular dysfunction as visible-light irradiation of lipofuscin causes lipid peroxidation, and production of hydrogen peroxide that can damage mitochondrial DNA in RPE cells (Rozanowska et al., 1995; Liang and Godley, 2003). Moreover, chronic oxidative stress induced by the photoreactive lipofuscin can contribute to age-dependent impairment of RPE phagocytosis (Olchawa et al., 2017). Intracellular accumulations of lipofuscin and melanolipofuscin in AMD would contribute to oxidative stress in the RPE, promoting RPE dysfunction (Haralampus-Grynaviski et al., 2003; Rozanowska et al., 2004).

Extracellular waste accumulations: Drusen and reticular pseudodrusen

One of the important pathological manifestations of AMD is the presence of waste deposits in and around the RPE. Extracellular deposits in AMD include drusen, which accumulate between the RPE and the choroidal blood supply, and RPD, which are subretinal deposits that are observed in some cases of AMD. Histologically drusen are associated with RPE cellular changes and loss of RPE integrity (Schlanitz et al., 2019). Analysis of drusen composition has identified a variety of molecules, including RPE cellular components, immune- and/or inflammation-associated proteins, lipids and carbohydrates (Hageman et al., 2001). RPE derived components of drusen include: RPE fragments, lipofuscin and melanin, complement activator and amyloid beta (Aβ) (Sarks et al., 1999; Hageman et al., 2001; Johnson et al., 2002). Lipoprotein containing lipid transporter, ApoE is also proposed to be secreted by the RPE, and to be retained by the less permeable Bruch's membrane, and may contribute to the formation of medium drusen (Mullins et al., 2000; Pikuleva and Curcio, 2014).

Immunogenic components are also apparent in drusen and may contribute to the recruitment of choroidal derived immune cells such as MPs. The presence of complement factors and several immune system proteins has been reported in drusen (Johnson et al., 2000; Mullins et al., 2000; Anderson et al., 2002). CFH and other complement components such as complement component 5 (C5) and C9 which are important for triggering innate immune cell activation and inhibition of self-damage have been identified in drusen (Mullins et al., 2000; Russell et al., 2000; Fett et al., 2012; Crabb, 2014). These findings correlate with genetic association studies, in which polymorphisms in the genes for complement components have been identified as a risk factor for AMD (e.g., CFH) (Edwards et al., 2005; Hageman et al., 2005), and hint that changes in MP interaction with complement-tagged cellular waste may be a driver of disease development. Additionally, vitronectin, a major drusen constituent, is a plasma and RPE derived extracellular matrix glycoprotein and may play a role in inhibiting complement-induced MP cell damage (Preissner, 1991; Hageman et al., 1999; Crabb et al., 2002). Cell membrane-associated protein complex human leukocyte antigen DR (HLA-DR) is also present in drusen and is thought to be derived from MPs, specifically dendritic cells from the choroid (Russell et al., 2000; Hageman et al., 2001). The presence of these immune factors likely contributes to the recruitment of choroidal derived MPs and accumulation of immune cells associated with drusen lesions in AMD (Combadière et al., 2007; Sennlaub et al., 2013; Levy et al., 2015; Silverman and Wong, 2018).

Unlike drusen, to date very little research has been completed on the make-up of RPD. Histologically, the subretinal presence of RPD is associated with RPE and photoreceptor disruption (Greferath et al., 2016). Clinical data from intermediate AMD patients indicate that RPD are associated with decreased photoreceptor function (Flamendorf et al., 2015), choroidal changes (Keenan et al., 2020), and over time with increased retinal thinning and degeneration (Chiang et al., 2020). The histological studies that have been undertaken show RPD to contain similar components to drusen such as photoreceptor outer segment debris including opsins; lipid in the form of unesterified cholesterol; RPE fragments (melanolipofuscin granules); ApoE, a protein important for lipid trafficking; vitronectin; and the immunogenic protein, CFH (Rudolf et al., 2008; Greferath et al., 2016; Wu et al., 2022). Interestingly, β-amyloid as well as a range of complement factors and immune markers, including C3, C5a, cluster of differentiation (CD) molecules CD11β and CD102, were not detected histologically and may not be present in RPD, highlighting a distinction between this type of deposit and classical drusen (Greferath et al., 2016). Further work is needed in this area to confirm the components of RPD and how they arise. However, despite the lack of certain immune related

deposits, MPs particularly microglia/macrophages have found to be associated with RPD suggesting that the innate immune system is associated with the presence of these abnormal subretinal deposits (Greferath et al., 2016).

What is controversial about the origin of these extracellular deposits, drusen and RPD, is whether deposition is a causative event or consequence of RPE degeneration and MP recruitment. Early studies using electron microscopy suggest that primary degeneration of the RPE is partly accountable for the formation of drusen (Farkas et al., 1971; Green and Key, 1977). However, others have suggested that drusen hinder the diffusion of oxygen and nutrients from the choroid to the retina, driving RPE degeneration (Hageman et al., 2001; Anderson et al., 2002; Rattner and Nathans, 2006). The immunogenic composition of drusen and to some extent RPD, suggest they are extracellular waste that are tagged for removal by local MPs, but this process comes with a cost. The debris likely induces ongoing local inflammation and immune activation by gathering chemokines and cytokines with the potential for "collateral damage" to nearby healthy cells. It is likely that a combination of both RPE dysfunction teamed with MP failure to clear extracellular deposits with age that leads to continued accumulation of waste in the form of drusen and RPD, driving the cycle of disease progression. In the next sections, we will consider the role of MPs in healthy eyes and in AMD.

Mononculear phagocytes and the ocular innate immune system

Origins of ocular mononuclear phagocytes

Mononuclear phagocytes are a dominant cell population of the innate immune system and have been widely reported to participate in the homeostatic regulation and the pathogenesis of disease within the mammalian retina. They comprise four cell types from the myeloid lineage of blood cells: blood monocytes, dendritic cells, tissue macrophages and retinal microglia, all of which have been implicated in the pathogenesis of AMD (Ransohoff and Cardona, 2010). Blood monocytes are a population of circulating mononuclear leukocytes (white blood cells) originated from hematopoietic stem cells in the bone marrow (Geissmann et al., 2003; Ransohoff and Cardona, 2010). In the postnatal period, the stem cell-derived myeloid progenitors produced in the bone marrow give rise to common monocyte-dendritic cell progenitors. These progenitors are released into the peripheral blood circulation to form a reservoir of myeloid cell precursors, and are transported to tissues for cytokine-driven cellular differentiation (Geissmann et al., 2003; Ransohoff and Cardona, 2010). Dendritic cells share the same lineage as blood monocytes, also being derived from monocyte-dendritic cell progenitors, yet their differentiation from monocytes remains debatable (Geissmann et al., 2003; Ransohoff and Cardona, 2010). Macrophages can be derived from blood monocytes, or from undefined MP progenitors in the circulation. Microglia, despite being identified as a type of mononuclear leukocytes, and sharing many similar phenotypical and functional features as monocytes and macrophages, are derived from hematopoietic progenitors in the embryonic yolk sac during development (Mildner et al., 2007; Ginhoux et al., 2010). Reminiscent of brain microglia, retinal microglia originate from microglial precursors or circulating monocytes, which invade the retinal tissue via the vitreal surface or ciliary margin within the embryonic and early postnatal life before the blood retinal barrier is finalized (Barron, 1995; Marin-Teva et al., 1998; Santos et al., 2008; Ranawat and Masai, 2021).

Change in peripheral blood monocytes in aging and age-related macular degeneration

Peripheral blood monocytes change with age, leading to an increased vulnerability to infection and the development of inflammatory diseases such as atherosclerosis and cancer and these changes may contribute to the development of AMD (**Figure 3**). Peripheral MP trafficking from bone marrow to blood, and responses to bacterial infection and phagocytosis are all reduced with age (Blacher et al., 2022). In intermediate and late-stage AMD, there is an increase in the number of peripheral blood monocytes suggesting these cells play a role in disease progression (Xue et al., 2021). In AMD, peripheral MP phagocytosis is significantly reduced irrespective of disease stage. Intermediate and late-stage AMD patients and those patients with RPD, all display reduced MP phagocytosis compared to healthy age-matched controls (Gu et al., 2021). Further investigation of expression of surface markers that are important in regulating leukocyte adhesion, migration, and phagocytosis (integrins CD11b and CD11c) show reduced expression in peripheral monocytes of late-stage AMD patients, both GA and nAMD (Gu et al., 2021). Importantly, these integrins form complexes with CD18 to form complement receptor 3 (CR3, CD11b/CD18) and complement receptor 4 (CR4, CD11c/CD18), respectively (Lukacsi et al., 2017). These receptors are both recognized to play an important role in phagocytosis and are reduced in peripheral MPs of late AMD. Further evidence supporting a reduction in peripheral MPs comes from work showing CD34, a marker of hemopoietic stem cells, is reduced in those with late AMD, implying that the capacity for differentiation of hemopoietic stem cells into monocytes is also reduced in those with late AMD (Gu et al., 2021). Alternatively, studies investigating the surface expression of molecules known to be important in phagocytosis, P2X purinoceptor 7 (P2X7) and CD33, report increased expression

in monocytes of late-stage AMD patients (Gu et al., 2021). The role of P2X7 on MPs in AMD is further indicated by genetic studies which suggest inheritance of a loss of function P2X7 receptor variant combined with P2X purinoceptor 4 (P2X4) variant increases the risk of developing AMD, likely due to a reduction in the ability of peripheral blood monocytes and microglia to phagocytose debris (Gu et al., 2013). As MP phagocytosis of debris would be critical to removal of subretinal and drusen deposits, a reduction in this aspect of MP function would contribute to AMD development and progression.

As mentioned previously, chemokines and their receptors have key roles in the movement of immune cells and are implicated in a wide range of inflammatory diseases, including AMD. Evaluation of expression of four chemokine receptors (CCR1, CCR2, CCR5, and CXCR3) in CD14 + peripheral blood monocytes in patients with GA and nAMD showed that monocytes have increased expression of CCR5 in GA and that CXCR3 expression is increased in both GA and nAMD (Krogh Nielsen et al., 2020). CCR5 expression was low on monocytes of healthy controls as it is generally not expressed under homeostatic conditions (Krogh Nielsen et al., 2020), but an increase in expression on monocytes has been shown to occur during acute inflammation (Castanheira et al., 2019), suggesting a role for this chemokine receptor in ongoing inflammatory response in late-stage AMD. CXCR3 is involved in leukocyte migration and induces cytoskeletal and integrin changes that facilitate movement to areas of inflammation (Karin, 2020), suggesting that these cells may migrate differently in late-stage AMD. In line with this, in a smaller study (n = 9 AMD vs. n = 9 healthy controls) expression of other chemokine receptors involved in cell migration, CCR1 and CCR2 receptor expression on peripheral blood monocytes may be upregulated in late-stage nAMD (Anand et al., 2012), however this was not observed in a larger sample study (Krogh Nielsen et al., 2020). More work is required to carefully evaluate all the chemokine receptors expressed on peripheral blood MPs and determine if there are alterations in expression in AMD. Future work in this area may highlight important systemic changes in circulating MPs that contribute to AMD development and progression.

Changes in retinal microglia in aging and age-related macular degeneration

The tissue resident MPs of the retina, microglia, are found in the nerve fiber layer, inner plexiform layer and outer plexiform layer of the healthy eye, where they are closely associated with the vasculature, neuronal synapses and glia. During aging, abnormal accumulation of microglia in the subretinal space occurs in both humans and mice (Xu et al., 2008; Ma et al., 2013). Microglia that accumulate in the subretinal space display a less ramified morphology with round cell bodies, shorter dendrites and less branching, suggestive of an activated phenotype (Xu et al., 2008; Damani et al., 2011; Ma et al., 2013). The recruitment of microglia to the subretinal space is thought to occur secondarily to RPE and photoreceptor dysfunction, to aid removal of photoreceptor outer segment debris (Combadière et al., 2007; Chinnery et al., 2012). Additionally, the activity of intraretinal microglia is altered with age. Time-lapse live imaging of resident microglia in the outer plexiform layer shows microglia have decreased process mobility in aged mice (Damani et al., 2011). Since aged microglia are less mobile, this may prolong the presence of microglia in the subretinal space, potentially contributing to photoreceptor and RPE pathology.

In AMD, the sustained presence of microglia/MPs in the subretinal space and microglial accumulation of lipofuscin may potentiate RPE injury and photoreceptor degeneration (Combadière et al., 2007; Xu et al., 2008; Chinnery et al., 2012; Ma et al., 2013). Like aged tissue, in AMD, subretinal microglia are bloated and have fewer processes suggesting activation (**Figure 3**; Penfold et al., 1997; Combadière et al., 2007). Histopathological examinations of human donors with GA show abnormal microglia/MPs in the subretinal space and the photoreceptor layer, which are enlarged, morphologically activated and contain photoreceptor components (rhodopsin) in their cytoplasm (Gupta et al., 2003; Combadière et al., 2007). Activated microglia/MPs may promote further photoreceptor degeneration in GA, as the loss of cones adjacent to atrophic regions has been linked to their accumulation in the subretinal space (Buschini et al., 2011; Eandi et al., 2016) and these activated microglia produce pro-inflammatory cytokines and nitric oxide which may be toxic to neurons (Gupta et al., 2003; Srinivasan et al., 2004; Zhang et al., 2005).

Evidence from mouse models where the blood retinal barrier is intact, but components of the immune system are mutated, hint at an important and specific role for subretinal microglia in age-related RPE and photoreceptor dysfunction. Mice lacking Ccl2, which is important for RPE recruitment of MPs (Ambati et al., 2003; Vessey et al., 2015); P2X7-receptor, which is important for MP phagocytosis (Vessey et al., 2017); and Cx3cr1 – mouse study not human, which is expressed solely by MPs (Combadière et al., 2007), all show subretinal microglia associated with RPE damage and retinal dysfunction that is reminiscent of early AMD in aged animals relative to age-matched controls. This suggests that perturbations in the function, recruitment and retention of subretinal microglia has the potential to contribute to RPE and photoreceptor failure with age. However, due to a lack of specific markers, differentiating subretinal microglia from infiltrating MPs is difficult. Despite evidence indicating a role for inflammation in AMD, the differential contribution of retinal microglia vs. peripheral monocytes/macrophages in the progression to the advanced stages of AMD in humans is unclear. Thus, in future sections, which detail the inflammatory changes in MPs in the subretinal space and their interaction with the RPE, microglia will be referred to as MPs unless their origin is explicitly clear.

Maintenance of homeostasis via immune regulation

The healthy RPE secretes immunosuppressive factors that inhibit activation of MPs and even promotes macrophage death (Taylor et al., 2015). Peripheral blood MPs and resident choroidal MPs such as macrophages are present in the choroidal vasculature interface with Bruch's membrane (Cherepanoff et al., 2010). However, the integrity of the blood retinal barrier blocks the entrance of peripheral blood MPs into the healthy retina. Within the retina, resident MPs, the microglia are found primarily in the synaptic layers of the retinal neurons and are not present in the photoreceptor layers or the sub-retinal space between the photoreceptor outer segments and the RPE. Hence, the subretinal space of healthy eyes is devoid of MPs, and there is no direct cell-cell contact between the MPs and RPE cells in the subretinal space.

The RPE contributes to the immune regulation of the retina via the release of anti-inflammatory factors including complement inhibitors (e.g., CFH) and cytokines, such as IL-10 (D'Orazio and Niederkorn, 1998; Langmann, 2007; Luo et al., 2013). IL-10 expression from MPs themselves has been implicated as playing an important role in maintaining homeostasis and immune privilege. For example, pigment epithelial derived factor (PEDF) released from the RPE increases IL-10 production by macrophages (Zamiri et al., 2006). Further recruitment and activation of MPs, particularly microglia is inhibited by IL-10, by reducing expression of antigen-presenting molecules such as monocyte MHC II (**Figure 3A**; D'Orazio and Niederkorn, 1998). Even under stress, the RPE tries to maintain an anti-inflammatory environment. Advanced glycation end-product (AGE) application, which induces oxidative stress, causes RPE cells in culture to upregulate expression of anti-inflammatory cytokines and receptors IL-9, IL-10, IL-13, and IL-1ra (Lin et al., 2013). IL-9 protects against RPE proliferation and apoptosis (Demoulin and Renauld, 1998) and IL-13 generally inhibits pro-inflammatory cytokine synthesis (Wynn, 2003). IL-1ra binds with comparable affinities for both IL-1α and IL-1β to the IL-1 receptor, without activating the receptor, playing a role in sopping up the overt inflammatory function of IL-1β (Gabay et al., 2010). The RPE cell also expresses Fas ligand which can induce apoptosis of inflammatory cells (Jorgensen et al., 1998). These immunomodulatory factors are likely a few of the mechanisms by which the RPE and MPs suppress MP recruitment and activation in the healthy retina.

Mononuclear phagocyte migration to the retinal pigment epithelium and retention

In healthy eyes and with age, choroidal MPs such as macrophages are not found within Bruch's membrane or closely associated with the RPE (Cherepanoff et al., 2010). However, in early AMD, MPs including macrophages are recruited to Bruch's membrane drusen and basal laminar deposits and begin to express inducible nitric oxide synthase (iNOS), a marker of MP activation (Cherepanoff et al., 2010). As AMD progresses, in GA, MPs continue to express iNOS and to be associated with Bruch's membrane. In early stages of subclinical CNV, MPs are associated with the new choroidal vessels (Cherepanoff et al., 2010). In late-stage CNV, MPs are found associated with Bruch's membrane, the new vessels and within the retina. On the subretinal side, with age, MPs are occasionally found between the photoreceptor outer segments and RPE. However, in AMD, MPs are associated with RPD (Greferath et al., 2016; Wu et al., 2022) and the degenerating RPE (Wu et al., 2022). The proximity of MPs with the RPE waste deposits on both the choroidal and subretinal side in early and late AMD indicates the importance of these macrophages in waste clearance.

Damaged RPE cells and the deposition of waste material containing inflammatory molecules can induce the migration of MPs. RPE cells express surface receptors for sensing and responding to the exposure of cytokines and in turn rapidly release soluble chemoattractant inflammatory mediators to direct the trafficking of immune cells to the injured site (Elner et al., 1991; Hageman et al., 2001; Ma et al., 2017; Natoli et al., 2017). CCL2, also known as monocyte chemoattractant protein-1, is well known to be involved in the recruitment and retention of CCR2 bearing MPs to sites of dysfunction. CCL2 is present in higher concentration in the aqueous humor of human eyes with AMD (Kramer et al., 2012; Lechner et al., 2017). In cell culture studies, direct cell-cell contact between human RPE and inactivated monocytes causes a significantly larger production of CCL2 than cell co-culture with physical separation (Yoshida et al., 2001; Bian et al., 2003). This suggests that the presence of MPs associated with the RPE, drives further recruitment of MPs via the CCL2-CCR2 axis. Thrombin, a clotting factor which extravasates at sites of blood retinal barrier breakdown, can also enhance the secretion of CCL2 and IL-8 from RPE cells (Yoshida et al., 2001). Thus, the breakdown of the blood retinal barrier as occurs even in early AMD may predispose eyes to excessive recruitment of monocytes to sites of RPE dysfunction.

In cell culture studies, direct contact between human RPE cells and inactivated monocytes also causes the secretion of IL-8 by the RPE, compared to the co-culture of human RPE cells with monocytes separated by a filter (Yoshida et al., 2001; Bian et al., 2003). IL-8 is a cytokine associated with chemotaxis of immune cells to sites of damage and subsequent phagocytosis of damage, as well as being a mediator of angiogenesis (Koch et al., 1992; Harada et al., 1994). Polymorphisms in the IL-8 promotor, IL-8-251AA, are associated with an increased risk of AMD (Goverdhan et al., 2008). The upregulated secretion of IL-8 during a cell-cell contact co-culture suggests that like CCL2, RPE release of IL-8 is involved in recruiting MPs to sites of RPE dysfunction.

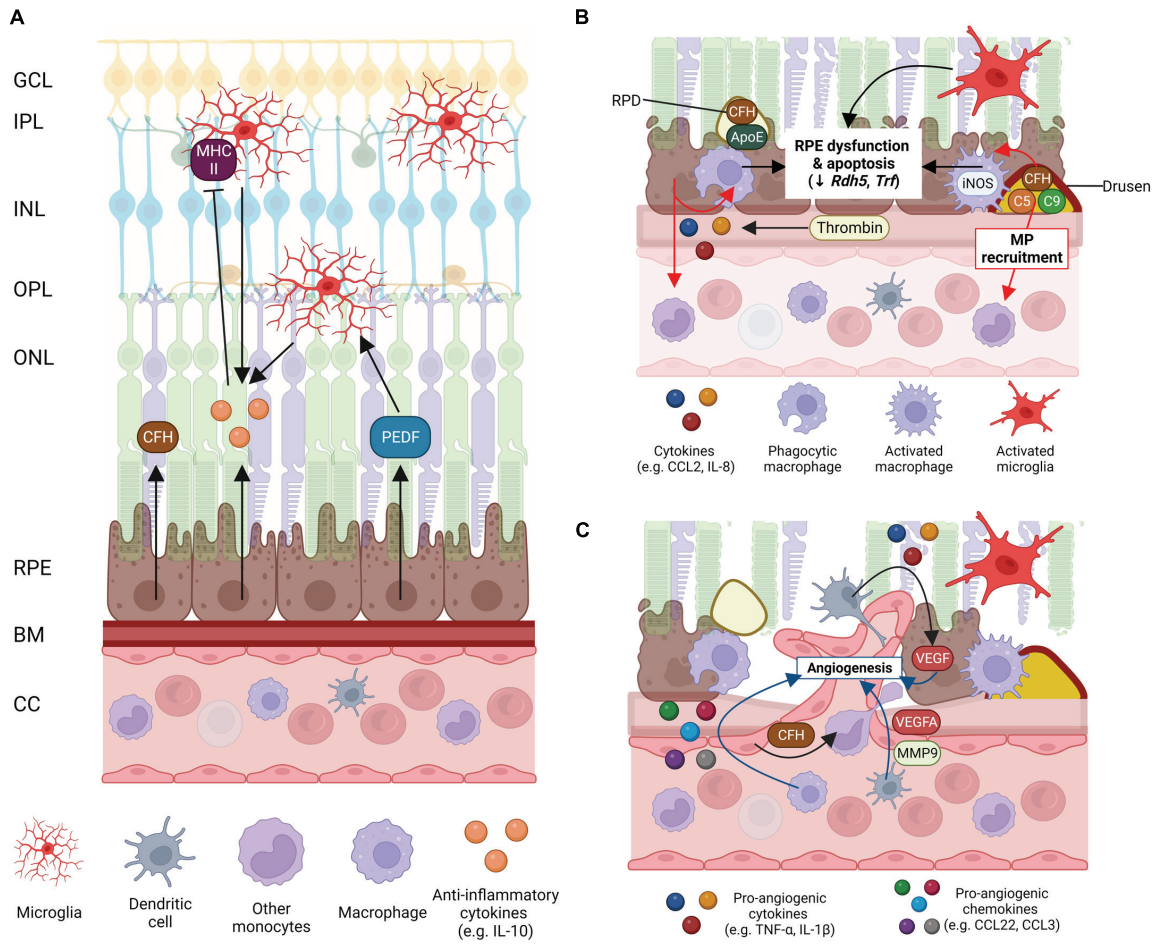

FIGURE 3
Schematic of mononuclear phagocyte (MP) interactions with the ocular tissues in health eyes and late-stage age-related macular degeneration (AMD). **(A)** Healthy posterior eye, showing transverse section of the retinal layers, the retinal pigment epithelium (RPE), Bruch's membrane (BM), and vascular supply (the choriocapillaris, CC). The location of the mononuclear phagocytes (MPs) is indicated including retinal tissue resident microglia associated with the neuronal synaptic layers (nerve fiber layer MPs not shown) and MPs in the choroid, including dendritic cells, macrophages and other monocytes. RPE expression of immunosuppressive cytokines (e.g., IL-10), growth factors (e.g., PEDF) and immune factors (e.g., CFH) are shown. **(B)** Schematic of late-stage AMD, geographic atrophy, showing loss of photoreceptors and RPE cells, and deposition of large drusen. The RPE expresses chemokines, e.g., CCL-2 and IL-8 to recruit immune cells to areas of damage. Microglia within the retina are activated, recruited to damaged RPE cells and RPD and activated iNOS-positive macrophages on the choroidal side are associated with the damaged RPE and drusen containing immunogenic complement pathway factors. Activated MP interaction with the RPE can contribute to RPE dysfunction and apoptosis. **(C)** Schematic of late-stage neovascular AMD showing choroidal neovascularization (CNV), loss of photoreceptors and RPE cells, and deposition of large drusen. Microglia within the retina are activated. Peripheral circulating MPs, dendritic cells are activated and associated with damaged RPE releasing VEGF and MMP-9 to drive new vessel development and are also able to enter the retina via new leaky vessels. There is an increase in expression of pro-inflammatory chemokines and cytokines by MPs and the RPE which drives angiogenesis and contributes to RPE cell dysfunction and death. Some of this illustration was started from a BioRender Template and content and stylistic modifications were made.

Para-inflammation interactions between the retinal pigment epithelium and mononuclear phagocytes in aging and age-related macular degeneration

Once MPs are recruited to the RPE and retained, a process of para-inflammation ensues. Para-inflammation is an adaptive response in which tissue-resident or recruited MPs generate low-grade inflammation and is essential for maintaining tissue homeostasis and restoring tissue function. This process occurs with age and in early AMD, when the RPE and retina are stressed from a low-degree of noxious insults (Medzhitov, 2008; Xu et al., 2009). Since para-inflammation is thought to be an intermediate state between basal homeostasis and classic inflammation, upregulation of expression of anti-inflammatory molecules (discussed in the section on homeostasis) may help maintain retinal

health by suppressing the inflammatory phenotypes of MPs (discussed in the section on pathological interactions below). In the early stages of AMD, there is likely to be a continuum of homeostatic and pro-inflammatory pathways activated.

Cell culture studies of MPs, co-cultured with RPE cells provide clues as to how these cells interact. Due to the immunosuppressive property of RPE cells, activated immune cells are likely to be eliminated when they are in close contact with RPE cells (Jorgensen et al., 1998). MPs have also been suggested to promote RPE cell survival and even proliferation, however, whether RPE cells are able to proliferate to repair areas of degeneration is not clear. It is generally accepted that RPE are terminally differentiated cells, but in mice, there is some evidence of proliferation in areas of lesions generated by a laser (Jobling et al., 2015) and some studies suggest that low grade proliferation in aged tissues may repair tissue damage, as a response to RPE cell death with age (Chen et al., 2016). Cell culture studies suggest that cell-cell contact between the RPE and monocytes/retinal microglia can induce the proliferation of RPE cells (Osusky and Ryan, 1996; Ma et al., 2009). However, this may prompt the RPE cells to lose integrity in morphology and intercellular adhesion, and form irregular clumps instead of a monolayer organization (Ma et al., 2009). Whether such an interaction whereby MPs have the potential to promote RPE survival and proliferation occurs *in vivo* is yet to be determined.

Pathological interactions between the retinal pigment epithelium and mononuclear phagocytes in aging and age-related macular degeneration

The balance between para-inflammation and inflammation may be key to development of AMD. Genetic studies indicate regulation of the innate immune system's alternative complement pathway confers increased risk of disease development. Indeed, an over-reactive alternative complement pathway due to mutations in CFH and C3, as well as downstream effectors such as C5 have been suggested to tip a patient into a "complement hyperinflammatory phenotype" (Whitcup et al., 2013). It is likely that failure to suppress the inflammatory MP response during basal para-inflammation contributes to disease progression in some cases of AMD. Over time, overt inflammatory interactions between MPs and the RPE occur and may drive AMD progression.

The direct interaction between RPE cells and MPs can induce pro-inflammatory cytokine production. Components of drusen from donor AMD patients and changes in accumulation of AluRNA (RNA expression of abundant short, repetitive DNA elements characterized initially by the action of Arthrobacter luteus (Alu) restriction endonuclease) in the RPE of GA patients have been shown to drive NLRP activation and inflammasome expression by MPs and the RPE, respectively (Doyle et al., 2012; Tarallo et al., 2012; Yerramothu et al., 2018). Inflammasome activation is an innate immune system mechanism that can induce pyroptosis, an inflammatory form of programmed cell death usually activated in response to infection, that is distinct to apoptosis and necroptosis (Cookson and Brennan, 2001). NLRP activation of the inflammasome results in cleavage of pro-caspase-1 to caspase-1 and subsequent cleavage of pro-interleukin-1β (pro-IL-1β) and pro-IL-18 into their mature pro-inflammatory forms (Cookson and Brennan, 2001).

In RPE samples from human patients with GA, expression of *Nlrp3* and *Il-18* mRNA was found to be increased relative to normal age-matched controls (Tarallo et al., 2012). Further analysis of protein samples from RPE of GA patients confirmed that in addition to NLRP3 increases, PYCARD (PYD And CARD Domain Containing), pro-caspase-1 and cleaved caspase-1, and downstream effectors of IL-18, including interleukin 1 receptor associated kinase 3 and 4 (IRAK3- and -4) were all increased, suggesting inflammasome activation in the RPE contributes to RPE dysfunction in GA (Tarallo et al., 2012). Another study, which did not isolate RPE specifically, but microdissected regions of photoreceptor and RPE cells from lesion areas of both GA and nAMD and healthy control samples, also found increases in mRNA expression of NLRP3, pro-IL-1β and pro-IL-18 in late-stage AMD (Wang et al., 2016). Studies using RPE cell culture models without MP co-culture suggest that NLRP3 inflammasome activation drives RPE cell damage, including mitochondrial damage and may contribute to AMD pathogenesis (Wang et al., 2016). Although the most likely source of inflammatory mediators, the role of inflammasome activation in MPs in human patients with AMD has not been studied as heavily. A study of the effect of drusen components on human peripheral blood mononuclear cells (PBMCs), which would be the primary source of peripheral MPs with access to the basal RPE, suggests that these cells are a potential source of inflammasome mediators independently of the RPE (Doyle et al., 2012). In this study, drusen components were isolated and used to treat peripheral blood MPs and this induced inflammasome activation and production of IL-1β and IL-18 (Doyle et al., 2012). In line with this, recent single cell RNA-seq analysis of MPs from AMD patients suggested NLRP3 is upregulated in infiltrating inflammatory macrophages (Voigt et al., 2022), implicating these cells as a likely source of inflammasome driven inflammatory mediators.

Further cell culture studies point to an important role of activated MPs in driving inflammation and RPE cell dysfunction and death. Activated MPs have been found

to negatively impact RPE function causing a reduction in expression of *Otx2* (orthodenticle homeobox 2), *Rdh5* (retinol dehydrogenase 5), *Ttr* (transthyretin), and *Trf* (transferrin) in cultured RPE cells (Mathis et al., 2017). *Rdh5* and *Ttr* are involved in recycling of vitamin A for rods photoreceptors, while *Trf* is important for iron transport in RPE cells. This decrease in the expression of genes essential for RPE function suggests pro-inflammatory, activated MP interaction with the RPE can contribute to RPE dysfunction (Mathis et al., 2017). Additionally, cell-cell contact between RPE cells and activated MPs can cause apoptosis of RPE cells. Both bone marrow derived macrophages and microglia from mouse retina, that have been activated by inflammatory cytokines such as TNF-α, IFN-γ, and IL-1β, cause cultured mouse RPE cells to enter apoptosis (Devarajan et al., 2016). Similar findings have been reported in co-culture of human RPE cells and human activated monocytes, with a large number of RPE cells entering apoptosis through caspase-3 activation (Elner et al., 1992; Yang et al., 2011). Overall, pro-inflammatory, activated MPs when in contact with RPE cells can cause the death of the RPE, which may lead to dysfunction and failure in nearby remaining RPE cells perpetuating AMD disease progression.

Angiogenesis and subretinal fibrosis

Mononuclear phagocytes such as microglia have been suggested to play an integral role in angiogenesis during development (Checchin et al., 2006) and they are implicated in new vessel growth in nAMD (Jackson et al., 1997; Ambati and Fowler, 2012; Marneros, 2021). A recent study using single cell RNA-seq on human samples of retina/RPE/choroid from the macula of healthy control and AMD patients (intermediate AMD or CNV, not GA) has shed some light on changes in the MP populations within the eye in AMD and hints at a potential role for MPs in angiogenesis (Voigt et al., 2022). Based on previously described transcriptomes of MPs, three populations of MPs were identified in the retina/RPE/choroid complex: tissue resident macrophages, likely microglia; dendritic cells and inflammatory monocytes (Voigt et al., 2022). Of these, choroidal dendritic cells of AMD patients showed upregulation of both *VEGFA* and matrix metallopeptidase 9 (*MMP9*) (Voigt et al., 2022). Both genes are important for angiogenesis, suggesting that MPs may contribute directly to new vessel growth. The inflammatory macrophage subclass was found to upregulate paired immunoglobulin like 2 receptor alpha (*PILRA*) and ATP binding cassette subfamily A member 1 (*ABCA1*), which like ApoE, is important for cholesterol trafficking. Finally, the vascular cell classes (arteries, veins, and choriocapillaries) showed upregulation of *COL8A1* (collagen type VIII alpha 1 chain) collagen expression, which suggests extracellular matrix remodeling, and upregulation in CFH in the alternative complement pathways, which could modulate MP interaction with the vascular bed (Voigt et al., 2022). The change in interaction between MPs and the vascular bed coupled with an upregulation of angiogenic factors in MPs, such as MMP9 and VEGFA, suggests that MPs may play a prominent role in CNV development, even prior to overt CNV pathology.

Additionally, MPs namely monocytes and derived macrophages recruited in CNV have been suggested to play a role in angiogenesis by secreting pro-angiogenic TNF-α, and IL-1β, which may promote expression of VEGF from the RPE and MPs (Leibovich et al., 1987; Oh et al., 1999; Cousins et al., 2004). The vitreous of patients with nAMD has increased pro-IL-1β and IL-1β relative to age-matched controls (Zhao et al., 2015). While the role of IL-1β in promoting angiogenesis is relatively well supported (Voronov et al., 2014), the role of IL-18 in nAMD has proven slightly controversial. IL-18 may play a protective role in limiting nAMD lesions in mouse models of CNV (Doyle et al., 2012), while other studies have shown it contributes to RPE degeneration (Tarallo et al., 2012). Generally, studies investigating CNV models in mice highlight a role for NLRP3 activation and MP generated IL-1β, but not necessarily IL-18, in nAMD lesion size and development (Marneros, 2021). The vitreous of patients with nAMD has also been found to contain higher levels of growth-related oncogene (GRO), CCL22, and CCL3 (Agrawal et al., 2019). Both CCL22 and CCL3 are chemokines that have been shown to be secreted by macrophages and induce angiogenesis (Agrawal et al., 2019), while GRO is a chemotactic chemokine that has been found to modulate inflammation and angiogenesis in diabetic retinopathy (Schoenberger et al., 2012).

Mononuclear phagocytes have also been implicated in fibrosis, the end stage of nAMD. Fibrosis is characterized as a wound healing process which involves deposition of extracellular matrix proteins driven by activated inflammatory cells and fibroblasts recruited to the damaged site (Little et al., 2018). This process has been suggested to be a primary reason for the failure of anti-VEGF therapies in arresting vision loss in nAMD progression. MPs, especially choroidal macrophages, are associated with CNV and fibrotic lesions in nAMD (Grossniklaus et al., 2000; Cherepanoff et al., 2010; Lad et al., 2015). MPs can trigger the expression of integrins α1 and α5 on the RPE surface via TNF-α production, promoting the RPE cells to migrate on fibronectin and collagen type I leading to fibrotic scarring (Jin et al., 2000; Kent and Sheridan, 2003; Ishikawa et al., 2016). Additionally, MPs have been suggested to directly contribute to fibrosis by transitioning to myofibroblasts (Little et al., 2018). Histological assessment of

fibrosis within nAMD lesions and mouse studies of laser induced nAMD suggest that C3 and transforming growth factor beta (TGF-β) can induce MPs to transition to myofibroblasts, with 20–30% of infiltrating macrophages expressing the myofibroblast marker, α-smooth muscle actin, in lesion sites (Little et al., 2018). Treatment of a laser induced mouse model of nAMD with an antifibrotic agent, a novel cinnamyl anthranilate (OCX063), has been shown to reduce lesion size and fibrosis driven via the TGF-β pathway alluding to the potential for treatments targeting TGF-β pathways as an adjunct therapy for nAMD (Brandli et al., 2022).

Conclusion

Age-related macular degeneration is a multigenic disease associated with a range of environmental risk factors including aging and lifestyle factors. RPE dysfunction and pro-inflammatory MPs have been found to play an important role in the progression of AMD, from early/intermediate stage to advanced forms GA and nAMD. Crosstalk between MPs and the RPE contributes to the pathological changes observed in AMD and the ensuing inflammatory microenvironment can promote RPE cell dysfunction and death, as well as breakdown of blood retinal barrier. The factors that drive MPs to exert a detrimental role in AMD, rather than serving as a protective response against AMD pathology, are many and are still being defined. In the future, determining the MP factors that promote homeostasis and subtle para-inflammation that aid an aging RPE vs. those that promote an overt pro-inflammatory response will likely provide a pathway for developing therapies to slow vision loss in AMD.

Author contributions

JW, JM, AB, UG, AJ, EF, and KV: manuscript writing and editing. All authors contributed to the article and approved the submitted version.

Funding

This work was supported by the National Health and Medical Research Council (Synergy Grant: APP1181010, APP1138253, and APP2011200).

Conflict of interest

The authors declare that the research was conducted in the absence of any commercial or financial relationships that could be construed as a potential conflict of interest.

Publisher's note

All claims expressed in this article are solely those of the authors and do not necessarily represent those of their affiliated organizations, or those of the publisher, the editors and the reviewers. Any product that may be evaluated in this article, or claim that may be made by its manufacturer, is not guaranteed or endorsed by the publisher.

References

Ach, T., Huisingh, C., McGwin, G., Messinger, J. D., Zhang, T., Bentley, M. J., et al. (2014). Quantitative Autofluorescence and Cell Density Maps of the Human Retinal Pigment Epithelium. *Investig. Opthalmol. Vis. Sci.* 55:4832. doi: 10.1167/iovs.14-14802

Ach, T., Tolstik, E., Messinger, J. D., Zarubina, A. V., Heintzmann, R., and Curcio, C. A. (2015). Lipofuscin redistribution and loss accompanied by cytoskeletal stress in retinal pigment epithelium of eyes with age-related macular degeneration. *Investig. Ophthalmol. Vis. Sci.* 56, 3242–3252. doi: 10.1167/iovs.14-16274

Adhi, M., Lau, M., Liang, M. C., Waheed, N. K., and Duker, J. S. (2014). Analysis of the thickness and vascular layers of the choroid in eyes with geographic atrophy using spectral-domain optical coherence tomography. *Retina* 34, 306–312. doi: 10.1097/IAE.0b013e3182993e09

Agrawal, R., Balne, P. K., Wei, X., Bijin, V. A., Lee, B., Ghosh, A., et al. (2019). Cytokine Profiling in Patients With Exudative Age-Related Macular Degeneration and Polypoidal Choroidal Vasculopathy. *Investig. Ophthalmol. Vis. Sci.* 60, 376–382. doi: 10.1167/iovs.18-24387

Ambati, J., Anand, A., Fernandez, S., Sakurai, E., Lynn, B. C., Kuziel, W. A., et al. (2003). An animal model of age-related macular degeneration in senescent Ccl-2- or Ccr-2-deficient mice. *Nat. Med.* 9, 1390–1397. doi: 10.1038/nm950

Ambati, J., and Fowler, B. J. (2012). Mechanisms of age-related macular degeneration. *Neuron* 75, 26–39. doi: 10.1016/j.neuron.2012.06.018

Ambati, J., Atkinson, J. P., and Gelfand, B. D. (2013). Immunology of age-related macular degeneration. *Nat. Rev. Immunol.* 13, 438–451. doi: 10.1038/nri3459

Anand, A., Sharma, N. K., Gupta, A., Prabhakar, S., Sharma, S. K., Singh, R., et al. (2012). Single nucleotide polymorphisms in MCP-1 and its receptor are associated with the risk of age related macular degeneration. *PLoS One* 7:e49905. doi: 10.1371/journal.pone.0049905

Anderson, D. H., Mullins, R. F., Hageman, G. S., and Johnson, L. V. (2002). A role for local inflammation in the formation of drusen in the aging eye. *Am. J. Ophthalmol.* 134, 411–431. doi: 10.1016/s0002-9394(02)01624-0

Baehr, W., Wu, S. M., Bird, A. C., and Palczewski, K. (2003). The retinoid cycle and retina disease. *Vis. Res.* 43, 2957–2958. doi: 10.1016/j.visres.2003.10.001

Barron, K. D. (1995). The microglial cell. A historical review. *J. Neurol. Sci.* 134, 57–68. doi: 10.1016/0022-510x(95)00209-k

Bhatia, S. K., Rashid, A., Chrenek, M. A., Zhang, Q., Bruce, B. B., Klein, M., et al. (2016). Analysis of RPE morphometry in human eyes. *Mol. Vis.* 22, 898–916.

Bhutto, I., and Lutty, G. (2012). Understanding age-related macular degeneration (AMD): Relationships between the photoreceptor/retinal pigment epithelium/Bruch's membrane/choriocapillaris complex. *Mol. Aspects Med.* 33, 295–317. doi: 10.1016/j.mam.2012.04.005

Bian, Z. M., Elner, S. G., Yoshida, A., and Elner, V. M. (2003). Human RPE-monocyte co-culture induces chemokine gene expression through activation of

MAPK and NIK cascade. *Exp. Eye Res.* 76, 573–583. doi: 10.1016/s0014-4835(03)00029-0

Bianchi, E., Scarinci, F., Ripandelli, G., Feher, J., Pacella, E., Magliulo, G., et al. (2013). Retinal pigment epithelium, age-related macular degeneration and neurotrophic keratouveitis. *Int. J. Mol. Med.* 31, 232–242. doi: 10.3892/ijmm.2012.1164

Bird, A. C., Bressler, N. M., Bressler, S. B., Chisholm, I. H., Coscas, G., Davis, M. D., et al. (1995). An international classification and grading system for age-related maculopathy and age-related macular degeneration. The International ARM Epidemiological Study Group. *Surv. Ophthalmol.* 39, 367–374.

Blacher, E., Tsai, C., Litichevskiy, L., Shipony, Z., Iweka, C. A., Schneider, K. M., et al. (2022). Aging disrupts circadian gene regulation and function in macrophages. *Nat. Immunol.* 23, 229–236. doi: 10.1038/s41590-021-01083-0

Bloch, S. B., Lund-Andersen, H., Sander, B., and Larsen, M. (2013). Subfoveal fibrosis in eyes with neovascular age-related macular degeneration treated with intravitreal ranibizumab. *Am. J. Ophthalmol.* 156, 116–124.e1. doi: 10.1016/j.ajo.2013.02.012

Boulton, M., and Dayhaw-Barker, P. (2001). The role of the retinal pigment epithelium: Topographical variation and ageing changes. *Eye* 15, 384–389. doi: 10.1038/eye.2001.141

Brandli, A., Khong, F. L., Kong, R. C. K., Kelly, D. J., and Fletcher, E. L. (2022). Transcriptomic analysis of choroidal neovascularization reveals dysregulation of immune and fibrosis pathways that are attenuated by a novel anti-fibrotic treatment. *Sci. Rep.* 12:859. doi: 10.1038/s41598-022-04845-4

Buschini, E., Piras, A., Nuzzi, R., and Vercelli, A. (2011). Age related macular degeneration and drusen: Neuroinflammation in the retina. *Prog. Neurobiol.* 95, 14–25. doi: 10.1016/j.pneurobio.2011.05.011

Castanheira, F., de Lima, K. A., Cebinelli, G. C. M., Sonego, F., Kanashiro, A., Colon, D. F., et al. (2019). CCR5-Positive Inflammatory Monocytes are Crucial for Control of Sepsis. *Shock* 52, e100–e106. doi: 10.1097/SHK.0000000000001301

Checchin, D., Sennlaub, F., Levavasseur, E., Leduc, M., and Chemtob, S. (2006). Potential role of microglia in retinal blood vessel formation. *Investig. Ophthalmol. Vis. Sci.* 47, 3595–3602. doi: 10.1167/iovs.05-1522

Chen, H., Lukas, T. J., Du, N., Suyeoka, G., and Neufeld, A. H. (2009). Dysfunction of the retinal pigment epithelium with age: Increased iron decreases phagocytosis and lysosomal activity. *Investig. Ophthalmol. Vis. Sci.* 50, 1895–1902. doi: 10.1167/iovs.08-2850

Chen, M., Rajapakse, D., Fraczek, M., Luo, C., Forrester, J. V., and Xu, H. (2016). Retinal pigment epithelial cell multinucleation in the aging eye - a mechanism to repair damage and maintain homoeostasis. *Aging Cell* 15, 436–445. doi: 10.1111/acel.12447

Cherepanoff, S., McMenamin, P., Gillies, M. C., Kettle, E., and Sarks, S. H. (2010). Bruch's membrane and choroidal macrophages in early and advanced age-related macular degeneration. *Br. J. Ophthalmol.* 94, 918–925. doi: 10.1136/bjo.2009.165563

Chiang, T. T., Keenan, T. D., Agron, E., Liao, J., Klein, B., Chew, E. Y., et al. (2020). Macular Thickness in Intermediate Age-Related Macular Degeneration Is Influenced by Disease Severity and Subretinal Drusenoid Deposit Presence. *Investig. Ophthalmol. Vis. Sci.* 61:59. doi: 10.1167/iovs.61.6.59

Chinnery, H. R., McLenachan, S., Humphries, T., Kezic, J. M., Chen, X., Ruitenberg, M. J., et al. (2012). Accumulation of murine subretinal macrophages: Effects of age, pigmentation and CX3CR1. *Neurobiol. Aging* 33, 1769–1776. doi: 10.1016/j.neurobiolaging.2011.03.010

Ciulla, T. A., Harris, A., and Martin, B. J. (2001). Ocular perfusion and age-related macular degeneration. *Acta Ophthalmol. Scand.* 79, 108–115. doi: 10.1034/j.1600-0420.2001.079002108.x

Combadière, C., Feumi, C., Raoul, W., Keller, N., Rodéro, M., Pézard, A., et al. (2007). CX3CR1-dependent subretinal microglia cell accumulation is associated with cardinal features of age-related macular degeneration. *J. Clin. Investig.* 117, 2920–2928. doi: 10.1172/jci31692

Cookson, B. T., and Brennan, M. A. (2001). Pro-inflammatory programmed cell death. *Trends Microbiol.* 9, 113–114. doi: 10.1016/s0966-842x(00)01936-3

Cousins, S. W., Espinosa-Heidmann, D. G., and Csaky, K. G. (2004). Monocyte activation in patients with age-related macular degeneration: A biomarker of risk for choroidal neovascularization?. *Arch. Ophthalmol.* 122, 1013–1018. doi: 10.1001/archopht.122.7.1013

Crabb, J. W. (2014). The Proteomics of Drusen. *Cold Spring Harbor. Perspect. Med.* 4:a017194. doi: 10.1101/cshperspect.a017194

Crabb, J. W., Miyagi, M., Gu, X., Shadrach, K., West, K. A., Sakaguchi, H., et al. (2002). Drusen proteome analysis: An approach to the etiology of age-related macular degeneration. *Proc. Natl. Acad. Sci. U. S. A.* 99, 14682–14687. doi: 10.1073/pnas.222551899

Curcio, C. A., and Millican, C. L. (1999). Basal linear deposit and large drusen are specific for early age-related maculopathy. *Arch. Ophthalmol.* 117, 329–339. doi: 10.1001/archopht.117.3.329

Curcio, C. A., Johnson, M., Huang, J. D., and Rudolf, M. (2009). Aging, age-related macular degeneration, and the response-to-retention of apolipoprotein B-containing lipoproteins. *Prog. Retin. Eye Res.* 28, 393–422. doi: 10.1016/j.preteyeres.2009.08.001

Damani, M. R., Zhao, L., Fontainhas, A. M., Amaral, J., Fariss, R. N., and Wong, W. T. (2011). Age-related alterations in the dynamic behavior of microglia. *Aging Cell* 10, 263–276. doi: 10.1111/j.1474-9726.2010.00660.x

Demirs, J. T., Yang, J., Crowley, M. A., Twarog, M., Delgado, O., Qiu, Y., et al. (2021). Differential and Altered Spatial Distribution of Complement Expression in Age-Related Macular Degeneration. *Investig. Ophthalmol. Vis. Sci.* 62:26. doi: 10.1167/iovs.62.7.26

Demoulin, J. B., and Renauld, J. C. (1998). Interleukin 9 and its receptor: An overview of structure and function. *Int. Rev. Immunol.* 16, 345–364. doi: 10.3109/08830189809043001

Detrick, B., and Hooks, J. J. (2020). "The RPE Cell and the Immune System," in *Retinal Pigment Epithelium in Health and Disease*, eds A. K. Klettner and S. Dithmar (Cham: Springer International Publishing), 101–114.

Devarajan, G., Niven, J., Forrester, J. V., and Crane, I. J. (2016). Retinal Pigment Epithelial Cell Apoptosis is Influenced by a Combination of Macrophages and Soluble Mediators Present in Age-Related Macular Degeneration. *Curr. Eye Res.* 41, 1235–1244. doi: 10.3109/02713683.2015.1109129

D'Orazio, T. J., and Niederkorn, J. Y. (1998). A novel role for TGF-beta and IL-10 in the induction of immune privilege. *J. Immunol.* 160, 2089–2098.

Doyle, S. L., Campbell, M., Ozaki, E., Salomon, R. G., Mori, A., Kenna, P. F., et al. (2012). NLRP3 has a protective role in age-related macular degeneration through the induction of IL-18 by drusen components. *Nat. Med.* 18, 791–798. doi: 10.1038/nm.2717

Eandi, C. M., Charles Messance, H., Augustin, S., Dominguez, E., Lavalette, S., Forster, V., et al. (2016). Subretinal mononuclear phagocytes induce cone segment loss via IL-1beta. *Elife* 5:e16490. doi: 10.7554/eLife.16490

Edwards, A. O., Ritter, R. III, Abel, K. J., Manning, A., Panhuysen, C., and Farrer, L. A. (2005). Complement factor H polymorphism and age-related macular degeneration. *Science* 308, 421–424. doi: 10.1126/science.1110189

Elner, S. G., Elner, V. M., Pavilack, M. A., Todd, R. F. III, Mayo-Bond, L., Franklin, W. A., et al. (1992). Modulation and function of intercellular adhesion molecule-1 (CD54) on human retinal pigment epithelial cells. *Lab. Investig.* 66, 200–211.

Elner, S. G., Strieter, R. M., Elner, V. M., Rollins, B. J., Del Monte, M. A., and Kunkel, S. L. (1991). Monocyte chemotactic protein gene expression by cytokine-treated human retinal pigment epithelial cells. *Lab. Investig.* 64, 819–825.

Farkas, T. G., Sylvester, V., and Archer, D. (1971). The ultrastructure of drusen. *Am. J. Ophthalmol.* 71, 1196–1205. doi: 10.1016/0002-9394(71)90963-9

Ferris, F. L. III, Fine, S. L., and Hyman, L. (1984). Age-related macular degeneration and blindness due to neovascular maculopathy. *Arch. Ophthalmol.* 102, 1640–1642. doi: 10.1001/archopht.1984.01040031330019

Ferris, F. L. III, Wilkinson, C. P., Bird, A., Chakravarthy, U., Chew, E., Csaky, K., et al. (2013). Clinical classification of age-related macular degeneration. *Ophthalmology* 120, 844–851. doi: 10.1016/j.ophtha.2012.10.036

Fett, A. L., Hermann, M. M., Muether, P. S., Kirchhof, B., and Fauser, S. (2012). Immunohistochemical localization of complement regulatory proteins in the human retina. *Histol. Histopathol.* 27, 357–364. doi: 10.14670/HH-27.357

Flamendorf, J., Agron, E., Wong, W. T., Thompson, D., Wiley, H. E., Doss, E. L., et al. (2015). Impairments in Dark Adaptation Are Associated with Age-Related Macular Degeneration Severity and Reticular Pseudodrusen. *Ophthalmology* 122, 2053–2062. doi: 10.1016/j.ophtha.2015.06.023

Fu, Z., Kern, T. S., Hellstrom, A., and Smith, L. E. H. (2021). Fatty acid oxidation and photoreceptor metabolic needs. *J. Lipid Res.* 62:100035. doi: 10.1194/jlr.TR120000618

Gabay, C., Lamacchia, C., and Palmer, G. (2010). IL-1 pathways in inflammation and human diseases. *Nat. Rev. Rheumatol.* 6, 232–241. doi: 10.1038/nrrheum.2010.4

Gao, H., and Hollyfield, J. G. (1992). Aging of the human retina. Differential loss of neurons and retinal pigment epithelial cells. *Investig. Ophthalmol. Vis. Sci.* 33, 1–17.

Geissmann, F., Jung, S., and Littman, D. R. (2003). Blood monocytes consist of two principal subsets with distinct migratory properties. *Immunity* 19, 71–82. doi: 10.1016/s1074-7613(03)00174-2

Ginhoux, F., Greter, M., Leboeuf, M., Nandi, S., See, P., Gokhan, S., et al. (2010). Fate mapping analysis reveals that adult microglia derive from primitive macrophages. *Science* 330, 841–845. doi: 10.1126/science.1194637

Golestaneh, N., Chu, Y., Xiao, Y. Y., Stoleru, G. L., and Theos, A. C. (2017). Dysfunctional autophagy in RPE, a contributing factor in age-related macular degeneration. *Cell Death Dis.* 8:e2537. doi: 10.1038/cddis.2016.453

Goverdhan, S. V., Ennis, S., Hannan, S. R., Madhusudhana, K. C., Cree, A. J., Luff, A. J., et al. (2008). Interleukin-8 promoter polymorphism -251A/T is a risk factor for age-related macular degeneration. *Br. J. Ophthalmol.* 92, 537–540. doi: 10.1136/bjo.2007.123190

Grassmann, F., Kiel, C., Zimmermann, M. E., Gorski, M., Grassmann, V., Stark, K., et al. (2017). Genetic pleiotropy between age-related macular degeneration and 16 complex diseases and traits. *Genome Med.* 9:29. doi: 10.1186/s13073-017-0418-0

Green, W. R., and Key, S. N. III (1977). Senile macular degeneration: A histopathologic study. *Trans. Am. Ophthalmol. Soc.* 75, 180–254.

Greferath, U., Guymer, R. H., Vessey, K. A., Brassington, K., and Fletcher, E. L. (2016). Correlation of Histologic Features with In Vivo Imaging of Reticular Pseudodrusen. *Ophthalmology* 123, 1320–1331. doi: 10.1016/j.ophtha.2016.02.009

Grossniklaus, H. E., Cingle, K. A., Yoon, Y. D., Ketkar, N., L'Hernault, N., and Brown, S. (2000). Correlation of histologic 2-dimensional reconstruction and confocal scanning laser microscopic imaging of choroidal neovascularization in eyes with age-related maculopathy. *Arch. Ophthalmol.* 118, 625–629. doi: 10.1001/archopht.118.5.625

Gu, B. J., Baird, P. N., Vessey, K. A., Skarratt, K. K., Fletcher, E. L., Fuller, S. J., et al. (2013). A rare functional haplotype of the P2RX4 and P2RX7 genes leads to loss of innate phagocytosis and confers increased risk of age-related macular degeneration. *FASEB J.* 27, 1479–1487. doi: 10.1096/fj.12-215368

Gu, B. J., Huang, X., Avula, P. K., Caruso, E., Drysdale, C., Vessey, K. A., et al. (2021). Deficits in Monocyte Function in Age Related Macular Degeneration: A Novel Systemic Change Associated With the Disease. *Front. Med.* 8:634177. doi: 10.3389/fmed.2021.634177

Guillonneau, X., Eandi, C. M., Paques, M., Sahel, J. A., Sapieha, P., and Sennlaub, F. (2017). On phagocytes and macular degeneration. *Prog. Retin. Eye Res.* 61, 98–128. doi: 10.1016/j.preteyeres.2017.06.002

Gupta, N., Brown, K. E., and Milam, A. H. (2003). Activated microglia in human retinitis pigmentosa, late-onset retinal degeneration, and age-related macular degeneration. *Exp. Eye Res.* 76, 463–471. doi: 10.1016/s0014-4835(02)00332-9

Hageman, G. S., Anderson, D. H., Johnson, L. V., Hancox, L. S., Taiber, A. J., Hardisty, L. I., et al. (2005). A common haplotype in the complement regulatory gene factor H (HF1/CFH) predisposes individuals to age-related macular degeneration. *Proc. Natl. Acad. Sci. U. S. A.* 102, 7227–7232. doi: 10.1073/pnas.0501536102

Hageman, G. S., Luthert, P. J., Victor Chong, N. H., Johnson, L. V., Anderson, D. H., and Mullins, R. F. (2001). An integrated hypothesis that considers drusen as biomarkers of immune-mediated processes at the RPE-Bruch's membrane interface in aging and age-related macular degeneration. *Prog. Retin. Eye Res.* 20, 705–732. doi: 10.1016/s1350-9462(01)00010-6

Hageman, G. S., Mullins, R. F., Russell, S. R., Johnson, L. V., and Anderson, D. H. (1999). Vitronectin is a constituent of ocular drusen and the vitronectin gene is expressed in human retinal pigmented epithelial cells. *FASEB J.* 13, 477–484. doi: 10.1096/fasebj.13.3.477

Harada, A., Sekido, N., Akahoshi, T., Wada, T., Mukaida, N., and Matsushima, K. (1994). Essential involvement of interleukin-8 (IL-8) in acute inflammation. *J. Leukoc Biol.* 56, 559–564.

Haralampus-Grynaviski, N. M., Lamb, L. E., Clancy, C. M. R., Skumatz, C., Burke, J. M., Sarna, T., et al. (2003). Spectroscopic and morphological studies of human retinal lipofuscin granules. *Proc. Natl. Acad. Sci. U. S. A.* 100, 3179–3184. doi: 10.1073/pnas.0630280100

Hassell, J. B., Lamoureux, E. L., and Keeffe, J. E. (2006). Impact of age related macular degeneration on quality of life. *Br. J. Ophthalmol.* 90, 593–596. doi: 10.1136/bjo.2005.086595

Heckenlively, J. R., Hawes, N. L., Friedlander, M., Nusinowitz, S., Hurd, R., Davisson, M., et al. (2003). Mouse model of subretinal neovascularization with choroidal anastomosis. *Retina* 23, 518–522. doi: 10.1097/00006982-200308000-00012

Hettich, C., Wilker, S., Mentlein, R., Lucius, R., Roider, J., and Klettner, A. (2014). The retinal pigment epithelium (RPE) induces FasL and reduces iNOS and Cox2 in primary monocytes. *Graefes Arch. Clin. Exp. Ophthalmol.* 252, 1747–1754. doi: 10.1007/s00417-014-2742-z

Hogan, M. J. (1972). Role of the retinal pigment epithelium in macular disease. *Trans. Am. Acad. Ophthalmol. Otolaryngol.* 76, 64–80.

Hogan, M. J., and Alvarado, J. (1967). Studies on the human macula. IV. Aging changes in Bruch's membrane. *Arch. Ophthalmol.* 77, 410–420. doi: 10.1001/archopht.1967.00980020412022

Holz, F. G., Bellman, C., Staudt, S., Schutt, F., and Volcker, H. E. (2001). Fundus autofluorescence and development of geographic atrophy in age-related macular degeneration. *Investig. Ophthalmol. Vis. Sci.* 42, 1051–1056.

Inana, G., Murat, C., An, W., Yao, X., Harris, I. R., and Cao, J. (2018). RPE phagocytic function declines in age-related macular degeneration and is rescued by human umbilical tissue derived cells. *J. Transl. Med.* 16:63. doi: 10.1186/s12967-018-1434-6

Ishikawa, K., Kannan, R., and Hinton, D. R. (2016). Molecular mechanisms of subretinal fibrosis in age-related macular degeneration. *Exp. Eye Res.* 142, 19–25. doi: 10.1016/j.exer.2015.03.009

Jackson, J. R., Seed, M. P., Kircher, C. H., Willoughby, D. A., and Winkler, J. D. (1997). The codependence of angiogenesis and chronic inflammation. *FASEB J.* 11, 457–465.

Jin, M., He, S., Worpel, V., Ryan, S. J., and Hinton, D. R. (2000). Promotion of adhesion and migration of RPE cells to provisional extracellular matrices by TNF-alpha. *Investig. Ophthalmol. Vis. Sci.* 41, 4324–4332.

Jobling, A. I., Guymer, R. H., Vessey, K. A., Greferath, U., Mills, S. A., Brassington, K. H., et al. (2015). Nanosecond laser therapy reverses pathologic and molecular changes in age-related macular degeneration without retinal damage. *FASEB J.* 29, 696–710. doi: 10.1096/fj.14-262444

Johnson, L. V., Leitner, W. P., Rivest, A. J., Staples, M. K., Radeke, M. J., and Anderson, D. H. (2002). The Alzheimer's A beta -peptide is deposited at sites of complement activation in pathologic deposits associated with aging and age-related macular degeneration. *Proc. Natl. Acad. Sci. U. S. A.* 99, 11830–11835. doi: 10.1073/pnas.192203399

Johnson, L. V., Ozaki, S., Staples, M. K., Erickson, P. A., and Anderson, D. H. (2000). A potential role for immune complex pathogenesis in drusen formation. *Exp. Eye Res.* 70, 441–449. doi: 10.1006/exer.1999.0798

Jorgensen, A., Wiencke, A. K., La Cour, M., Kaestel, C. G., Madsen, H. O., Hamann, S., et al. (1998). Human retinal pigment epithelial cell-induced apoptosis in activated T cells. *Investig. Ophthalmol. Vis. Sci.* 39, 1590–1599.

Joyal, J. S., Sun, Y., Gantner, M. L., Shao, Z., Evans, L. P., Saba, N., et al. (2016). Retinal lipid and glucose metabolism dictates angiogenesis through the lipid sensor Ffar1. *Nat. Med.* 22, 439–445. doi: 10.1038/nm.4059

Karin, N. (2020). CXCR3 Ligands in Cancer and Autoimmunity, Chemoattraction of Effector T Cells, and Beyond. *Front. Immunol.* 11:976. doi: 10.3389/fimmu.2020.00976

Keenan, T. D., Klein, B., Agron, E., Chew, E. Y., Cukras, C. A., and Wong, W. T. (2020). Choroidal Thickness and Vascularity Vary with Disease Severity and Subretinal Drusenoid Deposit Presence in Nonadvanced Age-Related Macular Degeneration. *Retina* 40, 632–642. doi: 10.1097/IAE.0000000000002434

Kent, D., and Sheridan, C. (2003). Choroidal neovascularization: A wound healing perspective. *Mol. Vis.* 9, 747–755.

Kim, S. Y., Sadda, S., Pearlman, J., Humayun, M. S., de Juan, E. Jr., Melia, B. M., et al. (2002). Morphometric analysis of the macula in eyes with disciform age-related macular degeneration. *Retina* 22, 471–477. doi: 10.1097/00006982-200208000-00012

Klaver, C. C., Kliffen, M., van Duijn, C. M., Hofman, A., Cruts, M., Grobbee, D. E., et al. (1998). Genetic association of apolipoprotein E with age-related macular degeneration. *Am. J. Hum. Genet.* 63, 200–206. doi: 10.1086/301901

Kliffen, M., van der Schaft, T. L., Mooy, C. M., and de Jong, P. T. (1997). Morphologic changes in age-related maculopathy. *Microsc. Res. Tech.* 36, 106–122. doi: 10.1002/(SICI)1097-0029(19970115)36:2<106::AID-JEMT4<3.0.CO;2-N

Koch, A. E., Polverini, P. J., Kunkel, S. L., Harlow, L. A., DiPietro, L. A., Elner, V. M., et al. (1992). Interleukin-8 as a macrophage-derived mediator of angiogenesis. *Science* 258, 1798–1801. doi: 10.1126/science.1281554

Kramer, M., Hasanreisoglu, M., Feldman, A., Axer-Siegel, R., Sonis, P., Maharshak, I., et al. (2012). Monocyte chemoattractant protein-1 in the aqueous humour of patients with age-related macular degeneration. *Clin. Exp. Ophthalmol.* 40, 617–625. doi: 10.1111/j.1442-9071.2011.02747.x

Kroemer, G. (2015). Autophagy: A druggable process that is deregulated in aging and human disease. *J. Clin. Invest.* 125, 1–4. doi: 10.1172/JCI78652

Krogh Nielsen, M., Subhi, Y., Molbech, C. R., Falk, M. K., Nissen, M. H., and Sorensen, T. L. (2020). Chemokine Profile and the Alterations in CCR5-CCL5 Axis in Geographic Atrophy Secondary to Age-Related Macular Degeneration. *Investig. Ophthalmol. Vis. Sci.* 61:28. doi: 10.1167/iovs.61.4.28

Kumar, M. V., Nagineni, C. N., Chin, M. S., Hooks, J. J., and Detrick, B. (2004). Innate immunity in the retina: Toll-like receptor (TLR) signaling in human retinal

pigment epithelial cells. *J. Neuroimmunol.* 153, 7–15. doi: 10.1016/j.jneuroim.2004.04.018

Kunchithapautham, K., and Rohrer, B. (2007). Apoptosis and autophagy in photoreceptors exposed to oxidative stress. *Autophagy* 3, 433–441. doi: 10.4161/auto.4294

Lad, E. M., Cousins, S. W., Van Arnam, J. S., and Proia, A. D. (2015). Abundance of infiltrating CD163+ cells in the retina of postmortem eyes with dry and neovascular age-related macular degeneration. *Graefes Arch. Clin. Exp. Ophthalmol.* 253, 1941–1945. doi: 10.1007/s00417-015-3094-z

Langmann, T. (2007). Microglia activation in retinal degeneration. *J. Leukoc Biol.* 81, 1345–1351. doi: 10.1189/jlb.0207114

Lechner, J., Chen, M., Hogg, R. E., Toth, L., Silvestri, G., Chakravarthy, U., et al. (2017). Peripheral blood mononuclear cells from neovascular age-related macular degeneration patients produce higher levels of chemokines CCL2 (MCP-1) and CXCL8 (IL-8). *J. Neuroinflammation* 14:42. doi: 10.1186/s12974-017-0820-y

Leibovich, S. J., Polverini, P. J., Shepard, H. M., Wiseman, D. M., Shively, V., and Nuseir, N. (1987). Macrophage-induced angiogenesis is mediated by tumour necrosis factor-alpha. *Nature* 329, 630–632. doi: 10.1038/329630a0

Leveillard, T., Philp, N. J., and Sennlaub, F. (2019). Is Retinal Metabolic Dysfunction at the Center of the Pathogenesis of Age-related Macular Degeneration?. *Int. J. Mol. Sci.* 20:762. doi: 10.3390/ijms20030762

Levy, O., Calippe, B., Lavalette, S., Hu, S. J., Raoul, W., Dominguez, E., et al. (2015). Apolipoprotein E promotes subretinal mononuclear phagocyte survival and chronic inflammation in age-related macular degeneration. *EMBO Mol. Med.* 7, 211–226. doi: 10.15252/emmm.201404524

Liang, F. Q., and Godley, B. F. (2003). Oxidative stress-induced mitochondrial DNA damage in human retinal pigment epithelial cells: A possible mechanism for RPE aging and age-related macular degeneration. *Exp. Eye Res.* 76, 397–403. doi: 10.1016/s0014-4835(03)00023-x

Lim, L. S., Mitchell, P., Seddon, J. M., Holz, F. G., and Wong, T. Y. (2012). Age-related macular degeneration. *Lancet* 379, 1728–1738. doi: 10.1016/S0140-6736(12)60282-7

Lin, T., Walker, G. B., Kurji, K., Fang, E., Law, G., Prasad, S. S., et al. (2013). Parainflammation associated with advanced glycation endproduct stimulation of RPE in vitro: Implications for age-related degenerative diseases of the eye. *Cytokine* 62, 369–381. doi: 10.1016/j.cyto.2013.03.027

Little, K., Ma, J. H., Yang, N., Chen, M., and Xu, H. (2018). Myofibroblasts in macular fibrosis secondary to neovascular age-related macular degeneration - the potential sources and molecular cues for their recruitment and activation. *Ebiomedicine* 38, 283–291. doi: 10.1016/j.ebiom.2018.11.029

Liu, J., Copland, D. A., Theodoropoulou, S., Chiu, H. A. A., Barba, M. D., Mak, K. W., et al. (2016). Impairing autophagy in retinal pigment epithelium leads to inflammasome activation and enhanced macrophage-mediated angiogenesis. *Sci. Rep.* 6:20639. doi: 10.1038/srep20639

Liversidge, J. M., Sewell, H. F., and Forrester, J. V. (1988). Human retinal pigment epithelial cells differentially express MHC class II (HLA, DP, DR and DQ) antigens in response to in vitro stimulation with lymphokine or purified IFN-gamma. *Clin. Exp. Immunol.* 73, 489–494.

Luhmann, U. F., and Ali, R. R. (2012). Local vs. systemic mononuclear phagocytes in age-related macular degeneration and their regulation by CCL2-CCR2 and CX3CL1-CX3CR1 chemokine signalling. *Adv. Exp. Med. Biol.* 723, 17–22. doi: 10.1007/978-1-4614-0631-0_3

Lukacsi, S., Nagy-Balo, Z., Erdei, A., Sandor, N., and Bajtay, Z. (2017). The role of CR3 (CD11b/CD18) and CR4 (CD11c/CD18) in complement-mediated phagocytosis and podosome formation by human phagocytes. *Immunol. Lett.* 189, 64–72. doi: 10.1016/j.imlet.2017.05.014

Luo, C., Zhao, J., Madden, A., Chen, M., and Xu, H. (2013). Complement expression in retinal pigment epithelial cells is modulated by activated macrophages. *Exp. Eye Res.* 112, 93–101. doi: 10.1016/j.exer.2013.04.016

Ma, W., Coon, S., Zhao, L., Fariss, R. N., and Wong, W. T. (2013). A2E accumulation influences retinal microglial activation and complement regulation. *Neurobiol. Aging* 34, 943–960. doi: 10.1016/j.neurobiolaging.2012.06.010

Ma, W., Zhang, Y., Gao, C., Fariss, R. N., Tam, J., and Wong, W. T. (2017). Monocyte infiltration and proliferation reestablish myeloid cell homeostasis in the mouse retina following retinal pigment epithelial cell injury. *Sci. Rep.* 7:8433. doi: 10.1038/s41598-017-08702-7

Ma, W., Zhao, L., Fontainhas, A. M., Fariss, R. N., and Wong, W. T. (2009). Microglia in the mouse retina alter the structure and function of retinal pigmented epithelial cells: A potential cellular interaction relevant to AMD. *PLoS One* 4:e7945. doi: 10.1371/journal.pone.0007945

Marin-Teva, J. L., Almendros, A., Calvente, R., Cuadros, M. A., and Navascues, J. (1998). Tangential migration of ameboid microglia in the developing quail retina: Mechanism of migration and migratory behavior. *Glia* 22, 31–52. doi: 10.1002/(sici)1098-1136(199801)22:1<31::aid-glia4<3.0.co;2-b

Marmorstein, A. D. (2001). The polarity of the retinal pigment epithelium. *Traffic* 2, 867–872. doi: 10.1034/j.1600-0854.2001.21202.x

Marneros, A. G. (2021). Role of inflammasome activation in neovascular age-related macular degeneration. *FEBS J.* [Epub ahead of print]. doi: 10.1111/febs.16278

Mathis, T., Housset, M., Eandi, C., Beguier, F., Touhami, S., Reichman, S., et al. (2017). Activated monocytes resist elimination by retinal pigment epithelium and downregulate their OTX2 expression via TNF-α. *Aging Cell* 16, 173–182. doi: 10.1111/acel.12540

Matsubara, J. A., Tian, Y., Cui, J. Z., Zeglinski, M. R., Hiroyasu, S., Turner, C. T., et al. (2020). Retinal Distribution and Extracellular Activity of Granzyme B: A Serine Protease That Degrades Retinal Pigment Epithelial Tight Junctions and Extracellular Matrix Proteins. *Front. Immunol.* 11:574. doi: 10.3389/fimmu.2020.00574

McBain, V. A., Kumari, R., Townend, J., and Lois, N. (2011). Geographic atrophy in retinal angiomatous proliferation. *Retina* 31, 1043–1052. doi: 10.1097/IAE.0b013e3181fe54c7

McLeod, D. S., Grebe, R., Bhutto, I., Merges, C., Baba, T., and Lutty, G. A. (2009). Relationship between RPE and choriocapillaris in age-related macular degeneration. *Investig. Ophthalmol. Vis. Sci.* 50, 4982–4991. doi: 10.1167/iovs.09-3639

Medzhitov, R. (2008). Origin and physiological roles of inflammation. *Nature* 454, 428–435. doi: 10.1038/nature07201

Mildner, A., Schmidt, H., Nitsche, M., Merkler, D., Hanisch, U. K., Mack, M., et al. (2007). Microglia in the adult brain arise from Ly-6ChiCCR2+ monocytes only under defined host conditions. *Nat. Neurosci.* 10, 1544–1553. doi: 10.1038/nn2015

Miller, J. W. (2013). Age-related macular degeneration revisited–piecing the puzzle: The LXIX Edward Jackson memorial lecture. *Am. J. Ophthalmol.* 155, 1–35.e13. doi: 10.1016/j.ajo.2012.10.018

Mitchell, S. L., Ma, C., Scott, W. K., Agarwal, A., Pericak-Vance, M. A., Haines, J. L., et al. (2021). Plasma Metabolomics of Intermediate and Neovascular Age-Related Macular Degeneration Patients. *Cells* 10:3141. doi: 10.3390/cells10113141

Mitter, S. K., Song, C., Qi, X., Mao, H., Rao, H., Akin, D., et al. (2014). Dysregulated autophagy in the RPE is associated with increased susceptibility to oxidative stress and AMD. *Autophagy* 10, 1989–2005. doi: 10.4161/auto.36184

Mullins, R. F., Russell, S. R., Anderson, D. H., and Hageman, G. S. (2000). Drusen associated with aging and age-related macular degeneration contain proteins common to extracellular deposits associated with atherosclerosis, elastosis, amyloidosis, and dense deposit disease. *FASEB J.* 14, 835–846.

Nakaizumi, Y., Hogan, M. J., and Feeney, L. (1964). The Ultrastructure of Bruch's Membrane. 3. The Macular Area of the Human Eye. *Arch. Ophthalmol.* 72, 395–400. doi: 10.1001/archopht.1964.00970020395018

Natoli, R., Fernando, N., Madigan, M., Chu-Tan, J. A., Valter, K., Provis, J., et al. (2017). Microglia-derived IL-1beta promotes chemokine expression by Muller cells and RPE in focal retinal degeneration. *Mol. Neurodegener.* 12:31. doi: 10.1186/s13024-017-0175-y

Oh, H., Takagi, H., Takagi, C., Suzuma, K., Otani, A., Ishida, K., et al. (1999). The potential angiogenic role of macrophages in the formation of choroidal neovascular membranes. *Investig. Ophthalmol. Vis. Sci.* 40, 1891–1898.

Olchawa, M. M., Furso, J. A., Szewczyk, G. M., and Sarna, T. J. (2017). Lipofuscin-mediated photic stress inhibits phagocytic activity of ARPE-19 cells; effect of donors' age and antioxidants. *Free Radic. Res.* 51, 799–811. doi: 10.1080/10715762.2017.1380307

O'Leary, F., and Campbell, M. (2021). The blood-retina barrier in health and disease. *FEBS J.* doi: 10.1111/febs.16330

Oshima, Y., Oshima, S., Nambu, H., Kachi, S., Hackett, S. F., Melia, M., et al. (2004). Increased expression of VEGF in retinal pigmented epithelial cells is not sufficient to cause choroidal neovascularization. *J. Cell. Physiol.* 201, 393–400. doi: 10.1002/jcp.20110

Osusky, R., and Ryan, S. J. (1996). Retinal pigment epithelial cell proliferation: Potentiation by monocytes and serum. *Graefes Arch. Clin. Exp. Ophthalmol.* 234, S76–S82. doi: 10.1007/BF02343052

Osusky, R., Dorio, R. J., Arora, Y. K., Ryan, S. J., and Walker, S. M. (1997). MHC class II positive retinal pigment epithelial (RPE) cells can function as antigen-presenting cells for microbial superantigen. *Ocul. Immunol. Inflamm.* 5, 43–50. doi: 10.3109/09273949709085049

Penfold, P. L., Liew, S. C., Madigan, M. C., and Provis, J. M. (1997). Modulation of major histocompatibility complex class II expression in retinas with age-related macular degeneration. *Investig. Ophthalmol. Vis. Sci.* 38, 2125–2133.

Pikuleva, I. A., and Curcio, C. A. (2014). Cholesterol in the retina: The best is yet to come. *Prog. Retin. Eye Res.* 41, 64–89. doi: 10.1016/j.preteyeres.2014.03.002

Preissner, K. T. (1991). Structure and biological role of vitronectin. *Annu. Rev. Cell. Biol.* 7, 275–310. doi: 10.1146/annurev.cb.07.110191.001423

Ranawat, N., and Masai, I. (2021). Mechanisms underlying microglial colonization of developing neural retina in zebrafish. *Elife* 10:e70550. doi: 10.7554/eLife.70550

Ransohoff, R. M., and Cardona, A. E. (2010). The myeloid cells of the central nervous system parenchyma. *Nature* 468, 253–262. doi: 10.1038/nature09615

Rashid, A., Bhatia, S. K., Mazzitello, K. I., Chrenek, M. A., Zhang, Q., Boatright, J. H., et al. (2016). RPE Cell and Sheet Properties in Normal and Diseased Eyes. *Adv. Exp. Med. Biol.* 854, 757–763.

Rattner, A., and Nathans, J. (2006). Macular degeneration: Recent advances and therapeutic opportunities. *Nat. Rev. Neurosci.* 7, 860–872. doi: 10.1038/nrn2007

Rizzolo, L. J. (2014). Barrier properties of cultured retinal pigment epithelium. *Exp. Eye Res.* 126, 16–26. doi: 10.1016/j.exer.2013.12.018

Rofagha, S., Bhisitkul, R. B., Boyer, D. S., Sadda, S. R., Zhang, K., and Group, S. U. S. (2013). Seven-year outcomes in ranibizumab-treated patients in ANCHOR, MARINA, and HORIZON: A multicenter cohort study (SEVEN-UP). *Ophthalmology* 120, 2292–2299. doi: 10.1016/j.ophtha.2013.03.046

Rogers, A. H., Martidis, A., Greenberg, P. B., and Puliafito, C. A. (2002). Optical coherence tomography findings following photodynamic therapy of choroidal neovascularization. *Am. J. Ophthalmol.* 134, 566–576. doi: 10.1016/s0002-9394(02)01566-0

Rozanowska, M., Jarvis-Evans, J., Korytowski, W., Boulton, M. E., Burke, J. M., and Sarna, T. (1995). Blue light-induced reactivity of retinal age pigment. In vitro generation of oxygen-reactive species. *J. Biol. Chem.* 270, 18825–18830. doi: 10.1074/jbc.270.32.18825

Rozanowska, M., Pawlak, A., Rozanowski, B., Skumatz, C., Zareba, M., Boulton, M. E., et al. (2004). Age-related changes in the photoreactivity of retinal lipofuscin granules: Role of chloroform-insoluble components. *Investig. Ophthalmol. Vis. Sci.* 45, 1052–1060. doi: 10.1167/iovs.03-0277

Rudolf, M., Malek, G., Messinger, J. D., Clark, M. E., Wang, L., and Curcio, C. A. (2008). Sub-retinal drusenoid deposits in human retina: Organization and composition. *Exp. Eye Res.* 87, 402–408. doi: 10.1016/j.exer.2008.07.010

Russell, S. R., Mullins, R. F., Schneider, B. L., and Hageman, G. S. (2000). Location, substructure, and composition of basal laminar drusen compared with drusen associated with aging and age-related macular degeneration. *Am. J. Ophthalmol.* 129, 205–214. doi: 10.1016/s0002-9394(99)00345-1

Saddala, M. S., Lennikov, A., Mukwaya, A., Fan, L., Hu, Z., and Huang, H. (2019). Transcriptome-wide analysis of differentially expressed chemokine receptors, SNPs, and SSRs in the age-related macular degeneration. *Hum. Genom.* 13:15. doi: 10.1186/s40246-019-0199-1

Salzmann, M., and Brown, E. V. L. (1912). *The anatomy and histology of the human eyeball in the normal state: Its development and senescence*. Chicago, IL: University of Chicago Press.

Santos, A. M., Calvente, R., Tassi, M., Carrasco, M. C., Martin-Oliva, D., Marin-Teva, J. L., et al. (2008). Embryonic and postnatal development of microglial cells in the mouse retina. *J. Comp. Neurol.* 506, 224–239. doi: 10.1002/cne.21538

Sarks, J. P., Sarks, S. H., and Killingsworth, M. C. (1988). Evolution of geographic atrophy of the retinal pigment epithelium. *Eye* 2, 552–577. doi: 10.1038/eye.1988.106

Sarks, J. P., Sarks, S. H., and Killingsworth, M. C. (1997). Morphology of early choroidal neovascularisation in age-related macular degeneration: Correlation with activity. *Eye* 11, 515–522. doi: 10.1038/eye.1997.137

Sarks, S. H. (1976). Ageing and degeneration in the macular region: A clinico-pathological study. *Br. J. Ophthalmol.* 60, 324–341. doi: 10.1136/bjo.60.5.324

Sarks, S. H., Arnold, J. J., Killingsworth, M. C., and Sarks, J. P. (1999). Early drusen formation in the normal and aging eye and their relation to age related maculopathy: A clinicopathological study. *Br. J. Ophthalmol.* 83, 358–368. doi: 10.1136/bjo.83.3.358

Schlanitz, F., Baumann, B., Sacu, S., Baumann, L., Pircher, M., Hitzenberger, C. K., et al. (2019). Impact of drusen and drusenoid retinal pigment epithelium elevation size and structure on the integrity of the retinal pigment epithelium layer. *Br. J. Ophthalmol.* 103, 227–232. doi: 10.1136/bjophthalmol-2017-311782

Schoenberger, S. D., Kim, S. J., Sheng, J., Rezaei, K. A., Lalezary, M., and Cherney, E. (2012). Increased prostaglandin E2 (PGE2) levels in proliferative diabetic retinopathy, and correlation with VEGF and inflammatory cytokines. *Investig. Ophthalmol. Vis. Sci.* 53, 5906–5911. doi: 10.1167/iovs.12-10410

Schultz, H., Song, Y., Baumann, B. H., Kapphahn, R. J., Montezuma, S. R., Ferrington, D. A., et al. (2019). Increased serum proteins in non-exudative AMD retinas. *Exp. Eye Res.* 186:107686. doi: 10.1016/j.exer.2019.05.026

Seddon, J. M., Reynolds, R., Yu, Y., Daly, M. J., and Rosner, B. (2011). Risk models for progression to advanced age-related macular degeneration using demographic, environmental, genetic, and ocular factors. *Ophthalmology* 118, 2203–2211. doi: 10.1016/j.ophtha.2011.04.029

Semba, R. D., Moaddel, R., Cotch, M. F., Jonasson, F., Eiriksdottir, G., Harris, T. B., et al. (2019). Serum lipids in adults with late age-related macular degeneration: A case-control study. *Lipids Health Dis.* 18:7. doi: 10.1186/s12944-018-0954-7

Sennlaub, F., Auvynet, C., Calippe, B., Lavalette, S., Poupel, L., Hu, S. J., et al. (2013). CCR2(+) monocytes infiltrate atrophic lesions in age-related macular disease and mediate photoreceptor degeneration in experimental subretinal inflammation in Cx3cr1 deficient mice. *EMBO Mol. Med.* 5, 1775–1793. doi: 10.1002/emmm.201302692

Silverman, S. M., and Wong, W. T. (2018). Microglia in the Retina: Roles in Development, Maturity, and Disease. *Annu. Rev. Vis. Sci.* 4, 45–77. doi: 10.1146/annurev-vision-091517-034425

Solomon, S. D., Lindsley, K., Vedula, S. S., Krzystolik, M. G., and Hawkins, B. S. (2019). Anti-vascular endothelial growth factor for neovascular age-related macular degeneration. *Cochrane Database Syst. Rev.* 3:CD005139. doi: 10.1002/14651858.CD005139.pub4

Sreekumar, P. G., Reddy, S. T., Hinton, D. R., and Kannan, R. (2022). Mechanisms of RPE senescence and potential role of alphaB crystallin peptide as a senolytic agent in experimental AMD. *Exp. Eye Res.* 215:108918. doi: 10.1016/j.exer.2021.108918

Srinivasan, B., Roque, C. H., Hempstead, B. L., Al-Ubaidi, M. R., and Roque, R. S. (2004). Microglia-derived pronerve growth factor promotes photoreceptor cell death via p75 neurotrophin receptor. *J. Biol. Chem.* 279, 41839–41845. doi: 10.1074/jbc.M402872200

Stevens, T. S., Bressler, N. M., Maguire, M. G., Bressler, S. B., Fine, S. L., Alexander, J., et al. (1997). Occult choroidal neovascularization in age-related macular degeneration. A natural history study. *Arch. Ophthalmol.* 115, 345–350. doi: 10.1001/archopht.1997.01100150347006

Strauss, O. (2005). The retinal pigment epithelium in visual function. *Physiol. Rev.* 85, 845–881. doi: 10.1152/physrev.00021.2004

Sugita, S. (2009). Role of ocular pigment epithelial cells in immune privilege. *Arch. Immunol. Ther. Exp.* 57, 263–268. doi: 10.1007/s00005-009-0030-0

Sunness, J. S. (1999). The natural history of geographic atrophy, the advanced atrophic form of age-related macular degeneration. *Mol. Vis.* 5:25.

Tarallo, V., Hirano, Y., Gelfand, B. D., Dridi, S., Kerur, N., Kim, Y., et al. (2012). DICER1 loss and Alu RNA induce age-related macular degeneration via the NLRP3 inflammasome and MyD88. *Cell* 149, 847–859. doi: 10.1016/j.cell.2012.03.036

Tarau, I. S., Berlin, A., Curcio, C. A., and Ach, T. (2019). The Cytoskeleton of the Retinal Pigment Epithelium: From Normal Aging to Age-Related Macular Degeneration. *Int. J. Mol. Sci.* 20:3578. doi: 10.3390/ijms20143578

Taylor, A. W., Dixit, S., and Yu, J. (2015). Retinal Pigment Epithelial Cell Line Suppression of Phagolysosome Activation. *Int. J. Ophthalmol. Eye Sci.* 2, 1–6.

Tserentsoodol, N., Gordiyenko, N. V., Pascual, I., Lee, J. W., Fliesler, S. J., and Rodriguez, I. R. (2006). Intraretinal lipid transport is dependent on high density lipoprotein-like particles and class B scavenger receptors. *Mol. Vis.* 12, 1319–1333.

Ts'o, M. O., and Friedman, E. (1967). The retinal pigment epithelium. I. Comparative histology. *Arch. Ophthalmol.* 78, 641–649. doi: 10.1001/archopht.1967.00980030643016

Vessey, K. A., Gu, B. J., Jobling, A. I., Phipps, J. A., Greferath, U., Tran, M. X., et al. (2017). Loss of Function of P2X7 Receptor Scavenger Activity in Aging Mice: A Novel Model for Investigating the Early Pathogenesis of Age-Related Macular Degeneration. *Am. J. Pathol.* 187, 1670–1685. doi: 10.1016/j.ajpath.2017.04.016

Vessey, K. A., Jobling, A. I., Tran, M. X., Wang, A. Y., Greferath, U., and Fletcher, E. L. (2022). Treatments targeting autophagy ameliorate the age-related macular degeneration phenotype in mice lacking APOE (apolipoprotein E). *Autophagy* 18, 2368–2384. doi: 10.1080/15548627.2022.2034131

Vessey, K. A., Waugh, M., Jobling, A. I., Phipps, J. A., Ho, T., Trogrlic, L., et al. (2015). Assessment of retinal function and morphology in aging Ccl2 knockout mice. *Investig. Ophthalmol. Vis. Sci.* 56, 1238–1252. doi: 10.1167/iovs.14-15334

Voigt, A. P., Mullin, N. K., Mulfaul, K., Lozano, L. P., Wiley, L. A., Flamme-Wiese, M. J., et al. (2022). Choroidal Endothelial and Macrophage Gene Expression in Atrophic and Neovascular Macular Degeneration. *Hum. Mol. Genet.* 31, 2406–2423. doi: 10.1093/hmg/ddac043

Voronov, E., Carmi, Y., and Apte, R. N. (2014). The role IL-1 in tumor-mediated angiogenesis. *Front. Physiol.* 5:114. doi: 10.3389/fphys.2014.00114

Wakatsuki, Y., Shinojima, A., Kawamura, A., and Yuzawa, M. (2015). Correlation of Aging and Segmental Choroidal Thickness Measurement using Swept Source Optical Coherence Tomography in Healthy Eyes. *PLoS One* 10:e0144156. doi: 10.1371/journal.pone.0144156

Wang, Y., Hanus, J. W., Abu-Asab, M. S., Shen, D., Ogilvy, A., Ou, J., et al. (2016). NLRP3 Upregulation in Retinal Pigment Epithelium in Age-Related Macular Degeneration. *Int. J. Mol. Sci.* 17:73. doi: 10.3390/ijms17010073

Whitcup, S. M., Sodhi, A., Atkinson, J. P., Holers, V. M., Sinha, D., Rohrer, B., et al. (2013). The role of the immune response in age-related macular degeneration. *Int. J. Inflam.* 2013:348092. doi: 10.1155/2013/348092

Wolf-Schnurrbusch, U. E., Enzmann, V., Brinkmann, C. K., and Wolf, S. (2008). Morphologic changes in patients with geographic atrophy assessed with a novel spectral OCT-SLO combination. *Investig. Ophthalmol. Vis. Sci.* 49, 3095–3099. doi: 10.1167/iovs.07-1460

Wu, Z., Fletcher, E. L., Kumar, H., Greferath, U., and Guymer, R. H. (2022). Reticular pseudodrusen: A critical phenotype in age-related macular degeneration. *Prog. Retin. Eye Res.* 88:101017. doi: 10.1016/j.preteyeres.2021.101017

Wynn, T. A. (2003). IL-13 effector functions. *Annu. Rev. Immunol.* 21, 425–456. doi: 10.1146/annurev.immunol.21.120601.141142

Xu, H., Chen, M., and Forrester, J. V. (2009). Para-inflammation in the aging retina. *Prog. Retin. Eye Res.* 28, 348–368. doi: 10.1016/j.preteyeres.2009.06.001

Xu, H., Chen, M., Manivannan, A., Lois, N., and Forrester, J. V. (2008). Age-dependent accumulation of lipofuscin in perivascular and subretinal microglia in experimental mice. *Aging Cell* 7, 58–68. doi: 10.1111/j.1474-9726.2007.00351.x

Xue, C. C., Cui, J., Gao, L. Q., Zhang, C., Dou, H. L., Chen, D. N., et al. (2021). Peripheral Monocyte Count and Age-Related Macular Degeneration. The Tongren Health Care Study. *Am. J. Ophthalmol.* 227, 143–153. doi: 10.1016/j.ajo.2021.03.010

Yang, D., Elner, S. G., Chen, X., Field, M. G., Petty, H. R., and Elner, V. M. (2011). MCP-1–Activated Monocytes Induce Apoptosis in Human Retinal Pigment Epithelium. *Investig. Opthalmol. Vis. Sci.* 52:6026. doi: 10.1167/iovs.10-7023

Yannuzzi, L. A., Freund, K. B., and Takahashi, B. S. (2008). Review of retinal angiomatous proliferation or type 3 neovascularization. *Retina* 28, 375–384. doi: 10.1097/IAE.0b013e3181619c55

Yannuzzi, L. A., Negrao, S., Iida, T., Carvalho, C., Rodriguez-Coleman, H., Slakter, J., et al. (2001). Retinal angiomatous proliferation in age-related macular degeneration. *Retina* 21, 416–434. doi: 10.1097/00006982-200110000-00003

Yerramothu, P., Vijay, A. K., and Willcox, M. D. P. (2018). Inflammasomes, the eye and anti-inflammasome therapy. *Eye* 32, 491–505. doi: 10.1038/eye.2017.241

Yoshida, A., Elner, S. G., Bian, Z. M., Kunkel, S. L., Lukacs, N. W., and Elner, V. M. (2001). Thrombin Regulates Chemokine Induction during Human Retinal Pigment Epithelial Cell/Monocyte Interaction. *Am. J. Pathol.* 159, 1171–1180. doi: 10.1016/s0002-9440(10)61793-2

Young, R. W. (1967). The renewal of photoreceptor cell outer segments. *J. Cell. Biol.* 33, 61–72. doi: 10.1083/jcb.33.1.61

Young, R. W. (1987). Pathophysiology of age-related macular degeneration. *Surv. Ophthalmol.* 31, 291–306. doi: 10.1016/0039-6257(87)90115-9

Yu, B., Egbejimi, A., Dharmat, R., Xu, P., Zhao, Z., Long, B., et al. (2018). Phagocytosed photoreceptor outer segments activate mTORC1 in the retinal pigment epithelium. *Sci. Signal.* 11:eaag3315. doi: 10.1126/scisignal.aag3315

Zamiri, P., Masli, S., Streilein, J. W., and Taylor, A. W. (2006). Pigment epithelial growth factor suppresses inflammation by modulating xmacrophage activation. *Investig. Ophthalmol. Vis. Sci.* 47, 3912–3918. doi: 10.1167/iovs.05-1267

Zhang, C., Shen, J. K., Lam, T. T., Zeng, H. Y., Chiang, S. K., Yang, F., et al. (2005). Activation of microglia and chemokines in light-induced retinal degeneration. *Mol. Vis.* 11, 887–895.

Zhang, Y., Cross, S. D., Stanton, J. B., Marmorstein, A. D., Le, Y. Z., and Marmorstein, L. Y. (2017). Early AMD-like defects in the RPE and retinal degeneration in aged mice with RPE-specific deletion of Atg5 or Atg7. *Mol. Vis.* 23, 228–241.

Zhao, M., Bai, Y., Xie, W., Shi, X., Li, F., Yang, F., et al. (2015). Interleukin-1beta Level Is Increased in Vitreous of Patients with Neovascular Age-Related Macular Degeneration (nAMD) and Polypoidal Choroidal Vasculopathy (PCV). *PLoS One* 10:e0125150. doi: 10.1371/journal.pone.0125150

Zinn, K., and Benjamin-Henkind, J. (1979). "Anatomy of the Human Pigment Epithelial Cell," in *The Retinal Pigment Epithelium*, eds K. M. Zinn and M. F. Marmor (Cambridge, MA: Harvard University Press), 3–31.

Frontiers in Neuroscience

Provides a holistic understanding of brain function from genes to behavior

Part of the most cited neuroscience journal series which explores the brain - from the new eras of causation and anatomical neurosciences to neuroeconomics and neuroenergetics.

Discover the latest Research Topics

See more →

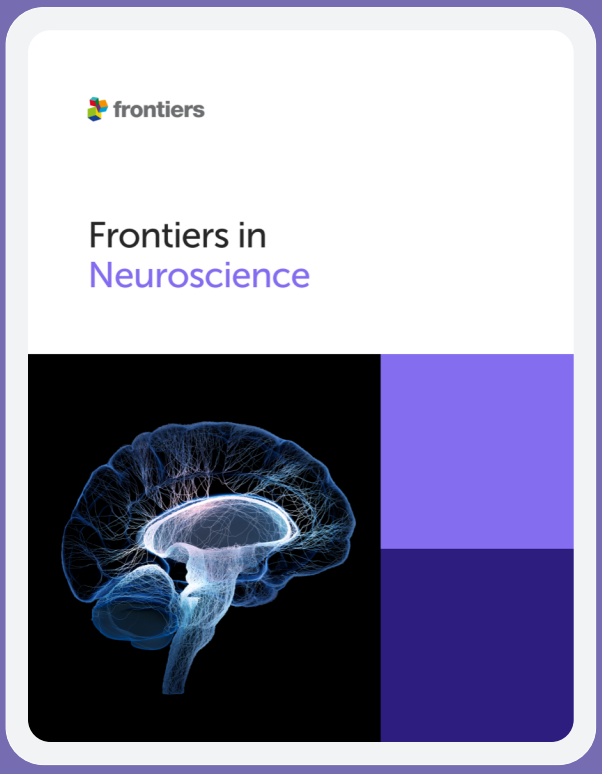

Frontiers

Avenue du Tribunal-Fédéral 34
1005 Lausanne, Switzerland
frontiersin.org

Contact us

+41 (0)21 510 17 00
frontiersin.org/about/contact